# Radiation Doses and Associated Risks from X-ray Guided Cardiac Catheterization Procedures in Children and Young Adults

Richard William Harbron, MSc, BSc

Doctor or Philosophy

Newcastle University, Institute of Health and Society

May 2016

Abstract:

Cardiac catheterizations are an essential procedure in the management of patients with congenital and acquired heart conditions. However, associated radiation doses are often high, raising concerns over potentially increased cancer risks. Neither the radiation doses, nor the associated risks, have been adequately investigated in young people undergoing these procedures.

A cohort was established of around 13,500 patients aged under 22 years who have undergone cardiac catheterizations in England. Organ doses were estimated based on a dosimetry system utilising data from Monte Carlo simulations. Doses were highest for the lungs (median: 17.6 millisieverts, mSv) and heart (13.6 mSv), while doses to bone marrow (2.6 mSv) and the thyroid (0.7 mSv) were relatively low. Radiation doses have fallen by a factor of up to ten during the study period. The results were compared to equivalent figures derived from physical measurements. Uncertainties in dose estimates were calculated. These were around ±30%, though were potentially much higher for breast dose.

The risk of cancer in relation to estimated doses was calculated using BEIR VII risk models. For examinations conducted using modern equipment, these risks are around 1 in 1700. A small epidemiological analysis was performed, suggesting a nearly threefold increased risk of cancer in the cohort, compared to the general UK population. There are a number of reasons to suggest that this increase was primarily not related to radiation exposure, most notably the large impact of transplantation and likely associated immunosuppressant use. Despite the high cancer incidence, the overall survival in the cohort was high, at around 91% after 30 years.

Conclusion: The study provides the first large scale estimation of organ doses from cardiac catheterizations among this age group. Rates of cancer among this patient group are high, although this is appears to be mostly due to factors other than radiation exposure.

Acknowledgements:
I am grateful to my supervisors, Professor Mark Pearce, Dr Jane Salotti, and Dr Claire-Louise Chapple. Thank you to Katherine Kirton and Emma Thompson for helping to transcribe paper records and numerous other things. Thank you to Richard Hardy for help with IT issues, cancer registry matching and database linkage. I am also grateful for the advice of assessors Dr Richard McNally and Dr Kevin Robson.

I also wish to acknowledge the help of radiographers, physicists, cardiologists and radiologists who have acted as local collaborators or provided information and advice: Clare McLaren, Dr Kieran McHugh, Dr John O'Sullivan, John Crompton, Steve Charlton, Johnson Mukanganiki, Ian Birch, Michaela Moore, Michelle Young, Dr Eva Dougeni, Chris Archer, Susan Reed, Mike Dunn, Ian Honey, Dr Laurence Abernethy and Dawn Smith. There are others who have helped but I never caught the name of. I also wish to thank Dr Amy Berrington de González of the National Cancer Institute, Bethesda, for advice on risk modelling and epidemiological analysis and Dr Hélène Baysson, Dr Marie-Odile Bernier, Dr Serge Dreuil and Serine Barnaoui of the Institute for Radiological Protection and Nuclear Safety in Paris for discussions on study design, dosimetry and previous publications. Thank you also to Morven Brown, Kay Mann, Lynn Driscoll, Louise Tanner, Dr Kate Best and Audrey Atkinson.

Funding:
The study received funding from the British Heart Foundation (Project Grant no. PG/15/1/31217)

# Table of Contents

# List of figures and tables:

# List of abbreviations used in this thesis:

AP: antero-posterior

ASD: atrial septal defect

AV: aortic valve

BEIR: Biological Effects of Ionizing Radiation

CT: computed tomography

E: effective dose

EAR: elevated absolute risk

EPS: electrophysiology study

ERR: elevated relative risk

FPD: flat panel detector

H: equivalent dose

HVL: half value layer

II: image intensifier

ICRP: International Commission for Radiological Protection

ICRU: International Commission on Radiological Units and measurements

IEC: International Electrotechnical Commission

kVp: peak kilovoltage

LAR: lifetime attributable risk

LNT: linear-no-threshold

mGy: milligray

mSv: millisievert

NHL: non-Hodgkin's lumphoma

PDA: patent ductus arteriosus

PV: pulmonary valve

$P_{KA}$: kerma area product

PA: posteroanterior

PVR: pulmonary vascular resistance

RFA: radiofrequency ablation

SIR: standardised incidence ratio

SMR: standardised mortality ratio

TGA: transposition of the great arteries

TLD: thermoluminescent dosemeter

UNSCEAR: United Nations Scientific Committee on the Effects of Atomic Radiation.

# 1: Introduction

This study examines the radiation doses and associated risks from cardiac catheterizations. These are procedures used for diagnosing and treating congenital and acquired heart conditions using a wire-like tube threaded through blood vessels under the guidance of a type of x-ray imaging called fluoroscopy. The procedure is an essential part of the management of congenital heart disease [1, 2]. The ability to diagnose and treat various congenital heart conditions using cardiac catheterizations comes at the price of a relatively high radiation exposure, which is associated with an increased lifetime risk of developing cancer [3]. However, epidemiological evidence of the cancer risks from cardiac catheterizations is limited to a few small, inconclusive studies [4-6]. Risk estimates are currently based on age-adjusted models derived from studies of Japanese atomic bomb survivors [7], suggesting a lifetime risk of cancer mortality from paediatric cardiac catheterization procedures of around 0.08% [8] (1 in 1250). The recent findings of increased risk of leukaemia following CT scans in childhood [9] are compatible with these estimates. However, along with a large scope for dose variation from one procedure to the next [10, 11], cardiac catheterizations result in a unique energy deposition pattern, with a high dose being delivered to a small volume. The transferability of risk estimates derived from CT or atomic bomb survivors may, therefore, be unreliable.

Faced with this uncertainty, researchers have turned to biodosimetric methods in which DNA damage is directly assessed from blood samples acquired following exposures [12-14]. These results indicate that the risks may be considerably higher than thought – around 0.4% [12]. This finding emphasises the need for a direct epidemiological assessment of the cancer risks specifically from cardiac catheterizations. Such an approach requires the following components; (1) establishing a well-characterised cohort of patients who have undergone cardiac catheterization procedures, (2) determination of the radiation doses these patients have received and (3) long-term follow-up of the cohort to assess cancer incidence and establish a dose/risk relationship. The rationale for focusing specifically on young patients is that the relatively low incidence of cancer in young people combined with the relative lack of confounding factors of cancer in this age range allows a greater statistical power in epidemiological analysis and longer follow-up time available for study. Furthermore, young patients with congenital heart conditions often undergo multiple procedures, resulting in potentially large cumulative doses. Information on

radiation doses from paediatric cardiac catheterizations is currently limited (previous research is reviewed in Chapter 2).

The following sections introduce the basic principles of fluoroscopy, before describing the application of this type of x-ray imaging in cardiology. Finally, a brief summary of the current knowledge of the risks from low dose exposure to x-rays is provided.

### *1.1: Fluoroscopy*

Fluoroscopy is an x-ray imaging system, developed soon after the discovery of x-rays by Röntgen in 1895 [15], that produces immediately viewable, dynamic, movie-like images [16]. This contrasts with general radiography (i.e. 'normal' x-ray imaging) in which a static image is recorded on film, which must be processed before viewing. As the dose per single image or 'frame' (akin to the frame of a movie reel) is relatively low, fluoroscopy is useful for situations in which simple verification of position is required without the need for high image quality. Such applications include orthopaedic surgery (alignment of screws and nails etc.), barium studies and the positioning of intravascular catheters. Most fluoroscopy systems also allow higher quality 'cine acquisition' imaging. The use of the word 'cine' harks back to the olden days where images were recorded on rolls of cine film for later viewing, although modern imaging systems record the images digitally. Acquisitions usually involve administration of iodine-based contrast agent (i.e. 'x-ray dye') which increases the attenuation properties of blood, increasing contrast between enhanced vessels and surrounding soft tissues. Other contrast agents, such as barium, may also be used, though not intravenously. Non-acquisition fluoroscopy is not usually permanently recorded, although modern equipment often features a 'fluoro-grab' function in which fluoroscopic images can be recorded. Despite this capability, the vast majority of recorded images are acquisitions and most fluoroscopic images are essentially lost forever once the procedure ends.

Fluorescent materials absorb x-ray photons before re-emitting the absorbed energy as new photons at visible light wavelengths. Briefly, this process occurs when an orbiting electron of the fluorescent material is excited by a secondary electron liberated by an x-ray, elevating it to the conduction band. The electron becomes trapped in the forbidden gap, before returning to a lower energy level, emitting a photon of visible light [17]. These visible light emissions from the fluorescent layer

can be viewed by the human eye as an image, although under normal x-ray fluence the intensity of light emitted is still quite low, producing an unacceptably dim image [17]. Modern fluoroscopy systems (post 1950s) utilise a sort of night-vision scope called an image intensifier to amplify this signal (Figure 1.1). Light photons emitted by the fluorescent layer strike a photocathode releasing electrons, which are accelerated by a 25-30 kV electric field onto an output screen where they are again converted into photons of visible light. The efficiency of the photocathode is around 10% [18], with around 300 electrons being released for a 60 keV incident x-ray photon. Further intensity gain is achieved by the demagnification of the image [18], as the output screen is around ten times smaller than the input screen. Under 'magnification mode' a larger output window size is used, meaning greater x-ray fluence is required to maintain the same signal strength [19]. Output from the image intensifer can be recorded by a video camera and immediately displayed on a television monitor. Alternatively, images may be recorded digitally, or on x-ray film to produce a permanent record.

The most commonly used fluorescent material is caesium iodide (CsI), arranged in closely packed needle-like crystal columns that function as 'light pipes' to channel fluorescence photons towards the photocathode without divergence [16]. This allows a relatively thick CsI crystal to be used without compromising spatial resolution. Furthermore, the k-edges of 36.0 keV (Cs) and 33.2 keV (I) correspond to typical photon energies used in diagnostic imaging [17], resulting in a high fractional absorption of x-rays ($\eta \approx 0.85$) [20] and high quantum detective efficiency (DQE). For each 60 keV x-ray photon absorbed, around 3000 violet light photos of 420 nm wavelength (≈ 3 eV) are emitted [16].

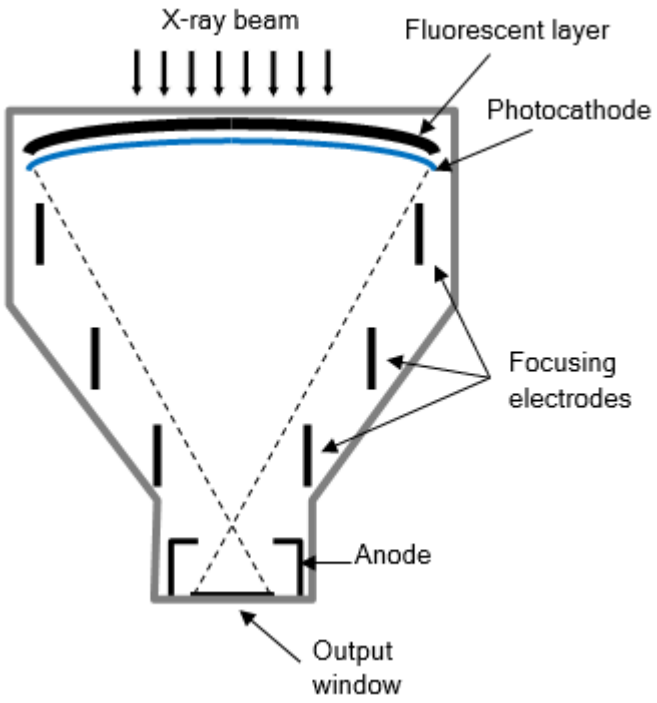


**Figure 1.1: Main features of an image intensifier. Figure credit: author**

In recent years, image intensifiers have begun to be replaced by digital, or 'flat panel' detectors (FPD). FPDs have also replaced film-screen and (to a certain extent) computed radiography (CR) detection methods in general radiography. In this sense the distinction between fluoroscopy and general radiography has become somewhat blurred. There are two types of FPD; 'Indirect conversion' digital detectors are comprised of a CsI fluorescent layer backed by an integrated active matrix array (AMA) of hydrogenated amorphous silicon (a-Si:H) [18] (Figure 1.2). Light photons emitted by the CsI layer release charge carriers (electrons or holes) in the a-Si:H layer which are stored in local capacitors and in turn read sequentially [20]. In 'direct conversion' digital detectors, x-ray photons are converted to electrons by an amorphous selenium (a-Se) photoconductive layer, backed by an integrated a-Si AMA layer. Direct conversion detectors allow improved spatial resolution compared to indirect conversion detectors, as measured by the modulation transfer function (MTF). However, with a relatively low k-edge of 13 keV, a-Se detectors have a poorer fractional absorption of x-rays ($\eta \approx 0.6$), meaning the dose efficiency, defined by the DQE, is lower [20].

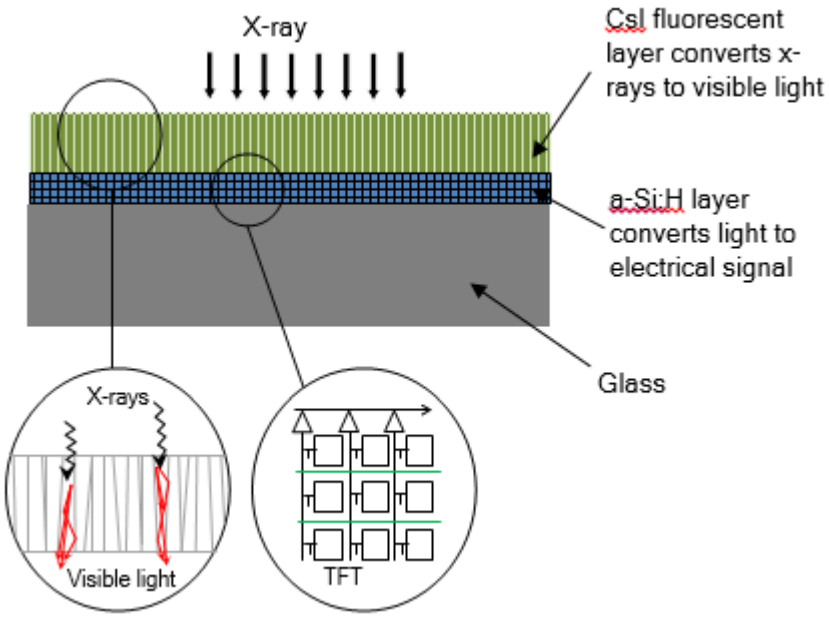


**Figure 1.2: Cross section of indirect conversion digital detectors. Figure credit: author**

FPDs have a more uniform response across the detector area than image intensifier-based systems, with no distortion and minimal veiling glare [19, 21, 22]. The impact of FPDs on radiation doses is difficult to determine, with research suggesting no impact, reduced doses [21, 22] and increased doses, compared to image intensifiers. The methodology of such studies invariably involves comparison of entire systems, of which the detector is just one component. If the x-ray tube, collimator, table, filtration and generator are also different, changes to dose indicators, such as kerma area product ($P_{KA}$, defined in Chapter 2) should not be attributed to the detector alone. Patient dose for a given value of $P_{KA}$ is strongly dependent on beam energy (see Chapter 4). Therefore a 'dose reduction', as represented by reduced $P_{KA}$, may not indicate a true change to patient dose if beam energy has changed between systems.

In most modern fluoroscopy systems, the detector and x-ray tube are joined together in a 'C-arm' configuration (actually it looks more like a 'G' or 'Ω') (Figure 1.3), with separate monitors providing real-time image display. Most systems have two such C-arms; one frontal (anterior-posterior, or AP) and one lateral. This so-called 'bi-plane' arrangement allows rapid switching between frontal and lateral imaging without the need to rotate the C-arm. Each C-arm, whether single or bi-plane, can be rotated around the patient and angled in the cranial-caudal direction to provide an almost limitless range of imaging angles known as projections. A collimation device is attached to the x-ray tube. This allows the size of the x-ray field to be adjusted. In

most cases, the field is rectangular, though older machines have circular or octagonal collimation. An ionisation chamber may also be fitted to the x-ray tube. This collects charged produce from ionisation of air by the x-ray beam, allowing the calculation of kerma area product. This is described in more detail later.

**Figure 1.3: A biplane fluoroscopy machine (Siemens Axiom Artis BC). The device pointing in from the left is the lateral x-ray tube, while the device facing this, on the right, is the lateral image intensifier. The frontal x-ray tube is obscured from view, underneath the table. Photo credit: Author**

Fluoroscopic equipment is manufactured by a number of companies, including General Electric, Siemens, Philips, Toshiba and Shimadzu. In this study, the large majority of machines were made by Philips and Siemens, with the latter dominating in the last ten years. Various configurations of *Siemens Axiom Artis* equipment were used for a large proportion of more recently acquired data. The letters following the name '*Artis*' provide more details on the equipment; d=digital (flat panel) detectors, F=floor mounted, B=Biplane, C=cardiology [23]. In all cases, an antiscatter grid is fitted to the entrance surface of the detector and can easily be removed.

Fluoroscopic equipment has evolved considerably over recent decades. It is possible to define three generations of machines based on detector type, beam energy and

other factors. In this study, data on procedures carried out using different machines will be analysed separately to explore the impact of technological factors on doses.

1st generation: Image intensifier detectors, fixed aluminium filtration, fixed antiscatter grid. Limited control of frame rates. E.g. Siemens BICOR and Angioscop.

2nd generation: Image intensifier detectors, fixed aluminium and copper filtration, fixed grid. Limited control of frame rates. E.g. Siemens BICOR Plus, BICOR TOP, Philips Integris H3000/5000.

3rd generation: Usually flat panel detectors, aluminium and variable copper filtration, removable grid, large range of frame rates and program settings. E.g. Siemens Axiom Artis/Artis Zee.

*1:2 Cardiac Fluoroscopy*

Cardiac catheterizations are a fluoroscopically guided procedure used for diagnosing and treating various congenital (i.e. those present at birth) or acquired heart conditions. Intravascular catheters are thin, wire-like tubes inserted into the body via blood vessels and used in the diagnosis and treatment of a range of conditions. The catheter is advanced from an entry point in a peripheral blood vessel - usually the femoral or radial artery - to the region of interest under fluoroscopic x-ray guidance. Once the heart has been catheterised, iodine based contrast agent can be directly injected into the heart. The relatively high atomic number of iodine (Z=53) increases attenuation (particularly by photoelectric absorption) of enhanced blood relative to surrounding tissues, thus increasing subject contrast. In fluoroscopy, the greyscale is usually reversed, with respect to radiography, meaning attenuating structures such as contrast enhanced vessels and bone appear relatively dark.

Catheterization of the chambers or blood vessels of the heart, known as cardiac catheterization was first conducted by Werner Forßmann on himself in 1929 [22]. The procedure allows a range of diagnostic and therapeutic procedures to be carried out, including coronary angiography, physiological measurements, angioplasty, and closure of septal defects. An overview of the most common cardiac catheterization procedures is provided below:

*Coronary Angiography:* Visualisation of the coronary circulation requires localised administration of contrast agent using a catheter. Pathology identified, such as vascular stenosis, may be treated by balloon inflation and/or stent insertion, known

collectively as percutaneous coronary intervention (PCI) [24]. Patients receiving a heart transplant are at risk of an accelerated form of coronary artery disease called coronary allograft vasculopathy, which can progress without clinical symptoms [25]. Consequently, transplant patients often undergo regular (i.e. yearly) coronary angiography.

*Heart Biopsy:* In endomyocardial heart biopsy (EMBx) procedures, a piece of tissue from the right ventricle of the heart is removed using a catheter with jaws called a bioptome [26]. EMBx procedures are usually carried out to assess for signs of rejection in recipients of heart transplants and are often combined with coronary angiography procedures. In contrast to most other procedures, the catheter is usually inserted via the jugular vein [26].

*Patent Ductus Arteriosus (PDA) occlusion:* The ductus arteriosus is a shortcut between the pulmonary artery and the arch of the aorta (Figure 1.4) that normally closes at birth. A failure of closure may be treated by trans-catheter delivery of a coil or mesh 'Amplatzer' device [27]. The procedure is highly effective, with few complications [28]

*Atrial Septal Defect (ASD) closure:* An ASD is a shortcut between the right and left atria (Figure 1.4), allowing oxygenated blood to flow directly to the right side of heart, thus bypassing the systemic circulation. ASDs may lead to right ventricular hypertrophy, paradoxical emboli and heart failure. Closure of ASDs may be achieved by surgery or trans-catheter implantation of an umbrella-like occlusion device. This procedure was first carried out by King and Mills in 1976 [29] and has been shown to have a similar success rate to surgery, though with a lower complication rate (7.2% verses 24%) and shorter hospital stay [30]. Some ASDs are 'fenestrated' and comprised of several holes in the septum. ASDs may be created deliberately (iatrogenic) to relieve symptoms of transposition of the great arteries (TGA) [1]. This procedure, called an atrial septostomy, was first performed by Rashkind *et al* in 1966 [31] and provides immediate relief from the symptoms of TGA until an switch operation is performed.

*Coarctation repair:* A coarctation of the aorta (COA) is a narrowing of the aorta in the region of the ductus arteriosus (arch of aorta area). It may be treated by endovascular balloon inflation or stent insertion [32-35]. Coarctations sometimes return (re-coarctation), requiring further treatment. The procedure is also used to treat coarctations developing post-operatively [1].

*Electrophysiology studies (EPS) and Radiofrequency ablation (RFA):* EPS procedures are used to investigate the electrical conduction pathways in the heart and can be used to locate the source of cardiac arrhythmias. These arrhythmias, such as that caused by Wolff-Parkinson-White (WPW) syndrome, can then be treated using radiofrequency ablation, first used in the late 1980s [30]. A current is passed through a catheter placed in contact with a region of myocardium suspected as being the source of the arrhythmia, causing thermal damage of the tissue [24].

*Valvuloplasty:* In cases where the aortic valve (AV) or pulmonary valve (PV) is narrowed (stenosis), a balloon may be inflated to improve blood flow. Balloon valvotomy of pulmonary stenosis was first performed in 1982 by Kan and colleagues [36] and is considered a safe and effective method of relieving obstruction, with a single procedure providing relief for decades or even a lifetime [1]. Aortic valvuloplasty was first performed in 1984 by Lababidi *et al* [37]. The procedure is considered more dangerous and less effective than pulmonary valvuloplasty [1].

*Pulmonary artery angioplasty:* Narrowed pulmonary arteries can be made more patent through balloon inflation and stent insertion. The procedure was first performed by Lock and colleagues in 1981 on newborn lambs [38] before being used in humans in 1983 [39]. The procedure is commonly employed in patients with Tetralogy of Fallot (a condition involving four distinct pathologies of the heart), and while usually effective, may occasionally result in haemodynamic instability or vascular rupture. Mortality has been reported at 0.2% [1].

*Pacemaker insertions:*

Not strictly a catheterization, fluoroscopy is also used to guide the implantation of the wires for pacemakers. Beginning in 1970, many patients were given plutonium ($^{238}$Pu) powered pacemakers, designed to reduce or eliminate the need for power source replacement [40]. These pacemakers were cost effective and relatively free of complications [41, 42], though are now unnecessary due to improvements in battery life.

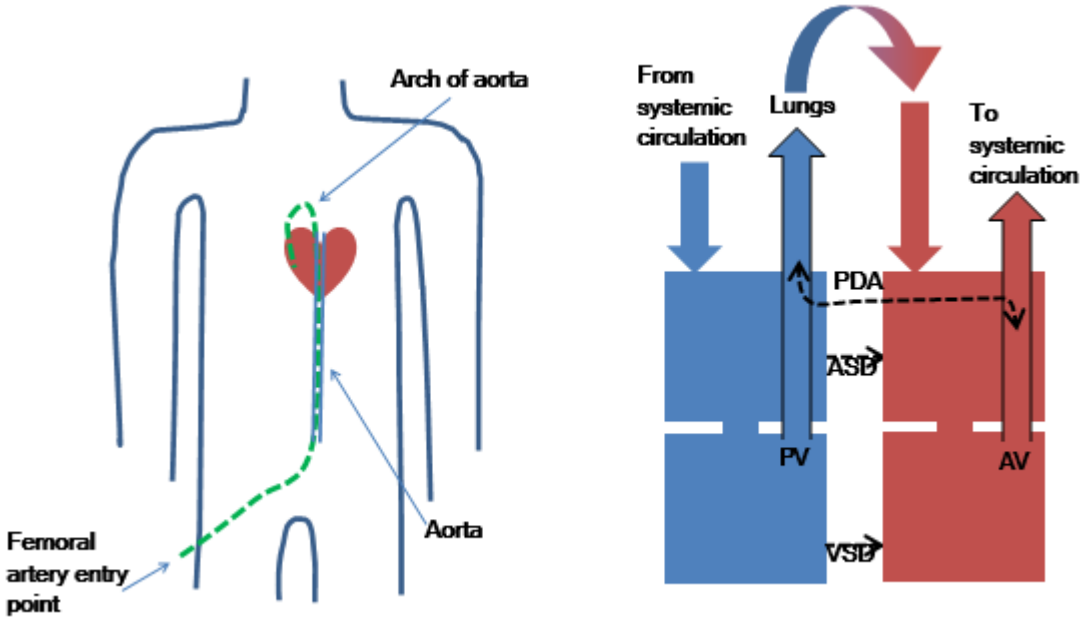


**Figure 1.4: Catheterisation of the heart (left) and a schematic diagram of the heart (right). AV=aortic valve, PV=pulmonary valve. Figure credit: author**

### 1.3: Risks from x-rays

X-rays are a form of electromagnetic radiation, sufficiently energetic to cause ionisation of atoms or molecules [43] (a more complete description can be found in Appendix 1). Ionisation within cells may lead to breakage of DNA, either directly or indirectly via hydrolysis and subsequent oxidative stressing by reactive oxygen species [16]. DNA damage may result in cell killing or cell mutation. The former is only significant when occurring to a sufficient extent to cause a noticeable tissue deficit known as a 'tissue reaction' [44]. A well-known tissue reaction, familiar to millions of British holidaymakers, is sunburn - a radiation injury caused by ultraviolet radiation. X-rays may also cause sunburn (or erythema), along with injuries to deeper lying tissues, although the doses required for these effects (>2 Gray) are much larger than those typical of diagnostic imaging (<50 milligray) [16].

In contrast to cell killing, a single mutated cell may, theoretically, undergo malignant transformation, leading to the later development of cancer [45, 46]. For over sixty years, the preferred model for describing the relationship between radiation dose and associated risk has remained the linear-no-threshold (LNT) model [3, 44, 47]. This assumes two things; firstly that there is no threshold dose below which there is no risk of developing cancer, and secondly that the risk increases in linear proportion to dose. The LNT model was originally ‘conceived’ to describe hereditary effects of

radiation following research by Muller and Mott-Smith on fruit flies in the 1920s [48]. Muller campaigned for decades for the LNT model to be adopted as the underlying principle of radiation protection, finally convincing the United States National Academy of Sciences in 1955 [49]. Although the early concerns of hereditary effects of radiation were later found to be overly pessimistic [50], the LNT model became the preferred choice to describe the induction of cancer in exposed individuals.

An analogy for the LNT relationship is the lottery; a single ticket is all it takes to win the jackpot. This may be very unlikely but the 'risk' of winning increases linearly with the number of tickets bought (Figure 1.5). Also the size of the jackpot does not increase with the number of tickets bought (this isn't strictly true as each ticket adds to the jackpot fund, but buying ten tickets instead of one certainly would not give you a ten times larger prize).

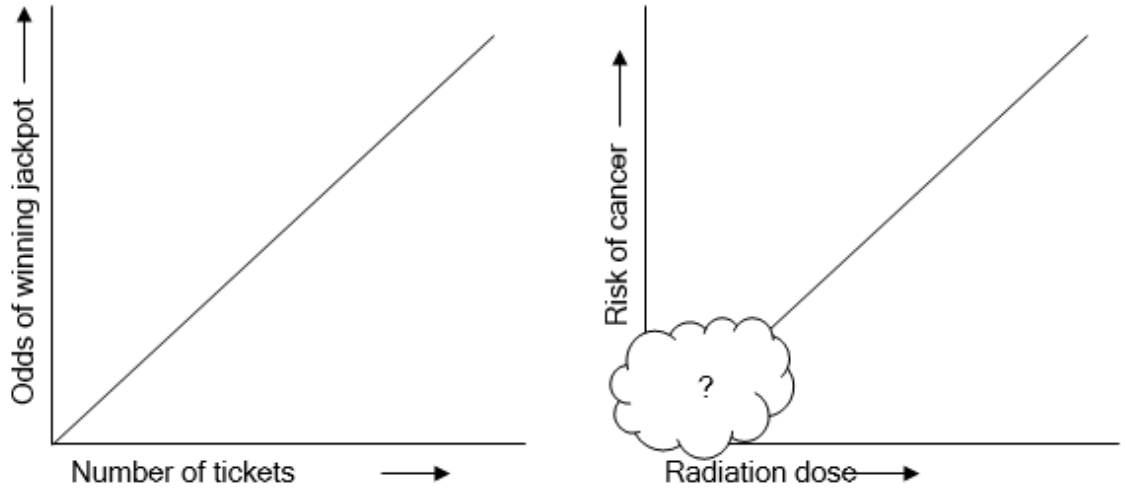


**Figure 1.5: The Linear-no-threshold model describing the relationship between radiation dose and cancer, and between lottery tickets and 'risk' of winning the jackpot. Figure credit: author**

The chances of winning the lottery jackpot seem trivially small – about 1:45 million. Yet since 1994 about 3700 people in Britain have struck it lucky [51], by virtue of the huge number of people playing. The same logic can be applied in radiation protection; Even though the risks of developing cancer from radiation exposures may appear trivially small to an individual (typically ranging from 1 in 1000 to 1 in 1 million for diagnostic dose levels [52]), a non-trivial cancer burden on society may be expected if sufficiently large numbers of people are exposed. In 2004, the number of excess cancer cases induced by diagnostic medical radiation procedures in the UK

was estimated to be around 700 [53]. This figure was based on the assumption that the LNT model correctly describes the dose-risk relationship between radiation and cancer. However, this assumption is difficult to prove.

Radiation induced cancers are not histologically distinct from those associated with numerous other risk factors [3] – smoking, diet, lifestyle, genetic factors, viruses etc. Excess cancers in populations exposed to radiation can be difficult to detect above background variation. Currently, the best available evidence of the cancer risks from low doses of radiation – the cohort of survivors of the nuclear bombings of Hiroshima and Nagasaki – can only detect a significant excess risk above doses of around 100-200 millisieverts (mSv) [7], where an approximately linear relationship is seen. The magnitude of excess risk at dose levels typical of medical diagnostic and interventional examinations (below around 50 mSv) can only be estimated by downward extrapolation, assuming a linear-no-threshold relationship. This practice remains controversial [46, 54-57] and other models have been advocated (Figure 1.6). The 'hormesis' model, a popular subject of the journal *Dose Response*, assumes exposure to low doses decreases cancer incidence compared to background levels. The 'bi-modal' model proposed by Busby [58] relates more to internal exposures from radioactive substances and assumes that small doses are especially dangerous. The 'threshold' model, supported by the French Academy of Sciences [59] implies that cellular defence mechanisms successfully eliminate risk at low doses, meaning that radiation doses typical of normal background levels or diagnostic medical exposures carry no or negligible risk.

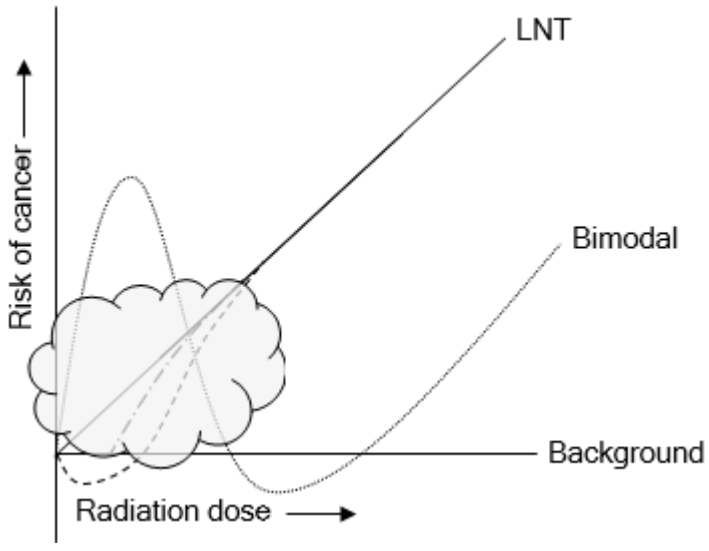


**Figure 1.6: Alternative models to LNT (solid line) include threshold (dot-dash), and hormesis (dashes). Figure credit: author**

This uncertainty is unfortunate as the central principle of radiation protection – that of justification – involves weighing up the potential risks from radiation exposures against the diagnostic or therapeutic benefit for the patient [52, 60]. The uncertainty in the magnitude of risks from low dose exposures to ionising radiation is relevant to all forms of medical radiation exposures, including cardiac catheterizations.

### 1.4: Study rationale

Cardiac catheterizations undoubtedly play a vital role in the management of congenital and acquired heart conditions. Because these procedures involve often lengthy exposure to x-rays, there are concerns over the potential for long term health effects, most notably an excess risk of developing cancer. Currently, information on the radiation doses from cardiac catheterizations is limited and risks can only be estimated by extrapolation of the known risks at higher doses. Uncertainties in the magnitude of doses and associated risks result in difficulty in justification and optimisation of all medical radiation studies, including cardiac catheterizations. The study aim was to estimate radiation doses from these procedures based on data recorded at the time of the examination, then estimate the risks using existing risk models and epidemiological analysis.

The aims of the PhD were as follows;

1. Estimate the radiation doses from x-ray guided cardiac catheterizations conducted on children and young adults with congenital heart disease.
2. Estimate the risk of cancer in relation to these doses.

Objectives:

1. Establish a cohort of people with congenital heart disease who have undergone cardiac catheterizations.
2. Produce a dosimetry system capable of estimation of organ doses from details recorded at the time of examinations.
3. Estimate radiation associated cancer risks using existing risk models.
4. Conduct a direct epidemiological analysis of these risks by matching cohort members with cancer registry data.

## 1.5: Structure of thesis

The following chapter will be a literature review of evidence of the effects of low doses of ionising radiation and the doses likely to be delivered from cardiac catheterizations. Later chapter will discuss the establishment of a retrospective cohort, dose estimation, risk estimation and epidemiological analysis. Each of these four chapters will be subdivided into methods, results and discussion, thus making them like self-contained studies. This organisation was an alternative to putting methods for each type of analysis in the same place, followed by the results for each type etc.

# Chapter 2: Literature review

A review was conducted of previously published research in two main areas; (1) existing knowledge of the radiation doses from cardiac catheterizations in children and young adults, including evaluations of various methodologies for estimating organ doses and effective dose, and (2) epidemiological studies assessing the potential cancer risks following exposures to ionising radiation. The search methodologies used are described separately for each of these areas.

## *2.1: Dosimetry*

The following sections describe the various measures of radiation dose referred to in this study, before reviewing previously published data on doses specific to x-ray guided cardiac catheterizations.

### *2.1.1: Measures of radiation dose*

Information was primarily obtained from the International Commission on Radiation Units and measurements (ICRU) [61, 62], along with textbooks on diagnostic imaging and radiotherapy physics [16, 43]. Measures of radiation dose include absorbed dose (D), equivalent dose (H), effective dose (E) and kerma (K). Different measures (particularly equivalent and effective) are often simply described as 'dose' or have the same units, which can lead to confusion [63]. Almost all previously published assessments of doses in cardiac catheterizations are based on kerma area product ($P_{KA}$), also known as dose area product (DAP), and fluoroscopic screening time. Both should be regarded as 'dose indicators' rather than as a true measure of absorbed dose to patient organs.

*Absorbed dose:* The fundamental measure of the biological effect of ionising radiation is the absorbed dose (D), which is defined as the mean energy imparted [by ionising radiation] ($d\bar{E}$) to mass *dm* of material:

$$D = \frac{d\bar{E}}{dm}$$

**Equation 2.1**

The SI unit of absorbed dose is the gray (Gy) defined as one joule (J) of energy absorbed per kilogram of material. The older unit of the 'rad' represents 100 ergs per gram [43], therefore 1 Gy = 100 rad, or 1 rad = $10^{-2}$ Gy or 1 cGy. Absorbed dose can

be related to the average mass absorption coefficient ($\bar{\mu}_{en}/\rho$) and the energy fluence ($\psi$):

$$D = \psi \cdot \left(\frac{\bar{\mu}_{en}}{\rho}\right)$$

**Equation 2.2**

Absorbed dose, as a point measurement (denoted by the derivative notation), is suitable for describing localised (i.e. partial organ or cell-level) exposures such as tumour dose in radiotherapy or *in vitro* experiments. It may be used to estimate stochastic risk provided the amount and type of tissue involved is defined. Localised diagnostic dose levels are typically in the 0-50 mGy range [64]. At a dose of 1 mGy, each cell nucleus is crossed by an average of 1 secondary electron track [65]. The mean dose ($D_m$) to a specific organ or tissue of mass $m_t$ can be defined as:

$$D_m = \frac{1}{m_t} \cdot \int_{m_t} D \cdot dm$$

**Equation 2.3**

*Equivalent dose:* The absorbed dose required to produce a certain biological endpoint varies between different types of radiation, such as photons, neutrons or alpha particles [66]. This is taken into account by the equivalent dose (H), which is defined as the mean dose to organ T by radiation type R ($D_{T,R}$), multiplied by a weighting factor $w_R$ designed to takes into account varying biological effectiveness of the radiation type. For photons and electrons, the value of $w_R$ is 1, while for protons it is 2 and for alpha particles or fission products it is 20. For exposures involving multiple radiation types, the equivalent dose is defined as the sum of each contribution:

$$H_T = \sum_T W_R \cdot D_{T,R}$$

**Equation 2.4**

Or, combined with equation 2.3, above:

$$H_T = \sum_T W_R \cdot \left(\frac{1}{m_T} \cdot \int_{m_T} D \cdot d_m\right)_{T,R}$$

**Equation 2.5**

Note that the earlier measure of ‘dose equivalent’ is not organ averaged. Equivalent dose is designed for estimation of stochastic risks from radiation exposures. As dose is averaged over the whole organ; equivalent dose is not suitable for evaluation of acute radiation effects or tumour dose in radiotherapy. In the case of estimation of stochastic effects, assuming a linear dose response, this averaging out should make no difference as the total energy imparted remains the same. Equivalent dose will be used to describe organ doses in this thesis, rather than ‘mean absorbed dose’ in gray. Although the units of equivalent dose (sieverts) are the same as for effective dose (described below), the distinction between these two measures will always be made clear.

*Effective dose:* It is difficult to compare the stochastic risk from localised exposures of different parts of the body (e.g. a chest x-ray compared to a CT scan of the head), or to compare exposures of the same body part but with different exposure patterns (e.g. a cardiac CT scan with a cardiac nuclear medicine scan). One way to avoid this problem is to simply average out a localised dose over the whole body. The problem of the 'mean whole body dose' approach is that the stochastic risk of cancer induction varies from one tissue to another. The effective dose (E) is designed to account for this variation by the application of specific weighting factors for each tissue ($W_T$). Effective dose is defined as the sum of the equivalent dose to each organ ($H_T$) multiplied by its respective tissue weighting factor ($w_T$).

$$E = \sum H_T \cdot w_T$$

Equation 2.6

Weighting factors are calculated by the International Commission on Radiological Protection (ICRP) [44], based on the risk of cancer induction for each organ and adjusted for associated lethality, quality of life and years of life lost (Table 2.1). Organs that are remote from the site of irradiation will only receive a small equivalent dose (mainly due to scattering) and therefore contribute little to the effective dose, even if the weighting factor for that organ is high. Effective dose is used to estimate stochastic risks for populations, rather than individuals.

| Organ/tissue | ICRP 60 [67] | ICRP 103 [44] |
|---|---|---|
| Bone marrow | 0.12 | 0.12 |
| Lungs | 0.12 | 0.12 |
| Colon | 0.12 | 0.12 |
| Stomach | 0.12 | 0.12 |
| Breasts | 0.05 | 0.12 |
| Thyroid | 0.05 | 0.04 |
| Liver | 0.05 | 0.04 |
| Oesophagus | 0.05 | 0.04 |
| Bladder | 0.05 | 0.04 |
| Salivary Glands | - | 0.01 |
| Brain | - | 0.01 |
| Skin | 0.01 | 0.01 |
| Bone surface | 0.01 | 0.01 |
| Remainder | 0.05 | 0.12 |
| Gonads | 0.20 | 0.08 |
| Total | 1.0 | 1.0 |

**Table 2.1: Effective dose tissue weighting factors.**

*Kerma:* The kerma, or KERMA (Kinetic Energy Released per unit MAss), not to be confused with korma (a lightly spiced, coconut-based curry), is the sum of the initial kinetic energies of secondary electrons liberated by uncharged ionising radiation ($dE_{tr}$) in material of mass *dm* [43].

$$K = \frac{dE_{tr}}{dm}$$

**Equation 2.7**

Like absorbed dose, kerma is measured in gray and the two measures can closely approximate each other. The energy transfer coefficient ($\bar{\mu}_{tr}$) defines the fraction of photon energy transferred to secondary electrons, in the form of kinetic energy, per unit thickness of material [43]. Kerma can be calculated from this figure, divided by the material's density (i.e. the mass energy transfer coefficient, $\bar{\mu}_{tr}/\rho$) and the photon energy fluence ($\psi$):

$$K = \psi \cdot \left(\frac{\bar{\mu}_{tr}}{\rho}\right)$$

**Equation 2.8**

Comparing this to the equivalent calculation for absorbed dose (Equation 2.2), it can be shown that:

$$\left(\frac{\bar{\mu}_{en}}{\rho}\right) = \left(\frac{\bar{\mu}_{tr}}{\rho}\right)(1 - \bar{g})$$

**Equation 2.9**

Where g is the fraction of energy lost to radiative processes. For photon radiation under 1 MeV, g is less than 0.4% [68], thus at diagnostic energy levels (usually <100 keV), the numerical values of kerma and absorbed dose are approximately the same. Differences between kerma and absorbed dose are shown in Figure 2.1.

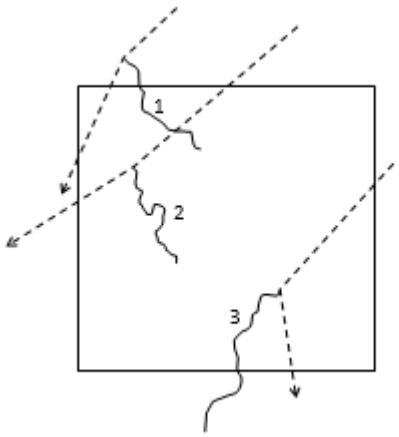


**Figure 2.1: X-rays (dashed lines) liberate secondary electrons (continuous lines) both inside and outside the volume of interest. The electron contributing track 1 is released outside the volume, thus does not contribute to the kerma, but imparts some of it's energy within the volume, thus contributing to absorbed dose. Electron 3 is released inside the volume, thus does contribute to kerma, though imparts some of its energy outside the volume. Figure credit: author**

Kerma can be divided into collision kerma ($K_{col}$) and radiative kerma ($K_{rad}$). The former results from soft and hard collisions with atoms, while the latter includes losses due to Bremsstrahlung interactions and electron/positron pair annihilation [69]. The latter process cannot occur when photon energies are below 1.02 MeV (i.e. twice the rest mass of an electron/positron), while Bremsstrahlung emissions are relatively unimportant in materials with a low atomic number, being proportional to $Z^2$ [43]. Thus at diagnostic photon energies, $K_{col}$ is the dominant component of total kerma.

*Dose indicators:*

All measures of dose thus far described are time consuming or impossible to measure *in vivo*, requiring some form of dose measuring device to be placed on or within the patient. None are routinely measured in clinical practice, or are readily

available for historic examinations. Kerma area product, given the symbol $P_{KA}$ by ICRU [70] (or KAP), is approximately equal to absorbed dose in air multiplied by beam area in a plane perpendicular to the beam central axis. $P_{KA}$ is either measured by a large area transmission ionisation chamber fitted to the exit port of the x-ray tube, or alternatively, estimated based on exposure factors. $P_{KA}$ has the advantage of being routinely recorded for almost all general radiographic and fluoroscopic x-ray exposures. The following section describes the principles of physical acquisition of $P_{KA}$, before outlining the relationship with patient dose.

Ionisation of air molecules occurs along the tracks of electrons liberated by x-ray photons passing through the chamber. Positive and negative ions move toward their respective collecting plates, producing a current measured by an electrometer (Figure 2.2). Under the assumption of electronic equilibrium (see figure 1), the exposure (X) can be calculated. This is defined by ICRU as *dQ/dm*, where *dQ* is the absolute value of the total charge of ions of one sign produced in [dry] air when all electrons and positrons liberated or created by photons in air of mass *dm* are completely stopped in air [62]. Exposure is measured in Coulombs per kilogram (C/kg), though the older unit of the Röntgen (R) is sometimes encountered, where 1 R = 2.58 $x10^{-4}$ C/kg.

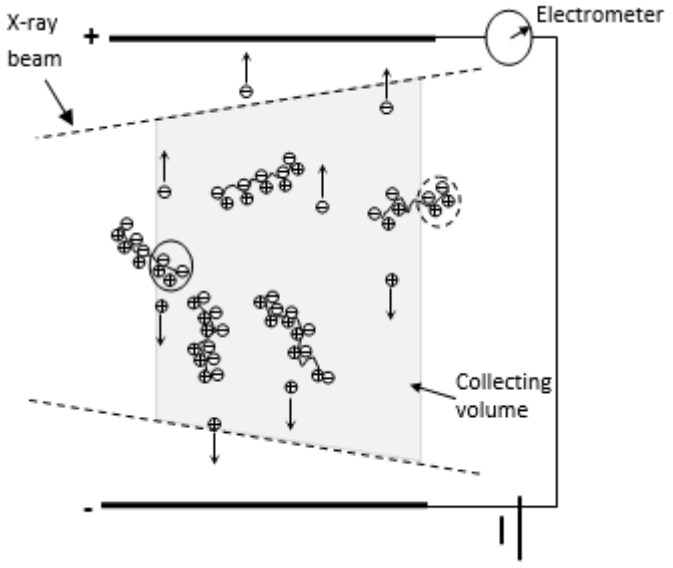


**Figure 2.2: Electrons liberated by x-ray photons generate ion pairs, which are collected by positively and negatively charged plates. For charged particle equilibrium to occur, collected ion pairs created by electrons liberated outside the volume (solid circle) must equal those not collected, created by electrons liberated within the volume (dashed circle).** Figure credit: author

The *exposure area product* (EAP), measured in R·$cm^2$, is approximately equal to exposure multiplied by area irradiated (A) defined by the collimators. As beam

intensity is uneven (e.g. due to the anode heel effect), EAP is more properly defined as the integral of X with respect to area:

$$EAP = \iint_A X(x,y)\,dx\,dy$$
$$\approx X \cdot A$$

**Equation 2.10**

The most recent estimate of the mean energy required to produce a single ion pair in air ($\overline{W}$) is 33.97 electronvolts (eV) [71], or 5.442 x $10^{-18}$ J. The average energy to produce one unit of charge, in Coulombs, is defined as $(\overline{W}/e)\ J/C$, where e is the charge of a single electron (1.602 x $10^{-19}$ C). Therefore:

$$\left(\frac{\overline{W}}{e}\right) = \left(\frac{33.97(eV/ion\ pair) \cdot 1.602 \text{ x } 10^{-19}(J/eV)}{1.602 \text{ x } 10^{-19}\ (J/ion\ pair)}\right) [8]$$

= 33.97 J/C

**Equation 2.11**

By multiplying the exposure (in C/kg) by this figure, the energy released by the x-ray beam per unit mass of air (i.e the air kerma) can be determined. As radiative losses (i.e. due to Bremsstrahlung interactions) are not accounted for, the result is more accurately described as *air collision kerma* ($K_{col,air}$):

$$K_{col,air} = X \cdot \left(\frac{\overline{W}}{e}\right)$$
$$= X \cdot 33.97$$

**Equation 2.12**

Kerma area product, or rather *collision kerma area product*, is the integral of air collision kerma with respect to area:

$$P_{KA} = \iint_A K_{col,air}(x,y)dx\,dy$$
$$\approx K_{air} \cdot A$$

**Equation 2.13**

The units of $P_{KA}$ are Gy·cm$^2$. Smaller doses are often quoted as cGy·cm$^2$, mGy·cm$^2$, or µGy·m$^2$. Some authors quote doses in R·cm$^2$, which can be converted to Gy·cm$^2$ by multiplying by 8.764 x$10^{-3}$ (i.e. the product of 2.58 x$10^{-4}$ (C/kg)/R and 33.97 J/C). The absorbed dose in air ($D_{air}$) can be defined as follows:

$$D_{air} = K_{col,air} \cdot (1 - g)$$

**Equation 2.14**

As mentioned previously, g is the fraction of energy lost to radiative processes. As this fraction is very small at diagnostic energy levels, collision air kerma can reasonably be considered approximately equal to absorbed dose in air. $P_{KA}$ and *dose area product* (DAP) are essentially the same thing, although in reality it is the former that is actually being measured.

Kerma area product is almost independent of distance from the source. This can easily be appreciated by considering that area is proportional to the square of distance (d) from the source ($A \propto d^2$), while x-ray intensity (I) is inversely proportional to the square of distance ($I \propto 1/d^2$). The product of both should therefore be constant, though, in reality, scattered and extrafocal radiation result in a small level of distance dependence [72].

It is important to understand that $P_{KA}$ is an *indicator* or patient dose rather than an absolute measure in itself. The relationship between $P_{KA}$ and patient dose is strongly dependent on a range of parameters, in particular beam energy, projection angle and patient size (this relationship is explored in depth in the Chapter 4). Comparison of $P_{KA}$ figures acquired using different equipment, patient sizes or examination types requires caution. Still, useful observations can be made from such dose indicators that will have important implications for studies of doses and associated risks.

*Calibration and uncertainty:*

$P_{KA}$ meters must be regularly calibrated to national standards. Quoted allowable uncertainties range from 7% [73] to 35% [74]. The International Electrotechnical Commission (IEC) recommend a combined uncertainty of 25% for $P_{KA}$ and air kerma measurements [75]. The International Atomic Energy Agency (IAEA) [76] describe the following calibration process, consisting of two steps; (1) measuring the air kerma at a distance $d_r$ from the focus (i.e. the part of the anode acting as the x-ray source), and (2) moving the device to a second position, downstream from a circular or square lead aperture with a known diameter at a distance $d_a$ from the focus. The calibration factor, $N_{PKA,Q}$ is then defined as:

$$N_{P_{KA,Q}} = \frac{KA(d_r/d_a)^2}{M_{KAP}k_{TP}^{KAP}}$$

**Equation 2.15**

Where $M_{KAP}$ is the reading obtained by the meter [76]. An alternative 'tandem' method has been described by Pöyry *et al* [77] and Toroi *et al* [78] in which both the field $P_{KA}$ meter to be calibrated and the reference meter are placed in the beam together.

### *Air Kerma:*

The air kerma ($K_{air}$) at a particular distance from the source can be calculated by simply dividing $P_{KA}$ by the beam area at that distance. This provides a method of estimating patient skin dose using $P_{KA}$, without resorting to the placement of dose measuring devices on the patient's skin. The location of the skin is estimated using the methodology of the IEC [79], who define the 'international reference point' as being at a location along the central axis of the x-ray beam 15 cm above (i.e. 'upstream' from) the isocentre between source and detector [74]. However, to provide a true estimate of entrance skin dose (ESD), the backscattering of x-rays and secondary electrons from deeper lying tissues must be taken into account, in the form of a backscatter factor (BSF). The BSF, defined as the ratio of air kerma at the patient surface to the air kerma at the same distance in the absence of the patient, increases with beam quality, field size and (slightly) focus-skin distance [70], typically ranging from 1.3 to 1.5 for a 25 x 25 cm field [80].

Even if accounting for backscatter, skin dose estimates provide no information on the distribution of dose over the patient's skin [74]. The beam is rarely in a fixed position throughout the procedure [81], meaning energy is imparted over a wider area of skin than suggested by the beam area.

## *2.1.2: Previously published data on doses*

A previous review was published by Neofotistou in 2001 [10] of reported doses from adult and paediatric cardiac catheterizations. A large number of new studies have been published since this review and the figures quoted by Neofotistou can considered to be unreliable (for example, the author misquoted figures from two out of the three studies in which paediatric doses were reported). A new review of published doses was therefore required. This served a number of purposes; (1)

assess the magnitude and variation in doses, (2) identify factors affecting doses, and (3) evaluate the potential to estimate organ doses from the information likely to be obtainable from participating hospitals.

Literature on doses was identified by searching Medline and Pubmed. Search terms were 'cardi*', 'catheteri*', 'fluoroscop*', 'dos*', 'paediatric', 'pediatric' and 'child*'. The reference list of identified papers was searched for further relevant publications. Most of these studies focus specifically on either childhood or adult exposures, with average age of patients in the latter group typically over 60 years. Some studies focus on all patients with congenital heart disease (CHD). These tend to be predominantly children, though studies may also include some patients followed into adulthood [82, 83]. Forty seven studies were initially identified as being relevant. Five studies reported methodologies for calculating organs doses or effective dose, rather than doses from clinical examinations [84-88]. Two studies focussed on risks but provided no information on doses [89, 90]. Forty studies were identified in which doses were reported.

A summary of reported dose indicators is provided in table 2.2. A number of observations stand out. Firstly, average $P_{KA}$ is seen to vary with procedure type; figures were typically highest for right ventricular outflow tract (RVOT) dilatation and lowest for atrial septal defect (ASD) occlusions and endomyocardial heart biopsies. Secondly, there is a strong trend of increasing $P_{KA}$ with increasing patient size (either mass or age); this is unsurprising given the increased x-ray output required to maintain the same intensity at the detector as attenuator thickness increases, and also the increased beam area required to include the region of interest. Thirdly, an enormous variation in $P_{KA}$ is seen between different studies; for example, there is a more than 50-fold variation in median $P_{KA}$ for interventional procedures in studies by Ait Ali *et al* [13] and Smith *et al* [22].

Regarding the third observation, there are a number of possible explanations. Firstly, the ages of patients vary between studies. Given the tenfold or more increase in examination $P_{KA}$ between newborns and young adults, a small difference in the average age of study subjects could explain a sizeable difference in average $P_{KA}$. Yet large variations are seen even where data are stratified by patient age or mass. Interestingly, there is a tendency for $P_{KA}$ to explode upwards to very high values (over 80 Gy·cm²) for larger patient sizes in some studies (e.g. Verghese [82], Glatz [91],

Ghelani [83]), but not in others (e.g. Barnaoui [92], McFadden [93], Martinez [94]), where the increases in $P_{KA}$ with patient size are relatively restrained.

A second reason for variation in $P_{KA}$ is that studies may include a different mix of procedure types. If a particular hospital specialises in complex procedures such as valve replacements, this could result in an unusually high average $P_{KA}$ where data for all procedure types are presented together. However, large discrepancies remain, even where studies are stratified by procedure type. For example, a 10-60 fold variation in median $P_{KA}$ for ASD occlusions was seen between studies led by Barnaoui [92], and Verghese [82], depending on age group. The screening times of the latter study are longer, but to a much smaller extent than the increase in $P_{KA}$.

A third explanation for $P_{KA}$ variation relates to equipment differences. This includes not only the model of fluoroscopic equipment used, (e.g. Siemens Axiom Artis, Philips Integris etc.), but also includes the way the machine is set up, including frame rates, dose rate and antiscatter grid usage. Here, the desire to reduce radiation doses conflicts with the desire to obtain satisfactory image quality [95]. The signal-to-noise ratio (SNR) quantifies the 'graininess' of the image by relating useful signal to random quantum fluctuations in photon fluence [96]. Photon counting statistics conform to a Poisson distribution [95], meaning variance ($\sigma^2$) is equal to the square root of photon count (N). Thus SNR is $N/\sqrt{N}$, which simplifies to $\sqrt{N}$ [16]. At this superficial level, 'image quality' is subject to a law of diminishing returns – to increase SNR by a factor of 2, photon fluence, and hence patient dose, would need to be increased by a factor of $2^2$. This relationship does not take into account the ability of the imaging system to process useful signal and noise – a characteristic described by the system's 'detective quantum efficiency' (DQE) – essentially a frequency dependent measure of image quality per unit dose [16, 97]. The DQE, and the related measure of 'effective DQE' (eDQE) take into account a range of other factors in addition to photon count, including handling of electronic noise, focal spot size and control of scattered radiation [97]. Post-acquisition image processing techniques, such as recursive filtering, may also improve image quality for a given dose [98, 99]. Thus, increased image quality does not necessarily come at the expense of increased dose [96].

| Study (Collection date) | Subjects | Median age/weight | Age/weight range | Median FT (mins) [IQR] | Median DAP (Gy·cm²) [IQR] | Mean DAP (Gy·cm²) [SD] | Median DAP per unit weight (Gy·cm²/kg) [IQR] |
|---|---|---|---|---|---|---|---|
| **Combined diagnostic** | | | | | | | |
| Campbell (1997)(MD 1)* | 18 | | 4m - 20y | 4.4 [R: 1.4-28.2] | 5.22 [R: 0-22.84] | 7.25 [7.75] | |
| Campbell (1997) (MD 2)* | 26 | | | 5.4 [R: 2.4-42.2] | 2.31 [R: 0.62-6.34] | 2.64 [1.57] | |
| Schultz (published 2003) §§ | 18 | | | | 4.45 | | |
| Bacher (published 2005) (0.2 mm Cu) ** | 15 | 2.4 y | 0.1-8.8 y | 4.9 [R: 0.5-14.5] | 5.48 [R: 1.14-14.61] | | |
| Bacher (published 2005) (0.4 mm Cu) ** | 13 | 1.3 y | 0.1-9.2 y | 3.9 [R: 1.6-33.2] | 3.37 [R: 0.96-13.99] | | |
| Martinez (2007) | 58 | | <1 y | | | 1.9 [0.3] $$$ | |
| | | | 1-5 y | | | 4.2 [0.9] $$$ | |
| | | | 5-10 y | | | 4.2 [0.9] $$$ | |
| | | | 10-16 y | | | 8.6 [2.7] $$$ | |
| Al Haj (2000-2002) | 60 | | 0-12 y | | | 7.77 [14.3] | |
| Dragusin (>2005) | 9 | | 1–30 d | 11 [ 18, 6] | 2.7 [ 2.3, 4.1] | | |
| | 27 | | 1-12 m | 6 [ 4, 11] | 2.5 [ 1.2, 5.4] | | |
| | 19 | | 1-3 y | 10 [ 8, 14] | 5.1 [ 3.1, 8] | | |
| | 24 | | 3-5 y | 8 [ 5.25, 14] | 5.8 [ 2.9, 9.4] | | |
| | 34 | | 5-10 y | 8 [ 5.75, 10.5] | 7.1 [ 4.4, 12.3] | | |
| | 13 | | 10-15 y | 5 [ 3, 16.5] | 9.9 [ 3.5, 16.6] | | |
| Beels (published 2009) | 17 | 1.77 y | 0-11.8 y | 8.3 [R: 0.6-27.4] | 5.55 [R: 0.7-16.6] | | |
| Yakoumakis (published 2009) | 42 | | 1 d-14 y | | | | |
| Karambatsakidou(1999-2004) | 139 | | 0-0.5 y | | | 3.7 [2.6] | |
| | | | 0.5-2.5 y | | | 6.0 [5.8] | |
| | | | 2.5-7.5 y | | | 7.6 [9.5] | |
| | | | 7.5-12.5 y | | | 15.9 [12.9] | |
| | | | 12.5-18 y | | | 37.9 [52.3] | |
| Onnasch (1998-2003) | 1106 | 11.0 kg | 1.7-115 kg | | | | 0.28 [75%: 0.5] |
| Ait Ali (2007) | 13 | 0.7 y | 0.4-11 y | | 14 [12, 28] | 20.85 [16.9] | |
| Gherardi (2008-2009) | 210 | | 0-15.6 y | 7.5 [R: 0.3-55] | 3.2 [R: 0.2-21.0] | | |
| Watson (2009-2010) | 50 | | 0-18 y | 16 | 12.00 [R: 3-143] | | |
| Watson (2009-2010) ## | 23 | | <1 y | | | | |
| El Sayed (published 2012) | 46 | 4.17 y | | | | 3.78 [2.5] | |
| Verghese (2005-2009) | 242 | | <1 y | 26 | 7.43 [4.33, 14.43] | | |
| | 134 | | 1-4 y | 26 | 13.99 [8.52, 22.22] | | |
| | 85 | | 5-9 y | 20 | 16.47 [9.04, 24.94] | | |
| | 130 | | 10-15 y | 19 | 34.15 [15.84, 60.29] | | |
| | 212 | | >16 y | 25 | 82.84 [34.31, 184.02] | | |

| | | | | | | | |
|---|---|---|---|---|---|---|---|
| Ubeda (published 2012) | 76 | | <1 y | | 1.0 $$$ | 1.1 $$$ | |
| | 80 | | 1-5 y | | 1.5 $$$ | 1.8 $$$ | |
| | 39 | | 5-10 y | | 2.2 $$$ | 2.8 $$$ | |
| | 30 | | 10-16 y | | 7.9 $$$ | 9.0 $$$ | |
| | 225 | | 0-16 y | | 1.5 $$$ | 2.7 $$$ | |
| Ubeda (published 2012) (normal) | 35 | | | | | 1.8 $$$ | |
| Ubeda (published 2012) (complex) | 45 | | | | | 3.5 $$$ | |
| McFadden (published 2013) | 159 | | 0.1-15.3 y | [4.6, 11.5] | [1.40, 5.87] | 2.94 $ | |
| Glatz (2009-2013) | 671 | | < 5 kg | 15 [ 9, 23] | 2.24 [ 1.16, 3.49] | | |
| | | | 5-12.5 kg | 16 [ 11, 26] | 4.18 [ 2.72, 6.63] | | |
| | | | 12.5-25 kg | 13 [ 9, 20] | 9.45 [ 5.75, 15.52] | | |
| | | | 25-45 kg | 14 [ 8, 22] | 27.22 [ 15.63, 42.90] | | |
| | | | 45-65 kg | 14 [ 10, 25] | 55.95 [ 34.32, 90.71) | | |
| | | | >65 kg | 16 [ 10, 21] | 89.59 [ 49.19, 147.84] | | |
| | | | All | 15 [ 10, 23] | 6.12 [ 2.72, 23.3] | | |
| Barnaoui (2010-2011) | 93 | | <6.5 kg | 7 [R: 0.3-45] | 2 [R: 0.3-8.1] | 2.7 [2] | |
| | 58 | | 6.5-14.5 kg | 6 [R: 0.3-25] | 2 [R: 0.02-11.5] | 2.9 [2.8] | |
| | 61 | | 14.5-25.5 kg | 4.5 [R: 1-23] | 2.6 [R: 0.37-14.2] | 3.9 [3.3] | |
| | 47 | | 25.4-43.5 kg | 5.4 [R: 1-25] | 5.8 [R: 0.7-16.6] | 6.3 [4.3] | |
| | 29 | | >43.5 kg | 7.5 [R: 2.5-45] | 12.8 [R: 3.4-37.5] | 16.4 [10.8] | |
| Kobayashi (2008-2013) | 510 | 3.6 kg | < 5 kg | 14 [ 8, 22] | 2.28 [ 1.22, 4.20] | | |
| | 1429 | 9.5 kg | 5-20 kg | 14 [ 9, 20] | 5.40 [ 2.86, 9.57] | | |
| | 498 | 27.4 kg | 20-45 kg | 12 [ 7, 17] | 14.49 [ 6.74, 26.74] | | |
| | 314 | 58 kg | 45-80 kg | 11 [ 7, 18] | 40.06 [ 15.69, 81.68] | | |
| | 76 | 92 kg | >80 kg | 12 [ 7, 19] | 103.47 [ 28.11, 158.74] | | |
| | 2827 | | All <18 y | 13 [75%: 20] | | | 0.59 [75% 1.05] |
| Borik (2007-2014) | 1224 | | Children | 11 [R: 0-181] | 4.75 [R: 0.01-338.18] | | 0.39 [R: 0-92.98] |
| Ubeda (2011-2013) | 200 | | 0-16 y | 9.9 [75%: 15.8] | 1.5 [75%: 2.9] $$$ | 2.7 | 0.1 [75%: 0.16] $$$ |
| | | | 0-1 y | [75%: 17.1] | [75%: 1.17] $$$ | | |
| | | | 1-5 y | [75%: 14.9] | [75%: 1.74] $$$ | | |
| | | | 5-10 y | [75%: 19.1] | [75%: 2.83] $$$ | | |
| | | | 10-16 y | [75%: 17.4] | [75%: 7.74] $$$ | | |
| Corredoira (2009-2013) ### | 34 | | 0-1 y | | 1.80 [0.92, 4.10] | 2.75 | |
| | 47 | | 1-5 y | | 4.67 [2.84, 10.44] | 6.17 | |
| | 25 | | 5-10 y | | 6.03 [3.12, 14.48] | 17.4 | |
| | 45 | | 10-16 y | | 15.56 [3.23, 29.56] | 24.93 | |
| | 21 | | 16-20 y | | 25.44 [7.43, 53.34] | 34.07 | |
| | 172 | | All <20 y | | 5.26 [2.31, 16.16] | 15.44 | |

| **Heart biopsy** | Subjects | Med age/weight | Range | Median FT | Median $P_{KA}$ | Mean $P_{KA}$ | Median $P_{KA}$/kg |
|---|---|---|---|---|---|---|---|
| Verghese (2005-2009) | 30 | | <1 y | 8 | 1.69 [ 0.99, 2.82] | | |
| | 112 | | 1-4 y | 7 | 2.66 [ 1.45, 4.84] | | |
| | 105 | | 5-9 y | 7 | 6.38 [ 2.89, 11.98] | | |
| | 224 | | 10-15 y | 8 | 15.14 [ 8.39, 31.10] | | |
| | 283 | | >16 y | 8 | 18.53 [ 8.52, 39.05] | | |
| Glatz (2009-2013) (Right Heart ± biopsy) | 301 | | 5-12.5 kg | 9 [ 6, 18] | 2.10 [ 0.89, 3.43] | | |
| | | | 12.5-25 kg | 7 [ 5, 12] | 4.84 [ 2.67, 9.90] | | |
| | | | 25-45 kg | 7 [ 5, 15] | 9.68 [ 4.64, 19.05] | | |
| | | | 45-65 kg | 8 [ 5, 12] | 17.71 [ 8.75, 32.04] | | |
| | | | >65 kg | 7 [ 5, 11] | 30.02 [ 12.67, 49.21] | | |
| | | | All < 22 y | 7.8 [5-14] | 9.00 [3.43, 20.87] | | |
| Kobayashi (2008-2013) | 4 | 4.2 kg | < 5 kg | 7 [ 5: 10] | 1.13 [ 0.51, 1.73] | | |
| | 394 | 14.8 kg | 5-20 kg | 8 [ 4, 12] | 3.91 [ 0.97, 10.63] | | |
| | 425 | 31.1 kg | 20-45 kg | 7 [ 4, 12] | 7.56 [ 1.66, 24.07] | | |
| | 293 | 54.7 kg | 45-80 kg | 6 [ 3 :10] | 13.41 [ 1.80, 48.96] | | |
| | 56 | 91.3 kg | >80 kg | 4 [2, 8] | 7.95 [ 3.12, 40.95] | | |
| | 1172 | | All <18 y | 7 [75%: 11] | | | 0.26 [75%: 0.79] |
| Borik (2007-2014) | 710 | | | 5 [R: 2-28] | 27.89 (*sic*) [R: 0.1-83.43] | | 0.1 [R: 0.01-1.08] |
| Sutton (2011-2012) | 45 | | | 3.7 [R: 1.2-9] | 0.16 [R: 0.04–1.45] | | |

| **Coronary angiography** | Subjects | Med age/weight | Range | Median FT | Median $P_{KA}$ | Mean $P_{KA}$ | Median $P_{KA}$/kg |
|---|---|---|---|---|---|---|---|
| Tsapaki (2007) | 18 | | 0-1 y | 9.4 [R: 3.4-11.1] | 1.9 [R: 0.1-3.2] | | |
| | | | 1-10 y | 3.1 [R: 1.1-6.6] | 1.15 [R: 0.1-10.7] | | |
| | | | >10 y | 4.1 [R: 2.4-21.1] | 4.1 [R: 0.7-36.7] | | |
| | 18 | | All | 4.0 [R: 1.1-21.2] | 2.1 [R: 0.1-36.7] | | |
| Glatz (2009-2013) | 179 | | 12.5-25 kg | 14 [ 11, 19] | 12.35 [ 8.54, 24.43] | | |
| | | | 25-45 kg | 15 [ 11, 20] | 26.98 [ 17.59, 40.61] | | |
| | | | 45-65 kg | 15 [ 11, 20] | 54.76 [ 36.61, 80.82] | | |
| | | | >65 kg | 16 [ 13, 21] | 89.77 [ 71.26, 112.43) | | |
| | | | All | 15 [ 11, 20] | 31.80 [ 16.83, 63.50] | | |

| **PDA occlusion** | Subjects | Med age/weight | Range | Median FT | Median $P_{KA}$ | Mean $P_{KA}$ | Median $P_{KA}$/kg |
|---|---|---|---|---|---|---|---|
| El Sayed (published 2012) | 18 | | | | | 10 | |
| Schultz (published 2003) §§ | 12 | | | | | 18.8 | |
| Verghese (2005-2009) | 61 | | 1-4 y | 17 | 8.00 [5.58, 14.30] | 9 [8] | |
| | 20 | | >16 y | 34 | 110.18 [56.51, 271.45] | | |
| Al Haj (2000-2002) | 41 | | 0-13 y | | | 23.21 [10.1] | |
| Glatz (2009-2013) | 92 | | 5-12.5 kg | 10.5 [8, 13] | 2.63 [1.78, 3.53] | | |
| | | | 12.5-25 kg | 9 [8, 15] | 5.56 [3.52, 9.85] | | |
| | | | All | 11 [9, 16] | 3.52 [2.29, 7.09] | | |
| Bacher (published 2005) | | | | | | | |
| Onnasch (1995-2003) | 165 | | | | | | mean=0.35 [75%: 0.37] |
| Smith (2005-2009) | 140 | | <18 y | 6 [ 4, 9] | 1.52 [ 0.78, 2.52] | | |
| Yakoumakis (published 2009) | 10 | | 4.8 m - 13 y | | | | |
| Yakoumakis (published 2013) & | 16 | | 7-11 y | | 9.5 [R: 7.8-11.2] | 9.5 [0.1] | |
| Barnaoui (2010-2011) | 23 | | <6.5 kg | 6.5 [R: 2-23.4] | 2.1 [R: 1-7.1] | 2.8 [1.8] | |
| | 85 | | 6.5-14.5 kg | 3 [R: 0.5-20] | 1.4 [R: 0.39-9.7] | 1.9 [1.4] | |
| | 29 | | 14.5-25.5 kg | 3 [R: 1.3-17] | 2.8 [R: 0.3-7.5] | 3.1 [2] | |
| | 8 | | 25.4-43.5 kg | 3 [R: 2-9.3] | 4.3 [R: 0.8-11.2] | 5.3 [3.9] | |
| | 6 | | >43.5 kg | 2 [R: 1-4.5] | 10.8 [R: 0.6-20.1] | 11.5 [7] | |
| | 98 | | All | 3 [0.5, 23.4] | 1.8 [R: 0.3-20.1] | 2.8 [2.9] | |
| Ghelani (2009-2013) § | 130 | | <1 y | 15 [75%: 21] | 5 [75%: 8] | | |
| | 294 | | 1-4 y | 10 [75%: 16] | 7 [75%: 12] | | |
| | 60 | | 5-9 y | 11 [75%: 15] | 13 [75%: 22] | | |
| | 38 | | 10-15 y | 12 [75%: 17] | 33 [75%: 85] | | |
| | 25 | | >15 y | 24 [75%: 33] | 96 [75%: 151] | | |
| Kobayashi (2008-2013) (coils) | 283 | | All <18 y | 8 [75%: 13] | | | 0.31 [75%: 0.53] |
| Kobayashi (2008-2013) (device) | 467 | | All <18 y | 11 [75%: 16] | | | 0.42 [75%: 0.71] |
| Song (published 2014) | 20 | 2.1 y | 0.5-7 y | 5.67 [R: 2.1-33.0] | 6.47 [R: 1.29-90.01] | 13.71 [20.21] | Mean=0.62 |
| Borik (2007-2014) | 266 | | Children | 8 [R: 3-92] | 2.54 [R: 0.38-181.31] | | 0.18 [R: 0.04-2.51] |
| | 87 | | 0-10 kg | | 1.37 [R: 0.38-18.93] | | 0.19 [R: 0.05-2.08] |
| | 122 | | 10-20 kg | | 2.45 [0.48, 12.38] | | 0.17 [R: 0.04-0.86] |
| | 34 | | 20-30 kg | | 4.11 [R: 0.91-19.48] | | 0.17 [R: 0.04-0.91] |
| | 25 | | >30 kg | | 20.87 [R: 2.94-181.31] | | 0.37 [R: 0.07-2.51] |
| Keiller (2012-2013) | 52 | | | | | 3.19 [R: 1.87-10.52] | |
| Ubeda (published 2012) (coils) | 20 | | | | | 1.5 $$$ | |
| Ubeda (published 2012) (device) | 117 | | | | | 2.1 $$$ | |
| Ubeda (2011-2013) (coils) | 42 | | | 6.0 [75%: 9.1] | 0.6 [75%: 1.2] $$$ | 0.9 $$$ | |
| Ubeda (2011-2013) (device) | 84 | | | 9.8 [75%: 13.6] | 1.0 [75%: 1.9] $$$ | 1.7 $$$ | |

| **ASD and PFO occlusion** | Subjects | Med age/weight | Range | Median FT | Median $P_{KA}$ | Mean $P_{KA}$ | Median $P_{KA}$/kg |
|---|---|---|---|---|---|---|---|
| Bacher (published 2005) | | | | | | | |
| Onnasch (1995-2003) (ASD) | 259 | | | | | | mean=0.42 [75%: 0.50] |
| Onnasch (1995-2003) (PFO) | 21 | | | | | | mean=0.23 [75%: 0.30] |
| Yakoumakis (published 2009) | 15 | | 1.5-18 y | | | | |
| El Sayed (2012) | 15 | | | | | 10 [10] | |
| Verghese (2005-2009) | 29 | | 1-4 y | 30 | 21.97 [ 16.14, 30.48] | | |
| | 40 | | 5-9 y | 31 | 28.16 [ 14.31, 39.78] | | |
| | 27 | | 10-15 y | 34 | 74.92 [ 44.19, 105.82] | | |
| | 99 | | > 16 y | 28 | 98.71 [60.97, 153.41] | | |
| Smith (2005-2009) | 49 (114?) | | <18 y | 8 [ 4, 14] | 2.82 [ 1.28, 4.93] | | |
| Yakoumakis (published 2013) & | 19 | | 6-11 y | | 40.3 [R: 17.3-58.3] | 39.9 [1.2] | |
| Glatz (2009-2013) | 97 | | 5-12.5 kg | 16 [ 11, 24] | 5.03 [ 2.97, 6.61] | | |
| | | | 12.5-25 kg | 14 [ 12, 22] | 7.28 [ 4.80, 9.32] | | |
| | | | 25-45 kg | 24 [ 12, 31] | 16.21 [ 11.87, 24.33] | | |
| | | | 45-65 kg | 18 [ 12, 27] | 30.63 [ 14.33, 43.53] | | |
| | | | >65 kg | 17 [ 13, 27] | 58.93 [ 33.79, 107.01] | | |
| | | | All | 15 [12, 25] | 10.38 [6.29, 28.78] | | |
| Barnaoui (2010-2011) | 4 | | 6.5-14.5 kg | 5.6 [R: 0.6-7] | 1.8 [R: 0.1-3] | 1.7 [1.2] | |
| | 25 | | 14.5-25.5 kg | 1 [R: 0.8-7] | 0.7 [R: 0.1-2.9] | 0.8 [0.6] | |
| | 13 | | 25.4-43.5 kg | 1.5 [R: 0.5-20] | 1.1 [R: 0.4-6.8] | 2 [2.2] | |
| | 12 | | >43.5 kg | 2.5 [R: 1-11] | 2.8 [R: 1-15] | 4.5 [4.4] | |
| | 54 | | All | 1.8 [0.5-20] | 0.9 [0.1-15] | 2 [2.7] | |
| Ghelani (2009-2013) § | 219 | | 1-4 y | 18 [75%: 27] | 9 [75%: 17] | | |
| | 180 | | 5-9 y | 16 [75%: 24] | 14 [75%: 25] | | |
| | 127 | | 10-15 y | 17 [75%: 27] | 39 [75%: 67] | | |
| | 194 | | >15 y | 20 [75%: 31] | 89 [75%: 204] | | |
| Kobayashi (2008-2013) | 568 | | All <18 y | 15 [75%: 23] | | | 0.41 [75: 0.71] |
| Song (published 2014) | 17 | 4.9 y | 2.0-18 y | 6.55 [R: 4.1-54.1] | 4.85 [R: 1.70-21.21] | 10.71 [8.35] | Mean=0.33 |
| Borik (2007-2014) | 345 | | Children | 8 [R: 2-95] | 5.04 [R: 0.34-244.56] | | 0.21 [R: 0.02-3.67] |
| | 6 | | 0-10 kg | | 2.91 [R: 1.78-8.82] | | 0.31 [R: 0.22-0.89] |
| | 141 | | 10-20 kg | | 2.83 [R: 0.34-42.68] | | 0.16 [R: 0.02-2.13] |
| | 80 | | 20-30 kg | | 4.71 [R: 1.93-29.87] | | 0.22 [R: 0.08-1.36] |
| | 118 | | >30 kg | | 12.70 [R: 1.93-244.56] | | 0.23 [R: 0.06-3.69] |
| Ubeda (published 2012) | 9 | | | | | 4.3 $$$ | |
| Keiller (2012-2013) | 19 | | | | | 4.95 [R: 2.08-33.23] | |
| Haas (2012-2013) | 19 | 30 kg | | 6.9 [ 4.6, 9.0] | 6.78 [ 3.52, 10.15] | 10.48 [14.45] | 0.16 [ 0.11, 0.39] |
| Haas (2013) | 31 | 26 kg | | 5.5 [ 3.8, 9.3] | 1.12 [ 0.68, 3.67] | 2.84 [3.51] | 0.04 [ 0.03, 0.07] |

| **Aorta dilatation / coarctation repair** | Subjects | Med age/weight | Range | Median FT | Median $P_{KA}$ | Mean $P_{KA}$ | Median $P_{KA}$/kg |
|---|---|---|---|---|---|---|---|
| Al Haj (2000-2002) | 24 | | 0-13 y | | | 11.35 [24.3] | |
| Yakoumakis (published 2009) | 10 | | 2 m - 12 y | | | | |
| El Sayed (published 2012) | 6 | | | | | 42.5 [18.18] | |
| Smith (2005-2009) (balloon) | 9 | | | 8 [ 5, 11] | 2.37 [ 1.44, 5.42] | | |
| Smith (2005-2009) (stent) | 21 | | | 12 [ 9, 14] | 27.10 [ 9.98, 50.12] | | |
| Verghese (2005-2009) | 42 | | <1 y | 34 | 12.98 [ 8.27, 22.92] | | |
| | 34 | | >16 y | 36 | 123.02 [78.54, 258.73] | | |
| Glatz (2009-2013) | 86 | | < 5 kg | 18 [14, 20] | 2.73 [ 2.02, 3.84] | | |
| | | | 5-12.5 kg | 18 [14, 24] | 4.34 [ 2.53, 6.90] | | |
| | | | All | 19 [14, 24] | 4.84 [2.61, 17.70] | | |
| Ghelani (2009-2013) § | 202 | | <1 y | 21 [75%: 32] | 7 [75%: 14] | | |
| | 36 | | 1-4 y | 23 [75%: 35] | 20 [75%: 30] | | |
| | 38 | | 5-9 y | 22 [75%: 33] | 41 [75%: 65] | | |
| | 79 | | 10-15 y | 20 [75%: 26] | 96 [75%: 170] | | |
| | 93 | | >15 y | 24 [75%: 36] | 200 [75%: 340] | | |
| Ubeda (published 2012) | 70 | | | | | 2.2 $$$ | |
| Kobayashi (2008-2013) (angioplasty) | 182 | | All <18 y | 15 [75%: 21] | | | 0.66 [75%: 1.07] |
| Kobayashi (2008-2013) (stent) | 112 | | All <18 y | 16 [75%: 23] | | | 0.90 [75%: 1.59] |
| Borik (2007-2014) (angioplasty) | 120 | | | 11 [R: 4-66] | 4.79 [R: 0.35-194.65] | | 0.43 [R: 0.07-4.47] |
| Borik (2007-2014) (stent) | 52 | | | 15 [R: 7-65] | 32.92 [R: 1.49-291.54] | | 0.80 [R: 0.13-4.48] |

| **Aortic Valvuloplasty** | Subjects | Med age/weight | Range | Median FT | Median $P_{KA}$ | Mean $P_{KA}$ | Median $P_{KA}$/kg |
|---|---|---|---|---|---|---|---|
| Smith (2005-2009) | 30 | | | 21 [ 16, 28] | 2.35 [ 0.90, 7.28] | | |
| Verghese (2005-2009) | 43 | | <1 y | 30 | 9.57 [6.29, 15.24] | | |
| Glatz (2009-2013) | 26 | | All | 30 [ 22, 32] | 11.18 [ 4.70, 63.42] | | |
| Ghelani (2009-2013) § | 155 | | <1 y | 25 [75%: 34] | 7 [75%: 11] | | |
| | 27 | | 1-4 y | 21 [75%: 33] | 19 [75%: 37] | | |
| | 22 | | 5-9 y | 22 [75%: 30] | 21 [75%: 28] | | |
| | 65 | | 10-15 y | 28 [75%: 36] | 93 [75%: 137] | | |
| | 27 | | >15 y | 23 [75%: 39] | 116 [75%: 187] | | |
| Kobayashi (2008-2013) | 138 | | All <18 y | 18 [75%: 26] | | | 0.80 [75%: 1.27] |

| | | | | | | | |
|---|---|---|---|---|---|---|---|
| Borik (2007-2014) | 138 | | Children | 13 [R: 4-61] | 3.4 [R: 0.14-110.91] | | 0.42 [R: 0.08-2.11] |
| | 72 | | 0-10 kg | | 1.45 [R: 0.14-7.09] | | 0.31 [R: 0.08-1.25] |
| | 20 | | 10-20 kg | | 0.48 [R: 0.05-19.55] | | 0.42 [R: 0.09-1.28] |
| | 7 | | 20-30 kg | | 14.72 [R: 7.38-32.22] | | 0.57 [R: 0.26-1.41] |
| | 39 | | >30 kg | | 44.54 [R: 8.05-110.91] | | 0.77 [R: 0.24-2.11] |
| Ubeda (published 2012) | 30 | | | | | 2.0 $$$ | |
| Ubeda (2011-2013) | 13 | | | 11.0 [75%: 13.5] | 0.6 [75%: 2.3] $$$ | 2.6 $$$ | |

| **Pulmonary valvuloplasty** | Subjects | Med age/weight | Range | Median FT | Median $P_{KA}$ | Mean $P_{KA}$ | Median $P_{KA}$/kg |
|---|---|---|---|---|---|---|---|
| Al Haj (2000-2002) | 44 | | 0-13 y | | | 9.96 [15.1] | |
| Yakoumakis (published 2009) | 11 | | 3.6 m - 8.5 y | | | | |
| Smith (2005-2009) | 63 | | <18 y | 11 [ 8, 18] | 1.23 [ 0.57, 2.03] | | |
| Verghese (2005-2009) | 86 | | <1 y | 28 | 7.97 [4.59, 13.55] | | |
| Glatz (2009-2013) | 75 | | <5 kg | 19 [ 12, 30] | 2.41 [ 1.65, 3.10] | | |
| | | | 5-12.5 kg | 24 [ 16, 32] | 4.71 [ 3.13, 7.06] | | |
| | | | All | 19 [12, 30] | 4.05 [2.33, 14.34] | | |
| Ghelani (2009-2013) § | 303 | | <1 y | 21 [75%: 35] | 4 [75%: 9] | | |
| | 64 | | 1-4 y | 19 [75%: 30] | 10 [75%: 18] | | |
| | 24 | | 5-9 y | 13 [75% 20] | 16 [75%: 23] | | |
| | 35 | | 10-15 y | 15 [75% 22] | 44 [75%: 98] | | |
| | 35 | | >15 y | 28 [75% 42] | 198 [75%: 448] | | |
| Kobayashi (2008-2013) | 342 | | All <18 y | 14 [75%: 20] | | | 0.56 [75%: 0.95] |
| Borik (2007-2014) | 286 | | Children | 15 [R: 1-131] | 1.63 [R: 0.22-188.47] | | 0.28 [R: 0.01-3.45] |
| | 216 | | 0-10 kg | | 1.14 [R: 0.22-12.22] | | 0.27 [R: 0.06-3.44] |
| | 40 | | 10-20 kg | | 3.56 [R: 0.91-40.39] | | 0.24 [R: 0.08-3.11] |
| | 9 | | 20-30 kg | | 7.48 [R: 5.49-11.56] | | 0.34 [R: 0.22-0.42] |
| | 22 | | >30 kg | | 50.90 [R: 0.87-188.47] | | 0.99 [R: 0.01-3.45] |
| Song (published 2014) | 16 | 4.8 y / 18 kg | | 9.8 [R: 5.1-21.0] | 6.20 [R: 3.80-10.68] | 7.11 [3.01] | |
| Ubeda (published 2012) | 61 | | | | | 1.2 $$$ | |
| Ubeda (2011-2013) | 29 | | | 12.4 [75%: 17.0] | 0.6 [75%: 0.9] $$$ | 0.9 $$$ | |

| **Combined interventional** | Subjects | Med age/weight | Range | Median FT | Median $P_{KA}$ | Mean $P_{KA}$ | Median $P_{KA}$/kg |
|---|---|---|---|---|---|---|---|
| Bacher (published 2005) (0.2 mm Cu) ** | 16 | 2 y | 0.2-10 y | | 4.72 [R: 2.82-20.44] | | |
| Bacher (published 2005) (0.4 mm Cu) ** | 16 | 2 y | 0.3-7.8 y | | 2.72 [R: 0.41-18] | | |
| Martinez (published 2007) | 79 | | <1 y | | | 2.4 [0.4] $$$ | |
| | | | 1-5 y | | | 4.4 [0.8] $$$ | |
| | | | 5-10 y | | | 8.6 [1.9] $$$ | |
| | | | 10-16 y | | | 17.8 [3.7] $$$ | |
| Dragusin (after 2005) | 12 | | 1–30 d | 16.5 [ 13.5, 24.3] | 4.8 [ 2.5, 6.5] | | |
| | 49 | | 1-12 m | 12 [ 9, 25] | 5.9 [ 3.7, 9.2] | | |
| | 29 | | 1-3 y | 16 [ 9.5, 24.5] | 7.5 [ 5, 12.5] | | |
| | 14 | | 3-5 y | 18 [ 10.75, 33.5] | 9.5 [ 5, 22.2] | | |
| | 31 | | 5-10 y | 21 [ 14, 26] | 17.1 [ 9.7, 27] | | |
| | 12 | | 10-15 y | 20 [ 16, 39.75] | 46.8 [ 28.7, 74.4] | | |
| Beels (published 2009) | 32 | 0.69 y | 0-10.8 y | | 2.7 [R: 0.1-31.7] | | |
| Karambatsakidou (1999-2004) | 110 | | 0-0.5 y | | | 3.2 [4.1] | |
| | | | 0.5-2.5 y | | | 2.6 [5.1] | |
| | | | 2.5-7.5 y | | | 7.8 [11.8] | |
| | | | 7.5-12.5 y | | | 10.0 [9.7] | |
| | | | 12.5-18 y | | | 34.2 [38.9] | |
| Onnasch (1998-2003) | 883 | 13.8 kg | 1.5-108 kg | | | | 0.35 [75%: 0.66] |
| Ait Ali (2007) | 5 | 14 y | 0.3-16 y | 24 [R: 13-26] | 93 [64, 99] | 109 [100.0] | |
| El Sayed (published 2012) | 61 | 7.84 y | 0–22 y | | | 13.24 [15.4] | |
| Smith (2000-2005) (old) *** | 444 | 2.19 y | 0-17.9 y | | 8.0 [R: 0.1-156.0] | | |
| Smith (2005-2009) (new) *** | 312 | 2.06 y | 0-17.9 y | | 1.76 [R: 0.03-125.15] | | |
| McFadden (published 2013) | 195 | | 0-16 y | [5.1, 15.4] | [1.37, 7.15] | 3.13 $ | |
| Glatz (2009-2013) | 816 | | < 5 kg | 19 [ 12, 32] | 2.58 [ 1.71, 3.67] | | |
| | | | 5-12.5 kg | 26 [ 14.5, 41] | 6.56 [ 3.46, 13.80) | | |
| | | | 12.5-25 kg | 24 [ 13, 44] | 12.96 [ 6.34, 31.28] | | |
| | | | 25-45 kg | 38 [ 24, 59] | 65.86 [ 2.43, 96.93) | | |
| | | | 45-65 kg | 24 [ 16, 45] | 85.14 [ 35.20–144.04) | | |
| | | | >65 kg | 36 [ 19, 51] | 158.41 [ 87.58, 389.69) | | |
| | | | All | 25 [ 14–43] | 10.51 [ 3.71, 43.15] | | |
| Kobayashi (2008-2013) | 680 | | < 5 kg | 18 [11, 31] | 2.78 [ 1.18, 6.10] | | |
| | 2231 | | 5-20 kg | 19 [ 11, 32] | 7.37 [ 3.36, 15.41] | | |
| | 767 | | 20-45 kg | 19 [ 11, 31] | 19.22 [ 8.37, 37.80] | | |
| | 500 | | 45-80 kg | 19 [ 12, 31] | 54.62 [ 23.70, 104.18] | | |
| | 90 | | >80 kg | 20 [ 12, 34] | 116.00 [ 65.09, 202.25) | | |
| | 4268 | | All <18 y | 19 [75%: 32] | | | 0.72 [75%: 1.51] |

| | | | | | | | |
|---|---|---|---|---|---|---|---|
| Ubeda (published 2012) | 74 | | <1 y | | 0.9 $$$ | 1.2 $$$ | |
| | 123 | | 1-5 y | | 1.4 $$$ | 1.7 $$$ | |
| | 58 | | 5-10 y | | 1.9 $$$ | 2.6 $$$ | |
| | 64 | | 10-16 y | | 4.5 $$$ | 7.1 $$$ | |
| | 319 | | 0-16 y | | 1.7 $$$ | 2.9 $$$ | |
| Ubeda (2011-2013) | 317 | | 0-16 y | 12.6 [75%: 20.6] | 1.2 [75%: 2.5] $$$ | 2.4 $$$ | 0.09 [75%: 0.17] $$$ |
| | | | 0-1 y | [75% 22.7] | [75%: 1.11] $$$ | | |
| | | | 1-5 y | [75% 20.6] | [75%: 1.90] $$$ | | |
| | | | 5-10 y | [75% 16.9] | [75%: 3.22] $$$ | | |
| | | | 10-16 y | [75% 23.1] | [75%: 8.68] $$$ | | |
| Corredoira (2009-2013) ### | 92 | | 0-1 y | | 1.91 [1.19, 3.14] | 3.19 | |
| | 158 | | 1-5 y | | 2.57 [0.86, 7.53] | 4.92 | |
| | 118 | | 5-10 y | | 6.09 [2.25, 14.18] | 11.52 | |
| | 176 | | 10-16 y | | 11.99 [3.77, 27.55] | 21.94 | |
| | 40 | | 16-20 y | | 39.74 [17.87, 91.12] | 57.06 | |
| | 584 | | All <20 y | | 4.87 [1.60, 15.05] | 14.68 | |

Table 2.1: Summary of dose indicators (kerma area product and screening time) for reviewed studies.

Notes: * Results given for two different operators, ** study conducted using two different levels of copper filtration, *** data presented for two equipment types, $ geometric mean, $$$ figures reduced to account for table attenuation, # doses presented in chart form only, ## subset of above group, ### study included cone beam CT elements for 38 diagnostic and 71 interventional procedures, & Organ doses for PDA, VSD and ASD occlusions calculated using 0, 10 and 10 year old phantoms, respectively, § Sample sizes are for DAP. The sample of examinations used for air kerma was smaller, presumably as not all procedures had an air kerma figure recorded, §§ It is not clear if the figures are median or mean.

Fryback and Thornbury [100] and Thornbury [101] propose six stages of efficacy of diagnostic imaging; these are (1) Technical capacity, (2) Diagnostic accuracy, (3) Diagnostic impact, (4) Therapeutic impact, (5) Patient outcomes, and (6) Societal outcomes. Barrett *et al* [95] state that the majority of research tends to focus on stage 2. There is insufficient evidence to determine whether higher radiation doses are associated with improved patient or societal outcomes (e.g. survival, quality of life, employment or burden on healthcare services). Although most papers investigating radiation doses from cardiac catheterizations make some mention of image quality, there is little to suggest a conscious decision to increase radiation doses in order to improve patient outcome. Higher doses are rarely acknowledged, partly because 'comparison with previous research' analyses tend to be limited to a handful of studies.

Returning to the question of why $P_{KA}$ varies so much between different published studies, a fourth potential explanation is measurement uncertainty and careless recording or reporting of dose indicators. It was noted that around half of reviewed publications make no mention of calibration of dose measuring equipment. Recorded $P_{KA}$ figures are subject to a typical uncertainty of ±15%, even when regularly calibrated to national standards. For uncalibrated dosemeters, this uncertainty may be sizably higher, though never to the extent of explaining a tenfold variation in doses. Confusion between units, for example between $\mu Gy \cdot m^2$ and $mGy \cdot cm^2$, could certainly explain a tenfold variation in doses. Smith *et al* [22] for example, quote $P_{KA}$ in the nonsensical units of "$mGy/cm^2$", giving the impression of extraordinarily low doses, assuming units should be $mGy \cdot cm^2$. The correct units of measurement of $\mu Gy \cdot m^2$ were obtained by consulting with medical physics staff at the same hospital (who were unaware the study had been conducted) (Ian Honey, 2013, personal communication). Borik *et al* [102] misquote the results of Smith by a factor of 10, leading to the incorrect conclusion that their own $P_{KA}$ figures were lower.

There is no clear trend in $P_{KA}$ or screening time with study date. If anything, reported $P_{KA}$ figures are higher in more recently published data, although this observation involves comparison between studies rather than comparison of different eras at the same centre. Onnasch and colleagues [103] found a decrease in $P_{KA}$ per patient mass with the replacement of a Siemens Bicor/Digitron with a Philips Integris 5000BH system (0.618 verses 0.278 $Gy \cdot cm^2\ kg^{-1}$). This change involved a reduction

in frame rate from 50 $s^{-1}$ to 12.5-25 $s^{-1}$ and the use of additional copper filtration. A greater than fourfold reduction in $P_{KA}$ was reported in the previously mentioned study by Smith *et al* [22] following the installation of new equipment. Again, the newer machine was able to use a lower frame rate (typically 7.5-15 $s^{-1}$). This reduction in the fluoroscopic or acquisition frame rate can be associated with a proportional reduction in dose [104], without sacrificing SNR. In many cases, frame rates are dictated by the heart rate of the individual undergoing the procedure, which for children can often exceed 100 beats per minute (BPM). Overall, there does appear to be a trend of reduced frame rates in more recent publications. Quoted fluoroscopic frame rates were typically 12.5 $s^{-1}$, though rates of up to 50 $s^{-1}$ were reported.

From the above discussion it is apparent that a wide, and largely unacknowledged gulf in doses, as represented by $P_{KA}$, exists between different centres. In particular, a number of large studies with sample sizes of several thousand examinations have reported unexpectedly large $P_{KA}$ figures in recent years. Most such studies are based in the United States, though it should be noted that other American studies have reported very low doses [105, 106], while some European studies have reported very high doses [13, 107]. A common mistake made by authors is to conduct only a limited comparison of their own data with previous research, often incorrectly reaching the conclusion that their doses are satisfyingly low. Studies reporting high $P_{KA}$ also tend to have large sample sizes, thus could argue that their figures represent a true picture of the radiation doses from these procedures, with lower doses being explainable by small sample sizes and publication bias (i.e. authors more likely to report doses if they are low).

### *2.1.3: Derivation of organ doses and effective dose from $P_{KA}$*

Kerma area product is a dose indicator, somewhat akin to the number of bullets fired from a gun. It provides no implicit information on how x-rays interact with the patient. This limitation is rarely acknowledged in publications, with $P_{KA}$ often simply referred to as 'dose'. $P_{KA}$ can however be used to provide estimates patient dose, including effective dose (E) and equivalent dose to individual organs (H). These are derived using $E/P_{KA}$ or $H/P_{KA}$ conversion factors calculated using either Monte Carlo (MC) computer simulations [86, 87, 108] or physical measurements in human tissue equivalent phantoms [84] (Figure 2.3). These phantoms are described in Chapters 4

and 7. Estimation of effective dose from entrance surface dose measurements has been found to be less reliable [109].

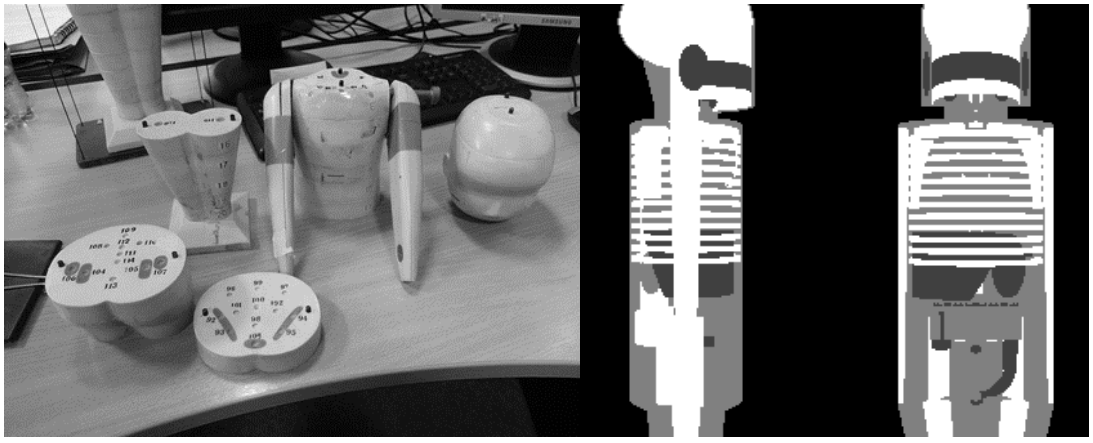

**Figure 2.3: An anthropomorphic phantom used for physical methods dosimetry, and a mathematical phantom used for Monte Carlo simulations (PCXMC 2.0). Photo credit: author**

A summary of $E/P_{KA}$ conversion factors is given in Tables 2.3 and 2.4. The most basic derivations of $P_{KA}$ are simple one-size-fits-all, age and mass independent conversion factors to relate total examination $P_{KA}$ to effective dose. Such simple estimates, used in both adult and paediatric studies [13, 110], should be avoided as it can be shown that effective dose is strongly dependent on patient age or mass [108]. In general, effective dose per unit $P_{KA}$ decreases with increasing patient age [86, 92], presumably due to a smaller proportion of patient tissues being close to the beam entrance. Consequently, where $P_{KA}$ values were converted to effective dose, the trend of increased 'dose' with age was less pronounced or even reversed, with the highest effective doses sometimes occurring in infants [111].

| | | Onnasch [103] PA+Lat combined $ * | Barnaoui [92] PA/lateral $$ | Karambatsakidou [112] PA/PA+Lat combined $ | Schmidt [86] PA/Lat $ | Axelsson [84] PA/LAT $ |
|---|---|---|---|---|---|---|
| Beam energy | | 65 kV, 3.0 mm Al | 70 kV, 3.0 mm Al, 0.3 mm Cu | 60-85 kV, 6 mm Al, 0.4/0.2 mm Cu | 65 kV, 3.0 mm Al ** | 58-70 kV, 3.0 mm Al |
| Methodology | | Derived from Schmidt [86] | PCXMC v2.0 | Modified from Schmidt [86] | PCXMC v1.3 | Physical measurements |
| Patient age (years) | 0 | 3.09 (3.4 kg) | 3.5/3.5 | 3.7/3.7 | 2.05/2.34 | - |
| | 1 | 1.03 (9.2 kg) | 2.1/1.6 | 1.9/1.9 | 0.82/1.16 | 1.8/1.4 |
| | 5 | 0.49 (19.0 kg) | 1.05/1.3 | 1.0/1.0 | 0.42/0.64 | 0.9/.07 |
| | 10 | 0.29 (32.4 kg) | 0.65/0.8 | 0.6/0.7 | 0.24/0.38 | - |
| | 15 | 0.17 (56.3 kg) | 0.35/0.4 | 0.4/0.4 | 0.13/0.22 | - |
| | 30 | 0.13 (73.2 kg) | - | - | 0.10/0.16 | - |

**Table 2.3: $E/P_{KA}$ conversion factors reported in different studies. Note: $ = ICRP 60 effective dose tissue weighting factors, $$ = ICRP 103. *The estimates for the Onnasch model are based on average weight at each age category, shown in brackets.**

| | | Glatz [91] PA/lateral $$ | Onnasch PA+Lat combined $ * |
|---|---|---|---|
| Beam energy | | Not stated | 65 kV, 3mm Al |
| Methodology | | PCXMC v2.0 | Derived from Schmidt [86] |
| Patient mass (kg) | <5 | 2.07/2.25 | 3.09 (3.4 kg) |
| | 5-12.5 | 0.91/1.04 | 1.06 (8.75 kg) |
| | 12.5-25 | 0.68/0.89 | 0.49 (18.8 kg) |
| | 25-45 | 0.47/0.60 | 0.26 (35 kg) |
| | 45-65 | 0.21/0.24 | 0.17 (55 kg) |
| | >65 | 0.18/0.16 | 0.13 (73.2 kg) |

**Table 2.4: $E/P_{KA}$ conversion factor stratified by mass. Note: $ = ICRP 60 effective dose tissue weighting factors, $$ = ICRP 103. *figures based on specified mass**

Dose estimates derived from $P_{KA}$ must therefore take patient size (age or mass) into account. This was done by Schmidt *et al* [86], who used Monte Carlo simulations (PCXMC v1.5) to produce tables of $E/P_{KA}$ conversion factors for individual projections and six different patient sizes, along with a separate table of relative adjustments to account for beam energy. No conversion factors were calculated for estimation of individual organ doses. The paper, published in 2000, provides beam energy

corrections that, while appropriate for fluoroscopic equipment of that era, are inadequate for modern equipment in which a greater thickness of added filtration is generally used. The data calculated by Schmidt were used by Onnasch and colleagues [103] to calculate a remarkably simple $E/P_{KA}$ conversion factor of 9.26 * ($P_{KA}$/kg). This figure, subsequently used by other studies [113, 114] is based on the mean of Schmidt's conversion factors for frontal (PA) and left lateral projections, and beam energy defined by a tube potential of 65 kV and 3 mm Aluminium filtration. These parameters represent a much lower beam energy than is used for equipment used in the last 10 years. Consequently, the $E/P_{KA}$ conversion factor developed by Onnasch will result in underestimates of effective dose (this will be investigated in the Chapter 4). Karambatsakidou *et al* [112] also use the data calculated by Schmidt to produce their own set of $E/P_{KA}$ conversion factors based on the mean of seven different projections using the frontal x-ray tube. A separate conversion factor was used for the lateral tube output. A beam energy correction was applied, based on values recorded for clinical examinations. Effective dose estimates obtained using these conversion factors were compared with those obtained from reconstructions of examinations using Monte Carlo simulations and detailed, exam specific, beam angle and beam energy data. The agreement between these two methodologies was high, with variation less than 10% for 48 out of 52 examinations. This is encouraging as it suggests dose estimates based on limited data are comparable to those with detailed data.

More recently, Barnaoui *et al* [92] used Monte Carlo simulations (PCXMC v2.0) to produce a set of $E/P_{KA}$ conversion factors for two beam projections (PA and left lateral), based on a beam energy more representative of modern equipment (70 kV, 3 mm of Aluminium and 0.3 mm of Copper). These conversion factors are similar to those of Karambatsakidou *et al* [112]. It is noted that effective dose estimates by Barnaoui used the tissue weighting factors from ICRP 103, rather than ICRP 60. The weighting factor for the breasts was increased in the more recent report from 0.08 to 0.12. Furthermore, the heart was included in the 'other' tissues category. Consequently, effective dose estimates using ICRP 103 weighting factors are greater than those using ICRP 60 by between 10 and 16% depending on patient size [112]. The previously mentioned study by Glatz et al [91] also estimated effective doses, again using PCXMC V2.0 Monte Carlo simulations. These $E/P_{KA}$ conversion factors

were lower than those calculated by other studies. The assumed beam energy and field sizes were not stated, making comparison difficult.

Two studies led by Yakoumakis were reviewed [107, 115], with the latter study reporting considerably higher effective doses (almost ten times higher for ASD occlusions), despite the same equipment being used. It should be noted that the methodology of these studies was not the same, with the former estimating effective dose based on surface dose measurements and the latter using $P_{KA}$. The latter study also estimated organ doses, although the actual conversion factors used were not stated.

Conversion factors to relate equivalent $P_{KA}$ to organ doses ($H/P_{KA}$) were developed by Axelsson *et al* [84] for a number of different projection angles. The methodology used by Axelsson was different to that used by the studies describe above, in that they used physical dose measurements in anthropomorphic phantoms rather than Monte Carlo computer simulations. Unfortunately, the range of beam angles (six) and phantom sizes (two) was very narrow, and no corrections for variable beam energy were investigated. A recent study by Kawasaki *et al* [116] calculated organ doses and effective dose for two beam angles (PA and lateral) and two patient sizes (0 and 1 years). While the equipment was a modern, 3$^{rd}$ generation machine (Philips Allura 9), the range of beam angles and patients sizes was overly limited. Other $H/P_{KA}$ conversion factors were developed by Stern *et al* [87] and Streulens *et al* [88] using MC simulations, though only for adult patients.

None of the previously developed $E/P_{KA}$ or $H/P_{KA}$ conversion factors described above are adequate for the purposes of this study, due to (1) the narrow range of patient sizes studied, (2) the lack of organ dose estimates, and (3) the limited range of beam energies studied. A new dosimetry system needs to be developed in which organ doses can be rapidly estimated for a large number of cohort members based on limited data recorded at the time of the examination and held within hospital clinical records. Ideally, examination data can be fed directly into the dosimetry system, i.e. in the form of a spreadsheet, with dose estimates outputted in a readily analysable form. The dosimetry system needs to be able to estimate doses for a large range of patient sizes, from prematurely born babies to adults, and for a large range of beam energies. Information on examination type also needs to be incorporated, as this will affect the likely beam angles used.

*2.1.4: Biodosimetry*

As an alternative to physical dose measurements, a number of studies have investigated the biological impact of medical radiation by measuring DNA damage itself. The initial response to a DNA double strand break is the phosphorylation of histone variant H2AX, to form 'γ -H2AX' [117, 118]. Foci of γ-H2AX can be detected using an antibody specific to this phosphorylated form of H2AX and immunofluorescence techniques. This technique has the advantage of allowing detection of DNA damage occurring at much lower doses than other techniques [118], including those relevant to diagnostic imaging. A number of studies have been conducted in which blood samples taken from patients following medical irradiation are analysed using γ-H2AX techniques. Beels and co-workers [12] compared risk estimates based on organ doses calculated using patient specific MC simulation with estimates based on γ-H2AX foci in peripheral blood T lymphocytes obtained before and immediately following diagnostic catheterization procedures of 48 paediatric subjects. In that study, a supralinear relationship between dose and γ-H2AX foci was found, implying the same dose response for DNA double strand break induction. This, the authors argued, suggests an under-estimation of the cancer risks by linear extrapolation using the linear no-threshold (LNT) model by a factor of four. A similar supralinear dose response was reported by Ojima *et al* [119] following *in vitro* irradiation of normal human fibroblasts to doses from 1.2 to 200 mGy. The authors attributed this pattern to the influence of gap-junction mediated bystander signalling between cells, as pre-treatment with lindane (an inhibiter of gap-junction communication) produced a linear dose response.

Geisel and colleagues [14] found a significant increase in γ-H2AX foci (representing 0.29±0.18 DSBs per lymphocyte) following adult diagnostic conventional coronary catheterizations (CCA) and cardiac CT procedures (n=56 for each modality). After 24 hours however, DSB numbers had returned to background levels. A significant correlation was found between dose and γ-H2AX foci for both CCA ($r=0.862$, $P<0.001$) and CT ($r=0.951$, $P<0.001$). The authors estimated that this level of biological effect was 1.8 times greater than predicted from effective dose, though the dose-response did not appear to exhibit the supralinear relationship noted by Beels [12]. In another study by Ait-Ali *et al* [13], a significant increase in micronucleus levels compared to baseline levels was found following diagnostic (11‰ vs 7‰, n=13) and

therapeutic procedures (9‰ vs 5‰, n=5), though without any apparent relationship with DAP (r=0.1, p=0.74).

While interesting, these findings need to be interpreted with caution. Beels's finding of 'hypersensitivity' refers to the early endpoint of DSB induction, rather than later endpoints of cell-killing or cancer induction. The suggestion that a supralinear dose response for DSBs also implies the same relationship for diagnosable cancer may be overly pessimistic. Research by Rothkamm [117] and later by Collis [120] and Grudzenski [121] suggests that DNA repair efficiency is reduced at low doses and possibly absent below around 5 mGy. When cultures were allowed to proliferate, damaged cells appeared to be eliminated. In this sense, 'hypersensitivity' may indicate excess cell-killing rather than cancer risk. Unfortunately Beels did not investigate persistence of γ-H2AX foci at later times following irradiation, thus allowing damage response to be assessed.

The suggestion by Beels [12] and Andreassi [122] that cancer risks determined through direct analysis DNA damage were four times higher than 'expected' is also dubious, given that 'expected' risks are based on observational studies, albeit ones that lack statistical power at low doses. If, as Andreassi [122] suggests, the supralinear DNA damage relationship detected by Beels is due to the impact of 'bystander' effects, in which irradiated cells influence their neighbours by means of the release of various genotoxic factors into the surrounding medium, why should such effects be specific to cardiac catheterizations? Surely if bystander effects do indeed play a role in cancer development following radiation exposure, such effects would have occurred following the exposures from which 'expected' risks are based, including studies of nuclear bombing survivors. There is currently no suggestion that bystander effects only occur at low doses, with some research even suggesting the reverse [123].

### *2.1.5: Summary of dosimetry review*

The published data on radiation doses from paediatric cardiac catheterizations suggests a wide variation, not only from one hospital or procedure type to the next, but also within individual hospitals and for the same procedure. This strongly suggests that the use of non-individualised 'typical' doses will be insufficient for an epidemiological analysis of the cancer risks. A patient and examination-type specific

system of dosimetry therefore needs to be attempted. Research suggests that an individualised estimation of organ doses based on limited examination data is plausible, though this needs to be investigated further. Biodosimetry studies have suggested that the risk from exposures may be higher than expected, but this is based on the early end-point of DNA damage and not cancer itself. To study this latter endpoint in relation to human exposures, epidemiological analysis is required. A review of relevant studies will be described next.

### *2.2: Epidemiology*

Epidemiological analysis of populations exposed to elevated levels of ionising radiation have the advantage of allowing assessment of the final outcome of cancer rather than a single endpoint such as DSB induction. A large number of epidemiological studies have been conducted. However, none of these provide conclusive evidence of risks at dose levels below 50-100 mGy. Some could be interpreted as suggesting high risks at low doses [124], some low [125], while others are consistent with decreased risks compared to spontaneous incidence (hormesis) [126]. The results of the same studies can be shown to be consistent with seemingly opposing viewpoints. Doss [127], for example, uses the data from the atomic bombing survivors' study (discussed below) to provide evidence of hormesis by adjusting background rates, while other authors have used the same study as evidence in support of the linear no threshold model [46].

Epidemiological analysis requires some form of dose estimation, although the standard of such estimates varies considerably, from individualised estimates to average doses applied across the whole study population or sub-groups (e.g. geographical areas) [128]. Studies with individualised dose estimated were preferred, to so-called 'ecological' studies with non-individualised estimates.

The primary sources for the epidemiology literature review were the reports of the National Academy of Sciences Committee on the Biological Effects of Ionising Radiation (BEIR VII) [3], United Nations Scientific Committee on the Effects of Atomic Radiation (UNSCEAR) [45, 129] and International Commission for Radiological Protection (ICRP) [44]. The reference lists for these reports were searched for relevant publications. Papers identified using PubMed as citing and

cited by these papers were also obtained. Review papers investigating the risks from low dose exposures were also obtained [46, 54, 55, 130] and the reference lists searched.

### *2.2.1: The Life Span Study*

The most informative study of the long-term cancer risk from exposures to ionising radiation remains the cohort of Japanese survivors of the nuclear bombings of Hiroshima and Nagasaki in 1945, known as the Life Span Study (LSS). The bombs dropped on both cities were fission weapons, but had different designs. The Nagasaki bomb, known as the “Fat Man”, used a sub-critical core of plutonium-239 ($^{239}$Pu) surrounded by conventional explosives, which when detonated produced an inward pressure on the core causing it to turn supercritical. The Hiroshima bomb, known as the “Little Boy”, used a sub critical hollow “bullet” of Uranium-235 ($^{235}$U) which was propelled down an artillery barrel by conventional explosives into a second “target” of $^{235}$U, again causing super-criticality. The resulting fission process resulted in the conversion of around 1 g and 0.6 g of mass into energy by the Nagasaki and Hiroshima bombs respectively - equivalent to 21,000 and 16,000 tons of TNT [131]. This is easily appreciated using Einstein's relation, $E=mc^2$, where 1 g of mass is shown to be equivalent to roughly 90 trillion joules.

Radiation doses to inhabitants of the cities were largely due to release of a flash of so-called ‘prompt radiation’ - gamma photons and neutrons from the fission process itself. This was followed by around 5 seconds of ‘delayed’ radiation due to further fission of radioactive products in the fireball [132]. In both cases, the intensity of radiation decreased with distance from the epicentre due to divergence according to the inverse square law, and atmospheric scattering and absorption. Further, more minor, sources of radiation exposure were due to neutron activation of ground and building materials (absorbing neutrons and becoming radioactive) and ‘fallout’, i.e. unexploded uranium, plutonium or fission products settling to the Earth. Around 90% of radiation exposure was due to photons and 10% due to neutrons.

The Lifespan study has the advantage of individualised dose estimates [133], although these have evolved considerably since 1945. The first meaningful estimates were calculated in 1957 and known as T57D (T standing for tentative), followed by a second in 1965 (T65D), a third in 1986 (DS86) and a fourth in 2002 (DS02) [132].

Both the total dose at a given distance, and the relative proportions of this dose due to photons and neutrons have changed with successive iterations. Clearly, the situation of survivors had the potential to change considerably during the 5 seconds of primary radiation exposure. Once standing houses were blown down, thus altering the shielding characteristics for someone inside. People were knocked over or spun around, changing their orientation relative to the epicentre. To improve dose estimates, replicas of typical Japanese houses were exposed to nuclear explosions in the Nevada desert [132].

The LSS includes 86,611 individuals of both sexes and all ages exposed to a wide range of doses, with a mean whole body dose of 0.2 Gy [46], with 74,440 (79%) receiving less than 0.1 Gy [7]. Increased incidence has been detected for solid cancers (ERR=0.42 $Sv^{-1}$ 95% CI: 0.32, 0.53) and leukaemia (ERR=3.1 $Sv^{-1}$ 95% CI: 1.8, 4.3). These estimates of risk per sievert (equivalent dose), based on the most recent dosimetry system (DS02) were around 8% lower than those based on the previous dosimetry system (DS86) [134]. The dose response for solid tumours is consistent with linearity without threshold, though Preston and colleagues [134] detected a significant upward curvature in the first report since the DS02 dosimetry was implemented. In the most recent analysis, the lowest dose range in which a significantly increased ERR for solid cancers was observed was 0 – 0.2 Sv [7], though an earlier report by Preston *et al* found a significant increase for cancer mortality in the 0-0.125 Sv range [135]. A linear-quadratic model provides the best fit for leukaemia incidence and mortality [130, 133].

In addition to the lack of statistical power to detect cancer risks below around 100-200 mSv, there are a number of other limitations of the LSS. Firstly, as background incidence rates vary considerably between populations and ethnic groups, the ability to transfer risk estimates derived from a very homogenous Japanese sample to other populations is problematic [45]. As a large proportion of the male population of Japan was conscripted into the army at the time of the bombings, the populations of Hiroshima and Nagasaki had a relatively large proportion of females. Risk estimates per sievert are dependent on the radiobiological effectiveness (RBE) weighting factor applied to neutrons, which is set at 10. Suggestions have been made that the RBE should be higher [59], leading to correspondingly increased dose estimates and reduced risk per unit dose. For example, in an analysis of the LSS data, Kellerer *et al*

[136] detected a significantly increased risk estimate for organs located closer to the body surface with a neutron RBE of up to 100. Furthermore, the energy of gamma ray photons originating from the nuclear bomb blasts was relatively high compared to those of diagnostic x-rays (typically 30-100 keV). The radiobiological effectiveness of low energy photons is thought to be higher [137, 138], meaning risk per unit dose may be correspondingly higher also.

### *2.2.2: Environmental and occupational exposures*

Populations and workforces exposed to elevated radiation levels represent an alternative opportunity to study cancer risks from exposures. Theoretically, a large dose protracted over a long period of time can be viewed as a succession of infinitesimally small exposures. If observed, elevated cancer risks in such populations would not be consistent with the concept of a low dose threshold below which there is no risk.

Cardis *et al* [139] conducted a pooled analysis of mortality among 407,391 nuclear workers from 15 countries, exposed to an average cumulative dose of 19.4 mSv. A significantly raised ERR of 0.97 $Sv^{-1}$ was found for all cancers except leukaemia (95% CI: 0.14, 1.97), while a non-significantly raised ERR for leukaemia was found (1.93 $Sv^{-1}$, 95% CI: <0, 8.47). The study has drawn comment concerning the potential confounding effect of smoking and the unusually high ERR among Canadian workers [140, 141]. A reanalysis of the Canadian data was conducted by Zablotska *et al* [142], finding a much greater solid cancer ERR among workers employed between 1956 and 1964 (7.78 $Sv^{-1}$, 95% CI: 1.88, 19.5) than for those employed after 1964 (-1.20 $Sv^{-1}$, 95% CI: -1.47, 2.39). Excluding the Canadian data from the 15-country study, the ERR for solid cancers is reduced to 0.58 $Sv^{-1}$ (95% CI: -01.0, 1.39) [143], which is reasonably close to the linear ERR mortality estimate from the LSS of 0.32 $Sv^{-1}$ [130]. A significant increase in mortality for leukaemia was found by Muirhead and colleagues [144](ERR $Sv^{-1}$ = 1.71, 95% CI: 0.06, 4.29) among 174,500 UK nuclear workers. The mortality ERR for all malignancies except leukaemia was also raised (0.28 $Gy^{-1}$ 95% CI: 0.02, 0.56). A more recent study was conducted by Leuraud *et al* [145] on a subset of the 15-country study, focusing on 308,297 radiation-monitored workers in the UK, USA, France, receiving a mean yearly bone marrow dose of 1.1 mGy. Mortality was significantly raised for leukaemia

(ERR=2.96 $Gy^{-1}$, 95 CI: 1.17, 5.21), but not for non-Hodgkin lymphoma (ERR=0.47 $Gy^{-1}$, 95% CI: -0.76, 2.03). This same group of workers was subject to a further study by Richardson *et al* [146] examining cancer mortality for all sites except leukaemia. A significantly elevated risk was found (ERR=0.48 $Gy^{-1}$, 95% CI: 0.2, 0.79). This risk is 50% lower than reported in the above-mentioned study by Cardis *et al* [143], though still a little higher than that of the LSS (0.32 $Sv^{-1}$). These studies suggest an association between radiation and excess risk of cancer persisting at low doses, especially for leukaemia. However these studies all focused on adults, and may be biased to some extent by a 'healthy worker effect'. The results may be more relevant to the cardiologists, nurses and radiographers conducting cardiac catheterizations, rather than the patients themselves.

Residents of a number of areas exposed to elevated radiation levels as a result of natural radioactivity or industrial pollution have also been studied. A significantly increased ERR for solid cancer mortality of 0.61 $Gy^{-1}$ (95% CI: 0.04, 1.27) was observed among people residing in the Techa River region of Russia between 1950 and 1960 [147]. There was a suggestion that ERR increased with increasing age at first exposure (p=0.05) and attained age (p=0.10). A similar finding was reported in a study by Bauer *et al* [148] of residents of the Semipalatinsk region of Kazakhstan, who were exposed to radiation from nuclear weapons testing fallout. For all solid cancers, an ERR of 1.77 $Sv^{-1}$ was reported (95% CI: 1.35, 2.27). Chen *et al* [126] studied residents of the Yangiang region in Southern China who receive an estimated yearly effective dose of 6.4 mSv from elevated background radiation levels. No increase in cancer mortality was detected, compared to a control area where residents received a mean yearly effective dose of 2.4 mSv (relative risk= 0.99, 95% CI: 0.87, 1.14). In particular, relative risks were less than unity for a number of cancer sites previously linked to radiation exposure, including the lungs, stomach, breasts and thyroid.

Kendall and colleagues [149] matched 27,447 children living in Great Britain who developed cancer with 36,793 cancer-free controls. Radiation doses were estimated based on the mother's residence at the time of the child's birth and a national survey of natural background radiation levels [150]. For leukaemia, a significantly raised relative risk of 1.12 per mSv cumulative bone marrow dose from gamma radiation was found (95% CI: 1.03, 1.22). Relative risk increased monotonically with

increasing bone marrow dose, becoming significantly raised above around 4 mGy. The trend was driven by lymphoid leukaemia (RR=1.13, 95% CI: 1.02, 1.24), with lower risks for myeloid leukaemia (RR=1.05, 95% CI: 0.87, 1.28). For all cancers except leukaemia, the ERR was non-significantly negative up to cumulative doses of around 12 mGy (Figure 2.4). Lest this be interpreted as evidence of hormesis, it should be noted that these doses were protracted, thus if a hormesis effect or low dose threshold does exist, it is likely to be in the region of a few nanosieverts. A similar study, based in Switzerland, was conducted by Spycher *et al* [151], involving 2,093,660 children aged under 16 years. A significant increase in incidence was found for all cancers combined (hazard ratio (HR) = 1.64, 95% CI:1.13, 2.37) and leukaemia (HR= 2.04, 95% CI: 1.11, 3.74) for children residing in areas with background dose rates of greater than 200 nSv per hour (≈1.75 mSv per year) compared to less than 100 (≈0.88 mSv per year). The negative risks for moderate dose rates found in the UK study described above were not seen in the Swiss study. No corresponding increase was found for lymphoma (HR=0.91, 95% CI: 0.29, 2.86). Both the UK and Swiss studies are consistent with the 'no-threshold' component of the LNT model, at least for leukaemia.

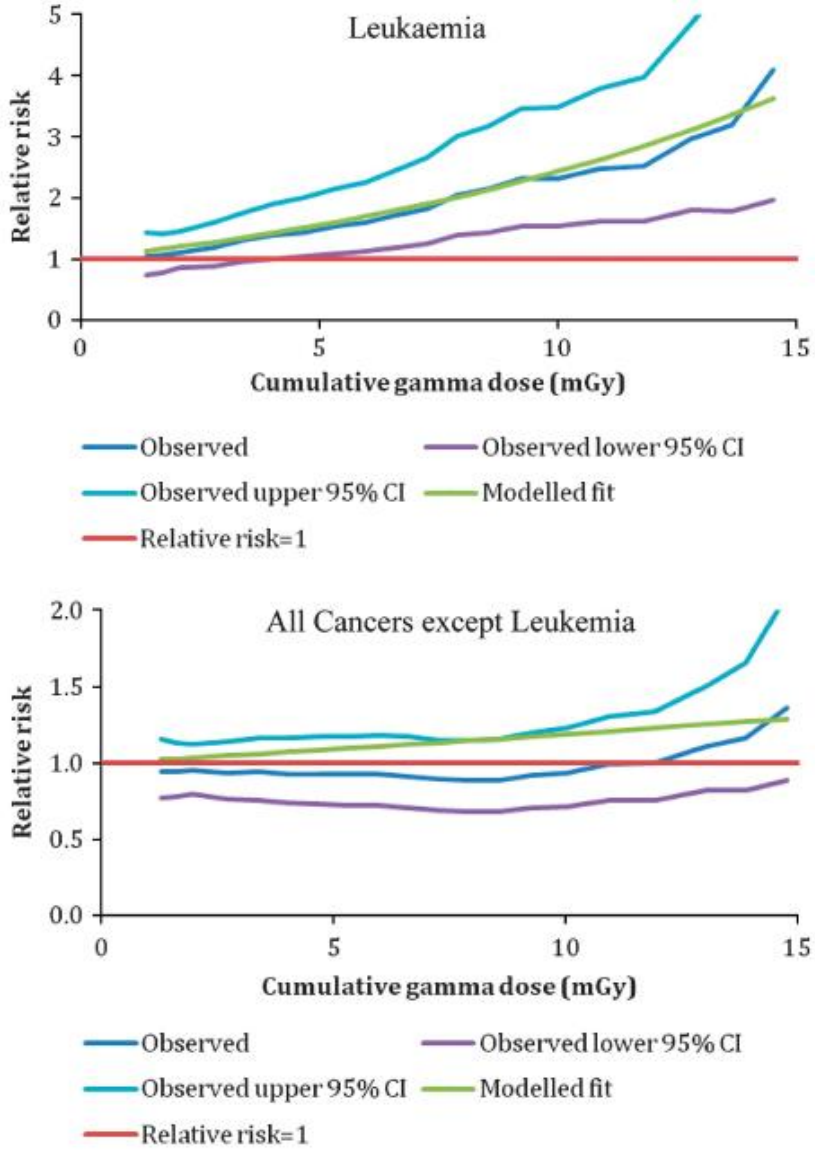


**Figure 2.4: Relative risk of leukaemia and all other cancers in relation to cumulative background dose. Reprinted by permission from Macmillan Publishers Ltd: Leukaemia, Kendall et al [146], copyright 2013**

### *2.2.3: Medical exposure studies*

Well over a hundred studies have been published investigating the cancer risk from radiation administered for medical diagnosis or treatment [3]. Such studies have the advantages of reasonably well defined exposure characteristics (i.e. dose, site of irradiation), relevance of low-energy and low linear energy transfer (LET) radiation, and medical records with long term follow-up. Medical exposures also typically produce a highly non-uniform dose distribution [130], in contrast to the whole-body doses from the Japanese atomic bomb exposures. The major disadvantage of

medical radiation studies is that of 'confounding by indication' [45]. Medical exposures should be carried out for a reason, such as illness or injury, which itself may be associated with increased long-term cancer risk. In other words, it is not clear if observed effects are due to the radiation itself or the need for radiation. Confounding by indication cannot be eliminated through large sample sizes. The association between the number of examinations of a particular type conducted and the number other examinations (e.g. fluoroscopy, nuclear medicine) or interventions including brain surgery could also influence results.

A small number of studies have attempted to directly assess the cancer risks from cardiac catheterizations. Modan *et al* [6] reviewed 674 Israeli children who underwent these procedures between 1950 and 1970. Dose records were unavailable for 90% of cohort members. A standardised incidence ratio (SIR) of 2.3 (95% CI: 1.2, 4.1), based on 11 cases compared to 4.75 expected, including 4 lymphomas and 3 melanomas. At least six of the tumours occurred in locations remote from the heart (testis, prostate, bladder, inguinal lymph nodes and melanomas of the groin and lower limb). The location of the others was not clear, either. A further interesting feature was that all cancers occurred in males, who represented 56% of the cohort. The results are unusual, though with such a small sample size, they could easily be attributed to chance. Spengler *et al* [4] conducted a retrospective cohort study on 4861 children receiving cardiac catheterisations between 1946 and 1968 in Ontario, Canada. After 13 years of follow-up, 5 cancer deaths were observed compared to 4.8 expected. A further study using the same cohort (reduced to 3915 members due exclusions of subjects living outside the study area) by McLaughlin *et al* [5] reported a standardised mortality ratio (SMR) of 1.2 (90% CI: 0.6, 2.3) based on 7 cancer deaths verses 5.7 expected, and SIR of 0.75 (0.3, 1.2) based on 13 cancer cases observed verses 17.3 expected. Again, a number of cancers were reported in sites remote from the heart including the tongue, testis (two cases), prostate, ovary, cervix, colon and brain. The small sample sizes, limited dosimetric information and lack of dose response analysis of these studies limits the ability to draw conclusions.

Several studies have been conducted focusing on two cohorts of patients (Massachusetts, USA and Canada) treated with fluoroscopically guided pneumothorax therapy for tuberculosis (TB). These treatments were conducted 2 or 3 times per month for around 2 years, resulting in mean cumulative doses of around

0.8 – 1 Gy to the lungs and 0.54 – 0.96 Gy to the breasts. Exposures were similar to cardiac fluoroscopy in terms of dose rate, photon energy and patient position (predominantly posterior-anterior). A significant increase in breast cancer incidence and mortality among both cohorts has been reported [152-155].

Despite the lungs receiving a particularly high dose, lung cancer mortality was not raised for the exposed group in either Massachusetts (SMR = 0.8 for both male and female) [154] or Canada (Relative risk=1.00, 95% CI: 0.94, 1.07) [156] – findings grossly inconsistent with the seven-fold increase predicted by Gofman and Tamplin based on estimated doses [157]. There are a number of possible explanations for these findings; (1) bias due to smoking, (2) modification of risk by TB, or (3) fractionation of large doses reduces or eliminates risk. The final point is plausible, though inconsistent with evidence of nuclear workers [139] or underground miners in which increased lung cancer risk has been associated with chronic, highly fractionated exposures. In the former case, a significant increase in lung cancer mortality (ERR = 1.8 $Sv^{-1}$ 95% CI: 0.26, 4.01) was reported, though the authors state that a confounding effect due to smoking "may be partly but not entirely responsible" for the figure.

The only study to evaluate all cancer sites among TB patients was conducted by Davis and colleagues using the Massachusetts cohort [154]. No overall increase in cancer mortality was detected – the SMR was increased for some sites but not for others. These patterns are often reversed when male and female data are compared. The SMR was non-significantly raised for female leukaemia (1.4, based on 9 cases) but not for male (1.0, based on 8 cases). It is therefore extremely difficult to draw conclusions from the TB fluoroscopy data that are applicable to cardiac fluoroscopy.

Patients suffering from the spinal deformity scoliosis are subjected to frequent radiological investigations to monitor curvature. Ronckers and colleagues [158] studied 3010 women examined an average of 26.8 times between 1912 and 1945, receiving a mean breast dose of 120 mGy (range = 0.05 – 1110 mGy). Based on a median follow-up of 35.5 years, a borderline significant ERR of 2.86 ($P$= 0.058) for breast cancer was detected. A significantly higher risk was reported for women with first or second degree relatives diagnosed with breast cancer (ERR = 8.37 $P$=0.03). Raised risk was only apparent for patients receiving a cumulative breast dose of greater than 200 mGy (mean dose per fraction of 7.46 mGy). No other cancer sites

were investigated. This is unfortunate as the dose levels and site of irradiation are reasonably similar to cardiac catheterizations.

Weiss and colleagues [125] studied 14,556 patients treated between 1935 and 1957 with radiotherapy for ankylosing spondylitis (an inflammatory spinal disorder). The mean whole body dose was high (2.64 Gy), with the greatest localised doses to the spine. The average follow up was 25 years. Cancer mortality for all sites was significantly increased (ERR= 0.18 $Gy^{-1}$) between 5 and 24.9 years after treatment, with risks decreasing beyond 25 years (ERR=0.11 $Gy^{-1}$). A significant dose response was seen for cancers of the oesophagus, colon, pancreas, bones and connective tissues, prostate, bladder and kidney, along with non-Hodgkin's lymphoma, multiple myeloma and leukaemia. A small increase in lung cancer mortality was detected (ERR=0.09 $Gy^{-1}$, 95% CI: 0.03, 0.15), while stomach cancer mortality was non-significantly decreased (ERR= -0.004, 95% CI: -0.05, 0.05). The lack of increased breast cancer risk (ERR=0.08 $Gy^{-1}$ 95% CI: -0.30, 0.65) may possibly be due to hormonal changes induced by the high dose to the ovaries [3]. The high doses limit the relevance of this study to cardiac catheterizations, although the limited effect on lung and stomach cancer is intriguing.

Hildreth and co-workers [159] compared extrathyroid tumour risk in 2856 infants therapeutically irradiated for enlarged thymus between 1926 and 1957 with 5053 unexposed siblings. A significant increase in incidence of malignant tumours of the skin and breast was noted (RR=2.0), along with benign tumours of the bone, nervous system, salivary glands, skin, and breast (RR=2.2). Further studies by Shore *et al* focused specifically on thyroid tumours among 2657 exposed individuals and 4833 unexposed siblings [160-162]. Thyroid doses ranged from 0.03 to over 8 Gy, with 62% receiving under 0.5 Gy. A significant increase was found for malignant tumours (ERR=10.0 $Gy^{-1}$ 95% CI: 5, 23) and benign adenomas (ERR=6.3 $Gy^{-1}$ 95% CI: 3.7, 11.2), with excess risk persisting for at least 40-45 years post-irradiation. Dose response was linear for malignant tumours and for adenomas up to 6 Gy, after which a downward curvature was seen. Although the doses were relatively high and location of irradiation more superior, these findings have relevance to cardiac catheterizations and demonstrate the sensitivity of the thyroid to cancer induction in childhood.

### *2.2.4: Computed tomography studies*

Computed tomography (CT) is a diagnostic examination in which axial cross-sectional images are produced by reconstruction of attenuation data obtained from multiple angles around the patient [163]. Based on existing knowledge, the effective dose for cardiac or chest CT (1-8 mSv [111, 164-167]) is similar, albeit somewhat lower, to that of cardiac catheterizations (2-12 mSv [91, 111, 164]), although the pattern of dose distribution is not the same. In CT, the beam rotates around the patient resulting in a relatively uniform dose distribution, while in cardiac catheterizations, exposures may involve only a single beam angle, focused in the same place, resulting in more uneven dose distribution to large organs such as the lungs. In addition, the peak tube potential used in CT (120 – 140 kVp) is higher than fluoroscopy (typically 60-80 kVp).

To date, five epidemiological studies have been conducted examining the excess cancer risks following CT scans in young people. Pearce *et al* [9] conducted a retrospective observational study of nearly 180,000 children and adolescents scanned by CT between 1985 and 2002. After around 15 years of follow-up, a significant association between radiation dose and incidence of leukaemia (ERR=36 $Gy^{-1}$ 95% CI: 5, 120) and brain tumours (ERR=23 $Gy^{-1}$, 95% CI: 10, 49) was detected (in relation to red bone marrow and brain doses, respectively). The authors quote equivalent figures from the LSS of 45 $Sv^{-1}$ for leukaemia (95% CI: 16, 188) and 6.1 $Sv^{-1}$ for brain tumours (95% CI: 0.1, 63.9) in the 0-19 years age group, suggesting the study findings are very similar to the LSS for leukaemia and four times higher for brain tumours. However the CT study ERR for leukaemia includes myelodysplastic syndrome (MDS), which is not generally regarded as a form of leukaemia [168] and not included in the LSS risk estimate. Excluding MDS from the CT study results, the ERR is reduced to less than half that of the LSS at 19 $Sv^{-1}$ and no longer statistically significant. Even including MDS, risks for leukaemia were lower than reported in the previously mentioned study by Kendal *et al* [149] in relation to natural background radiation. Pearce *et al* found the risk of brain tumours to increase with increasing age at exposure, ranging from 5 $Gy^{-1}$ at 0-5 years to 41 $Gy^{-1}$ after 15 years. This finding, while not unprecedented, contrasts with the LSS [169] and studies of children irradiated for tinea capitis [170] and skin haemangioma [171] in which the reverse pattern was suggested. There was a suggestion that females were at a greater risk

than males of brain tumours following CT scans (ERR of 28, verses 16, p=0.085). Again, the reverse pattern was observed among the LSS cohort (p=0.02) [169].

As stated above, the ERR estimates derived by Pearce *et al* were higher than those of the LSS by a factor of around four. The LSS figures are themselves higher, by a factor of between five and ten, those derived from studies of brain tumours following radiotherapy for previous cancer in childhood [172]. These studies provide limited evidence of excess risk of brain tumours below doses of around 10 Gy [173-175]. A systematic review of benign second tumours by Kutsenko *et al* [176] found significantly raised incidence only where the primary tumour was of the brain, 'other central nervous system', thyroid and acute lymphoblastic leukaemia (all sites in which cranial radiotherapy is used). The association is stronger for meningioma, in which a reasonably linear dose response is seen, compared to glioma [129, 174]. Pearce *et al* [9] suggest a mean absorbed dose to the brain from CT scans of around 60 mGy in childhood could triple the risk of brain tumours. This increase in risk is comparable to that following radiotherapy doses of over 10 Gy [172].

The UK CT study, and others following, was reviewed by Walsh *et al* [177] and Boice [178] who both raise concerns over the potential for confounding by indication, as well as the combining of MDS with leukaemia. No effort was made to identify subjects with diseases such as neurofibromatosis or tuberous sclerosis, both of which are an indication for CT and a major risk factor for brain tumour development [179, 180]. A recent study by Meulepas *et al* [181] estimated the confounding bias introduced by various cancer predisposing conditions. The study concludes that relative risks for leukaemia are not meaningfully confounded by such conditions, while brain tumour risks may be overestimated due to tuberous sclerosis.

Following the UK CT study by Pearce *et al* [9], Mathews *et al* [124] conducted a data linkage analysis of 680,211 Australian patients receiving CT scans at ages 19 or under, between 1985 and 2005, compared to 10,259,569 unexposed individuals. With a mean follow-up duration of 9.3 years, cancer incidence in the exposed group was 24% greater than in the unexposed group (incidence rate ratio (IRR) = 1.24, 95% CI: 1.20, 1.29 for all cancers). This increase, the authors state, is 'mostly due to irradiation'. Increases in almost all sites of cancer were found, including those with limited previous association with radiation, such as Hodgkin's lymphoma and melanoma [182, 183], but no increase was found for breast cancer (IRR = 0.99) and

lymphoid leukaemia (0.96), both of which are strongly associated with radiation [45, 178]. IRR figures were also calculated based on the number of years since first exposure. These were 1.35, 1.25, 1.14 and 1.24 for 1-4, 5-9, 10-14 and >15 years since the first scan respectively. This pattern of a large excess of cancers occurring soon after exposure, followed by a decrease is not consistent with the findings of the LSS or studies of second cancers following radiotherapy, in which a median latency between exposure and cancer diagnosis of around 20 is typically seen [184] [185]. The decision to use a latency period of only 1 year for solid tumours is not adequately justified and lacks biological plausibility. Again, no effort was made to remove potential confounding diseases.

Huang and colleagues [186] studied cancer incidence ascertained from insurance records among 24,418 subjects undergoing CT scans of the head while aged under 18 years between 1998 and 2006 in Taiwan, compared to 97,668 unexposed individuals. For all cancer types combined, no significant increase was seen among the exposed cohort (hazard ratio = 1.29, 95% CI 0.90-1.85). A significant increase in brain tumours was found (HR=2.56, 95% CI 1.44-4.54), based on 19 cases, of which 14 were benign. A significant trend of increased brain tumour risk with scan frequency was noted, though based on an extremely limited number of cases (a single case in the 3 or more scans group). Radiation doses were not estimated. Furthermore, the authors did not include non-head CT exposures in their analysis. However, unlike the studies by Pearce and Mathews described above, the Taiwanese CT study team have at least attempted to address the issue of confounding by indication by excluding patients with certain conditions. The exclusions are somewhat inexhaustive though; not including tuberous sclerosis, ataxia telangiectasia or Li Fraumeni syndrome. This, combined with the small sample size and short latency period of 2 years (based on limited evidence not specific to brain tumours) renders the Huang study of limited value.

Journy *et al* [187] investigated cancer incidence among 67,274 children who underwent CT scans before the age of 10 in France between 2000 and 2010. As with the Taiwanese study, Journy et al attempted to address the issue of confounding by indication by identifying patients with known cancer predisposing conditions. The study is limited by the very short median follow-up time of 4 years, though has the advantage over the Huang study [186] of providing dose estimates based on

examination protocols. The results presented by Journy are difficult to interpret. While apparently suggesting a decrease in ERR after adjusting for predisposing conditions, the ERR for children without such conditions appears to be higher than the unadjusted ERR for the whole cohort, while the ERR for children with predisposing conditions is close to zero. This, argue and Cardis and Bosch de Basea [188] and Muirhead [189] , implies the ERR is modified by predisposing factors rather than confounded. Furthermore, the study acquired data from specialist hospitals, where the rate of underlying predisposing conditions was relatively high [189].

Krille *et al* [190] conducted a study investigating cancer incidence among 44,584 German children exposed to 71,073 CT scans between 1980 and 2010. Again, efforts were made to exclude subjects with conditions predisposing for cancer or those examined for suspected cancer. Non-significantly raised incidence of leukaemia (SIR = 1.72, 95 % CI: 0.89, 3.01) and CNS tumours (SIR=1.35, 95% CI: 0.54, 2.78) was found. A significant risk for all cancers combined was observed (SIR=1.54, 95% CI: 1.05, 2.19), based on 31 observed cases verses 20.1 expected. This increase was driven to some extent by an increase in lymphoma (SIR=1.85, 95% CI: 0.68, 4.02). A dose response was obtained by calculating the hazard ratio (HR). A significantly increased HR was found for brain tumours (1.008 per mGy, 95% CI: 1.004, 1.013), but not for leukaemia (HR=1.009 $mGy^{-1}$, 95% CI: 0.981, 1.037) and for all tumours combined (HR=0.986 $mGy^{-1}$, 95% CI: 0.944, 1.030).

Most recently, a re-examination of the UK CT study was conducted by Berrington de González *et al* [191], who analysed pathology reports, radiologist reports and comments written in the radiology information system (RIS) to identify predisposing conditions and pre-existing tumours. Previously unreported cancers were found to have the largest impact, resulting in a reduction in ERR for brain tumours by 50% and for leukaemia by 15%. Pre-disposing conditions were not associated with a decrease in ERR as they did not appear to be related to CT exposure.

| | ERR per Gy (95% CI) | |
|---|---|---|
| **Study** | **Brain tumours** | **Leukaemia** |
| **Life Span study *** | 6 (0, 64) | 45 (16, 188) |
| **Pearce [9]** | 23 (10, 49) | 19 (-12, 79) |
| | | 36 (5, 120) $ |
| **Berrington [191] excluding previous cancers.** | 10 (2, 26) | 20 (-11, 29) $ |
| **Berrington [191] excluding PFs** | 27 (10, 65) | 34 (5, 129) |
| **Mathews [124]** | 21 (14, 29) | 35 (0, 77) |
| **Journy [187] (unadjusted for PF)** | 22 (-16, 61) | 57 (-79, 193) |
| **Journy [187] (adjusted for PF)** | 12 (-13, 37) | 47 (-65, 159) |

**Table 2.5: Summary of elevated relative risk (ERR) for brain tumours and leukaemia (excluding myelodysplastic syndrome) for 5 CT studies. * Figures reported by Pearce *et al [9]*. $ including myelodysplastic syndrome, PF=predisposing factor.**

### *2.2.5: In Utero exposures*

Prior to 1956, many pregnant mothers were examined by x-ray pelvimetry for obstetric planning purposes. This procedure was restricted following concerns of hereditary effects in the offspring of the irradiated foetus [192]. Although such risks appear to have been overly pessimistic, the abandonment of pelvimetry was later associated with a significant decrease in childhood cancer in the following years [193] in the Oxford Study of Childhood Cancers. Based on an estimation of doses per image and the total number of images acquired during pregnancy, the mortality ERR was estimated by Mole [192] as 0.038 per mGy (95% CI: 0.007, 0.079) and Bithell as 0.051 $mGy^{-1}$ (95% CI: 0.028, 0.076). The latter estimate is influenced by an upturn in RR beyond 1967, which Doll and Wakeford [193] argue is likely to be artificial. The authors calculate an EAR of 6% $Gy^{-1}$; though acknowledge uncertainty in the exact value. A later study by Wakeford and Little [194] revised this figure to 8% $Gy^{-1}$.

The results of the Oxford study have been used as evidence in support of linearity of dose response as low as 10 mGy [46], having the advantages of x-ray energies relevant to diagnostic imaging and the lack of confounding by indication issues (i.e. the unborn child was not being treated for a pre-existing condition). Nonetheless, the risk estimates are dependent on non-individualised reconstructions of doses delivered decades earlier, resulting in significant uncertainty. Furthermore, the findings are not consistent with those of the LSS in which no significant increase in

childhood cancer was detected among 753 subjects receiving *in utero* exposures of over 10 mGy [193]. A more recent study of 8000 offspring of pregnant workers of the Mayak nuclear weapons facility in Russia, receiving a mean dose of 54.5 mGy [195] found no significant increase in solid cancers (ERR= -0.1 $Gy^{-1}$, 95% CI: <-0.1, 4.1) or leukaemia (ERR= -0.8 $Gy^{-1}$, 95% CI: <-0.8, 46.9) in offspring.

It is interesting that an increase in almost all cancer sites was detected in the Oxford study, including those cancers not normally induced by radiation [193]. The different level of cell proliferation, immune system development and level of gap-junction intercellular communication in embryonic tissues should limit the applicability of the Oxford findings to the wider population [59].

### *2.2.6: The effect of age*

Age at exposure modifies the risk of radiation induced cancer and will have an important bearing on the current study. For all sites combined, a pattern of decreasing risk with increasing age at exposure is generally assumed [3, 44]. Such assumptions, while having reasonable evidential support, have become something of a cliché, forming part of the standard preamble of almost all published papers on paediatric imaging and radiation doses. In reality, evidence of the effect of age at exposure on radiation induced cancer risk is far from conclusive. More recent analysis of the LSS data suggests the possibility of a 'U'-shaped relationship, with risks initially falling with age at exposure, before rising in middle age [169]. Analysis between individual cancer sites lacks statistical power [196], though there is a suggestion that for some sites, the risk of radiation induced cancer is higher among adults than previously supposed [197]. Confidence intervals are wide, however, and cannot be narrowed as data collection for individuals exposed in middle age is complete (i.e. all have now died) [198].

Other epidemiological studies, studies of nuclear industry workers have failed to find any modifying effect of age at exposure [9, 139, 148]. Analyses of cancer mortality among residents of the Techa River and Semipalatinsk regions suggests an increase in risk with increased age at exposure [147, 148]. The most recent analysis by the United Nations Scientific Committee on Atomic Radiation (UNSCEAR) [129] concludes that children are at a greater risk than adults for 25% of tumour types,

including thyroid cancer and leukaemia, at the same risk as adults for 15% of tumour types, including liver cancer, and at a lower risk for 10% of tumour types, including lung cancer. For 20% of tumour types, including oesophageal cancer, the data are insufficient to draw conclusions [129].

It appears that most radiation induced cancers develop at ages at which they would normally be expected to occur in the general population [132]. For example, where children receive radiotherapy for primary cancer, second cancers developing in the following years (i.e. where the patient is still a child or young adult) tend to be other 'childhood' cancers, such as sarcomas, leukaemia and brain tumours [185, 199]. With longer follow-up, breast and colon second cancers develop [200, 201]. Only where follow-up times are sufficient to include cohort members who have reached around 40 years, are 'adult' second cancers such as lung and stomach found. Among the atomic bombing survivors, excess cases of lung, stomach, breast and liver cancer were close to zero at 35 years, rising to maximum levels at age 80 or above [135, 169]. While there is a suggestion that the latency period between exposure and cancer diagnosis is reduced at high doses [45], there is little evidence that radiation can somehow 'force' the early development in children of tumours normally associated with adulthood. Cancers of many of the most heavily irradiated sites from cardiac catheterizations (lungs, oesophagus, stomach and liver) are exceptionally rare before 30 years of age, with incidence rates generally less than 1 case per 100,000, per year [202, 203]. This presents an important challenge for an epidemiological analysis; in order to detect the cancers most likely to be induced by cardiac catheterizations, the follow-up time would need to be long. With short follow-up times (i.e. less than 20 years), observed cancers are all likely to be those normally occurring in childhood, notably leukaemia and lymphoma.

### *2.2.7: Summary of epidemiology review*

Previous attempts at epidemiological assessment of the cancer risks from cardiac catheterizations lack sufficient statistical power and have limited or non-existent dosimetry. Currently, risks from these procedures can only be estimated based on the findings from studies of other exposures, most notably the Life Span Study. The applicability of these findings to cardiac catheterizations is debateable as the doses and exposure patterns are different. There is therefore a need for a direct

epidemiological analysis of radiation associated cancer risks among patients undergoing these procedures. There are however a number of significant challenges, in particular the issue of confounding by indication and the long follow-up time required to detect the cancers most likely to be induced.

### *2.3: Conclusion*

Previously published assessments of the radiation doses from cardiac catheterizations in young people are inadequate, being mainly restricted to simple surveys of kerma area product, with little or no assessment of dose to the patient. Studies have suggested that estimation of patient dose using $P_{KA}$ is possible, though this needs to be explored in greater detail. Epidemiological evidence of the cancer risks at low doses remains inconclusive. The uncertainty in both the radiation doses and associated risks from cardiac catheterizations is problematic in terms of justification and optimisation. This necessitates further research.

# Chapter 3: Analysis of Cohort Data:

The following chapter describes the establishment of a retrospective cohort of children and young adults who have undergone x-ray guided cardiac catheterizations in the UK, along with an analysis of data received from participating hospitals. These data included kerma area product ($P_{KA}$), fluoroscopic screening time (ST) and air kerma (skin dose estimates). Such dose indicators have limited usefulness in risk estimation or epidemiological analysis, though offer the opportunity for comparison with previously published research and can be used to evaluate and explain variation in doses between hospitals and to set so-called 'reference doses'. The estimation of organ doses and associated cancer risks using these data will be covered in later chapters.

## *3.1: Research Governance*

A favourable ethical opinion was gained for the study from the National Research Ethics Service (NRES) Committee North East - Newcastle & North Tyneside 2 ethics committee (10/H0907/47). In addition, Confidentiality Advisory Group (CAG) approval for obtaining patient identifiable data without individual patient consent was obtained (ECC 7-04(j)/2010). Each committee was provided with yearly updates of study status. Where data were obtained from hospitals, local Research and Development (R&D) department approval was also obtained. Cohort members were assigned an anonymous identification code. After these were assigned, the dataset containing patient names was stored in a relational database that could only be accessed from within the Sir James Spence Institute at Newcastle University. Analysis was conducted on anonymised data wherever possible. The study was retrospective in nature, extending from 2014 to as far back as data were recorded. Once data were acquired from a participating hospital, collection at that site was terminated.

## *3.2: Data collection methodology*

The cohort was created by identifying all the hospitals in the UK carrying out cardiac catheterizations on children and young adults. These procedures are performed on adults at most hospitals throughout the United Kingdom. However, procedures on children and young adults are limited to 14 centres, carrying out between 100 and

500 procedures per year [2] (Table 3.1). Some of these are dedicated children's hospitals while others are general hospitals. All hospitals were contacted by the author, except for two hospitals in which prior agreement to supply data had been obtained. Various strategies were used. A list of e-mail addresses of local medical physicists was obtained and these staff contacted. Job advertisements for catheterization laboratory staff were searched for possible contacts. Collaborators already involved in the study where in some cases able to identify staff at other hospitals who could help. R&D approval to obtain data was obtained from 7 hospitals. At the time of writing, 6 hospitals had provided data. These were reasonably well distributed throughout England (Figure 3.1), giving representation for Southern, Midlands and Northern regions. One further hospital had agreed to participate but has not yet sent any data (though cooperation has been maintained).

To be eligible for inclusion in the cohort, subjects needed to be aged under 22 years at the time of the first recorded examination. Procedures conducted after the patient reached 22 years were retained, though were not analysed in this study. Patients undergoing Hickman or PICC (Peripherally Inserted Central Catheter) line insertions or pericardial effusion drainage, in the absence of other cardiac catheterizations, were excluded. These procedures were not regarded as true cardiac catheterizations, and, in the case of PICC and Hickman insertions, often signify existing malignancy as they are used for chemotherapy administration or marrow transplants [204, 205]. Patients with congenital heart conditions who reach adulthood may continue to be cared for by paediatric cardiologists and may undergo catheterizations in children's hospitals. Consequently, data obtained from paediatric hospitals often contained a small number of records for patients examined as adults.

| Hospital: | Contacted | Replied | R&D approval obtained | Data obtained |
|---|---|---|---|---|
| Great Ormond Street Hospital, London * | Yes | Yes | Yes | Yes |
| Alder Hey Children's Hospital, Liverpool* | Yes | Yes | Yes | Yes |
| Glenfield Hospital, Leicester | Yes | Yes | Yes | Yes |
| Evelina Children's Hospital, London * | Yes | Yes | Yes | Yes |
| Freeman Hospital, Newcastle-upon-Tyne | Yes | Yes | Yes | Yes |
| John Radcliffe Hospital, Oxford | Yes | Yes | Yes | Yes |
| Birmingham Children's Hospital * | Yes | Yes | Yes | Awaiting |
| Manchester Royal Infirmary | Yes | Yes | Failed | |
| Leeds General Hospital | Yes | Yes - declined | | |
| Glasgow Hospital for Sick Children * | Yes | Yes | Applied | |
| Southampton General Hospital | Yes | No response | | |
| The Bristol Royal Hospital for Children * | Yes | Yes | Lost contact | |
| Royal Brompton and Harefield Hospital | Yes | No response | | |
| Royal Belfast Hospital for Sick Children * | Yes | Yes | Lost contact | |

**Table 3.1: Data acquisition status for 14 UK hospitals carrying out cardiac catheterizations in children and young adults. * Specialist children's hospitals.**

**Figure 3.1: Location of hospitals providing data (yellow) and centres from which no data were obtained at the time of writing (red). Figure credit: author**

The data provided by participating hospitals were variable. Some centres recorded examination details in paper logbooks, while others recorded it electronically. A description of the data available at each participating hospital is provided below. A summary is provided in Table 3.2. Note that the total number of patients in the cohort is smaller than the sum of individual hospitals, as some patients underwent

procedures at more than one hospital. Table 3.3 shows details of equipment used at each hospital. All machines were biplane. These details will be explored in much greater detail in the 'supporting information' chapter. From the remainder of this thesis, all hospitals will be anonymized, and will be referred to as Hospitals 1-6. Fluoroscopic equipment was confirmed with local medical physics staff to have undergone at least yearly quality assurance (QA) testing, including $P_{KA}$ measuring device calibration. QA reports were obtained for machines, where available.

*Hospital 1*

Hospital 1 provided by far the largest amount of data in the study (36% of examinations). Data were recorded in paper form in multiple log books, which extended back as far as 1994. The logbooks were transcribed at Newcastle University. Procedures were carried out in several different laboratories, often with different equipment. Post 2002, recorded details were relatively extensive, including bi-plane $P_{KA}$, estimated skin doses and clinical details including indications for the procedures (i.e. why it was being carried out). For examinations conducted in lab 1 between 1994 and 2000, the recording of $P_{KA}$ was sporadic, quoted for 32% of procedures. Between 2000 and 2002, only screening time was recorded.

*Hospital 2*

Data were obtained for procedures carried out between 2004 and 2013. During this time period, two machines were used – a Philips Integris BH3000 up to 2008 and a Siemens Artis Zee after this date. Data were not available prior to 2004. Boxes of cine film from procedures as far back as the late 1960s were located, each containing the patient name and screening time, but no $P_{KA}$ or procedure type. These data were not acquired due to the limited information content and time required for gathering. More recent examinations up to 2004 were recorded on CDs, with dose information written on the CD packaging. Unfortunately, in a bid to save space, these CDs were transferred to large spools and all packaging was discarded without the information being recorded. Examination details were recorded in paper log books. On agreement with the named local collaborator and local R&D team, data from these were obtained by photographing each page of the book at Hospital 2 and transcribing these photographs at Newcastle University. The fluoroscopy equipment used at Hospital 2 reports doses as bi-plane $P_{KA}$ figures, but these were only

recorded in logbooks as total $P_{KA}$ (i.e. frontal and lateral beams combined). Hospital 2 records the beam angles used for each examination along with short, free-text descriptions of procedure type and the clinical details of the patient.

*Hospital 3:*

Data were available from 2004 onwards and in electronic form. Doses were recorded as total $P_{KA}$ figures. Procedure types were recorded in good detail and secondary procedure types (i.e. a second exam done at the same time) were also recorded. Patient age, height and mass were also recorded.

*Hospital 4*

The data obtained from the Hospital 4 were unusual in that dose indicators were not recorded on the Radiology Information System (RIS). A download of RIS data for procedures carried out since 1991 was obtained, along with a separate file containing dose indicators recorded using a monitoring system developed by the local medical physics department from 1993 to 2014. $P_{KA}$ figures were adjusted by a calibration factor and for table attenuation. Unfortunately a large number of procedures recorded in the RIS data (n=4728) were not present in the dose file (n=1769). Dose details were only obtained for patients under age 16 years. Furthermore, the procedure types were found to be vague. Most procedures (75%) were simply listed in the dose file as 'A.PAE'. It was observed that radiographers tended to use this procedure code for virtually all cardiac catheterizations, regardless of what the actual procedure type was. In the RIS file, most procedures were simply listed as an 'angiocardiogram'. $P_{KA}$, where recorded was in the form of biplane figures for 70% of procedures. The remainder were recorded as a single total figure. Dose data were recorded sporadically. In particular, between 2006 and 2011, $P_{KA}$ was recorded for only 26 out of 984 (2.6%) procedures.

*Hospital 5:*

Data were obtained from the Radiology Information System (RIS) in electronic form and included total examination $P_{KA}$ figures and screening time. Patient mass or height were not recorded. Procedure type was reasonably detailed, though lacked clinical details. There were 130 entries in which it appeared that the patient had undergone two identical examinations on the same day, both with the same screening time, but different $P_{KA}$. Where dose figures were identical, the second

entry was assumed this was a duplicate entry and removed. Where the figures were different, they were combined to produce a single procedure.

*Hospital 6*

Data were recorded in log books at Hospital 6, but unfortunately these were discarded some years prior to the study. Procedures carried out after May 2006 were recorded electronically and details were obtained in an Excel file. Data included patient age, but not height or mass. Only the patient's surname was included, which limited the usefulness of the Hospital 6 data for cancer registry matching.

| Hospital (date range) [laboratory number] | No. of exams | No. Of patients | % with $P_{KA}$ (with biplane $P_{KA}$) | % with ST | % with Mass | % with Height | Age | Exam type | Clinical info |
|---|---|---|---|---|---|---|---|---|---|
| **Hospital 1 (1994-00) [1]** | 2067 | 4753 | 32% (30%) | 98% | 96% | 0% | Yes | Yes | Yes |
| **Hospital 1 (1999-02) [2]** | 1040 | | 96% (96%) | 97% | 98% | 95% | Yes | Yes | Yes |
| **Hospital 1 (2000-02) [1]** | 183 | | 0% (0%) | 100% | 71% | 14% | Yes | Yes | Yes |
| **Hospital 1 (2002-08) [1]** | 3196 | | 97% (97%) | 98% | 98% | 85% | Yes | Yes | Yes |
| **Hospital 1 (2007-10) [4]** | 725 | | 98% (98%) | 99% | 91% | 68% | Yes | Yes | Yes |
| **Hospital 2 (2004-08)** | *1640* | *3655* | 92% (0%) | 91% | 87% | 0% | Yes | Yes | Yes |
| **Hospital 2 (2008-13)** | *2012* | | 90% (0%) | 91% | 93% | 0% | Yes | Yes | Yes |
| **Hospital 3 (2008-13)** | 1407 | 1611 | 94% (0%) | 94% | 99% | 81% | Yes | Yes | No |
| **Hospital 3 (2004-08)** | 842 | | 94% (0%) | 92% | 100% | 86% | Yes | Yes | No |
| **Hospital 4 (1991-03)** | 2666 | 2983 | 46% (37%) | 45% | 41% | 40% | Yes | Yes | No |
| **Hospital 4 (2003-14)** | 2863 | | 19% (9%) | 19% | 17% | 17% | Yes | Yes | No |
| **Hospital 5 (2005-13)** | 737 | 674 | 97% (0%) | 94% | 0% | 0% | Yes | Yes | No |
| **Hospital 6 (2006-13)** | 356 | 313 | 58% (0%) | 60% | 13% | 10% | Yes | Yes | No |
| **Total:** | 19734 | 13,564 | 67% (33%) | | | | | | |

**Table 3.2: Summary of data acquired from participating hospitals. Note that many hospitals replaced equipment during the data collection period at least once. These separate 'eras' are recorded as separate lines in the table. ST= screening time.**

| Hospital (date range) [laboratory number] | Manufacturer and model | Antiscatter Grid | Tube potential (kVp) | Filtration | Frame rates ($s^{-1}$) | Detector type |
|---|---|---|---|---|---|---|
| **Hospital 1 (1994-2000) [lab 1]** | Siemens BICOR Biplane | Fixed | Unknown | Al | Cont (f) 30-60 (a) | II |
| **Hospital 1 (1999-2002) [lab 2]** | Toshiba Infinix CX Biplane | Fixed | 50-125 | Al+? | 25-30 (f) 25-30 (a) | II |
| **Hospital 1 (2000-2002) [lab 1]** | Unknown | Unknown | Unknown | Unknown | Unknown | Unknown |
| **Hospital 1 (2000-2008) [lab 1]** | Siemens Axiom Artis BC Biplane | >10 kg | 58-125 | Al + Cu | 10-15 (f) 15 (a) | II |
| **Hospital 1 (2007-2010) [lab 4]** | Siemens Axiom Artis dBC Biplane | >10 kg | 58-125 | Al + Cu | 10-15 (f) 15 (a) | FPD |
| **Hospital 2 (2004-2008)** | Philips Integris BH3000 | Always | Unknown | Al + Cu | Unknown | II |
| **Hospital 2 (2008-2013)** | Siemens Artis Zee Biplane | Always | 58-125 | Al + Cu | 10-15 (f) 30 (a) | FPD |
| **Hospital 3 (2004 - 2013)** | Siemens HICOR Biplane | Fixed | Unknown | Al + Cu | 10 (f) 30 (a) | II |
| **Hospital 3 (2004-2008)** | Siemens Axiom Artis dFC Biplane | >10 kg | 58-125 | Al + Cu | 12.5 (f) 30 (a) | FPD |
| **Hospital 4 (1991-2003)** | Siemens Coroskop C Biplane | Fixed | Unknown | Al | Unknown | II |
| **Hospital 4 (2003-2014)** | Siemens Axiom Artis BC Biplane | >10 kg | 58-125 | Al + Cu | 7.5 (f) 15-30 (a) | II |
| **Hospital 5 (2005-2013)** | Siemens Axiom Artis Biplane | Unknown | 58-125 | Al + Cu | 7.5-15 (f) ? (a) | FPD |
| **Hospital 6 (2006-2013)** | Siemens Axiom Artis dBC Biplane | Unknown | 58-125 | Al + Cu | Unknown | FPD |

**Table 3.3: Equipment used at participating hospitals. Note: II=image intensifier, FPD=flat panel detectors, Cu=copper, Al=aluminium, f=fluoroscopy, a=acquisitions.**

### *3.3: Data checking procedure*

For all cohort data, a systematic process was used to detect, and correct where appropriate, data entry errors. This process was especially important for data extracted from log books.

1. Where $P_{KA}$ was reported as biplane figures as well as a 'total' $P_{KA}$, the frontal and lateral figures were added to check if it matched the 'total' quoted in log book. The radiographer calculates the total $P_{KA}$ figure through mental arithmetic. The sum of frontal and lateral figures was considered more reliable and used in cases of discrepancies (57 entries at Hospital 1).

2. Estimated skin dose is calculated by dividing $P_{KA}$ by beam area. The $P_{KA}$ should always be higher than skin dose, otherwise the field size would be smaller than 1

$cm^2$. Skin doses were higher than $P_{KA}$ in 41 cases (all at Hospital 1), where it was assumed the respective figures had been entered into the wrong columns.

3. Body mass index (BMI) was calculated, where mass and height were recorded. This is defined as:

$$\frac{Mass\ (kg)}{Height^2(m)}$$

Individuals with a BMI of over 35, defined by the World Health Organisation as being 'obese class II' [206] (severely obese) were investigated. In most cases, a typing error was responsible, typically a missing decimal point. In 28 cases, the mass and height appeared to have been written the wrong way round. Units of height varied between centimetres and metres. After corrections, where possible, 19 patient mass entries were considered unreliable and deleted. A record of the quoted figure was recorded in the comments column. In all of these cases, a reliable patient age was recorded.

4. Divide total $P_{KA}$ by screening time. A very high dose per unit screening time may be due to the patient being obese. The $P_{KA}$/time figure was therefore divided by patient mass. In 13 cases, the $P_{KA}$/min/kg was considered unusually high or low.

5. Calculate age by subtracting date of birth from date of examination. Negative ages were investigated. After corrections, where possible, 5 patients had unresolved negative ages.

6. Plot the date of examination against entry number as entered in the log book. The examination dates should increase steadily. Any outliers suggest the date was entered incorrectly. Exams were always presented in chronological order. For missing examination dates, a date was assigned based on that of the previous examination.

7. Where biplane $P_{KA}$ and skin doses are provided, calculate the ratio between PA and lateral $P_{KA}$ and between PA and lateral skin dose. The ratios should be approximately the same. This process was not always possible for procedures with low doses. The skin dose from Hospital 1 was recorded in integer units of mGy, with doses less than 1 mGy being recorded as 0.

All discrepancies were first highlighted in red in the database and investigated further. In some cases, the problem could be corrected. The most common problems were transcription errors. In many cases, details had been written in the wrong columns (e.g. a height of 3 cm and a mass of 40 kg). These were corrected and a note made of the original data entry. Unresolved discrepancies were mostly due to illegible handwriting.

### *3.4: Data analysis methodology*

Data were obtained for 20,078 procedures carried out for which a valid procedure type was available. Kerma area product was recorded for 13,654 of these procedures. Data obtained for procedures carried out at the same hospital but using different equipment were analysed separately (i.e. the same date ranges shown in Table 3.). These different 'eras' corresponded with the three generations of fluoroscopic equipment outlined in the Introduction chapter (section 1.1). All statistical analysis was carried out using MATLAB (versions 2011a and 2013a, Mathworks, Natick, USA) using anonymised data (only age, mass, dose indicators and anonymous ID number). A MATLAB function was written that automatically sorts the data into different procedure type categories, stratifies by patient age or mass and produces summary statistics. The results are automatically saved as an Excel file for viewing.  Each examination was numerically coded into four overall categories:

1. Diagnostic: All procedures in which the aim was to find out what is wrong with the patient or to monitor a condition, but without any form of therapeutic intervention.
2. Interventional: All procedures that involve "doing something" to the heart or surrounding vessels with the aim of changing heart function. This includes stent insertion, balloon dilatation, closure of anomalous ducts or vessels, or ablation. The interventional category includes procedures with both diagnostic and therapeutic elements and attempts at intervention that failed.
3. Pacemaker procedures, including wire and battery replacements.
4. Other: All other procedures involving cardiac fluoroscopy. This included biopsies and those procedures difficult to categorise as either diagnostic or interventional.

The above groups were then sub-divided into more specific procedure types:

1. Atrial septal defect (ASD) occlusion
2. Patent ductus arteriosus (PDA) occlusion
3. Pulmonary valve (PV) angioplasty
4. Aortic valve (AV) angioplasty
5. Pulmonary artery (PA) angioplasty
6. Coarctation (COA) angioplasty
7. Electrophysiology studies (EPS) with or without radiofrequency ablation (RFA)
8. Endomyocardial biopsy (EMBx)
9. Coronary angiography
10. Valve replacements
11. Pulmonary vascular resistance (PVR) studies.
12. Pacemaker procedures
13. Atrial septostomy
14. Unspecified valve angioplasty (PV or AV)
15. Right ventricular outflow tract (RVOT) angioplasty
0. Unspecified or other procedure types not listed above.

Descriptions of these procedures can be found in the Introduction chapter. The final procedure type '0' included procedures rarely carried out, such as collateral embolization or ventricular septal defect (VSD) occlusion. The procedure types provided by hospitals were sometimes too vague to categorize the procedure. This was the case for 1323 procedures carried out at the Hospital 4, listed simply as 'A.PAE'. These procedures were also classed as type 0. Note that certain procedures, such as valve replacements and heart biopsies are typically only carried out at certain specialist hospitals.

The coding system also included a separate column to indicate multiple procedures being carried out during the same catheterization. In many cases these were relatively minor procedures such as insertion of a central venous catheter. These were coded as '1' and included in the analysis of doses for individual procedure types. Where two distinct, non-minor procedure types were carried out, such as ASD occlusion and valve angioplasty, these were coded as '2' and excluded from analysis of individual procedure types but included in the broader interventional or diagnostic groups.

Cohort data were analysed by total $P_{KA}$, screening time, patient mass and age, $P_{KA}$ per kilogram ($P_{KA}$/kg) and by broad exam category and specific procedure type. Bi-plane $P_{KA}$ and skin dose figures were analysed where recorded. Data were stratified by mass using the same groups as Glatz *et al* [91]. Age was stratified using the same groups as Kobayashi *et al* [207] and Verghese *et al* [82] with the addition of an extra 16-18 years group. Examinations with zero doses were excluded from the analysis, as were examinations in which data were considered unreliable, mostly due to difficult handwriting (n=29). A Lilliefors test [208] was applied to determine whether $P_{KA}$ data were normally distributed. Data were not found to be normally distributed for any of the hospitals from which data were acquired, and were always right skewed. Therefore median and interquartile range statistics were chosen as the primary representation of $P_{KA}$ data.

### *3.5: Results*

Tables 3.4 to 3.6 present mean $P_{KA}$, along with median $P_{KA}$, screening time and (where available) skin doses and the percentage of total $P_{KA}$ originating from the frontal (PA) output, for all procedure types combined, stratified by age, presented for each hospital and equipment era separately. Skin dose is recorded in both frontal and lateral planes. The figures reported here are the median of whichever figure was the highest in each examination, rather than the median of both planes combined (a common, though ultimately unhelpful practice). Tables 3.7 and 3.8 show median $P_{KA}$ for different procedure types for all patient ages combined, again separately for different hospitals and eras. Categories in which fewer than ten procedures were carried out are not shown. More detailed tables with stratification by both mass and procedure type are provided in the appendix, along with equivalent tables stratified by mass. The following sections discuss various elements of the data separately.

| Hospital, era | Dose indicator | Patient age range | | | | | | |
|---|---|---|---|---|---|---|---|---|
| | | <1 y | 1-5 y | 5-10 y | 10-16 y | 16-18 y | >18 y | All |
| HOSPITAL 1 1994 - 2000 | Median $P_{KA}$ [IQR] | 12.2 [7 : 18.7] | 23.7 [14.9 : 35.9] | 35.6 [21.1 : 61.8] | 69.9 [28.1 : 117] | 105 [64.3 : 179.7] | 112.8 [77.6 : 150.3] | 26.8 [13.1 : 61.9] |
| | Mean $P_{KA}$ [St Dev] | 15.8 [14.1] | 29.7 [23] | 47.2 [40] | 94.5 [101.5] | 137.6 [107.7] | 125.8 [91.1] | 50.5 [67.9] |
| | Median $P_{KA}$/kg [IQR] | 2.35 [1.49 : 3.89] | 2.02 [1.27 : 3.04] | 1.7 [1.1 : 2.57] | 1.8 [0.9 : 2.68] | 2.19 [1.3 : 3.26] | 1.82 [1.35 : 2.38] | 2 [1.24 : 3.07] |
| | Median % PA [IQR] | 71% [64 : 78] | 67% [57 : 75] | 62% [50 : 68] | 61% [50 : 70] | 60% [49 : 70] | 62% [49 : 73] | 66% [55 : 74] |
| | Median skin dose [IQR] | n/a | n/a | n/a | n/a | n/a | n/a | n/a |
| | Screening time [IQR] | 17.4 [11 : 25.9] | 19.5 [12.4 : 29.7] | 18.9 [11.9 : 29.7] | 20.1 [9.8 : 34] | 18.7 [13.3 : 30.6] | 19.9 [12.6 : 25.7] | 18.9 [11.6 : 29.7] |
| | n | 166 | 179 | 124 | 111 | 32 | 29 | 641 |
| HOSPITAL 1 1999 - 2001 | Median $P_{KA}$ [IQR] | 4.4 [2.4 : 7.8] | 9.1 [5.2 : 16.4] | 13.7 [7.5 : 26.8] | 26.6 [11.6 : 57.5] | 43.2 [24.3 : 102.4] | 95 [47.7 : 126.5] | 10.3 [5 : 25.5] |
| | Mean $P_{KA}$ [St Dev] | 7.3 [10] | 15.7 [29.2] | 20.5 [23.3] | 45.2 [53.1] | 63.9 [55.7] | 89.5 [48.1] | 23.9 [38.1] |
| | Median $P_{KA}$/kg [IQR] | 0.87 [0.44 : 1.55] | 0.76 [0.41 : 1.34] | 0.66 [0.34 : 1.11] | 0.65 [0.31 : 1.24] | 0.87 [0.46 : 1.7] | 1.44 [1.01 : 1.92] | 0.76 [0.39 : 1.32] |
| | Median % PA [IQR] | 68% [56 : 78] | 68% [53 : 81] | 65% [49 : 81] | 71% [50 : 100] | 67% [56 : 85] | 78% [52 : 82] | 68% [53 : 82] |
| | Median skin dose [IQR] | n/a | n/a | n/a | n/a | n/a | n/a | n/a |
| | Screening time [IQR] | 10.9 [5.7 : 18.2] | 12.9 [6.6 : 19.9] | 10.2 [5.3 : 15.7] | 10.8 [6.3 : 19.4] | 12.9 [7.2 : 21.8] | 17.5 [11.1 : 27] | 11.3 [6.2 : 19.2] |
| | n | 248 | 291 | 184 | 214 | 44 | 12 | 993 |
| HOSPITAL 1 2002-2008 | Median $P_{KA}$ [IQR] | 0.8 [0.5 : 1.5] | 1.2 [0.5 : 2.4] | 2.2 [0.9 : 4.7] | 5 [2 : 12.3] | 7.8 [2.9 : 16.9] | 8.2 [3.8 : 28.8] | 2.1 [0.8 : 5.9] |
| | Mean $P_{KA}$ [St Dev] | 1.2 [1.1] | 1.9 [2] | 3.8 [5.1] | 9.7 [12.9] | 12.8 [14.7] | 23.1 [45.3] | 5.8 [11.4] |
| | Median $P_{KA}$/kg [IQR] | 0.16 [0.09 : 0.29] | 0.1 [0.04 : 0.21] | 0.1 [0.04 : 0.2] | 0.12 [0.05 : 0.26] | 0.15 [0.06 : 0.29] | 0.14 [0.08 : 0.46] | 0.12 [0.05 : 0.25] |
| | Median % PA [IQR] | 55% [41 : 68] | 58% [38 : 80] | 59% [37 : 88] | 53% [35 : 83] | 49% [32 : 79] | 53% [38 : 82] | 55% [37 : 79] |
| | Median skin dose [IQR] | 15 [9 : 27] | 16 [8 : 30] | 24 [11 : 49] | 46 [22 : 109] | 75 [29 : 138] | 72 [39 : 215] | 26 [12 : 61] |
| | Screening time [IQR] | 11.1 [7.3 : 18.5] | 10.2 [6.1 : 18.3] | 10.4 [6.2 : 19.4] | 10.3 [6.1 : 18] | 10.2 [5.4 : 17.3] | 12.7 [7.5 : 22.7] | 10.4 [6.2 : 18.4] |
| | n | 502 | 737 | 549 | 969 | 233 | 49 | 3039 |
| HOSPITAL 1 2007-2010 | Median $P_{KA}$ [IQR] | 0.6 [0.4 : 0.9] | 1.2 [0.6 : 2.3] | 2.3 [1 : 5.8] | 9.8 [3.6 : 19.2] | 10.1 [3.3 : 26.5] | 10.8 [3.5 : 24.2] | 2.1 [0.8 : 8.3] |
| | Mean $P_{KA}$ [St Dev] | 1 [1.8] | 1.9 [2.1] | 6.5 [18.2] | 17.7 [23.8] | 18.5 [23.3] | 17.6 [24.5] | 8.7 [18.3] |
| | Median $P_{KA}$/kg [IQR] | 0.1 [0.06 : 0.18] | 0.09 [0.05 : 0.2] | 0.1 [0.05 : 0.24] | 0.19 [0.09 : 0.38] | 0.17 [0.06 : 0.44] | 0.21 [0.07 : 0.59] | 0.12 [0.06 : 0.26] |
| | Median % PA [IQR] | 59% [45 : 69] | 70% [49% : 83%] | 65% [40 : 80] | 57% [43 : 75] | 68% [55 : 84] | 85% [61 : 99] | 62% [46 : 78] |
| | Median skin dose [IQR] | 11 [7 : 18] | 17 [9 : 31] | 28 [12 : 64] | 78 [38 : 161] | 93 [27 : 186] | 98 [32 : 176] | 26 [11 : 79] |
| | Screening time [IQR] | 8.3 [5.5 : 14.2] | 10.1 [5.5 : 17] | 10.5 [5.4 : 18.3] | 10.6 [6.9 : 20.1] | 10.1 [5.3 : 19.6] | 10.6 [5.6 : 30] | 10.1 [6.1 : 17.5] |
| | n | 129 | 170 | 135 | 196 | 67 | 5 | 702 |

Table 3.4: Summary statistics for all procedures combined at Hospital 1, for 4 eras of data collection. $P_{KA}$ is quoted in Gy·cm², skin doses are quoted in mGy.

| Hospital, era | Dose indicator | Patient age range | | | | | | |
|---|---|---|---|---|---|---|---|---|
| | | <1 y | 1-5 y | 5-10 y | 10-16 y | 16-18 y | >18 y | All |
| Hospital 3 2004-2008 | Median $P_{KA}$ [IQR] | 3 [1.7 : 5.3] | 5.1 [2.9 : 8.5] | 6.5 [2.7 : 13] | 8.9 [3.6 : 19.4] | 9.4 [4.8 : 19.2] | 18.5 [5.3 : 33] | 4.8 [2.4 : 9.9] |
| | Mean $P_{KA}$ [St Dev] | 4.3 [4.4] | 6.5 [5.5] | 9.7 [9.7] | 16.3 [20.8] | 13 [13.1] | 22.9 [21.1] | 9.1 [12.7] |
| | Median $P_{KA}$/kg [IQR] | 0.52 [0.34 : 0.95] | 0.39 [0.24 : 0.7] | 0.26 [0.12 : 0.54] | 0.19 [0.07 : 0.43] | 0.15 [0.08 : 0.31] | 0.26 [0.08 : 0.63] | 0.36 [0.18 : 0.67] |
| | Screening time [IQR] | 12.4 [7.4 : 18.9] | 12.5 [8.1 : 20.6] | 13.2 [7.1 : 23] | 18.6 [12.8 : 28.7] | 13.5 [6.2 : 20] | 11.5 [6.8 : 21.5] | 13.5 [7.9 : 22.1] |
| | n | 245 | 193 | 97 | 122 | 40 | 40 | 737 |
| Hospital 3 2008-2013 | Median $P_{KA}$ [IQR] | 0.8 [0.5 : 1.4] | 1.6 [0.9 : 3.2] | 2.7 [1.4 : 6.9] | 7.5 [3 : 15.2] | 6.9 [2.1 : 16.9] | 19.1 [7 : 35.9] | 2.1 [0.8 : 6.6] |
| | Mean $P_{KA}$ [St Dev] | 1.3 [1.8] | 2.7 [3.3] | 7 [17.9] | 12.2 [14.5] | 15.3 [23.8] | 34.6 [49.2] | 7.4 [18] |
| | Median $P_{KA}$/kg [IQR] | 0.14 [0.08 : 0.25] | 0.14 [0.08 : 0.25] | 0.13 [0.06 : 0.26] | 0.15 [0.07 : 0.33] | 0.1 [0.04 : 0.29] | 0.29 [0.1 : 0.51] | 0.14 [0.07 : 0.29] |
| | Screening time [IQR] | 10.8 [7.3 : 18.3] | 10.7 [6.6 : 18.4] | 12 [7.7 : 18.2] | 14.7 [8.6 : 25] | 12.9 [7.8 : 21.2] | 14.3 [8.7 : 24] | 11.8 [7.5 : 19.9] |
| | n | 345 | 354 | 185 | 247 | 87 | 71 | 1289 |
| Hospital 2 2004-2008 | Median $P_{KA}$ [IQR] | 3.6 [1.9 : 6.4] | 6.2 [3.7 : 11.6] | 9.1 [4.4 : 16.6] | 16.4 [7.4 : 34.1] | 23.2 [10.7 : 46.3] | 5.6 [2.7 : 32.1] | 6.7 [3.2 : 15.6] |
| | Mean $P_{KA}$ [St Dev] | 6.7 [11.3] | 9.7 [11.1] | 13.7 [15] | 25 [28.9] | 54.3 [163.9] | 16.8 [19.8] | 14.8 [42] |
| | Median $P_{KA}$/kg [IQR] | 0.62 [0.37 : 1.3] | 0.5 [0.31 : 0.95] | 0.42 [0.2 : 0.8] | 0.4 [0.19 : 0.73] | 0.49 [0.23 : 0.75] | 0.1 [0.04 : 0.56] | 0.5 [0.28 : 0.95] |
| | Screening time [IQR] | 9.2 [5.6 : 14.2] | 9.1 [6.1 : 14.5] | 10.1 [5.5 : 18.2] | 10.1 [6 : 17.1] | 12.5 [7.3 : 17.2] | 2.4 [1.1 : 12.4] | 9.6 [5.8 : 15.6] |
| | n | 407 | 469 | 249 | 280 | 77 | 8 | 1490 |
| Hospital 2 2008-2013 | Median $P_{KA}$ [IQR] | 2.3 [1 : 4.1] | 3.8 [2.5 : 6.9] | 6.5 [3.6 : 11.4] | 14.7 [6.6 : 29.9] | 14 [6.2 : 29.7] | 7.4 [2.6 : 11.8] | 4.7 [2.4 : 10.7] |
| | Mean $P_{KA}$ [St Dev] | 3.3 [4] | 5.6 [5.5] | 9 [8.5] | 21.6 [21.1] | 23.4 [27.4] | 11.4 [13.4] | 9.6 [14.3] |
| | Median $P_{KA}$/kg [IQR] | 0.42 [0.24 : 0.79] | 0.34 [0.21 : 0.57] | 0.32 [0.17 : 0.51] | 0.33 [0.16 : 0.62] | 0.24 [0.11 : 0.54] | 0.13 [0.04 : 0.19] | 0.35 [0.19 : 0.61] |
| | Screening time [IQR] | 8 [4.8 : 14.5] | 7.1 [4.9 : 12.3] | 7.6 [4.6 : 11.9] | 10.3 [6.1 : 17.1] | 9.9 [7 : 19.2] | 5.4 [4 : 11.4] | 8.2 [5 : 14] |
| | n | 476 | 607 | 250 | 374 | 81 | 15 | 1803 |

Table 3.5: Summary statistics for all procedures combined at Hospitals 2 and 3, for two eras of data collection. $P_{KA}$ is quoted in Gy·cm².

| Hospital, era | Dose indicator | Patient age range | | | | | | |
|---|---|---|---|---|---|---|---|---|
| | | <1 y | 1-5 y | 5-10 y | 10-16 y | 16-18 y | >18 y | All |
| Hospital 4 1993-2003 | Median $P_{KA}$ [IQR] | 3.2 [1.8 : 5.4] | 5 [2.8 : 8.8] | 8.4 [4.3 : 14.7] | 16.2 [7.8 : 35.9] | 18.4 [6.5 : 32.6] | - | 6.4 [3.1 : 13.7] |
| | Mean $P_{KA}$ [St Dev] | 5.3 [8.5] | 7.2 [7.6] | 12.8 [15] | 26.2 [27.4] | 23.5 [19.5] | - | 12.5 [17.9] |
| | Median $P_{KA}$/kg [IQR] | 0.64 [0.39 : 1.07] | 0.47 [0.24 : 0.79] | 0.41 [0.21 : 0.68] | 0.42 [0.22 : 0.8] | 0.36 [0.14 : 0.63] | - | 0.49 [0.25 : 0.84] |
| | Median % PA [IQR] | 0.71 [0.6 : 0.86] | 0.69 [0.54 : 0.89] | 0.68 [0.46 : 2] | 0.66 [0.5 : 0.94] | 0.71 [0.51 : 0.93] | - | 0.69 [0.53 : 0.92] |
| | Screening time [IQR] | 9.9 [5 : 16.3] | 9.4 [5.6 : 16] | 11 [5.8 : 20] | 14.5 [7 : 26.2] | 12.5 [5.1 : 24.1] | - | 10.9 [5.9 : 19.2] |
| | n | 275 | 394 | 255 | 271 | 30 | 0 | 1225 |
| Hospital 4 2003-2014 | Median $P_{KA}$ [IQR] | 0.5 [0.3 : 1.1] | 1.4 [0.7 : 2.5] | 2.2 [1 : 4.7] | 7.6 [4.3 : 11.6] | 7.6 [4.9 : 9.6] | - | 1.7 [0.6 : 4.7] |
| | Mean $P_{KA}$ [St Dev] | 1.4 [4.4] | 2.3 [3.8] | 4 [5.7] | 10.9 [12.9] | 7.1 [3.3] | - | 4.2 [7.9] |
| | Median $P_{KA}$/kg [IQR] | 0.1 [0.05 : 0.18] | 0.11 [0.07 : 0.2] | 0.11 [0.05 : 0.17] | 0.16 [0.1 : 0.23] | 0.16 [0.12 : 0.19] | - | 0.12 [0.07 : 0.2] |
| | Median % PA [IQR] | 0.51 [0.44 : 0.65] | 0.56 [0.38 : 0.68] | 0.52 [0.41 : 0.65] | 0.56 [0.43 : 0.91] | 1 [1 : 1] | - | 0.54 [0.43 : 0.69] |
| | Screening time [IQR] | 10.8 [5.2 : 18.6] | 10.4 [6 : 18] | 9.1 [6 : 13.7] | 10 [7.3 : 16] | 7.1 [5.3 : 13.7] | - | 10.1 [6 : 16.8] |
| | n | 145 | 164 | 116 | 110 | 9 | 0 | 544 |
| Hospital 5 2005-2013 | Median $P_{KA}$ [IQR] | 0.8 [0.4 : 1.5] | 1.5 [0.7 : 3.8] | 1.4 [0.4 : 5.7] | 2 [0.6 : 11.3] | 2.6 [0.9 : 10.4] | 3.96 [0.98 : 48.77] | 1.3 [0.5 : 3.9] |
| | Mean $P_{KA}$ [St Dev] | 1.4 [2] | 3.7 [5.5] | 6.4 [16] | 13.7 [45.9] | 8.9 [17.8] | 32.09 [46.08] | 6.9 [24.9] |
| | Screening time [IQR] | 11.5 [6.5 : 22.5] | 8.6 [4.7 : 17.2] | 10.1 [5.8 : 24.5] | 15.5 [8.2 : 23.4] | 16.8 [9.2 : 31.6] | 15.4 [7.9 : 27.47] | 11.7 [6.5 : 22.6] |
| | n | 161 | 167 | 93 | 130 | 41 | 20 | 612 |
| Hospital 6 2006-2013 | Median $P_{KA}$ [IQR] | 0.7 [0.4 : 1.1] | 0.9 [0.6 : 1.8] | 1.5 [0.7 : 3] | 3.4 [1.4 : 8.4] | 1.2 [0.3 : 3.7] | 3.53 [1.64 : 5.52] | 1.2 [0.6 : 2.9] |
| | Mean $P_{KA}$ [St Dev] | 0.9 [0.9] | 1.5 [1.4] | 2.2 [2] | 9.8 [18.4] | 7.4 [27.7] | 7.39 [17.17] | 3.5 [11.8] |
| | Screening time [IQR] | 10.2 [6.2 : 17.2] | 9.5 [7.3 : 15.9] | 12.6 [8.7 : 16.5] | 9.3 [3 : 18.1] | 7.5 [3.2 : 10.1] | 10.15 [6.44 : 14.11] | 10.1 [6.4 : 16.2] |
| | n | 91 | 116 | 41 | 39 | 26 | 47 | 360 |

Table 3.6: Summary statistics for all procedures combined at Hospitals 4, 5 and 6. $P_{KA}$ is quoted in Gy·cm².

| Procedure | Hospital and data collection period | | | | | |
|---|---|---|---|---|---|---|
| | Hospital 1 94-00 | Hospital 1 99-01 | Hospital 1 02-08 | Hospital 1 07-10 | Hospital 3 04-08 | Hospital 3 08-13 |
| **Other** | 26 [13 : 55.5] | 14.3 [6 : 28.5] | 1.5 [0.4 : 3.9] | 1.4 [0.7 : 4.8] | - | - |
| **Interventional** | 27.1 [13.8 : 54.2] | 7.6 [3.7 : 18.4] | 1.7 [0.7 : 5.8] | 2.2 [0.7 : 9.7] | 4.7 [2.5 : 9.8] | 2.2 [0.8 : 8.3] |
| **Diagnostic** | 68.9 [22.3 : 132.6] | 11.6 [6.3 : 29.4] | 3.2 [1.5 : 7.4] | 2.8 [1 : 8.3] | 5.1 [2.8 : 10] | 1.9 [0.9 : 5] |
| **ASD occlusion** | - | 6.3 [2.7 : 21.9] | 0.8 [0.5 : 1.7] | 1.3 [0.4 : 4.1] | 5.3 [2.1 : 8] | 3.2 [1.3 : 8.9] |
| **PDA occlusion** | 27.1 [14.4 : 45] | 6.2 [3.4 : 12] | 0.8 [0.5 : 1.3] | 0.7 [0.5 : 1.3] | 3.4 [2.5 : 5.3] | 1.1 [0.6 : 2.2] |
| **PV plasty** | 16.9 [13.2 : 27.2] | 6 [2.8 : 10.7] | 1 [0.6 : 2] | 0.8 [0.5 : 2] | 3.4 [2.1 : 7.1] | 0.7 [0.4 : 1.2] |
| **AV plasty** | - | 6.9 [4.3 : 21.6] | 1.2 [0.7 : 4.6] | 4 [0.6 : 13.1] | 5.2 [1.5 : 7.4] | 2 [0.6 : 6.2] |
| **PA plasty** | 34.1 [26.9 : 154.9] | 19.4 [8.3 : 40.6] | 4.7 [2 : 9.2] | 4.6 [1.8 : 8.8] | 11.1 [8.3 : 28.5] | 7.2 [3 : 13.8] |
| **COA repair** | - | 7.8 [5.1 : 26.4] | 1.7 [0.7 : 3.4] | 3.7 [0.5 : 10.6] | 3.5 [2 : 10.1] | 6.4 [1.2 : 24.3] |
| **EPS/RFA** | 70.6 [46.8 : 147.4] | 77.8 [24.1 : 144.8] | 3.3 [1.2 : 7.3] | 3.5 [1.6 : 9] | 4.3 [2 : 9.2] | 3.6 [1.7 : 7.1] |
| **Biopsy** | 5.5 [3 : 32.4] | 5.4 [1.7 : 10.9] | 0.7 [0.3 : 1.8] | 1.2 [0.7 : 3.3] | - | - |
| **Coronaries** | 100.7 [62.9 : 149.2] | 17.1 [9.7 : 33.6] | 4.8 [2.5 : 11.1] | 5.4 [1.9 : 11.9] | - | - |
| **PVR/Pressures** | - | - | 1.3 [0.4 : 3.7] | 1.4 [0.6 : 5.4] | - | - |
| **Valve replace** | - | - | - | 37.9 [27 : 77.4] | - | - |
| **Pacemaker** | 18.5 [8.8 : 51.8] | - | 1.6 [0.8 : 2.9] | - | 2.6 [1.4 : 11.8] | 0.7 [0.3 : 2] |
| **Septostomy** | 3.5 [2.8 : 7] | 2.1 [0.8 : 28.9] | 2.1 [0.9 : 7.9] | - | - | - |

Table 3.7: Median $P_{KA}$ [interquartile range] for individual procedure types for all patient sizes combined, for different eras at Hospitals 1 and 3. Note, 'plasty' can refer to ballooning and/or stent insertion. Only figures where at least 10 procedures were conducted are presented.

| Procedure | Hospital and data collection period | | | | | |
|---|---|---|---|---|---|---|
| | Hospital 2 04-08 | Hospital 2 08-13 | Hospital 4 93-03 | Hospital 4 03-14 | Hospital 5 05-13 | Hospital 6 06-13 |
| **Other** | 6.6 [3.1 : 14.6] | 5.5 [2.5 : 10.8] | 6.3 [3.2 : 13.5] | 1.3 [0.6 : 3.2] | 0.6 [0.2 : 2] | 0.9 [0.5 : 2.4] |
| **Interventional** | 7.2 [3.6 : 16.7] | 4.3 [2.3 : 10.9] | 6.8 [2.6 : 16.1] | 1.1 [0.5 : 2.6] | 1.3 [0.6 : 3.9] | 1.2 [0.6 : 2.7] |
| **Diagnostic** | 5 [2.4 : 14] | 5.8 [3 : 10.5] | 8.3 [6.3 : 19.3] | 4.8 [2.7 : 9.3] | 2.6 [0.9 : 8.5] | 1.5 [0.7 : 3.4] |
| **ASD occlusion** | 6.9 [4.8 : 14] | 4.4 [2.7 : 8.4] | - | - | 1.5 [0.7 : 3.8] | 0.5 [0.5 : 1] |
| **PDA occlusion** | 6.2 [3.8 : 11.1] | 3.2 [2.4 : 4.8] | - | - | 1.1 [0.6 : 2.2] | 0.4 [0.4 : 0.8] |
| **PV plasty** | 4.5 [2.5 : 8.6] | 2.7 [1.7 : 4.7] | - | - | - | - |
| **AV plasty** | 7.9 [3.3 : 30.5] | 2.1 [1.1 : 5] | - | - | - | - |
| **PA plasty** | 17.8 [7 : 28.8] | 11.5 [5.9 : 21.8] | - | - | - | - |
| **COA repair** | 6.2 [2.9 : 16.4] | 3.2 [2.5 : 6.2] | - | - | 6.1 [1 : 27.7] | - |
| **EPS/RFA** | 16.7 [9 : 30.5] | 12 [5.3 : 27] | 17.4 [7.7 : 42.7] | - | 1.1 [0.5 : 2.2] | 1.6 [0.9 : 3.5] |
| **Biopsy** | - | - | - | - | - | - |
| **Coronaries** | - | - | 9.8 [6.5 : 17.3] | 4.8 [2.7 : 9.3] | 2.3 [0.6 : 14.3] | 2.1 [0.9 : 4.2] |
| **PVR/Pressures** | - | 8.7 [3 : 11.4] | - | - | - | - |
| **Valve replace** | - | - | - | - | - | - |
| **Pacemaker** | 3 [2.2 : 11.7] | 2.2 [1 : 6.1] | - | - | 0.3 [0.2 : 0.5] | - |
| **Septostomy** | 1.2 [0.6 : 4.6] | 0.4 [0.2 : 1] | - | - | 0.3 [0.2 : 1.5] | - |

Table 3.8: Median $P_{KA}$ [interquartile range] for individual procedure types for all patient sizes combined, for different eras at Hospitals 2, 4, 5 and 6 Only figures where at least 10 procedures were conducted are presented.

### *3.5.1: Kerma area product*

$P_{KA}$ was generally in the range 0 to 20 Gy·cm², though occasionally reached 100 Gy·cm² or higher, particularly for older procedures. Four procedures had a $P_{KA}$ of greater than 500 Gy·cm², with two being over 1000 Gy·cm². In one of these, the patient was a large 18 year old female (93 kg). The other was for an average sized 17 year old female (51 kg) undergoing a procedure with 53.1 minutes of fluoroscopic screening. For the most recently conducted examinations using 3rd generation equipment, the median $P_{KA}$ across all patient sizes and procedure types ranged from 1.2 to 4.7 Gy·cm² depending on the hospital - a near fourfold variation. Restricting to procedure conducted using Siemens Axiom Artis machines (all hospitals except Hospital 2), this range was reduced to 1.2 to 2.1 Gy·cm² – a less than two fold variation. $P_{KA}$ was almost always positively correlated with patient mass. Spearman's rank correlations are shown in Table 3.9 for most recent era procedures conducted at the four hospitals with the largest sample sizes. Exceptions tended to only occur where only a limited number of procedures were included in a particular category, such as 'other' procedures at Hospital 3, or if procedures were only carried out over a limited range of ages, such as electrophysiology studies (EPS) at Hospital 2.

Median $P_{KA}$ varied between procedure types, tending to be highest for ballooning and/or stenting of the pulmonary arteries and (more recently) trans-catheter valve replacement. The lowest doses were for atrial septostomies and closures of patent ductus arteriosus (PDA) and atrial septal defect (ASD).

The ranking of procedures by $P_{KA}$ was not the same at different hospitals, or even at the same hospitals for different eras. For example, among the most regularly conducted procedures, aortic valve (AV) angioplasty procedures had the lowest median $P_{KA}$ at Hospital 2 (2008-2013 data) but the highest at Hospital 1 (2007-2010). The exception in this variation in ranking was for pulmonary artery angioplasty procedures, which were consistently among the highest doses. Where carried out, endomyocardial biopsies were usually associated with low doses when carried out in isolation. At least 10% of coronary angiography procedures also included a heart biopsy as part of a yearly transplant review examination. Coronary angiography is increasingly performed with intravascular ultrasound (IVUS), which is regarded as the most sensitive imaging modality in the detection of coronary allograft vasculopathy [209].

| Procedure type: | Hospital 1, 2002-2008 | | | Hospital 2, 2008-2013 | | | Hospital 3, 2008-2013 | | | Hospital 4, 2003-2011 | | |
|---|---|---|---|---|---|---|---|---|---|---|---|---|
| | Mass and $P_{KA}$ | Mass and ST | $P_{KA}$/kg and age | Mass and $P_{KA}$ | Mass and ST | $P_{KA}$/kg and age | Mass and $P_{KA}$ | Mass and ST | $P_{KA}$/kg and age | Mass and $P_{KA}$ | Mass and ST | $P_{KA}$/kg and age |
| **Other** | 0.47 p=<0.01 | -0.03 p=0.38 | -0.02 p=0.45 | 0.43 p=<0.01 | -0.10 p=0.07 | -0.26 p=<0.01 | 0.03 p=0.23 | -0.23 p=0.05 | -0.21 p=0.08 | | | |
| **Combined interventional** | 0.64 p=<0.01 | 0.12 p=<0.01 | 0.06 p=0.02 | 0.63 p=<0.01 | 0.16 p=<0.01 | -0.12 p=<0.01 | 0.76 p=<0.01 | 0.10 p=0.01 | 0.29 p=<0.01 | 0.45 p=<0.01 | -0.07 p=0.54 | -0.08 p=0.48 |
| **Combined diagnostic** | 0.72 p=<0.01 | -0.14 p=<0.01 | -0.0 p=0.85 | 0.61 p=<0.01 | -0.08 p=0.16 | -0.15 p=<0.01 | 0.71 p=<0.01 | 0.00 p=0.97 | 0.14 p=<0.01 | 0.67 p=<0.01 | -0.37 p=<0.01 | -0.24 p=<0.01 |
| **ASD occlusion** | 0.57 p=<0.01 | 0.04 p=0.61 | 0.12 p=0.11 | 0.51 p=<0.01 | -0.02 p=0.82 | -0.06 p=0.56 | 0.73 p=<0.01 | 0.10 p=0.28 | 0.37 p=<0.01 | | | |
| **PDA occlusion** | 0.39 p=<0.01 | -0.01 p=0.78 | -0.30 p=<0.01 | 0.31 p=<0.01 | -0.09 p=0.11 | -0.36 p=<0.01 | 0.61 p=<0.01 | 0.02 p=0.77 | 0.12 p=0.13 | | | |
| **Pulmonary valvuloplasty** | 0.67 p=<0.01 | 0.04 p=0.63 | -0.08 p=0.37 | 0.34 p=<0.01 | -0.26 p=<0.01 | -0.36 p=<0.01 | 0.61 p=<0.01 | -0.09 p=0.46 | 0.10 p=0.40 | | | |
| **Aortic valvuloplasty** | 0.81 p=<0.01 | -0.00 p=0.97 | -0.10 p=0.44 | 0.79 p=<0.01 | 0.28 p=0.03 | 0.14 p=0.30 | 0.92 p=<0.01 | 0.28 p=0.05 | 0.49 p=<0.01 | | | |
| **Pulmonary artery angioplasty** | 0.69 p=<0.01 | -0.06 p=49 | 0.00 p=0.94 | 0.62 p=<0.01 | 0.13 p=0.14 | -0.10 p=0.23 | 0.76 p=<0.01 | -0.03 p=0.78 | 0.29 p=<0.01 | | | |
| **Coarctation repair** | 0.80 p=<0.01 | 0.00 p=0.95 | -0.10 p=0.46 | 0.78 p=<0.01 | 0.07 p=0.6 | -0.32 p=0.02 | 0.85 p=<0.01 | 0.05 p=0.69 | 0.53 p=<0.01 | | | |
| **EPS ± ablation** | 0.43 p=<0.01 | -0.02 p=0.75 | 0.05 p=0.45 | 0.35 p=<0.01 | 0.10 p=0.12 | -0.15 p=0.01 | | | | | | |
| **Heart biopsy** | 0.67 p=<0.01 | -0.07 p=0.17 | 0.15 p=0.005 | | | | | | | | | |
| **Coronary angiography** | 0.79 p=<0.01 | 0.07 p=0.11 | 0.25 p=<0.01 | | | | | | | 0.85 p=<0.01 | -0.01 p=0.93 | 0.15 p=0.21 |

Table 3.9: Correlation between $P_{KA}$ and other parameters for most recent era data at four hospitals. Note the 2002-2008 data at Hospital1 were preferred to 2007-2010 data due to much larger sample size. ST=screening time

As mentioned previously, $P_{KA}$ was not normally distributed and exhibited a right-skewed distribution, with a large number of procedures delivering a $P_{KA}$ and a small number of procedures delivering very high $P_{KA}$ (i.e. over 100 Gy·cm²). The distribution was investigated in greater detail for the 2002-2007 data collected at Hospital 1, by plotting percentiles in 1% intervals on a log scale (Figure 3.2). The relative ranking of $P_{KA}$ between procedure types was shown to be reasonably constant across the range of percentiles.

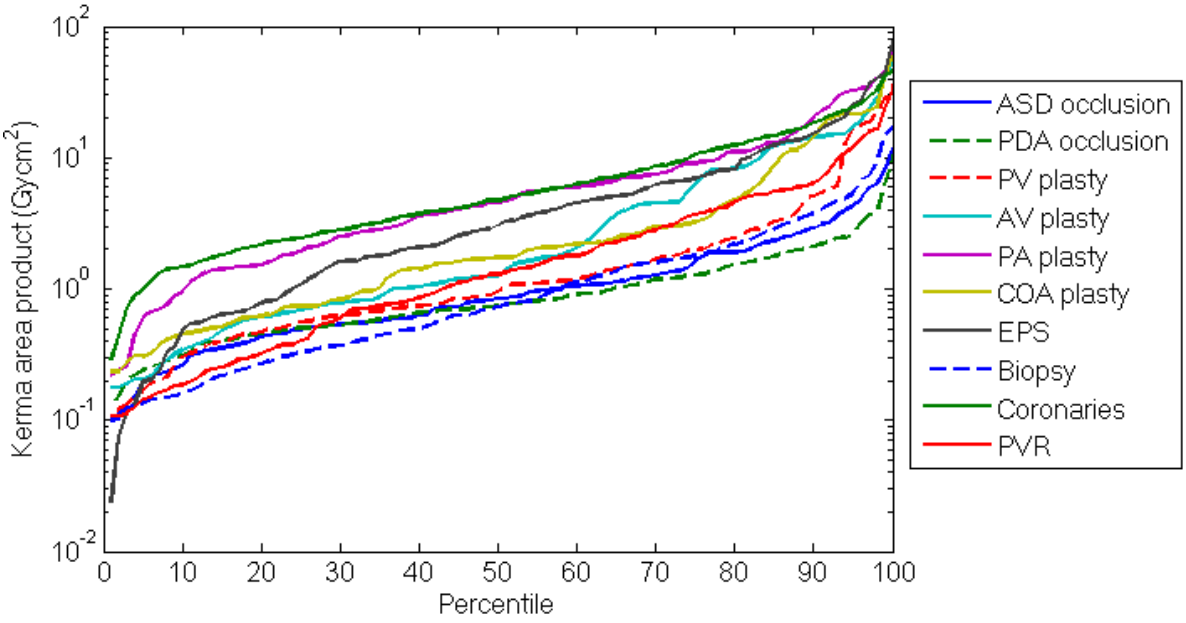


**Figure 3.2: Distribution of doses for various procedure types at Hospital 1 (2002-2008 data)**

The most striking feature of Tables 3.4 to 3.8 is the fall in $P_{KA}$ with successive 'eras', at hospitals where equipment was replaced during the study period. In all but one case, these falls were significant (Wilcoxon test for all procedure types combined p=<0.01). The exception was between 2002-2008 and 2007-2010 eras at Hospital 1 (p=0.116). These represented two catheterization laboratories, both equipped with Siemens Axiom Artis machines. The machine in Lab 1 (02-08 data) was equipped with image intensifier (II) detectors, while Lab 4 (07-10 data) had flat panel detectors (FPDs). The median $P_{KA}$ for all procedure types combined is identical for the II and FPD machines (2.1 Gy·cm²), while the corresponding figures for interventional procedures were significantly higher in the FPD equipped Lab 4 (1.66 verses 2.40 Gy·cm², Wilcoxon test: p=0.03). When this was analysed further, it was found that a large proportion of procedures carried out using the FPD equipped machine were

high-dose valve replacements. For 2007, 38% of interventional procedures in the FPD lab were valve replacements, while very few of these procedures were done in the II lab. Carrying out the same analysis, but excluding valve replacement procedures, the apparent increase in interventional $P_{KA}$ associated with the FPD machine disappeared and there was no significant difference in $P_{KA}$ associated with the transition between II and FPD ($p=0.22$).

Further analysis of the fall in $P_{KA}$ with study date was conducted by calculating median $P_{KA}$ by year of procedure. This was conducted for all procedure types combined, as the number of individual procedure types carried out in a particular year was often small. These results suggest that $P_{KA}$ tended to fall suddenly upon installation of new equipment, though there was also some suggestion of a fall in $P_{KA}$ within eras as well. These patterns are shown in Figures 3.3 to 3.5 for Hospitals 1, 2 and 3, respectively. Analysis of $P_{KA}$ by year was difficult for the Hospital 4 data due to the sporadic nature of data recording. New equipment was installed in 2003, but doses were recorded for hardly any procedures until 2011, while procedures carried out at Hospitals 5 and 6 were conducted on a single piece of equipment. $P_{KA}$ fluctuated quite wildly between 1994 and 1997 at Hospital 1, increasing from around 21 Gy·cm² to nearly 40 Gy·cm² between 1995 and 1996, before falling. The reasons for this are unclear and there was no corresponding pattern for screening times (also shown in the same figure), though these figures unexpectedly increased themselves in 1999 before falling in 2000.

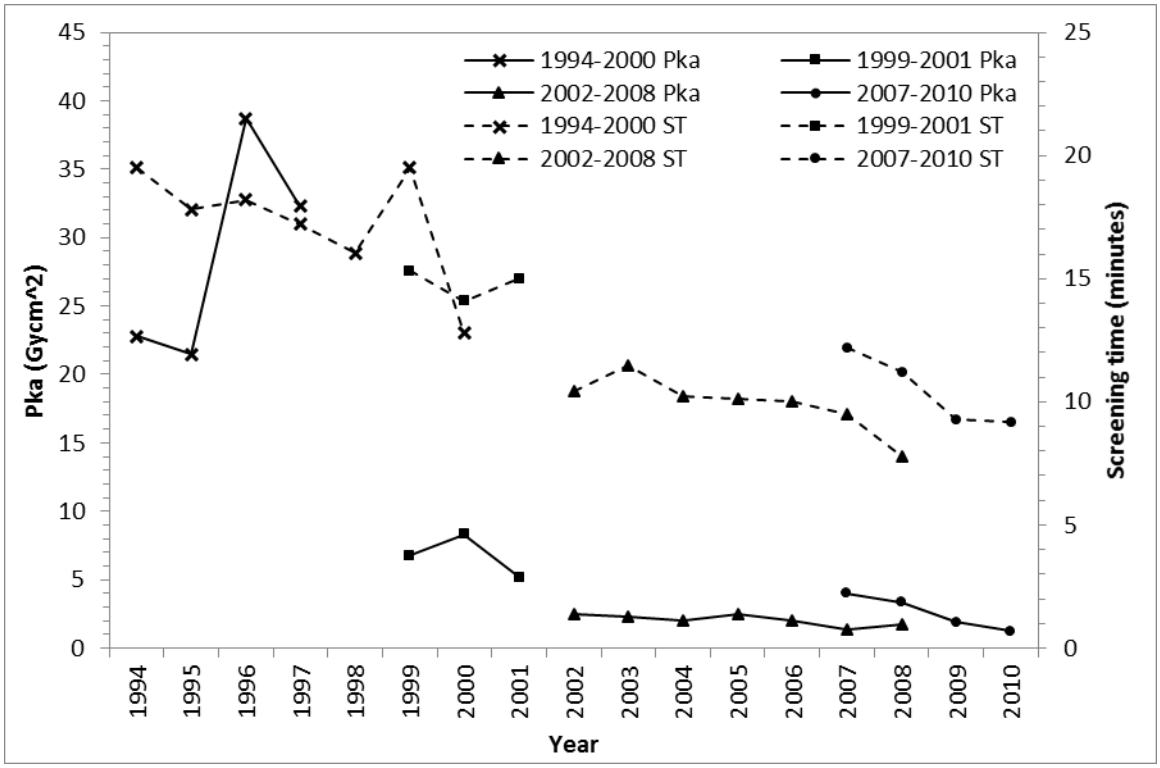


Figure 3.3: Median $P_{KA}$ and screening times (ST) for all procedures combined by year, at Hospital 1, between 1994 and 2010. Only years in which figures for more than 50 procedures were carried out are shown.

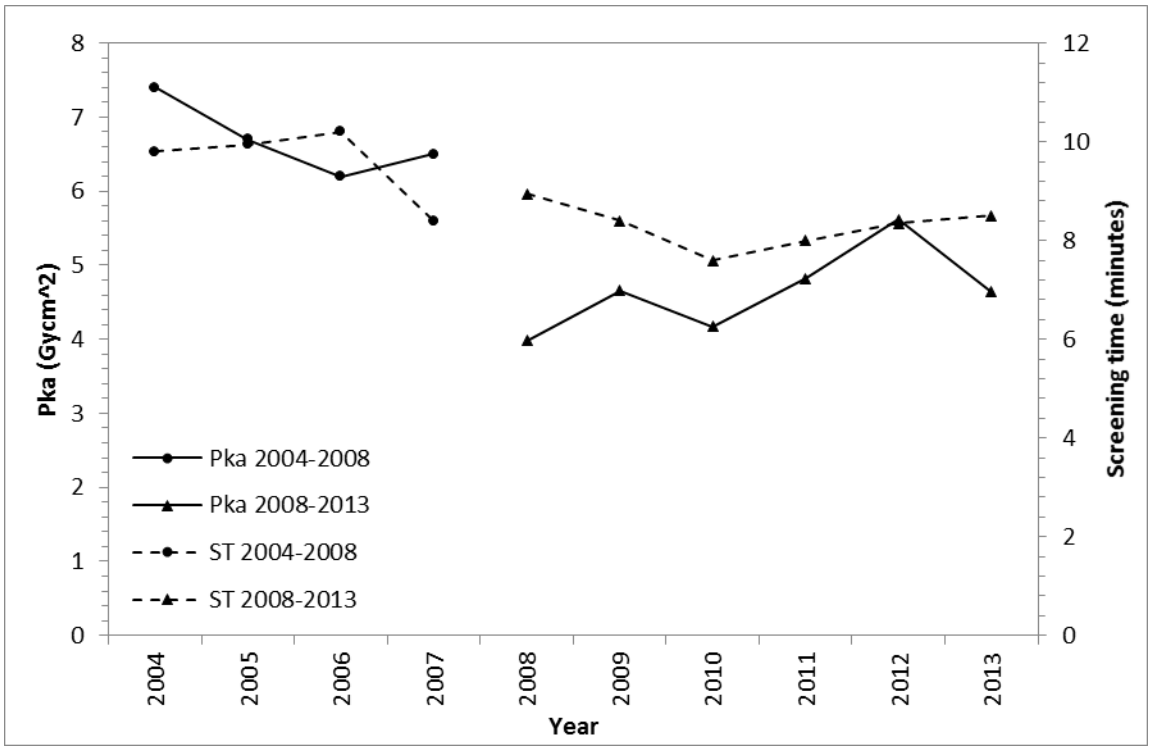


Figure 3.4: Median $P_{KA}$ and screening times (ST) for all procedures combined by year, at Hospital 2, between 2004 and 2013.

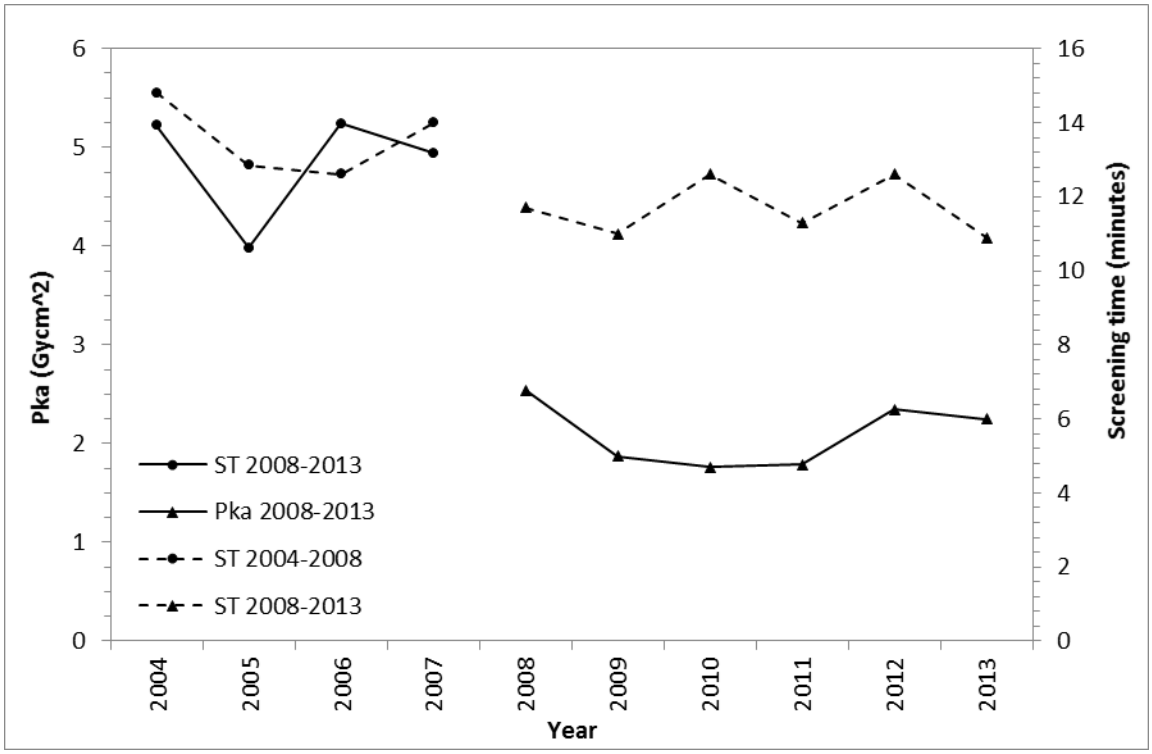


**Figure 3.5: Median $P_{KA}$ and screening times (ST) for all procedures combined by year, at Hospital 3, between 2004 and 2013**

For all procedures, the percentage of $P_{KA}$ originating from the frontal (PA), x-ray tube, recorded at Hospital 1, was around 60%. This figure varied with data collection era, being 66% between 1994 and 2000 (lab 1), 68% between 1999 and 2001 (lab 2) and 55% between 2002 and 2008 (lab 1). A similar fall in this proportion was seen at the Hospital 4 Hospital, from 69% between 1993 and 2003, to 54% after 2003. A small but statistically significant negative correlation was found between total dose and the percentage of this figure originating from the frontal x-ray tube (across all procedure types at Hospital 1, Spearman's r= -0.12, p=<0.01). In other words, where doses are high, laterally orientated projections tend to be more responsible than frontally orientated projections.

### *3.5.2: Fluoroscopic screening time*

As with $P_{KA}$, the distribution of screening times was right skewed (Figure 3.6). The large majority of procedures had screening times below around 30 minutes, while a small number of procedures involved lengthy screening, extending to one hour or more. For the most recently acquired data, median screening times for all procedure

types and patient sizes combined occupied a reasonably narrow range, from 8.2 to 11.8 minutes. As with $P_{KA}$, there was a tendency for screening times to fall between successive eras. This pattern was found for all hospitals with different equipment eras and was seen for almost all individual procedure types. As seen in Figures 3.3 to 3.5, screening time has tended to fall more steadily, without the pronounced falls occurring with the installation of new equipment, seen for $P_{KA}$. At Hospital 1, a significant fall in screening time was seen between 2001 and 2002 corresponding to changing equipment (Wilcoxon test p=0.0001). An unexplained spike in median screening times was seen at Hospital 1 in 1999, before times fell in 2000 to below pre-1998 levels.

In contrast to $P_{KA}$, correlation between mass and screening time for individual procedure types tended to be weak (range was -0.37 to +0.28) though occasionally significant (Table 3.9), especially for overall procedure categories (diagnostic, interventional and other). These correlations were both positive and negative, and not consistent between hospitals. The overall impression was a lack of strong relationship between patient size and fluoroscopic screening time. Less variation in median screening times – generally by a factor of no more than two - was found between different hospitals than for $P_{KA}$. Screening time was relatively poorly correlated with median doses at different hospitals. In fact, the hospital with the highest median doses for the most recent data (Hospital 2) had the shortest median screening times.

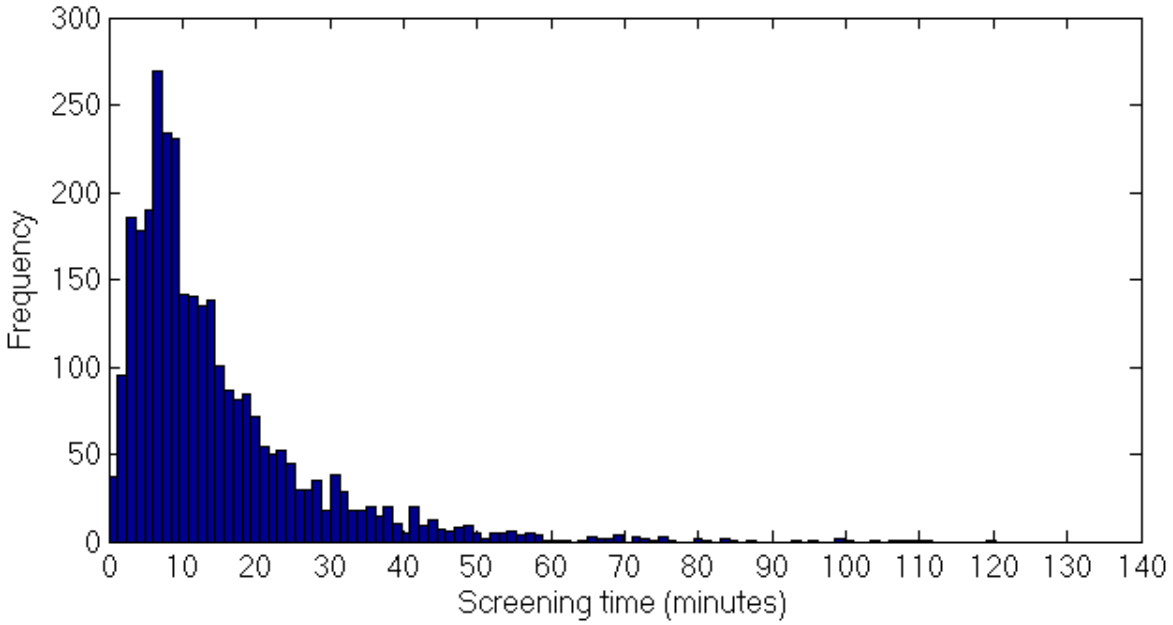


**Figure 3.6: Histogram of screening times (all procedures combined), at Hospital 1, 2002-08**

### *3.5.3: Skin Dose estimates*

Estimated skin doses (i.e. air kerma) were available for 3640 examinations conducted at Hospital 1. These figures were generally in the range 0-200 mGy, with a median for all procedure types and patient ages combined of 26 mGy. Skin dose estimates in any one plane exceeded 1000 mGy in six examinations, and 2000 mGy in one examination. No skin doses were recorded for procedures conducted on older generation equipment, meaning it was not possible to assess trends with time. Like $P_{KA}$, skin doses increased with patient mass/age (correlation coefficients were +0.89 and +0.91 for interventional and diagnostic procedures respectively for 2002-2008 data). This upward trend with age was smaller than that for $P_{KA}$, increasing by a factor of around 10 from the smallest to the largest patient size groups for skin dose, compared to around 20 for $P_{KA}$.

### *3.5.4: $P_{KA}$ normalised by mass*

Patient mass was recorded for most examinations at Hospitals 1 to 4, but not Hospitals 5 or 6. Where $P_{KA}$ was divided by patient mass ($P_{KA}$/kg), the median of this figure was found to vary with age/mass category. The nature of this pattern varied between hospitals or different eras at the same hospital. In some cases $P_{KA}$/kg was seen to steadily increase or decrease, while in others a U-shaped or bimodal pattern

was observed (Figure 3.7). The correlation between $P_{KA}$/kg and mass category tended to be either strongly negative or strongly positive, for example, -0.92 between 2004 and 2008 for all procedures combined at Hospital 3, and +0.93 between 2008 and 2013 at the same hospital. It was found that in addition to replacing fluoroscopic equipment in 2008, a new policy of omitting the antiscatter grid for patients less than 10 kg was implemented. Similar patterns were observed for both procedure categories (diagnostic or interventional) and individual procedure types, although analysis of the latter is often hindered by small sample sizes. A similar situation was found for other hospitals. Where antiscatter grids were used for all patient sizes, $P_{KA}$/m was highest in the 0-1 year age group and tended to be negatively correlated with patient age. Where antiscatter grids were omitted for small patients, $P_{KA}$/m tended to increase with patient size or display a lop-sided 'U' or 'J' shaped pattern. Where $P_{KA}$/kg figures were further normalised by screening time (Figure 3.8), i.e. ($P_{KA}$/kg)/min, the above patterns become even more pronounced. A clear distinction was seen between datasets depending on grid usage.

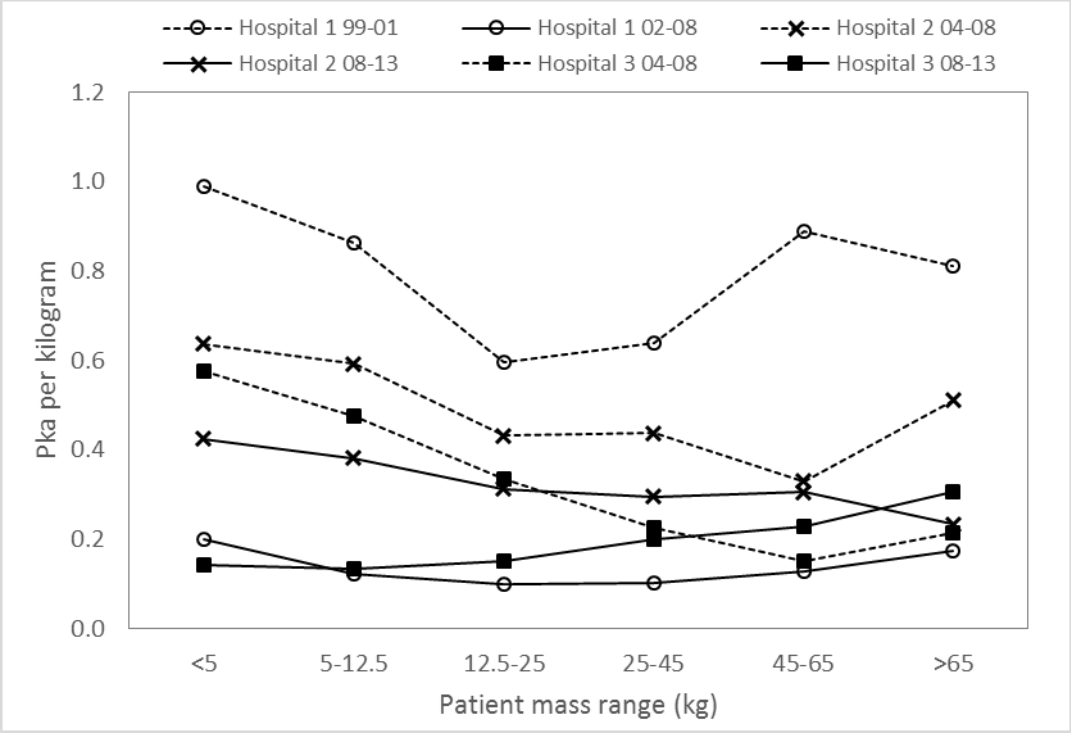


Figure 3.7: $P_{KA}$ normalised by mass for two different eras at three hospitals.

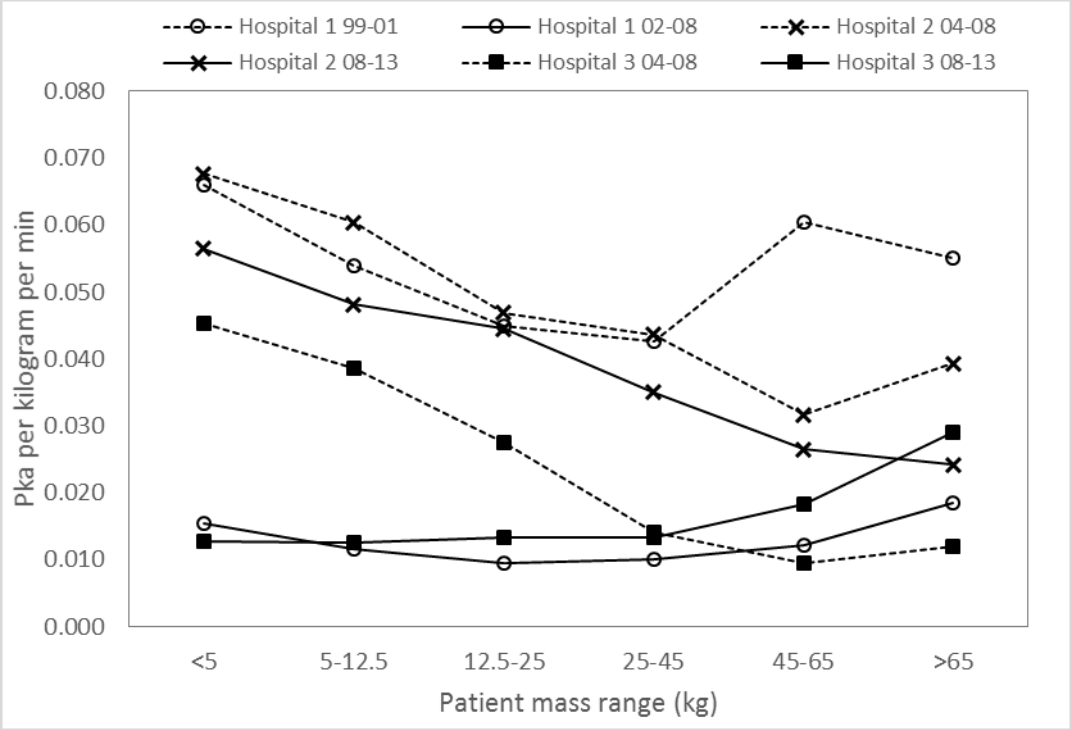


**Figure 3.8: $P_{KA}$/kg further normalised by screening time (per minute)**

*3.3.5: Number of procedures per patient*

A function was written in MATLAB to identify patients undergoing multiple procedures on different dates (i.e. not including situations in which a patient has two or more procedure types during the same catheterizations on the same day). Across the whole cohort, the mean number of procedures per patient was 1.5 (median=1). As with $P_{KA}$, the distribution was right skewed. The majority (75.8%) of patients underwent a single recorded examination during the study period, while 13.6% underwent two procedures. 79 patients (0.6%) underwent 10 or more procedures. All but one of these patients were examined at Hospitals 1 and 4, which are the two centres carrying out paediatric heart transplants in the UK [210]. The maximum number of procedures recorded for a single patient was 38. Figure 3.9 shows the percentage of patients undergoing a particular number of procedures, separated into transplant (Hospitals 1 and 4) and non-transplant hospitals (all others). The mean number of procedures per patient during the study period was 1.7 at transplant hospitals and 1.3 at non-transplant hospitals. For the latter group, a large majority of patients (82.4%) underwent a single recorded procedure. This analysis is limited by the follow-up period of the study, which was considerably longer for Hospital 4 and Hospital 1 than other hospitals. Calculations were repeated for patients born within

the study period, though the results were virtually unchanged, with a mean number of procedures per patient of 1.5 (1.6 and 1.3 for transplant and non-transplant hospitals respectively).

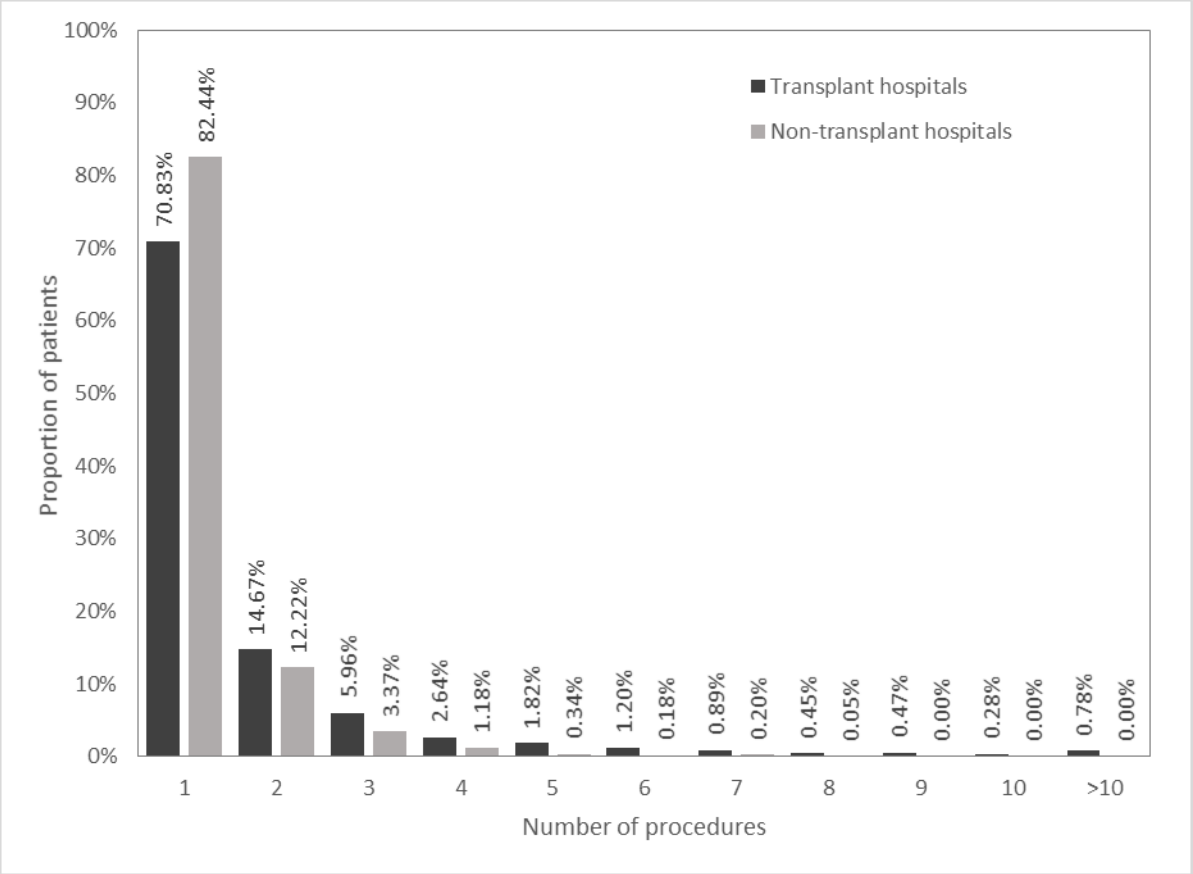


**Figure 3.9: Number of examinations per patient. Data are presented for the whole cohort.**

### *3.5.6: Clinical history and indication for procedure*

The reason for carrying out the cardiac catheterization procedure was recorded at Hospitals 1 and 2 (7973 examinations). Clinical information was searched for the following terms; transplant (Tx, HTx), Down's syndrome (Trisomy 21), Tetralogy of Fallot (TOF, T4), transposition of the great arteries (TGA), hypoplastic left or right heart syndrome (HLH, HLHS, HRH, HRHS) Norwood procedure (surgery carried out for hypoplastic left heart), Fontan procedure (surgery for patients with a single ventricle) and valve atresias (pulmonary, aortic, tricuspid or mitral). The first two of these conditions are associated with known increased risk of cancer [211, 212], while the remainder (as well as transplantation) are associated with significantly decreased

survival [213-216]. These conditions are not mutually exclusive, with some patients suffering from more than one condition. The most common combinations were transplant and Tetralogy of Fallot (13 patients) and Tetralogy with Down syndrome (8 patients).

The percentage of examinations carried out on patients with these conditions differed between the two hospitals (Table 3.10). In particular, Hospital 1 carried out a much greater number of examinations on transplant patients (23% of total procedures). The mean number of procedures carried out for these indication groups was calculated. This figure was higher for transplant patients (4.1) compared to others (1.3 to 2.2). Patients with Down's syndrome usually only underwent a single catheterization. It should be noted that there are a number of shortcomings of the above analysis. Firstly, only two participating hospitals record information on indications. Secondly, there is a reliance on the radiographer noting such details in examination records – the absence of the search terms in the comments column does not imply the patient does not have the conditions searched for, simply that they were not recorded. Consequently, the figures in Table 3.10 are likely underestimates of the presence of these conditions among cohort members. Again, this will have implications for epidemiological analysis.

| | Hospital 1 | | Hospital 2 | | Both | |
|---|---|---|---|---|---|---|
| **Condition** | **n** | **% patients** | **n** | **% patients** | **n** | **% patients** |
| **Heart transplant** | 456 | 9.4% | 14 | 0.5% | 471 | 6.0% |
| **Tetralogy of Fallot** | 231 | 4.8% | 121 | 4.0% | 352 | 4.5% |
| **TGA** | 222 | 4.6% | 242 | 8.0% | 464 | 5.9% |
| **Down syndrome** | 26 | 0.5% | 56 | 1.8% | 82 | 1.0% |
| **Norwood procedure** | 25 | 0.5% | 23 | 0.8% | 48 | 0.6% |
| **Fontan procedure** | 47 | 1.0% | 68 | 2.2% | 115 | 1.5% |
| **Hypoplastic left heart** | 21 | 0.4% | 25 | 0.8% | 46 | 0.6% |
| **Hypoplastic right heart** | 9 | 0.2% | 37 | 1.2% | 46 | 0.6% |
| **Pulmonary atresia** | 141 | 2.9% | 74 | 2.4% | 215 | 2.7% |
| **Tricuspid atresia** | 19 | 0.4% | 27 | 0.9% | 46 | 0.6% |
| **Mitral atresia** | 5 | 0.1% | 4 | 0.1% | 9 | 0.1% |
| **Aortic atresia** | 1 | 0.0% | 0 | 0.0% | 1 | 0.0% |

Table 3.10: Indication for procedures at Hospital 1 and Hospital 2. Percentages represent the proportion of patients at the respective hospital with each condition. TGA = Transposition [of the] Great Arteries.

### *3.5.7: Imaging mode*

Fluoroscopic imaging may be in the form of high quality 'cine' acquisitions or non-acquisition fluoroscopy. $P_{KA}$ is recorded separately for these imaging modes at Hospital 2 between 2004 and 2008, allowing the respective proportions to be analysed. This information was later utilised in the estimation of organ doses from $P_{KA}$. Overall, the mean proportion of $P_{KA}$ from fluoroscopy was 0.82 (median = 0.85). This proportion was higher for interventional (median=0.86) rather than diagnostic procedures (0.68). Individual interventions, such as ASD or PDA occlusions tended to utilise reasonably similar proportions of acquisition imaging (Table 3.11). For RFA and EPS procedures, the total $P_{KA}$ was usually entirely from non-acquisition fluoroscopy. A small, but significant, positive correlation was found between total examination $P_{KA}$ and the percentage of this figure originating from fluoroscopy rather than cine acquisitions (Spearman's r=0.17, p<0.01).

| | Proportion of total $P_{KA}$ from fluoroscopy | |
|---|---|---|
| **Procedure type:** | **Median [IQR]** | **Mean [SD]** |
| **All interventional** | 0.86 [0.77-0.96] | 0.84 [0.15] |
| **All diagnostic** | 0.68 [0.53-0.80] | 0.68 [0.21] |
| **Other** | 0.67 [0.55-0.81] | 0.67 [0.19] |
| **ASD occlusion** | 0.98 [0.94-1.00] | 0.95 [0.08] |
| **PDA occlusion** | 0.83 [0.75-0.89] | 0.80 [0.12] |
| **AV plasty** | 0.85 [0.78-0.91] | 0.84 [0.10] |
| **PV plasty** | 0.85 [0.78-0.90] | 0.81 [0.15] |
| **PA plasty** | 0.82 [0.71-0.86] | 0.82 [0.13] |
| **COA procedures** | 0.78 [0.64-0.87] | 0.74 [0.17] |
| **EPS ± RFA** | 1.00 [1.00-1.00] | 0.97 [0.09] |

**Table 3.11: Proportion of $P_{KA}$ from fluoroscopy at Hospital 2. IQR = interquartile range, SD = standard deviation.**

### *3.5.8: Beam angle*

Beam angles were also recorded at Hospital 2, for acquisitions only. These data will be utilised in greater detail in the 'supporting information' chapter and will be analysed here with respect to $P_{KA}$. The majority of acquisitions were in the posteroanterior (48%) or lateral projections (35%), with the remainder made up mainly of left/right anterior oblique (both 3%) and other unspecified oblique views.

Table 3.12 shows the Spearman's rank correlation between $P_{KA}$ and the percentage of acquisitions in a particular projection, per examination. Analysis was carried out for both total $P_{KA}$ and that resulting from acquisition exposures only. In each case, $P_{KA}$ was normalised by mass to reduce (but not eliminate, see above) the impact of patient size. No strong correlations between usage of particular beam projections and $P_{KA}$/kg were found (r ranged from -0.34 to +0.22). There was a tendency for usage of the PA projection to be negatively correlated with dose and oblique projections to be positively correlated, although neither of these observations was consistent between different procedure types. Also shown in Table 3.12, a positive correlation was always present between $P_{KA}$/kg and the number of cine acquisitions. This was expected, though not inevitable as a single acquisition can still result in a large dose if lengthy. The direction of correlation was almost always consistent between acquisition $P_{KA}$/kg and total $P_{KA}$/kg verses number of acquisitions or percentage usage of different projections. In the former case, positive associations tended to be greater and more significant.

| | | No. of acquisitions | % in PA | % in Lateral | % in RAO | % in LAO | % in RAO/CR | % in LAO/CR | % in Long Axis |
|---|---|---|---|---|---|---|---|---|---|
| **PDA occlusion** | Acquisition $P_{KA}$/mass | 0.62** | -0.20* | -0.13 | 0.18** | 0.07 | | | |
| | Total $P_{KA}$/mass | 0.49** | -0.24** | -0.02 | 0.22** | 0.09 | | | |
| **ASD occlusion** | Acquisition $P_{KA}$/mass | 0.38** | -0.34** | 0.12 | 0.2 | 0.1 | | | |
| | Total $P_{KA}$/mass | 0.16 | -0.06 | 0.04 | 0.11 | 0.08 | | | |
| **Coarctation angioplasty** | Acquisition $P_{KA}$/mass | 0.51** | 0.09 | -0.35* | 0.01 | 0.05 | | | |
| | Total $P_{KA}$/mass | 0.43** | 0.13 | -0.18 | 0.06 | -0.09 | | | |
| **Pulmonary artery angioplasty** | Acquisition $P_{KA}$/mass | 0.57** | 0.07 | 0.15 | 0.09 | -0.15 | 0.08 | 0.05 | |
| | Total $P_{KA}$/mass | 0.49** | 0.18 | 0.19 | 0.06 | -0.07 | 0.10 | 0.03 | |
| **Pulmonary valve angioplasty** | Acquisition $P_{KA}$/mass | 0.40** | -0.1 | -0.26** | 0.22* | 0.11 | 0.16 | 0.21* | |
| | Total $P_{KA}$/mass | 0.23* | -0.03 | 0 | 0.20* | 0.08 | -0.08 | 0.08 | |
| **Aortic valve angioplasty** | Acquisition $P_{KA}$/mass | 0.44** | -0.25 | -0.13 | 0.15 | | | | 0.37* |
| | Total $P_{KA}$/mass | 0.21 | 0.02 | -0.25 | -0.04 | | | | 0.24 |

**Table 3.12: Correlations between dose (either total or that arising from cine acquisitions only) and the number of acquisitions or proportion of acquisition $P_{KA}$ in different projections. ** Significant to 0.01 level, * significant to 0.05 level.**

### *3.5.9: Operating cardiologist*

The cardiologists and radiographers conducting the examination were recorded at Hospital 1. Variation in $P_{KA}$ and screening time according to the involvement of

different staff was investigated using a Kruskal-Wallis test for five of the most common procedure types. A Spearman's rank test was also performed to identify any correlation between dose/screening time and the number of procedures carried out for each operator. In both cases, $P_{KA}$ was normalised by mass to reduce the impact of variation in patient size on the results. For most examinations, more than one staff member was listed and it was not known who was actually at the controls. The results were characterised by mainly null findings. A significant difference in $P_{KA}$ was found for cardiologists for coronary angiography ($p=0.03$) and PDA occlusions ($p=0.02$), and for ASD occlusions for radiographers ($p=0.03$). A significant negative correlation was found between the number of coronary angiography procedures carried out by each operator and $P_{KA}$ (Spearman's $r=-0.17$, $p=<0.01$). No other significant correlations of this type were found.

### *3.6: Discussion*

The most significant finding of the analysis of $P_{KA}$ and screening times was the fall in these dose indicators with time. For $P_{KA}$, these falls tended to be associated with the installation of new equipment. The decrease was particularly pronounced at Hospital 1 between the 1994-2000 and 2002-2008 eras, where a fall in median $P_{KA}$ by a factor of around 20 was seen for all procedures combined. A more moderate decrease was seen between the 2004-2008 and 2008-2013 eras at Hospital 2 (1.42 fold) and Hospital 3 (2.5), though older, pre-2000 data were not available at these hospitals. There was some suggestion of a decrease in $P_{KA}$ within individual eras, along with a more steady decrease in screening times, as might be expected due to increased experience and technique refinement. This variation was relatively small, however, and not monotonic. Only a limited analysis of the variation in dose indicators between operators at a given hospital was possible. These results suggest inter-operator variation has a relatively minor impact on doses. The overall impression was that technological factors were the driving force behind the decline in dose indicators with time.

Technological factors include (1) improved detective quantum efficiency of detectors, (2) use of a different beam spectrum including the use of extra copper filtration, (3) ability to reduce frame rates for acquisitions and fluoroscopic imaging, (4) ability to remove antiscatter grids, (5) more dose efficient digital image processing techniques,

and (6) other features such as 'last frame hold' and lung shuttering. Referring to point 2, while the use of extra copper filtration is an effective dose reduction technique without impacting image quality [8, 217-219], the patient dose per unit $P_{KA}$ is higher as beam quality is increased (see Monte Carlo results chapter for more details). Consequently, the magnitude of decrease in patient dose may be exaggerated where doses are represented by $P_{KA}$ only. Lung shuttering takes into account the reduced density of the lungs compared to the mediastinum, by inserting aluminium filters to modulate the intensity of the x-ray beam and reduce lung dose. The impact of lung shuttering on $P_{KA}$ is difficult to judge as usage is not recorded in examination details. Improved image processing includes techniques such as recursive filtering or 'temporal filtering' [99], in which signal-to-noise ratio is improved by a weighted combination of the signal from previous frames. Alternatively, signals can be deconstructed into frequency bands called a 'Laplacian Pyramid' and filtered separately [99].

The introduction of digital flat panel detectors (FPDs) is associated with a number of advantages, including reduced geometric distortion, greater dynamic range, smaller physical size and improved dose efficiency [98, 220]. The latter point is controversial, with some studies finding little or mixed evidence of any advantage [21, 221]. Comparison requires caution, as FPDs are usually installed as part of a complete replacement of fluoroscopic equipment, including x-ray tube, generator, control panel and image processing software. Thus the fall in doses between eras at Hospitals 2 and 3, though associated with replacement of image intensifiers (IIs) with FPDs, should not be solely attributed to a difference in detectors. Median $P_{KA}$ was similar at Hospital 1 for ostensibly the same machine type, equipped with II detectors (2002-2008) and FPDs (2007-2010). Hospital 4, while continuing to use image intensifiers (as of 2015), delivered doses that are very similar to those of hospitals using FPDs. The conclusion by Davies *et al* [221] that FPDs do not confer "*an automatic improvement in image quality or dose efficiency*" is supported by the current study, at least for doses.

Antiscatter grids are used to reduce the impact of Compton scattering, and the associated reduction of image contrast, by selectively attenuating x-rays not traveling perpendicular to the grid septa [16]. This improvement in image quality comes at the expense of increased dose. As attenuator thickness increases, the amount of

material traversed by the beam, and thus opportunities for scattering, also increases. Conversely, for 'small' patients, the amount of scattering is often considered sufficiently minor to allow removal of the grid, resulting in a significant increase in dose efficiency [222, 223]. The definition of 'small' is open to debate. Partridge *et al* [224] recommend "*that the gridless imaging should be the default technique for adults and children and in most installations*". This conclusion appears to have been reached based on a rather limited range of procedure types and a subjective assessment of image quality. Tapiovaara and colleagues [217] reported improved dose efficiency where the grid was removed for the smallest patient size studied (3 years) but not for larger patients (10 and 15 years). The usage/omission of an antiscatter grid should only impact on doses for patients below 5 years of age (i.e. small patients where grids are removed), though lower $P_{KA}$, $P_{KA}$/kg and ($P_{KA}$/kg)/min figures are seen beyond these ages. This suggests grid usage patterns are not solely responsible for variation in these figures between hospitals. Participating hospitals in this study tended to report grid removal for patients under 'around 10 kg', though admitted often omitting them for larger patients (McLaren C, personal communication 2014). Thus the reduction in $P_{KA}$ and $P_{KA}$/kg associated with grid removal may not be restricted only to the smallest patients.

The variation in $P_{KA}$ between individual procedure types was expected as different procedures have different levels of complexity and involve the use of different beam angles. Furthermore, some procedures such as atrial septostomy and ASD closure involve the combined use of fluoroscopy and trans-oesophageal echo (TOE) ultrasound [225, 226], and tend to deliver lower doses. In fact, most atrial septostomies conducted at Hospital 3 where done entirely under TOE guidance with no x-ray exposure. The procedures associated with the highest doses were valve replacements, although this procedure is carried out infrequently. Despite the high doses, the procedure is a relatively complication-free alternative to surgery in patients with pulmonary valve regurgitation [227]. At most hospitals, median $P_{KA}$ figures for 'interventional' procedures were lower than those for 'diagnostic'. In some previous studies, the reverse was found [91, 103, 113, 207]. However, while grouping procedures into such large categories is statistically convenient, it is ultimately arbitrary and unhelpful. For example, stenting of the coronary arteries would have a lot more in common with a purely diagnostic visualisation of the same vessels than with other interventional procedures such as ASD occlusion.

Furthermore, the individual procedure types included within each category are not the same at each hospital. Coronary angiography (diagnostic), for example, is usually only carried out at hospitals specialising in heart transplants. Valve replacements (interventional) were only regularly conducted at Hospital 1. It might be expected that the relative ranking of procedure types by $P_{KA}$ would be fairly constant between centres, i.e. the procedures associated with the lowest doses at one hospital would be the lowest at all the others as well. This pattern was not observed however - even at the same hospital over multiple eras. The reasons for this are not clear, though possibly related to local expertise and technique preferences.

A trend of increasing average $P_{KA}$ with increased patient size or mass was seen for almost all procedure types at all hospitals. This finding was consistent with previous research [82, 91, 92, 207, 228]. The increase in $P_{KA}$ with patient size can be explained by (1) increased patient thickness requires a greater x-ray output to produce the same exposure at the detector, and (2) a larger beam area is required to cover the cardiac region as the patient grows.

For all procedures combined, there was a near fourfold variation in median $P_{KA}$ between different hospitals. This variation is smaller than that suggested by previous research (see literature review), where a greater than tenfold variation was seen. The reasons why there is a smaller variation within the UK this are unclear. Standardisation of training for cardiologists is a potential factor, although concerns have been raised over the lack of formal training courses for these staff [229]. Monitoring of dose indicators is carried out by Public Health England, for the purposes of setting reference doses (discussed later). The sharing of such information could potentially help to standardise dose levels between centres, however, paediatric cardiac catheterizations are not included within published reports [230, 231]. Interestingly, no association between $P_{KA}$ and the number of procedures carried out at a particular hospital was found. In fact the lowest doses were recorded at Hospital 6, which carried out the fewest procedures.

Normalising $P_{KA}$ by patient mass has previously been advocated in several studies [103, 207] as a way a standardising dose reporting and setting of reference levels. Kobayashi *et al* [4] suggest that "*growth dependent variation in $P_{KA}$ is successfully eliminated by normalizing $P_{KA}$ by body weight*". This conclusion appears to be based

on the lack of strong correlation between $P_{KA}$/kg and patient age (r ranging from -0.079 to 0.014). This finding was not replicated in the current study, where $P_{KA}$/kg was found to vary with patient age in a number of distinctive patterns depending on equipment type and, it seems, antiscatter grid usage. It should be noted that the data described by Kobayashi were acquired from 16 hospitals, encompassing a range of equipment types. These were combined together to produce a single dataset of 8267 procedures. Each machine type may respond to changes in patient size differently, while some hospitals may omit an antiscatter grid for small patients with others keeping it in. The lack of an overall pattern when data have been combined into a single sample is perhaps unsurprising. Combining data from multiple hospitals may produce large sample sizes, but an inevitable consequence is the blurring out of patterns and loss of useful information. Furthermore, in their claim that that normalising $P_{KA}$ by body weight eliminates variation in $P_{KA}$ with age, Kobayashi and colleagues [207] appear to have made the mistake of assuming the lack of correlation between two datasets implies *there is no relationship*. This is not necessarily true - a U-shaped relationship results in a correlation coefficient of zero, either for Spearman's or Pearson's methods. Correlation coefficients should not be used alone to determine if $P_{KA}$/kg is somehow independent of patient size. The measure of $P_{KA}$/kg is indeed a useful indicator of dose, reducing the impact of patient size but not eliminating it. The findings of the current study thus do not support the recommendation by Kobayashi *et al* that $P_{KA}$/kg is suitable for establishing reference levels, at least not in isolation and not as single figure for all patient sizes. Further discussion of reference levels is provided below.

The majority of patients in the cohort underwent a single procedure. This finding was replicated when analysis was restricted to patients born within the study period. This has positive implications for epidemiological analysis as it suggests the possibility of missing procedures is relatively small. Data on clinical conditions were limited to only two hospitals, although a certain degree of inferences can be made from the examination type alone. For example, a patient undergoing closure of a ventricular septal defect must be suffering from this anomaly. There is, however, no guarantee that this condition was isolated and not part of a wider disease pattern such as Tetralogy of Fallot. Information on clinical conditions will also have a significant bearing on future epidemiological analysis of this or similar cohorts. Patients with HLH or those undergoing transplants or Norwood procedures have reduced life

expectancies [89, 211, 232], while transplant and Down syndrome patients are at an increased risk of developing lymphoma and leukaemia, respectively [211, 212, 233].

The analysis of skin dose estimates was limited to examinations conducted at Hospital 1 after 2002. These figure suggest the risk of acute skin injuries, thought to occur following localised doses of above 2 Gray [16, 44, 234, 235], is extremely small for paediatric cardiac catheterizations carried out using modern equipment. Only a single patient received a skin dose in any one plane of greater than 2 Gy for a single procedure. Skin doses were not recorded for procedures conducted prior to 2002, for which $P_{KA}$ was higher by a factor of up to 20. The use of copper filtration in modern equipment has the effect of almost entirely removing low energy photons (<30 keV) from the x-ray beam and reducing skin dose by 58% (based on 0.35 mm Cu) [236]. Thus skin doses for older equipment in which no copper filtration is used may be higher than suggested by the ratio of $P_{KA}$. Skin dose estimates are subject to considerable uncertainties relating to the distance from the source at which the patient's entrance skin surface is expected to be found (i.e. the 'international reference point'). The beam area varies according to the square of the distance from the source, thus a 10% error in estimation of the location of the reference point equates to a greater than 20% error in skin dose.

### *3.6.1: Comparison with previous publications*

Previous publications reporting $P_{KA}$ and screening times from paediatric cardiac catheterizations were discussed in the literature review. These figures will now be re-examined in the light of the data from the current study. It should be again emphasised that comparison of dose indicators with previous studies is difficult as each study involves a different equipment types, range of patient sizes and procedure types. Recent era data from Hospitals 1 (2002-2008), 2 and 3 were preferred in these comparisons, due to the large sample sizes and detailed examination type information (lest this be interpreted as 'cherry picking' in order to provide more favourable comparisons with other studies, it should be noted that doses at Hospitals 4, 5 and 6 Hospitals were lower – see Tables 3.7 and 3.8).

The majority of previously published data are for procedures conducted in the last 10 years with little data with which to compare early era doses at Hospital 1 and Hospital 4. The doses from between 1994 and 2001 at Hospital 1 were compatible

with those quoted by Boothroyd *et al* in 1997 [228] (presented for frontal tube output only) but much higher than those reported by Rassow *et al* [108] for data acquired from 1994 to 1996. For both diagnostic and interventional categories, recent era $P_{KA}$ figures were compatible with the results of studies led by Martinez [94], Dragusin [237] and McFadden [93] when adjusted for age, and with Barnaoui *et al* [92] for diagnostic, ASD occlusion and PDA occlusion procedures. Where normalised by mass, $P_{KA}$ figures were higher than those presented by Ubeda *et al* [223] by a factor ranging from 1.3 to 3.5 (The $P_{KA}$ figures presented in Ubeda's study, based in Chile, are exceptionally low, compared to almost all previous research). These investigations were relatively small, with sample sizes of no more than a few hundred procedures.

A number of large studies have been recently published in which stratification of $P_{KA}$ by age or mass for individual procedure types was sufficient to allow meaningful comparisons. Firstly, Verghese *et al* [2] reported $P_{KA}$ and air kerma for 3365 procedures conducted at Boston Children's Hospital using Siemens Axiom Artis units with flat panel detectors. Given the modern equipment, one would expect the reported $P_{KA}$ figures to be comparable to those of the current study. Instead they are considerably higher. For diagnostic procedures, the median $P_{KA}$ reported by Verghese *et al* was higher than equivalent figures at Hospital 1 (2002-2008 data) by a factor of 5.1 to 8.8 depending on age range. For individual procedure types, the discrepancy is larger. For example, the median $P_{KA}$ quoted by Verghese *et al* for ASD occlusions is higher than that recorded at Hospital 1 by a factor of between 34 and 40. It is noted that quoted doses also include those acquired before the implementation of the new radiation protection policy, where $P_{KA}$ was reduced by a factor ranging from 4 to 52%. Fluoroscopic screening times were longer than those of the current study by a factor of around 2; insufficient to explain the much greater $P_{KA}$.

Glatz and colleagues [1] reported $P_{KA}$ for 2265 procedures carried out at Philadelphia Children's Hospital, using a Siemens Artis Zee unit between 2009 and 2011. Again, despite a range of effective dose reducing measures being implemented, including reduced frame rates and antiscatter grid removal where appropriate, the quoted $P_{KA}$ figures were much higher than those of the current study. For all procedure types combined, the median $P_{KA}$ quoted by Glatz *et al* was higher than equivalent figures for the most recent era in the current study by a factor of between 1.6 and 6.3

depending on hospital. For individual procedure types, the discrepancy in $P_{KA}$ was even greater, being higher for ASD occlusions by a factor of up 20 compared to the current study. As with Verghese, the screening times are longer, but by an insufficient extent to explain the discrepancy in doses.

A recent study by Ghelani *et al* [83] in which data from 2713 examinations were acquired from 7 American centres, reported median $P_{KA}$ and air kerma levels higher still than Verghese or Glatz (two of the included centres were Philadelphia and Boston Children's Hospitals). The median $P_{KA}$ for ASD occlusions in the 10-15 year age category was 93 $Gycm^2$, compared to 2.0 at Hospital 1 between 2002 and 2008. For all ages, ASD doses were higher than those of the current study by a factor ranging from 4.7 to 24.7 depending on hospital. The discrepancies for other procedures were somewhat smaller, with median $P_{KA}$ figures reported by Ghelani being higher by a factor of 2.2 to 9.2 for PDA occlusions, 6.8 to 10.1 for aortic valvuloplasty, 5.0 to 16.8 for coarctation repair and 2.6 to 10.1 for pulmonary valvuloplasty, depending on hospital. Again, screening times were approximately twice as long as those of the current study.

The previously mentioned study by Kobayashi et al [4] acquired data from 16 centres giving a sample of 8267 procedures. No analysis of variation between each of the participating centres or equipment types was performed. The procedure specific $P_{KA}$/kg figures reported by in the study were higher than those of the current study using modern equipment by a factor of 2.2 to 6 for combined interventional procedures, 1.3 to 3.7 for diagnostic procedures, 2.0 to 10.3 for ASD occlusions, 2.5 to 5.3 for aortic valvuloplasty and 1.3 to 4.7 for pulmonary valvuloplasty, depending on hospital. Another, more recent study by Borik *et al* [102], acquired data on 5196 cases conducted at the Toronto Hospital for Sick Children. Doses, as represented by $P_{KA}$ and $P_{KA}$/kg where closer to those of the current study, being broadly similar to figures recorded at Hospital 2 after 2008, but higher than equivalent figures at Hospitals 1 and 3.

Few studies have been conducted with which skin dose estimates can be compared. Frustratingly, most authors have combined figures from both imaging planes into a single 'cumulative air kerma' figure. In such cases, it can be assumed that the maximum skin dose in any single plane can be no less than 50% of the cumulative figure. Skin doses reported in the previously mentioned study by Glatz *et al* [91] were

higher than those of the current study by a similar factor to their $P_{KA}$ figures. Single plane doses of greater than 2000 mGy occurred in 4.3% of interventional procedures overall. For patients over 65 kg, these levels were exceeded in 32.9% of all interventional procedures and 58% of PA angioplasty procedures. The skin doses reported by Verghese and colleagues [82] were also greater than those of the current study by a similar factor to $P_{KA}$. For patients over age 16, the median cumulative skin doses for *'distal R or L angioplasty or stent', 'RVOT dilatation and or stent' and 'Prox R or L angioplasty and or stent'* were 4.52 Gy (IQR: 2.94, 8.48), 4.55 (1.96, 5.54) and 4.84 Gy (3.08, 5.51) respectively. For these procedures, the 'median maximum' dose (i.e. the median of whichever plane delivered the highest skin dose) must be at least 2.25 Gy, thus over the supposed threshold for observable skin reactions [234]. The authors do not comment on the frequency of skin injuries at the study hospital. The skin doses reported by Sawdy et al [238] for 1310 procedures carried out over a 3 year period are especially difficult to interpret. It is not clear what the units of measurement are – data presented in tables are written in the unit of 'R', which presumably means Roentgen (a unit of exposure often recorded by older equipment), while the text refers to the same figures in 'mGy'. Nor is it clear if figures are combined for both planes, or are the maximum of both (as in this study). The authors report that 15 patients received radiation burns during the study period. Skin injuries were the first recorded adverse effects of exposure to ionising radiation, reported within 6 months of the discovery of x-rays in 1895 [16]. The findings of the current study suggest that acute skin reactions from cardiac catheterizations carried out using modern equipment are extremely unlikely in children, at least in the UK. Skin cancer, however, appears inducible by radiation, albeit mostly in less dangerous forms such as basal cell carcinoma, rather than malignant melanoma [45]. It is important, therefore, that epidemiological analyses of cancer risks following cardiac catheterizations include the identification of skin cancers.

In the literature review, it was speculated that the high doses reported in recent studies led by Glatz [91], Verghese [82], Ghelani [83] and Kobayashi [207] could be a true representation of doses from modern cardiac catheterizations, and that the low doses of other studies could be explained by small sample sizes and publication bias (only publishing if doses are low). The findings of the current study, presented in this chapter, ought to suggest otherwise. While it is tempting to speculate that mistakes have been made in quoting $P_{KA}$ data, for example confusing mGy·cm² with μGy·m², it

is unlikely that four large studies could have made the same mistake. If the $P_{KA}$ figures quoted in the above mentioned studies were to be reduced by a factor of 10, they would become inexplicably low. The units of measurement were confirmed individually for all six hospitals in the current study and were consistent. The discrepancy in doses, as represented by $P_{KA,}$ is almost certainly real. However, it is not possible to claim that high doses are 'too high' – that would imply a proven net disadvantage, with the radiation-associated detriment (i.e. increased risk of cancer) outweighing the improved image quality associated with higher doses.

*3.7: Limitations and uncertainties*

The most important limitation of the data described in this chapter is the variable quality from one hospital to the next. Most notably, a large proportion of examinations conducted at the Hospital 4 lacked any form of dose indicator and lacked sufficient information on procedure type. This has implications for dose estimation as knowing the procedure type allows the likely beam angles used to be predicted. Procedure type information is also useful for epidemiological analysis as it allows inferences on confounding factors and survival rates.

The number of patients without sufficient personal details to allow cancer registry matching (full name, date of birth, or NHS number) is also a concern. Much of the cohort (i.e. from Hospitals 1 and 2) was established from handwritten records, rather than computer-based RIS records. A number of spelling discrepancies were only identified because the patient had multiple entries. For patients examined only once, the risk of misspelled names is increased. Such cohort members, if they have indeed developed a tumour, may not be identified as such by the cancer registry. This could potentially lead to an under-ascertainment of cancer incidence in this patient group. Data obtained electronically may also include data entry errors – it is just as easy to enter data into the wrong column (e.g. mixing up $P_{KA}$ and ST) or to place a decimal point in the wrong place.

Kerma area product is typically subject to an uncertainty of ±15% where regularly calibrated. All $P_{KA}$ meters were subjected to regular quality assurance (QA) testing. Calibration factors were applied to $P_{KA}$ data where provided. The spike in $P_{KA}$ in 1996 at Hospital 1 (Figure 3.) could potentially be due to measurement error, although this is impossible to confirm or rule out. A calibration factor for the lateral tube (1.13) was

provided for 1995 but not 1996. The reliability of older data is an important concern for future epidemiological analysis.

The automatic gathering of examination data for the purpose of national audits has been discussed [239, 240]. This is, in principle, a very attractive prospect, but requires rigorous attention to quality assurance. The automatic archiving of dose indicators, including 'structured dose reports' recorded by most modern fluoroscopic equipment, could be valuable in radiation protection and (providing sufficient details are recorded) epidemiological research, while also reducing the workload for radiographers. The latter point may not necessarily be a good thing though; manual recording of dose indicators may help to enforce a culture of awareness of radiation doses among radiography staff.

*3.8: Reference levels*

Mention must be made of so called ‘reference’ levels. These are often referred to as ‘diagnostic reference levels’ (DRLs) [241], although their applicability need not be restricted to purely diagnostic procedures. Reference levels are supposed to represent typical doses for a particular procedure, usually defined using median or third quartile doses obtained from audits of $P_{KA}$, skin dose, fluoroscopy time or (in CT), dose length product. In particular, reference levels should serve as an investigation level where these figures are being consistently exceeded. The above discussion of the large variation in $P_{KA}$ between published studies ought to illustrate the danger of failing to compare local dose indicators with those delivered elsewhere. Ironically, many of the studies reporting the highest $P_{KA}$ levels had the specific objective of setting reference levels themselves [83, 207]. This undermines the usefulness of the reference level concept. The setting of local reference doses that would be considered exceptionally high elsewhere provides little incentive for optimisation.

Most reference levels are based on $P_{KA}$, usually referred to in publications simply as ‘dose’, with little or no appreciation for what this figure actually represents. As described in Chapter 2, $P_{KA}$ is derived from the charge produced in a known mass of air as the x-ray beam passes through, and thus represents dose (or more specifically collision air kerma) *in air* – not to the patient. Although $P_{KA}$ can indeed be related to patient dose (this will be exploited extensively in this study), this relationship is highly variable, depending on conditions including patient size, beam angle and beam

energy. Equal $P_{KA}$ figures may equate to greatly different patient doses. So what's the use of reference levels based on something so tentatively related to patient dose as $P_{KA}$? Without efforts to stratify $P_{KA}$-based reference levels by patient size, exam type (and hence likely beam angles) and equipment type (defining beam energy) these figures are of limited usefulness. If such variables are accounted for, then the result will be a large number of different reference levels. This may be an unattractive prospect for those who like to keep radiation protection simple, but the alternative of one-size-fits-all reference levels for all procedure types combined would be of little value and could potentially be misleading. The use of $P_{KA}$ stratified by mass for reference levels is advocated as a solution by Kobayashi *et al* [207] and Onnasch *et al* [103], though as demonstrated above, $P_{KA}$/kg is not constant across the range of patient sizes studied. Therefore normalising $P_{KA}$ by mass does not eliminate the need for any form of patient size stratification of reference levels. The $P_{KA}$ data presented in this thesis may be used as the basis for the establishment of reference levels, but only in the fully stratified, procedure specific form presented in the appendix. Any form of 'averaging out' to produce simplified reference levels is not recommended.

### *3.9: Conclusion*

A cohort was established from data on around 13,500 patients undergoing around 20,000 procedures at six hospitals in the UK. The quality of these data were variable. In particular, a large number of procedures conducted at the Hospital 4 Hospital had no dose indicator recorded.

Doses, as represented by $P_{KA}$, screening times and skin doses have decreased over the timeframe of data collection. This appears to be mainly due to equipment related factors. The figures collected in this study were low compared to several recently published American surveys. Variation in $P_{KA}$ was seen between individual centres providing data, although the magnitude of this variation is somewhat less that suggested in previous publications.

It should again be emphasised that $P_{KA}$ and screening time are only indicators of patient dose. For a more thorough analysis, including cumulative doses over multiple procedures and the associated risks, it is necessary to estimate organ doses. The following chapters describe the use of Monte Carlo computer simulations to establish

the relationship between $P_{KA}$ and organ doses over a range of beam angles and x-ray energies, and the use of this information to construct a dosimetry system for rapid dose calculation for cohort members. Further chapters describe the use of estimated organ doses for assessment of long term risks of cancer.

# Chapter 4: Computational Dosimetry:

The following chapters describe the process of using kerma area product ($P_{KA}$) (defined in Chapter 2), recorded for cardiac catheterizations, to estimate patient dose. The dosimetric modelling process was comprised of four components, each of which are covered in separate chapters:

1. A systematic analysis of the relationship between kerma area product ($P_{KA}$) and organ doses using Monte Carlo simulations, for a large range of beam angles, beam energies and patient sizes (this chapter)
2. A process for utilising the above data for calculation of doses for cohort members based on available examination data (Chapter 5).
3. Collection of supporting data on beam angles and beam energy used in clinical practice for use in dose models (Chapter 6).
4. Verification of computer simulated doses using physical dosimetry (Chapter 7).

Monte Carlo (MC) computer simulations were chosen as the primary method of dose estimation due to the ability to rapidly calculate doses to multiple organs over a broad range of exposure conditions. Thousands of possible combinations of beam angle, patient size and x-ray energy were investigated, therefore accounting for each combination using physical measurements would be extremely time consuming.

When estimating dose to organs based on limited data recorded at the time of the examination (i.e. procedure type, patient age/mass and $P_{KA}$ only), the uncertainty in dose estimates due to deviations from expected beam angles or energy needed to be estimated. Part of the dosimetric modelling process was to determine the sensitivity of organ doses to small changes to these factors. A further aim was to determine if correction factors to adjust organ doses could be applied as a single scaling factor or would need to be a continuous function of other factors (e.g. beam rotation).

## *4.1: Monte Carlo Methodology*

Monte Carlo (MC) simulations are based on computer modelling of multiple random interactions between x-ray photons and matter [242], to produce the photon equivalent of flipping a coin a great many times (the name Monte Carlo refers to the region of Monaco and reflects the stochastical nature of gambling). Instead of heads

or tails, photon trajectories are modelled according to the known laws of physics, including photoelectric absorption, Compton scattering and Rayleigh scattering. The number of photon trajectories simulated can be variable, ranging from $10^3$ to $10^8$ [16]. In this study, the software used for Monte Carlo computer simulations was PCXMC version 2.0 [242]. This is a commercial code developed especially for calculating doses from diagnostic medical exposures with photon energies of 150 keV and below. PCXMC uses phantoms representing various ages (new born, 1, 5, 10, 15 and 30 years (Figure 4.1), modified from the phantom originally reported by Cristy and Eckerman [243]. Modifications include the addition of an oesophagus and improved alignment of the head and neck region [242]. The phantoms are hermaphrodites. It is not possible to produce gender specific dose calculations (other than simply omitting breast dose). Characteristics of each phantom are given in Table 4.1. The crude nature of the Cristy phantom is widely acknowledged [244].

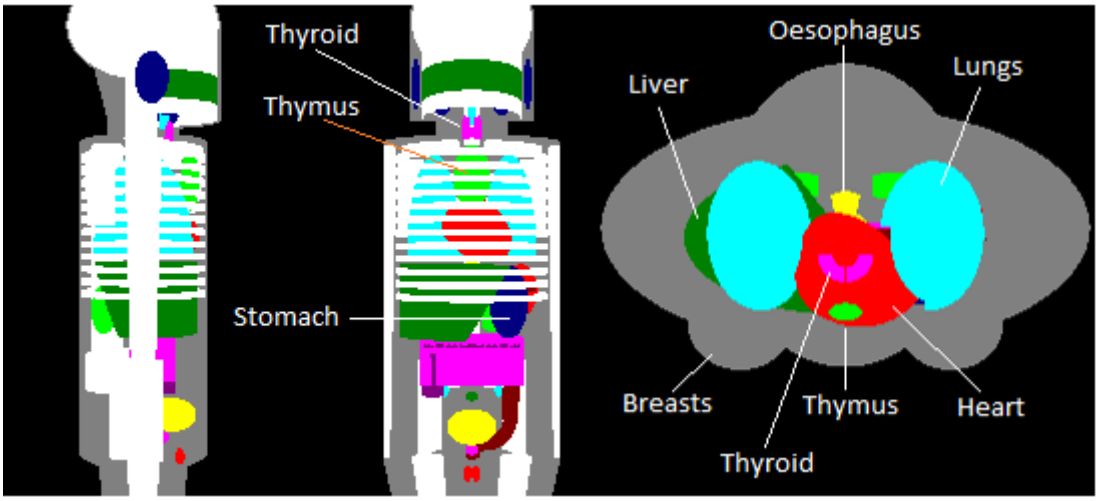


**Figure 4.1: 5-year old mathematical phantom used in PCXMC 2.0. The right hand image is displayed as if looking down from above, achieved by using maximum caudal beam angulation and removing head organs. Figure credit: author annotated PCXMC screengrab.**

| Phantom size | Mass (kg) | Height (cm) | Trunk height (cm) | Trunk thickness (cm) |
|---|---|---|---|---|
| Newborn | 3.0 | 50.9 | 21.6 | 9.8 |
| 1 Year | 9.2 | 74.4 | 30.7 | 13 |
| 5 Years | 19.0 | 109.1 | 40.8 | 15 |
| 10 Years | 32.4 | 139.8 | 50.8 | 16.8 |
| 15 Years | 56.3 | 168.1 | 63.1 | 19.6 |
| Adult | 73.2 | 178.6 | 70 | 20 |

**Table 4.1: Phantom characteristics in PCXMC 2.0. Data obtained from Tapiovaara and Siiskonen [242]**

PCXMC has been used extensively in diagnostic medical radiation dosimetry, including for estimation of doses from cardiac catheterizations [85, 86, 91, 92, 107]. The results of such simulations in PCXMC show good agreement with the general purpose Monte Carlo code MCNP, while the former is considerably more convenient to use [85]. Good agreement has also been found between PCXMC and the results of Stern *et al* [87] for coronary angiography examinations [245], and with the results of Hart *et al* [246] for a range of x-ray energies and examinations, including chest imaging [245, 247]. Brady [248] found that agreement between computational and physical measurements of effective dose from CT scans was higher for PCXMC than for other programs, including those specifically designed for CT dose estimation.

PCXMC calculates doses to 29 different organs and tissues along with effective dose using ICRP 60 [67] and ICRP 103 [44] weighting factors. Organ doses are presented as the mean dose to the whole tissue and are thus numerically identical to the equivalent dose (H) for that organ. This includes dose to the skin; it is not possible to calculate localised skin doses for the irradiated area in PCXMC, nor is it possible to calculate 'partial' organ doses, such as unilateral breast or lung doses. Only doses to active bone marrow, breasts, heart, lungs, lymph nodes, oesophagus, liver, stomach and thyroid were utilised in the dosimetry system, along with effective dose (ICRP 103 factors) and mean absorbed dose to the whole body. Although other organs such as the bladder, colon and salivary glands are susceptible to radiation induced cancer [45], these organs are well outside the exposed area and thus receive little radiation dose. Other organs such as the uterus are of little interest in an epidemiological study of low radiation doses. Incorporating additional organs into the dosimetry system (described in Chapter 5) is especially time consuming, as each requires its own separate set of corrections for beam energy. These organs were not

analysed separately in this study, although the doses were incorporated into effective dose.

Lymph nodes are not themselves simulated in PCXMC phantoms. Instead, lymph node dose is calculated by a weighted sum of doses to other tissues using the following relationship [242]:

$$D_{lymph\ node} = D_{small\ intestine} + 0.13 \cdot D_{extrathoracic\ airways} + 0.08 \cdot D_{salivary\ glands} + 0.05 \cdot D_{thyroid} + 0.04 \cdot D_{oesophagus} + 0.03 \cdot D_{stomach} + 0.15 \cdot D_{pancreas} + 0.10 \cdot D_{gall\ bladder} + 0.07 \cdot D_{lungs} + 0.05 \cdot D_{total\ body} + 0.04 \cdot D_{heart} + 0.01 \cdot D_{testes}$$

**Equation 4.1**

Neither the thymus nor active bone marrow or the spleen are included in the above equation. Although not considered to be 'nodes', these tissues are regarded primary organs of the lymphatic system [249]. It is unclear what the impact of these assumptions in lymph node locations is. Currently, evidence of an association between lymphoma and radiation exposure is limited [7, 45] and it is not possible to determine which tissues need to be irradiated to induce this disease (if indeed this is possible).

PCXMC does not allow circular or irregularly shaped x-ray fields and cannot be used to assess the impact of beam equalising filters such as lung 'shutters' designed to adjust for the lower density of the lungs compared to the mediastinum. Nor does PCXMC allow organ density to be changed, meaning it is not possible to examine the impact of contrast enhancement on doses. This is not a trivial matter. Research suggests organ doses from CT scans can vary by 10-100% depending on contrast agent administration, due to the effect on tissue density [250, 251]. The issue of contrast agents is also discussed in the 'Future Research' chapter.

Aside from featuring pre-set 'standard' phantoms representing different age groups, PCXMC allows the height and mass (i.e. weight) of these phantoms to be adjusted over a limitless range. To account for increased mass, the program adopts a cosmological inflation model in which all organs expand like balloons, visceral organs and bones alike (Figure 4.2). This approach is unsupported by evidence and has no basis in reality. Some level of pathological enlargement of some viscera can occur (e.g. cardiomegaly, hepatomegaly or emphysema) and rare conditions in which bone

enlargement occurs also exist (e.g. Paget's disease), but never in the manner suggested by PCXMC. The primary reasons for altered mass for a given height are the variable deposition of adipose tissue (fat) and muscle size, neither of which is modelled in PCXMC. Given this limitation, the majority of analysis was restricted to the standard, pre-set phantom sizes based on average heights, weight and thickness of the general population.

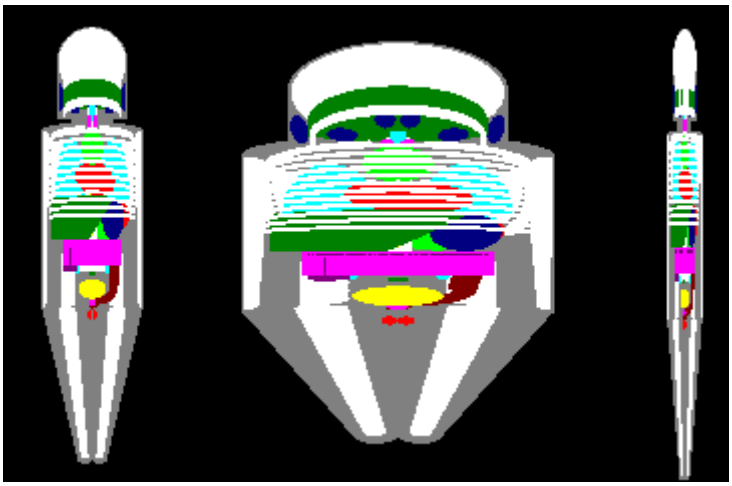

**Figure 4.2: Standard 5 year old phantom (left), adjusted to have a greater and smaller mass for a given height. Note the unrealistic expansion or contraction of bones, especially the skull. Figure credit: author created screengrabs**

PCXMC can be operated automatically using a macro code in Microsoft Excel (2010 edition, Microsoft Corporation, Redmond, Washington). The 'Autocalc' macro [252] allows relevant parameters such as patient and beam characteristics to be inputted in an Excel worksheet. A particular combination of parameters can simply be copied and pasted as multiple rows in the workbook to produce a large number of simulations in which a single parameter, such as beam angle or energy, is adjusted one step at a time. This is ideal for simulation of doses over a large range of beam angles and energies. The initial autocalc macro code restricts simulations to a 16° anode angle, copper and aluminium filtration and 20,000 photons per simulation, but these parameters can be changed by editing the macro script.

For effective dose and equivalent dose to most organs, simulation errors were found to decrease with increasing phantom age (Figure 4.3). These errors were generally less than 3% for effective dose and doses to certain tissues such as bone marrow and lymph nodes and heart (Figure 4.4). Errors were much higher for tissues receiving relatively low doses due to being located well outside the irradiated field,

such as the thyroid (up to 80%) and testicles (up to 100%). Thyroid dose errors increased with increasing phantom age (Figure 4.5). This is most likely to be due to increased distance from the irradiated field and hence lower dose due to scattered radiation.

Dose errors for tissues lying deep to the entrance surface, such as the breasts in postero-anterior (PA) beam projections, were higher than those for tissues lying close to the entrance surface. As these tissues are of interest in risk modelling and epidemiological analysis, measures to reduce large errors were investigated. It was found that increasing the input dose simply resulted in a linear scaling of calculated organ doses and did not affect estimated error. Increasing the number of simulated photon interactions *does* result in a decrease in error (Figures 4.3 to 4.6), but also increases the simulation time (2, 7, 15 and 150 seconds per simulation for 10, 50 and 100 thousand and 1 million photons respectively). Figures 4.3 to 4.5 also show the doses for each photon count. These figures are almost identical at a given phantom size for the heart, in which errors are below 3%. However a large variation in breast and thyroid dose is apparent depending on the number of photons used in the simulation.

The autocalc macro defaults to simulation for all photon energies, up to 150 keV. Simulation time can be reduced by editing the macro to restrict simulated photons to match the tube potentials being investigated. A maximum mean error of 3% for effective dose and 10% for breast dose could be achieved using 40,000 photons for phantoms adult, 15 and 10 year old patients, while 50,000 photons were sufficient for the 5 year and 1 year phantoms. For the neonate phantom, 100,000 photons were used. These simulations were used for initial investigations on the effects of changes to various parameters. For the final dosimetry system (described in Chapter 5), a set of ‘reference’ data based on single beam energy combination was used. For the reference data, a lower level of error was desired, and simulations were run using 1 million photons (50 times the pre-set level). These simulations took over two weeks to complete, running day and night. The result was simulation errors being reduced to generally less than 1%.

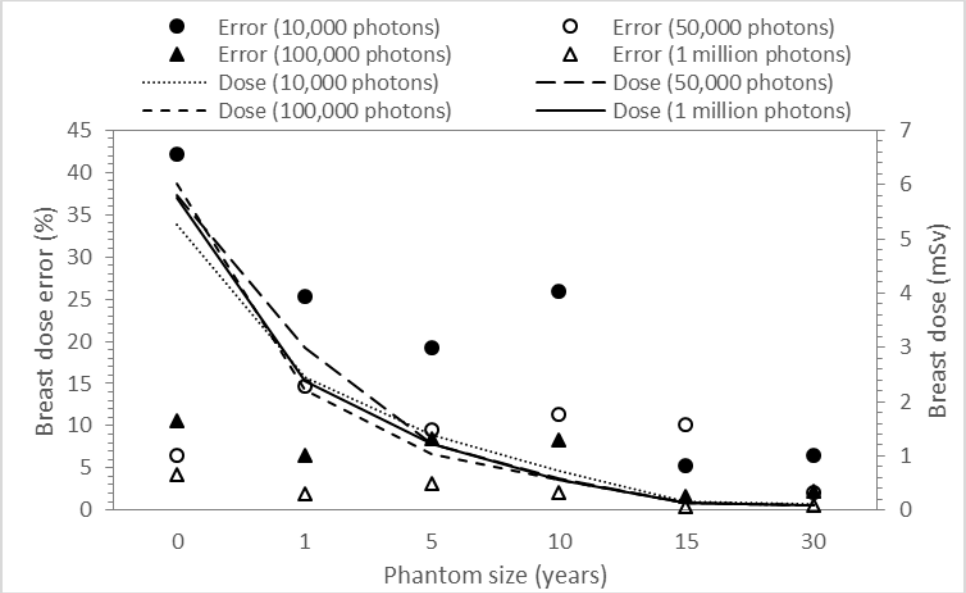


Figure 4.3: Breast dose simulation errors at each phantom age for different number of simulated photons.

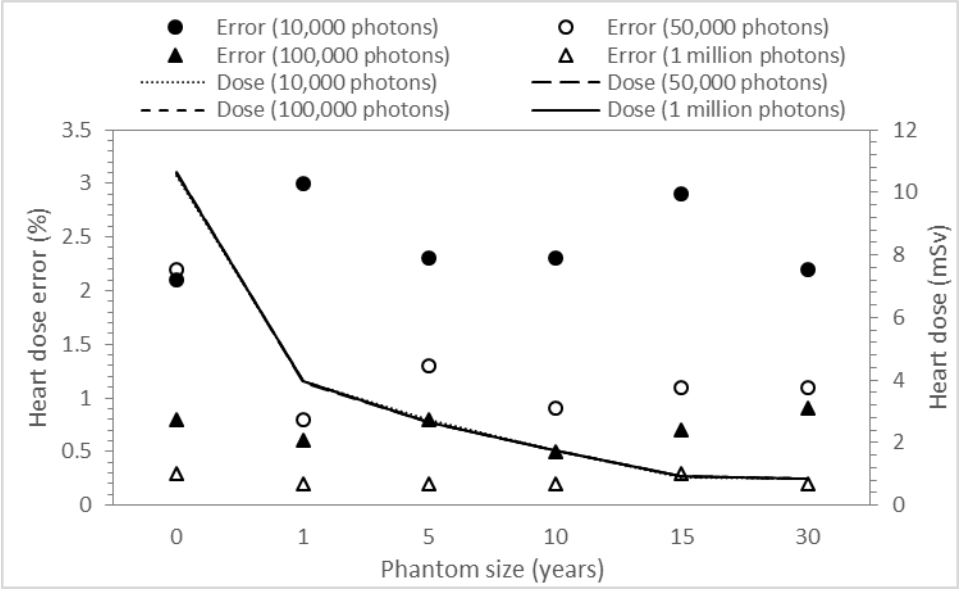


Figure 4.4: Heart dose simulation errors at each phantom age for different number of simulated photons.

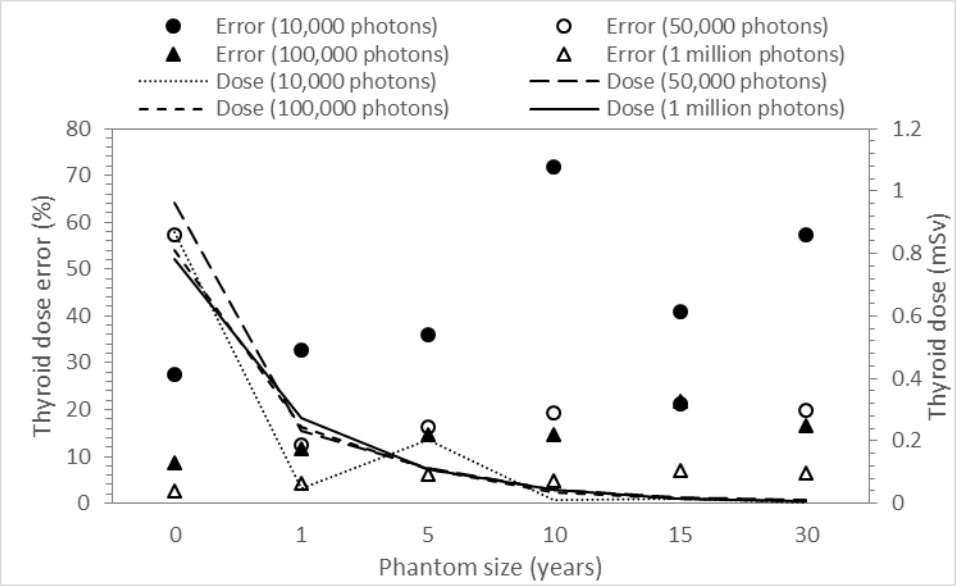


**Figure 4.5: Thyroid dose simulation errors at each phantom age for different number of simulated photons.**

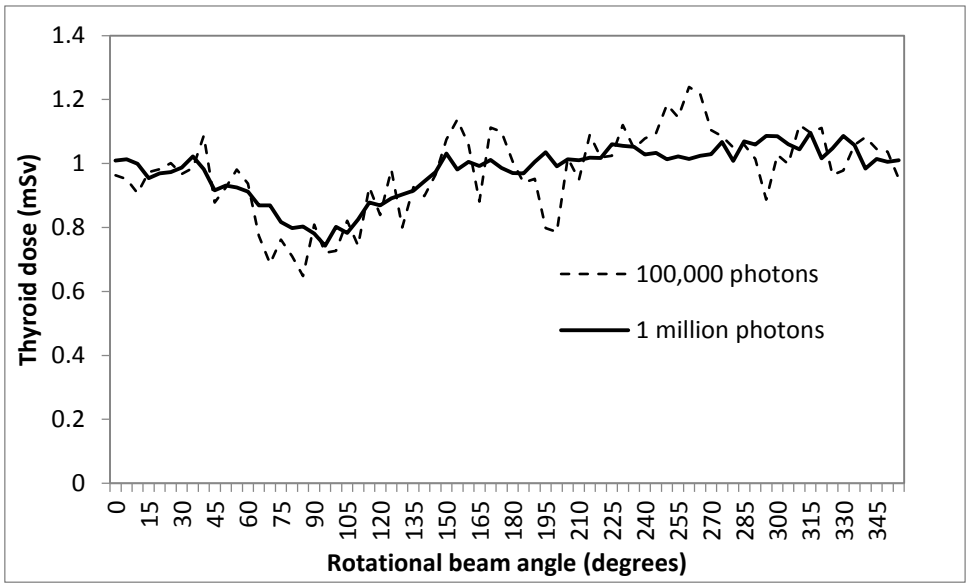


**Figure 4.6: Thyroid dose as a function of beam angle for 0 year phantom at 70 kVp and 0.2 mm Cu for simulations using 100,000 and 1 million photons (mean errors of 10.1 and 2.5%, respectively). The latter simulations were used as reference data.**

It is easy to accidently calculate and input doses calculated from previous simulations. To avoid this possibility, each simulation was given a unique identification number, and simulation files were deleted after doses were calculated and inputted into Excel spreadsheets.

The input dose for simulations was always in the form of kerma area product, set at 1000 mGy·cm$^2$ (1 Gy·cm$^2$), meaning that the results were always presented as equivalent organ doses (in mSv) per unit $P_{KA}$ (PCXMC uses the units of 'mean organ dose' in mGy). Changes to the following parameters were investigated:

- Beam angle in both rotational (around the patient) and cranio-caudal (head to foot) directions
- Central ray location
- Field size (collimation)
- Focus-skin distance (FSD) – the distance between the x-ray source and the patient.
- Beam energy (tube potential and filtration)
- Patient size (the six phantom sizes in Table 4.1)

Initially, the x, y and z beam coordinates were adjusted to ensure that the heart was in the centre of the irradiated field for all angles. Beam area was set to include the entire heart and a small surrounding region (Figure 4.7). The arms were omitted from the phantom for all projections (in clinical practice, the arms are elevated above the head to avoid obscuring the heart in the lateral projection). The focus-skin distance was initially set at 80 cm. PCXMC uses a default anode angle of 16°. This was changed to 12°, based on manufacturer's specifications for fluoroscopy equipment from used equipment vendors [253]. In particular, an anode angle of 12° is used for Siemens Axiom Artis units, which were the most commonly used fluoroscopic machine at participating hospitals. The impact of using different anode angles was also investigated.

For this thesis, the beam angle (or projection angle) terminology described in Appendix 1 will be used. A 'posteroanterior' (PA) beam projection is one that enters the back and exits the front, an 'anteroposterior' (AP) beam is the reverse of this. In bi-plane machine, both PA and AP projection utilise the frontal x-ray tube. A 'left lateral' beam enters the right hand side and exits the left. These correspond to rotational beam angles of 90°, 270° and 180° respectively in PCXMC. A distinction is made between 'PA orientated projections', meaning beam angles that are approximately in the PA projection, and 'straight PA' which means exactly PA and achieved with a vertical beam which the patient supine. A similar distinction is made between 'laterally orientated' and 'straight lateral' projections. It should also be noted

that cardiologists often refer to the PA projection as ‘AP’ [86]. This convention will not be used in this thesis.

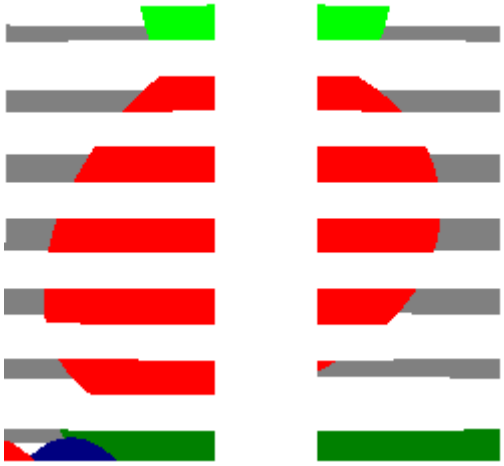

**Figure 4.7: The exposed region for new-born child in PA projection (90°). The lungs are not shown. The dark green feature below the heart is the stomach, the white bars represent the ribs and spine, while the light green shape above the heart is the thymus. Figure credit: author created screengrab**

Rotational beam angle was investigated as a function of full 360° rotation around the patient in 5° intervals, resulting in a set of 72 Monte Carlo simulations. Each of these sets was repeated at different cranio-caudal beam angulations ranging from 55° caudal to 55° cranial (also in 5° intervals). Greater angulations in either direction were not calculated, as the head or pelvis is projected over the heart rendering the image clinically useless. The combination of rotation around the patient and cranio-caudal angulations produced 1656 simulations representing a near complete range of possible beam angles. This ‘full projection set’ was the starting point from which all other changes to parameters were investigated.

To investigate the impact of changes to beam energy, peak tube potential in kilovolts (kVp) was varied from 50 to 100 kVp at 10 kVp intervals. The typical range in clinical practice was around 58-90 kVp (see Chapter 6: Supporting Data). Aluminium filtration was kept constant at 2.5 mm, while copper (Cu) filtration was set at 0, 0.1, 0.2, 0.3, 0.6 and 0.9 mm for each tube potential interval. Thus 36 different combinations of beam energy were investigated. The impact of beam energy on organ doses was calculated for all 1656 projection angles to determine whether conversion factors needed to be projection specific or could be applied as a single figure regardless of beam angle.

The effect of variation in patient size was investigated by calculating doses for the 6 different pre-set phantoms listed in Table 4.1. For each of these phantom sizes, doses were calculated for the full set of 1656 projection angles and 36 different beam energy combinations. This resulted in a total of 1656 * 36 * 6 = 357,696 different MC simulations. Further investigation of the effect of patient size was difficult due to the unrealistic manner in which PCXMC handles changes to mass for a given height. If the mass is increased, the heart size is also increased, meaning the beam area must be adjusted to include the same region. Nonetheless, some separate simulations were carried out to assess the potential effect of under- or overweight patient characteristics on dose estimates. Phantom mass was adjusted to approximate 5$^{th}$ and 95$^{th}$ percentiles of body mass index (BMI) obtained from the Royal College of Paediatrics and Child Head (RCPCH) [254]. BMI is not used for children below 2 years, so for phantoms representing new born and 1 year, the 5$^{th}$ and 95$^{th}$ percentiles of mass were used. The beam area was collimated to the heart border following each size adjustment. This process was repeated for both straight PA and left lateral beam projections.

To investigate the effects of changes to focus-skin distance (FSD), central ray location and field size, a reduced set of beam angles were used, with intervals in the cranio-caudal direction increased to 10°. Beam energy was restricted to a central value of 70 kV and 0.2 mm Cu filtration, and extreme values of 50 kV/0.0 mm Cu and 100 kV/0.9 mm Cu. All investigations were carried out using each of the 6 pre-set phantom sizes.

Changes to field size were investigated by increasing or decreasing the height and width of the field in 1 cm intervals. The relative impact of this 1 cm increase would be larger for smaller patients (i.e. it would cover a greater proportion of the body), so extra simulations were run at ±0.5 cm for the new born phantom. In addition, a separate set of large field simulations were carried out designed to include most of the lungs. Such large field sizes are used in clinical practice to visualise the pulmonary circulation. In these cases, the central ray location was positioned slightly superior to the heart to include the aortic arch and avoid inclusion of the liver and stomach within the primary field.

Focus-skin distance was adjusted over the range of 40-120 cm in 20 cm intervals using the standard field size. The impact of variation in the location of the x-ray beam

central ray was investigated by adjusting x, y and z coordinates in 2 cm intervals until the heart was no longer included within the primary field. This process was repeated for a limited range of beam angles.

## *4.2: Results*

### *4.2.1: Beam angle*

The influence of beam angle on dose was seen to vary considerably between different organs, which are discussed individually below. Note that *situs solitis* is assumed (organs in their normal positions). Some patients may have unusual organ arrangements including *dextrocardia* (right sided heart) [249] and *situs inversus* (all organs are on the opposite side of the body to normal).

The figures showing the effect of beam angle throughout this chapter are presented for over the full range of rotational beam angles, but at a reduced range of cranio-caudal angles to improve clarity. All figures are for a phantom representing a 15 year old individual (56.3 kg). The patterns shown are generally similar for other phantom sizes. Any significant differences are described.

*Bone Marrow:*

Active bone marrow (ABM) is contained within long bones (arms and legs) and the axial skeleton (spine, ribs, skull, and sternum) [255], which is predominantly posteriorly located. In the phantoms used in PCXMC, ABM is uniformly distributed through the matrix of bones [247], rather than being located in the medullary canal or sandwiched between two layers of compact bone as occurs in reality [255]. The distribution of ABM throughout the skeleton, according to data presented by Cristy [256], is taken into account. Equivalent dose to active bone marrow (ABM) (i.e. averaged over all ABM in the body) was found to be higher for PA orientated projections (Figure 4.8). Two peaks in ABM dose either side of the straight PA projection were noted in the results of simulations for phantoms representing 0, 1 and 5 year old individuals (see Figure 4.31 later in chapter), and can be explained by greater inclusion of one scapula (shoulder blade) within the primary beam. These peaks are not seen for 10 year, 15 year and adult phantoms, because the scapulae are so widely spaced that they are not included within the primary beam unless the

field size is especially large (see field size results, later). Compared to other tissue types, ABM dose shows relatively little variation with beam angle in the cranio-caudal direction.

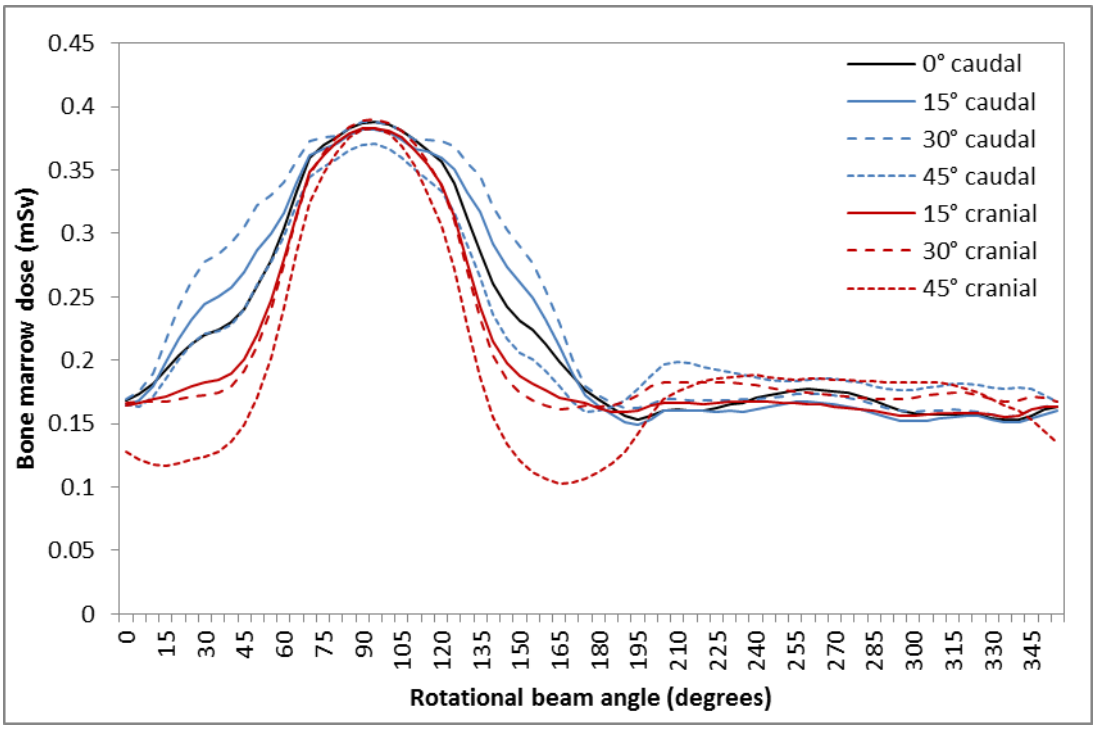


**Figure 4.8: Bone marrow dose per unit $P_{KA}$ as a function of beam angle.**

*Breasts:*

Breast doses are calculated by PCXMC as the mean of both breasts and it is not possible to determine these doses individually. In contrast to ABM dose, breast dose was found to be much higher for AP orientated projections than PA, owing to the more anterior location of the breasts (Figure 4.9). The large dip in breast dose occurring for straight AP projections occurs because the beam passes in between the right and left breasts, excluding both from the primary beam. The transition in breast dose between AP and PA projections is considerably more abrupt than is seen for ABM dose. This is particularly striking between rotational beam angles of 165° and 195° and 345° to 15°, between which breast dose increases by a factor of 13 (56 kg phantom). Breast dose is also sensitive to changes in cranio-caudal beam angulation, being highest where little such angulation is present.

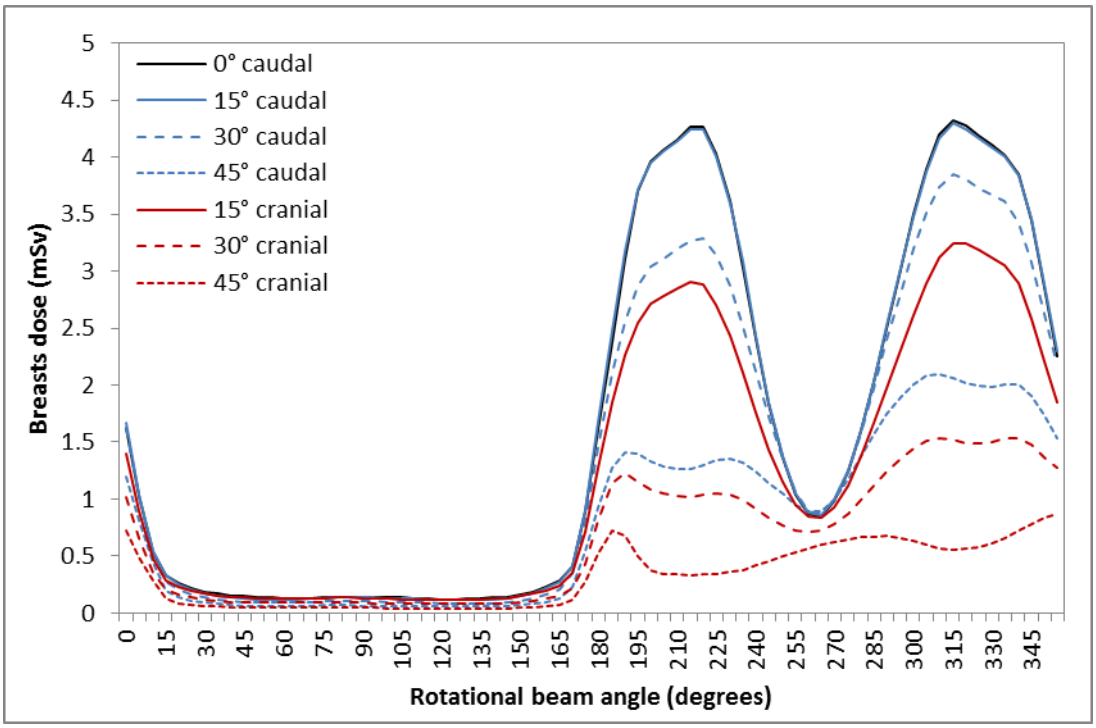


**Figure 4.9: Breast dose per unit $P_{KA}$ as a function of beam angle. Note the pronounced 'cliff' in breast dose between around 170 to 190°.**

At certain ages, a pronounced 'spike' in breast dose was seen at rotational beam angles of around 195-210° (i.e. approximately laterally orientated with some rotation towards the anterior), with a smaller spike at around 350-355° (Figure 4.10). These features were present over the full range of beam angulations in the cranio-caudal direction. The spikes were only noted for simulations using 0 and 10 year old phantoms. Simulation errors were excluded as the cause because the spikes were still present when simulations were run at 1 million photons, where breast dose errors were less than 1% (i.e. a lot less than the size of the spike). It was noted that at the specified beam location coordinates, the irradiated field extended beyond the anterior chest wall. The coordinates of the x-ray beam were adjusted, decreasing the y coordinate so that the beam no longer included the anterior chest wall (Figure 4.11). This was found to eliminate the dose spike. It should be noted, however, that beam angles orientated in the 195-210° range are never seen in clinical practice (these beam angles are described in the 'Supporting Information' chapter, later), therefore the 'spike' was of little consequence in dose estimations for clinical

examinations. The impact of inclusion of the chest wall in the primary beam will be explored further in section 4.2.4.

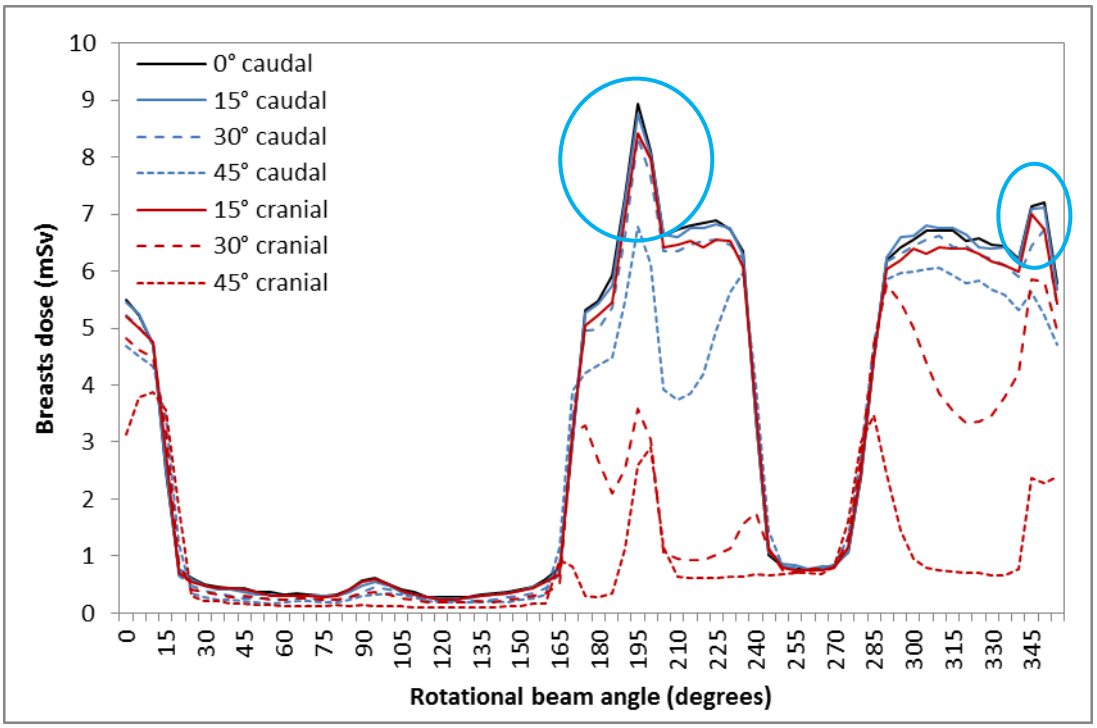


Figure 4.10: Breast dose for 10 year phantom size (32.4 kg) as a function of beam angle, showing spikes.

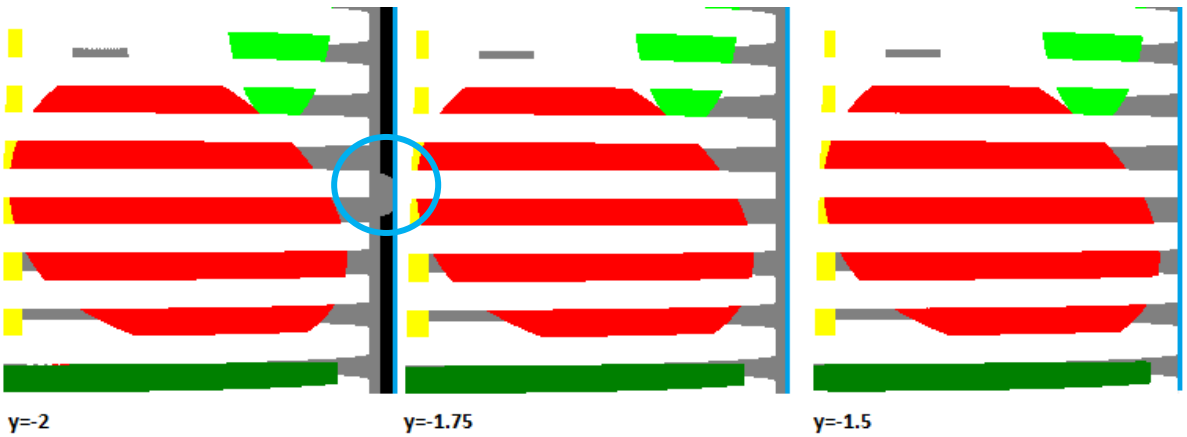


Figure 4.11: Anatomy inclusion at three different y coordinates by beam central ray. The thin blue line on the right hand side of each image delineates the beam edge. The projection of one breast outside the chest wall (blue circle) appears to be the cause of the dose spikes. Image credit: author screengrabs

*Heart:*

The heart is an anterior lying organ, found slightly to the left of the midline. Consequently, heart dose is higher for AP orientated projections (between around 220-300° in PCXMC) and higher for right lateral than left lateral projections (Figure 4.12). In clinical practice, it is common to use beam projections in which the heart is closest to the detector to reduce magnification distortion and geometric unsharpness (i.e. PA and left lateral projections). This means the heart is shielded to some extent by other organs and dose is often lower than the lungs or breasts, despite the organ being located entirely within the irradiated field. For almost all rotational angles, dose to the heart was found to be greater where no cranial or caudal beam angulation was present. This is because cranio-caudal angulation increases the thickness of preceding tissue traversed by the beam before the heart is reached.

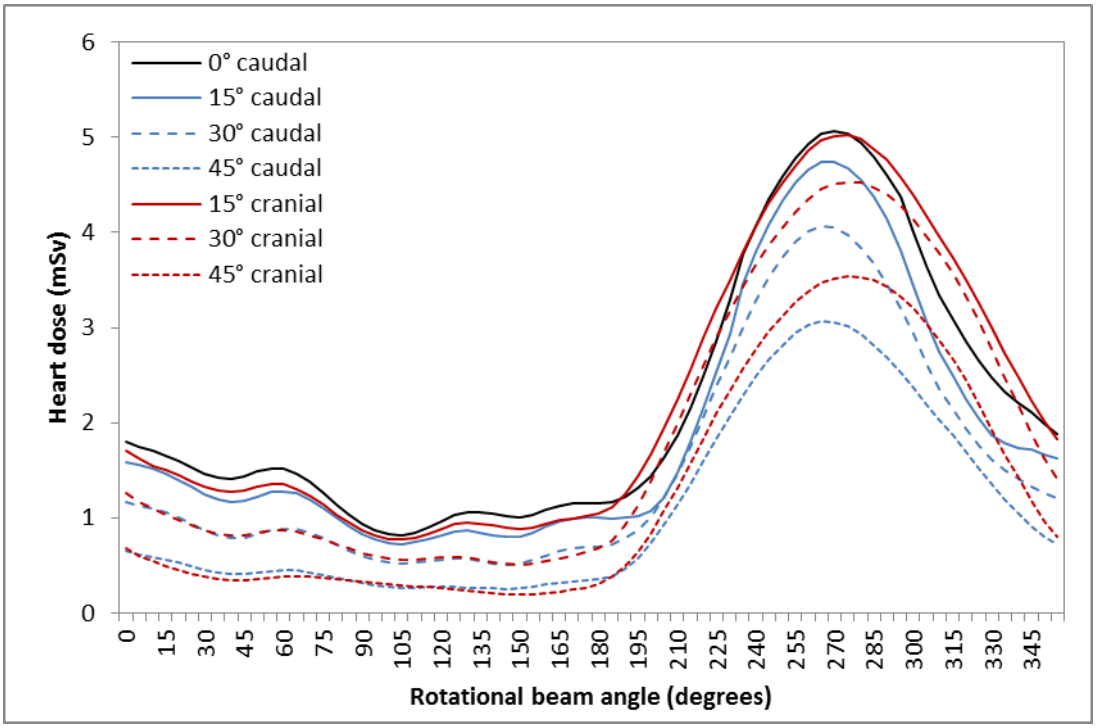


**Figure 4.12: Heart dose per unit $P_{KA}$ as a function of beam angle.**

*Liver:*

The liver lies inferior to the heart and is predominantly located on the right hand side of the body [249]. Consequently, liver dose is highest in the left lateral projection. Liver dose was found to be especially sensitive to changes in cranio-caudal angulation compared to other organs (Figure 4.13). A particularly striking feature of

Figure 4.13 is the peak in liver dose occurring with cranial angulation and a rotational angle between 130-200°, in which case the beam passes through the liver before reaching the heart. Such beam angles are rarely used in clinical practice, however.

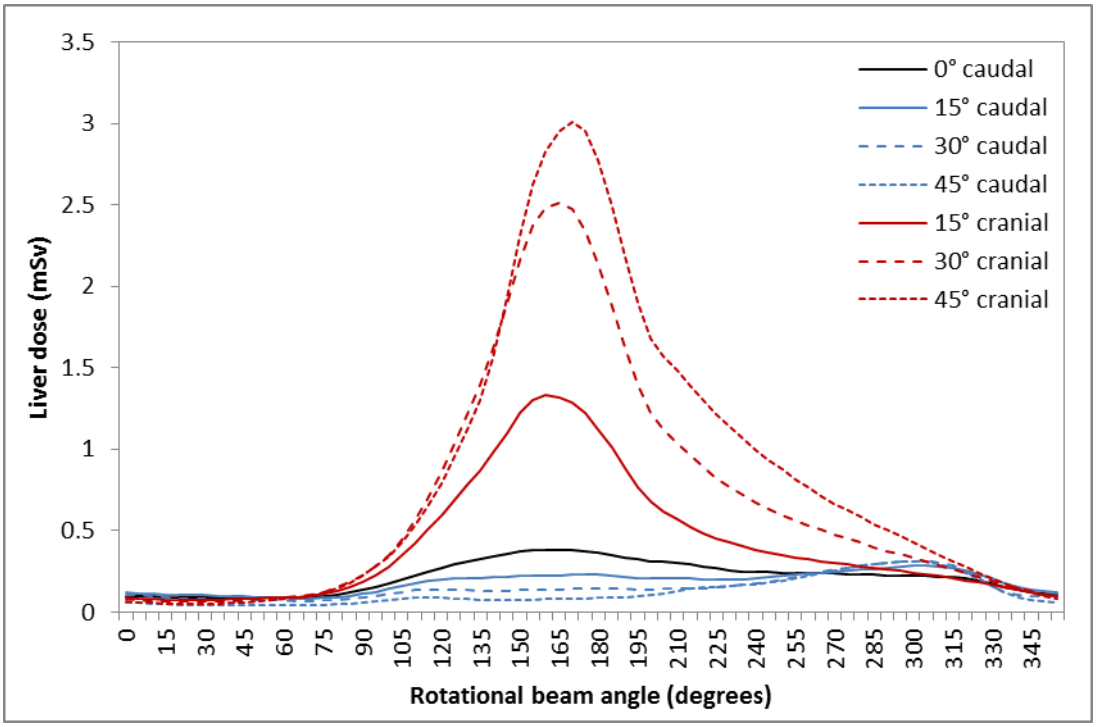


**Figure 4.13: Liver dose per unit $P_{KA}$ as a function of beam angle.**

*Lymph nodes:*

As the organs used to estimate dose to this tissue are spread around the body, lymph node dose shows relatively little variation with beam angle compared to other tissues (Figure 4.14). Caudally orientated beam projections resulted in lower doses per unit $P_{KA}$ than cranially orientated beams. Dose per unit $P_{KA}$ is generally low and comparable to that for bone marrow. It was noted earlier that neither active bone marrow nor the thymus are included in lymph node dose calculations in PCXMC, despite both being regarded as principle organs of the lymphatic system [249]. The thymus is located in the anterior and superior mediastinum, close to the heart, though sometimes extending superiorly as far as the thyroid [249] (seen in Figure 4.1 as the light green feature). The organ thus lies within the primary beam during cardiac catheterizations. The importance of the thymus in radiocarcinogenesis is currently unknown, however.

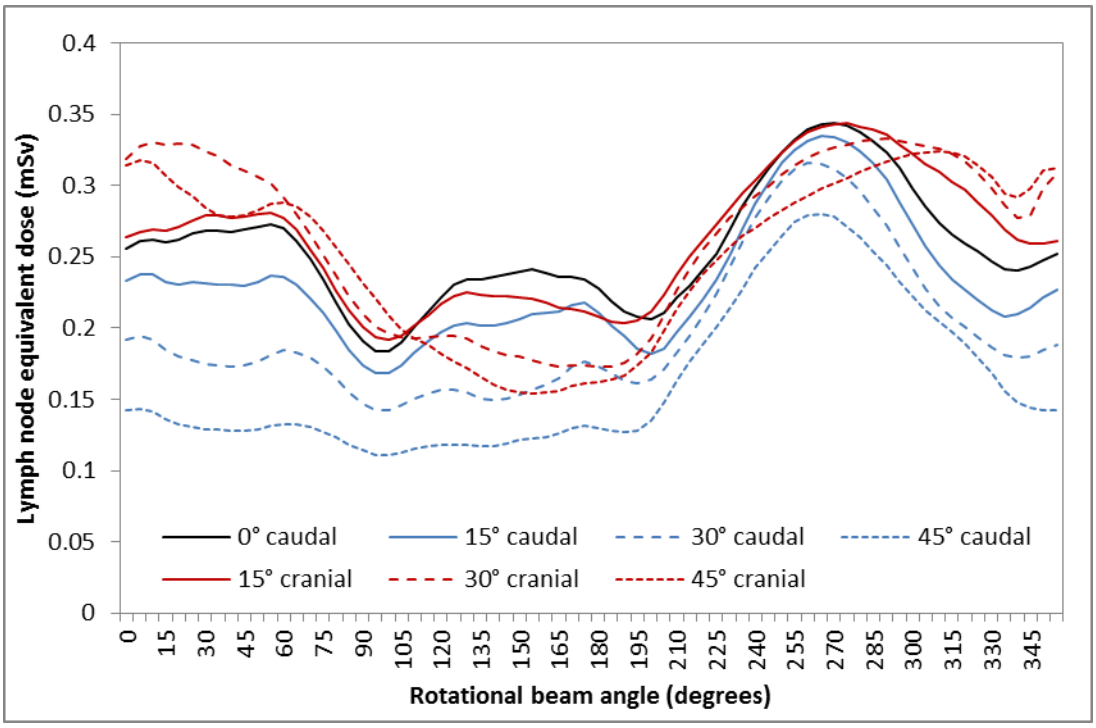


**Figure 4.14: Lymph node dose per unit $P_{KA}$ as a function of beam angle.**

*Lungs:*

Pronounced dips in lung dose per unit $P_{KA}$ were seen for straight PA and AP orientated projections in which exclusion of the lungs from the primary field is greatest (Figure 4.15). Overall, doses were higher in PA orientated projections, as a greater volume of the lungs is found in the posterior half of the body. Dose in left-laterally orientated projections was higher than for right laterals as the right lung is larger due to the presence of the heart on the left. Like the heart, doses were also higher for beams in which no cranial or caudal angulation was present. Lung doses were generally among the highest of all organ doses, regardless of projection angle.

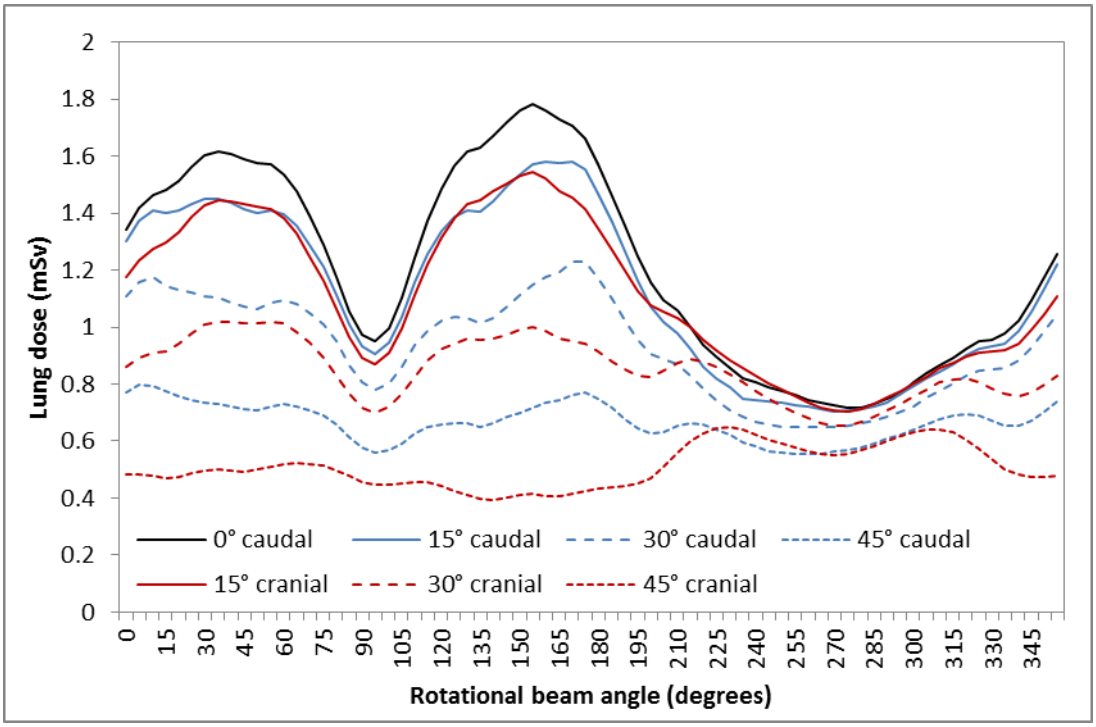


**Figure 4.15: Lung dose per unit $P_{KA}$ as a function of beam angle.**

*Oesophagus:*

The oesophagus is fairly centrally located, found anterior to the spine and posterior to the heart. It is within or close to the primary beam in most projection angles, though is always shielded to some extent by other organs. This shielding effect increases where cranio-caudal beam angulation is applied (Figure 4.16). In PCXMC, the oesophagus is modelled as being exactly central and directly anterior to the spine. In reality, the oesophagus may deviate to one side [257], in which the shielding provided by the spine for PA-orientated projections would be less. Thus oesophagus dose may be underestimated by PCXMC.

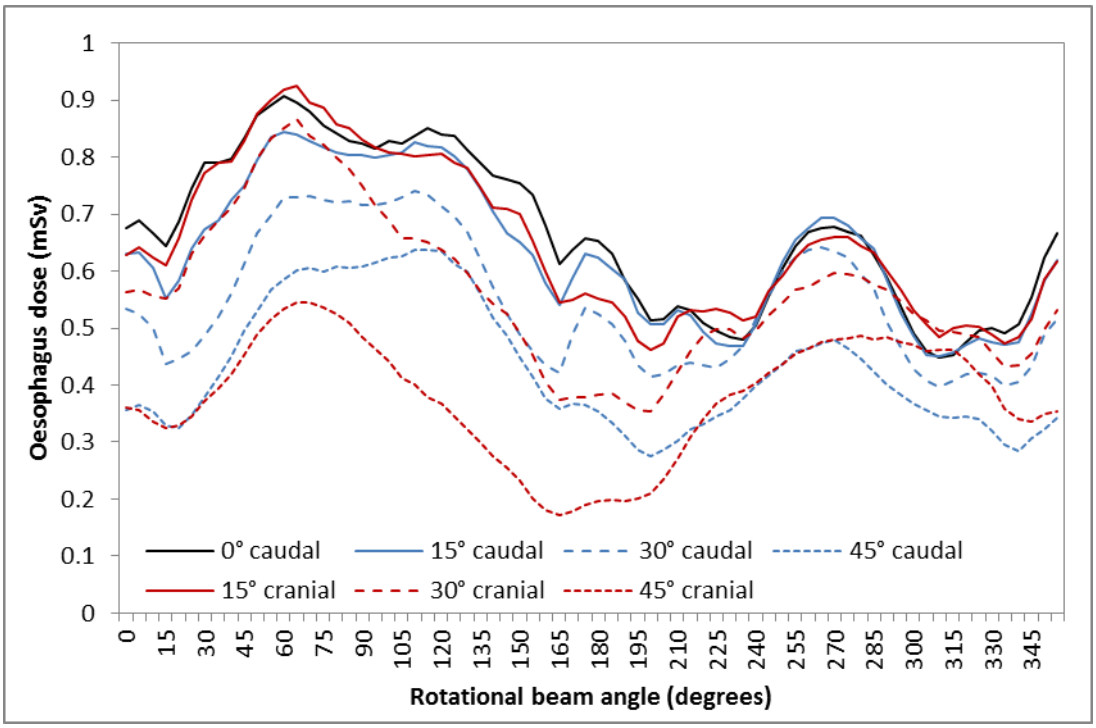


**Figure 4.16: Oesophagus dose per unit $P_{KA}$ as a function of beam angle.**

*Stomach:*

Like the liver, the stomach is located inferior to the heart and thus receives greater doses in cranially orientated projections (Figure 4.17). In contrast to the liver, stomach dose is higher in right lateral projections, owing to its predominantly left sided location. The stomach is approximately 'J' shaped in humans, however its size and shape is highly variable, tending to increase in the cranio-caudal dimension and decrease in the anterior-posterior dimension with increasing ponderal index (a measure of how 'lean' a person is) [258]. Tall, thin people have tall, thin stomachs. This variation is not reflected in the PCXMC mathematical phantoms, in which the stomach is modelled as an ovoid (dark blue in Figure 4.1). However, the pattern of higher stomach doses with cranial beam angulation should still be valid.

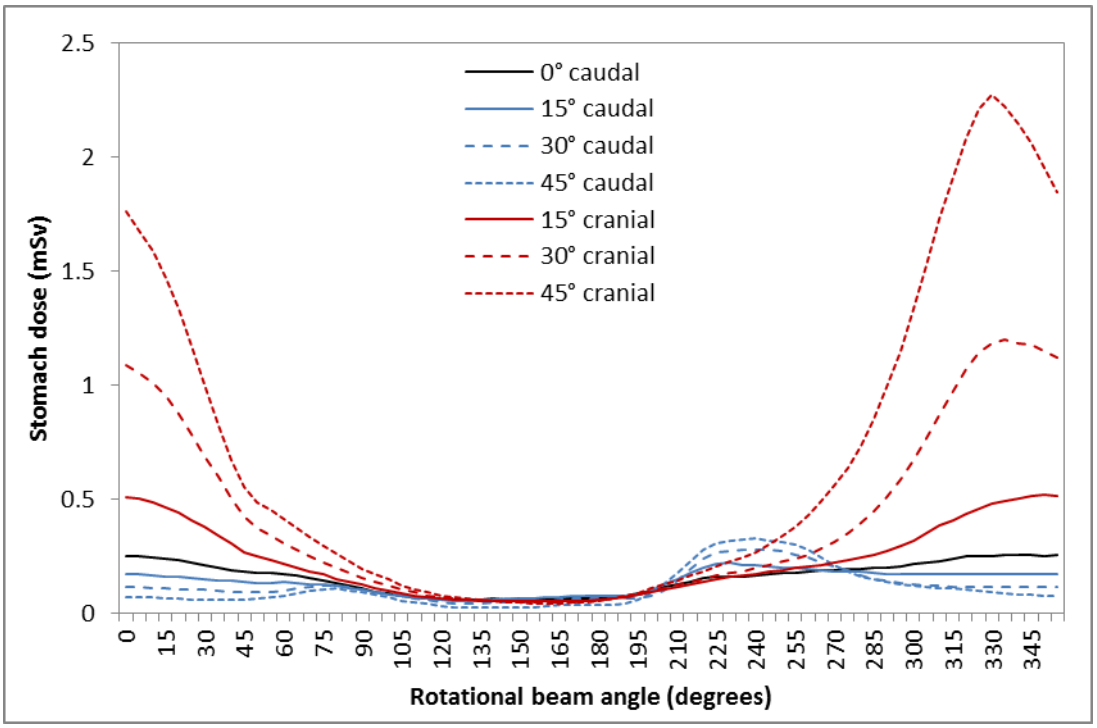


**Figure 4.17: Stomach dose per unit $P_{KA}$ as a function of beam angle.**

*Thyroid:*

The thyroid gland is located anterior to the trachea and superior to the sternal notch and should not be included in the primary radiation field in normal practice (although one study found cases where this did sometimes occur [259]). Consequently, thyroid dose is low, and almost entirely due to scattered radiation (extrafocal and leakage radiation are not simulated in PCXMC but are accounted for in physical measurements, described in a later chapter). Doses were found to be highest with large levels of cranial beam angulation (Figure 4.18), where the thyroid is closest to the primary field. Where the beam is angled cranially, thyroid dose is highest in laterally orientated projections, while for caudal beam angles dose is highest in AP and right posterior oblique orientated projections (Figure 4.19)

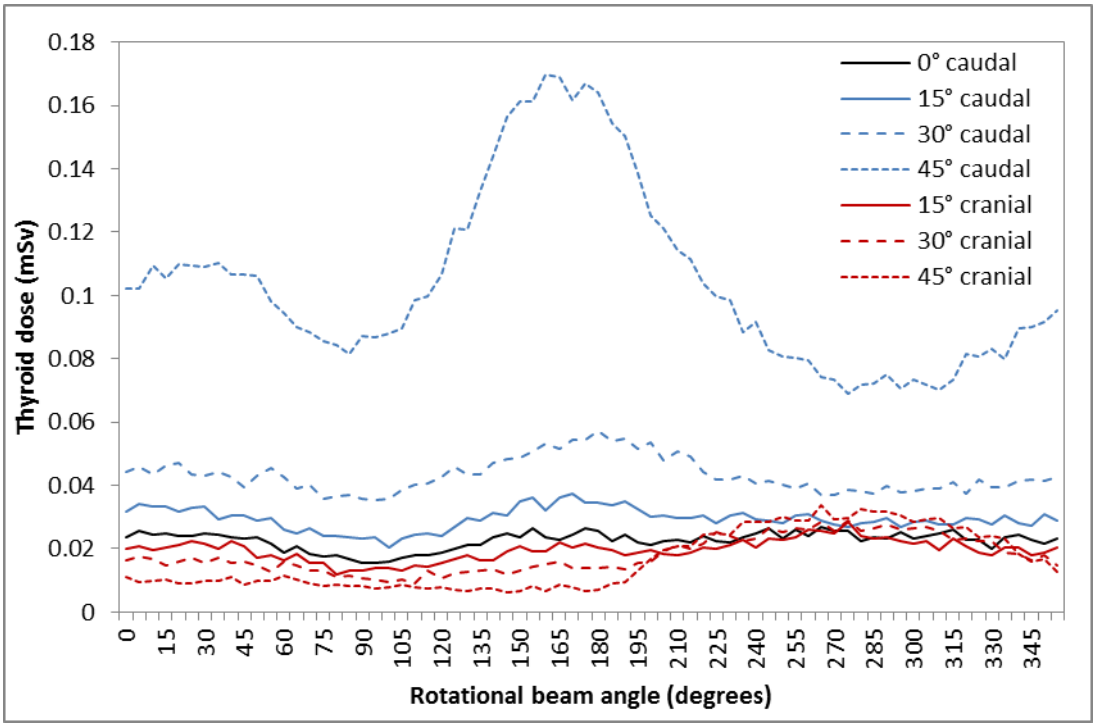


**Figure 4.18: Thyroid dose per unit $P_{KA}$ as a function of beam angle.**

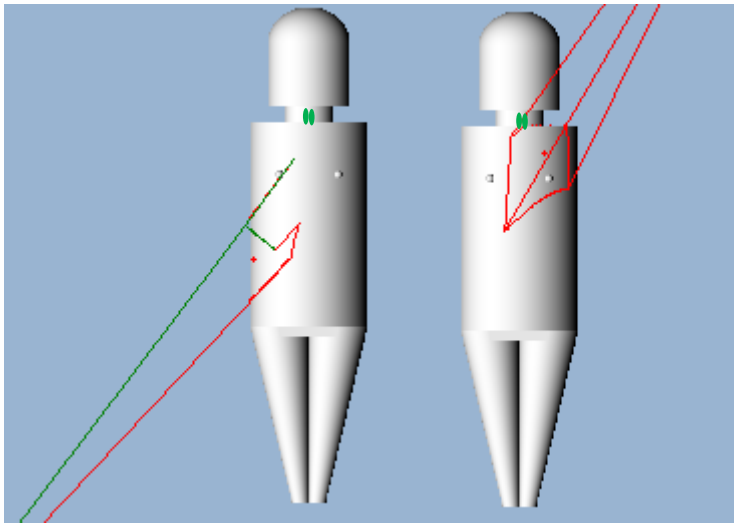

**Figure 4.19: Beam projections at which thyroid dose is highest (1 year old phantom). The position of the thyroid is shown (the green feature under the head). Image credit: author generated PCXMC screengrab**

*Gonads:*

The testes and ovaries are located well outside the primary radiation field for cardiac catheterizations and receive minimal scattered dose. Where femoral catheterization is used, the pelvic area may be briefly imaged for catheter guidance, although this

should not be necessary for most patients [259]. Calculated doses were almost zero, even for the most caudally angulated beam projections (i.e. those in which the gonads would be closest to the primary field).

*Effective dose:*

The effective dose (E) is strongly influenced by breast dose, owing to the proximity of the breasts to the irradiated field and the high tissue weighting factor (0.12 in ICRP 103 [44]). This can be appreciated by comparing Figure 4.9 and Figure 4.20 – the shape of the two curves is similar, though variation in effective dose with beam angle is less pronounced than for breast dose. Overall, there is a tendency for effective dose to be higher in more anteriorly orientated projections than posterior. As with the heart and lungs, effective dose per unit $P_{KA}$ is higher where no craniocaudal angulation is present. With large levels of cranial or caudal angulation, the variation in effective dose with rotational beam angle was found to be reduced. It should also be noted that effective dose is higher by around 20% for cardiac exposures where ICRP 103 [44] weighting factors are used as opposed to ICRP 60 [67]. This is principally due to the increased weighting for the breasts (0.12 instead of 0.05) and the inclusion of the heart into the 'other' tissue category.

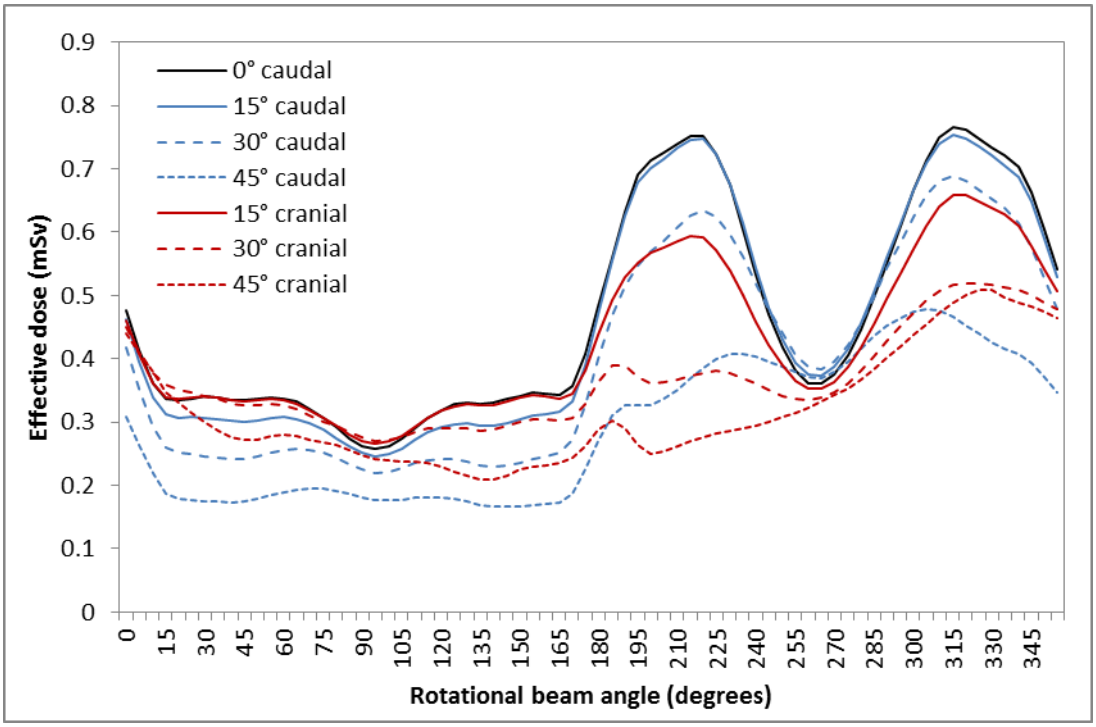


**Figure 4.20: Effective dose per unit $P_{KA}$ as a function of beam angle. Note the presence of the 'cliff' between170 to 190° and the dip between 220 and 290°, also seen for breast dose.**

*Average absorbed dose:*

The average absorbed dose to the whole body was also calculated. This was done to allow comparison with effective dose (which could also be considered a form of 'whole body' radiation dose measurement) and for use in risk models. Unlike effective dose or doses to individual organs, average absorbed dose was virtually independent of beam angle in either direction (Figure 4.21). Average absorbed dose was lower than effective dose by an average factor of around 1.8 across all beam angles and patient sizes. For beam angles commonly used in cardiac catheterizations, this factor is slightly reduced to around 1.7 (see Chapter 8). The difference between effective and average whole body dose illustrates the impact of the high density of radiosensitive organs in proximity to the heart. If such calculations are repeated for exposures of the extremities, the average absorbed dose is found to be higher than effective dose (for example, for a knee radiograph, the average absorbed dose calculated by PCXMC is higher than effective dose by a factor of 18).

By multiplying the average absorbed dose by phantom mass, the total energy imparted to the body, in Joules (J) can be estimated. The energy imparted per unit $P_{KA}$ increases slightly as phantom size is increased from 3.4 to 73.2 kg (0 to 30

years), ranging from 8.0 to 13.1 mJ  at 70 kV and 0.2 mm Cu, as a greater proportion of the beam is attenuated with greater material thickness.

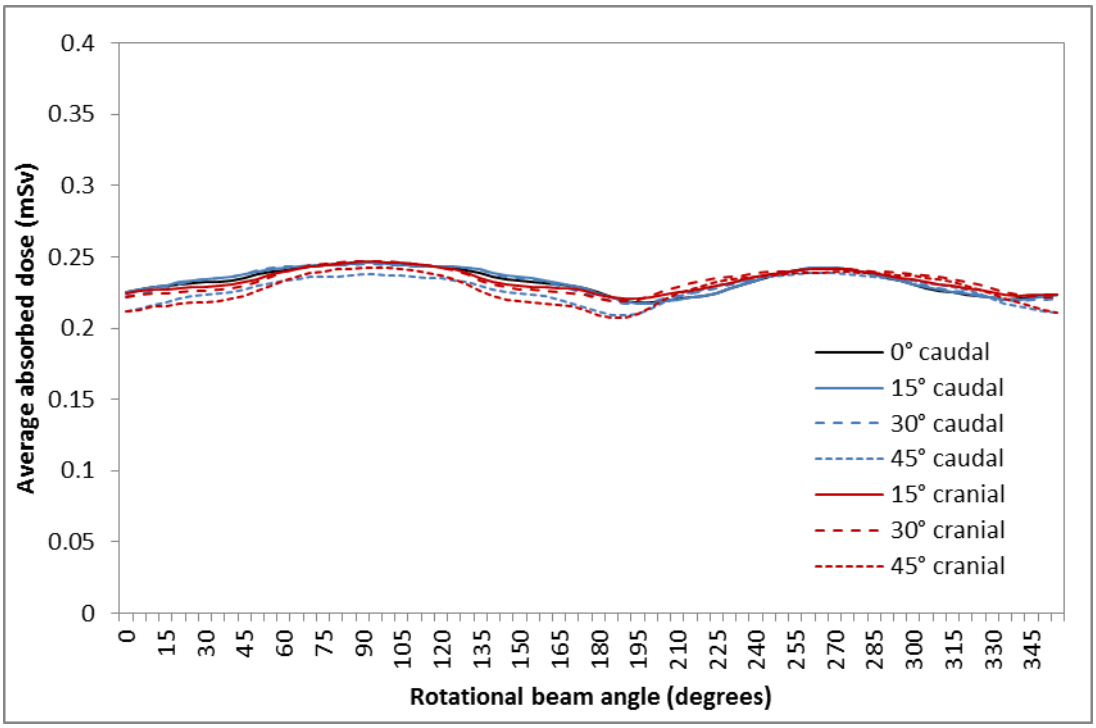


**Figure 4.21: Average absorbed dose per unit $P_{KA}$ as a function of beam angle**

### *4.2.2: Beam energy*

Doses to all organs per unit $P_{KA}$ were found to increase with increasing beam energy. This pattern can be characterised in different ways; by considering individual parameters affecting beam energy separately (i.e. tube potential, filtration and anode angle) or by using a single figure in which beam quality is characterised by the thickness of a given material required to reduce beam intensity by 50% - the so-called half-value layer (HVL), usually given in millimetres of aluminium (Al). The former measure is more informative while the latter is more convenient. In this study, HVL was calculated using SpekCalc [260], a commercially available program utilising Monte Carlo data calculated by Poludniowski and Evans [261, 262]. This allows calculation of beam spectra and associated half value layer from a range of parameters including tube potential, anode angle and thickness filters of various materials including air, aluminium and copper. The HVL methodology has a number of limitations. The same HVL can be achieved using very different parameters

(Figure 4.22). For example, a 1st HVL of around 3.5 mm Al is achieved using a tube potential of 110 kV with 2.5 mm Al filtration, and also using 40 kV, 2.5 mm Al and 0.9 mm copper filtration. The 2nd HVLs (i.e. the thickness reducing intensity by a further 50%) for these two situations are very different, at 5.75 and 3.62 mm respectively. The low kV situation results in a beam spectrum lacking the high kV 'tail' and is entirely due to Bremsstrahlung, with no characteristic emissions. As the patient is not made from aluminium, the characterisation of x-ray beams according to their interactions with aluminium is an approximation and can lead to errors in dose estimation (see Section 5.2).

When characterising by kV and filtration separately, the increase in organ dose with beam energy follows a pattern well described by a logarithmic or 3$^{rd}$ order polynomial (Figure 4.23). The rate of increase declines as beam energy is increased. The marginal increase in organ dose per unit $P_{KA}$ is especially large with initial addition of copper filtration (i.e. increased from zero to 0.1 or 0.2 mm). The effect of varying anode angle was generally small, with dose per unit $P_{KA}$ increasing by little more than 1% for each degree decrease in angle. The effect of beam energy on dose varied between organs (Figure 4.24), being greater for the thyroid, stomach and liver – tissues located mostly, or entirely, outside the primary field of irradiation - than for more evenly distributed organs such as bone marrow or the lungs. The implication of this finding is that corrections to adjust doses for beam energy must be organ specific. It was also found that the impact of changes to beam energy also increased with increasing phantom size. Examples of the ratio in dose between different beam energies are shown in Table 4.2. This implies that energy corrections must also take patient size into account.

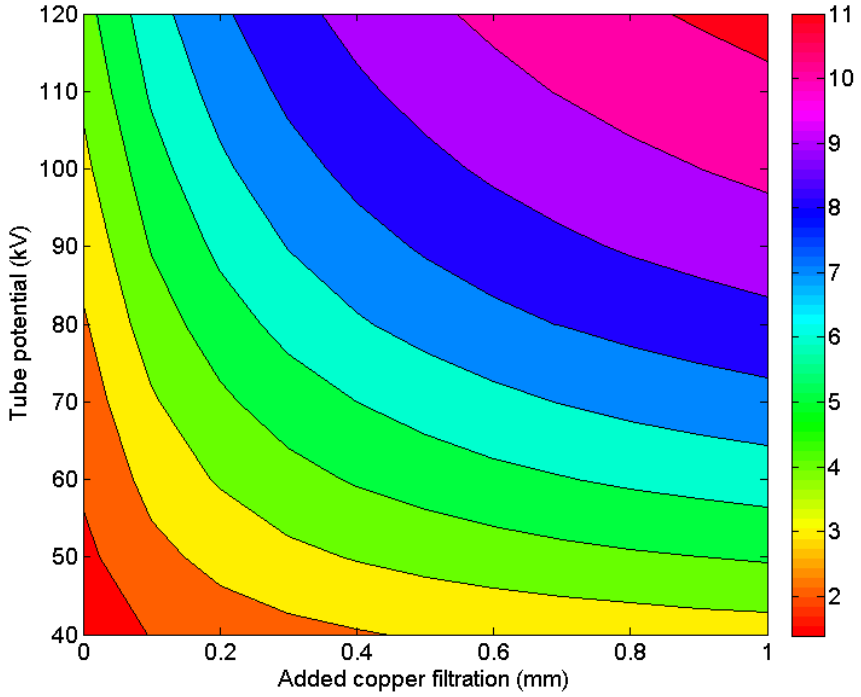


Figure 4.22: Using half value layer (HVL) to describe beam energy. Colours represent HVL in millimetres of aluminium as a function of tube potential and added copper filtration (assuming 2.5 mm Al filtration).

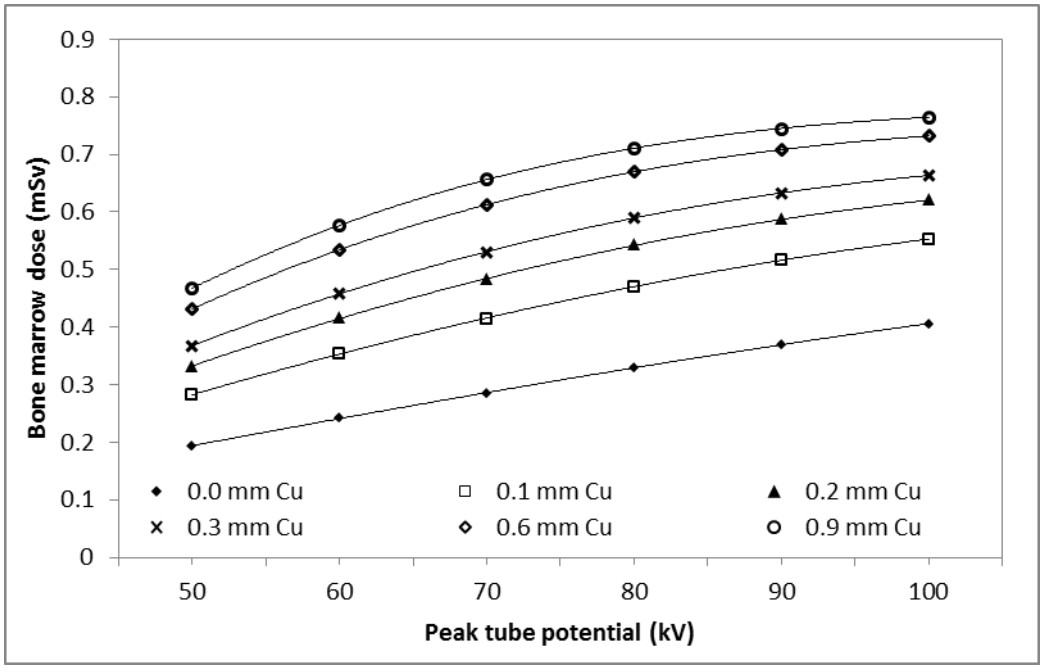


Figure 4.23: Bone marrow dose as a function of beam quality for various combinations of tube potential and added copper filtration. The phantom size is 10 years and beam angle is straight PA. Third order polynomial trend lines have been fitted.

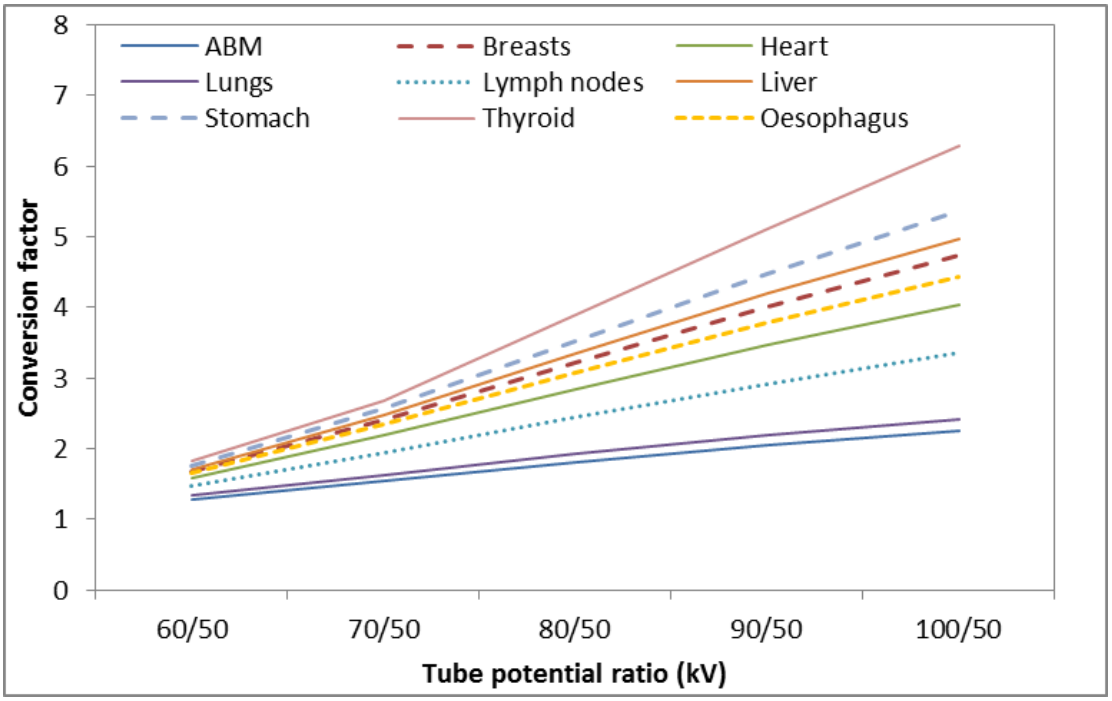


**Figure 4.24: The ratio in dose to different organs between high and low beam energy levels, represented by tube potential. Phantom size = 56 kg (15 years), beam angle is straight PA.**

| | Dose ratio | | |
|---|---|---|---|
| **Phantom size (kg)** | **Bone marrow** | **Breasts** | **Lungs** |
| 3.4 | 1.89 | 1.30 | 1.18 |
| 9.2 | 2.34 | 1.48 | 1.27 |
| 19.0 | 2.35 | 1.90 | 1.35 |
| 32.4 | 2.50 | 2.19 | 1.41 |
| 56.3 | 2.49 | 2.32 | 1.59 |
| 73.2 | 2.59 | 2.38 | 1.62 |

**Table 4.2: Ratio between dose at 100 kV/0.9 mm Cu and 70 kV/0.2 mm Cu for bone marrow, breasts and lungs for each phantom size. Beam angle is straight PA.**

The variation in dose with beam energy was also seen to be dependent on beam angle. This is best visualised by plotting the ratio between two beam quality values as a function of beam angle (Figure 4.25). The variation is greater for more unevenly distributed tissues (e.g. breasts and heart), i.e. these organs are found towards one side of the body (the anterior) rather than being evenly spread throughout the torso.

In the case of characterising by HVL, the variation in dose can also be described by a polynomial equation, although the closeness of fit is not precise (Figure 4.26). The

data points appear to be scattered around the polynomial in a seemingly random way, albeit with greater deviation as HVL is reduced towards 1.7 mm Al (corresponding to 50 kV, 2.5 mm Al and 0.0 mm Cu filtration). This distribution was explored in greater detail by plotting dose against HVL, while labelling data points according to filtration level. This showed that the distribution followed a more predictable 'saw-tooth' pattern (Figure 4.27). It was also noted that deviation of data points from the polynomial increased with increasing phantom size.

The average absorbed dose to the whole body increases with increasing beam energy, but the proportion of the beam absorbed correspondingly decreases (Figure 4.28). The rates of these changes vary with patient size; the rate of increase in average absorbed dose with beam energy increases with increasing patient size (Figure 4.29), while the decrease in the fraction of beam energy absorbed by the patient decreases with increasing patient size (Figure 4.30).

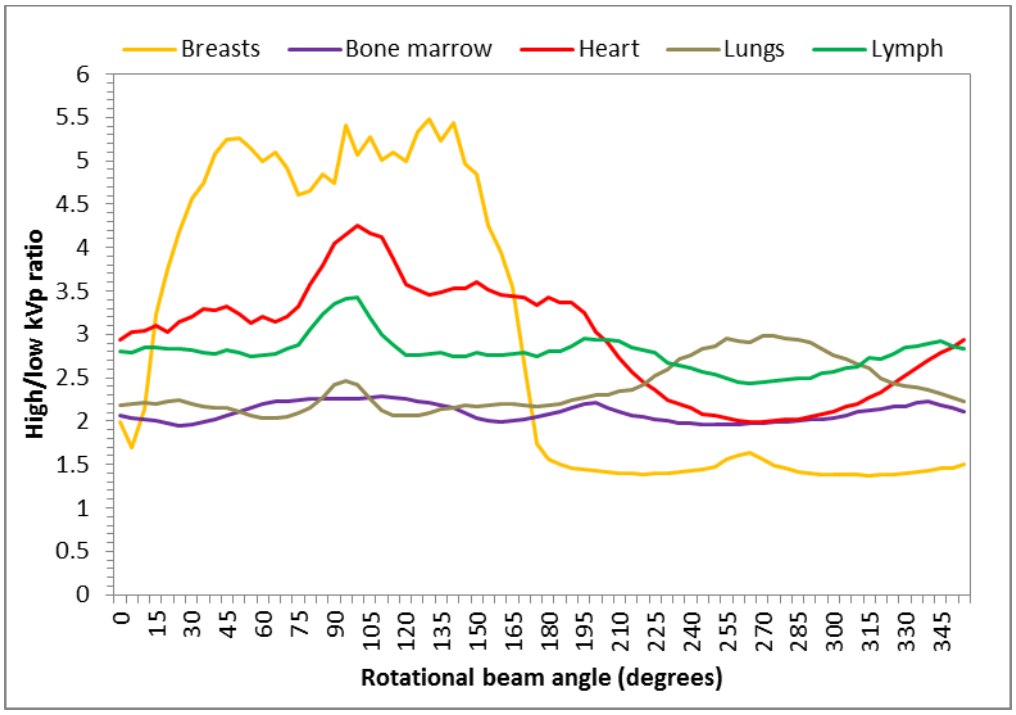


**Figure 4.25: Ratio between dose at 100 kVp and 50 kVp (0.0 mm Cu filtration) as a function of beam angle for different tissues. Phantom size is 15 years.**

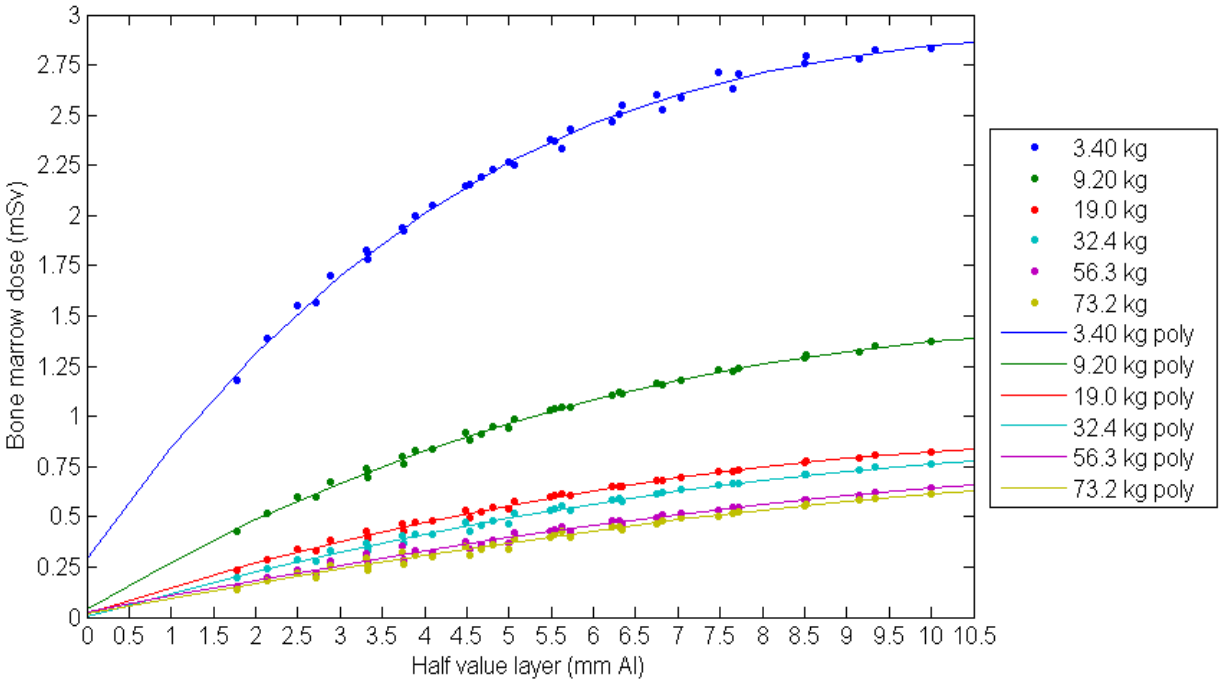


**Figure 4.26: Bone marrow dose as a function of half value layer for 6 phantom sizes. Third order polynomial trend lines have been fitted.**

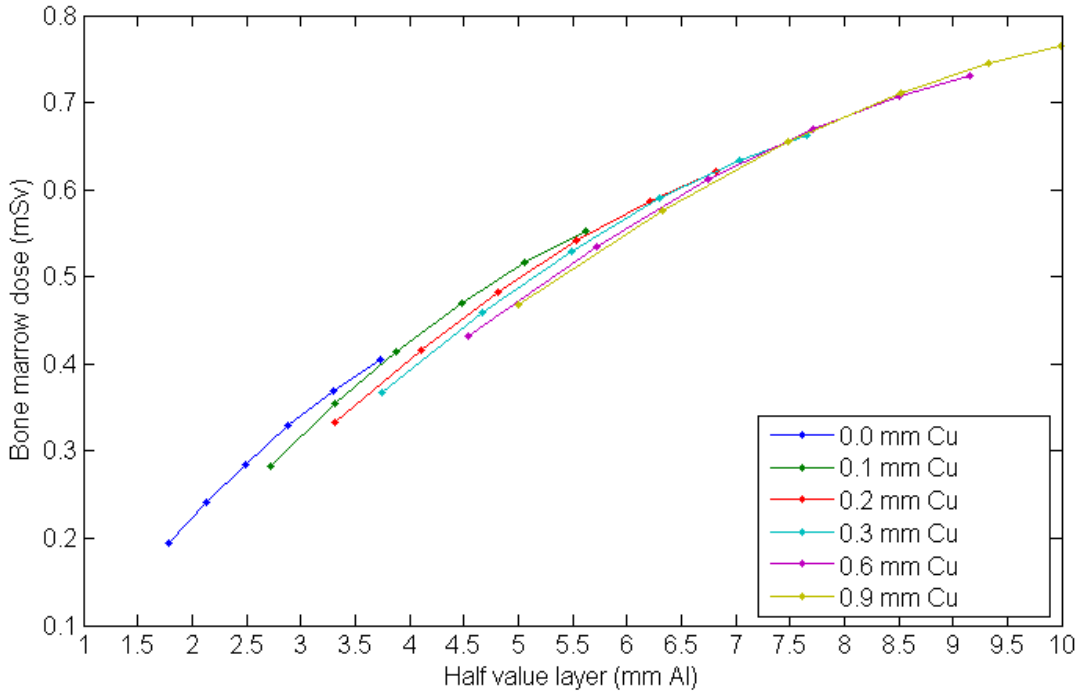


**Figure 4.27: Bone marrow dose as a function of HVL (10 year, 32.4 kg phantom) with different filtration levels displayed in different colours. Successive points for each colour represent different tube potentials, ranging from 50 to 100 kVp in 10 kVp intervals.**

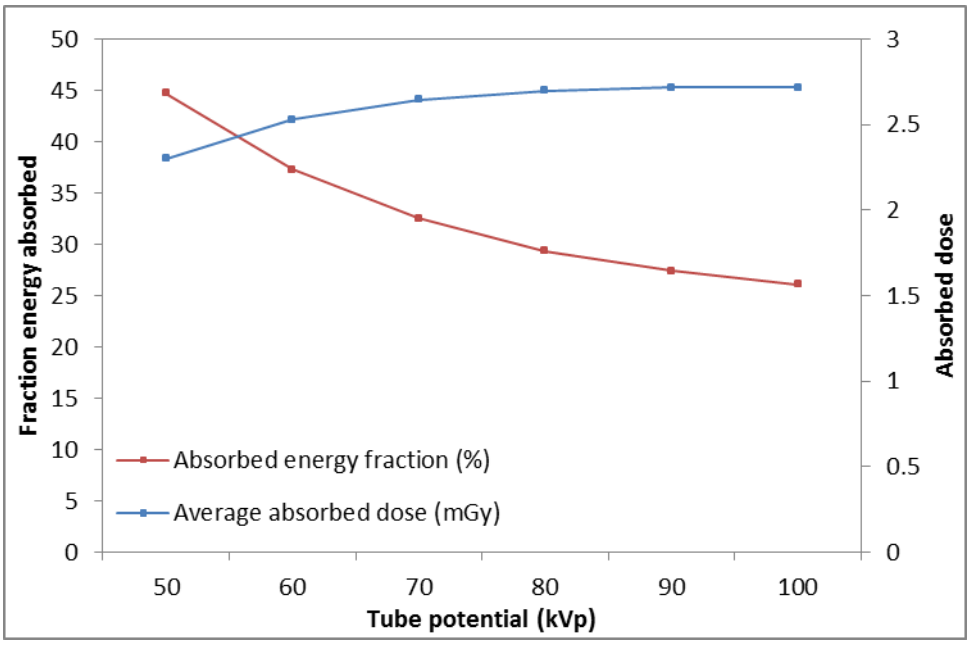


Figure 4.28: Variation in average absorbed dose to the whole body and the percentage of beam energy absorbed by the patient

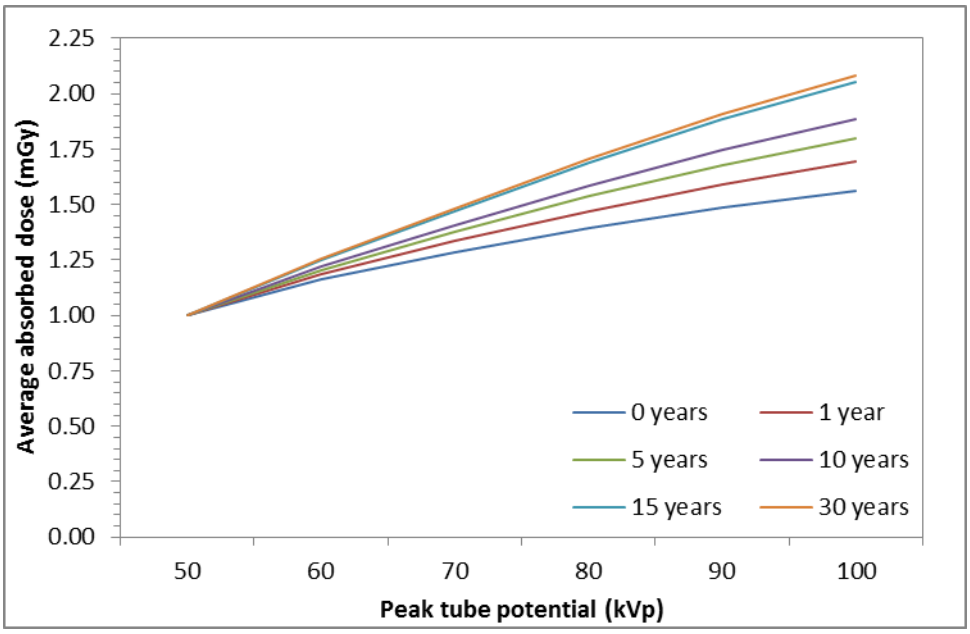


Figure 4.29: Variation in average absorbed dose to whole body with beam energy defined by tube potential, for 6 phantom sizes. Figures are presented relative to dose at 50 kV. Beam angle is 90°, with no cranio-caudal angulation applied (straight PA).

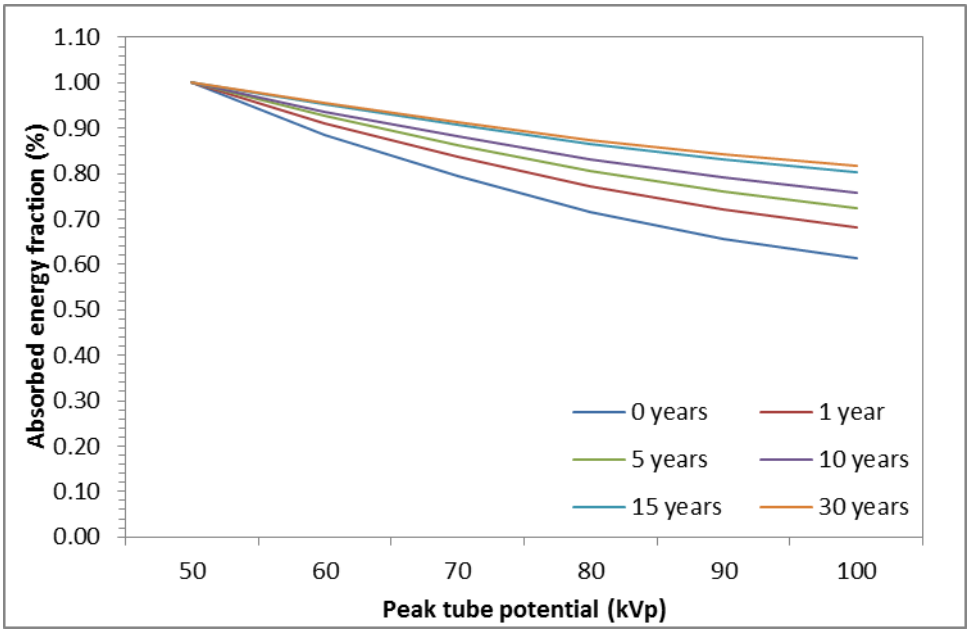


**Figure 4.30: Variation in the fraction of beam energy absorbed with tube potential, for 6 phantom sizes.**

### *4.2.3: Phantom size*

Dose per unit $P_{KA}$ was seen to decrease with increasing phantom size. This pattern was seen for all organs and beam angles. This is demonstrated in Figure 3.31, in which the variation in bone marrow dose with rotational beam angle is shown for each of the 6 simulated phantom sizes. Note that the shape of the curves for each patient size is approximately the same, although some details vary, such as the 'horns' on the peak for smaller phantom sizes (described earlier)

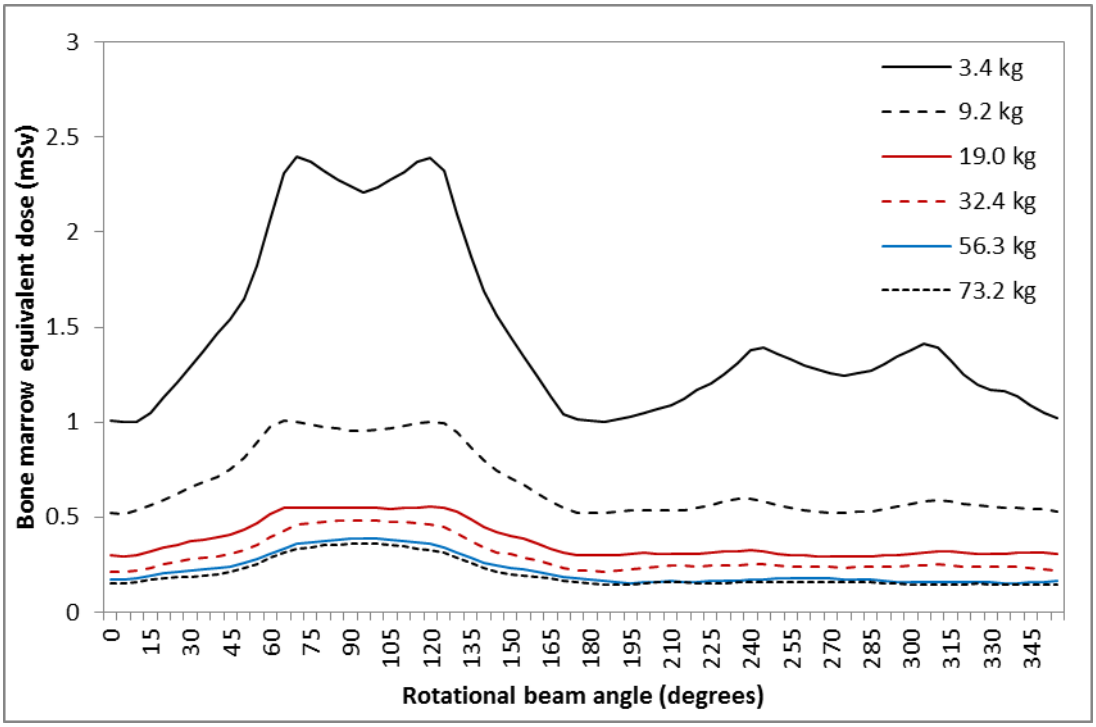


**Figure 4.31: Bone marrow dose as a function of beam angle at different simulated mass levels.**

There are a number of explanations for this pattern. X-rays are attenuated by tissues in a manner described by Beer's law [16], in which intensity (I) is reduced exponentially with increasing thickness (t) of material traversed:

$$I = I_0 e^{-\mu t}$$

**Equation 4.16**

Where $I_0$ is the initial intensity and μ is the linear attenuation coefficient. Thus, if a greater thickness of tissue is traversed before an organ is reached by the x-ray beam, the intensity will be lower. This can be seen in Figure 4.32 where distance A' is shorter than distance A. Consequently, the intensity of radiation at tissues lying close to the surface are higher than those at greater depth. Effectively, for smaller patients, organs lie closer to the surface and thus receive a greater intensity of radiation. As organ size increases, the mean intensity of radiation traversing it decreases. For organs lying partially or wholly outside the irradiated field, such as the stomach or thyroid, the distance between the organ and the field edge decreases with decreasing patient/phantom size. This is demonstrated in Figure 4.32, in which distance between the field edge and the out-of-field organ (B) is greater than the equivalent distance for the smaller patient (B'). The intensity of scattered radiation

reaching such out-of-field tissues would decrease with increasing distance (though not strictly according to the inverse-square-law, due to anisotropy of scatter).

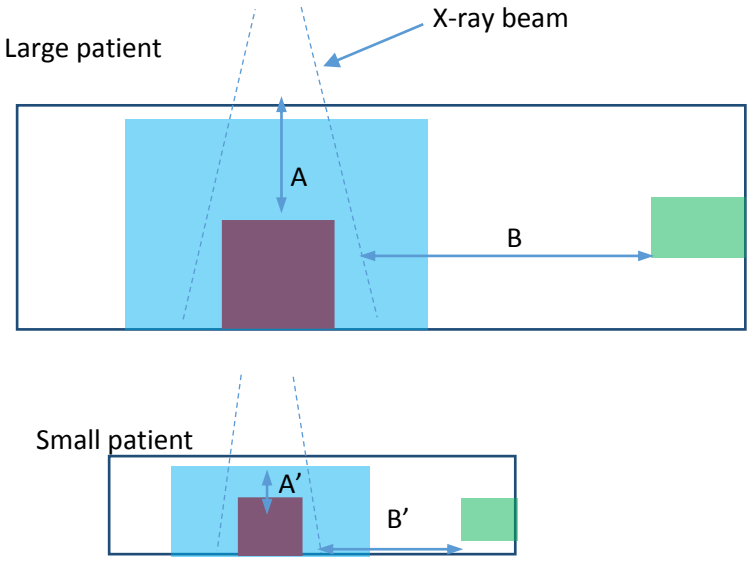


**Figure 4.32: Effect of patient size on organ doses. Entirely in-field (red), partially in-field (blue) and entirely out-of-field organs (green) are shown. Figure credit: author**

The relationship between dose and patient size was investigated by plotting effective dose and organ doses obtained at two different beam angles (90° and 180°, ie. PA and lateral) against mass using SPSS (Version 19, IBM).The beam energy was set at 70 kV and 0.2 mm Cu. Different curves were then fitted (figures 4.33 and 4.34). The closeness of fit for each curve varied between tissue types, although some general observations were apparent. It was found that an exponential curve provided a reasonable fit for masses greater than around 10 kg but tended to underestimate dose below this level. $R^2$ varied from 0.79 to 0.96. A logarithmic curve provided better estimation of doses for low masses, but underestimated doses for masses above around 50 kg (even predicting negative doses in some cases). $R^2$ ranged from 0.90 to 0.95. A power law relationship was found to produce the best overall fit across the full range of masses and did not predict negative doses. $R^2$ ranged from 0.93 to 0.99. Despite all three curve fits being statistically significant for all organs and beam angles tested, for the purposes of this study the closeness of fit was often less than satisfactory. This was to cause difficulties later when an attempt at applying a correction factor for patient mass was made (see Section 5.3 in Chapter 5).

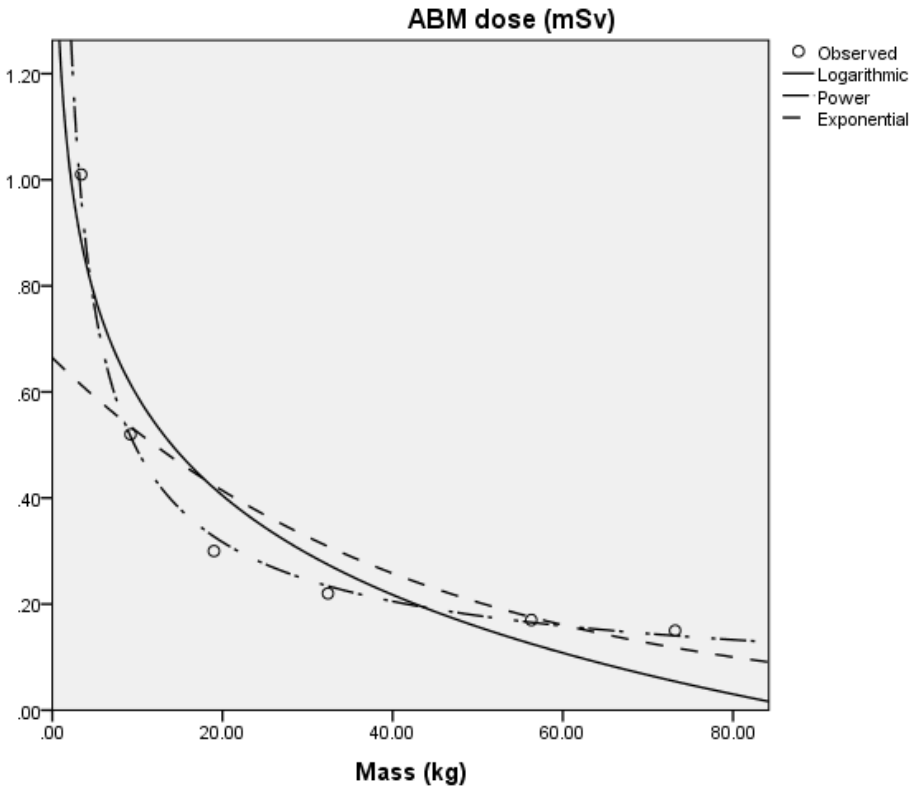


Figure 4.33: Simulated active bone marrow (ABM) dose, in millisieverts (y-axis), as a function of phantom mass with three models fitted (logarithmic, power and exponential). Beam angle = 180 degrees (straight left lateral).

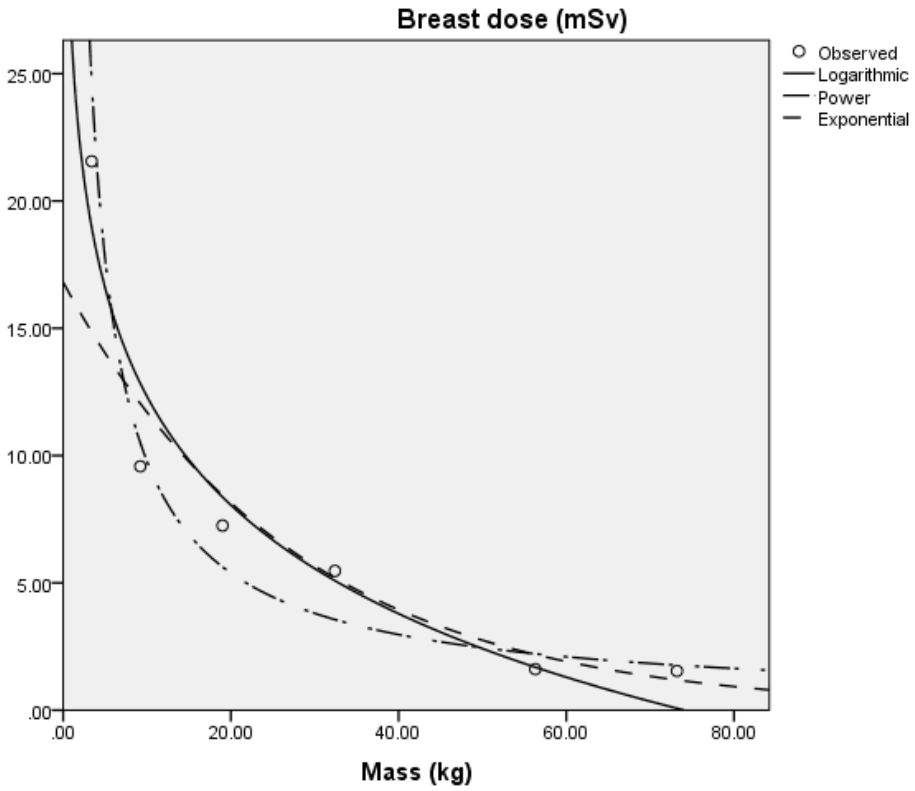


**Figure 4.34: Breast dose (y-axis) in mSv, as a function of mass with logarithmic, power law and exponential curves fitted. Beam angle = 180 degrees (straight left lateral).**

The values of the coefficient and exponent of the power law relationship describing variation in dose with patient mass were recorded as the beam quality was adjusted. Both were found to vary (Table 4.3) albeit in a well behaved manner and describable using a simple logarithmic relationship (Figure 4.35). In theory, this means that a conversion factor to adjust doses calculated at one patient size to any other size could be designed in which beam quality is accounted for. In general, the relative increase in organ dose with increased beam quality was greater as phantom size was increased.

| Tube potential: | 0.0 mm Cu | | 0.1 mm Cu | | 0.2 mm Cu | | 0.3 mm Cu | | 0.6 mm Cu | | 0.9 mm Cu | |
|---|---|---|---|---|---|---|---|---|---|---|---|---|
| | a | b | a | b | a | b | a | b | a | b | a | b |
| 50 kVp | 31.24 | -1.04 | 28.52 | -1.01 | 27.25 | -0.99 | 26.38 | -0.97 | 24.87 | -0.95 | 24.05 | -0.94 |
| 60 kVp | 28.51 | -1.00 | 25.84 | -0.97 | 24.51 | -0.95 | 23.63 | -0.94 | 22.12 | -0.91 | 21.30 | -0.90 |
| 70 kVp | 26.45 | -0.98 | 23.87 | -0.94 | 22.59 | -0.92 | 21.76 | -0.91 | 20.33 | -0.89 | 19.57 | -0.87 |
| 80 kVp | 24.71 | -0.95 | 22.31 | -0.92 | 21.13 | -0.90 | 20.37 | -0.89 | 19.09 | -0.87 | 18.42 | -0.85 |
| 90 kVp | 23.85 | -0.94 | 21.18 | -0.90 | 20.12 | -0.88 | 19.44 | -0.87 | 18.31 | -0.85 | 17.72 | -0.84 |
| 100 kVp | 22.37 | -0.92 | 20.37 | -0.89 | 19.42 | -0.87 | 18.80 | -0.86 | 16.42 | -0.84 | 16.03 | -0.83 |

**Table 4.3: Values of coefficient (a) and exponent (b) of conversion factor to adjust effective dose at 56 kg (15 years) to any other mass, as the level of copper (Cu) filtration and tube potential are adjusted.**

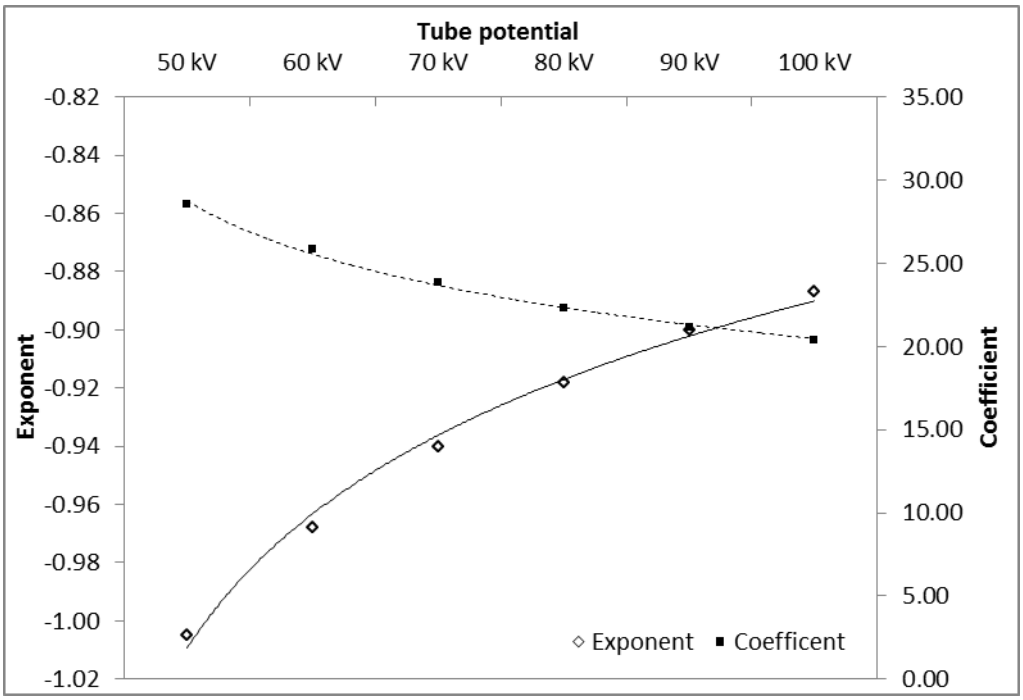


**Figure 4.35: Plot of values from table 4.3 at 0.1 mm Cu filtration with log trend lines fitted.**

The fraction of total beam energy absorbed increases with phantom size, ranging from 44.7% for the new born phantom, to 68.7% for the 30 year old phantom (70 kV and 0.2 mm added Cu filtration).

Analysis of the variation of dose due to changes in mass for a given height is hindered by the unrealistic phantom used in PCXMC. A few interesting observations could be made, however. In almost all cases, organ doses were seen to increase as phantom mass was reduced while height was kept constant, and decrease as mass was increased (Table 4.4). This variation in dose was generally around ±20% with

one standard deviation in BMI or mass. There was no clear relationship between this variation and phantom size. In some cases, thyroid dose was decreased for the smaller phantom BMI and increased for the larger BMI. Presumably this is because thyroid dose is entirely due to scatter originating from primary radiation field, therefore increasing the volume of material irradiated would increase opportunities for scatter.

The implication is that obese patients would receive lower organ doses *per unit* $P_{KA}$ than asthenic patients. Due to the limitations of the computational phantoms used in PCXMC, these findings were not incorporated into central dose estimates or associated uncertainties. Further investigation is required, ideally using patient specific phantoms derived from cross sectional imaging. This would require different Monte Carlo software (e.g. MCNP or GEANT) as PCXMC can only utilise the inbuilt phantoms based on the Christy model.

| Phantom age (mass) | Projection | Size change | Effective dose | Bone marrow | Breasts | Heart | Lungs | Lymph nodes | Oesoph | Thyroid | Liver | Stomach | Mean Dose |
|---|---|---|---|---|---|---|---|---|---|---|---|---|---|
| 0 years (3.4 kg) | PA | -1 SD # | 20% | 14% | 53% | 25% | 18% | 16% | 16% | 4% | 11% | 12% | 16% |
| | | +1 SD # | -16% | -13% | -31% | -23% | -17% | -15% | -16% | 4% | -9% | -5% | -14% |
| | Lateral | -1 SD # | 41% | 17% | 69% | 17% | 17% | 14% | 48% | -13% | 1% | 6% | 15% |
| | | +1 SD # | -26% | -14% | -40% | -19% | -15% | -14% | -8% | -4% | -4% | -8% | -14% |
| 1 year (9.2 kg) | PA | -1 SD # | 21% | 17% | 21% | 34% | 22% | 22% | 26% | 1% | 14% | 12% | 19% |
| | | +1 SD # | -17% | -12% | -40% | -23% | -16% | -15% | -19% | 13% | -13% | -14% | -13% |
| | Lateral | -1 SD # | 36% | 19% | 77% | 26% | 20% | 18% | 12% | 4% | 5% | 16% | 18% |
| | | +1 SD # | -12% | -43% | 85% | -59% | -52% | -56% | -58% | -62% | -46% | -59% | -54% |
| 5 years (19.0 kg) | PA | -1 SD | 27% | 18% | 102% | 33% | 23% | 21% | 26% | -12% | 15% | 17% | 19% |
| | | +1 SD | -18% | -10% | -29% | -22% | -20% | -17% | -17% | -26% | -14% | -13% | -13% |
| | Lateral | -1 SD | 24% | 18% | 32% | 30% | 19% | 20% | 19% | -16% | 7% | 21% | 19% |
| | | +1 SD | 36% | -11% | 131% | -20% | -21% | -19% | -26% | -13% | -7% | -12% | -15% |
| 10 years (32.4 kg) | PA | -1 SD | 17% | 13% | 16% | 24% | 18% | 18% | 22% | 9% | 13% | 11% | 14% |
| | | +1 SD | -25% | -18% | -50% | -34% | -24% | -24% | -24% | 6% | -22% | -25% | -20% |
| | Lateral | -1 SD | 12% | 13% | 3% | 23% | 16% | 17% | 22% | -12% | 5% | 25% | 14% |
| | | +1 SD | -28% | -20% | -56% | -31% | -16% | -17% | 24% | -32% | -10% | -24% | -19% |
| 15 years (56.3) | PA | -1 SD | 20% | 17% | 38% | 35% | 18% | 22% | 26% | -31% | 19% | 15% | 17% |
| | | +1 SD | -23% | -18% | -41% | -34% | -25% | -24% | -24% | -29% | -21% | -20% | -19% |
| | Lateral | -1 SD | 17% | 15% | 17% | 31% | 17% | 19% | 13% | -22% | 7% | 26% | 17% |
| | | +1 SD | -26% | -18% | -41% | -31% | -18% | -21% | -12% | 6% | -9% | -25% | -19% |

Table 4.4: Percentage variation in dose associated with adjusting phantom body mass index (BMI) by 1 standard deviation. # for 1 year and new born phantoms, mass is used rather than BMI.

*4.2.6: Field size*

$P_{KA}$ approximates the absorbed dose to air multiplied by beam area [70]. If $P_{KA}$ remains constant, an increase in field size must be matched by a decrease in dose. Most organs considered in this study are located partly within the irradiated field. For these organs, along with effective dose and average whole body dose, increasing field size increases the volume of the tissue within the field, but decreases dose to that volume. Theoretically, the result is invariance of organ dose per unit $P_{KA}$ with field size. In reality, due to the irregular shape of organs, organ doses do indeed vary with field size. This relationship was found to be complex, varying between different organs and beam angles. The overarching pattern is that increasing or decreasing field size depreciates or intensifies the variation in dose with beam angle, respectively. This can be seen in Figure 4.36, in which effective dose as a function of rotational beam angle is shown for three different field sizes (the 11x11 cm field is the same as that in Figure 4.20). Note that the variation is less pronounced for the largest field size – the 'cliff' between rotational angles of 160 and 190° has become a gentle hill. In this case, effective dose per unit $P_{KA}$ in the left lateral projection would be overestimated if the field size was underestimated.

Of the organs considered in this study, only the heart is entirely included within the irradiated field. In this case, the situation is relatively straightforward - as field size is increased, heart dose per unit $P_{KA}$ decreases Figure 4.37. For tissues lying entirely outside the primary beam, increasing the field size has the effect of decreasing the distance between the tissue and the field edge, and thus increases dose. Of the organs of interest in this study, only the thyroid gland is entirely out-of-field. A clear increase in thyroid dose was only seen for the largest field size, with moderate increases in field size having a negligible effect (Figure 4.38). Overall, field size has an important impact on organ doses calculated from $P_{KA}$ and needs to be taken into account in dose estimations and associated uncertainty analysis.

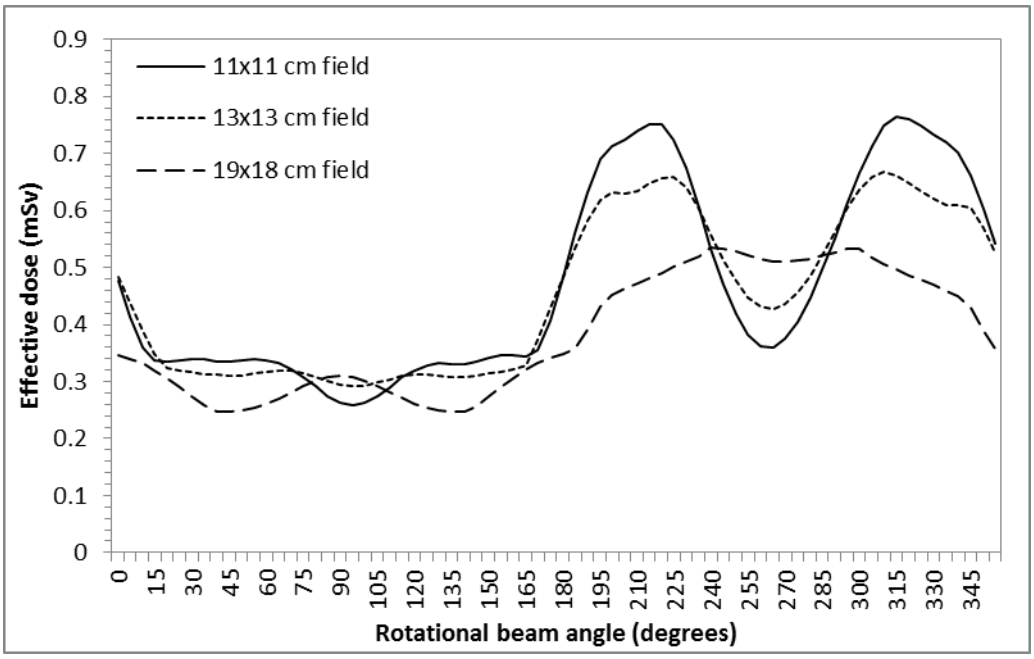


Figure 4.36: Effect of variation in field size on effective dose (15 year phantom).

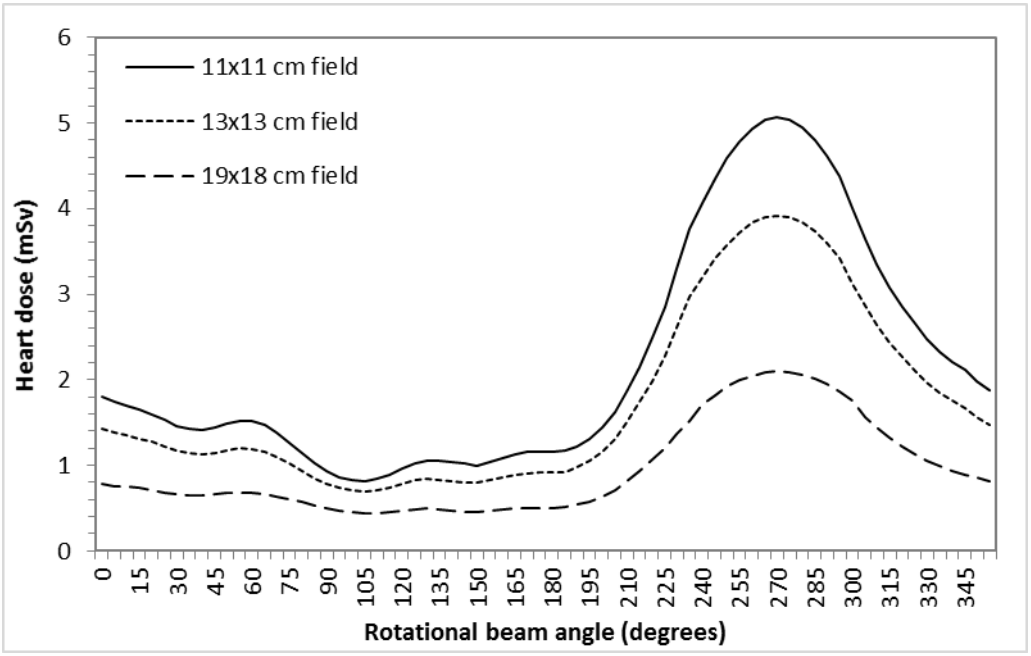


Figure 4.37: Effect of field size on heart dose (15 year phantom).

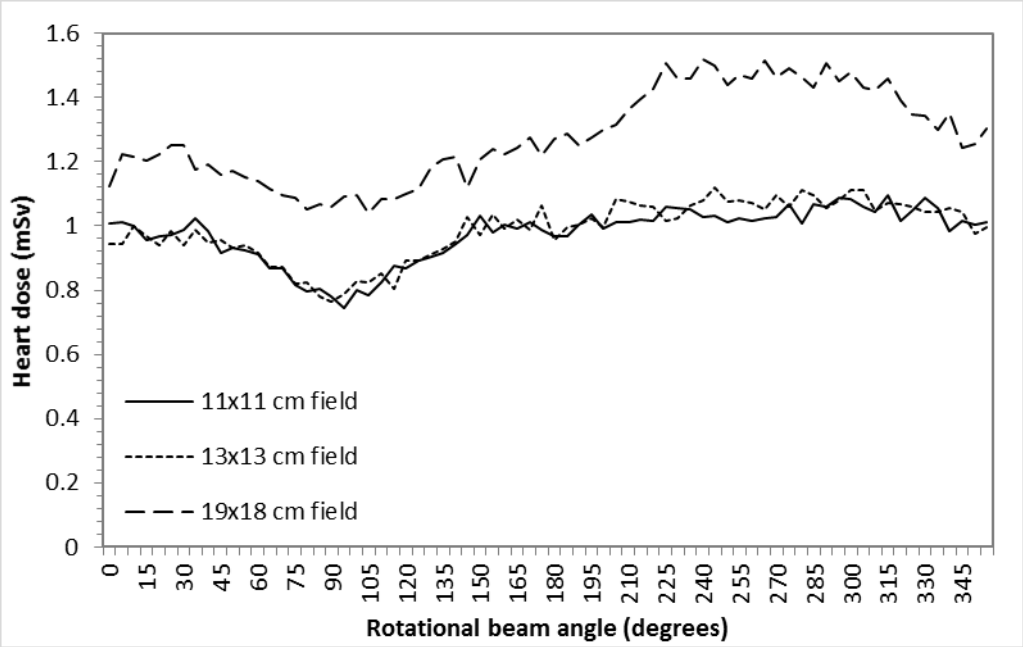


**Figure 4.38: Effect of field size on thyroid dose (new born phantom)**

*4.2.4: Central ray location*

In clinical practice, variation in central ray location is generally in the superior-inferior direction. Procedures involving the pulmonary trunk or the arch of the aorta tend to be centred a little higher than other procedures. Left to right translation is very limited. Occasionally, imaging of the left upper lobe area of the lungs is carried out during pacemaker insertions to check box position. For the lateral projection the beam centring point is also determined by the height of the table in relation to the x-ray beam central axis. Raising the table causes posterior translation of the central ray, while lowering the table results in anterior translation. Variation in organ doses as central ray location was adjusted was consistent with the anatomical distribution of respective tissues. Oesophageal dose was relatively insensitive to anterior-superior translation, while thyroid dose was found to increase sharply with increasingly superior beam centring. Conversely, stomach and liver doses increased sharply as the central ray was shifted inferiorly.

A fall of 89% in breast dose was seen in the lateral projection as the central ray was adjusted in the anterior-posterior direction, i.e. toward the front or back, defined by table height, relative to the patient, falling from around 5.5 to less than 1.0 mSv per unit $P_{KA}$ with a translation of only 2 cm (10 year phantom). This pattern is demonstrated in Figure 4.39 for two different field sizes. Where the field size was

increased, the variation in breast dose was smaller and the point of transition from high to low dose shifted in the positive y-axis direction (i.e. toward the back). According to these simulations, using an admittedly crude mathematical phantom, if the anterior chest wall is included within the primary field for laterally orientated projections, breast dose is very high. If it is excluded from the primary field, breast dose is close to that obtained in the PA projection. For other organs, the variation in dose with anterior-posterior translation in the lateral projection was reasonably small, generally varying by 20% or less. Images from a sample of 30 cardiac catheterizations conducted at Hospital 4 were reviewed and the level of inclusion of the anterior chest wall in the lateral projection was noted. In 20% of examinations, the anterior chest wall was entirely excluded from the exposed area, in 23% it was fully visible, while in the majority of cases (57%), the chest wall was partially visible. The exposed area in the majority of examinations was equivalent to positions 3 or 4 in Figure 4.39 (y-axis positions of -3.5 and -1.5 cm), thus corresponding to high or low breast doses.

Variation in breast dose in the lateral projection was further investigated by simulating the variation in dose with rotational beam angle with different combinations of field size and central ray position. In two cases, the field size was narrowed to completely exclude the anterior chest wall from the irradiated field. In one of these situations, the central ray was also translated posteriorly by 1 cm. This resulted in exclusion of a small part of the apex of the heart, though was still clinically plausible as the major vessels would be included within the field. In all four cases, the same pattern of a rapid rise in breast dose as the beam is rotated between into the lateral projection was seen (Figure 4.40). However, the angle at which breast dose begin to rise varied, occurring at greater angles for the ‘chest wall excluded’ situations. For an angle of 180° (i.e. a ‘straight left lateral’), this resulted in a greater than 3-fold difference in breast dose between these four situations. It can be seen from Figure 4.40 that breast dose in the left lateral projection can be as low at that in the straight PA projection, depending on the combination of central ray location and field size.

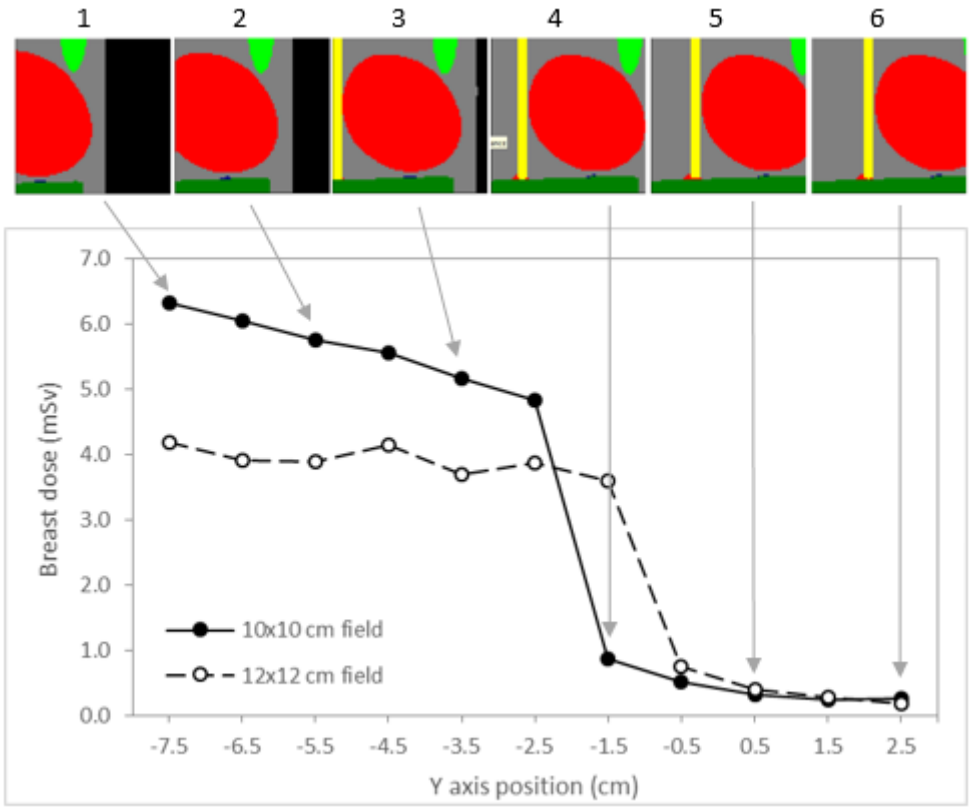


Figure 4.39: Variation in breast dose with central ray location. Simulated radiographs are shown for each corresponding position as beam is translated along the y-axis (anterior-posterior direction) from front to back.

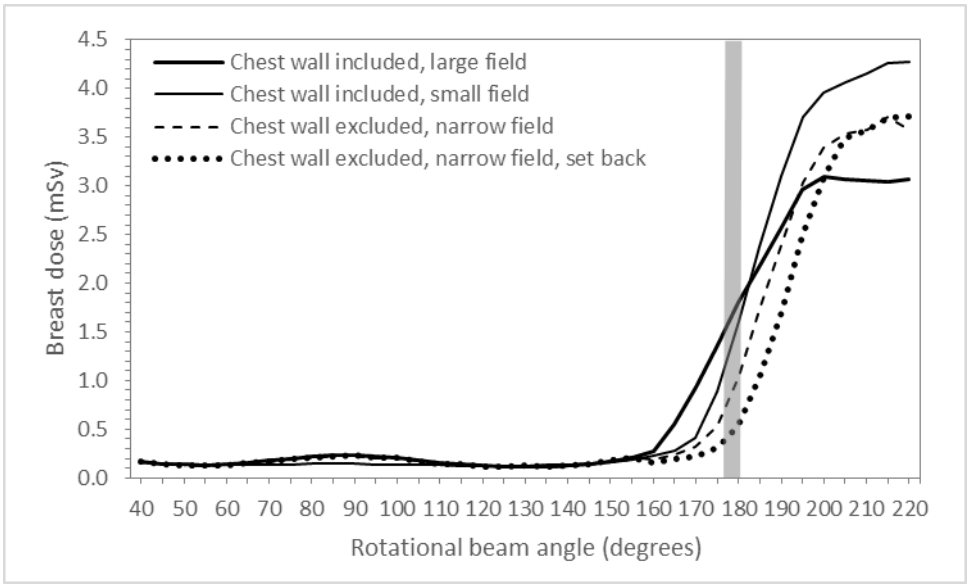


Figure 4.40: Breast dose as a function of beam angle (15 year old phantom) for different field sizes and central ray positions. The grey bar represents the left lateral projection. The PA projection is at 90°.

*4.2.5: Focus-skin distance*

Changes to the focus-skin distance (FSD), which is the distance between the x-ray source (i.e. the anode) and the patient's entrance surface, had relatively little impact on organ doses per unit $P_{KA}$. There was a small trend of reduced doses at shorter FSDs, although within the range of distances likely to be used in clinical practice (60-100 cm), these differences were almost negligible. The same pattern was seen for both beam qualities extremes, though a slightly larger variation in dose with FSD was seen at 100 kV and 0.9 mm Cu compared to 50 kV and 0.0 mm Cu. For example, the mean variation between bone marrow dose at the shortest and longest FSDs was 3.8% and 3.0% respectively. The variation in dose with FSD was lowest for the bone marrow (Figure 4.41) and highest for the heart (Figure 4.42). Increasing FSD is frequently listed among optimisation techniques in diagnostic imaging [263] and interventional fluoroscopy and can result in a modest reduction in effective dose [264]. The results described above should not be compared to such research as they represent dose *per unit* $P_{KA}$, rather than *per se*. Overall, a central value of FSD (80 cm) should suffice for dose estimations based on $P_{KA}$.

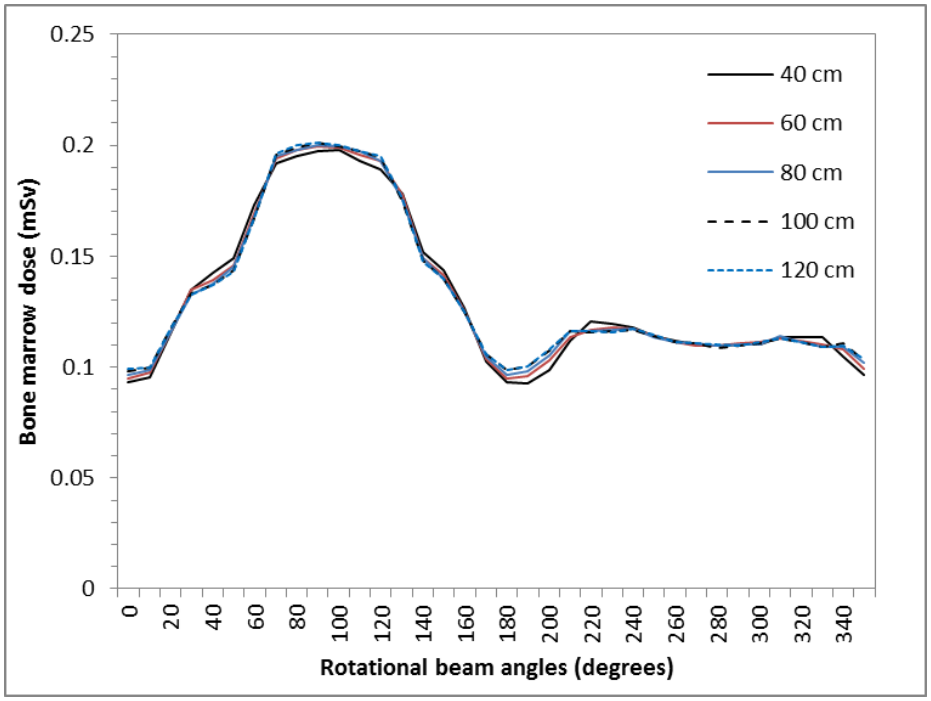


**Figure 4.41: Bone marrow dose as a function of rotational beam angle at different focus-skin distances.**

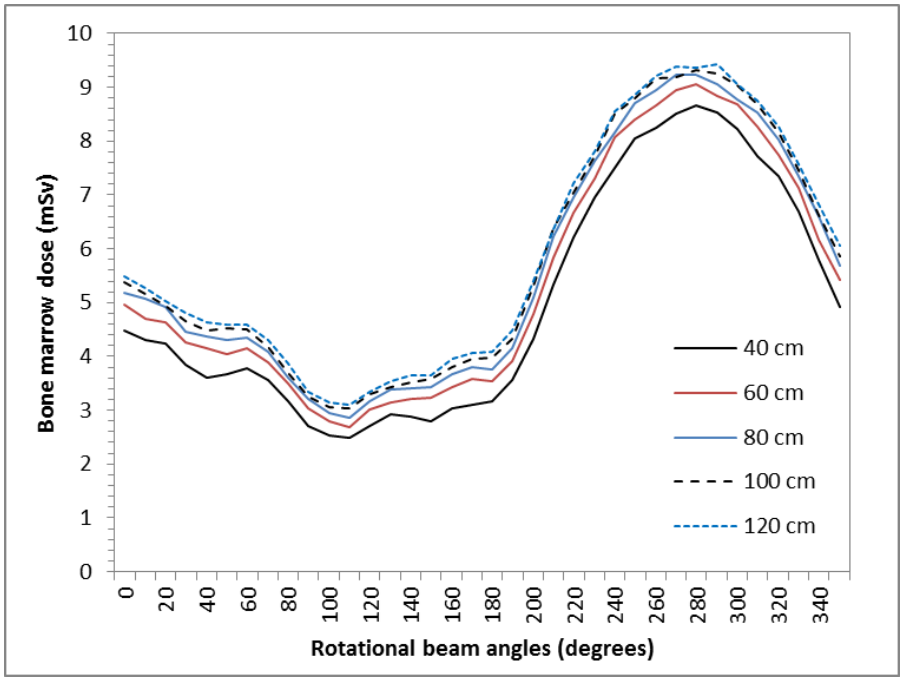


**Figure 4.42: Heart dose as a function of rotational beam angle at different focus-skin distances.**

*4.3: Comparison with previous research*

The previously published effective dose per unit $P_{KA}$ ($E/P_{KA}$) conversion factors summarised in the literature review were compared to those of the current study (Table 4.5). Conversion factors were similar to those of Barnaoui *et al* [92] and Karambatsakidou *et al* [112], though higher by a factor of around 2 than those of Schmidt *et al* [86] and Onnasch *et al* [103]. This difference is consistent with the effect of beam energy on dose per unit $P_{KA}$, as these latter two studies used relatively low energies for calculations. The $E/P_{KA}$ conversion factors quoted by Barnaoui *et al* are higher than those of the current study for the PA projection, but lower for the left lateral projection. The field sizes used by Barnaoui – a potential explanation for this variation - were not stated. It should be noted that four of the previous studies described here also used PCXMC Monte Carlo simulations to calculate $E/P_{KA}$ conversion factors. The figures reported by Kawasaki *et al* [116] were based on physical measurements. These figures are close to those of the current study for the 1 year phantom, but lower for the new born. The lateral/PA $E/P_{KA}$ ratio is similar, albeit slightly higher, than calculated in the current study.

| | | Onnasch et al PA+Lat combined $ | Barnaoui et al PA/lateral $$ | Karambat-sakidou et al PA+Lat combined $ | Schmidt et al PA/lateral $ | Kawasaki et al PA/Lateral $$ | This study PA/lateral $$ |
|---|---|---|---|---|---|---|---|
| Beam energy | | 65 kV, 3mm Al | 70 kV, 3.0 mm Al, 0.3 mm Cu | | 65 kV, 3mm Al | 70-73 kV, 1 mm Al, 0.4 mm Cu | 70 kV, 3.0 mm Al, 0.3 mm Cu |
| Phantom age (years) | 0 | 3.09 | 3.5/3.5 | 3.7 | 2.05/2.34 | 2.2/4.0 | 3.5/5.28 |
| | 1 | 1.03 | 2.1/1.6 | 1.9 | 0.82/1.16 | 1.4/2.7 | 1.60/2.62 |
| | 5 | 0.49 | 1.05/1.3 | 1.0 | 0.42/0.64 | | 0.84/1.69 |
| | 10 | 0.29 | 0.65/0.8 | 0.6 | 0.24/0.38 | | 0.49/1.11 |
| | 15 | 0.17 | 0.35/0.4 | 0.4 | 0.13/0.22 | | 0.26/0.48 |
| | 30 | 0.13 | - | - | 0.10/0.16 | | 0.20/0.39 |

**Table 4.5: Comparison of effective dose per unit $P_{KA}$ conversion factors, between this and previous publications. Note: $=ICRP 60 weighting factors, $$=ICRP 103.**

The only authors to use an alternative Monte Carlo code were Streulens *et al* [88], who used MCNP-X (v2.5.0), along with two voxel phantoms based on cross sectional images, known as 'Laura' and 'Golem' [265]. This allowed doses to be calculated separately for males and females (not possible using PCXMC). The analysis was restricted to adults, with no paediatric phantoms used. Simulations were conducted using a range of beam energies, represented by HVL, from 2.5 to 11.5 mm, allowing detailed comparison of the calculated effect of x-ray energy on doses. The overall pattern is the same for both studies, i.e. dose per unit $P_{KA}$ increases with increasing energy, tending to level off above around 9 mm Al. There is a close agreement in the magnitude of this variation in the PA projection (0-13%), though not for the left lateral projection, in which Streulen's data suggest a 15-45% greater increase in dose per millimetre increase in HVL. Despite this, estimated effective dose for the lateral projection in the current study was higher by 38%, while for the PA projection, figures varied by around 2% (Figure 4.43). Streulens *et al* calculated doses to individual organs, as well as effective dose. There is no overall pattern of agreement between studies; heart dose per unit $P_{KA}$ was higher in Streulens's paper, while breast dose was lower. The overall agreement was approximately ±30%.

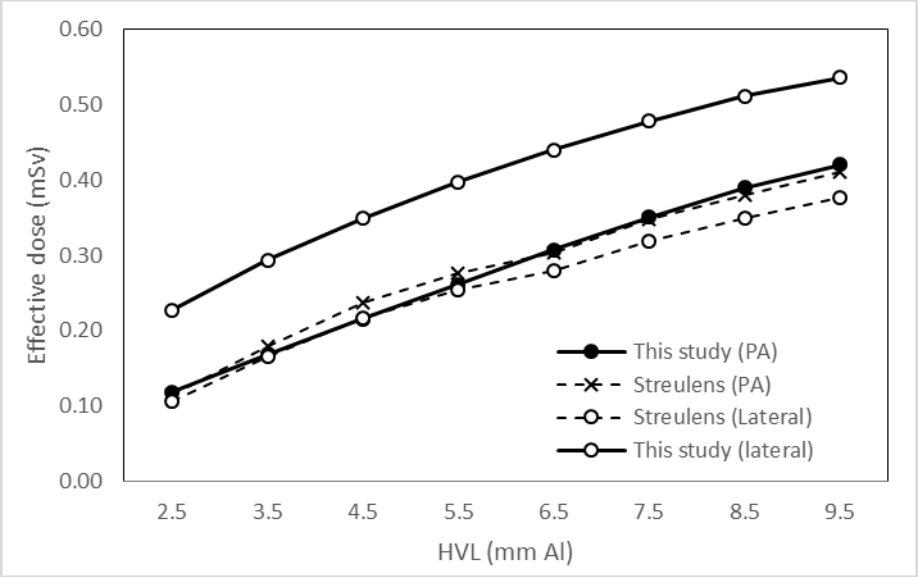


**Figure 4.43: Effective dose per unit $P_{KA}$ for two projections, calculated over a range of beam energies, by the current study and by Streulens et al.**

*4.4: Conclusion*

The relationship between kerma area product and patient dose was found to vary sufficiently with beam angle, beam energy, phantom size and field size that these parameters need to be taken into account in dose estimations derived from $P_{KA}$. Although a measure of patient size is usually recorded for clinical examinations (e.g. height, mass, age), details of beam angle and energy are not routinely recorded. These parameters must therefore be estimated, based on examination type and equipment type and uncertainty in these estimates must be taken into account. A somewhat smaller impact was found for changes in focus-skin distance, and anode angle. The largest variation in dose for a given value of $P_{KA}$ was for the breasts in the lateral projection. Even small changes to beam angle, field size or central ray location can result in a large difference in dose.

# Chapter 5: Dosimetry system development

The Monte Carlo simulation data described in Chapter 4 were represented in a large number of table matrices describing simulations done at 1656 discrete values of beam angle, 36 beam energy combinations and six different phantom sizes. Essentially, these are conversion factors, representing organ doses per unit $P_{KA}$ ($H/P_{KA}$). Similar tabulated conversion factors have been previously published [84, 86, 88], albeit over a more limited range of conditions. This chapter describes the incorporation of Monte Carlo data into a MATLAB-based dosimetry system, called 'Cardiodose', capable of rapid estimation of individual organ doses for large cohorts by picking the right conversion factor. There are two reasons why this dosimetry system was developed, as opposed to running individual Monte Carlo simulations for each examination for cohort members: (1) MC simulations are slow to set up and execute, and (2) PCXMC is a relatively expensive piece of software that can only be installed on one computer. A dosimetry system that utilises MC data, but does not require doing new simulations would not require a PCXMC licence, improving accessibility. Future versions of the dosimetry system can be written as self-executable files, not requiring MATLAB either. Ultimately, the development of Cardiodose paid dividends, as the dose estimation process needed to be repeated several times during the study as new data were obtained.

The Cardiodose function was designed to be able to estimate organ doses for any specified projection angle, x-ray beam energy or patient size. If beam angle or energy data were not available, then some way of estimating these parameters based on examination and equipment type was needed. The gathering of data on beam energy and projection angles used in clinical practice is described in Chapter 6: Supporting information.

## *5.1: Beam angle*

Conversion factors to relate $P_{KA}$ to organ doses were stored in the form of tables with 23 rows and 72 columns. The rows represented cranio-caudal angles from 55° caudal to 55° cranial, in 5° intervals, while the columns represented rotational angles, ranging from 0 to 360°, also in 5° intervals. A simple linear scaling approach was used to convert the specified beam angle to the correct table row/column number. For specified beam angles between the 5° intervals, a linear interpolation approach

was used. This is relatively straightforward and has the advantages of computational simplicity and fidelity to the original simulated data. The main disadvantages of linear interpolation are the large volume of data required (all of it) and the problem of high simulation errors for certain tissues resulting in noisy data. The latter problem could be addressed by running MC simulations with a greater photon count, although this is even more time consuming.

An alternative to the above approach involved encoding the 23x72 tables as polynomial equations. A polynomial describes a function (i.e. organ dose as a function of beam angle) as the sum of a number of 'building blocks', each raised to a non-negative integer power and multiplied by a coefficient [266]. The degree of the polynomial (n) is represented by the building block raised to the highest power.

$$D = c_n x^n + c_{n-1} x^{n-1} + \cdots + c_2 x^2 + c_1 x^1 + c_0 x^0$$

Equation 5.17

In theory, even complex functions can be described by a polynomial equation, although the number of degrees required may be large – in this case between 8 and 20 (Figure 5.1). The polynomial method has the advantage of smoothing out noisy data, reducing the need to run lengthy simulations. Additionally, even complicated polynomials require much less file-space than tables. Although the idea of describing a large table of numbers in a single equation is rather elegant, there are several significant problems with the polynomial approach. Firstly, the beam angle in two directions must be accounted for (rotational and cradio-caudal). It is possible to create a 2-dimensional surface polynomial, although this is significantly more complex and would require so many elements it would eliminate any advantages of reduced data storage. Secondly, the evaluation of polynomials is computationally slower than linear interpolation, increasing the time to estimate doses for a large number of examinations. A third problem was the difficulty in applying further correction factors to adjust for beam quality and patient size. It was principally for this latter problem that the polynomial method was abandoned in favour of linear interpolation.

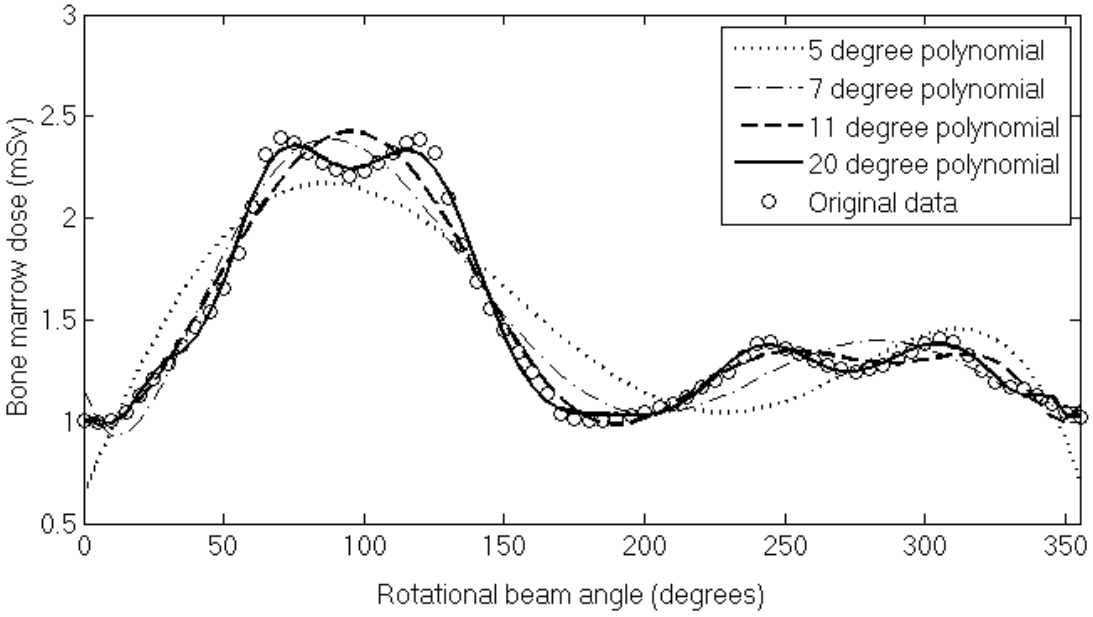


**Figure 5.1: Variation in dose with beam angle can be described using a polynomial equation. Circles represent data from Monte Carlo simulations at discrete beam angle intervals.**

For each examination type, the range of beam angles used was encoded in an *n* by 4 matrix for incorporation into the dosimetry system, where *n* represents the number of different beam angles used. An example is shown below:

$$\begin{bmatrix} 90 & 0 & 0.5 & t \\ 180 & 0 & 0.4 & 0 \\ 120 & 10 & 0.1 & t \end{bmatrix}$$

The first and second columns represent the rotational and cranio-caudal beam angles respectively. The third column represents the proportion of the total $P_{KA}$ spent in each projection. This could be adjusted to match projections used at different hospitals. The fourth column was added as a later modification and allows reduction of dose by a particular specified factor. This was used to correct for attenuation for the presence of the x-ray table (t). The estimation of this 'table reduction factor' is described in section 6.2.6.

Each procedure type was given its own beam angle matrix. The values used in the matrix were based on data described in the following chapter on supporting information. The matrices are stored in the MATLAB function code and can easily be edited (see third page of appendix 4; matrices are written on a single line, with semicolons separating each row of the matrix, and commas separating the columns).

### *5.2: Beam energy*

The dosimetry system needed to take beam energy into account. As with projection angle, the simplest option would be to linearly interpolate between the simulated energy levels to produce a dose estimate at any specified beam quality. Again, this has the disadvantage of requiring a huge volume of data to be incorporated into the dosimetry system – 36 big tables of data, each about 60 kilobytes in size, for each phantom size and each organ type. A second approach involves starting with dose at a single 'reference' beam quality and applying a conversion factor to adjust for any other beam quality. The advantages of this approach include reduced data storage requirements, and that simulations at the 'reference' beam quality could be run using a very large number of photons, leading to reduced simulation errors and less noisy data. This approach also allows different field sizes to be incorporated as different sets of 'reference' data. A further advantage is that correction factors could be designed to account for other beam quality parameters (i.e. not just tube potential and copper filtration). A number of immediate questions arise: (1) how should beam quality be described? (2) What should the 'reference' quality be? (3) Could a single conversion factor be applied for all beam angles, or would it need to vary with beam angle? These questions are addressed in the following sections.

#### *5.2.1: Half value layer encoding*

Even if inherent filtration is assumed to be fixed, accounting for both added filtration and kVp results in complicated conversions. For example, dose variation with added filtration is also dependent on kVp and *vice versa*. As with beam angle, the combination of kVp and filtration can be treated as a surface and described by a multi-variable polynomial equation. However, if other factors such as voltage ripple and inherent filtration were also taken into account, then these conversions would become extremely complex. As mentioned in the Computational Dosimetry chapter (section 4.2.2), beam energy can also be described by half value layer (HVL). This addresses the above problem by describing beam quality as a single figure that allows all influencing factors to be taken into account.

The reference HVL was set at 4.8 mm Al, corresponding to 70 kV, 2.5 mm Al and 0.2 mm Cu filtration. This ansatz was chosen simply because it represented a relatively central beam quality from which to convert to other beam energies (values seen in

clinical practice appeared to range from around 3 to 6.5 mm Al – see Chapter 6). The errors associated with correction to other beam energies were calculated as the reference HVL was adjusted from 1.78 to 9.99 mm Al (where errors were defined as a deviation from values obtained from doing an individual Monte Carlo simulation). Such errors were indeed minimal at 4.8 mm, though this is to some extent immaterial when beam angle specific energy conversions are applied, in which errors are consistently very small. The HVL conversion factor was applied in the form of a $4^{th}$ order, single variable polynomial equation.

### *5.2.2: Beam angle dependence*

As seen in the Computational Dosimetry chapter (section 4.2.2), the effect of beam energy varied quite strongly with phantom size and organ type, therefore correction factors needed to be specific to each. In previous Monte Carlo based attempts at dosimetry for cardiac catheterizations by Schmidt *et al* [86] and Streulens et al [88], different conversion factors were used to adjust for beam quality for each of the beam angles represented. In general, beam quality correction factors for organs that are fairly evenly or symmetrically distributed such as the lungs, lymph nodes or bone marrow, are relatively insensitive to changes to beam angle. For organs that are more localised on one aspect of the body such as the heart and breasts, the correction factor is considerably more sensitive to beam angle.

Three approaches were investigated:

1. A single conversion factor polynomial for all 1656 beam angles based on the mean value of conversion factors across these angles.
2. A partially beam-angle-specific conversion factor, with a separate polynomial for each of the 23 different cranio-caudal beam angles, but each one of these averaged over the range of rotational beam angles (or vice versa).
3. Fully beam angle specific conversion factors, with a separate polynomial for each of the 1655 different simulated beam angles.

The first and second approaches were found to result in large deviations from the results of individual simulations with the specified beam energy, especially for the heart and breasts. The fully beam angle specific approach was considerably more accurate (Figure 5.2). The computational time required to calculate dose to a

particular organ was found to be identical for all three methods (0.012 s). The size of the correction factor files was 1 kilobyte (kB) for the first approach, 6kB for approach two, and 367 kB for approach three. The files are much bigger, but there is no tremendous burden associated with having beam angle specific energy corrections. It would be desirable to have a simple dosimetry system, but ultimately accuracy (in terms of fidelity to the original Monte Carlo simulation data) is the most important consideration. Therefore the beam angle specific approach was adopted for all organs.

As shown in Figure 5.2, the beam angle specific correction approach still results in a small level of 'error' in the sense of a difference between doses calculated by the dosimetry system and those obtained from doing individual MC simulations. This error is due to the use of half value layer to describe beam energy as opposed to using separate kV and filtration figures. Struelens *et al* [88] claim that dose estimates derived from the 'HVL method' deviate a maximum of 5% from those derived from the exact spectrum. This is encouraging, though a separate analysis was conducted to confirm this.

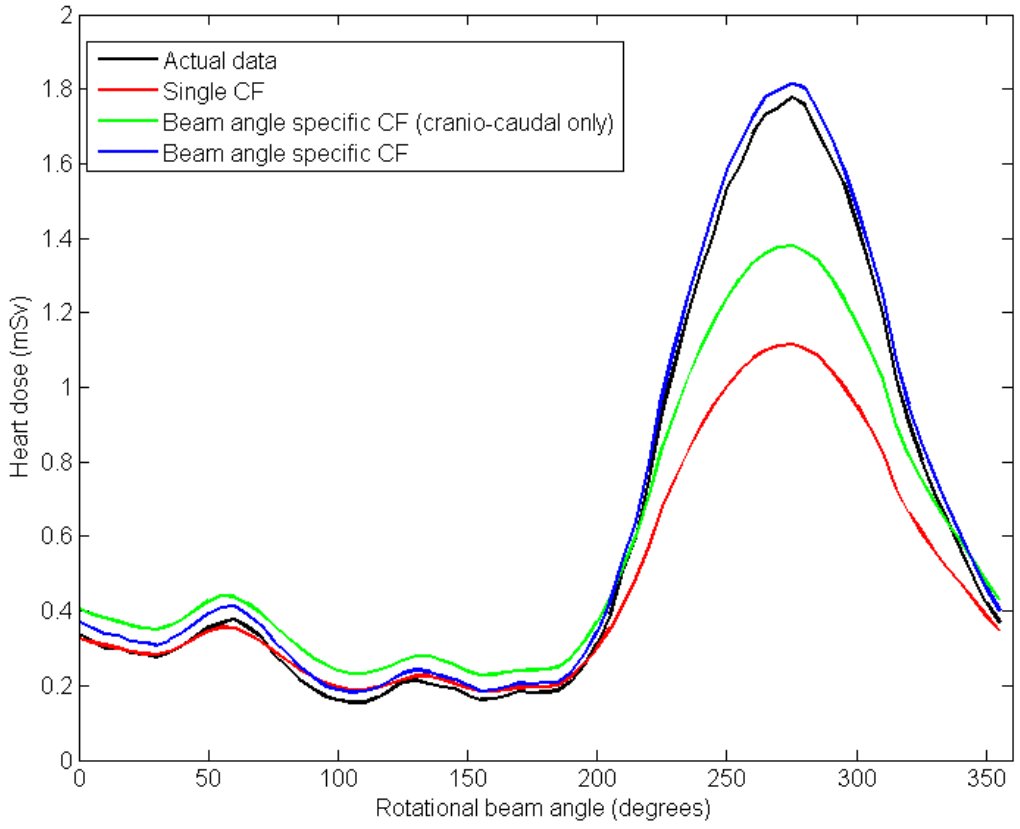


**Figure 5.2: Different approaches to beam energy correction for heart dose.**

A function was written in MATLAB to compare doses calculated using each of the 36 separate kVp and Cu combinations with those calculated using corresponding HVLs. This process was carried out across the full range of beam angles in the rotational direction (0-355° in 5 degree intervals) and 11 cranio-caudal beam angles (-50°, to +50° in 10° intervals) and for each phantom size and for each organ type. The errors resulting from the use of HVL as opposed to separate kV and Cu figures decreases with increasing HVL and increases with increasing phantom size. An example of these errors is shown in Figure 5.3, for bone marrow dose. The largest errors of over 10% occur for high kV/low Cu combinations for 56.3 and 73.2 kg phantoms. For HVLs of greater than 5.5 mm, errors are generally less than 5%. Such errors were considered an acceptable price to pay for the computational simplicity and greater flexibility of the HVL approach.

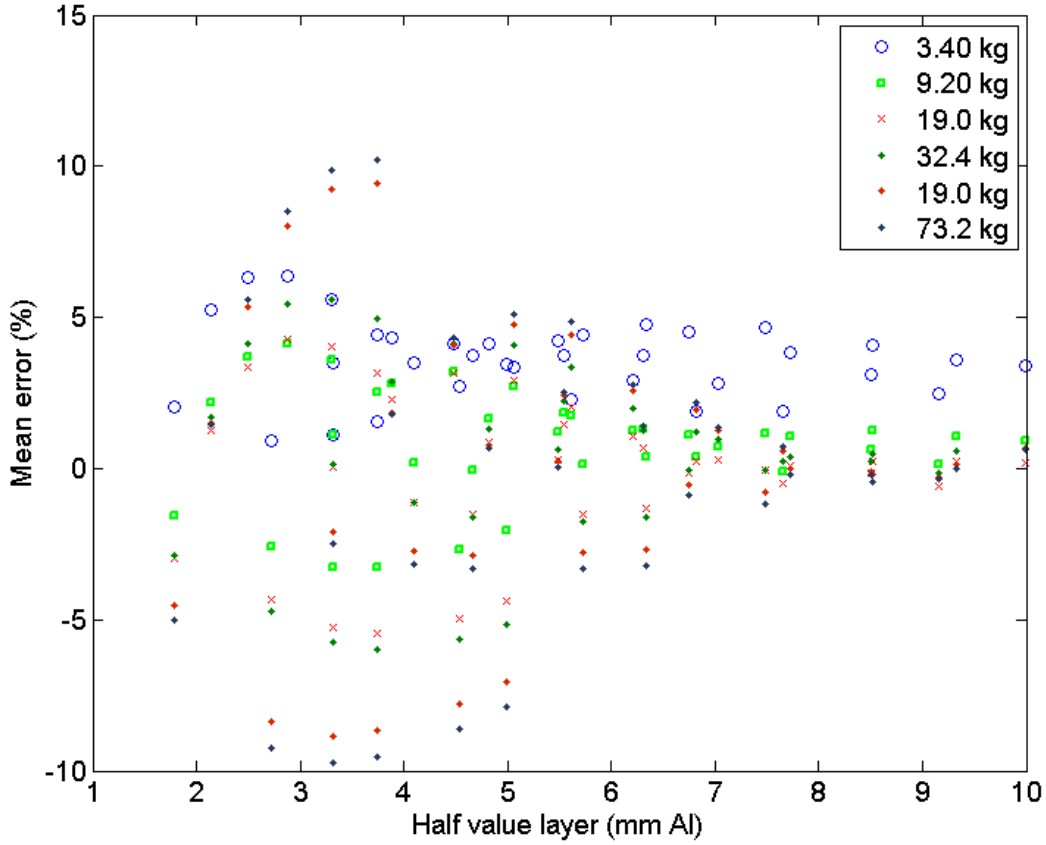


**Figure 5.3: Dosimetry system 'errors' as a function of HVL for bone marrow dose (mean across all rotational beam angles, 0 degree cranio-caudal rotation).**

*5.3: Patient size*

The dosimetry system also needed to be able to adjust for variable patient size. The relationship between dose and patient size can be assessed by age, mass (weight),

height, or body mass index (BMI). Age and mass data were available for nearly all patients in the cohort, but height information (and therefore ability to calculate BMI) was only recorded at a limited number of centres. Characterising patients by age would need to assume they were of 'normal' size (i.e. close to the 50th centile on growth charts) and not under or overweight. Secondly, problems arise when accounting for prematurely born patients who effectively have a negative age. This is not a problem when characterising by mass, which can be lower than 1 kg for extreme low birth weight (ELBW) neonates [254, 267, 268]. Clearly the same body mass can be achieved by being tall and asthenic or being short and sthenic, meaning mass characterisation could still be potentially inaccurate.

As discussed in the Computational Dosimetry chapter (section 4.2.3), a power law was found to provide the best description of the relationship between dose and phantom size. It was found that the coefficient (*a*) and exponent (*b*) of this relationship varied with beam quality. In principle, a conversion factor ($cf_m$) based on this power law could be applied to the dose estimate at a particular 'reference mass' to allow conversion to dose at any other specified mass, providing that *a* and *b* were themselves a function of beam quality, i.e. $cf_m = a \cdot m^b$. This beam quality adjusted power law correction factor was investigated by comparing actual simulated doses at a particular mass with those estimated using the correction factor. Large errors were found (Figure 5.4), principally because the values of *a* and *b* also varied with beam angle. Effectively, the curve representing dose as function of beam angle changes shape as mass is varied. To address this problem, separate power law conversion factors for each possible beam angle were calculated. This approach was also found to be inadequate, mostly due to the imperfect fit of the power law curve to actual data. A further modification of the power law, in the form $cf_m = a \cdot m^{b+c}$ was also investigated but this tended to significantly underestimate doses at large masses. If mass is not available then patient age would need to be used to represent patient size. Using the power law correction, the dose tends to infinity as patient age approaches zero.

Because of these errors, the conversion factor approach to adjusting for patient size was abandoned and replaced by interpolation between the discrete simulated mass levels. This approach has the advantages of simplicity and the avoidance of gross errors, though predictions of negative doses for larges masses still occur. Different

methods of interpolation were investigated; linear interpolation, power law interpolation, and a modified power law of the form $a^{b+c}$. An example of these methods is shown in Figure 5.5 for bone marrow. Clearly the modified power law method provides a very poor fit to simulated values. The simple power law provides a good fit to simulated data below 30 kg, but begins to underestimate dose beyond this level. All size-adjustment models predict doses that continually fall, beyond the largest simulated patient size of 73.2 kg (30 years). This results in the prediction of negative doses for especially large patients (i.e. above 100 kg). To avoid this, no further adjustment for patient size was applied for patient masses of 80 kg or more.

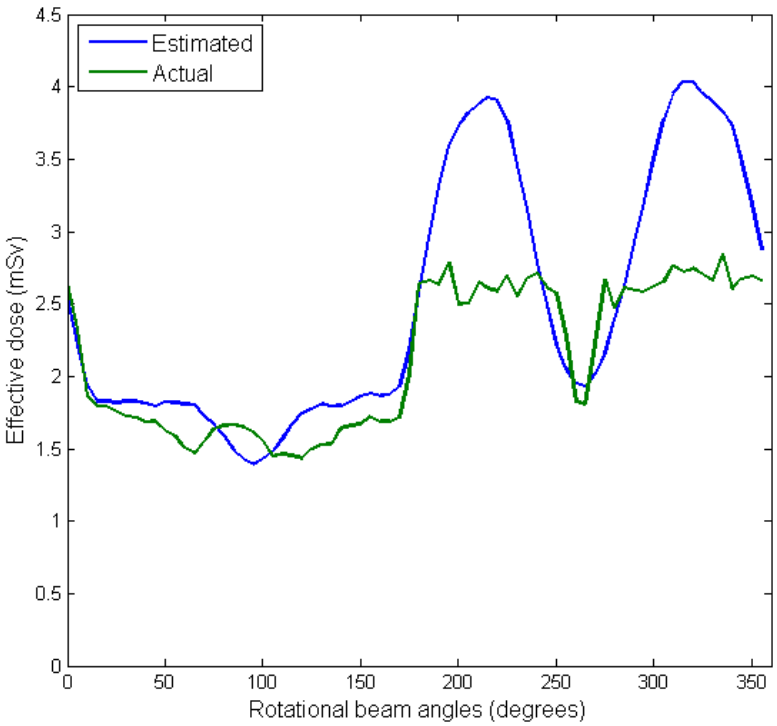


**Figure 5.4: Actual simulated effective dose at 1 year (9 kg) (green) plotted against estimated effective dose calculated by conversion from dose polynomial at 10 years (32 kg) using beam quality specific power law (blue).**

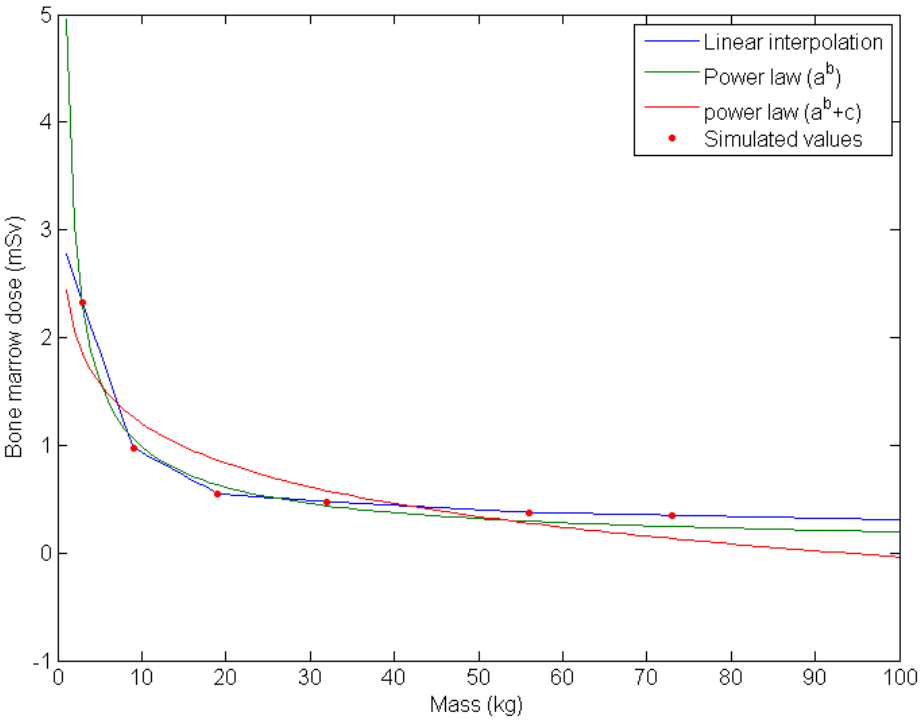


**Figure 5.5: Various interpolation methods to obtain doses between simulated values.**

### *5.4: Field size*

Different field sizes were incorporated as different sets of 'reference data'. This allowed more accurate dose estimation for examinations in which the pulmonary vessels need to be visualised (many examinations including pulmonary artery stenting, valvuloplasty, PDA occlusions and various diagnostic procedures). The only limitation of including extra field sizes was that energy corrections were calculated for the 'standard' field size, rather than for other sizes. Upon investigation, it was found that there is indeed a small field size dependence on energy corrections, though the errors associated with using a single energy correction for all field sizes was relatively small compared with not correcting for field size at all. Thus three extra field sizes were added, representing 1 cm and 2 cm larger fields and a 'large' field in which the whole thorax was included.

### *5.5: Further modifications*

The Cardiodose function was modified several times during the study. The first version used the polynomial approach to selecting beam angles and non-beam-angle-specific energy corrections. The second version replaced the polynomials with

linear interpolation, while the third added beam-angle-specific energy corrections. The ability to calculate doses based on age if no mass was recorded was added. Extra organs were gradually added during development as well as different field sizes. All field sizes use the same energy corrections as the 'standard' field size. A further modification was to utilise biplane $P_{KA}$ figures, where available. Initially, the Cardiodose function had a separate piece of code to calculate the dose to each organ. At first, the methods used for energy corrections were not the same for each organ (i.e. some were beam angle specific, others were not). Once these were standardised, a single *for* loop was created to calculate dose to all organs. This did not significantly affect the speed of the function (0.143, verses 0.148 seconds per line) but did reduce the length of code by around 50% and reduce the number of files needed.

### *5.6: Summary of dosimetry system*

Cohort data is inputted in the form of an Excel file containing anonymous ID number, $P_{KA}$ (either total or separate frontal and lateral figures), mass (or age if not available), examination type, field size, beam energy (defined by HVL) and (if known) precise beam angles. The Cardiodose function estimates doses to organs through the following process:

1. Dose per unit $P_{KA}$ at the desired beam angle is obtained by linear interpolation between conversion factors at 5° intervals. This process is done for each of the simulated patient sizes, to give 6 figures representing dose per unit $P_{KA}$ at the specified beam angle for a beam energy of 4.8 mm Al. If beam angles are not specified, these are estimated based on examination type. This process is covered in the next chapter.

2. Apply the beam energy correction factor based on the HVL polynomial to each of the 6 figures calculated in step 1, to adjust for beam energies other than 4.8 mm Al. The process of determining the correct HVL to use is also described in the next chapter.

3. Linear interpolation between doses at the 6 patient sizes to give dose per unit $P_{KA}$ at the specified mass. If mass isn't specified, patient age is used instead (again, using linear interpolation).

4. Multiply this figure by the $P_{KA}$ for specified beam angle. If the beam passes through the table, a transmission factor is applied, unless this is already accounted for.

5. Repeat for all beam angles used in the examination. The total examination dose is obtained as the sum of doses from different beam angles.

6. Repeat steps 1-5 for each organ.

The only ‘errors’ (in the sense that results differed from those obtained from running an individual PCXMC simulation using the same parameters) were due to the use of HVL to describe beam quality as opposed to the exact spectrum.

### *5.7: Conclusion*

A dosimetry system was developed that utilises Monte Carlo simulations to provide rapid organ dose estimates based on limited data recorded at the time of the examination. The dosimetry system requires information on beam angles and beam energy used in clinical practice to be incorporated. The gathering of these data will be described in the next chapter.

# Chapter 6: Supporting Data for Dosimetry System

The dosimetry system described in the previous chapter requires information on projection angles and beam energy used for clinical examinations of cohort members. Unfortunately, such information is difficult to acquire and is rarely reported in published studies, or quoted too imprecisely. For example, Streulens *et al* [88] state that beam energy used in cardiac fluoroscopy, as represented by half value layer, is between 2.5 and 11.5 mm Al – a range encompassing practically every possible combination of exposure factors. This chapter is concerned with the gathering of relevant information, estimating the central values of beam energy and projection angles, analysis of how reliable these estimates are, and analysis of how variation from expected values may affect calculated organ doses. The methodology, results and discussion of the beam energy analysis will be presented first, followed by the same for projection angles.

## *6.1: Beam energy*

The energy of x-ray photons used in fluoroscopy (or any other form of x-ray imaging) is defined by a number of parameters described below:

*Peak tube potential:* Measured in kilovolts (kV). Defines the maximum kinetic energy of electrons, in kiloelectronvolts (keV) arriving at the anode and thus available for conversion into radiant energy of x-ray photons [43]. All fluoroscopic equipment allows tube potential to be varied. Usually, the machine adjusts kV, along with tube current, automatically to reflect attenuator thickness in order to maintain an approximately constant signal-to-noise ratio [16].

*Filtration:* Both added and inherent filtration (i.e. the x-ray tube housing) is designed to selectively absorb low energy x-rays, resulting in a 'hardening' of the x-ray beam and an increase in mean photon energy. Aluminium filtration (Al, Z=13) is usually kept constant and designed to ensure a minimum thickness of 2.5 mm in order to remove very low energy photons. In modern machines, additional copper (Cu, Z=29) filtration is used. The thickness of copper is sometimes varied automatically, tending to decrease as tube potential is increased [269]. In other machines, added filtration is maintained at a constant level determined by program mode. For Siemens equipment, the capability of variable filtration, known as "*CAREfilter*" and first

introduced in 1994, is utilised for all "*Artis*" equipment (*Axiom* and *Zee*) [270]. Other filtration materials are employed by Toshiba and Shimadzu, including Gold (Au, Z=79) and Tantalum (Ta, Z=73) [271]. Older machines tend to lack the capability of variable filtration, though allow still tube potential to be adjusted.

*Voltage waveform:* X-ray tubes utilise an alternating current. A rectifier is used to ensure voltage at the anode stays positive with respect to the cathode, avoiding electrons bombarding the cathode during the reverse cycle [43]. Voltage is never constant, however, tending to 'ripple' in a manner dependent on the method of rectification. Ripple ranges from 100% for a single phase, self-rectified generator, down to less than 10% for 3-phase/12 pulse or high frequency inverter generators [16]. All the equipment used for examinations in this study used high frequency generators. The impact of voltage ripple on beam energy was considered negligible.

*Anode angle:* Average photon energy increases slightly as anode angle is decreased, presumably as photons generated within a narrow-angle anode must pass through a greater thickness of tungsten before exiting. For example, the HVL (half value layer) calculated using SpekCalc (described in section 4.2.2), was 2.13, 2.07, 2.04, 2.01, and 1.98 mm Al at 8, 10, 12, 14 and 16° respectively (60 kV, 2.5 mm Al). Where the beam is heavily filtered, the impact of anode angle on beam energy is negligible. Despite this, information on anode angle is readily available from manufacturers' specifications, therefore can easily be incorporated into beam energy estimates. The impact of anode angle was briefly discussed in Chapter 4 (section 4.2.2).

A number of sources of information on the beam energies used in cardiac catheterizations were investigated. Firstly, patent applications [272], used equipment vendors such as medwow.com [253] and sales brochures [270] provide some details on the anode angle, generator type, tube potential range and filtration, though no details on the actual thickness of attenuator at which values change. Secondly, an American Association of Physics in Medicine task group (AAPM 125) [271] conducted a study investigating automatic fluoroscopic controls, though for a limited range of machines (one per manufacturer). The data provided on exposure conditions were insufficient and there is no guarantee that the machines tested by the AAPM group were set up in the same way as those used for examination of cohort members. The group did not investigate both acquisitions and fluoroscopic

exposures (in fact it is unclear which of these imaging modes was used). Likewise, a study by Li [269] provides some information concerning the operation of a single machine (Siemens Axiom Artis dBA) but no others. A third source of information was quality assurance (QA) reports, authored by local medical physics staff around the UK and obtained with the cohort data. These reports generally focus on characteristics such as threshold contrast detail, comparison of nominal and measured kV, image distortion and dose rate. Tests of the variation in output with attenuator thickness (usually sheets of copper), where reported, were insufficiently detailed.

More information was required for the purposes of this study. Two approaches were used; (1) An experimental method in which machine response to variable thicknesses of water equivalent material was investigated, and (2) obtaining data recorded for clinical examinations, in the form of structured dose reports or image metadata. Analysis of variation of kV, Cu and associated HVL was carried out for both patient age and mass (structured dose reports) and PMMA thickness (experimental measurements). Information on older equipment was gathered from previously published research, especially that relating to paediatric cardiac catheterizations.

It should be noted that even with these data, uncertainties still exist. The kVp and filtration values chosen by the machine depend on user-selected program mode (different settings designed to optimise for various examination types and patient sizes). These program modes may be changed by users or with software upgrades during the lifetime of the machine and were not always the same at different hospitals. Furthermore, x-ray output may vary over the lifetime of the tube with anode wear.

### *6.1.1: Methodology*

The following sections describe the methodology for physical measurements and obtaining data from structured dose reports and image metadata. In both cases, filtration and tube potential were combined to produce a single HVL using Spekcalc. A description of this software, along with the advantages and limitations of the HVL method are given in Chapter 4.

### *1. Physical measurements:*

The response of fluoroscopic equipment to changing patient size was experimentally investigated using a methodology similar to the previously mentioned AAPM report [271] (Figure 6.1). Sheets of polymethylmethacrylate (PMMA, i.e. plexiglass) water equivalent material were used to simulate a patient of varying thickness (the density of PMMA is 1.18 g/cm$^3$). The equipment types investigated were:

1. *Siemens Axiom Artis BC* biplane unit with image intensifier detectors.
2. *Siemens Artis Zee* biplane with flat panel detectors

The c-arm was positioned in the vertical orientation with the x-ray tube pointing upwards (i.e. typical of a PA projection). The table top was positioned to be 15 cm below the isocentre of the beam. The table cushion was left in place. Slabs of PMMA material were added in 2 cm intervals up to a maximum of 26 cm. At each thickness, fluoroscopic, and then digital acquisition exposures were initiated and maintained until a steady value of tube potential and added filtration was reached (about 3 seconds). The value of both figures was recorded. When the maximum thickness of PMMA was reached, the process was reversed, with slabs being removed one by one. This was to determine if the same filtration and tube potential values were used for the same PMMA thickness depending on whether the thickness had increased or decreased to that level. Anecdotal evidence suggested they would not be the same. Both gridded and non-gridded conditions were evaluated along with different field sizes and imaging modes.

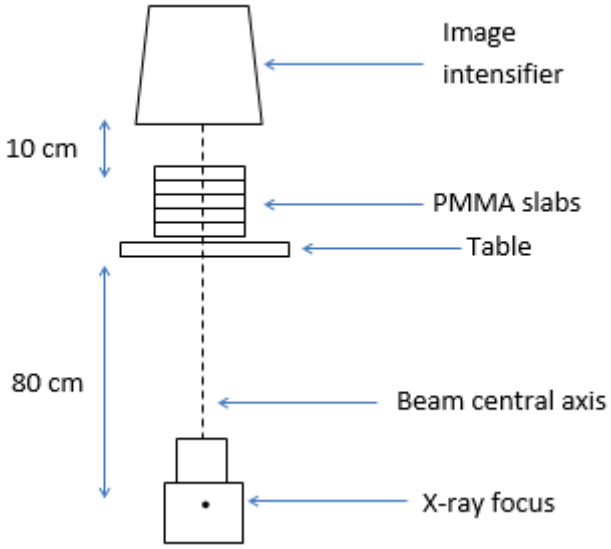


**Figure 6.1: Experimental set up for physical measurements. Figure credit: author**

### *2. Structured dose reports and PACS images:*

A second methodology involved obtaining details on tube potential and filtration recorded for cardiac catheterizations carried out in clinical practice. Since 2009, Siemens fluoroscopic equipment automatically records a 'CAREreport' [270], which includes details of dose ($P_{KA}$ and, sometimes, skin dose), beam angle, field size, frame rate, tube potential and added copper filtration for each digital acquisition. More limited details are recorded for fluoroscopy - doses are reported for each bi-plane output but not for individual beam angles. The Axiom Artis records kV but not filtration, while the Artis Zee records neither, regrettably. Program mode is not recorded in dose reports. In addition to structured dose reports, information on tube potential and program mode could be obtained from images stored on the PACS network. This information was easier to obtain, but lacked details of added filtration used for examinations, and patient mass.

## *6.1.2: Results*

Results are discussed below, first for the physical measurements (presented separately for the two machines studied), followed by the results of the dose report analysis.

**Physical measurements - Axiom Artis:** For acquisitions (Figure 6.2) an increase in tube potential with PMMA thickness was found. This increase was relatively steady and monotonic, ranging from 60 to over 90 kV. Added Cu filtration correspondingly decreased from 0.9 to 0.0 mm. For fluoroscopic exposures (Figure 6.3) this variation occurred in a more stepwise manner, with tube potential remaining below 60 kV up to a thickness of14 cm of PMMA before increasing to 66 kV at 16 cm. When the experiment was reversed, the 66 kV potential was maintained down to 12 cm PMMA thickness. Only three values of copper filtration were used for fluoroscopy - 0.3, 0.6 and 0.9 mm. Again there was a mismatch between results obtained for increasing and decreasing PMMA thickness, with 0.9 mm Cu being maintained to a greater thickness during the increase phase.

Where potential and filtration values were converted into a single HVL figure, a fall in HVL with increasing PMMA thickness was seen for acquisitions (Figure 6.4), but not for fluoroscopy. In the former case, the fall takes on a zigzag form, though could be reasonably approximated by a linear model. The highest value of HVL recorded was 6.3 mm Al, which occurred for cine-acquisitions at the smallest PMMA thickness (60 kV, 0.9 mm Cu) and for fluoroscopy between 14 and 20 cm of PMMA (66 kV, 0.6 mm Cu). The HVL for fluoroscopy remained above 6 mm Al up to a thickness of 22 cm and never dropped below 5.0 mm Al. The lowest HVL was 3.0 mm Al, which occurred for acquisitions at 22 cm of PMMA (82 kV, 0.0 mm Cu). The mean HVL across all thicknesses was 4.7 mm for acquisitions and 6.0 mm for fluoroscopy.

A weighted sum of both fluoroscopy and acquisition exposures was also calculated (Figure 6.4). Where the proportion of fluoroscopy was high (over 90%), the HVL was almost constant at around 6 mm Al, from 2 to 20 cm of PMMA, before falling to around 5.0 mm. This change was associated with the machine switching from 0.6 to 0.3 mm of Cu filtration for fluoroscopy. As the proportion of fluoroscopy is decreased, the HVL begins to fall with increased PMMA, though even for a fluoroscopy proportion of 70% the HVL did not fall below 5.6 mm for thicknesses less than 20 cm.

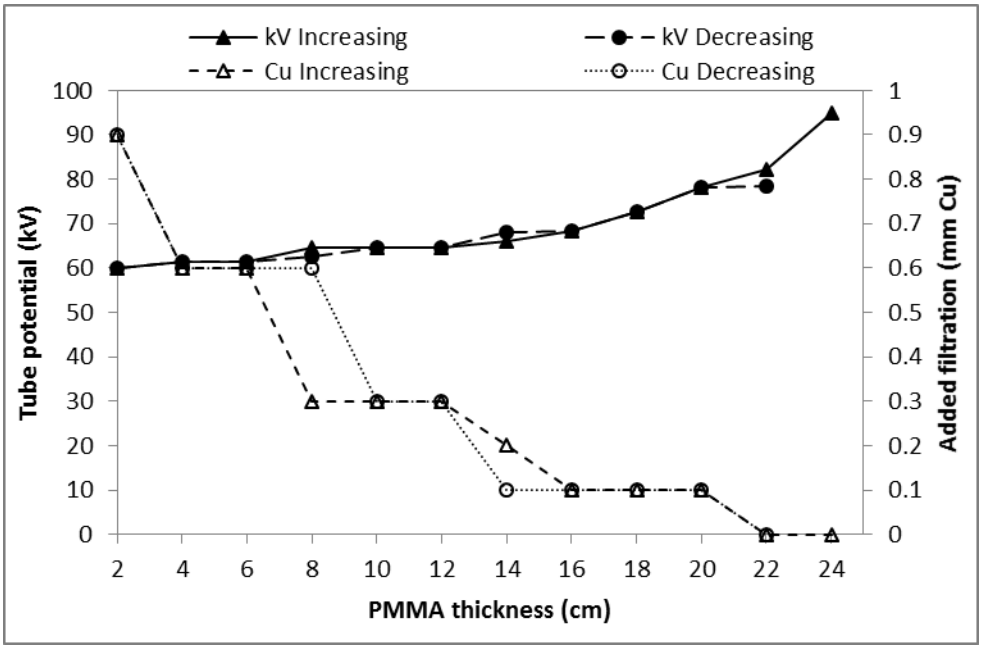


Figure 6.2: Copper filtration and tube potential as a function of PMMA thickness for acquisitions. Values acquired while increasing or decreasing PMMA thickness are shown

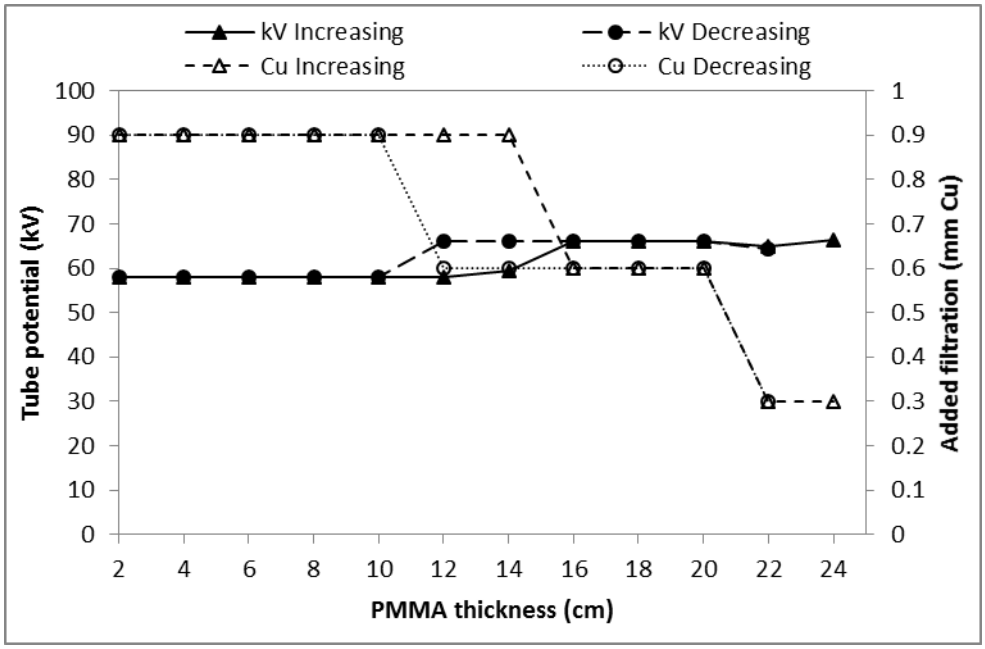


Figure 6.3: Copper filtration and tube potential as a function of PMMA thickness for fluoroscopy.

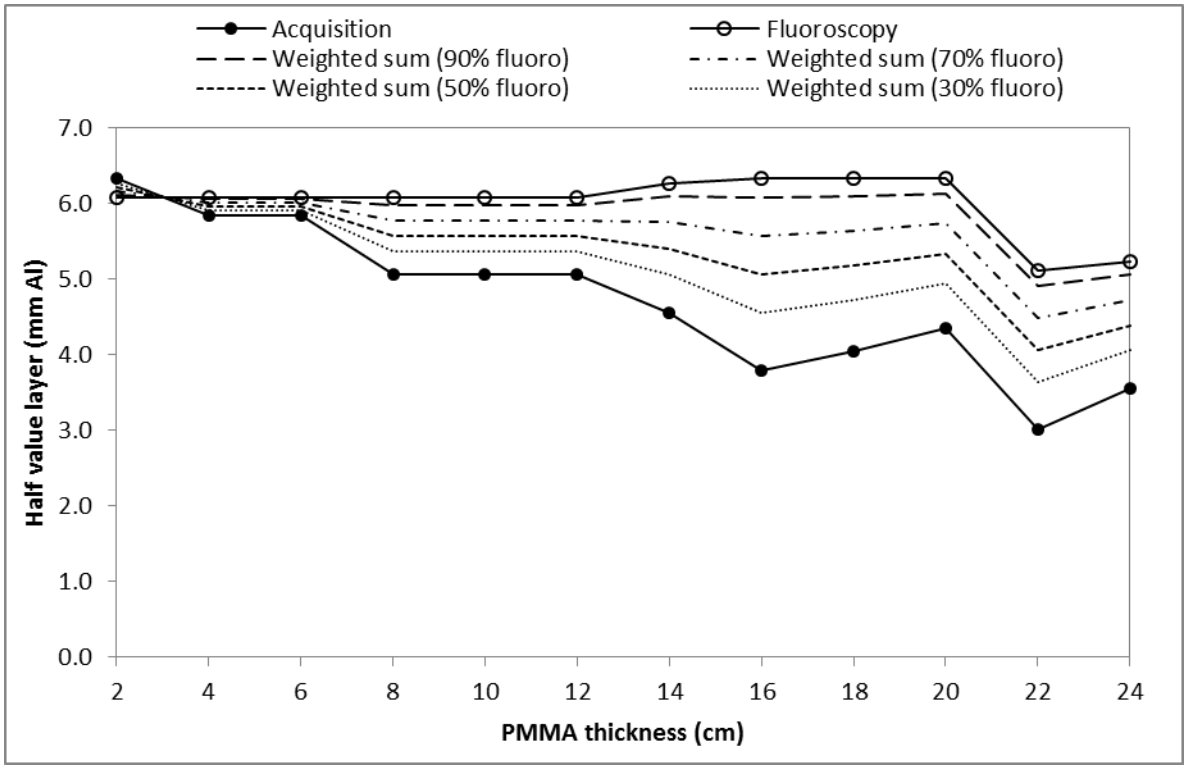


**Figure 6.4: Filtration and potential combined as single half value layer figure (increasing PMMA thickness) along with three different weighted sums of fluoroscopy and acquisitions.**

When the field size was decreased from 22 cm to 13 cm, tube potential and filtration changed more rapidly with increasing PMMA thickness (Figure 6.5), though the overall HVL was approximately the same between field sizes. When the antiscatter grid was omitted, the machine became relatively insensitive to changes in attenuator thickness, maintaining values of 58 kV and 0.9 mm Cu for most thicknesses of PMMA.

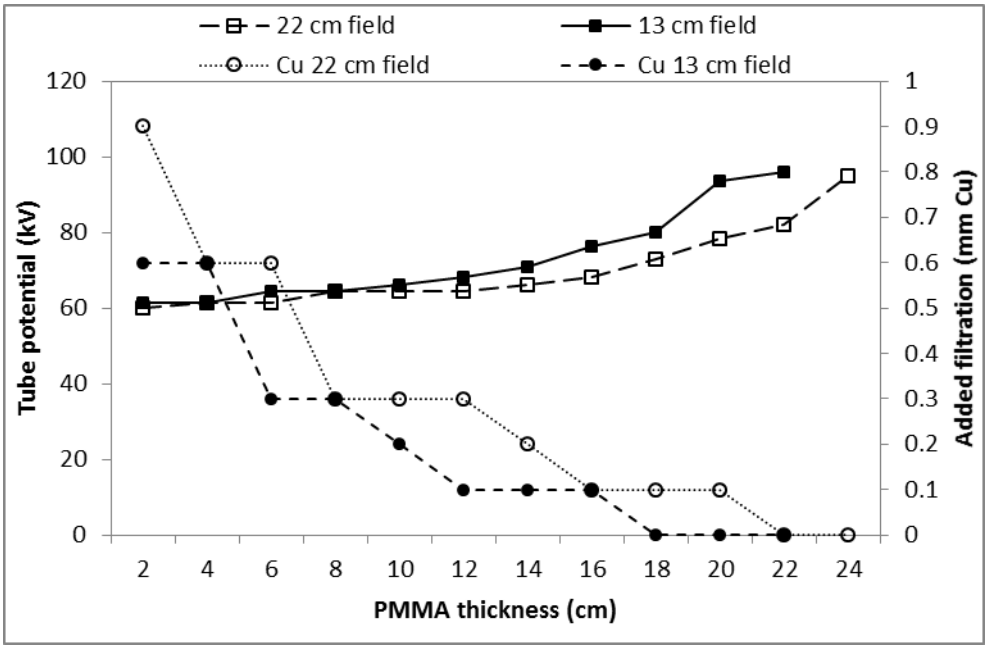


**Figure 6.5: Variation in fluoroscopic tube potential and added filtration for two different field sizes.**

*Physical measurements - Artis Zee:* In contrast to the Axiom Artis, the Zee adjusts fluoroscopic tube potential while usually maintaining a constant value of added copper filtration, which depends on the imaging mode. Three imaging modes are available, “FL card”, “FL – card” and “FL + card”. At Hospital 2, these modes correspond to added copper filtration of 0.2, 0.3 (0.6 for patients above 70 kg) and 0.1 mm respectively (D .Smith, Personal Communication). The machine defaults to “FL – card”, though the radiographer can switch to other modes to improve image quality if needed. At Hospital 4, these values were set at 0.6, 0.9 and 0.3 mm respectively.

As with the Axiom Artis, the tube potential was found to increase with attenuator thickness, but reached a plateau after which it usually remained constant (Figure 6.6). Where fluoroscopic kV and Cu values were converted into a single HVL figure, the pattern was the same as that for kV, reaching a plateau value and then remaining constant (Figure 6.7). Depending on imaging mode, HVL ranged from 3.1 to 8.6 mm Al, based on the Cu filtration at the Hospital 4.

Changing frame rates for a given program did not impact the way in which the machine adjusts kV and Cu with attenuator thickness. Increasing magnification resulted in a slightly greater kV for a given thickness of PMMA, reaching the plateau

value at a lower thickness. This is an interesting finding given that the Zee uses flat panel detectors (FPDs), rather than image intensifiers. In the latter case, decreasing the field size results in decreased minification gain, meaning output must be adjusted to maintain signal-to-noise ratio [98]. For FPDs, magnification can be achieved without the need to adjust exposure factors, though as noted by Nickoloff, manufacturers do tend to utilise greater photon fluence for smaller field sizes to compensate for the perceived reduction in SNR [98].

Only tube potential was recorded for acquisitions. As with fluoroscopic exposures, kV increased with PMMA thickness up to a plateau value and then remained constant. The lack of data on filtration prevented the calculation of HVL for acquisitions.

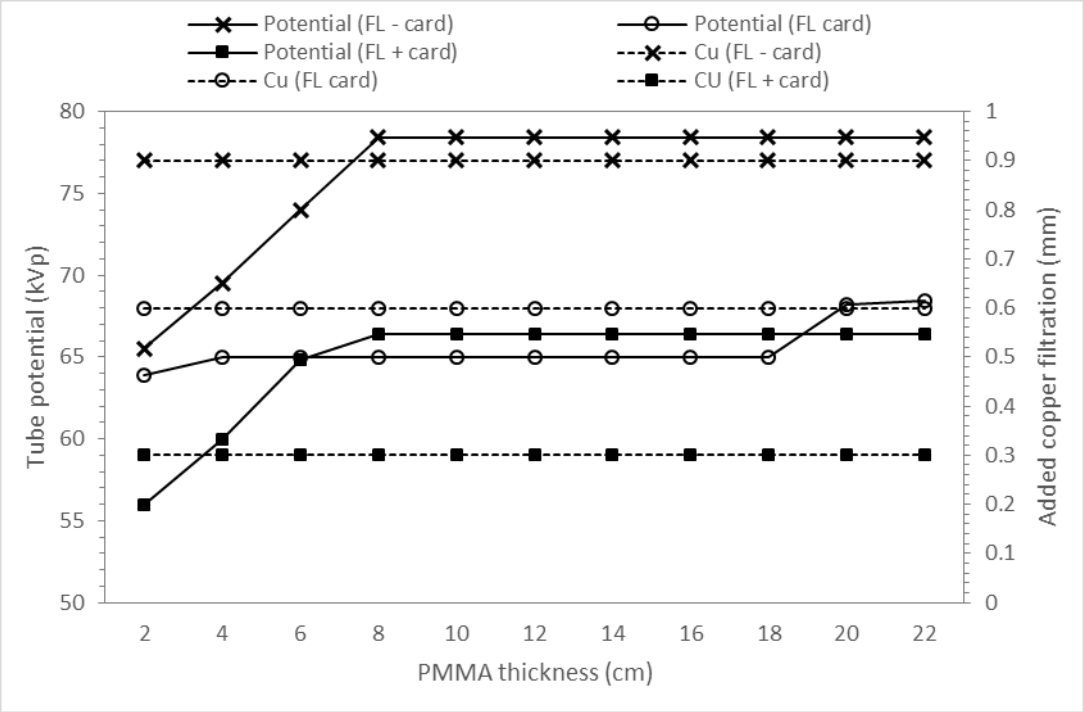


**Figure 6.6: Variation in fluoroscopic tube potential with PMMA attenuator thickness for Siemens Artis Zee machine.**

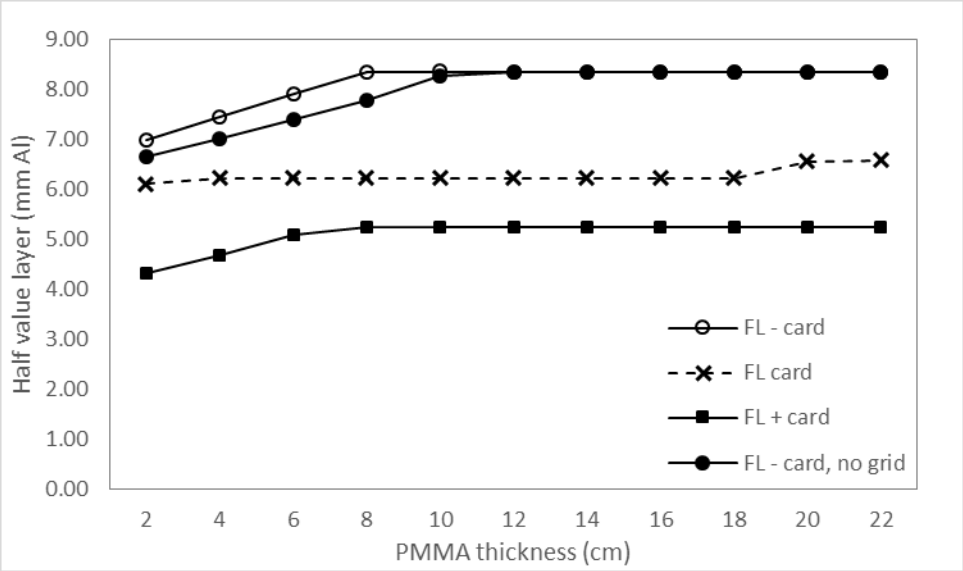


**Figure 6.7: Variation in fluoroscopic HVL with PMMA thickness for three different imaging modes. Data for the 'FL-card' are shown with and without an antiscatter grid fitted.**

### *Results: Structured dose reports and PACS images*

For Hospital 4, dose reports from 49 examinations were obtained, comprising a total of 387 acquisitions. These reports are not automatically sent to PACS and could only be accessed from the machine console in the catheterization laboratory. In addition to these, information for 169 examinations comprising 1307 acquisitions and stored sequences of fluoroscopy (known as 'fluoro grabs') was obtained from images stored on the PACS network. This gave a total of 218 examinations comprising 1694 acquisitions and fluoro grabs. These procedures were all conducted on the same Axiom Artis machine as used for the physical measurements described above. For Hospital 2 (Artis Zee, flat panel detectors), dose reports for 64 examinations comprising 324 acquisitions were obtained. Reports are sent to PACS and include patient age but not mass. Procedure type was recorded, but was found to be inaccurate.

*Axiom Artis machine at Hospital 4:* For acquisitions, filtration (dose reports only) again ranged from 0.0 to 0.9 mm Cu, while tube potential ranged from 60 to 125 kV. Most acquisitions were at two frame rates – 15 and 30 per second. At Hospital 4, the latter frame rate was reserved almost exclusively for digital subtraction angiography (DSA) runs. Across all angles, the mean thickness of added copper filtration was a

little higher for DSA compared to non-DSA acquisitions (0.19 verses 0.14 mm, p<0.01), with tube potential being correspondingly lower (67.5 verses 72.0, p<0.01). A relatively large proportion of the non-DSA acquisitions were in oblique projections, however. Where tube potential was compared for the same projection, mean kV was almost identical (e.g. 66.5 verses 66.3 for PA). The relationship between tube potential and patient age was best analysed by considering different beam projections separately. In each case, a general trend of increased kV with increasing patient age was seen (Figure 6.8), although variation in kV was larger between different projection angles than between ages for the same angle. Data for patients above 15 years was limited, therefore were combined into a single group.

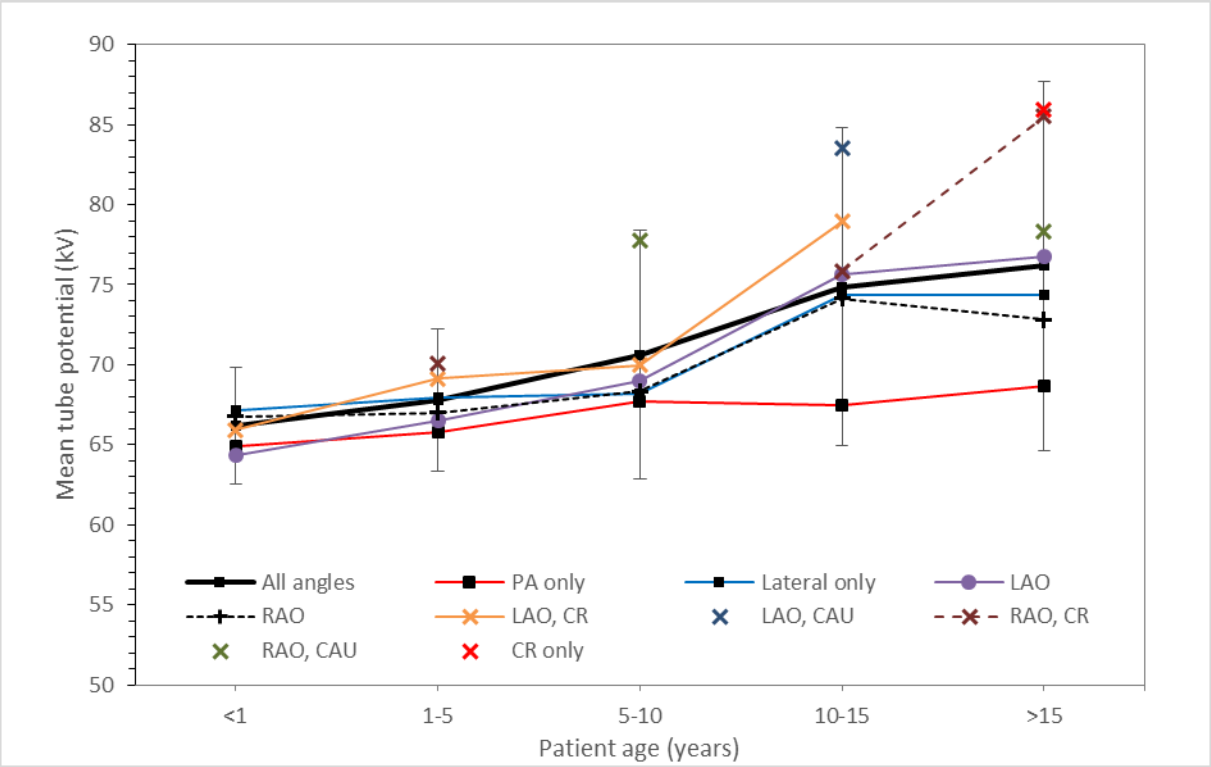


**Figure 6.8: Variation in mean tube potential with patient age for different beam angles. Error bars represent ± 1 standard deviation for the 'all angles' group. RAO/LAO = right/left anterior oblique.**

Analysis of HVL requires information on both tube potential and filtration. The latter figures were not recorded on PACS images, which greatly limits the sample of examinations from which overall beam energy can be analysed. To address this, the results of the experimental methodology previously described were combined with

the dose reports to provide estimates of filtration for examinations where it was not recorded. From the dose reports, a range of tube potential values were seen for each Cu thickness. A starting point for estimating the potential at which filtration changes was midway between the mean kV values for each Cu thickness (red markers in Figure 6.9. These figures were compared to corresponding figures derived from experimental methods, using the mean of both increasing and decreasing PMMA thickness phases (black markers in Figure 6.9). The agreement between these two methods was very high, with variation no greater than 1.3%. Taking the mean of the two methodologies yields estimated tube potentials above which added filtration of 0.0, 0.1, 0.2, 0.3 and 0.6 mm Cu is selected as 80, 68, 66, 64 and 61 kV respectively. Tube potentials of less than 61 kV were assumed to be associated with 0.9 mm Cu. This allows filtration and HVL to be estimated in cases where only the tube potential was known and increases the sample of procedures from which beam energy can be inferred from 49 to 218 examinations.

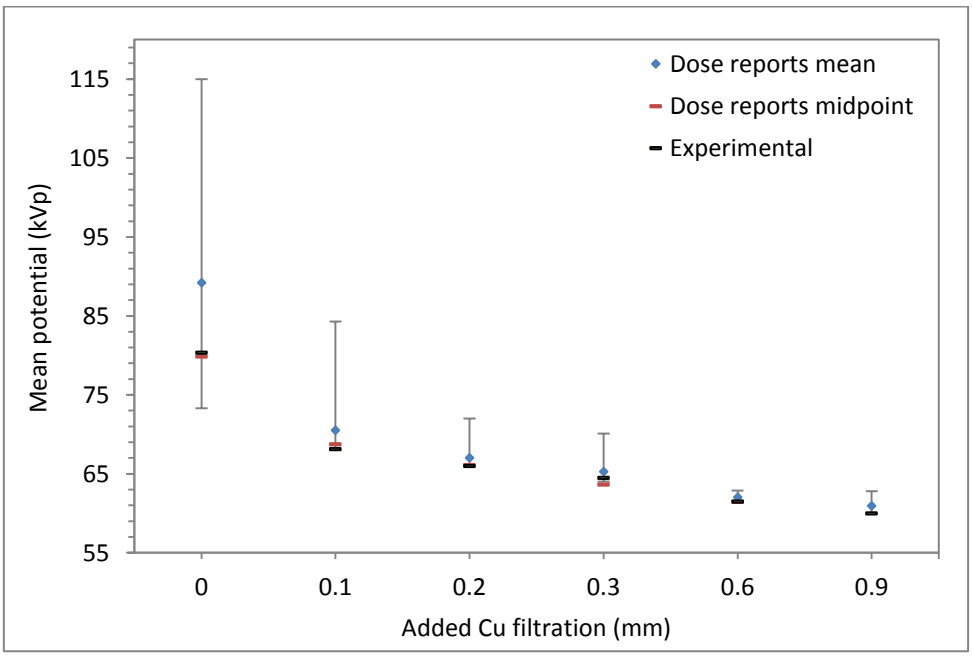


**Figure 6.9: Tube potential ranges for different levels of added copper filtration derived from structured dose reports. Up/down bars represent the range of tube potentials at which a particular thickness of copper filtration was associated.**

The results of these estimates are shown in Figure 6.10. It is evident that there is less variation in HVL between different beam angle projections than was apparent for

tube potential (Figure 6.8). This is due to the corresponding decrease in added copper filtration at higher tube potentials, thus restraining overall HVL to a reasonably narrow range of values (4-5 mm Al). Interestingly, HVL for the PA projection tended to be higher than for other angles, despite the tube potential generally being lower. The lowest HVL recorded was 2.7 mm Al. This minimum occurred for an oblique projection during a coronary angiography examination of a 9 year old patient. The highest value was 6.7 mm Al, occurring during a biopsy procedure on a 5-year old patient.

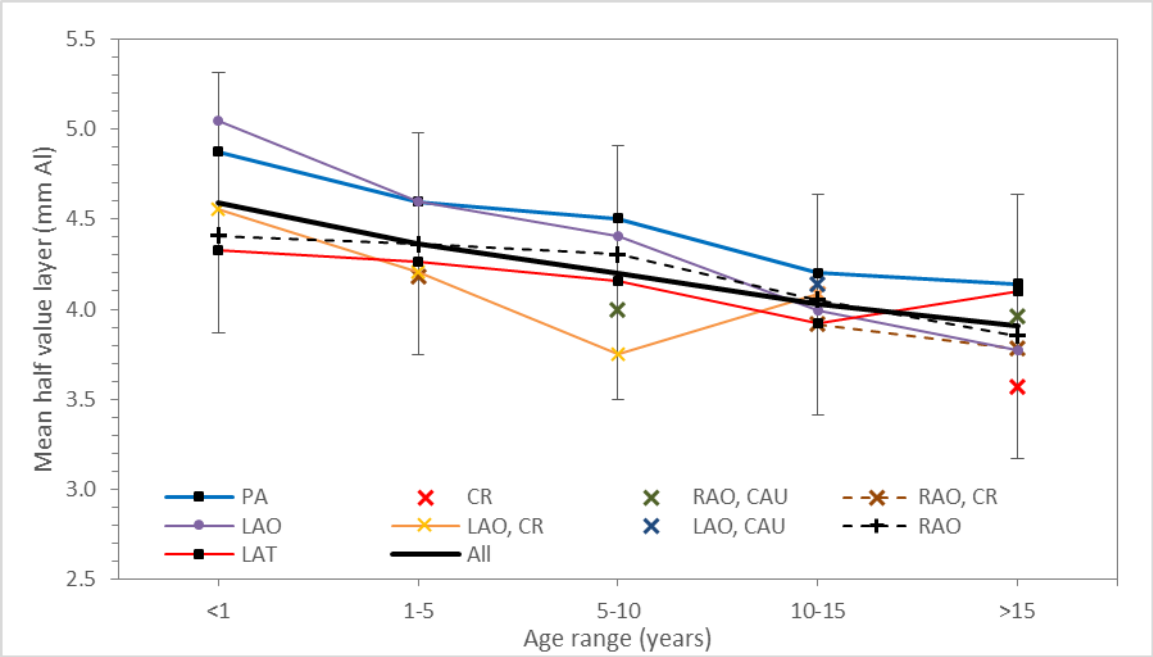


**Figure 6.10: Half value layer for different beam angles derived from tube potential recorded in dose reports and PACS images, and estimated added filtration. Error bars represent ± 1 standard deviation for the 'all beam angles' data. RAO/LAO = right/left anterior oblique.**

Fluoroscopic exposures were usually found to be at 7.5 frames per second and in one of two modes; 'fluoro low' or 'fluro normal', with the latter offering greater image quality. Across all beam angles, the mean tube potential for fluoroscopy was significantly lower than for acquisitions (63.3 verses 70.0 kV, $p<0.01$). Analysis of fluoroscopic exposures by specific beam projection was limited to comparison between frontal and lateral biplane outputs, with tube potential being significantly higher for the latter (64.9 verses 62.0 kV, $p<0.01$). These mean kV figures are somewhat misleading however; the majority (75%) of fluoroscopic exposures for

patients under 15 years are at one of two values - 58 or 66 kV, with few values in between. These two potentials were combined with 0.9 and 0.6 mm added Cu filtration respectively, both yielding a similar HVL (6.1 and 6.3 mm Al). For patients older than 15 years, there is evidence of increased use of tube potentials of 68 kV, with either 0.3 or 0.6 mm Cu (corresponding HVLs of 5.4 and 6.5 mm Al respectively). Tube potentials of 70 kV or more were also recorded, though there is little data from which to determine the filtration thickness at these potentials.

***Siemens Artis Zee machine at Hospital 2:*** For most acquisitions, the *Artis Zee* was found to use 0.1, 0.2 or 0.3 mm of copper filtration. No acquisitions were found in which either less than 0.1 mm or greater than 0.6 mm was used. For all projection angles combined, tube potential generally ranged from 61 to 72 kV. There was a trend of increasing kV with increased patient age, though without the corresponding decrease in Cu seen with *Axiom Artis* equipment. Acquisitions were at three frame rates – 7.5, 15 and 30 per second. Across all ages and beam angles, the mean thickness of copper for these frame rates was 0.35, 0.25 and 0.13 mm respectively. When this pattern was explored in greater detail by stratifying by age, the same pattern was observed. Judging from the results of physical measurements, however, it is the imaging mode associated with the frame rate (which was not recorded in dose reports), rather than the frame rate *per se* that is responsible for this variation.

Where kV and Cu figures were combined to produce a single HVL for acquisition data, the mean value across all beam angles and patient sizes was 4.5 mm Al, ranging from 3.6 to 7.1 mm. In contrast to the Axiom Artis, there was a tendency of HVL to rise with increasing patient beyond 10 years (Figure 6.11), presumably due to the maintenance of a single value of copper filtration thickness as tube potential is increased. There were insufficient data available to analyse variation in beam energy with projection angle beyond PA, lateral and combined oblique angles. As with the Axiom Artis, HVL tended to be higher in the PA projection than oblique or lateral projections. The apparent wide variation in HVL with beam angle for patients aged over 15 years should be interpreted with caution as the sample of acquisitions was small for this group (5 oblique. 7 PA and 11 lateral). Due to the maintenance of at least 0.1 mm added copper filtration, the Artis Zee tends to avoid HVLs of less than 3.6 mm Al.

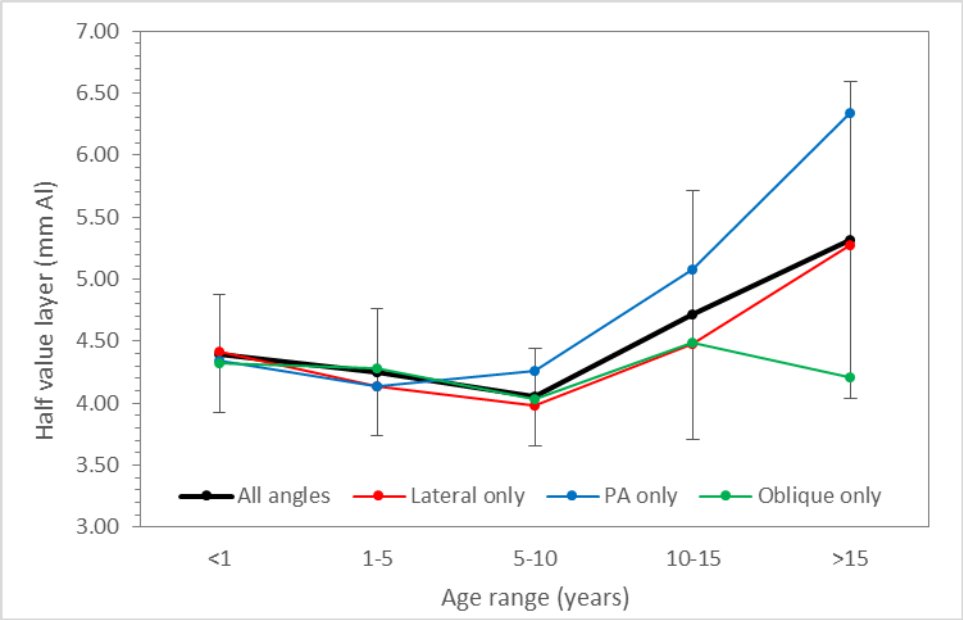


**Figure 6.11: Siemens Artis Zee: Half value layer (mm Al) for acquisitions for different patient age ranges. Error bars represent ± one standard deviation for all angles.**

### *6.1.3: Beam energy for older equipment*

Although the majority of the examinations in the study were conducted using *Siemens Axiom Artis* or *Artis Zee* equipment, other, older machines were also used, such as the *Philips Integris*, *Toshiba Infinix CB* and *Siemens BICOR (biomedical imaging core)* or *Hlcor*. These machines did not record structured dose reports and were not available for carrying out physical measurements on. Some technical details were found on websites selling used equipment, such as medwow.com [253]. Further information could be gathered from previous publications. A summary of these details is provided in Table 6.1

In most cases, information on filtration and tube potential is very limited or entirely absent. The most detailed account of the latter is provided by Rassow *et al* [108] for a *Siemens Angioskop* biplane fluoroscopy system, in which kV values for different beam angles were recorded for both acquisitions and non-acquisition fluoroscopy, with and without zoom. An 'effective voltage' was calculated as a weighted average of these different modes for a range of different patient ages. For the frontal output, the effective voltage ranged from 54.5 kV (0-0.02 years) to 67.0 kV (15-21 years), while for the lateral output, the equivalent figures ranged from 63.6 to 83.5 kV. Using

the quoted total filtration of 2.5 mm Al, this range of 54.5 to 83.5 kV corresponds to a half-value-layer of 1.9 to 3.1 mm Al.

The most commonly reported filtration values for *Philips Integris* machines (either 3000 or 5000) is 1.5 mm Al plus either 0.2 or 0.4 mm Cu. Trianni *et al* [21] report the use of 0.1 mm Cu where fluoroscopy is restricted to 12.5 pulses $s^{-1}$ and 0.0 mm for 25 pulses $s^{-1}$. Over a range of tube potentials 60 to 80 kV, this corresponds to a HVL of between 4.0 and 5.0 mm Al. The *Siemens Coroskop TOP* utilises the *CAREfilter* system of variable copper filtration, while the earlier *Coroskop C Hicor* does not [273]. The *Bicor TOP* is described by Yakoumakis *et al* [107] as using 3.5 mm Al plus 0.22 mm Cu filtration, and a tube potential of between 55 and 70 kV. This corresponds to a HVL of between approximately 4.2 and 5.5 mm Al. The Bicor Plus machine is described by Al Haj *et al* (2008) as having an overall HVL of 3.5 mm Al, although it is unclear how this was measured.

| Study (publication year) | Equipment: | Filtration: | Tube potential (kV) |
|---|---|---|---|
| Calkins (1991) [274] | Siemens Angioscop D | Not stated | 70-109 |
| Schueler (1994) [275] | GE Fluoricon 300 | HVL=3.2 mm Al @ 80 kVp | >60-70, up to 120 |
| Ross (1997) [276] | Siemens HICOR | Not stated | Not stated |
| Boothroyd (1997) [228] | Siemens BICOR Biplane. | Not stated | Not stated |
| Broadhead (1997) [277] | Siemens Coroskop C Biplane | 3 mm (Al?) assumed | 80 ± 4 assumed |
| | Philips Polydiagnost C2 (monplane?) | | |
| Axelsson (1999) [84] | Philips Optimus 2000 | 3.00 mm Al | 67 (a), 58-70 (f) |
| Rassow (2000) [108] | Siemens ANGIOSCOP bi-plane and SIRECON II | 2.5 mm Al | Not stated |
| Kuon (2003) [278] | Philips Integris H3000 | 1.5 mm Al, 0.4 mm Cu | Not stated |
| Bacher (2005) [8] | Philips Integris BH5000 biplane | 1.5 mm Al + 0.2 mm Cu | Not stated |
| | | 1.5 mm Al + 0.4 mm Cu | Not stated |
| Trianni (2005) [21] | Philips Integris 3000 | 0.1 mm Cu (12.5 p/s), 0.0 mm (25 p/s) | Not stated |
| Onnasch (2007) [103] | Siemens biplane BICOR/Digitron, 50 fps. | Not stated | Not stated |
| | Philips biplane DCI/LARC system. | Not stated | Not stated |
| | Dec 1997 Philips Integris 5000BH, 12.5, 25 or 50 fps | ≈1.5 mm Al, 0.2/0.4 mm Cu | Not stated |
| Al Haj (2008) [279] | Siemens BICOR plus biplane (COA dilitation, PV, PDA occlusion, diag). | Not stated. Beam HVL=3.5 mm Al | 80 (f), 66 (a) |
| | GE bi-plane (septostomy, embolisation and RFA | Not stated | 80 (f), 70 (a) |
| Beels (2009) [12] | Philips Integris BH5000 biplane | 1.5 mm Al, 0.4 mm Cu | Not stated |
| Karambatsakidou (2009 and 2013) [112] [107] | Philips Integris H 5000C | 6 mm Al + 0.4 mm Cu (f), and 6 mm Al + 0.2/0.04 mm Cu (a) | 65-70 (f), 60-65 (a) |
| Yakoumakis (2009) [115] | Siemens BICOR TOP II | 3.5 mmAl + 0.22 mm Cu | 55-70 |
| Ait Ali (2010) [13] | Philips Integris H5000C monoplane | Not stated | Not stated |
| Chida (2010) [280] | Siemens BICOR Plus. | ? + auto 0.1/0.2 mm Cu | 70 kVp |
| Watson 2012 [167] | Philips Integris BH5000 biplane | Not stated | Not stated |
| McFadden (2013) [281] | Siemens BICOR TOP biplane | 2.5 mm Al | Not stated |

Table 6.1: Tube potential and filtration details of older generation equipment quoted in previous publications of doses from cardiac catheterisations

### 6.1.4: Discussion (Beam energy)

Beam energy was found to be variable, not only between different fluoroscopic equipment manufacturers and models, but for the same machine under different conditions, such as imaging mode, field size and frame rates. Some general patterns can be observed, although a degree of uncertainty will still exist. The most suitable approach was therefore to estimate a central beam energy value and set associated uncertainty limits. Structured dose reports were considered to provide the most reliable source of data on tube potential used for fluoroscopic imaging, and both tube potential and added filtration for acquisitions. Physical measurements were used as the source of information on fluoroscopic filtration. As the typical x-ray energies used in these two acquisition modes is different, the value (or values) of HVL used in organ dose estimates must take into account the proportion of total $P_{KA}$ as fluoroscopy and acquisitions. Hospital specific fluoroscopy proportions were used where such information was available (i.e. Hospitals 2 and 4). The beam energy values used for dose estimates are described below for different equipment types:

*Artis Zee:* There was insufficient evidence of variation in x-ray energy with beam angle to warrant the definition of projection-specific HVL estimates. Based on structured dose reports from Hospital 2, the mean proportion of total $P_{KA}$ originating from fluoroscopy ($p_f$) across all procedure types was 0.75 (this compares to 0.82 for 2004-2008 data user older equipment). For diagnostic and interventional procedures, $p_f$ was 0.67 and 0.77 respectively. There are insufficient data to allow further stratification of $p_f$ by procedure type, though for electrophysiology studies (EPS) and pacemaker insertions, a $p_f$ of 0.95 was considered appropriate. The HVL values used for dose estimates at Hospital 2 are shown in Table 6.2, and assume the use of "FL – card" mode with 0.3 mm Cu applied for all fluoroscopic imaging and 0.6 mm Cu for patients over 70 kg. The lower and upper HVL limits, were based on 5$^{th}$ and 95$^{th}$ percentiles of values for acquisitions. The upper limit for patients over 10 years was fixed at 7.1 mm.

| Patient size in years (kg) | Intervention ($p_f$ = 0.77) | Diagnostic ($p_f$ = 0.67) | EPS, Pacemakers ($p_f$ = 0.95) |
|---|---|---|---|
| <1 (<9.2) | 5.2 [4.6 : 6.1] | 5.1 [4.3 : 5.9] | 5.4 |
| 1-5 (9.2-19) | 5.5 [5.0 : 6.5] | 5.3 [4.5 : 6.1] | 5.8 |
| 5-10 (19-32.4) | 5.7 [5.5 : 6.5] | 5.5 [4.7 : 6.3] | 6.1 |
| 10-15 (32.4-56.3) | 5.9 [5.5 : 7.1] | 5.7 [5.3 : 7.1] | 6.1 |
| >15 (>56.3) | 6.0 [5.0 : 7.1] | 5.9 [4.9 : 7.1] | 6.2 |
| >70 y (>70 kg) | 7.7 [5.2 : 8.2] | 7.4 [5.1 : 8.2] | 8.2 |
| Mean (all sizes) | 5.7 | 5.5 | 5.9 |

**Table 6.2: Assumed half value layers (mm Al) used to estimate doses for procedures carried out using Siemens Artis Zee equipment at Hospital 2.**

**Siemens Axiom Artis:** Again, there appears to be little basis for beam angle specific HVL estimates. Values for all angles combined, with associated uncertainty limits were deemed sufficient. The majority of fluoroscopic exposures were at either 58 kV (0.9 mm Cu) or 66 kV (0.6 mm Cu), yielding HVLs of 6.0 and 6.2 mm Al respectively. The higher tube potentials seen for larger patients may yield a higher or lower HVL depending on the filtration applied, data on which was rather limited. There is reasonable justification in utilising a patient size independent HVL for fluoroscopy of 6.1 mm Al, at least up to 15 years and probably beyond.

Overall HVL figures calculated as a weighted sum of fluoroscopic and acquisition components are shown in Table 6.3 for proportions of fluoroscopy ranging from 0 (i.e. entirely acquisitions) to 1.0 (entirely fluoroscopy). Where hospital specific data on $P_f$ was available, these were utilised. From structured dose reports at Hospital 4, the mean proportion of total examination $P_{KA}$ from fluoroscopy was 0.41 for all examination types combined, and 0.49 and 0.36 for interventional and diagnostic procedure categories respectively. For EPS, biopsy and pacemaker insertion procedures, the proportion $P_{KA}$ from fluoroscopy was set at 0.95. The assumed half value layers used for dose estimations using Siemens Axiom Artis machines, taking into account uncertainty in HVL for acquisitions and fluoroscopy, along with uncertainty in the proportions of total $P_{KA}$ in these two operating modes are given in Table 6.4. Uncertainties were based on 5$^{th}$ and 95$^{th}$ percentiles of HVL, calculated at -0.8 mm and +1.1 mm. The same values were used for all patient sizes as there was little suggestion of variation with age or mass.

| | Proportion of total output as fluoroscopy | | | | | | | | | | |
|---|---|---|---|---|---|---|---|---|---|---|---|
| Patient size in years (kg) | 0.0 | 0.1 | 0.2 | 0.3 | 0.4 | 0.5 | 0.6 | 0.7 | 0.8 | 0.9 | 1.0 |
| <1 (<9.2) | 4.6 | 4.7 | 4.9 | 5.0 | 5.2 | 5.3 | 5.5 | 5.6 | 5.8 | 5.9 | 6.1 |
| 1-5 (9.2-19) | 4.4 | 4.5 | 4.7 | 4.9 | 5.1 | 5.2 | 5.4 | 5.6 | 5.8 | 5.9 | 6.1 |
| 5-10 (19-32.4) | 4.2 | 4.4 | 4.6 | 4.8 | 5.0 | 5.2 | 5.3 | 5.5 | 5.7 | 5.9 | 6.1 |
| 10-15 (32.4-56.3) | 4.0 | 4.2 | 4.4 | 4.6 | 4.9 | 5.1 | 5.3 | 5.5 | 5.7 | 5.9 | 6.1 |
| >15 (>56.3) | 3.9 | 4.1 | 4.3 | 4.6 | 4.8 | 5.0 | 5.2 | 5.4 | 5.7 | 5.9 | 6.1 |

**Table 6.3: Central estimates of half value layer (mm Al) for different patient sizes and various proportions of fluoroscopy for Siemens Axiom Artis equipment.**

| | Procedure type | | |
|---|---|---|---|
| Patient size in years (kg) | Interventional | Diagnostic | EPS, Pacemakers |
| <1 (<9.2) | 5.3 [4.5 : 6.3] | 5.1 [4.3 : 6.2] | 6 [4.6 : 6.3] |
| 1-5 (9.2-19) | 5.2 [4.4 : 6.3] | 5.0 [4.2 : 6.1] | 6 [4.6 : 6.3] |
| 5-10 (19-32.4) | 5.2 [4.4 : 6.3] | 4.9 [4.1 : 6.0] | 6 [4.4 : 6.3] |
| 10-15 (32.4-56.3) | 5.1 [4.3 : 6.2] | 4.8 [4.0 : 5.9] | 6 [4.4 : 6.3] |
| >15 (>56.3) | 5.0 [4.2 : 6.1] | 4.7 [3.9 : 5.8] | 6 [4.4 : 6.3] |

**Table 6.4: Assumed half value layers (mm Al) used to estimate doses for procedures carried out using Siemens Axiom Artis equipment. The figures in square brackets represent upper and lower uncertainty limits.**

The effect of the upper and lower beam energy uncertainty limits, expressed as percentages, are shown in Table 6.5 for each organ type and each patient. Uncertainty was seen to vary between organs, being highest for the stomach and thyroid, and lowest for the lungs and active bone marrow. Uncertainties also increased with increasing patient size and varied with beam angle. The figures in Table 6.6 represent the mean uncertainty over a range of beam angles from straight PA to left lateral in 30° intervals. The uncertainty for all organs and patient sizes was ±12.5%.

*Siemens BICOR / BICOR Plus / HICOR/ Coroskop:* A central HVL value of 4.8 mm was chosen, based on 65 kV and 0.22 mm Cu and 3.5 mm Al filtration. The lower uncertainty limit was set at 3.5 mm Al, based on the lowest reported tube potential of 60 kV and no copper filtration. The upper limit was set at 5.9 mm Al, assuming maintenance of 0.22 mm Cu, and the maximum reported tube potential of 80 kV. There are few details available from which to estimate HVL for the older generation BICOR machine used at Hospital 1 prior to 2000 (i.e. not the more recent BICOR Plus or TOP machines), although copper filtration did not appear to be used. The

central HVL was set at 3.0 mm Al, assuming a central tube potential of 75 kV, 3.5 mm Al filtration and no copper. The lower limit of 2.0 mm Al assumed a reduced aluminium filtration of 2.5 mm and a potential of 60 kV. The upper limit was set at 4.0 mm Al. The upper limit was based on a potential of 100 kV, with 3.5 mm Al filtration. A HVL of 3.0 mm was also used for the Siemens Coroskop C used at Hospital 4 until 2003, based on the limited description of the machine in a paper by Broadhead *et al* [277]. For the purposes of effective dose estimation, the authors assumed 3 mm of aluminium filtration and a tube potential of around 80 kV. The same upper and lower HVL limits were used as for the BICOR machine described above.

Percentage variations in dose due to HVL uncertainties for 2$^{nd}$ and 1$^{st}$ generation equipment are shown in Tables 6.6 and 6.7 respectively.

| Patient age (mass) | Uncertainty | Effective dose | ABM | Breasts | Heart | Lungs | Lymph | Oesophagus | Thyroid | Liver | Stomach | Average dose |
|---|---|---|---|---|---|---|---|---|---|---|---|---|
| <1 y (<9.2 kg) | Lower | -8% | -8% | -9% | -9% | -6% | -9% | -10% | -13% | -9% | -12% | -7% |
| | Upper | 8% | 8% | 10% | 9% | 5% | 9% | 10% | 15% | 9% | 13% | 7% |
| 1-5 y (9.2-19 kg) | Lower | -9% | -10% | -8% | -12% | -8% | -11% | -12% | -17% | -11% | -15% | -9% |
| | Upper | 10% | 12% | 7% | 14% | 8% | 14% | 15% | 23% | 13% | 19% | 10% |
| 5-10 y (19-32 kg) | Lower | -10% | -11% | -8% | -14% | -9% | -13% | -14% | -19% | -13% | -17% | -10% |
| | Upper | 12% | 13% | 10% | 17% | 10% | 16% | 18% | 24% | 16% | 22% | 11% |
| 10-15 y (32-56 kg) | Lower | -10% | -12% | -7% | -15% | -10% | -15% | -17% | -20% | -15% | -18% | -11% |
| | Upper | 13% | 15% | 10% | 19% | 12% | 19% | 23% | 28% | 19% | 25% | 13% |
| 15-18 y (>56 kg) | Lower | -13% | -13% | -10% | -18% | -13% | -16% | -18% | -24% | -18% | -22% | -12% |
| | Upper | 17% | 16% | 12% | 24% | 15% | 22% | 26% | 38% | 24% | 33% | 14% |
| >18 y (>70 kg) | Upper | -13% | -13% | -10% | -18% | -13% | -17% | -19% | -23% | -17% | -21% | -12% |
| | Lower | 17% | 17% | 12% | 25% | 16% | 23% | 28% | 39% | 24% | 31% | 15% |

Table 6.5: Percentage uncertainties for Siemens Axiom Artis equipment, based on 5$^{th}$ and 95$^{th}$ percentiles of HVL.

| Patient age (mass) | Uncertainty | Effective dose | ABM | Breasts | Heart | Lungs | Lymph | Oesophagus | Thyroid | Liver | Stomach | Average dose |
|---|---|---|---|---|---|---|---|---|---|---|---|---|
| <1 y (<9.2 kg) | Upper | -30% | -31% | -27% | -38% | -27% | -36% | -39% | -46% | -37% | -45% | -29% |
| | Lower | 11% | 10% | 13% | 12% | 7% | 12% | 13% | 19% | 12% | 16% | 9% |
| 1-5 y (9.2-19 kg) | Upper | 12% | 14% | 9% | 16% | 10% | 15% | 17% | 26% | 15% | 22% | 11% |
| | Lower | -35% | -37% | -29% | -44% | -33% | -42% | -45% | -52% | -42% | -52% | -35% |
| 5-10 y (19-32 kg) | Upper | 13% | 15% | 11% | 19% | 11% | 18% | 20% | 28% | 18% | 24% | 13% |
| | Lower | -39% | -39% | -34% | -49% | -36% | -45% | -50% | -64% | -46% | -55% | -37% |
| 10-15 y (32-56 kg) | Upper | 14% | 16% | 10% | 21% | 13% | 20% | 24% | 30% | 21% | 27% | 14% |
| | Lower | -34% | -41% | -19% | -50% | -39% | -48% | -52% | -60% | -50% | -58% | -38% |
| 15-18 y (>56 kg) | Upper | 18% | 17% | 13% | 25% | 16% | 23% | 27% | 40% | 25% | 34% | 15% |
| | Lower | -43% | -41% | -34% | -54% | -43% | -50% | -55% | -64% | -54% | -60% | -39% |
| >18 y (>70 kg) | Upper | 18% | 18% | 12% | 26% | 17% | 24% | 29% | 40% | 25% | 32% | 15% |
| | Lower | -43% | -42% | -33% | -54% | -44% | -51% | -56% | -62% | -52% | -59% | -39% |

Table 6.6: Percentage uncertainties for 2nd generation equipment (Philips Integris, Toshiba Infinix CB, Siemens Bicor plus/Hicor) based on uncertainty in HVL

| Patient age (mass) | Uncertainty | Effective dose | ABM | Breasts | Heart | Lungs | Lymph | Oesophagus | Thyroid | Liver | Stomach | Average dose |
|---|---|---|---|---|---|---|---|---|---|---|---|---|
| **<1 y (<9.2 kg)** | Upper | -20% | -23% | -12% | -30% | -20% | -28% | -31% | -35% | -29% | -35% | -22% |
| | Lower | 17% | 18% | 16% | 23% | 15% | 22% | 24% | 32% | 23% | 30% | 17% |
| **1-5 y (9-19 kg)** | Upper | -24% | -27% | -15% | -34% | -25% | -32% | -36% | -37% | -32% | -40% | -26% |
| | Lower | 21% | 23% | 17% | 30% | 19% | 27% | 30% | 38% | 27% | 38% | 21% |
| **5-10 y (19-32 kg)** | Upper | -30% | -29% | -28% | -38% | -28% | -35% | -39% | -58% | -35% | -44% | -27% |
| | Lower | 24% | 25% | 20% | 34% | 22% | 31% | 36% | 56% | 32% | 42% | 23% |
| **10-15 y (32-56 kg)** | Upper | -23% | -30% | -9% | -39% | -30% | -36% | -38% | -48% | -39% | -48% | -28% |
| | Lower | 20% | 27% | 10% | 36% | 25% | 33% | 38% | 50% | 35% | 46% | 24% |
| **15-18 y (>56 kg)** | Upper | -32% | -30% | -24% | -42% | -33% | -38% | -42% | -47% | -42% | -46% | -28% |
| | Lower | 28% | 26% | 20% | 40% | 28% | 36% | 42% | 56% | 40% | 49% | 24% |
| **>18 y (>70 kg)** | Upper | -32% | -31% | -24% | -42% | -34% | -39% | -44% | -57% | -40% | -47% | -29% |
| | Lower | 28% | 27% | 20% | 41% | 29% | 37% | 43% | 49% | 38% | 47% | 24% |

Table 6.7: Percentage uncertainties for 1st generation equipment (Siemens Bicor and Coroskop) based on uncertainty in HVL.

**Philips Integris:** Again, information is limited to a few previous publications (Table 6.1). A central HVL of 4.8 mm Al was selected, corresponding to a tube potential of 70 kV, fixed aluminium filtration of 1.5 mm Al and copper filtration of 0.3 mm (i.e. halfway between the commonly used values of 0.2 and 0.4 mm). A lower HVL uncertainty limit of 3.3 mm Al was used, based on 60 kV and 0.1 mm Cu. The upper HVL uncertainty was set at 6.3 mm Al, based on 0.4 mm of Cu and 80 kV. This range in HVL is thus the largest of all equipment types studied.

**Toshiba Infinix CB**: Tube potential was recorded for 50 procedures conducted using this machine at Hospital 1 between 1999 and 2001. The mean potential was 76 kV (range: 70 to 88). The anode angle was stated to be 8° by a used equipment vendor [253], but the filtration was unknown. A central HVL of 4.8 mm was again used for this machine, being typical of equipment of this era, with the same uncertainty limits as the Philips Integris (3.3 to 6.3 mm).

### *6.1.5: Limitations of beam energy analysis*

Only an image intensifier equipped Siemens Axiom Artis was studied, while in reality both image intensifier and flat panel equipped machines are used in practice. It is unclear if the beam energy characteristics differ between the two detector types. Irrespective of detector type, scope for variation in beam energy exists for otherwise identical machines depending on setup and software upgrades. This is illustrated by the large difference in copper filtration thickness used for Siemens Artis Zee machines at Hospitals 2 and 4. The sample of examinations for which structured dose reports were obtained was quite small. Unfortunately, obtaining these reports was very time consuming. Future research could make use of automatic recording of imaging metadata.

Comparison of these findings with previous research is challenging. The previously mentioned AAPM report [271] provides limited details of imaging parameters, therefore it is difficult to determine equivalency of findings. A pattern of decreasing copper filtration and increasing tube potential with greater attenuator thickness was found in both the current and AAPM studies, although the thicknesses of PMMA at which these changes occur was not the same. The AAPM team noted an increase in tube potential from 58 to 66 kV with associated decrease in copper filtration from 0.9

to 0.6 at 7.6 cm of PMMA, while for the current study, this combination was not used until 16 cm was reached. The AAPM reports also suggests the use of 0.3 mm of copper occurs at a smaller thickness of PMMA (18 cm) than was found in the current study (22 cm). These variations support the comments above concerning uncertainty in beam energy due to differences in protocols and software upgrades.

### *6.2: Beam angles*

As with beam energy, previously published information on the beam angles used for cardiac catheterizations is limited. The following sections describe attempts to gather information on beam angles used in clinical practice along with the impact of uncertainty in beam angle on dose estimates. A description of the terminology used for describing x-ray beam angles is given in the appendix.

#### *6.2.1: Methodology*

Four sources of information on beam angles were used:

1. ***Projection angle questionnaire:***

The first investigation involved simply asking specialised cardiac radiographers which beam projections they used. A questionnaire was sent to radiographers working at participating hospitals, enquiring about typical beam angles used for various procedure types.

2. ***Logbook records:***

The beam angles used for each procedure were recorded at Hospital 2 from 2004 onwards. These were only recorded for acquisitions and not for non-acquisition fluoroscopy. In many cases, acquisitions are carried out in two beam angles simultaneously using the frontal and lateral x-ray tube. This allows iodinated contrast agent (which is osmotoxic and can cause renal damage and allergic reactions) to be injected as sparingly as possible.

3. ***Structured dose reports and PACS images:***

As well as recording tube potential and added filtration, the structured dose reports recorded by Siemens equipment also records beam angles. As with the angles recorded in log books at Hospital 2, only acquisition beam angles are listed. Images

stored on the PACS network display the same beam angle information as dose reports. The procedure names listed on PACS are often rather vague - many are entered under the non-specific name of “congenital anomaly study” - meaning it was difficult to search the PACS archive for specific procedure types. Consequently, a greater sample of procedures was obtainable for some procedures than for others.

*4. Biplane kerma area product:*

Hospitals 1 and 4 record $P_{KA}$ as separate figures for frontal and lateral x-ray tube outputs. This allows some information on beam projections to be inferred, including the proportion of total $P_{KA}$ in each angle.

Along with information on the beam angles used for different procedures, information on the proportion of the total examination dose originating from each of these angles is also required. This is relatively straightforward for examinations in which only straight PA and straight left lateral projections tend to be used; the proportions can be derived from the Biplane $P_{KA}$ data described above. The situation is more complex for examinations in which two or more projections involve the same x-ray tube (mainly pulmonary artery and coronary angiography procedures). Structured dose reports can help, but only provide information for acquisitions, not fluoroscopy.

### *6.2.2: Results*

Data obtained on beam angles will now be presented separately for each of the four methodologies described above:

*Beam quality questionnaire.*

The compiled results of the beam angle questionnaire are shown in Table 6.8. Unfortunately, there are a lot of gaps. In some cases the hospitals sent their own departmental protocols for various imaging procedures rather than filling out the questionnaire. Although this information was still useful, comparison between hospitals was difficult. Reported projections for aortic and pulmonary valvuloplasty, pulmonary vascular resistance (PVR) studies and atrial septostomy procedures were consistent (PA and lateral), as were those for electrophysiology studies (EPS), although the level of left anterior oblique angulation varied from 30 to 50°. Other differences including reported usage of a small level of oblique angulation for coarctation repairs and PDA closures. Reported coronary angiography beam angles

have been colour coded for easier comparison. All hospitals reported use of a 30° right anterior oblique (RAO) projection, a left anterior oblique (LAO) beam and a LAO beam with caudal angulation. The lateral projection was reported at Hospitals 2 and 3 but not at Hospital 4. The level of angulation varied between centres. It should be noted that coronary angiographies and endomyocardial heart biopsies are only regularly conducted at Hospitals 1 and 4, where transplant procedures are carried out.

| Hospital: | 4 | 4 | 2 | 3 | 1 |
|---|---|---|---|---|---|
| Source: | Radiographer | Cardiologist | Protocol | Protocol | Radiographer |
| Coronary angiography | RAO 20,<br>CR 40,<br>RAO 20/CAU 40,<br>LAO 50/CAU 30,<br>RAO 30,<br>LAO 30 | | LAO 30/CAU 40,<br>Lateral,<br>RAO 30,<br>LAO 60 | LAO 30/CAU 40, RAO 30,<br>RAO 30/CAU 25, LAO 60/CR 25,<br>LAO 60<br>Lateral<br>PA | AP Plane:<br>RAO 30<br>CAU 10<br><br>Lateral plane:<br>LAO 45<br>CR 20<br>LAO 60 |
| PDA closure | PA,<br>Lateral | RAO 30,<br>Lateral | | | RAO 25,<br>Lateral |
| ASD closure | PA,<br>Lateral | | | | PA,<br>Lateral |
| AV angioplasty | PA,<br>Lateral | | | | PA,<br>Lateral |
| PV angioplasty | PA,<br>Lateral | | PA,<br>Lateral | | PA,<br>Lateral |
| Heart biopsy | PA | | | | PA,<br>Lateral |
| PA angioplasty | | PA,<br>Lateral | LAO 25/CR 25 | | LAO 40/CR40<br>Lateral/CAU 10 |
| EPS | RAO 30,<br>LAO 50 | RAO 30,<br>LAO 30 | | RAO 30,<br>LAO 45 | PA |
| PVR | PA,<br>Lateral | | | | PA<br>Lateral |
| Atrial septostomy | PA,<br>Lateral | | | | PA,<br>Lateral |
| Pacemaker | PA | | | | PA, RAO 30,<br>LAO 30 |
| Coarctation repair | PA,<br>Lateral | PA,<br>Lateral | | | LAO 15,<br>Lateral |
| Any others | | LAO 30,<br>Lateral (arch aortogram) | | | |

**Table 6.8: Beam angles reported by staff at participating hospitals. Angles separated by a '/' represent both rotational and cranio-caudal angulation together for the same projection.**

*Logbook records of beam angles:*

Where all procedure types were analysed as a whole, 48% of acquisitions were listed as being in the PA projection, while 35% were in the left lateral projection. The remainder were various combinations of oblique beam angles, including right anterior oblique (3%) and left anterior oblique (3%). These proportions varied between procedure types (Figure 6.12). The majority of ASD occlusions, electrophysiology studies (EPS), radiofrequency ablations (RFA), and pacemaker procedures involved acquisitions only the PA projection. Procedures involving angioplasty of coarctations and pulmonary or aortic valve stenosis usually used PA and lateral projections only. More complex combinations of beam angles were used for angioplasty of the pulmonary arteries. These were usually anterior oblique angles with around 25° cranial angulation.

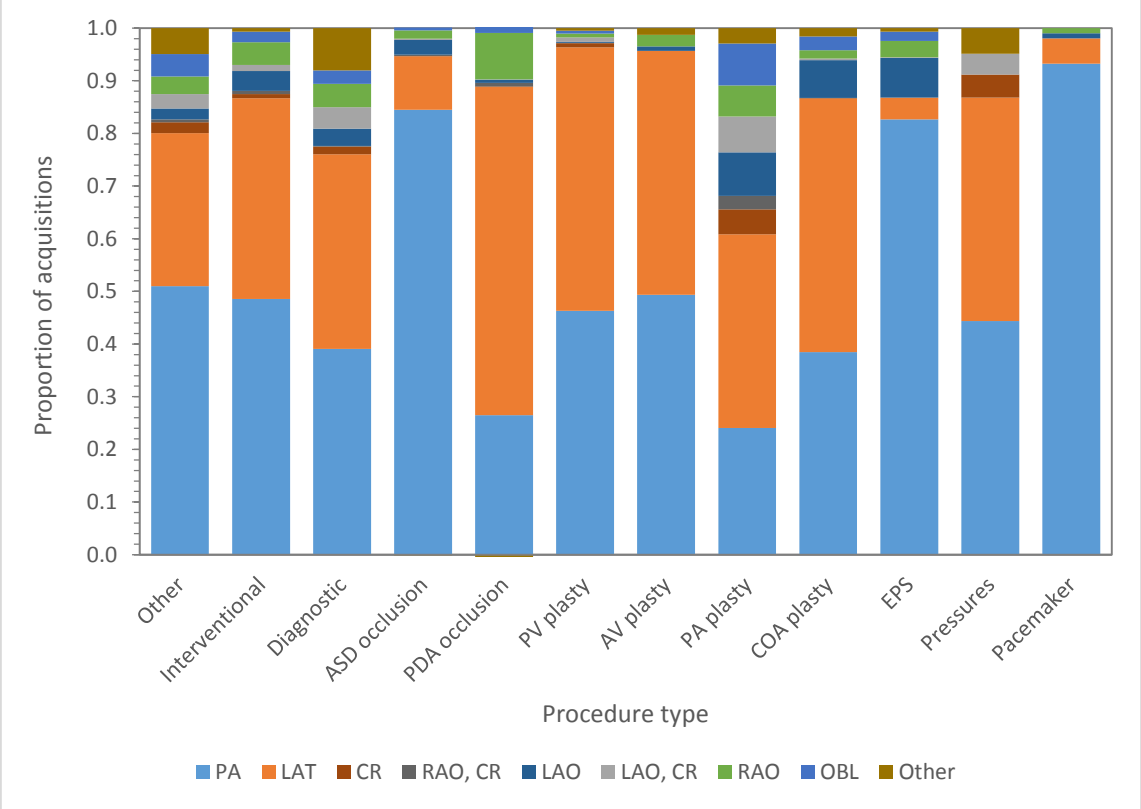


**Figure 6.12: Proportion usage of different imaging projections for acquisitions. CR=cranial, OBL=oblique, 'Sit up' and 'Long Axis' views are a combination of oblique and lateral projections**

*Structured dose reports and PACS images:*

Hospital 2: Details of 64 complete examinations comprising 324 acquisitions were recorded. Of all acquisitions, 85 were straight PA projections (26.2% of total), 147 were left laterals (45.4%), while 77 were oblique (28.4%). The proportion of acquisitions recorded in structured dose reports as being in either PA or lateral projections (71.6%) was lower than recorded in the logbooks (83%). Of all complete examinations recorded, 25 (39%) involved only PA, left lateral or both PA and lateral projections only. A further 6 examinations (9%) involved a single acquisition in an oblique projection with all other acquisitions in PA or lateral. All other examinations involved at least 2 acquisitions in an oblique projection. Analysis of the beam angles used for different examination types is difficult as the sample size is relatively small for individual procedures. For all diagnostic procedures combined, (111 acquisitions in total), 36 projections were PA (32.4%), 48 were lateral (43.2%) and 27 were oblique (24.3%). For combined Interventional procedures (178 acquisitions), 43 were PA (24.7%), 83 were lateral (46.6%) and 52 were oblique (29.2%). For three examinations of the pulmonary arteries, 5% of acquisitions were in the PA, projection were 43% lateral and 52% were oblique projections, typically with around 25° cranial and 25° left anterior oblique angulation. These angles are consistent with those reported in the questionnaires, although the proportion of acquisition in the PA projection is lower than suggested by logbook records.

*Hospital 4:* Dose reports for 49 examinations conducted using Siemens Axiom Artis machines were collected, along with details from 169 examinations stored on the PACS network. Figure 6.13 shows the proportion of acquisitions in various beam angles for nine of the most commonly conducted examinations, along with broad diagnostic, interventional and ‘other’ categories. There are a number of differences in these proportions to those shown in Figure 6.12, derived from logbook records of beam angles at Hospital 2. The main observation was the relatively lower use of the straight PA projection at the Hospital 4 and greater use of oblique projections. This was especially apparent for ASD occlusions in which PA projections were usually modified with a small right anterior oblique angle (around 10°), along with considerably greater usage of the left lateral projection. The use of the RAO and left lateral projections for PDA occlusions were consistent with the angles reported by

the cardiologist but not the radiographer (who stated PA and lateral). The projections used for aortic and pulmonary valvuloplasty were consistent with those of the questionnaire and Hospital 2 logbook records.

In terms of beam angles, coronary angiographies are relatively unusual procedures and deserve special attention. Straight PA and lateral projections tend to be avoided in favour of various oblique projections. In most cases, the procedure is purely diagnostic, with only one acquisition carried out in each projection angle. This contrasts with most other examination types in which one or two projections are favoured for the whole examination. Beam angle data was analysed from PACS images and structured dose reports for 40 coronary angiography procedures conducted at the Hospital 4. Ten different projections were identified; these were various combinations of right or left anterior oblique angles, with or without cranial or caudal angulation, plus occasional use of straight PA and left lateral projections (Figure 6.14). The most common of these, used in 90% of examinations, was a left anterior oblique angle with no cranial or caudal angulation (Figure 6.15). The straight left lateral projection was avoided in all but one examination. Dose (as represented by $P_{KA}$) was fairly evenly distributed between different projections.

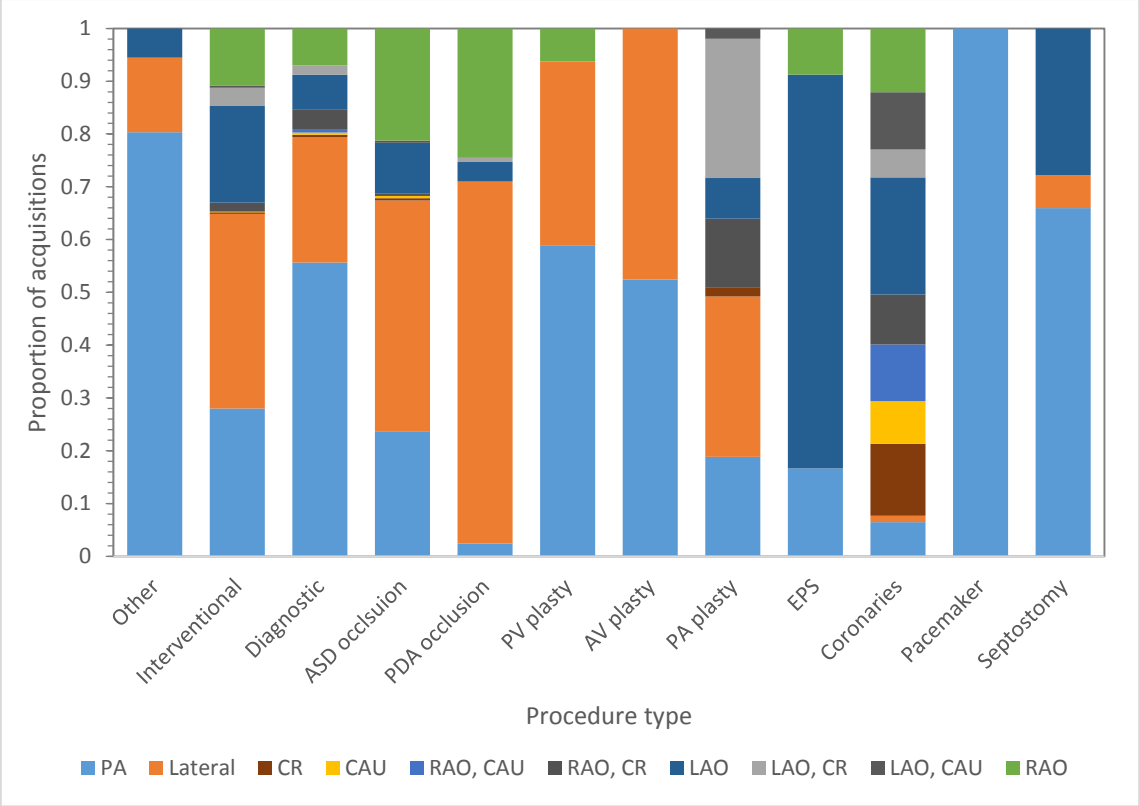


**Figure 6.13: Beam angles obtained from structured dose reports and PACS images at Hospital 4**

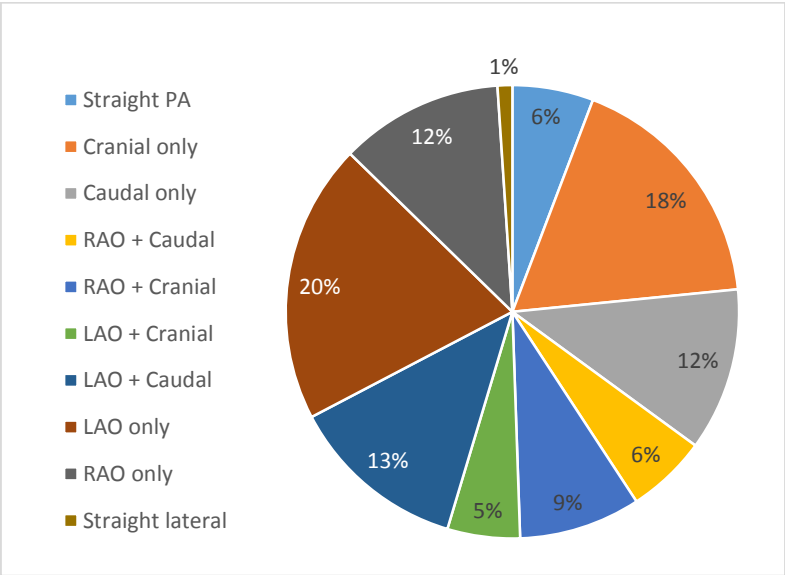


**Figure 6.14: Percentage of examination $P_{KA}$ originating from different projections for coronary angiography at Hospital 4.**

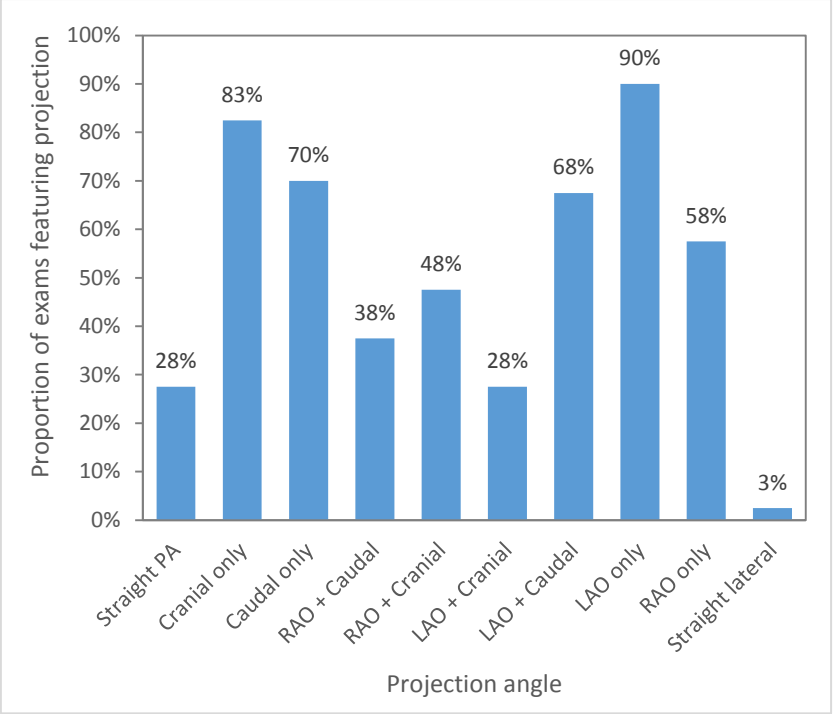


**Figure 6.15: Percentage of coronary angiography examinations in which a particular projection is used.**

### *Biplane $P_{KA}$*

Hospitals 1 and 4 record $P_{KA}$ as separate figures for frontal and lateral x-ray tube outputs. This allows some inferences to be made, particularly in regard to the proportions of total $P_{KA}$ in each projection, but provides little information on the actual beam angles used (i.e. output from the lateral tube does not necessarily imply the projection was a straight left lateral). The information is therefore more useful for examinations in which oblique projections tend to be avoided and most imaging is done in straight PA or lateral projections.

*Hospital 1:* For all procedures combined between 1994 and 2010, the mean and median proportions of total $P_{KA}$ originating from the frontal tube were both 0.61. These figures varied considerably between different procedures (Figure 6.16). Almost all total $P_{KA}$ for ASD occlusions and pacemaker insertions originated from the frontal tube, while the majority of $P_{KA}$ was from the lateral tube for coronary angiography and PDA occlusions. The proportions also varied with era. The proportion of $P_{KA}$ from the frontal tube tended to be lower between 2002 and 2008 (where the majority of data were acquired) than for other eras.

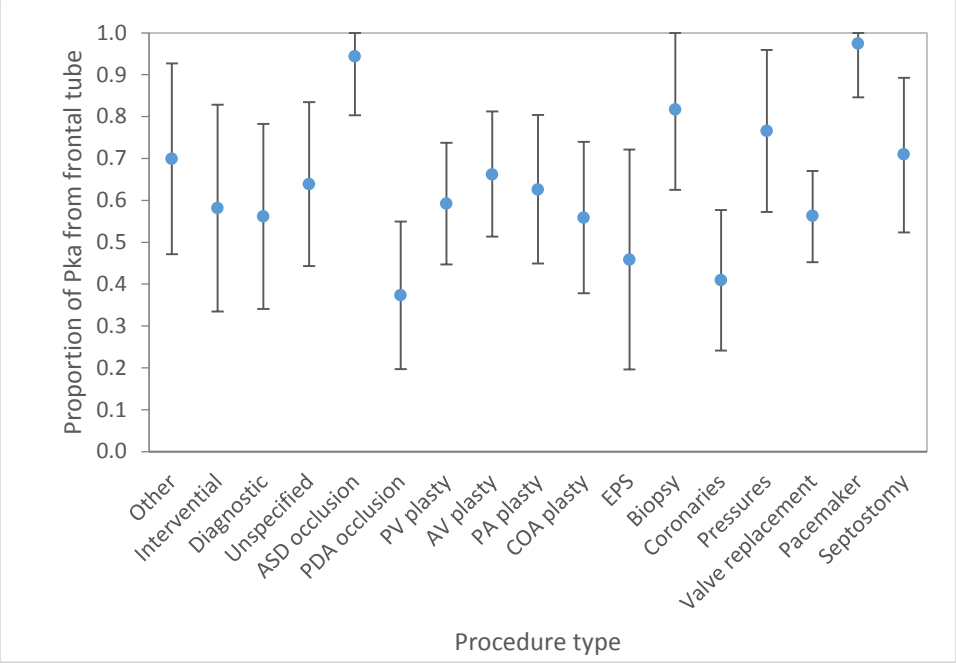


**Figure 6.16: Proportion of total $P_{KA}$ from the frontal x-ray tube for different procedures at Hospital 1 from 1994 to 2010. Error bars represent one standard deviation.**

***Hospital 4:*** Biplane $P_{KA}$ was recorded sporadically at Hospital 4. For 1126 procedures conducted from November1994 to May 2005, the mean and median proportions of $P_{KA}$ from the frontal tube were 0.61 and 0.62 respectively. These proportions are clearly very similar to those of Hospital 1 (mean and median were both 0.61), though the lack of detailed procedure type information prevents further analysis. Analysis of structured dose reports from Hospital 4 (which are considerably more reliable) demonstrated a proportion of total $P_{KA}$ from the frontal tube of 0.63. This could be analysed separately for fluoroscopy (0.73) and acquisitions (0.57).

***Hospital 2:*** Only total $P_{KA}$ figures were recorded in logbooks at Hospital 2, though a crude approximation of the relative involvement of frontal and lateral x-ray tubes could be obtained from the number of acquisitions involving each output. In this case, the proportion of acquisitions involving the frontal tube was 0.59 for all procedures combined. For most procedures and categories, a reasonable level of agreement was found with the mean proportions of total $P_{KA}$ from the frontal x-ray tube at Hospital 1 (Figure 6.17). This is especially significant considering these data were obtained using two different methodologies at two different hospitals. The largest differences are for pressure studies and EPS procedures. Is these cases, the reason for the discrepancy appears to be that these procedure generally do not involve

acquisitions (the same logic would also apply to pacemaker insertions, although the agreement between acquisitions and total $P_{KA}$ is very high in this case).

A further source of biplane information at Hospital 2 was the 64 structured dose reports obtained for procedures conducted between 2011 and 2014. Based on this source, the mean proportion of total $P_{KA}$ for all procedures combined from the frontal x-ray tube was 0.75 (0.88 for fluoroscopy and 0.53 for acquisitions). This proportion is higher than previously discussed figures derived from other sources, though the sample size was small and the procedure mix relatively limited.

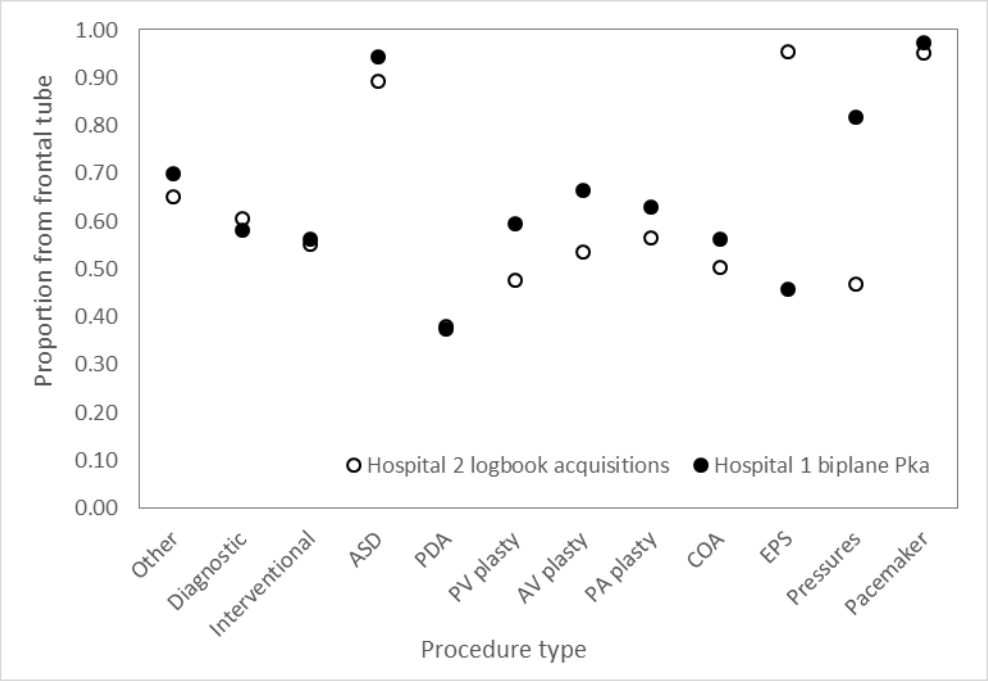


**Figure 6.17: Proportion of total $P_{KA}$ from the frontal tube at Hospital 1 compared to proportion of the number of acquisitions using the frontal tube at Hospital 2 (2004-2008). Data are presented for 3 procedure categories, plus nine common individual procedures.**

### *6.2.3: Discussion (beam angles)*

The four methodologies used to establish projection angles each have their own strengths and limitations. Structured dose reports and PACS images provide details of the exact beam angles used for acquisitions and the relative proportions of such, but lack information on the angles used for fluoroscopic exposures. Biplane $P_{KA}$ figures include fluoroscopy, but provide little information on angles other than whether the frontal or lateral x-ray tube was used. Questionnaires provide some

information on the variation in projections between centres but provide no information on the relative proportions of different angles. Lastly, logbook records of acquisition beam angles have the advantage of offering a very large sample size, but provide only a crude approximation of relative proportions.

A number of observations can be made. Firstly, the projections used vary between different procedure types. This was not unexpected as different beam angles are required to demonstrate different anatomical features such as heart chambers, vessels and valves. In some cases, more than one projection may be used to visualise a particular structure, giving scope for variation in beam angles between different hospitals or (potentially) between different cardiologists at the same hospital. As with beam energy, a degree of uncertainty in projection angles is unavoidable. This uncertainty will be quantified later in this chapter.

Analysis of structured dose reports suggests that a greater proportion of acquisitions have some form of oblique angulation than is suggested by questionnaire results and angles recorded in logbooks. One explanation is that a PA projection with a small amount of oblique angulation may be casually referred to as 'PA'. This appears to be the case for ASD occlusions, in which the use of a 15° LAO angulation was acknowledged as "pretty much standard practice to bring the atrial septum into profile" (S. Charlton, personal communication) by the same radiographer who listed the projections as being 'PA and Lateral' in the questionnaire. Both Hospitals 2 and 4 reported the use of oblique beam angles for EPS and ablation procedures, even though the majority of these examinations appeared to only involve the PA projection according to information recorded in logbooks. This could be explained by the fact that these procedures rarely involve acquisitions, meaning the figures recorded in logbooks (which are for acquisitions only) may not represent the angles in which the majority of irradiation occurred.

There was some scope for hospital specific beam angle combinations. This was more appropriate for hospitals in which good quality information on beam angles was obtained (Hospitals 1,2 and 4). In particular, the much greater use of the lateral projection for ASD occlusions at the Hospital 4 ought to be taken into account. Unfortunately, due to the limited examination type details recorded at this hospital, it was not possible to identify which procedures were ASD occlusions. Variation in coronary angiography beam angles was also seen between Hospitals 1 and 4.

However, this difference was based on radiographer reported angles, with no structured dose reports at Hospital 1 with which to compare.

A further hospital specific modification was the use of a 15° LAO angulation for coarctation repairs at Hospital 1, rather than straight PA. It can also be implied from Figure 6.17 that the relative usage of PA and lateral projections in pulmonary/aortic valvuloplasty and coarctation repair procedures varies somewhat between Hospitals 1 and 2. This may be true, although the methodologies used to determine the proportions shown in Figure 6. are different - biplane $P_{KA}$ for Hospital 1 and number of acquisitions for Hospital 2. The former may be considered more reliable as the number of acquisitions allow only limited inference of actual dose in any particular beam angle and does not include fluoroscopy.

### *6.2.4: Beam angles used for dose estimation*

There are a number of cardiac catheterizations that are difficult to define as any particular procedure type. For these 'unspecific cardiac catheterizations', the most realistic starting point when estimating likely beam angles would be a combination of straight PA and straight left lateral projections in proportions of 0.6 and 0.4 respectively. These are by far the most commonly used projection angles and the proportions are consistent with data from biplane $P_{KA}$ records and acquisition beam angles recorded for individual examinations. This configuration can be encoded in the following matrix used in cardiodose:

$$\begin{bmatrix} 90 & 0 & 0.6 & t \\ 180 & 0 & 0.4 & 0 \end{bmatrix}$$

For example, for a total examination $P_{KA}$ of 2.0 Gy·cm², 1.2 Gy·cm² would be applied in a beam angle of 90° (straight PA) and 0.8 Gy·cm² would be applied in a beam angle of 180° (straight left lateral). The 't' in the matrix means the table attenuation factor is applied for the first projection (PA) but not the second (lateral) Only the frontal output is modified by a table attenuation correction. The same beam angle matrix is also appropriate for coarctation angioplasty and pulmonary/aortic valvuloplasty procedures. Other examination types are listed below.

*Pulmonary artery angioplasty* – aside from coronary angiography, these procedures involve the most complex arrangement of beam angles. The matrix used is based on

beam angles reported by radiographers in proportions suggested by structured dose reports. The proportion for the left lateral beam (180°) is based on biplane $P_{KA}$ data.

$$\begin{bmatrix} 90 & 0 & 0.25 & t \\ 180 & 0 & 0.4 & 0 \\ 115 & -25 & 0.25 & t \\ 65 & -25 & 0.1 & t \end{bmatrix}$$

*ASD occlusion* – these predominantly involve the PA projection, with or without around 10° of right or left anterior oblique angulation. A small contribution from the left lateral projections was added, based on biplane data and acquisition beam angles:

$$\begin{bmatrix} 90 & 0 & 0.93 & t \\ 180 & 0 & 0.07 & 0 \end{bmatrix}$$

ASD occlusion (Hospital 4):

$$\begin{bmatrix} 90 & 0 & ? & t \\ 180 & 0 & ? & 0 \end{bmatrix}$$

*PDA occlusion* – this procedure usually involves PA and left lateral projections, although the small use of a right anterior oblique projection is also taken into account:

$$\begin{bmatrix} 90 & 0 & 0.3 & t \\ 180 & 0 & 0.6 & 0 \\ 60 & 0 & 0.1 & t \end{bmatrix}$$

*Pulmonary and aortic valvuloplasty, coarctation repair* – Almost all procedures utilised the PA and lateral projections only. The respective proportions of these angles were based on biplane $P_{KA}$ data recorded at Hospital 1. These proportions were different from those suggested by the analysis of beam angles recorded in Hospital 2 logbooks (Figure 6.12) although these latter data were considered less reliable, being based solely on the number of acquisitions rather than $P_{KA}$.

Pulmonary valvuloplasty:

$$\begin{bmatrix} 90 & 0 & 0.60 & t \\ 180 & 0 & 0.40 & 0 \end{bmatrix}$$

Aortic valvuloplasty:

$$\begin{bmatrix} 90 & 0 & 0.65 & t \\ 180 & 0 & 0.35 & 0 \end{bmatrix}$$

Coarctation repair:

$$\begin{bmatrix} 90 & 0 & 0.55 & t \\ 180 & 0 & 0.45 & 0 \end{bmatrix}$$

Coarctation repair (Hospital 4) – the use of a small left anterior oblique projection is accounted for:

$$\begin{bmatrix} 105 & 0 & 0.55 & t \\ 180 & 0 & 0.45 & 0 \end{bmatrix}$$

*Coronary angiography:* Angles were based on structured dose reports at Hospital 4, for the 5 most commonly used angles:

$$\begin{bmatrix} 70 & -40 & 0.2 & t \\ 70 & 40 & 0.2 & t \\ 140 & 30 & 0.2 & t \\ 50 & 0 & 0.2 & t \\ 130 & 0 & 0.2 & t \end{bmatrix}$$

*Endomyocardial biopsy* – Most imaging is done in the straight PA projection, though 72% of these procedures involved a small contribution of $P_{KA}$ from the left lateral projection. The majority of biopsies were conducted at Hospital 4 in which biplane information was recorded. In these cases, the proportions in the PA and lateral projections were as given by biplane figures. The following matrix was used in the absence of these data:

$$\begin{bmatrix} 90 & 0 & 0.89 & t \\ 180 & 0 & 0.11 & 0 \end{bmatrix}$$

*Electrophysiology study (EPS)* - this matrix was largely based on radiographer reported beam angles and proportions based on biplane $P_{KA}$ data:

$$\begin{bmatrix} 60 & 0 & 0.5 & t \\ 40 & 0 & 0.5 & 0 \end{bmatrix}$$

*Pressures and pulmonary vascular resistance studies and atrial septostomy* – proportions based on biplane $P_{KA}$ data:

$$\begin{bmatrix} 90 & 0 & 0.75 & t \\ 180 & 0 & 0.25 & 0 \end{bmatrix}$$

*Trans-catheter pulmonary valve replacement*: Based on radiographer reported beam angles. Proportions based on biplane $P_{KA}$ data:

$$\begin{bmatrix} 90 & 0 & 0.65 & t \\ 180 & 0 & 0.35 & 0 \end{bmatrix}$$

### *6.2.5: Errors and uncertainties*

Estimating the uncertainty in organ dose calculations based on variation in beam angles from those expected is challenging. The overall uncertainty encompasses variation in the angles themselves and their respective proportions. The situation is relatively simple for pulmonary and aortic valvuloplasty, valve replacement, coarctation repair, biopsies and pressure studies, which usually involve straight PA and straight left lateral projections. The usage of other beam angles in these procedures was considered negligible. Thus the uncertainty analysis needs only to focus on the variation in proportion between PA and lateral projections. Uncertainty in this proportion was initially based on two standard deviations, though this methodology was abandoned and replaced with 5$^{th}$ and 95$^{th}$ percentiles to allow calculation of separate upper and lower uncertainties and avoid situations in which lower uncertainty limits were greater than 100% (implying negative doses). PA/lateral proportions were obtained from bi-plane $P_{KA}$ figures recorded at Hospital 1 between 1994 and 2010. Total examination doses were calculated with the PA/lateral proportions set at median, 5$^{th}$ and 95$^{th}$ percentile values. The difference in resulting dose to each organ between median and 5$^{th}$/95$^{th}$ percentile proportions was calculated as a percentage figure. These figures are shown in Table 6.9 for pulmonary and aortic valvuloplasty, valve replacement, coarctation repair, biopsies and pressure studies combined. Uncertainties for individual procedures can be found in Appendix 4. As expected, uncertainties are highest for the breasts and relatively low for the lungs and lymph nodes. Uncertainties increase with increasing patient size and vary between the different procedure types. Where biplane $P_{KA}$ figures are recorded for a given procedure, the uncertainties in Table 6.9 are essentially reduced to zero. Thus the rather high beam angle uncertainties for endomyocardial biopsies are immaterial as these procedures were all conducted at hospitals in which biplane figures were recorded (Hospitals 1 and 4).

For other procedure types in which usage of more than two beam angles was recorded, a different process was used. Multiple procedures for each examination type were reconstructed using the beam angles recorded in structured dose reports and the doses calculated using cardiodose. All other parameters, including total examination $P_{KA}$, patient size and beam energy were kept constant. Total examination doses for each organ were obtained by summing the doses from the individual beam angles comprising the reconstructed procedure. Any variation in these doses was due to variation in beam angles and their associated proportions. Uncertainties were defined using the 5$^{th}$ and 95$^{th}$ percentiles of these figures and expressed as a percentage variation from the median. This process was repeated for six different patient sizes. The uncertainties for 'other' or unspecified examinations were calculated from the mean values of uncertainties for all procedures for which uncertainties were calculated. These uncertainties are shown in Table 6.10, for coronary angiography, PDA/ASD occlusions and pulmonary angioplasty combined.

Uncertainties for breast dose require special consideration. In the Computational Dosimetry chapter, it was demonstrated that depending on the combination of beam angle, field size and central ray position, breast dose in the lateral projection may be as low as that in the PA projection, or several times higher. For central dose estimates, the latter situation has been assumed, while the former must be regarded as clinically plausible (and desirable) and needed to be accounted for in uncertainty limits. Thus the lower limit for breast dose was set to be no higher than would be obtained if the entire procedure was conducted in the PA projection.

### 6.2.6: Table Reduction factor

For many projections, the x-ray table and mattress attenuate the x-ray beam before it reaches the patient. The only hospital known to apply a correction factor to 'raw' $P_{KA}$ data (i.e. as quoted by the equipment) to account for table attenuation is Hospital 4. For all other hospitals, it was assumed that no such factor was applied. Previous studies by Ubeda *et al* [282] and Martinez *et al* [94] have quoted transmission factors due to table and mattress attenuation of 0.81 and 0.82, respectively, i.e. reduction in beam intensity by 19% and 18%. Used equipment vendors [253] usually quote table attenuation, in terms of aluminium equivalence, at 1 mm. Beer's law was used to calculate the reduction in beam intensity, using quoted mass attenuation coefficients

of 0.37, 0.57 and 1.13 $cm^3/g$ at 50, 40 and 30 keV and a density of 2.7 $g/cm^3$ [16] (i.e. linear attenuation coefficients of 1.0, 1.5 and 3.1 $cm^3$, respectively). This yielded transmission factors of 0.90, 0.86 and 0.74 for 50, 40 and 30 keV beams, respectively. The mean of these three figures was 0.83, thus very close to the transmission factors quoted by Ubeda *et al* [282] and Martinez *et al* [94]. If the x-ray beam is angulated (i.e. not perpendicular to the table), the thickness of material traversed by the beam will be increased. The relative increase in thickness can be determined as $1 / \cos \theta$, where $\theta$ is the angulation away from perpendicular. The maximum oblique angulation was 40° ($2\pi/9$). This results in an increase in thickness of material traversed of 31% and an increase in table attenuation by 5.4%. The average transmission factor for angles ranging from 0° (i.e. perpendicular to the table) to 40° for the three x-ray energies was 0.81. This figure was used for organ dose calculations for all projections except straight left lateral. Most table surfaces are flat. The table used in Siemens Artis Zee systems is slightly concave, though by an insufficient extent to influence the above calculations.

### *6.3: Conclusion*

Information was gathered on the beam energy and projection angles used for cardiac catheterizations in clinical practice. Central values of these parameters were estimated from a range of sources, with structured dose reports being considered the most reliable. It is acknowledged that considerable uncertainty exists in these values. These uncertainties have been estimated from available data. The following chapter presents estimates of organ doses calculated using the 'Cardiodose' dosimetry system, utilising the information presented in this chapter.

| Age range (mass) | Uncertainty | Effective dose | Bone marrow | Breasts | Heart | Lungs | Lymph nodes | Oesophagus | Thyroid | Liver | Stomach | Average dose |
|---|---|---|---|---|---|---|---|---|---|---|---|---|
| **<1 years (<9.2 kg)** | Upper | 6% | 14% | 30% | 11% | 3% | 0% | 2% | 5% | 20% | 3% | 3% |
| | Lower | -3% | -20% | -18% | -7% | -3% | 0% | -2% | -4% | -14% | -3% | -4% |
| **1-5 years (9.2-19 kg)** | Upper | 11% | 11% | 39% | 16% | 1% | 3% | 7% | 5% | 30% | 4% | 1% |
| | Lower | -7% | -15% | -24% | -11% | -1% | -2% | -5% | -3% | -19% | -5% | -2% |
| **5-10 years (19-32.4 kg)** | Upper | 14% | 10% | 52% | 10% | 3% | 1% | 2% | 10% | 32% | 8% | 2% |
| | Lower | -9% | -15% | -31% | -7% | -1% | -1% | -1% | -7% | -21% | -11% | -3% |
| **10-15 years (32.4-56.3 kg)** | Upper | 18% | 14% | 67% | 7% | 2% | 2% | 1% | 7% | 31% | 10% | 4% |
| | Lower | -11% | -19% | -40% | -4% | -1% | -2% | -2% | -5% | -20% | -14% | -6% |
| **15-18 years (>56.3 kg)** | Upper | 15% | 14% | 78% | 4% | 5% | 3% | 7% | 13% | 35% | 14% | 3% |
| | Lower | -9% | -20% | -47% | -2% | -2% | -3% | -9% | -8% | -23% | -19% | -4% |
| **>18 years (>70 kg)** | Upper | 16% | 14% | 86% | 4% | 6% | 5% | 12% | 8% | 35% | 19% | 4% |
| | Lower | -10% | -21% | -51% | -6% | -3% | -6% | -16% | -4% | -23% | -26% | -5% |

Table 6.9: Upper and lower percentage uncertainties in organ dose due to variation in the proportion of PA and lateral projections. Figures are the average for Pulmonary/aortic valvuloplasty, coarctation repair, atrial septostomy, valve implantation and biospies.

| Age range (mass) | Uncertainty | Effective dose | Bone marrow | Breasts | Heart | Lungs | Lymph nodes | Oesophagus | Thyroid | Liver | Stomach | Average dose |
|---|---|---|---|---|---|---|---|---|---|---|---|---|
| **<1 years (<9.2 kg)** | Upper | 10% | 19% | 37% | 9% | 6% | 5% | 7% | 10% | 25% | 15% | 3% |
| | Lower | -11% | -22% | -37% | -13% | -3% | -4% | -7% | -9% | -15% | -15% | -3% |
| **1-5 years (9.2-19 kg)** | Upper | 12% | 15% | 47% | 14% | 7% | 5% | 7% | 10% | 29% | 12% | 1% |
| | Lower | -13% | -16% | -38% | -18% | -6% | -7% | -8% | -9% | -20% | -14% | -1% |
| **5-10 years (19-32.4 kg)** | Upper | 16% | 14% | 53% | 11% | 10% | 5% | 5% | 11% | 32% | 15% | 2% |
| | Lower | -17% | -15% | -42% | -17% | -10% | -8% | -6% | -12% | -22% | -16% | -1% |
| **10-15 years (32.4-56.3 kg)** | Upper | 18% | 18% | 49% | 13% | 9% | 7% | 8% | 11% | 35% | 21% | 4% |
| | Lower | -18% | -21% | -44% | -15% | -11% | -6% | -7% | -13% | -23% | -22% | -3% |
| **15-18 years (>56.3 kg)** | Upper | 13% | 19% | 44% | 15% | 12% | 8% | 9% | 16% | 41% | 28% | 2% |
| | Lower | -16% | -21% | -43% | -16% | -18% | -10% | -9% | -18% | -27% | -27% | -2% |
| **>18 years (>70 kg)** | Upper | 13% | 20% | 44% | 17% | 13% | 9% | 13% | 18% | 40% | 32% | 3% |
| | Lower | -15% | -21% | -44% | -13% | -17% | -7% | -14% | -20% | -27% | -36% | -2% |

Table 6.10: Upper and lower uncertainties for coronary angiography, PDA occlusions, ASD occlusions, and Pulmonary angioplasty

# Chapter 7: Physical dosimetry

This chapter describes the attempt to verify the findings of the previously described Monte Carlo simulations and Cardiodose dosimetry system using the alternative methodology of physical measurements conducted with anthropomorphic phantoms and thermoluminescent dosemeters (TLDs). Anthropomorphic phantoms are mannequins made from materials with similar x-ray interaction properties to human tissues [283]. They are designed to appear approximately similar to a living person when x-rayed, and usually have the capability to be disassembled to allow small dose measuring devices to be placed inside. A more detailed description of the phantoms used in this study, along with a description of thermoluminescent dosimetry is provided below.

## *7.1: Methodology*

Physical measurements were conducted using 'ATOM' anthropomorphic phantoms manufactured by CIRS (Norfolk, Virginia, USA) [284] (Figure 7.1). Five different phantom sizes were available, representing new-born, 1 year, 5 year, 10 year and 15 year old individuals. Conveniently, these are the same paediatric patient ages represented in PCXMC. ATOM phantoms are made from tissue equivalent epoxy resin, with no human remains [284] (some phantoms utilise a real human skeleton). The bone density varies with phantom size, from 1.41 to 1.6 g/cm$^3$ (electron density; 4.606 x10$^{23}$ to 5.030 x 10$^{23}$/cm$^3$). Human bones comprise an outer layer of dense cortical bone surrounding an inner core of spongy, trabecular bone [255]. ATOM bones are solid with a uniform density equal to the average of trabecular and cortical bone to simplify calculations and eliminate air voids [284]. The density of the lungs is 0.2 g/cm$^3$. All other soft tissue organs were of identical density (1.055 g/cm$^3$) [284]. This uniformity caused problems when positioning the phantoms as the heart was simply the space between the lungs and above the abdomen, and thus difficult to locate. Table 7.1 compares the characteristics of ATOM and PCXMC Monte Carlo phantoms. The phantoms are split into a number of 25 mm thick axial slices allowing them to be disassembled (Figure 7.1). Most slices are drilled with holes allowing dose measuring devices such as TLDs or metal oxide semiconductor field effect transistors (MOSFETs) to be placed inside. Most of the phantom sizes did not have holes drilled in positions representing the heart. Furthermore, only the new born and

1 year phantoms had arms and legs. The remaining phantoms only featured a torso (down to the proximal femora) and a head.

Figure 7.1: Disassembled 1 year ATOM phantom, showing numbered holes in which TLDs can be placed. The arms can also be disassembled. Photo: author

| Characteristic | Phantom | New born | 1 year | 5 years | 10 years | 15 years |
|---|---|---|---|---|---|---|
| **Total height (cm)** | ATOM | *51.0* | *75.0* | *110.0* | *140.0* | |
| | PCXMC 2.0 | 50.9 | 74.4 | 109.1 | 139.8 | 168.1 |
| **Total body mass (kg)** | ATOM | *3.5* | *10.0* | *19.0* | *32.0* | |
| | PCXMC 2.0 | 3.4 | 9.2 | 19.0 | 32.4 | 56.3 |
| **Torso width (cm)** | ATOM | *10.5* | *14.0* | *17.0* | *20.0* | |
| | PCXMC 2.0 | 10.9 | 15.1 | 19.6 | 23.8 | 29.7 |
| **Torso thickness (cm)** | ATOM | *9.0* | *12.0* | *14.0* | *17.0* | |
| | PCXMC 2.0 | 9.8 | 13.0 | 15.0 | 16.8 | 19.6 |
| **Soft tissue Density (g/cm³)** | ATOM | *1.06* | *1.06* | *1.06* | *1.06* | 1.06 |
| | PCXMC 2.0 | 1.04 | 1.04 | 1.04 | 1.04 | 1.04 |
| **Bone Density (g/cm³)** | ATOM | *1.4* | *1.5* | *1.5* | *1.6* | 1.6 |
| | PCXMC 2.0 | 1.22 | 1.4 | 1.4 | 1.4 | 1.4 |
| **Lung Density (g/cm³)** | ATOM * | *0.21* | *0.21* | *0.21* | *0.21* | 0.21 |
| | PCXMC 2.0 | 0.30 | 0.30 | 0.30 | 0.30 | 0.30 |

Table 7.1 Comparison of phantom characteristics for ATOM anthropomorphic phantoms and PCXMC Monte Carlo phantoms. * Lung density for ATOM phantoms is based on inhalation.

Thermoluminescent dosemeters are conceptually similar to the phosphor-based luminous paint on watch dials, in which radiant energy from visible light is absorbed, trapped, and re-emitted later as new visible light photons. TLDs used in x-ray dosimetry typically utilise a crystal of lithium fluoride (LiF) rather than phosphor. Incident x-ray photons provide energy to elevate electrons from the valance band to the forbidden gap whereupon they become stuck in 'traps' caused by the addition of impurities into the crystal. Excited electrons remain trapped until provided with sufficient energy in the form of heating (around 300°C) to escape the electron traps and reach the conduction band [43], after which they return to the valance band, accompanied by the emission of a visible light photon (direct transition from traps to the valance band is forbidden). The intensity of visible light photons emitted following heating is related to the absorbed dose to the TLD. The heating can be in the form of contact with a strip of hot metal, lasers/focused infrared bulbs or hot gas [285]. A controlled increase in heating during the reading process empties electron traps of increasing depth, producing a characteristic 'glow curve', measured using a photomultiplier tube [16].

The TLDs used were lithium fluoride, doped with magnesium and titanium (LiF:Mg,Ti) (Thermo Electron Corporation, Solon, OH). The effective atomic number of LiF (8.2) is comparable to that of soft tissue (7.4) [43], meaning x-ray interaction properties are reasonably similar. The electron traps are sufficiently deep to reduce spontaneous emptying at room temperatures to negligible levels [16]. TLDs have the advantages of small size, re-usability, low cost, and reasonably linear response to radiation at diagnostic dose levels and photon energies. TLDs are fiddly and extremely time consuming to use. The whole process of loading a phantom with TLDs, exposing, removing the TLDs and reading them can typically take 2 days.

Before measurements could be made, the TLDs needed to be calibrated. The entire batch of TLDs were calibrated twice, once at the beginning of the study, and a second calibration after the first phase of exposures (see Exposures section below). The calibration procedure produces a conversion factor for each TLD to convert the measured signal to absorbed dose in milligray. To begin, all TLDs were annealed using a dedicated oven (Model TLD-28, Pickstone Ovens, Thetford, Norfolk, UK) set at 400°, for 12 hours after which they were allowed to cool, undisturbed, for a further

36 hours. The annealing process empties electron traps of residual signal from previous irradiations or background exposure [285].

Following annealing, the TLDs were placed in individual heat sealed bags and attached to a jig designed to allow irradiation of TLDs equidistant from the radiation source (Figures 7.2 and 7.3). The source used to irradiate the TLDs was Caesium-137 ($^{137}$Cs), which decays by β- emission to barium-137 ($^{137}$Ba). Around 90% of the time, $^{137}$Cs decays to a metastable state ($^{137m}$Ba), followed by the emission of a gamma-ray of 661.6 keV [16]. In the remainder, $^{137}$Cs decays directly to $^{137}$Ba with no metastable state. The source was handled with a set of special tongs to maintain distance from the handler, and the time spent with the source was kept to a minimum once it was unshielded. The source was placed in the centre of the calibration jig so as to be equidistant from the TLDs. For the first calibration, this achieved using tape stretched across the jig (Figure 7.). The TLDs were irradiated with the $^{137}$Cs source for 4 Hours 30 minutes, 42 seconds, giving a mean total dose to each TLD of 11.11 mGy.

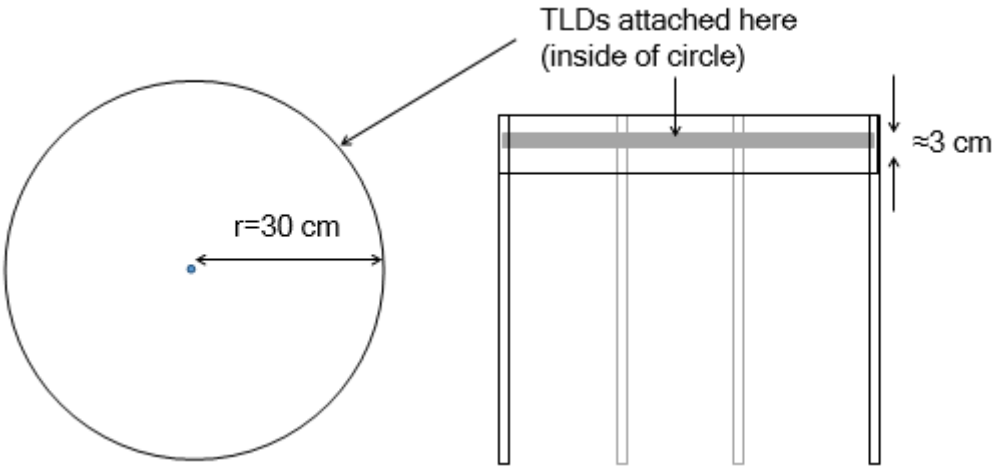


**Figure 7.2: Diagram of TLD calibration setup shown in Figure 7.3. Figure credit: author**

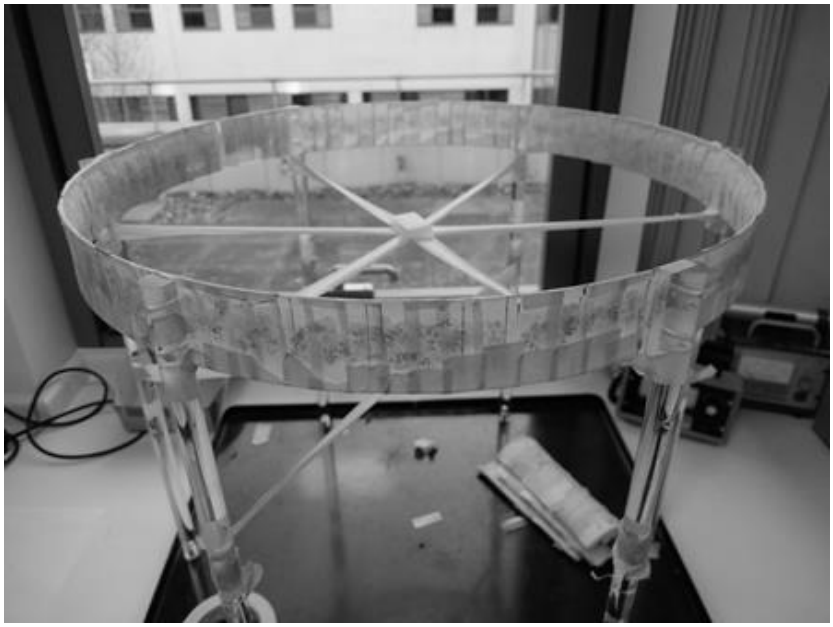

**Figure 7.3: TLD calibration jig as used for the first calibration. Note the tape method of finding the centre of the jig. Photo: author**

After exposure, TLDs were read to produce calibration factors. Each TLD chip responds slightly differently, therefore the calibration factor was specific to each numbered chip. Following calibration, all TLDs were annealed again before usage in dosimetry, using the same annealing protocol as the first time. Reading was carried out using a HARSHAW 5500 TLD reader (Thermo Electron Corporation, Solon, OH) [286], which uses hot nitrogen gas heating. The photomultiplier tubes of the reader are cooled, using cold liquid nitrogen. TLDs were read in batches of 50 at a time, with each batch taking around 35 minutes to read.

Errors in the TLD calibration process came from a number of sources. Firstly, the TLDs were not exactly equidistant from the source. The vertical spread of TLDs on the calibration apparatus was around ±1.5 cm. This results in a variation in the distance from the source of ±0.12% (Pythagoras):

$$Error = \left( \frac{\sqrt{30^2 \pm 1.5^2}}{30} \right) - 1$$

Secondly, the site of the source was found to be not exactly in the centre of the circle, varying from 29 to 31 cm. As beam intensity from a point source is proportional to the inverse square of distance from that source, this small variation in distance from 30 cm would result in a variation in intensity of around ±6.7%.

For the second calibration, a number of changes were made to reduce these uncertainties. Firstly, the tape method of finding the centre of the calibration jig was replaced by an aluminium pole, which reduced variation in distance between the source and TLDs. Secondly, the vertical spread of TLDs on the calibration jig was reduced to around 1 cm. Where the results of the first and second calibrations were compared, the mean absolute variation in calibration factor was 5% (median = 4%), with 1% of calibration factors varying by greater than 20%, 8% varying by greater than 10%, 39% varying by greater than 5% and 87% varying by more than 1%. The largest variation was 268% although this TLD was never used in any phantom irradiations. The mean and median signed variation in calibration factor between first and second calibrations were +0.4 and +1.1% respectively, therefore there was little evidence of a systematic difference.

### *7.1.1: Exposures*

TLDs were placed in all the holes representing the lungs, heart, stomach, liver, bone marrow, thyroid and breasts, using tweezers. A single TLD was placed in each hole. The organs represented by each hole in each phantom slice were determined from the manufacturers' loading schemes. The number or holes representing each organ generally increased with phantom size, from new born to 15 years - Lungs (15-33 holes), Bone marrow (49-67), oesophagus (2-4), liver (7-21), stomach (6-11), breasts (2 for all sizes), thyroid (2-4), heart (8-11).

Phantom exposures were split into two phases. The first phase involved exposing each of the five phantoms, separately, in two projection angles - straight posteroanterior (PA) and straight left lateral. The second phase focused on a single phantom size (10 years) and involved exposures in 7 projection angles ranging from PA to lateral in 10 to 25° intervals, along with a further exposure in the PA projection at a lower beam energy.

For the first phase, exposures were carried out using a Siemens Axiom Artis BC biplane unit at Hospital 4, with image intensifier detectors (Figure 7.4). The machine undergoes routine quality assurance (QA) testing every 12 months. A general use 'native' cardiac paediatric imaging protocol was used (30 frames per second for acquisitions). An antiscatter grid was fitted. The c-arm was positioned and the beam collimated to the region of interest by a specialist cardiac radiographer. This is rather

difficult due to the crude anatomy of the ATOM phantoms. Finding the heart, which is simply the gap between the lungs, is challenging compared to PCXMC, in which organs have been thoughtfully colour coded. The positioning process was guided by fluoroscopy rather than cine-acquisitions. The dose from this initial positioning was generally less than 0.01 Gy·cm$^2$ and regarded as negligible. The image intensifier was positioned as close as possible to the patient. The source-to-skin distance (SSD) was kept at approximately 80 cm.

The phantom was exposed in a single beam projection to a particular value of $P_{KA}$ which depended on phantom size: 1, 2, 5, 10 and 15 Gy·cm$^2$ for new born, 1, 5, 10 and 15 year old phantoms respectively. These values were chosen based on the organ dose per unit $P_{KA}$ derived from Monte Carlo simulations and designed to ensure a mean dose to the lungs and heart of at least 10 mGy. A remainder of 10 TLDs were saved to represent background exposures. The average doses recorded by these background TLDs were subtracted from the values recorded by TLDs placed in the phantoms. Following exposures, the phantoms were disassembled and the TLDs read (see below). The tube potential, added copper filtration and cumulative kerma area product were recorded.

This process was repeated in the second beam projection. Dose estimations for complete examinations could be reconstructed from these data by adding doses from each projection in a particular combination. By obtaining results in individual projections separately, the results could easily be compared to the results of Monte Carlo simulations.

**Figure 7.4: Position of new born phantom for the left lateral position. The arms are raised above the head as would be the case in clinical imaging. The bag over the x-ray tube is for infection control. An antiscatter grid (the black disk) is fitted to the image intensifier. Photo: author.**

For the second phase, exposures were carried out using a Philips BV300 mobile c-arm fluoroscopy machine located in the regional medical physics department at the Hospital 4. This machine undergoes quality assurance testing every 12 months. Unlike the Siemens Axiom Artis, this Philips BV300 utilises circular x-ray fields. A PTW (Freiburg, Germany) M2 Diamentor was attached for $P_{KA}$ measurements and was calibrated at the time of the exposures. The c-arm had no proper attachment for a $P_{KA}$ meter, meaning the device needed to be strapped on (Figure 7.5). For these exposures, the phantom was stood vertically, supported by a table. The phantom itself was rotated for each projection angle rather than the c-arm, which was maintained in the same position. Exposures were carried out in seven projections ranging from straight PA to straight left lateral (rotational angles 90° to 180° in PCXMC terminology). Cranio-caudal angulation was fixed at 0°. A $P_{KA}$ of 10 Gy·cm$^2$ was delivered for each exposure. Unlike the Axiom Artis machine, tube potential could be set manually and was fixed at 70 kV for all exposures investigating the effect of beam angle. The overall HVL of 4.8 mm Al was obtained from QA reports for this machine. This figure is the same as the central value used in Cardiodose.

The process was extremely time consuming, therefore dose to a more limited range of organs was calculated. These were the lungs, heart, oesophagus, breasts and thyroid (i.e. organs in the thoracic region). A second exposure in the straight PA projection was carried out using a tube potential of 60 kV to investigate the impact of beam energy on dose per unit $P_{KA}$.

**Figure 7.5: Setup for exposures using Philips BV300 mobile C-arm unit. Note the kerma area product meter strapped to the x-ray tube. Photo: author**

### *7.1.2: TLD reading*

The same HARSHAW 5500 TLD reader was used for TLD reading following exposures as was used following calibration. TLDs were read approximately the same length of time following exposures as they were following calibration exposures (as there were many TLDs to process, there was clearly a spread of reading times and there were numerous interruptions). Organ doses were calculated as the mean reading for all TLDs representing each tissue. For active bone marrow dose, a different approach was needed as the distribution of this tissue is uneven and varies with age. Information on age-specific bone marrow distribution was obtained from a paper by Cristy [256] (PCXMC Monte Carlo software uses the same approach). These proportions are summarised in Table 7.2. The mean TLD reading representing each of these regions of bone marrow was calculated before being multiplied by the

respective proportion from the Cristy data. The equivalent bone marrow dose (i.e. the average over the whole body) was calculated as the sum of these figures. Not all of the regions in Table 7.2 were simulated in the ATOM phantoms. The larger phantoms (5 years and above) did not have arms, or legs below the proximal femur. Dose values for these bones were assigned based on whichever bone containing TLDs was the closest (e.g. mandible = cervical vertebrae).

| | Age (years) | | | | | | |
|---|---|---|---|---|---|---|---|
| **Region:** | **0** | **1** | **5** | **10** | **15** | **25** | **40** |
| **Cranium** | 27 | 25.1 | 15.9 | 11.6 | 9.2 | 7.7 | 7.6 |
| **Mandible** | 2.5 | 2.4 | 1.6 | 1.1 | 0.9 | 0.8 | 0.8 |
| **Scapulae** | 2.7 | 2.7 | 2.7 | 2.9 | 3.3 | 2.9 | 2.8 |
| **Clavicles** | 0.8 | 0.8 | 0.9 | 0.9 | 1 | 0.8 | 0.8 |
| **Sternum** | 0 | 0.8 | 1.7 | 2.1 | 2.7 | 3 | 3.1 |
| **Ribs** | 9.2 | 8.9 | 8.8 | 10.9 | 13.6 | 15.2 | 16.1 |
| **Cervical vertebrae** | 3.4 | 2.8 | 2.2 | 2.7 | 3.3 | 3.7 | 3.9 |
| **Thoracic vertebrae** | 8.3 | 8.4 | 8.9 | 10.9 | 13.7 | 15.3 | 16.1 |
| **Lumbar vertebrae** | 2.4 | 4.3 | 6.8 | 8.4 | 10.5 | 11.7 | 12.3 |
| **Sacrum** | 0.1 | 2.4 | 5.5 | 6.7 | 8.4 | 9.4 | 9.9 |
| **Os coxae** | 9.2 | 11.1 | 13.1 | 15.6 | 18.5 | 19.5 | 17.5 |
| **Femora, upper half** | 3.7 | 4.1 | 6.8 | 9.4 | 9.2 | 7.4 | 6.7 |
| **Femora, lower half** | 3.7 | 3.9 | 6.3 | 6.1 | 2 | 0 | 0 |
| **Tibiae, fibulae, patellae** | 8.0 | 8.7 | 9 | 5.5 | 0 | 0 | 0 |
| **Ankle and foot bones** | 8.3 | 4.7 | 2.5 | 0 | 0 | 0 | 0 |
| **Humeri, upper half** | 2.3 | 2.4 | 2.4 | 2.5 | 3.1 | 2.5 | 2.3 |
| **Humeri, lower half** | 2.3 | 2.3 | 2.2 | 1.6 | 0.7 | 0 | 0 |
| **Ulnae and radii** | 2.5 | 2.5 | 2 | 1.1 | 0 | 0 | 0 |
| **Wrist and hand bones** | 3.6 | 1.9 | 0.9 | 0 | 0 | 0 | 0 |

**Table 7.2: Percentage distribution of active bone marrow as a function of age. Figures obtained from Cristy [253]. Note: 'Os Coxae' are the bones of the hip and pelvis.**

## *7.2 Results*

### *7.2.1: Phase 1*

The mean TLD readings per unit $P_{KA}$ for each organ are presented for PA and left lateral projections for each phantom size in Tables 7.3 and 7.4. In each case, equivalent figures calculated using Cardiodose are provided for comparison. Some

organ doses could not be calculated - on two occasions, the phantom's head fell off during transporting resulting in the loss of TLDs representing the thyroid.

The highest doses were for the lungs, oesophagus, heart and breasts. Doses to the thyroid, stomach and bone marrow were relatively low. Overall, organ doses calculated using physical measurements were higher than those estimated by Monte Carlo simulations. For the PA projection, the level of agreement between the two methodologies is reasonably high. Agreement was highest for the lungs, oesophagus and stomach and lowest for the liver and breasts. There is little suggestion of an association between phantom size and agreement between physical and Monte Carlo methods. For the left lateral projection, the doses calculated by physical measurements were higher than those of the Monte Carlo counterparts by an average factor of around 2.2. This discrepancy varied between organs, being highest for the liver and oesophagus and lowest for the breasts. Discrepancies were present across all ages – there is no suggestion of a closer match for smaller or larger phantom sizes. As with Monte Carlo simulations, organ doses per unit $P_{KA}$ decreased with increasing phantom size, except for the breasts in which the dose for the 1 year phantom was higher than for the new born. Again, a power law relationship tended to provide the best fit for this relationship.

| Phantom size (y) | Methodology | Organ | | | | | | | |
|---|---|---|---|---|---|---|---|---|---|
| | | ABM | Breasts | Heart | Lungs | Oesophagus | Thyroid | Liver | Stomach |
| 0 | Physical | 2.60 | 4.17 | 9.10 | 13.13 | 10.71 | 1.71 | 1.56 | 2.76 |
| | Cardiodose | 2.31 | 8.29 | 9.56 | 13.40 | 10.38 | 1.01 | 2.87 | 2.47 |
| 1 | Physical | 1.35 | 4.26 | n/a | 8.56 | 6.28 | 0.40 | 0.99 | 1.83 |
| | Cardiodose | 1.05 | 3.36 | 4.15 | 6.42 | 4.35 | 0.38 | 1.57 | 1.37 |
| 5 | Physical | 0.63 | - | n/a | 4.03 | 2.67 | - | 0.30 | 0.30 |
| | Cardiodose | 0.53 | 1.37 | 2.12 | 3.32 | 2.14 | 0.12 | 0.69 | 0.59 |
| 10 | Physical | 0.43 | 1.23 | 1.66 | 2.35 | 1.20 | 0.07 | 0.83 | 0.34 |
| | Cardiodose | 0.46 | 0.82 | 1.49 | 2.17 | 1.19 | 0.05 | 0.41 | 0.33 |
| 15 | Physical | 0.44 | 0.51 | n/a | 1.49 | 0.81 | 0.05 | 0.42 | 0.15 |
| | Cardiodose | 0.35 | 0.25 | 0.77 | 1.33 | 0.80 | 0.02 | 0.22 | 0.15 |

**Table 7.3: Organ doses (in mSv) per unit $P_{KA}$ calculated for the PA projection by physical methods compared to those estimated using Monte Carlo computer simulations.**

| Phantom size (y) | Methodology | Organ | | | | | | | |
|---|---|---|---|---|---|---|---|---|---|
| | | ABM | Breasts | Heart | Lungs | Oesophagus | Thyroid | Liver | Stomach |
| 0 | Physical | 2.45 | 4.83 | 30.71 | 24.29 | 19.26 | 2.01 | 14.13 | 7.33 |
| | Cardiodose | 1.00 | 20.50 | 15.20 | 11.60 | 7.90 | 1.00 | 3.50 | 1.80 |
| 1 | Physical | 1.11 | 9.32 | n/a | 14.09 | 17.65 | 0.45 | 1.51 | 3.15 |
| | Cardiodose | 0.55 | 10.00 | n/a | 6.05 | 4.15 | 0.35 | 2.05 | 0.80 |
| 5 | Physical | 0.83 | - | n/a | 8.15 | 6.99 | 0.20 | 1.29 | 0.64 |
| | Cardiodose | 0.30 | 7.30 | n/a | 3.98 | 2.66 | 0.14 | 1.36 | 0.39 |
| 10 | Physical | 0.78 | 5.81 | 3.99 | 3.78 | 2.22 | 0.16 | 2.34 | 0.26 |
| | Cardiodose | 0.22 | 5.27 | 2.46 | 2.34 | 1.18 | 0.07 | 0.76 | 0.21 |
| 15 | Physical | 0.38 | 0.46 | n/a | 2.37 | 1.23 | 0.06 | 1.94 | 0.14 |
| | Cardiodose | 0.15 | 1.77 | n/a | 1.30 | 0.52 | 0.02 | 0.52 | 0.06 |

**Table 7.4: Organ doses (mSv) per unit $P_{KA}$ calculated for the left lateral projection by physical methods compared to those estimated using Monte Carlo computer simulations.**

### *7.2.2: Phase 2*

Mean TLD readings for each projection angle and organ are given in Table 7.5 along with corresponding figures estimate using Cardiodose. A greater level of agreement was found between TLD readings and cardiodose estimates for phase 2 measurements than phase 1. In particular, the discrepancy between doses in the left lateral projection was considerably smaller. The mean dose across all beam angles was higher for physical measurements by 22%, 8% and 12% for the lungs, heart and oesophagus respectively. A poor agreement was found across most beam angles for breast dose. The sharp rise in breast dose predicted to occur around the left lateral projection by Monte Carlo simulations was not seen for physical measurements. Thyroid dose was around 100% higher for physical measurements, although the absolute difference was not large (i.e. both methodologies yielded small doses).

| | | Rotational beam angle (degrees) | | | | | | |
|---|---|---|---|---|---|---|---|---|
| **Organ** | **Methodology** | **90 (PA)** | **115** | **130** | **145** | **155** | **170** | **180 (Lat)** |
| **Lungs** | Physical | 2.75 | 2.81 | 2.88 | 2.80 | 2.44 | 2.48 | 2.63 |
| | Cardiodose | 1.78 | 2.22 | 2.45 | 2.72 | 2.77 | 2.57 | 2.29 |
| **Heart** | Physical | 1.36 | 1.51 | 1.52 | 1.72 | 2.15 | 2.22 | 2.54 |
| | Cardiodose | 1.72 | 1.63 | 1.92 | 1.94 | 2.04 | 2.23 | 2.24 |
| **Oesophagus** | Physical | 1.17 | 0.90 | 1.17 | 1.42 | 1.21 | 1.32 | 1.37 |
| | Cardiodose | 1.22 | 1.32 | 1.32 | 1.40 | 1.31 | 1.14 | 1.06 |
| **Breasts** | Physical | 1.39 | 0.57 | 0.49 | - | 0.70 | 0.90 | 0.92 |
| | Cardiodose | 0.56 | 0.27 | 0.28 | 0.34 | 0.45 | 2.94 | 5.48 |
| **Thyroid** | Physical | 0.09 | 0.13 | 0.12 | - | 0.08 | 0.08 | 0.08 |
| | Cardiodose | 0.04 | 0.05 | 0.06 | 0.06 | 0.06 | 0.06 | 0.06 |

**Table 7.5: Doses per unit $P_{KA}$ for five organs (in mSv) and various projection angles obtained from physical measurements, compared to estimates obtained using the cardiodose function based on Monte Carlo simulations.**

Organ doses per unit $P_{KA}$ at 60 kV were lower than at 70 kV by 15%, 17%, 32%, 12% and 38% for the lungs, heart, oesophagus, breasts and thyroid respectively, compared to equivalent dose reductions of 9%, 13%, 14%, 12% and 16% calculated using Cardiodose.

## *7.3: Discussion*

A number of discrepancies were found between physical measurements and Monte Carlo simulation based Cardiodose, although these varied between the two phases of measurements. Most notably, a large difference was found between cardiodose and physical measurements for the lateral projection where the Siemens Axiom Artis machine was used, but not when using the Philips BV300. There are a number of possible explanations; (1) differences in phantom density, (2) differences in phantom dimensions, i.e. width and thickness, (3) the discrete locations of TLDs within physical phantoms, and (4) measurement and calibration errors.

The density of soft tissues and bones are similar for PCXMC and ATOM phantoms (see Table 7.1 at the beginning of the chapter), except for the new born model, in which bone density is around 13% lower in PCXMC. Lung density, however, is significantly different, being around 43% higher in PCXMC. The effect of this difference in density was investigated analytically, by considering the reduction in x-

ray intensity (I) from its initial value ($I_0$) as it passes through an attenuator of thickness x, approximated by Beer's law:

$$I = I_0 e^{-\mu x}$$

Where μ is the linear attenuation coefficient, which is dependent on material and photon energy. The mean intensity through an attenuator of thickness $t$ is therefore:

$$\bar{I} = \frac{1}{t}\int_0^t I_0 e^{-\mu x}\, dx$$

$$= I_0 \frac{1}{t}\left(\frac{1}{\mu} - \frac{e^{-\mu t}}{\mu}\right)$$

Where μ is the linear attenuation coefficient, which is dependent on material and photon energy. A mass attenuation coefficient (μ/ρ) for ICRU-44 lung tissue of 0.227 $cm^2\, g^{-1}$ at 50 keV, quoted by the Physical Measurement Laboratory [287] was used. The linear attenuation coefficient was therefore obtained by multiplying this by the respective lung density values. Three lung densities were analysed based on the values used in PCXMC (0.3 g $cm^{-2}$), standard ATOM phantoms with inspiration lung density (0.21 g $cm^{-2}$), and ATOM phantoms with expiration lung density (0.5 g $cm^{-2}$). X-ray intensity relative to the initial unattenuated level as a function of lung thickness is shown in Figure 7.6, revealing a difference in attenuation patterns between different lung densities. Note that the attenuation curve for the PCXMC lung density lies approximately midway between the ATOM inspiration and expiration density curves. If the lung density is lower, then the x-ray beam will undergo less attenuation before reaching TLD locations in the lungs and other tissues. The resulting higher x-ray intensity at TLD positions would result in higher recorded doses. However, to account for a 100% increase in dose, the beam would need to traverse around 30 cm of lung tissue. The thickness of lung tissue traversed in the phantoms considered in this study was considerably less than 30 cm, especially for the new born phantom, in which the heart may be reached by the beam following the traversal of only around 2-3 cm of lung tissue. In this case, the intensity of radiation reaching the heart would be higher by little more than 10% for the low density lungs used in physical phantoms. Thus differences in lung density are unlikely to account for the large discrepancy in doses between MC and physical methodologies.

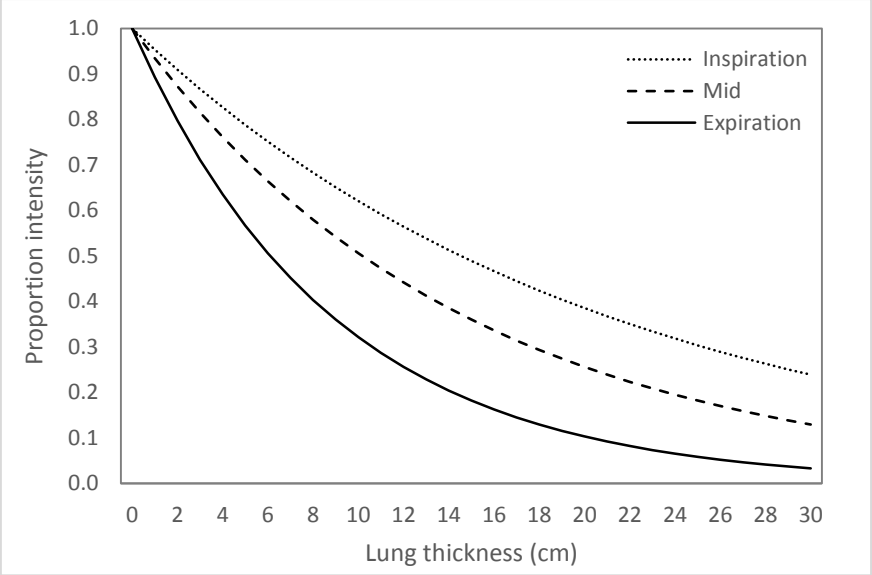


**Figure 7.6: Attenuation of a mono-energetic (50 keV) x-ray beam through lung tissues of three different densities – 0.21, 0.3 and 0.5 g cm$^{-3}$, representing different levels of inspiration.**

Aside from the difference in lung density, the ATOM phantoms, while having similar anterior-posterior thorax dimensions to the equivalent PCXMC mathematical phantoms, have somewhat narrower thoracic width (Table 7.1, again). This is especially the case for the 5 and 10 year old phantoms, in which the ATOM phantoms are 13% and 16% narrower respectively. The mean intensity to a given tissue decreases as the tissue thickness is increased. Based on the same Beer's law relationship above, the difference in mean x-ray intensity between thicknesses t and t' were calculated as follows:

$$\%\, difference = \frac{\left(\frac{1}{t}\int_0^t I_0 e^{-\mu x}\right) - \left(\frac{1}{t'}\int_0^{t'} I_0 e^{-\mu x}\right)}{\left(\frac{1}{t'}\int_0^{t'} I_0 e^{-\mu x}\right)} * 100$$

$$= \frac{I_0 \frac{1}{t}\left(\frac{1}{\mu} - \frac{e^{-\mu t}}{\mu}\right) - I_0 \frac{1}{t^1}\left(\frac{1}{\mu} - \frac{e^{-\mu t^1}}{\mu}\right)}{I_0 \frac{1}{t^1}\left(\frac{1}{\mu} - \frac{e^{-\mu t^1}}{\mu}\right)} * 100$$

Based on the difference is phantom widths, mean x-ray intensity should be higher for the narrower ATOM phantoms by between 3% and 15% depending on phantom size.

Variation in liver and stomach doses between physical and Monte Carlo methodologies may be related to the shape of the lungs represented in respective phantoms. In PCXMC, the diaphragm is flat (Figure 7.7). This happens to people

who have smoked for decades and have developed emphysema [288]. In normal, healthy individuals, the diaphragm is dome shaped, both in the sagittal and coronal planes [249]. The diaphragm does flatten during inspiration, but never to the extent shown in Figure 7.7. A more realistic lung shape is used in the ATOM anthropomorphic phantoms, with some TLD locations representing the liver and stomach being found superior to the lung bases. As the liver extends upwards to a greater degree in the ATOM phantoms, it would be expected that measured doses would be higher for cardiac imaging.

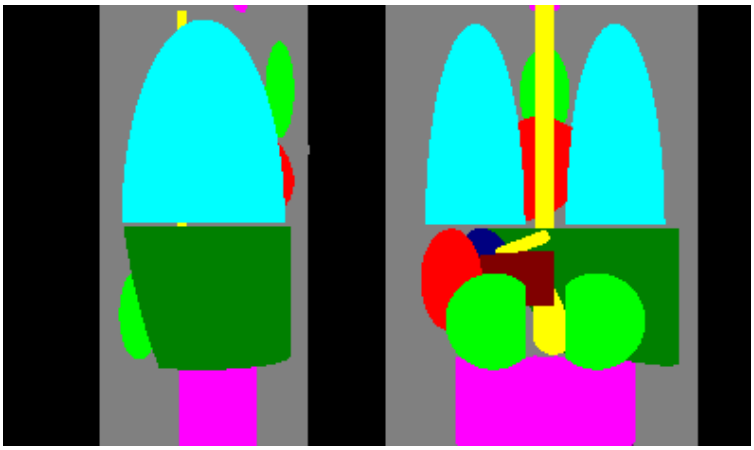

**Figure 7.7: The unrealistic relationship between the lungs and the liver in PCXMC 2.0. Image credit: author generated PCXMC screengrabs**

TLD calibration was only performed at a single energy (661 keV), and not repeated at photon energies more relevant to cardiac fluoroscopy (i.e. 30-100 keV). Brady [248] compared TLD calibration factors obtained using a linear accelerator at 6 MV with those obtained using a Therapax S3 SXRT superficial radiotherapy unit at 120 kV and 1.1 mm Al and 0.3 mm Cu filtration (HVL=8.1 mm Al). On average, the latter calibration factors were higher by 4.2%. Other general uncertainties in TLD dosimetry must also be considered. Nunn *et al* [289] found TLD response as a function of photon energy to differ from Monte Carlo simulations by up to 13%, due to complications in solid state physics of TLD materials. Harris *et al* [290] studied linearity of dose response for LiF:Mg:Ti (used in this study) and LiF:Mg:Cu:P TLD crystals. Although some departure from linearity was found, this occurred at large doses, approaching 5% at 400 cGy.

None of the variations in phantom dimensions and density and TLD calibration errors and uncertainties discussed above offers a satisfactory explanation for differences in recorded dose between computational and physical methodologies, either in isolation or when combined. Nor do these variations explain the difference in agreement of physical measurements with Monte Carlo results between the two phases of phantom exposures. The two machines used for physical measurements differ in a number of ways, including beam energy (Axiom Artis is higher) and field shape (BV300 fields are circular), though neither of these factors explain why the large discrepancies were found in the lateral projection only. The Axiom Artis used in the first phase of physical measurements is a biplane machine, while the Philips BV300 is not. Biplane machines have one capability not shared by single plane units – they can irradiate in two different projections at the same time. An unexpectedly large dose recorded for exposures in the lateral projection could be explained if the machine was also irradiating in the frontal plane. In fact, if the PA and lateral dose estimates derived using cardiodose are combined, the agreement with the lateral physical measurements using the Axiom Artis becomes close. The double-exposure problem would not have occurred for PA projection measurements as the lateral tube was always fully retracted.

### *7.3.1: Comparison with previous research*

Three other studies using physical measurements were compared. Firstly, Axelsson and colleagues [84] calculated organ doses for two different paediatric phantom sizes (1 and 5 years) and for 10 different beam angles, including straight PA and left lateral. Exposures were carried out using relatively old equipment (Philips Optimus 2000, Eindhoven, Netherlands), with a total filtration of 3.0 mm Al and a tube potential ranging from 58 to 70 kVp. Doses were measured using thermoluminescent dosemeters. In a second, more recent study, Barnaoui *et al* [92] calculated doses to the breasts, lungs, thyroid and oesophagus for 5 cardiac catheterizations, by reconstructing them using CIRS ATOM family phantoms. Doses were again measured using TLDs. For two of the reconstructions, multiple beam angles were used and it was not possible to determine the contribution to total organ dose from each projection. For the remaining three – two using the PA projection, and one using the left lateral projection, the results could be compared with those of the current

study. Finally, Kawasaki *et al* [116] calculated organ doses using 0 and 1 year CIRS ATOM phantoms, silver activated phosphate glass dosemeters and Philips Allura 9 fluoroscopy equipment , in two projection (PA and lateral).

The results of these studies, converted to organ dose per unit $P_{KA}$, are presented in Table 7.6, along with equivalent physical measurements from the current study. There is a greater level of agreement between the figures presented by Axelsson et al and those of the current study for the PA projection. Differences in beam energy would explain the degree to which doses for the 1 year phantom are higher in the current study (50-100%), but not for the 5 year phantom, in which there is an unexpectedly close agreement between the two studies. Discrepancies in liver and stomach doses are presumably due to different levels of collimation and beam centring. Doses for the lateral projection were generally much higher in the current study, by a factor greater than could be explained by beam energy alone. Dose to the oesophagus was 3.7 and 4.7 times higher in the current study for the 1 and 5 years phantoms respectively. This discrepancy is consistent with the earlier theory that doses for the lateral projection in the current study are overestimates due to exposure in two planes. The figures calculated by Barnaoui *et al* [92] were based on the same equipment as used in the current study, thus ought be more comparable. Doses per unit $P_{KA}$ are generally lower than those of the current study, however, most notably for the breasts. Only Kawasaki *et al* calculated organ doses for the new born phantom size. With the exception of the thyroid, doses were lower than those of the current study for both projections. This is despite the involvement of higher beam energy (HVL=6.4-6.7 mm Al). The overall patterns of higher doses for the lateral projection and lower doses with increasing phantom size were consistent, however.

| | | Posteroanterior | | | | Left lateral | | | |
|---|---|---|---|---|---|---|---|---|---|
| Age | Organ | Axelsson | Barnauoi | Kawasaki | This study | Axelsson | Barnauoi | Kawasaki | This study |
| 0 years | ABM | | | 1.7 | 2.6 | | | 1.8 | 2.5 |
| | Breasts | | | 4.0 | 4.7 | | | 11.8 | 4.8 |
| | Lungs | | | 6.0 | 13.1 | | | 9.8 | 24.3 |
| | Oesophagus | | | 6.0 | 10.7 | | | 11.2 | 19.3 |
| | Thyroid | | | 4.9 | 1.7 | | | 4 | 2.0 |
| | Liver | | | 0.9 | 1.6 | | | 2.2 | 14.1 |
| | Stomach | | | 0.7 | 2.8 | | | 1.3 | 7.3 |
| 1 year | ABM | 0.8 | | 0.9 | 1.4 | 1.1 | | 1.1 | 1.1 |
| | Breasts | 1.6 | 1.7 | 2.9 | 4.3 | 3.8 | | 9.4 | 9.3 |
| | Lungs | 6.3 | 5.5 | 4.4 | 8.6 | 8.5 | | 6.6 | 14.1 |
| | Oesophagus | 3.1 | 4.4 | 3.6 | 6.3 | 3.7 | | 6.9 | 17.7 |
| | Thyroid | 0.2 | 0.5 | 1.9 | 0.4 | 0.3 | | 2.3 | 0.5 |
| | Liver | 0.7 | | 0.7 | 1.0 | 2.6 | | 0.9 | 1.5 |
| | Stomach | 2.6 | | 0.6 | 1.8 | 4.1 | | 0.6 | 3.2 |
| 5 years | ABM | 0.8 | | | 0.6 | 0.4 | | | 0.8 |
| | Breasts | 1.8 | | | | 3.7 | 1.3 | | 17.0 |
| | Lungs | 4.1 | | | 4.3 | 2.3 | 4.7 | | 8.1 |
| | Oesophagus | 2.6 | | | 2.7 | 1.9 | 3.2 | | 7.0 |
| | Thyroid | 0.3 | | | | 0.3 | 0.6 | | 0.61 |
| | Liver | 0.4 | | | 0.3 | 0.6 | | | 1.3 |
| | Stomach | 0.2 | | | 0.3 | 0.1 | | | 0.6 |
| 15 years | ABM | | | | 0.4 | | | | |
| | Breasts | | 0.1 | | 0.5 | | | | |
| | Lungs | | 0.4 | | 1.5 | | | | |
| | Oesophagus | | 0.6 | | 0.8 | | | | |
| | Thyroid | | 0.1 | | 0.1 | | | | |
| | Liver | | | | 0.4 | | | | |
| | Stomach | | | | 0.2 | | | | |

**Table 7.6: Organ doses, in mSv, per unit $P_{KA}$ calculated using physical measurements in three previous studies, compared to the current.**

## *7.4: Partial organ doses*

The organ doses presented in this chapter represent the mean for the whole organ. However, energy would not be expected to be imparted evenly within large organs; the heart is in the left lower portion of the chest, therefore the left lower lobe of the lungs would be expected to receive a higher dose than other lobes, the distal oesophagus would receive a higher dose than the proximal, and the fundus of the stomach would receive a higher dose than the pylorus. The results of Monte Carlo simulations in PCXMC are always presented as mean organ doses and cannot be expressed as partial organ doses. Physical measurements in phantoms do not have this restriction, thus allow doses to be characterised in greater detail.

According to the linear no threshold (LNT) model describing the supposed relationship between radiation dose and associated risk of cancer, uneven dose distribution is immaterial – one lung receiving a mean dose of 10 mGy would result in the same risk as both lungs receiving 5 mGy each (assuming they are of equal size). The introduction of the concept of a 'dose and dose rate effectiveness factor' (DDREF) – a reduction in risks, typically by a factor of 1.5 or 2.0 [3, 44], where doses are less than 200 mGy or delivered at a low dose rate – could be interpreted as an admission that some level of non-linearity exists. If the left lung receives a dose of 250 mGy, while the right receives 50 mGy, then the equivalent lung dose would be 150 mSv and no DDREF would be applied, despite the left lung receiving more than 200 mGy. From an epidemiological perspective, partial organ dosimetry may allow alternative insights into the cancer risks from exposures. The uneven dose distribution within large organs should be matched by an uneven distribution of associated excess cancers. For example, if the dose to the left lower lobe of the lungs is consistently higher than for other lobes, then associated excess cases of lung cancer would be expected to occur more frequently in the left lower lobe than other lobes.

ATOM phantoms do not have delineated 'lobes' of the lungs, though it is straightforward to analyse dose separately for left and right lungs, as well and left and right breasts. The results of this analysis (Table 7.7), for phase 1 figures, show that the left lung receives a higher dose than the right in the PA projection, while the situation is reversed for the left lateral projection with the right lung receiving a considerably higher dose. The right/left lung dose ratio increases with phantom size for the lateral projection, ranging from 2.2 at 0 years to 10.1 at 15 years. For examinations in which a 50/50 proportion of PA and lateral projections is used, the right lung would receive a higher dose than the left, by a factor ranging from 1.6 to 5.4.

These patterns were similar for breast dose. The right breast receives a considerably higher dose than the left in the lateral projection. Left and right breast doses were almost identical in the PA projection for the 1 and 15 year phantoms, while the left breast received almost twice the dose of the right for the 10 year phantom.

| | | Lungs | | Breasts | |
|---|---|---|---|---|---|
| **Phantom size** | **Projection** | **R/L ratio** | **Mean R/L ratio** | **R/L ratio** | **Mean R/L ratio** |
| **0 years** | PA | 0.97 | 1.59 | n/a | n/a |
| | Lat | 2.22 | | 2.61 | |
| **1 year** | PA | 0.92 | 2.00 | 0.99 | 2.18 |
| | Lat | 3.08 | | 3.37 | |
| **5 years** | PA | 0.57 | 1.93 | n/a | n/a |
| | Lat | 3.29 | | 8.65 | |
| **10 years** | PA | 0.63 | 2.98 | 0.57 | 4.47 |
| | Lat | 5.33 | | 8.36 | |
| **15 years** | PA | 0.79 | 5.43 | 1.09 | 3.19 |
| | Lat | 10.06 | | 5.30 | |

**Table 7.7: Comparison of doses to left and right lungs and breasts**

Dose to the lungs was also analysed on a slice-by-slice basis. As would be expected, given the inferior location of the heart in the chest, dose increases towards the lung bases and decreases towards the apices. The ratio between apical and basal lung dose tended to be greater for the lateral projection, reaching a value of more than 11 in some cases (Figure 7.8). There was a small suggestion of a greater apex/base ratio with increasing phantom size, though the steepest gradient was found for the 10 year phantom.

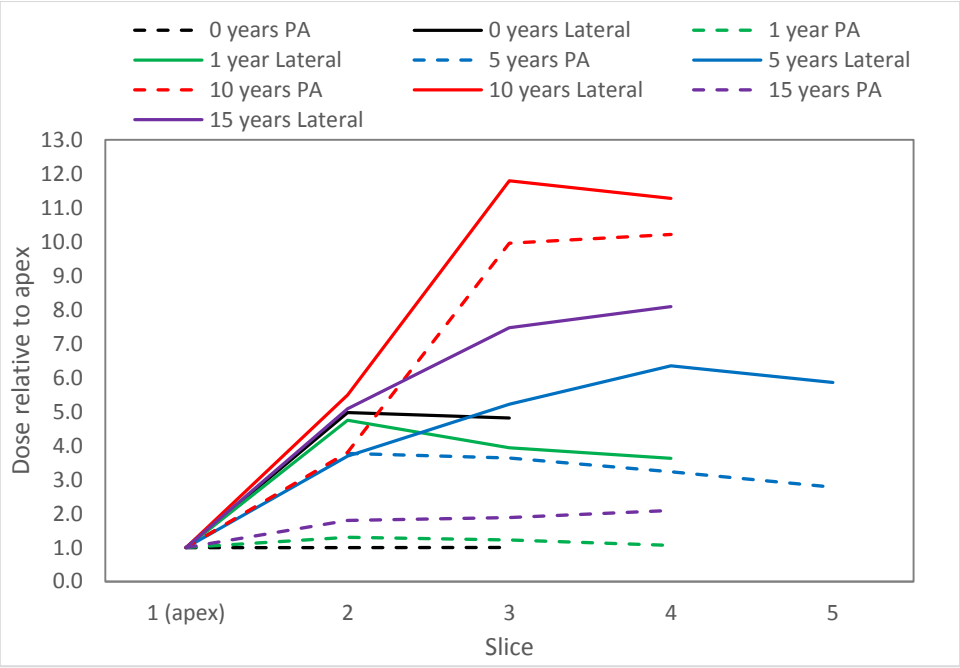


**Figure 7.8: Variation in lung dose with slice, relative to dose at the apex.**

*7.5: Conclusion*

The aim of this chapter was to verify the results of computational dosimetry (i.e. Monte Carlo simulations). This was only partially achieved. The results of the physical measurements were in reasonable agreement with MC-based Cardiodose in the PA projection, but were much higher in the lateral projection. A number of explanations are possible, including anatomical variation (differences in the size, shape and density of organs) and experimental error. The unusually high doses recorded for the left lateral projection using the biplane Siemens Axiom Artis were not replicated using the single plane Philips BV300. A likely explanation is that the phantoms were in fact irradiated using both imaging planes, resulting in approximately twice the anticipated dose.

# Chapter 8: Organ doses

With the 'Cardiodose' dosimetry system and supporting information on beam angles and x-ray energy in hand, organ doses could be estimated for cohort members using details recorded at the time of the examination. This chapter presents the results of such organ dose estimates, before comparing these figures to previous research and assessing uncertainties.

## *8.1: Methodology*

Equivalent doses to the breasts, lungs, oesophagus, thyroid, stomach, liver, bone marrow and heart, along with effective dose and mean whole body dose were estimated for 14,934 examinations where patient age (n=14,775) or mass (n=13,382), dose indicators (kerma area product or screening time) and examination type were recorded. Only data obtained from Hospital 1 had usable biplane $P_{KA}$ figures. Those recorded at Hospital 4 were not considered reliable and only total $P_{KA}$ (e.g. frontal and lateral combined) was utilised.

There were 1385 procedures conducted at Hospital 1 before 2000 where $P_{KA}$ was not recorded, but where screening time (ST) and patient mass or age were. Various methodologies for estimating $P_{KA}$ in these cases were investigated. Two linear models were calculated based on the median $P_{KA}$, where it *was* recorded in this era, per minute screening time, per kilogram body mass ($P_{KA}$/ST/kg), or per year of age ($P_{KA}$/ST/age). These models were calculated for different age ranges (Figure 8.1) and polynomials fitted, to provide alternative models. The four models were applied to situations in which $P_{KA}$ was recorded, allowing the difference between actual and estimated $P_{KA}$ to be determined.

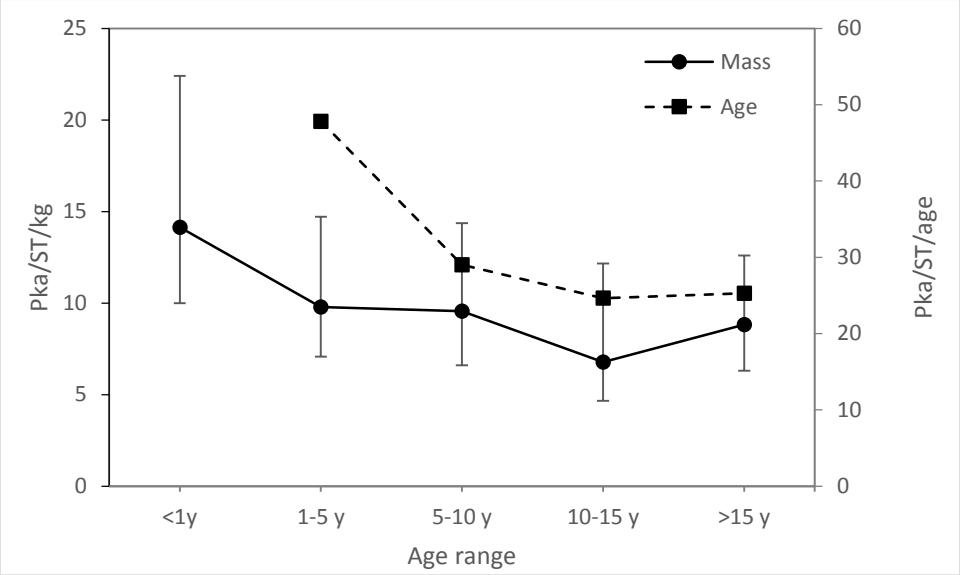


**Figure 8.1: Relationship between $P_{KA}$/ST/kg and $P_{KA}$/ST/age and patient size. The age model was restricted to beyond 1 year. Below this age, the model rises rapidly, tending to infinity as age approaches zero.**

The median absolute errors were 39%, 47%, 35% and 41% for the linear mass, linear age, polynomial mass and polynomial age models, respectively. The respective 95$^{th}$ percentiles for these errors were 133%, 223%, 147% and 166%. Both age models resulted in extremely large errors below 1 year, while for the mass polynomial model, errors for patients below 10 kg were similar to other ages. The mass polynomial was the preferred approach, although for 27 examinations in which mass was not recorded, the age polynomial model was used. The estimation of doses from screening time results in the introduction of large uncertainties, though was still preferable to simply assigning average doses to these examinations. This approach was unavoidable for a large number of procedures conducted Hospital 4, and will be described in section 8.5 of this chapter.

Cardiodose produces breast dose estimates for all patients, regardless of gender. All male patients in the cohort were identified and breast doses for these examinations were deleted. All breast doses were removed for patients examined at Hospital 6 as it was not possible to determine gender (neither sex nor Christian name were recorded). As with the raw $P_{KA}$ data, a MATLAB function was written to organise the output from Cardiodose to provide age, mass and procedure type stratification. Where patients underwent multiple procedures during the data collection period, these doses were added together to produce cumulative organ doses in addition to

individual examination doses. The total energy imparted to the patient, in millijoules (mJ), was calculated by multiplying the mean whole body dose by the patient mass.

*8.2: Results*

A summary of organ doses for all procedure types and from all hospitals combined is given in Table 8.1, stratified by both patient mass and age. More examinations are included in the age stratified data, and these figures are somewhat lower than where mass stratification is applied. These differences are due to the inclusion of examinations conducted at Hospitals 5 and 6, which not only lacked records of patient mass, but which also delivered generally low doses. Table 8.2 shows these data stratified by hospital and data collection era, but without mass stratification. More comprehensive tables with breakdown by procedure type and patient age are presented in appendix 3.

Across the whole cohort, where patient age was recorded, and excluding procedures with zero dose, the median effective dose was 5.0 mSv. The median effective dose was a little higher for males (5.3 mSv) compared to females (4.7). As with $P_{KA}$ and screening times, organ doses were right skewed, with mean doses being almost twice as high as median (10.2 and 8.9 mSv for males and females respectively). The distribution of effective dose is shown in Figure 8.2, which is stratified by procedure type (unspecified procedures are not included). Figures 8.3 and 8.4 show this distribution in greater detail for low dose and high dose regions respectively. The median cumulative effective dose, for the whole cohort, was 6.2 mSv, and 8.2, 20.6, 11.8, 8.8, 18.7, 19.2, 14.8 and 16.6 mSv for patients identified as having a history of transplantation, Tetralogy of Fallot, transposition of the great arteries, Down syndrome, Norwood procedure, Fontan procedure, hypoplastic ventricles and valve atresia, respectively.

A more detailed analysis was conducted of the procedures with especially high or low doses. There were 279 procedures delivering an effective dose of less than 0.2 mSv, of which 65 were pacemaker insertions/revisions, 50 were electrophysiology studies (EPS), 44 were heart biopsies and 80 were unspecified cardiac catheterizations. The large majority (91%) of these procedures were carried out using 3$^{rd}$ generation fluoroscopy machines. There were 898 procedures with an effective dose of less than 0.5 mSv; 105 pacemakers, 95 ASD occlusions, 156

EPS/ablations, 188 Biopsies and 213 unspecified. Again, 91% were carried out using 3rd generation equipment. There were 100 procedures delivering an effective dose of more than 100 mSv, 95 of which involved 1st and 2nd generation equipment. The majority of these procedures (n=63) were unspecified cardiac catheterizations. Fourteen procedures delivered an estimated effective dose of over 200 mSv.

The organs receiving the highest doses were the lungs (median for whole cohort =15.5 mSv), heart (11.8 mSv) and oesophagus (10.1 mSv). Estimated breast doses were high in examinations involving laterally orientated projections, but were low where these projections tended to be avoided. This was the case for a number of common procedure types including pacemaker insertions, biopsies (PA projection only), coronary angiography and EPS procedures. Doses to bone marrow and lymph nodes were relatively low at 2.3 and 3.0 mSv, respectively. For more recently acquired data, bone marrow doses were around 1 mSv. Thyroid doses were especially low and rarely exceeded 1 mSv for recent examinations.

The relationship between dose and patient size (age or mass) varied between organs. In general, the relationship is similar to that for $P_{KA}$ normalised by mass, tending to display a lop-sided 'U' shaped pattern overall (Figure 8.5). For those hospitals that omit antiscatter grids for small patients, organ doses tended to increase with increasing patient size. Dose to the thyroid and breasts were almost always seen to decrease with increasing patient size (Figure 8.6). The average absorbed dose to the body was also found to decrease with increasing patient size, while the total energy imparted increased (Figure 8.7). On average, the effective dose was higher than the mean whole body dose by a factor of 1.73 (standard deviation = 0.22, 5th/95th percentiles = 1.16/2.17).

Many of the patterns evident from analysis of organ doses are similar to those for $P_{KA}$. A fall in organ doses between successive data collection eras is apparent, although the magnitude of organ dose reduction is somewhat less than that for $P_{KA}$. For example, median effective dose was seen to fall by a factor of around 10 between 1994-2000 and 2002-2008 eras at Hospital 1 (Table 8.2), compared to a reduction by a factor of around 20 for $P_{KA}$.

| | Patient mass range (kg) | | | | | | |
|---|---|---|---|---|---|---|---|
| | <5 | 5-12.5 | 12.5-25 | 25-45 | 45-65 | >65 | All |
| **Effective dose** | 5.7 [2.1 : 15.3] | 6.2 [2.5 : 14.3] | 5.5 [2 : 13.3] | 5 [1.7 : 12.3] | 5 [1.9 : 12.2] | 5 [1.9 : 13] | 5.6 [2.1 : 13.5] |
| **Bone marrow** | 2.3 [0.9 : 6.2] | 2.3 [0.9 : 5.4] | 2.2 [0.9 : 5.1] | 2.6 [1 : 6.4] | 3.6 [1.4 : 8.3] | 5 [1.9 : 11.3] | 2.6 [1 : 6.2] |
| **Breasts** | 13.8 [5.3 : 37.3] | 16 [6.3 : 36.6] | 13.7 [4.5 : 33.5] | 11.2 [2.2 : 33.9] | 9.7 [1.6 : 28.3] | 6.5 [1.3 : 26.2] | 13.2 [4.1 : 33.6] |
| **Heart** | 13.7 [5.3 : 36.1] | 14.4 [5.7 : 31.9] | 12.3 [4.7 : 28.4] | 11.5 [4.5 : 27.5] | 12.1 [4.9 : 26.9] | 13.3 [5.2 : 28.5] | 13 [5.1 : 29.7] |
| **Lungs** | 16.9 [6.3 : 46.6] | 18.2 [7.2 : 42.4] | 16.6 [6.3 : 40.2] | 15.3 [5.5 : 37.4] | 17.3 [6.7 : 40.4] | 16.9 [6.5 : 39.8] | 17 [6.5 : 41.1] |
| **Lymph** | 3.5 [1.3 : 9] | 3.8 [1.5 : 8.5] | 3.3 [1.3 : 7.6] | 2.8 [1.1 : 6.6] | 2.9 [1.1 : 6.5] | 3 [1.2 : 6.7] | 3.3 [1.3 : 7.6] |
| **Oesophagus** | 13.3 [5.1 : 33.6] | 13 [5.2 : 29] | 10.8 [4.2 : 25] | 8.7 [3.3 : 20.1] | 9.5 [3.9 : 20.8] | 10.6 [4.2 : 22.9] | 11.1 [4.3 : 25.6] |
| **Thyroid** | 1.2 [0.5 : 3.1] | 1.1 [0.4 : 2.3] | 0.7 [0.3 : 1.5] | 0.4 [0.2 : 0.9] | 0.3 [0.1 : 0.7] | 0.2 [0.1 : 0.4] | 0.6 [0.2 : 1.5] |
| **Liver** | 4.9 [1.9 : 12.6] | 6.2 [2.5 : 13.8] | 5.5 [1.9 : 12.5] | 4.1 [1.3 : 10.4] | 4.1 [1.3 : 10.4] | 4.4 [1.5 : 11.3] | 5.2 [1.8 : 12.2] |
| **Stomach** | 2.8 [1.1 : 7.1] | 3.1 [1.2 : 6.7] | 2.5 [1 : 5.5] | 1.9 [0.7 : 4.2] | 1.5 [0.6 : 3.3] | 1.6 [0.6 : 3.4] | 2.3 [0.9 : 5.3] |
| **n** | 1453 | 3759 | 3327 | 2095 | 1772 | 777 | 13183 |

| | Patient age range (years) | | | | | | |
|---|---|---|---|---|---|---|---|
| | **<1** | **1-5** | **5-10** | **10-16** | **16-18** | **18-22** | **All** |
| **Effective dose** | 5.5 [2.1 : 13.1] | 5.3 [2.1 : 12.9] | 5 [1.6 : 12.3] | 4.5 [1.5 : 11.2] | 4 [1.3 : 10.7] | 5.2 [1.5 : 15.6] | 5 [1.8 : 12.3] |
| **Bone marrow** | 2.1 [0.8 : 5.1] | 2 [0.8 : 4.8] | 2.1 [0.8 : 5.2] | 3 [1.1 : 7.1] | 3.3 [1.2 : 7.9] | 4.7 [1.3 : 12.2] | 2.3 [0.9 : 5.8] |
| **Breasts** | 13.4 [5.3 : 32.4] | 13.8 [5.2 : 33.6] | 11.6 [3.1 : 30.5] | 9.1 [1.6 : 28.1] | 6 [1 : 24.4] | 6.4 [1.9 : 35.1] | 11.8 [3.5 : 31.1] |
| **Heart** | 12.9 [5.1 : 30.5] | 12.1 [4.9 : 28.2] | 11.2 [4 : 26.8] | 11 [4.2 : 25.3] | 10.2 [3.6 : 23.5] | 12.2 [3.9 : 32] | 11.8 [4.5 : 27.7] |
| **Lungs** | 16.2 [6.1 : 38.9] | 15.8 [6.2 : 38.5] | 15.1 [5.2 : 37.2] | 14.8 [5.4 : 35.9] | 13.5 [4.7 : 34.3] | 17.6 [5.2 : 51.1] | 15.5 [5.7 : 37.7] |
| **Lymph** | 3.3 [1.3 : 7.8] | 3.2 [1.3 : 7.6] | 2.9 [1 : 7] | 2.6 [1 : 6] | 2.4 [0.9 : 5.7] | 3 [0.9 : 8.3] | 3 [1.1 : 7.1] |
| **Oesophagus** | 12.1 [4.7 : 28.5] | 10.7 [4.3 : 25.2] | 9.4 [3.3 : 22.4] | 8.4 [3.2 : 19.3] | 8.1 [2.9 : 18.3] | 9.8 [3.2 : 26.8] | 10.1 [3.9 : 23.7] |
| **Thyroid** | 1.1 [0.4 : 2.5] | 0.8 [0.3 : 1.8] | 0.5 [0.2 : 1.2] | 0.3 [0.1 : 0.7] | 0.2 [0.1 : 0.5] | 0.2 [0.1 : 0.7] | 0.6 [0.2 : 1.4] |
| **Liver** | 5 [1.9 : 11.6] | 5.6 [2.1 : 12.9] | 4.6 [1.4 : 11.2] | 3.8 [1.2 : 9.6] | 3.3 [0.9 : 9.5] | 4.5 [1.1 : 13.3] | 4.7 [1.6 : 11.3] |
| **Stomach** | 2.7 [1 : 6.2] | 2.5 [1 : 5.9] | 2.1 [0.8 : 4.9] | 1.5 [0.6 : 3.5] | 1.3 [0.5 : 2.9] | 1.6 [0.5 : 4.3] | 2.1 [0.8 : 4.9] |
| **n** | 3584 | 4164 | 2414 | 3261 | 819 | 375 | 14617 |

Table 8.1: Median estimated organ doses, in millisieverts [interquartile range] for whole cohort and all procedure types combined. The upper table presents figures stratified by mass, while the lower table presents figures stratified by age.

| Organ | Hospital 1 94-00 | Hospital 1 99-01 | Hospital 1 02-08 | Hospital 1 07-10 | Hospital 2 04-08 | Hospital 2 08-13 |
|---|---|---|---|---|---|---|
| **Effective dose** | 22.3 [13.6 : 35.7] | 11.9 [6.2 : 21.7] | 1.9 [0.8 : 4.2] | 2 [1 : 4.4] | 8.2 [4.6 : 14] | 6.5 [3.5 : 11.4] |
| **Bone marrow** | 10.3 [6.3 : 16.7] | 5.8 [2.9 : 10.8] | 1 [0.4 : 2.1] | 1 [0.5 : 2.6] | 3.5 [2 : 6.1] | 2.7 [1.5 : 4.8] |
| **Breasts** | 56 [26.3 : 96.5] | 26 [11.3 : 49.3] | 3.2 [1 : 9.7] | 3.6 [1.4 : 10.4] | 21.7 [11.1 : 37.9] | 17.2 [8.8 : 30.1] |
| **Heart** | 45.8 [28.4 : 73.3] | 27.8 [14.4 : 49.3] | 4.9 [2.2 : 10.3] | 5 [2.5 : 10.9] | 18.7 [10.7 : 31.3] | 15.4 [8.4 : 26.8] |
| **Lungs** | 70.2 [43.4 : 112.1] | 37.3 [19.7 : 67.7] | 6.1 [2.6 : 13] | 6.2 [3.1 : 14.1] | 24.6 [14.2 : 41.9] | 19.2 [10.5 : 33.6] |
| **Lymph** | 12.1 [7.4 : 19.7] | 7.3 [3.9 : 13] | 1.2 [0.5 : 2.6] | 1.3 [0.6 : 2.6] | 4.7 [2.7 : 7.9] | 3.8 [2.1 : 6.6] |
| **Oesophagus** | 38.9 [23.5 : 64.1] | 24.6 [12.9 : 42.9] | 4.2 [1.8 : 8.6] | 4.3 [2.2 : 8.8] | 16 [9.3 : 27.1] | 13.3 [7.2 : 22.9] |
| **Thyroid** | 2.1 [1 : 3.9] | 1.5 [0.7 : 2.8] | 0.2 [0.1 : 0.5] | 0.3 [0.1 : 0.5] | 1 [0.5 : 1.8] | 0.9 [0.4 : 1.6] |
| **Liver** | 18.4 [10.5 : 30.4] | 10.7 [5.3 : 19.8] | 1.7 [0.7 : 3.8] | 1.8 [0.8 : 4.1] | 7.9 [4.3 : 13.5] | 6.6 [3.4 : 11.3] |
| **Stomach** | 7.9 [4.6 : 13.4] | 5.6 [2.9 : 10.1] | 0.9 [0.4 : 1.9] | 0.9 [0.5 : 1.9] | 3.3 [1.9 : 5.8] | 2.8 [1.4 : 4.9] |
| **n** | 2137 | 1039 | 3204 | 719 | 1615 | 1992 |

| Organ | Hospital 3 04-08 | Hospital 3 08-13 | Hospital 4 93-03 | Hospital 4 03-13 | Hospital 6 06-13 | Hospital 5 05-13 |
|---|---|---|---|---|---|---|
| **Effective dose** | 6 [3 : 11.1] | 2.4 [1.3 : 4.9] | 7.4 [4 : 12.7] | 2.7 [1.5 : 5] | 1.4 [0.7 : 2.6] | 1.7 [0.6 : 4.6] |
| **Bone marrow** | 2.5 [1.4 : 4.7] | 1.1 [0.6 : 2.4] | 3.1 [1.7 : 5.6] | 1.3 [0.6 : 2.3] | 0.7 [0.3 : 1.1] | 0.7 [0.3 : 2.1] |
| **Breasts** | 15.9 [6.4 : 30.1] | 5.9 [2.3 : 12.8] | 20.3 [10.9 : 35.4] | 7 [3.9 : 12.9] | 3.5 [1.9 : 6.8] | 4.3 [1.5 : 11.8] |
| **Heart** | 14.2 [7.4 : 25.8] | 6.2 [3.2 : 11.5] | 15.2 [7.8 : 25.5] | 6.4 [3.5 : 11.8] | 3.2 [1.6 : 6] | 4.1 [1.5 : 11.2] |
| **Lungs** | 18.2 [9.5 : 32.9] | 7.6 [4 : 15.3] | 23.2 [12.4 : 39.4] | 8.3 [4.6 : 15.3] | 4.1 [2.2 : 7.8] | 5.1 [1.9 : 14.2] |
| **Lymph** | 3.5 [1.8 : 6.4] | 1.5 [0.8 : 2.8] | 4.1 [2.1 : 6.9] | 1.6 [0.9 : 2.9] | 0.8 [0.4 : 1.6] | 1 [0.4 : 2.8] |
| **Oesophagus** | 12.5 [6.3 : 22] | 5.2 [2.7 : 9.7] | 13 [6.8 : 22] | 5.4 [3.1 : 10] | 2.8 [1.4 : 5.3] | 3.6 [1.2 : 9.9] |
| **Thyroid** | 0.8 [0.3 : 1.6] | 0.3 [0.1 : 0.6] | 0.7 [0.3 : 1.4] | 0.4 [0.2 : 0.7] | 0.2 [0.1 : 0.4] | 0.2 [0.1 : 0.7] |
| **Liver** | 5.9 [2.7 : 10.9] | 2.4 [1.2 : 4.8] | 6.3 [3.3 : 10.7] | 2.5 [1.4 : 4.6] | 1.3 [0.7 : 2.6] | 1.6 [0.6 : 4.8] |
| **Stomach** | 2.7 [1.3 : 4.8] | 1.1 [0.6 : 2] | 2.7 [1.4 : 4.7] | 1.1 [0.7 : 2.2] | 0.6 [0.3 : 1.2] | 0.7 [0.2 : 2] |
| **n** | 842 | 1407 | 817 | 496 | 354 | 738 |

Table 8.2: Median organ doses in millisieverts [interquartile range] for all procedures and patient sizes combined, stratified by hospital and data collection era.

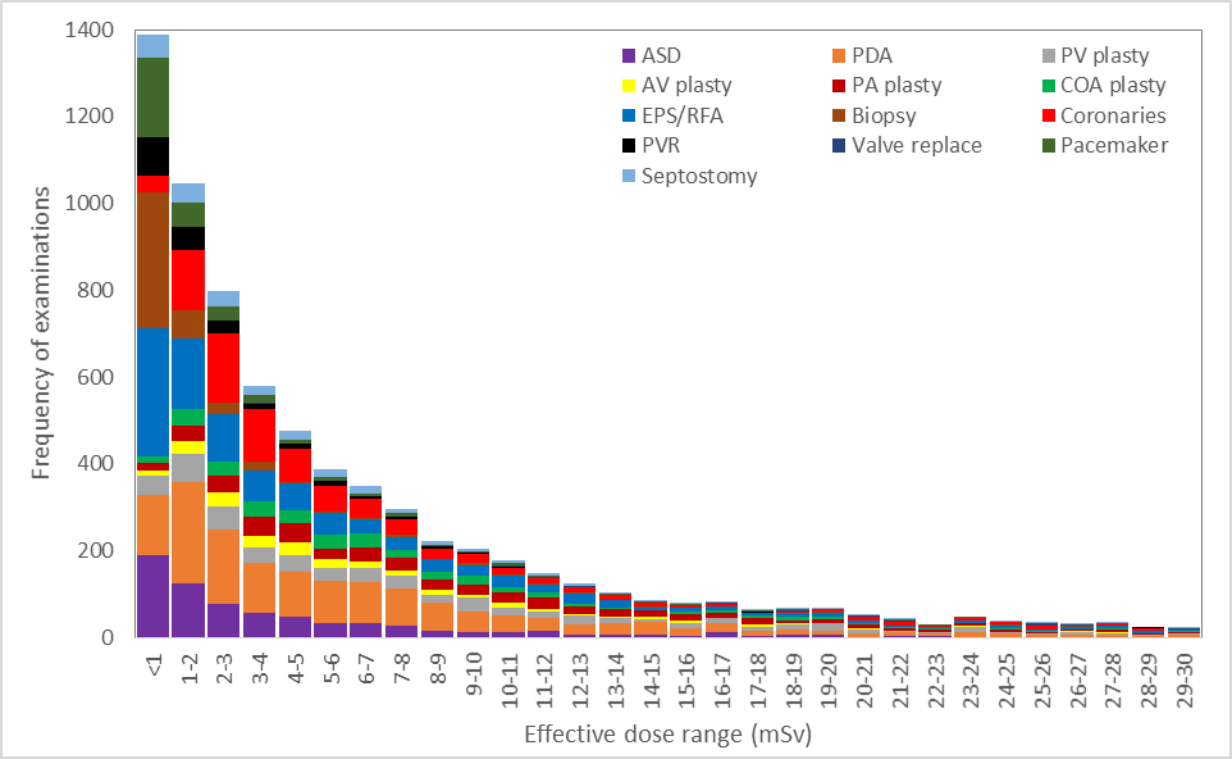


Figure 8.2: Distribution of effective doses, stratified by procedure type.

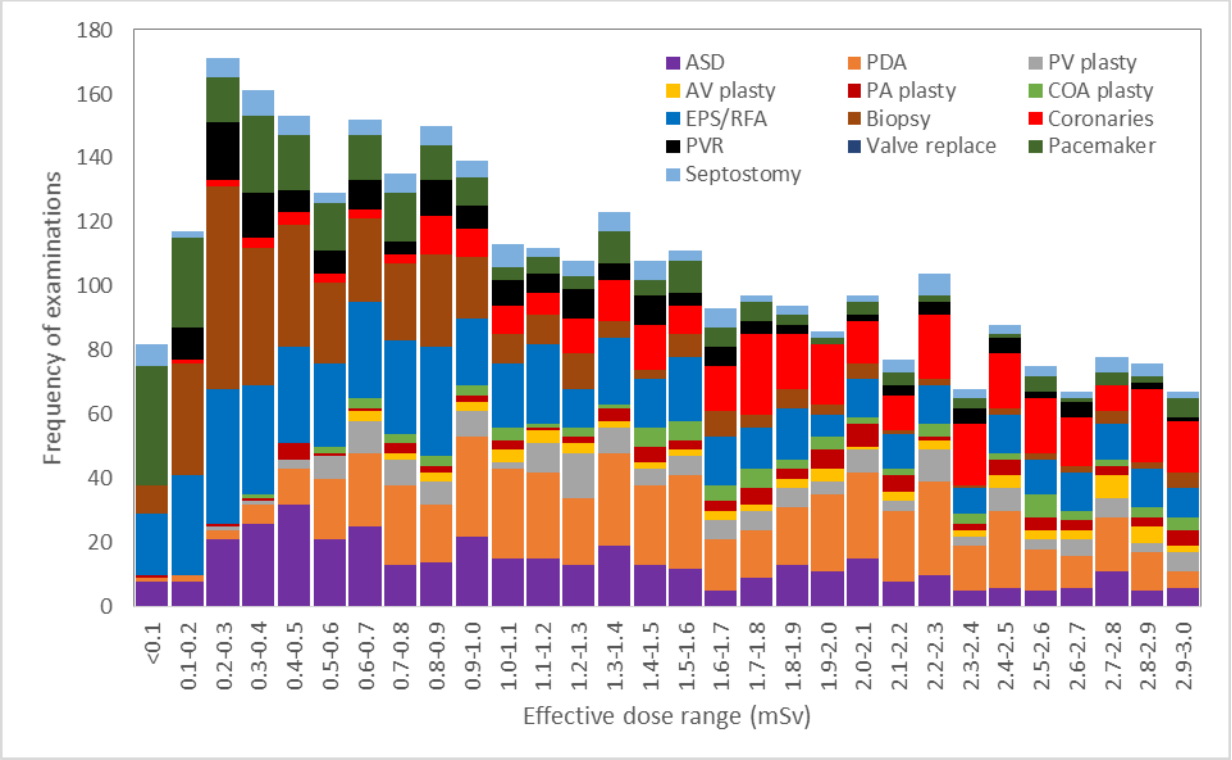


Figure 8.3: Distribution of effective doses in the 0-3.0 mSv range

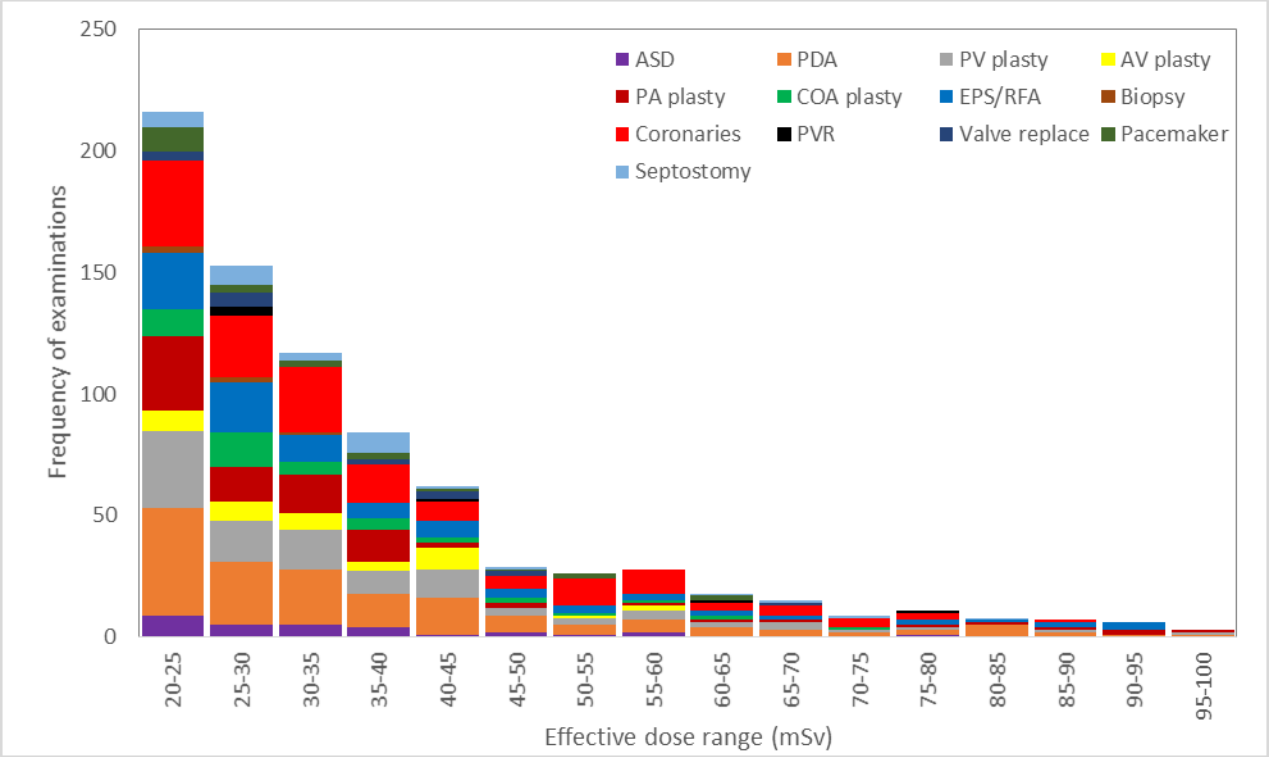


Figure 8.4: Distribution of effective doses between 20 and 100 mSv.

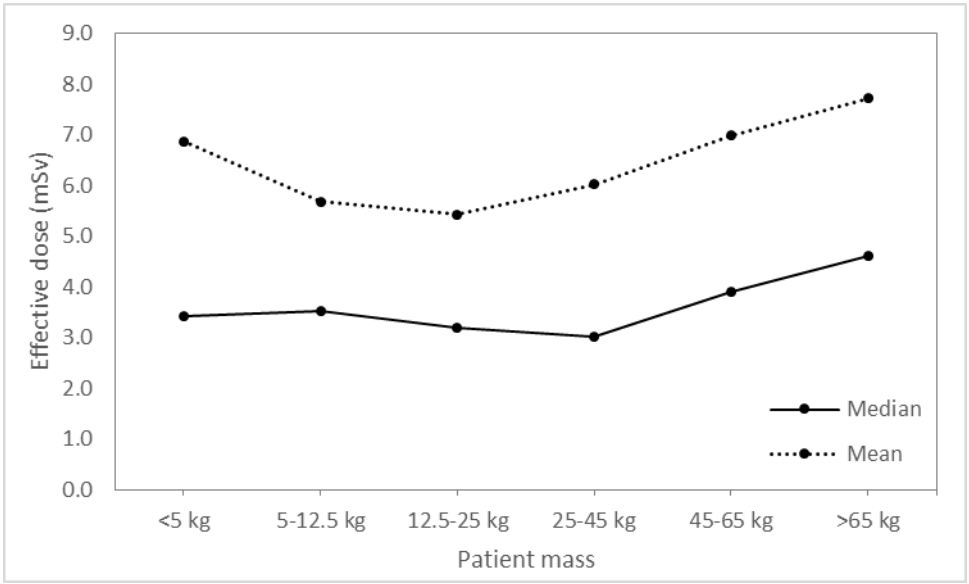


Figure 8.5: Median and mean effective dose for all procedure types combined, as a function of patient mass, for examinations conducted using Siemens Axiom Artis or Artis Zee machines.

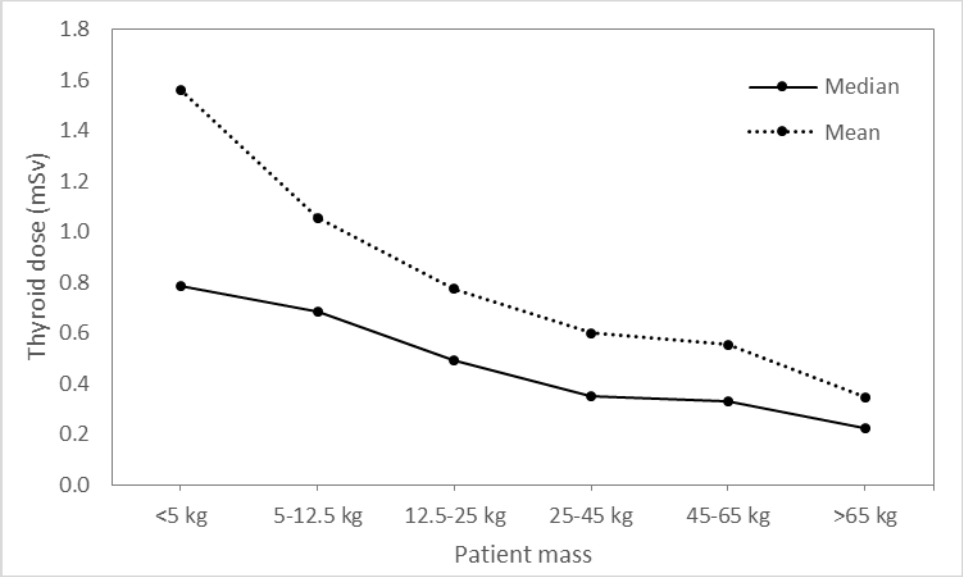


**Figure 8.6: Median and mean thyroid dose for all procedure types combined, as a function of patient mass, for examinations conducted using Siemens Axiom Artis or Artis Zee machines.**

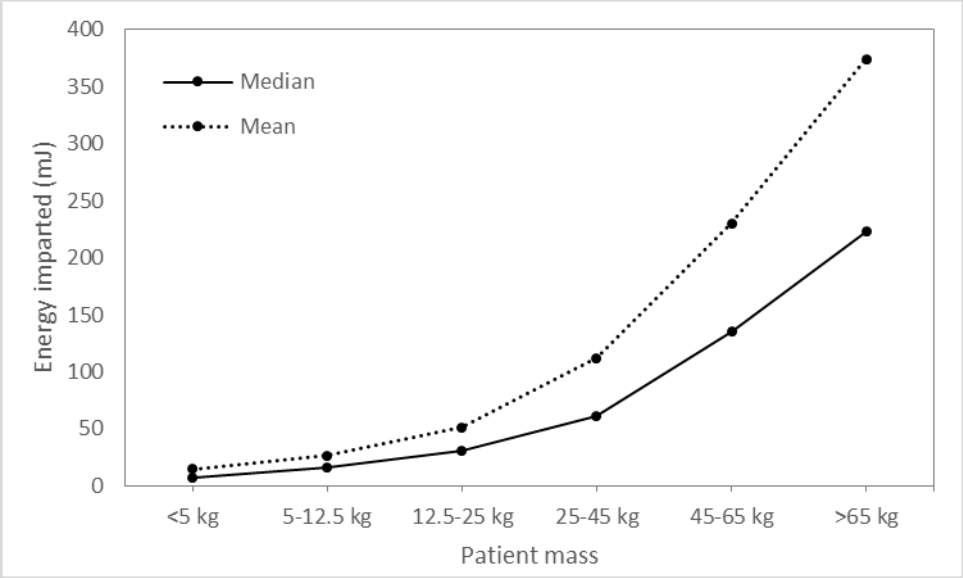


**Figure 8.1: Total energy imparted in millijoules for all procedure types combined, as a function of patient mass, for examinations conducted using Siemens Axiom Artis or Artis Zee machines.**

### *8.3: Discussion*

The finding that the breasts, oesophagus, heart and lungs receive the highest doses from cardiac catheterizations is unsurprising considering the thoracic location of the field of primary irradiation. The doses to these organs were very high for procedures

conducted before 2000 at Hospital 1, though have fallen to reasonably low levels with the installation of new equipment.

Cancers of the lungs and breasts have previously been strongly associated with radiation exposure [7, 139, 158, 291], with oesophageal cancer appearing to be more moderately inducible [7, 45]. While there is currently no evidence of the ability of radiation to induce cardiac tumours, there is evidence of an association between radiation exposure and other cardiovascular disease [3]. From an epidemiological perspective however, searching for evidence of heart disease among patients treated for heart disease is likely to be especially challenging. The relatively low doses to active bone marrow and the thyroid gland are significant findings as radiation exposure to both tissues is strongly associated with cancer development, especially in children [7, 292-294].

The relationship between patient size and organ doses is noteworthy. In Chapter 3 (section 3.5.1), it was noted that $P_{KA}$ is positively correlated with patient size (mass or age). The relationship between organ doses and patient size is more complex and was seen to vary between organs and the era in which the examination was conducted. The upturn in dose as patient size is reduced below around 10 kg (approximately 1 year) possibly suggests overexposure of small patients and a failure of equipment to properly adjust exposure factors to match attenuator thickness. The use of antiscatter grids for all patient ages was associated with a pattern of highest doses among the smallest patient sizes. Further research is warranted to determine if doses for these patients can be reduced without compromising image quality. The fall in thyroid dose with increasing patient size is most likely due to the increasing distance between the thyroid and the primary irradiation field. Effective dose was always higher than the average absorbed dose to the whole body. This is to be expected given the high density of organs with large effective dose tissue weighting factors in the chest region.

The effective doses for paediatric cardiac catheterizations carried out in the last 10 years were somewhat higher than those for cardiac computed tomography (CT) (Table 8.3). For example, Gherardi *et al* [111] estimate a median effective dose for paediatric cardiac CT of 1.7 mSv (IQR 0.8 : 2.4), while the equivalent figure calculated by Watson *et al* [167] was 0.74 mSv (range: 0.43–15.31). Doses from cardiac CT depend on the techniques used for gating (matching scan acquisition to

heart rhythm), tending to be lower for prospectively gated rather than retrospectively gated scans [165, 166]. Lee and co-workers [166] used a 1-year old ATOM anthropomorphic phantom and thermoluminescent dosemeters to calculate organ doses delivered by both 64 and 256 slice CT using different gating techniques (Table 8.3). Typical effective doses for cardiac CT of 1-3, 2-6 and 0.2-1.0 mSv were reported by Goo [165] for high pitch dual source scanning, retrospective gating and prospective gating protocols respectively. Thus there is a sizeable variation in quoted doses for cardiac CT depending on equipment and imaging protocol, although this variation appears smaller than that evidence for cardiac catheterization doses. As with fluoroscopy, there has been a fall in CT doses over the last two decades. Reasons for this include improved detectors, more dose efficient reconstruction algorithms and slice-by-slice exposure modulation (varying x-ray output to match local anatomy). Despite the potential to deliver lower doses, CT provides limited capability to conduct therapeutic intervention such as ballooning, stenting or duct closure.

| | 64 slice scanner | | 256 slice scanner | | |
|---|---|---|---|---|---|
| **Organ** | **NG** | **RGH** | **NG** | **RGH** | **PGA** |
| **ABM** | 1.67 | 5.27 | 2.4 | 7.5 | 1.17 |
| **Breast** | 2.34 | 7.35 | 3.6 | 10.74 | 2.04 |
| **Lung** | 2.26 | 7.5 | 3.16 | 10.66 | 1.8 |
| **Oesophagus** | 2.18 | 7.21 | 3.13 | 11.29 | 1.96 |
| **Thyroid** | 2.54 | 7.76 | 4 | 13.5 | 2.03 |
| **Liver** | 1.37 | 4.28 | 2.47 | 5.6 | 0.52 |
| **Stomach** | 2.15 | 6.47 | 2.6 | 9.95 | 1.39 |
| **Effective** | 1.49 | 4.66 | 2.15 | 6.87 | 1.12 |

**Table 8.3: Organ doses (in mSv) for cardiac CT reported by Lee *et al* [166]. NG = non-gated, RGH = retrospective gated helical, PGH = prospectively gated helical. Both 64 and 256 slice machines are models of Philips Brilliance scanner (Philips Healthcare, Cleveland, OH, USA).**

### *8.3.1: Comparison with previous research*

At the time of writing, very few assessments of organ doses from paediatric cardiac catheterizations have been carried out. A larger number of studies have estimated effective dose [8, 12, 13, 91, 92, 103, 108, 113], though, as noted in the literature review, many of these assessments were based on highly simplistic $E/P_{KA}$

conversion factors with little or no x-ray energy or beam angle adjustment. The often quoted $E/P_{KA}$ conversion factor calculated by Onnasch et al in 2007 [103] based on $P_{KA}$ normalised by mass, of 9.26 * ($P_{KA}$/kg) was re-examined in the light of the estimated effective doses calculated in the current study. For examinations conducted using 3rd generation equipment (Siemens Axiom Artis or Artis Zee), the effective dose per $P_{KA}$ per kilogram was calculated for 7202 examinations of all types. The mean E per $P_{KA}$/kg conversion factor was calculated as 20.7 (standard deviation = ±3.2) – more than twice the value of the coefficient reported by Onnasch. This difference is consistent with the use of higher beam energies than were assumed in the 2007 study. Although simplistic, the $E/P_{KA}$ conversion factor quoted by Onnasch offers the opportunity to provide rapid estimates of doses for a sample of examinations of mixed type where variation in beam angles is averaged out. The methodology was easily expanded to include figures for individual organs. These conversion factors are given in Table 8.4. They should be regarded as being unsuitable for dose estimation for individual procedures in which particular beam angle combinations are used.

| | Conversion factor | |
|---|---|---|
| **Organ** | **Mean [SD]** | **Median [IQR]** |
| **Bone marrow** | 11.0 [4.9] | 9.0 [7.7 : 14.0] |
| **Breasts** | 46.1 [15.8] | 48.5 [35.7 : 56.4] |
| **Heart** | 53.7 [19.2] | 48.9 [44.2 : 56.6] |
| **Lungs** | 65.2 [14.7] | 65.0 [57.6 : 70.9] |
| **Lymph nodes** | 13 [2.8] | 12.8 [11.8 : 14.0] |
| **Oesophagus** | 43.2 [8.2] | 42.7 [39.5 : 45.9] |
| **Thyroid** | 2.6 [0.9] | 2.7 [1.8 : 3.3] |
| **Liver** | 17.3 [5.3] | 17.9 [12.9 : 21.6] |
| **Stomach** | 11.1 [4.4] | 10.2 [8.5 : 11.4] |
| **Effective dose** | 20.7 [3.2] | 21.1 [19.3 : 22.9] |
| **Mean Dose** | 11.9 [2.2] | 11.9 [10.8 : 13.1] |

**Table 8.4: Conversion factors in the form of effective dose or organ dose (in mSv) per PKA per kilogram body mass. Note: SD=standard deviation, IQR=interquartile range.**

Organ doses for three procedure types (occlusion of ASD, PDA and ventricular-septal defect, VSD) were estimated by Yakoumakis and colleagues [107], using PCXMC V2.0. Very high mean effective doses of 40, 22 and 17 mSv were reported for ASD, PDA and VSD occlusions respectively. Where age matched, these doses are higher than those of the earliest data in the current study and higher than recent

era doses by a factor of almost 60. To further investigate, the doses for each procedure type were calculated in Cardiodose using the same patient size and total examination $P_{KA}$ reported by Yakoumakis *et al*, with beam angles, field size and x-ray energy being set at the same values as used in this study. VSD occlusions are not modelled in this study (the procedure is rarely carried out in the UK), therefore the 'unspecified' examination category was applied. This results of this comparison are shown in Table 8.5. There are a number of surprisingly large discrepancies between the two sets of figures, most notably for thyroid dose. Organ doses calculated by cardiodose were higher than those of Yakoumakis for PDA occlusions, and generally lower for ASD or VSD occlusions. The difference in dose estimates between Cardiodose and Yakoumakis are difficult to explain. The field sizes are similar between studies, as are the x-ray energies. The projection angles reported by Yakoumakis are difficult to interpret, though any variation is unlikely to be sufficient to explain the variation in doses. The study by Yakoumakis is the only one to provide breast dose estimates higher than those of the current study.

| | | | Organ | | | | | | | |
|---|---|---|---|---|---|---|---|---|---|---|
| **Procedure** | **Study** | **$P_{KA}$** | **ABM** | **Breasts** | **Heart** | **Liver** | **Lungs** | **Stomach** | **Thyroid** | **Effective** |
| **ASD occlusion (10 years)** | Yakoumakis | 39.9 | 9.9 | 141.1 | 146.8 | 40.8 | 63.7 | 50.6 | 4.1 | 40.0 |
| | Cardiodose | | 16.8 | 38.8 | 55.7 | 16.4 | 81.4 | 11.4 | 1.9 | 22.7 |
| **VSD occlusion (10 years)** | Yakoumakis | 17.5 | 5.2 | 61.7 | 67.6 | 24.2 | 35.7 | 29.9 | 5.6 | 22.0 |
| | Cardiodose | | 6.0 | 35.7 | 26.2 | 10.3 | 35.8 | 4.2 | 0.9 | 12.0 |
| **PDA occlusion (new born)** | Yakoumakis | 9.5 | 4.3 | 60.7 | 57.0 | 19.0 | 26.6 | 23.8 | 1.5 | 17.0 |
| | Cardiodose | | 13.8 | 106.0 | 101.9 | 35.8 | 108.1 | 19.4 | 8.9 | 39.1 |

**Table 8.5: Organ doses (in mSv) calculated by Yakoumakis et al, compared to those calculated using Cardiodose for the same examination type, patient size and total examination $P_{KA}$.**

Doses to the lungs, oesophagus, thyroid and breasts were estimated by Barnaoui *et al* [92] for 5 examinations by reconstructing the procedures using CIRS ATOM anthropomorphic phantoms. These results were compared to the physical measurements obtained in the current study in the preceding chapter. Further comparison was made by calculating doses for each of the 5 examinations

reconstructed by Barnaoui *et al,* using Cardiodose. The results of this comparison are presented in Table 8.6 and show a number of striking discrepancies. There is little suggestion of a systematic difference, except for thyroid dose, which is higher for all procedures in the Barnaoui study. The largest discrepancies were for the PDA occlusion procedure, particularly for the breasts and lungs which were 1217% and 357% higher, respectively, in the current study. For one procedure – a pulmonary valvuloplasty on a new born baby - the recorded thyroid dose was especially high (37 mSv), based on a $P_{KA}$ of 6.09 Gy·cm$^2$. This could only have occurred if the beam was collimated such that the thyroid was entirely within the primary field. Another unusual finding was a higher dose to the oesophagus for a PDA occlusion, than for the lungs (3.7 verses 2.2 mGy).

| | | Organ | | | |
|---|---|---|---|---|---|
| **Examination** | **Study** | **Breasts** | **Lungs** | **Oesophagus** | **Thyroid** |
| **PA angioplasty? (10 kg)** | Cardiodose | 9.0 | 9.0 | 6.2 | 0.5 |
| | Barnaoui | 4.2 | 13.3 | 10.6 | 1.3 |
| **Coronaries and biopsy (32 kg)** | Cardiodose | 2.6 | 19.7 | 12.1 | 0.9 |
| | Barnaoui | 21.0 | 42.7 | 26.0 | 1.0 |
| **PV plasty and VSD occlusion (3.5 kg)** | Cardiodose | 60.1 | 72.7 | 57.3 | 5.5 |
| | Barnaoui | 33.0 | 61.0 | 53.8 | 37.0 |
| **ASD occlusion (55 kg)** | Cardiodose | 2.1 | 7.4 | 4.1 | 0.1 |
| | Barnaoui | 4.0 | 14.6 | 10.0 | 2.0 |
| **PDA occlusion (19 kg)** | Cardiodose | 10.5 | 10.0 | 6.6 | 0.4 |
| | Barnaoui | 0.8 | 2.2 | 3.7 | 0.7 |

**Table 8.6: Organ doses (in mSv) calculated by Barnaoui et al [91] for five examinations, compared to doses calculated using Cardiodose using the same reported $P_{KA}$, patient mass and examination type.**

Keiller and Martin [295] estimated dose to the heart from 250 cardiac catheterization procedures (PDA and ASD occlusions, Radiofrequency ablations, 'balloon angioplasty' and 'cardiac catheter and angiography') conducted between 2012 and 2013 on patients aged 1 to 11 years. Heart dose was calculated from $P_{KA}$ using PCXMC V2.0 for 'typical procedures' and for the 'highest dose' for each examination type. It appears therefore that dose was not calculated for each individual procedure, but rather single simulations were conducted using average and maximum $P_{KA}$. Table 8.7 compares Keiller and Martin's results with those of the current study (Hospital 1 2002-2008). The former doses are considerably higher. This is primarily due to the higher $P_{KA}$, though heart dose per unit $P_{KA}$ is also higher, especially for

ASD occlusions. The main reasons for this difference appear to be a lower mean patient mass in the Keiller and Martin study and different beam energy (a Philips Allura Xper was used, with relatively heavy filtration and high kV, giving a half value layer of around 6.8 mm Al). The beam angles used are generally similar to those of the current study. Comparisons were not made for the 'cardiac catheter and angiography' and 'balloon angioplasty' procedures as it is not clear what these procedures actually are (many disparate procedures involve balloon angioplasty of some sort, and virtually all procedures involve angiography).

| Procedure type | Study | Mean $P_{KA}$ (Gy cm²) | Heart dose (mGy) | Mass (kg) | $H/P_{KA}$ |
|---|---|---|---|---|---|
| CC + Angiography | Keiller and Martin | 5.7 | 43 | 8.2 | 7.5 |
| | Hospital 1 (02-08) | - | - | - | - |
| PDA occlusion | Keiller and Martin | 3.2 | 31 | 11.8 | 9.7 |
| | Hospital 1 (02-08) | 1.8 | 6.7 | 14.1 | 5.6 |
| Radiofrequency ablation | Keiller and Martin | 4.3 | 13 | 46 | 3.0 |
| | Hospital 1 (02-08) | 10.1 | 19.9 | 53.0 | 2.5 |
| Balloon angioplasty | Keiller and Martin | 10.6 | 43 | 18.4 | 4.1 |
| | Hospital 1 (02-08) | - | - | - | - |
| ASD occlusion | Keiller and Martin | 5.0 | 23 | 21 | 4.6 |
| | Hospital 1 (02-08) | 4.4 | 7.4 | 28.6 | 2.3 |

**Table 8.7: Mean heart doses estimated by Keiller and Martin, compared to equivalent figures for the current study at Hospital 1 2002-2008. Note: CC+A is 'cardiac catheter + angiography'.**

The above comparison with previous studies reveals large differences in dose estimates, though these are not systematic, i.e. doses from the current study are not consistently higher or lower. Variation in dose estimates reaffirms the need for uncertainties stemming from variation in beam energy, projection angle and other factors from expected values to be incorporated into dose estimates and subsequent risk modelling. This process is described below.

### *8.4: Uncertainty modelling*

An assessment of the uncertainty in dose estimates is essential, especially in the case of estimating cardiac catheterization doses using limited data recorded at the time of the examination. Estimated doses are calculated from the product of $P_{KA}$ and a conversion factor to relate this figure to organ doses ($CF_T$). The overall uncertainty

in dose estimates (δD) can be calculated by adding in quadrature the uncertainty of $P_{KA}$ measurements ($\delta P_{KA}$) and uncertainty in the conversion factor ($\delta CF_T$):

$$\delta D = |D| \sqrt{\left(\frac{\delta P_{KA}}{P_{KA}}\right)^2 + \left(\frac{\delta CF_T}{CF_T}\right)^2}$$

The denominators in the above equation represent the recorded value of $P_{KA}$ and the central estimate of the conversion factor, whereas the numerators are the uncertainty of each. The value of $\delta P_{KA}$ was assumed to be fixed at ±15%:

$$\delta D = |D| \sqrt{(15\%)^2 + \left(\frac{\delta CF_T}{CF_T}\right)^2}$$

By adding in quadrature, the total uncertainty is dominated by the largest individual component (which is usually $\delta CF_T$), meaning $\delta P_{KA}$ makes little contribution. The uncertainty in $CF_T$ (the T stands for total) comprises the uncertainty in projection angle (δp) beam energy (δE), field size (δfs) and 'anatomical variation' (δa):

$$\delta CF_T = |CF_T| \sqrt{\left(\frac{\delta p}{a}\right)^2 + \left(\frac{\delta E}{E}\right)^2 + \left(\frac{\delta_{fs}}{fs}\right)^2 + \left(\frac{\delta a}{m}\right)^2}$$

The value of δE and δp are based on the 5th and 95th percentiles of dose per unit $P_{KA}$ over the range of energies and projection angles seen in clinical practice. These figures were defined in the supporting information chapter. As stated previously, where biplane $P_{KA}$ figures are recorded, δp is effectively reduced to zero for procedures involving only two projection angles such as valvuloplasty or pressure studies. The field size uncertainty was obtained by calculating doses using each of the 3 simulated field sizes used in cardiodose. In many cases, the field size used in dose estimations resulted in either the highest or lowest dose of the three sizes available. Consequently, the field size uncertainty usually only affected either the upper or lower uncertainty limit in isolation, rather than both.

The value of δa – the uncertainty due to 'anatomical variation' is not only potentially the largest but also the most difficult uncertainty to quantify. It encompasses variation in the size, shape and density of cohort members from the PCXMC phantoms used in dose calculations. This includes variation in lung density due to different levels of

inspiration and the potential change in organ density due to contrast agent administration.

The potential impact of lung density was apparent in the results of physical measurements, in which doses were higher than predicted by Monte Carlo simulations. Obtaining estimates of human lung density values is difficult as few published data exist. Woodard [296] quotes a single figure of 260 kg $m^{-3}$ (0.26 g $cm^{-3}$) for inspiratory lung density. Van Dyk *et al* [297] used computed tomography images to calculate mean inspiratory and expiratory lung densities of 0.36 and 0.20 g $cm^{-3}$ respectively at 5 years of age. The mean of these two values is 0.28 g $cm^{-3}$. The authors found an inverse linear relationship between age and lung density, with respective values at 80 years being 0.22 and 0.16 g $cm^{-3}$. A similar finding of decreased lung density with age was reached by Long and colleagues [298], who found an approximately 35% difference in mean Hounsfield Unit between inspiratory and expiratory breathing phases in children (-835 and -616 HU respectively). Further research by Brown *et al* [299] suggests that following termination of primary growth of new alveoli between 2 and 8 years of age, further 'growth' of the lungs is achieved by enlarging existing alveoli, leading to a gradual decline in lung density with age.

Lung density in both Monte Carlo and physical phantoms is fixed. Larger lungs are simply modelled by more lung tissue, rather than the same amount of lung tissue expanded to fill a larger volume, as seems to occur in reality [299]. PCXMC V2.0 assumes a single lung density of 0.3 g $cm^{-3}$, which appears to be designed to reflect a central level of inspiration. Adult 'RANDO' phantoms (The Phantom Laboratory, Salem, New York) have lung density of 0.32 g $cm^{-3}$ designed to "*closely [mimic] the density of lungs in a median respiratory state*" [300], while ICRU-44 lung tissue substitute has a density of 0.26 g $cm^{-3}$ [301]. As previously stated, ATOM phantoms are based on an inspiration density of 0.21 g $cm^{-3}$, with expiration lung densities of 0.50 g $cm^{-3}$ being available on special request.

Usually, cardiac catheterizations in children are carried out under general anaesthetic, with breathing controlled via a ventilator through an endotracheal tube [302]. During fluoroscopic exposures, the patient is allowed to breathe normally, therefore radiation exposures would be distributed over a range of lung densities from full inspiration to full expiration. During acquisitions, the anaesthetist can switch the ventilator off to reduce movement and improve image quality (S. Charlton,

personal communication). Thus for fluoroscopy at least, the 'central' lung density value of PCXMC appears more appropriate than the inspiration lung density of ATOM phantoms.

Even where patient age and breathing phase are fixed, lung density varies with location, being higher towards the posterior or hilum (location of the primary pulmonary arteries and veins) [298]. Blood makes up around 43% of lung mass [296]. If iodinated contrast agent has been administered, the density, and hence attenuating property of lung tissue will correspondingly increase. The impact of contrast agents on organ density and calculated doses has been studied with respect to radiotherapy [303-305], though little research has been carried out on the impact of dose estimation for diagnostic imaging. There is, therefore, insufficient information available to account for the impact of contrast agent administration in organ dose uncertainties.

Other research has focussed on the impact of more general changes in phantom size and shape between phantoms and organ doses. Zanki and colleagues [306] compared doses calculated using seven different adult phantom models (Adam, Eva, Golem, Donna, Helga, Irene, Frank, Visible Human and Voxelman) incorporated into Monte Carlo simulations. Variation in calculated doses for the breasts, lungs, oesophagus, thyroid, stomach and bone marrow were up to 30% "*for those directions of photon incidence where the organ is located at a shallower depth*" and 30-100% for "*photon beam directions from which the organs are averted*" [306]. Variation between models was related to photon energy, being highest below 30 keV and relatively low beyond 200 keV. A further study by Johnson *et al* [307] assessed variation in organ doses from adult cardiac catheterizations, calculated by Monte Carlo simulations (MCNPX 2.6.0) for 27 phantoms constructed using contour mapped CT images of real patients, compared to size-matched UF reference phantoms. The authors estimate a variability in dose calculations due to variation in organ size and location of 35-45%. Such errors can be reduced through the incorporation of contour mapped patient specific phantoms, especially in the case of organ attenuation, in which errors can be reduced by 20-60% [307]. However this approach is unthinkable for dose estimation in a cohort of thousands of patients. Obtaining cross sectional images is exceptionally time consuming and requires considerable cooperation from collaborating hospitals. Furthermore, such images

would need to be acquired at a similar age as cardiac catheterizations were carried out.

As such, dose estimation errors due to 'anatomical variation' ought to be accepted as unavoidable uncertainties and combined with uncertainties from other sources. Central dose estimates could be improved through more realistic phantom anatomy. Based on the previously discussed findings of Johnson *et al* [307], a potential value for δa is around 50%, which when combined with other uncertainties results in a total figure for δD of around ±60%, rising to ±80% where only screening time is recorded. These uncertainties are large, though considerably smaller than would be present without any form of examination specific dose indicator being incorporated, i.e. simply assigning an average dose for each procedure type. The figure for δa was considered too speculative to incorporate into dose estimates for the current study, however. Consequently, the doses presented in this thesis include all uncertainties except for those owing to anatomical variation. Examples are given in Table 8.8 for the 'unspecified' procedure category, in which errors represent the mean of those for all defined procedure types. Across all patient sizes, these errors are approximately ±25%. Combined uncertainties, stratified by patient size and procedure type are shown in Appendix 4.

In this discussion, individual sources or error have been largely treated as being independent of each other. This can be partly justified by the relatively small impact of projection angle on overall beam energy represented by HVL (Section 6.1.2, Figures 6.10 and 6.11). In reality, it is likely that the variation in beam energy is principally due to anatomical variation, i.e. differences in organ size, shape and density affect the level of beam attenuation, causing the machine to respond by adjusting tube potential and filtration accordingly. Furthermore, $P_{KA}$ measurement uncertainties may be influenced, to some extent, by beam energy. Uncertainty in the table transmission factor should also be considered. In particular, a single figure was used, rather than equipment/vendor specific factors. Some level of variation would be expected. The transmission factor is dependent on beam angle, though this variation was found to be quite small (see section 6.2.6). A more detailed analysis of the relationship between uncertainties is beyond the capabilities of the PCXMC Monte Carlo code and its crude phantoms and will be left as the subject of future research.

| Patient age (mass) | Limit | Effective dose | ABM | Breasts | Heart | Lungs | Lymph | Oesophagus | Thyroid | Liver | Stomach | Average dose |
|---|---|---|---|---|---|---|---|---|---|---|---|---|
| **<1 y (<9.2 kg)** | **Upper** | 19% | 24% | 41% | 34% | 17% | 17% | 18% | 20% | 32% | 22% | 17% |
| | **Lower** | -18% | -24% | -35% | -20% | -16% | -17% | -19% | -21% | -32% | -27% | -17% |
| **1-5 y (9.2-19 kg)** | **Upper** | 21% | 22% | 42% | 30% | 17% | 19% | 23% | 25% | 40% | 24% | 17% |
| | **Lower** | -20% | -22% | -40% | -24% | -17% | -19% | -20% | -25% | -28% | -26% | -17% |
| **5-10 y (19-32.4 kg)** | **Upper** | 25% | 23% | 59% | 41% | 18% | 20% | 24% | 24% | 44% | 27% | 19% |
| | **Lower** | -22% | -22% | -47% | -24% | -18% | -20% | -21% | -24% | -34% | -31% | -18% |
| **10-15 y (32.4-56.3 kg)** | **Upper** | 26% | 26% | 64% | 37% | 19% | 21% | 24% | 27% | 49% | 31% | 19% |
| | **Lower** | -23% | -26% | -56% | -24% | -19% | -21% | -22% | -27% | -37% | -35% | -19% |
| **15-18 y (>56.3 kg)** | **Upper** | 24% | 28% | 66% | 42% | 20% | 22% | 28% | 31% | 58% | 37% | 20% |
| | **Lower** | -24% | -26% | -63% | -26% | -22% | -23% | -25% | -33% | -47% | -42% | -19% |
| **>18 y (>70 kg)** | **Upper** | 25% | 28% | 70% | 41% | 21% | 23% | 28% | 30% | 61% | 40% | 20% |
| | **Lower** | -24% | -26% | -65% | -26% | -22% | -23% | -28% | -32% | -42% | -47% | -19% |

Table 8.8: Overall uncertainties (not including those due to anatomical variation) for 'unspecified' procedures. ABM = active bone marrow.

### *8.4.1: Comparison of dose estimates based on detailed and limited data*

To further investigate the accuracy of dose estimations, figures produced using Cardiodose and limited data (mass, single-plane $P_{KA}$ and examination type only) were compared to those produced by reconstructing 44 examinations conducted at Hospital 4 for which structure dose reports, containing beam angles, tube potential and added filtration, were available. Fluoroscopic exposures are only recorded in structured dose reports as the total $P_{KA}$ from frontal and lateral tubes, rather than in the form of individual beam angles. The beam angles used for fluoroscopy were assumed to be the same as those used for acquisitions. The proportion of fluoroscopic $P_{KA}$ in each beam angle was estimated from the respective proportions for acquisitions. Thus dose estimated obtained from 'detailed' data are still subject to uncertainties.

This analysis reveals reasonably good agreement between dose estimates obtained from limited and detailed examination data (Figure 8.8). The latter figures generally are within the upper and lower uncertainty limits for the former. For some organs, the detailed dose estimate is marginally outside the upper uncertainty limit. The median absolute error was 11%, while the median signed error was -8%, indicating a small systematic underestimation of doses by Cardiodose. The largest error in effective dose for a single examination was -37%. This finding that dose estimates obtained using limited examination data can be reasonable approximations of those using detailed data is consistent with that of Karambatsakidou *et al* [112], where the mean deviation in estimated effective dose between detailed and limited data methodologies was 5%.

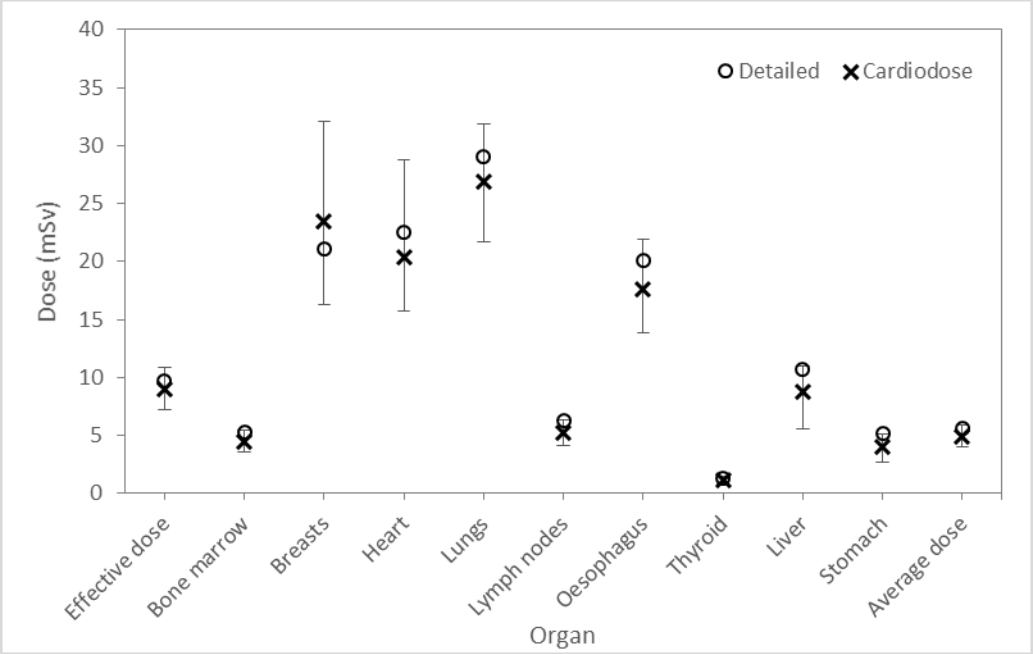


**Figure 8.8: Comparison of doses calculated using detailed beam angle data from structured dose reports with estimates derived from limited data using Cardiodose. Figures for each organ represent the mean dose for the sample of 44 examinations.**

### *8.5: Estimation of missing doses*

As noted in chapter 3, around 70% of procedures conducted at Hospital 4 had no recorded dose indicator (neither $P_{KA}$ nor even screening time). This presented a problem for the epidemiological analysis, considering patients examined at the Hospital 4 contributed around 23% of the total cohort (i.e. approximately 16% of the cohort had no dose estimates based on recorded data). The only option available was to estimate these missing doses from data where $P_{KA}$ was recorded. This is unsatisfactory, given the potential for enormous variation in doses from one procedure to the next. However, there was no alternative, other than to exclude these patients from the study. Comparable studies investigating the risks from CT scans have adopted a similar approach, using average doses for groups of scan types, adjusted for patient age and exposure era [9, 124, 187, 190].

The only individual procedure types in which a sufficiently large sample of examinations was available was for coronary angiographies (both 1993-2003 and >2003), and PDA occlusions (>2003 only). Missing doses were estimated based on the median figures for these groups. For all other procedures, estimated doses were based on the figures in Table 8.2, for each era. No patient size stratification was

applied, as there was little suggestion of a variation in organ doses with age at Hospital 4 (see age stratified organ dose tables in Appendix 3). There is a suggestion of an increase in coronary angiography dose with patient size, although this was not found to be significant (p=0.39) and the number of procedures in each size category was quite small.

| | All procedures | | Coronary angiography | | PDA occlusion |
|---|---|---|---|---|---|
| **Organ** | **93-03** | **Mar-13** | **93-03** | **Mar-13** | **Mar-13** |
| **Effective dose** | 7.4 [4 : 12.7] | 2.7 [1.5 : 5] | 8.5 [4.8 : 12.2] | 3.4 [2 : 5.2] | 2.7 [1.9 : 4.2] |
| **Bone marrow** | 3.1 [1.7 : 5.6] | 1.3 [0.6 : 2.3] | 3.8 [2.6 : 7.9] | 2 [1.2 : 3] | 0.9 [0.7 : 1.4] |
| **Breasts** | 20.3 [10.9 : 35.4] | 7 [3.9 : 12.9] | 21.3 [14.8 : 32.5] | 9.3 [5.2 : 14.7] | 7.4 [5.2 : 12.3] |
| **Heart** | 15.2 [7.8 : 25.5] | 6.4 [3.5 : 11.8] | 17.4 [9.8 : 26.6] | 8.6 [4.8 : 13.2] | 6.3 [4.8 : 9.7] |
| **Lungs** | 23.2 [12.4 : 39.4] | 8.3 [4.6 : 15.3] | 24 [14.1 : 41.8] | 10.6 [5.8 : 15.9] | 7.6 [5.4 : 12.1] |
| **Lymph** | 4.1 [2.1 : 6.9] | 1.6 [0.9 : 2.9] | 3.8 [2.1 : 6.1] | 1.8 [1 : 2.9] | 1.6 [1.1 : 2.4] |
| **Oesophagus** | 13 [6.8 : 22] | 5.4 [3.1 : 10] | 12 [7.1 : 20.5] | 6.7 [3.8 : 9.9] | 5.4 [3.8 : 7.9] |
| **Thyroid** | 0.7 [0.3 : 1.4] | 0.4 [0.2 : 0.7] | 0.4 [0.2 : 0.7] | 0.3 [0.2 : 0.4] | 0.4 [0.2 : 0.6] |
| **Liver** | 6.3 [3.3 : 10.7] | 2.5 [1.4 : 4.6] | 5.6 [3.1 : 9.1] | 2.7 [1.6 : 4.3] | 3 [1.9 : 4.6] |
| **Stomach** | 2.7 [1.4 : 4.7] | 1.1 [0.7 : 2.2] | 1.5 [0.7 : 2.5] | 0.9 [0.5 : 1.5] | 1.3 [0.8 : 1.9] |
| n | 817 | 496 | 19 | 69 | 18 |

**Table 8.8: Estimated organ doses (in mSv) for examinations at the Hospital 4, where $P_{KA}$ was not recorded.**

### *8.6: Conclusion*

Organ doses have been estimated for around 14,500 procedures. The organs receiving the highest doses are the lungs, heart, oesophagus and breasts. Doses to bone marrow, lymph nodes and the thyroid gland are relatively low. Organ doses have fallen significantly during the period of data collection, in a similar manner to the dose indicators presented in Chapter 3. The doses from cardiac catheterizations are similar to those for computed tomography, albeit slightly higher. The estimates presented in this chapter are subject to uncertainties due to variation in beam angle and x-ray energy from expected values. Further uncertainties are introduced by 'anatomical variation' – differences in organ size, shape and arrangement from that assumed in the phantoms used in Monte Carlo simulations and physical measurements. While the former uncertainties can be quantified and used to produce upper and lower uncertainty limits on dose estimates, uncertainties due to anatomical variation are difficult to determine without using patient specific phantoms. Based on previous research, however, such uncertainties may be around

±50%. The following chapter utilises organ doses to estimate excess cancer risks using existing risk models, derived mainly from survivors of the nuclear bombings of Hiroshima and Nagasaki.

## Chapter 9: Risk projection

The organ doses presented in the previous chapter can be used to estimate the lifetime risk of radiation induced cancer using models derived from previous studies of radiation exposures. The projection approach has the advantage of allowing risk estimation for small cohort sizes where epidemiological analysis would lack sufficient statistical power, or where follow-up time is limited. The largest source of data for risk models remains the cohort of survivors of the nuclear bombings of Hiroshima and Nagasaki [135, 308], though models may also incorporate data from other studies including pooled analyses of studies of thyroid [294] and breast cancer [309]. As discussed in the literature review, most epidemiological studies to date lack sufficient statistical power to detect excess cancer risks below doses of around 100 mSv, meaning risk estimation below this level can only be achieved through downwards extrapolation, assuming a linear-no-threshold (LNT) relationship between dose and risk.

The process of risk estimation has two stages: (1) calculation of excess relative risk (ERR) or excess absolute risk (EAR) in relation to a given dose, age at exposure, sex and attained age in the 'study' population, then (2) to transport these risks to a 'reference' population in terms of the lifetime attributable risk (LAR) of disease in relation to dose [310]. The ERR is equal to the rate of disease in the exposed population divided by the rate in the unexposed population, minus 1 [3]. Thus the ERR assumes cancer increases in proportion to the baseline rate [16]. However, the baseline rate varies from one population to another, depending on geographical location and ethnic group. Stomach cancer, for example, is more common in Japan than in America or Europe, while lung and breast cancer are less common in Japan [133]. Thus the application of ERR models derived from exposures in one such population (i.e. Japan) to other populations (i.e. UK) requires caution. The EAR represents the rate of incidence or mortality of the disease in the exposed population minus the corresponding rate in the unexposed population. This model assumes excess cancer is independent of baseline levels [16] and is thus better suited to application in populations differing from that from which the model was calculated [49] (e.g. European instead of Japanese).

A modification to the LNT model known as a 'dose and dose rate effectiveness factor' (DDREF) has been recommended by a number of organisations [3, 44, 45]. This

reduction in risks by a variable factor is applied where dose rates are below 0.1 mGy/min (regardless of total dose) or where the total dose is less than 200 mGy [45]. Such requirements were met for around 98% of examinations in the current study. Application of a DDREF effectively results in two linear slopes, one for low doses and one for high doses, and has remained unpopular with authors arguing for threshold or hormesis models [311]. Calculated values of DDREF have ranged from 1 to 35 depending on biological end points [49], though values in the range 1.5 to 2.0 are typical in cancer risk estimation from low doses [3, 44].

### *9.1: Risk projection theory*

The simplest approach to risk estimation is to use sex- and age-at-exposure averaged 'nominal risk coefficients', calculated by the International Commission for Radiological Protection (ICRP). For the general population, these are 5.5% per sievert for cancer and 0.2% for heritable effects [44]. For example, for an effective dose of 10 mSv, the cancer risk would be 0.0055% or approximately 1 in 2000. This risk model is for a 'reference person' – a hermaphrodite of no particular age. It is not designed to be applied to real patients of defined age and sex [312, 313], rather being designed for use in optimisation and radiation protection planning purposes (e.g. shielding requirements). There are a number of reasons why this is the case. Firstly, the tissue weighting factors used to calculate effective dose are age independent, despite the risk of cancer induction varying with age in a different manor for different tissues [196, 197]. Secondly, risk estimates and weighting factors are sex-averaged, despite the risk of radiation induced cancer being strongly sex dependent (risks are higher for females) [44]. Thirdly, the effective dose for a male patient would assume he had breasts. This is especially significant for cardiac imaging as breast dose has such a large impact on effective dose. Removing the impact of the breasts from calculated effective dose for males would require all the remaining weighting factors to be re-calculated. Effective dose should not be used for individualised risk modelling, although various authors have done this [8, 13, 89]. These studies will be discussed later in this chapter.

Appropriate risk estimation for individuals utilises age, sex and organ specific risk models. The Committee to Assess Health Risks from Exposure to Low Levels of Ionizing Radiation report on the Biological Effects of Ionizing Radiation (BEIR) 2006

report (BEIR VII phase 2) [3] describes models for estimating the ERR and EAR of cancer for a person of a given age following exposure to a given dose of radiation. Risks can be calculated for all solid cancers combined, or for certain individual cancer sites. Separate models are provided for leukaemia, in which a linear-quadratic dose response is assumed, based on epidemiological data [7].

The 'all solid cancers' model is based on the concept of 'mean colon dose' as a measure of radiation dose to the body. This is based on the whole-body nature of exposure following the nuclear bombings, as opposed to the highly localised exposures from cardiac catheterizations, where mean colon dose is lower than the mean whole body dose by a factor of around 5. Using mean colon dose as the primary measure of radiation dose from these procedures would result in large underestimates of risk.

For solid cancer sites, including lung, stomach and liver, the general form of the model for a given equivalent dose $D$, in Sieverts (Sv) is the following:

$$ERR = \beta_S \cdot D \cdot \exp(\gamma \cdot e^*) \cdot \left(\frac{a}{60}\right)^{\eta}$$

Equation 9.18

The variable $\beta_S$ is the ERR for exposure at age 30 years and attained age of 60 years, and is organ and sex-dependent. The parameters to the right of $D$ are designed to adjust this figure to other exposure ages and to adjust for attained age. The parameter $e$ represents age at exposure, $e^*$ is ($e$-30)/10 for ages below 30 and zero above this age, while $a$ represents the attained age. Organ-specific values of $\beta_S$ for males and females along with those of the age at exposure adjustment coefficient $\gamma$ and attained age exponent $\eta$ are given in table 9.1.

| Cancer Site | β male (95% CI) | β female (95% CI) | $\gamma$ | $\eta$ |
|---|---|---|---|---|
| Stomach | 0.21 (0.11, 0.40) | 0.48 (0.31, 0.73) | -0.30 | -1.4 |
| Colon | 0.63 (0.37, 1.1) | 0.43 (0.19, 0.96) | -0.30 | -1.4 |
| Liver | 0.32 (0.16, 0.64) | 0.32 (0.10, 1.0) | -0.30 | -1.4 |
| Lung | 0.32 (0.15, 0.70) | 1.40 (0.94, 2.1) | -0.30 | -1.4 |
| Breast | - | 0.51 (0.28, 0.83) | 0 | -2 |
| Prostate | 0.12 (<0, 0.69) | - | -0.30 | -1.4 |
| Uterus | - | 0.055 (<0, 0.22) | -0.30 | -1.4 |
| Ovary | - | 0.38 (0.10, 1.4) | -0.30 | -1.4 |
| Bladder | 0.50 (0.18, 1.4) | 1.65 (0.69, 4.0) | -0.30 | -1.4 |
| Other solid | 0.27 (0.15, 0.50) | 0.45 (0.27, 0.75) | -0.30 | -2.8 (-4.1, -1.5) |
| Thyroid | 0.53 (0.14, 2.0) | 1.05 (0.28, 3.9) | -0.83 | 0 |
| All solid cancers | 0.33 (0.24, 0.47) | 0.57 (0.44, 0.74) | -0.30 | 1.4 (-2.2, -0.7) |

**Table 9.1: Parameter values for incidence ERR model defined by the BEIR VII committee**

The effect of the negative value of $\gamma$ in the exponential term is that ERR estimates decrease with increasing age at exposure. The factor $e^{*}$ causes risk estimates to decrease until age 30, at which point they become constant. The evidential support for this feature of the model is limited. For all cancer sites combined, the risk does appear to decrease with increasing age at exposure [169, 314]. However, it is unclear if this pattern applies to individual sites. Most notably, there is reasonably strong evidence that the risk of lung cancer does not fall with age and may in fact increase [197, 314]. For this reason, the modelling process for lung cancer was repeated with the exponential term removed, meaning risks for all ages at exposure were equal to those at age 30 years. The same approach could be applied to other sites, although the evidence of the modifying effect of age on oesophageal and stomach cancer risks is inconclusive [129].

The negative value of the exponent of attained age (relative to age 60), η, results in decreasing ERR estimates with increasing attained age, consistent with epidemiological data [7]. For thyroid cancer, the zero value of $\eta$ means that the ERR is dependent only on age at exposure and not attained age [315] (i.e. the attained age term remains constant at 1). The model for the elevated absolute risk (EAR) takes the same form as the ERR model and is based on absolute risk per 10,000 person years at age 30 [3]. Values for the various parameters for the EAR model are given in Table 9.2.

The BEIR VII committee prefer a separate model for breast cancer, based on that developed by Preston and colleagues [309], defined for the relative risk model as:

$$ERR\ per\ Sv = \beta(\frac{a}{60})^2$$

**Equation 9.19**

While the absolute risk model is defined as:

$$EAR\ per\ Sv = 9.9\ \exp(-0.05 \cdot (e - 25)) \cdot (a/50)^{\eta}$$

**Equation 9.20**

Where *a* is the attained age and *e* is the age at exposure. The exponent $\eta$ is equal to 3.5 for attained ages of less than 50, and 1.0 thereafter.

There is no EAR model for thyroid cancer. The ERR model for this site is based on a pooled analysis conducted by Ron *et al* [294], and is defined as:

$$ERR\ per\ Sv = \beta \cdot \exp[-0.083(e - 30)]$$

**Equation 9.21**

Where $\beta$ is 0.53 for males and 1.05 for females.

The model for leukaemia was obtained from the BEIR VII report [3] as follows:

$$EAR\ or\ ERR\ per\ Sv = \beta_S(D + \theta \cdot D^2) \cdot exp[\gamma \cdot e^* + \delta \cdot log(t/25) + \phi \cdot e^* \cdot log(t/25)]$$

**Equation 9.22**

Where $\phi$, $\delta$ and $\theta$ are fitting parameters. This model has a linear quadratic form, as opposed to purely linear for other sites. The quadratic term is omitted for chronic exposures [315] (i.e. a purely linear dose response is assumed), though was kept in for this analysis as all exposures were considered acute.

| Cancer Site | β male (95% CI) | β female (95% CI | $\gamma$ | $\eta$ |
|---|---|---|---|---|
| Stomach | 4.9 (2.7, 8.9) | 4.9 (3.2, 7.3) | -0.41 | 2.8 |
| Colon | 3.2 (1.8, 5.6) | 1.6 (0.8, 3.2) | -0.41 | 2.8 |
| Liver | 2.2 (1.9, 5.3) | 1.0 (0.4, 2.5) | -0.41 | 4.1 (1,9, 6.4) |
| Lung | 2.3 (1.1, 5.0) | 3.4 (2.3, 4.9) | -0.41 | 5.2 (3.8, 6.6) |
| Breast | - | 9.9 (7.1, 14)* | -0.41 | 3.5 (<30 years)<br>1.1 (>30 years) |
| Prostate | 0.11 (<0, 1.0) | - | -0.41 | 2.8 |
| Uterus | - | 1.2 (<0, 2.6) | -0.41 | 2.8 |
| Ovary | - | 0.70 (0.2, 2.1) | -0.41 | 2.8 |
| Bladder | 1.2 (0.4, 3.7) | 0.75 (0.3, 1.7) | -0.41 | 6.0 (3.1, 9.0) |
| Other solid | 6.2 (3.8, 10.0) | 4.8 (3.2, 10.0) | -0.41 | 2.8 |
| Thyroid | - | - | -0.41 | - |
| All solid cancers | 22 (15, 30) | 28 (22, 36) | -0.41 | 2.8 (2.15, 3.41) |

**Table 9.2: Parameter values for incidence EAR model defined by BEIR VII committee. * Figures based on an erratum after publication of report.**

These BEIR VII risk models have been extensively critiqued by Calabrese and O'Connor [49], in particular highlighting the considerable difference in risk estimates derived using ERR and EAR methods. Kellerer *et al* [310] note that "radiation-risk estimates tend to be scrutinized to a level that is out of balance with their inherent degree of uncertainty", though noting later that such uncertainties should not justify a lack of rigour in risk modelling.

### *9.1.1: Risk Transport*

The ERR or EAR figures described above can be used to estimate the 'lifetime attributable risk' (LAR) of cancer from radiation exposure. Such estimates must take into account the probability of reaching a particular age, and, for ERR transport, background cancer rates. The LAR based on relative risk transport is defined by Kellerer *et al* [310] as:

$$LAR(D,e,s) = \int_{e+L}^{a_{max}} ERR(D,a,e,s) \cdot m(a,s) \cdot \frac{S(a,s)}{S(e,s)} da$$

**Equation 9.23**

This represents the sum of age-specific risks taking into account the probability of surviving to that age [315]. The parameter *m(a,s)* represents the sex specific spontaneous incidence rate as a function of age. *S(a,s)* represents the "survival function", which is the probability at birth, to reach age *a*, while the ratio *S(a,s)/S(e,s)*

represents the conditional probability of someone alive at age *e* of reaching age *a* [310]. Thus, at the time of exposure, the ratio *S(a,s)/S(e,s)* is equal to 1 and decreases with each successive year. In the case of LAR, *S(a,s)* represents the survival of an unexposed rather than exposed population, unlike the otherwise similar risk transport concept of 'risk of exposure influenced death' (REID), favoured by UNSCEAR. For doses below 0.1 Sv, the LAR and REID methods yield virtually the same results [3], while at 1 Sv, REID yields figures around 10% lower [310]. As doses in this study were almost always below 0.2 Sv, either figure could be used, although LAR was adopted as it is computationally simpler. The parameter *L* in the lower limit of integration represents the latency period for cancer development following radiation exposure. A value of L of five years was used in this study for solid cancers, and 2 years for leukaemia. These values are consistent with epidemiological studies [45], including the Life Span study.

In reality, each parameter is obtained at discrete intervals (i.e. per year or per decade), thus the integral form of this calculation reduces to a simple summation:

$$LAR(e) \approx \sum_{i=e+L}^{100} ERR_i \cdot m_i \cdot \frac{S_i}{S_e}$$

**Equation 9.24**

The second form of LAR is based on absolute risk transport and uses EAR rather than ERR. The absolute risk transport LAR can be defined by the BEIR VII committee [3] as:

$$LAR(D, e, a) = M(D, e, a, s) \cdot \frac{S(a, s)}{S(e, s)}$$

**Equation 9.25**

Where *M(D,e,a,s)* is the EAR resulting from dose *D* at age *a* exposure age *e* and sex *s*. Integrating this between the exposure age (plus the latency period, *L*) and $a_{max}$ (taken to be 100 years, as before), yields the overall lifetime attributable risk:

$$LAR(e) = \int_{e+L}^{a_{max}} M(D, e, a, s) \cdot \frac{S(a, s)}{S(e, s)} da$$

**Equation 9.26**

Again, this reduces to a simple summation:

$$LAR(e) \approx \sum_{i=e+L}^{100} EAR_i \cdot \frac{S_i}{S_e}$$

**Equation 9.27**

The key difference between this and the relative risk transport of LAR is the absence of the background rate, *m(a,s)*, in calculations, thus avoiding the problem of sensitivity of risk estimates on regional variation in background rates.

*9.2: Methodology*

Lifetime attributable risk of cancer incidence was calculated for all examinations for which organ dose estimates, based on recorded dose indicators, were available. LAR was not calculated for examinations conducted at Hospital 4 for which no dose indicators were recorded. A function was written in MATLAB that allows rapid calculation of LAR using data outputted by the Cardiodose dosimetry system. Estimates for EAR and ERR for cancers of the lungs, stomach, liver, breast, thyroid (ERR only) and all solid cancers combined, excluding thyroid and non-melanoma skin cancer, were based on the previously described models presented in the BEIR VII report [3] (Tables 9.1 and 9.2, earlier in this chapter). Fitting parameters for oesophageal cancer (not included in the BEIR VII report) were obtained from a paper by Berrington de González *et al* [315] describing 'RadRat' - a non-commercial web-based risk estimation tool developed by the US National Cancer Institute (NCI). This program allows cancer risks to be estimated from a given dose at a given age, using BEIR VII models. For both ERR and EAR methodologies, a DDREF of 1.5 was applied in all cases where organ doses were less than 200 mSv. A DDREF was not applied for leukaemia risk estimates as the reduced risk at low doses is already accounted for in the linear-quadratic model used for that site.

Figures for the survival function, *S(a)*, for England and Wales were obtained from the Office for National Statistics (ONS) [316] (Figure 9.2). These figures were available for males and females and presented for birth years of 1975, 2000 and 2010. The figures for 2000 were chosen as they represent a relatively central value of birth dates in the study cohort. These survival functions were for the general population, rather than people with congenital heart disease (CHD) who may have reduced life expectancy. The impact of an overestimation of survival is an overestimation of

radiation induced cancer risks. However, obtaining an equivalent *S(a)* function for CHD patients is challenging, as survival has only been studied up to 15-25 years of age, so far [214, 317]. The most complete source of information of survival of children born with congenital defects in the UK is that by Tennant *et al* [213], published in 2010 and based on data from the North of England. Survival to 20 years is quoted for a range of congenital heart conditions, including tetralogy of Fallot (TOF) and ventricular septal defect (VSD), as well as all CHD conditions combined (Figure 9.2) Another study was conducted by Olsen and colleagues [317] examining survival to 25 years for Danish children with CHD, again, for individual conditions along with all CHD conditions combined (Figure 9.2). These survival rates are considerably lower than the UK study at age 1 year (80%, rather than 92%), though the rate of change beyond this age is similar. The date range in the Danish study (1977 to 2005) was wider than that of the UK study (1985 to 2003)

These limited data were used to estimate lifetime survival functions for people with CHD beyond 20-25 years. Two approaches were considered. The first involved simply reducing the ONS survival function by a factor equal to the difference at the last age for which CHD survival is known. For the Tennant *et al* data [213], CHD survival is around 10% lower than background at 20 years, therefore survival beyond 20 years was extrapolated by reducing the ONS rate by 10%. The difference between background and CHD survival is not constant, however, tending to widen slightly with increasing age. The second approach involved establishing the relationship between CHD and background survival, fitting a linear model (Figure 9.1), then using this model to adjust ONS rates for survival beyond 20 years. The effect of the modified extrapolation was a reduction in estimated survival. This methodology is admittedly fairly crude, therefore risk estimates obtained using all 3 survival functions (ONS and 2 extrapolated CHD) will be presented. Furthermore, the estimated CHD survival functions are for all CHD conditions combined, when in reality survival varies between CHD subtypes [213, 317]. This should be unimportant where radiation associated cancer risks are calculated for the whole cohort, but would result in either over- or underestimation of risks for patients with specific conditions. This is especially so for patients undergoing transplants or with hypoplastic ventricles, in which survival is further reduced [211].

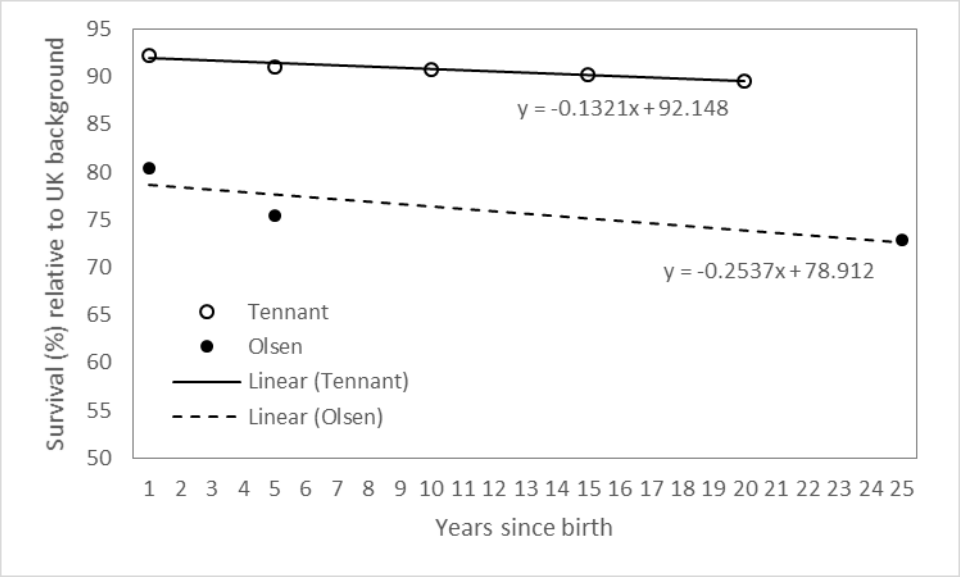


**Figure 9.1: Linear models describing relationship between survival for CHD and background UK rates (ONS)**

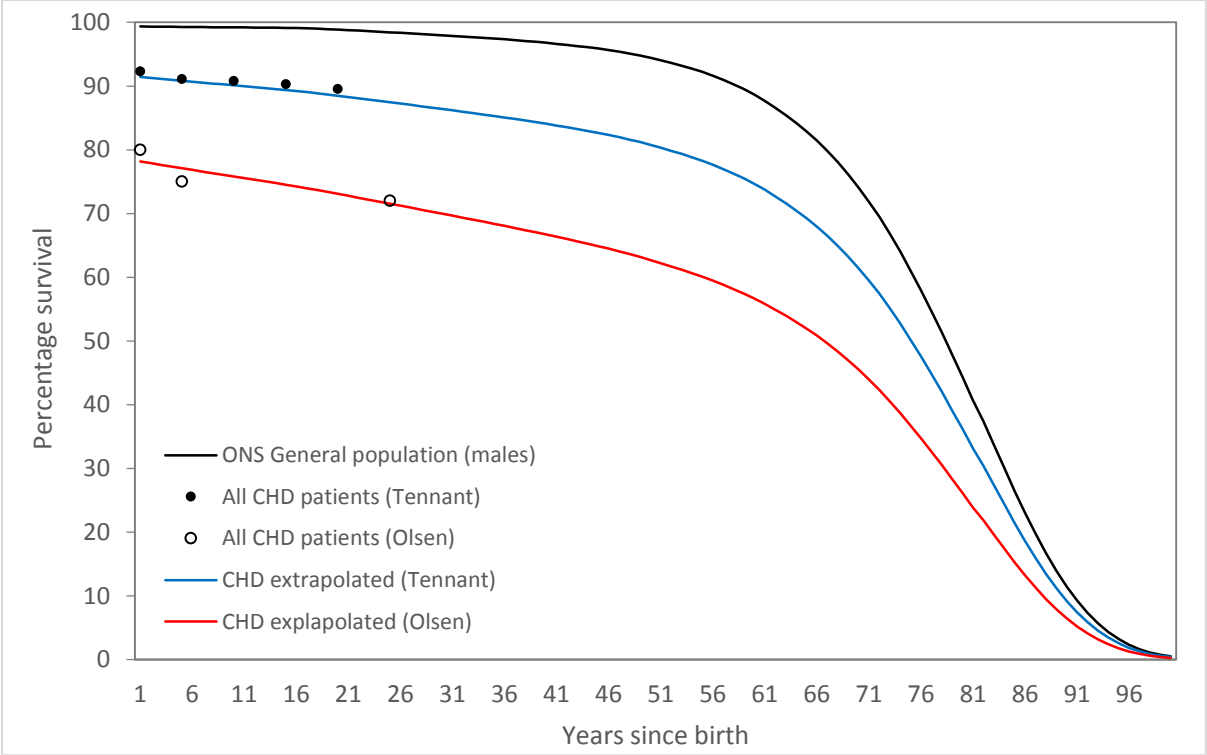


**Figure 9.2: Extrapolated survival curves for people with congenital heart disease, based on data from two studies.**

Returning to Equation 9.23 used to calculate LAR, cancer incidence rates, *m(a,s)*, for different regions of the UK population were obtained from Cancer Research UK [202]. These figures represent UK-wide rates, based on data from the Office for

National Statistics (England), Welsh Cancer Intelligence and Surveillance, Information Services Division Scotland and the Northern Ireland Cancer Registry. The dates of data provision for these registries were July 2013, May 2013, June 2013 and June 2013, respectively.

The results of the EAR and ERR transport methods were combined to produce a weighted sum, in linear space. These proportions, obtained from the BEIR VII committee report [3] and Berrington de Gonzalez *et al [315]* were 0.3 (EAR) and 0.7 (ERR) for stomach, liver, oesophagus and the 'all solid cancers' groups, while for lung cancer, these proportions were reversed. No weighting was applied for breast (EAR only) and thyroid cancer (ERR only).

*9.3: Results*

Summaries of median estimated lifetime attributable risks using EAR and ERR transport methodologies are shown in Tables 9.3 and 9.4 for male and female patients respectively. Each table presents risks calculated using three different survival functions; UK general population rates (ONS) and CHD survival rates based on the data presented by Tennant *et al* [213] and Olsen *et al* [317]. These figures represent all procedure types and all hospitals and data collection eras combined.

LAR based on relative risk transport was higher for lung and oesophageal cancer, leukaemia and the 'all solid cancers' group, while for cancers of the liver, stomach and breasts, the absolute risk transport method resulted in higher estimated LAR. Tables 9.5 and 9.6 present LAR estimates based on the weighted sum of EAR and ERR transports, for males and females, respectively. From now on, all analysis will focus on the weighted sum of these two transports, unless stated. The figures for the 'all solid cancers' group are based on the mean whole body dose and the 'all solid cancers' BEIR VII risk coefficients from Tables 9.1 and 9.2, while the 'summed solid' group is the sum of individual risks for individual sites, excluding leukaemia. The 'all solid cancers' LAR was lower than the 'summed solid' LAR for females by around 58%. For males, the central values for the 'all solid' and 'summed solid' groups were very similar, although the confidence intervals were more widely spaced for the latter. The 'summed solid' group includes thyroid cancer, while the 'all solid' model does not. The contribution from this site is minimal, however.

Estimated solid cancer risks were dominated by lung and breast cancer, with relatively small contributions from cancers of the oesophagus, stomach, liver or thyroid. Leukaemia risks were the fourth highest among individual sites, after oesophageal cancer. Estimated thyroid cancer risks were especially small, with central figures being close to zero. Omitting the exponential term from the BEIR VII models results in a reduction in lung cancer risks by a factor of around 2 for the ERR transport and almost 3 for the EAR transport. The overall effect of omitting the exponential term is a 40% and 29% reduction in the 'summed solid' cancer risk for males and females respectively.

The median LAR for all sites combined was higher for females than for males by a factor of 3.3. Excluding breast cancer from the analysis, female summed LAR remained higher than for males by a reduced factor of around 1.7. The difference between the 'all solid cancers' estimate and the 'summed solid' figure was also greater for females than males.

| | EAR transport | | | ERR transport | | |
|---|---|---|---|---|---|---|
| **Organ** | **ONS S(a)** | **Tennant S(a)** | **Olsen S(a)** | **ONS S(a)** | **Tennant S(a)** | **Olsen S(a)** |
| **Lung** | 38 [18 : 82] | 34 [16 : 75] | 30 [14 : 66] | 54 [26 : 119] | 50 [23 : 109] | 44 [21 : 96] |
| **Lung*** | 14 [7 : 31] | 13 [6 : 29] | 11 [5 : 25] | 21 [10 : 45] | 19 [9 : 42] | 17 [8 : 37] |
| **Stomach** | 8 [4 : 14] | 7 [4 : 13] | 6 [4 : 12] | 1 [1 : 2] | 1 [0 : 2] | 1 [0 : 1] |
| **Liver** | 9 [8 : 22] | 8 [7 : 20] | 7 [6 : 18] | 2 [1 : 4] | 2 [1 : 4] | 2 [1 : 3] |
| **Oesophagus** | 7 [1 : 16] | 6 [1 : 15] | 6 [1 : 13] | 13 [0 : 29] | 12 [0 : 27] | 11 [0 : 24] |
| **Breast** | n/a | n/a | n/a | n/a | n/a | n/a |
| **Thyroid** | n/a | n/a | n/a | 1 [0 : 3] | 1 [0 : 2] | 1 [0 : 2] |
| **Leukaemia** | 8 [1 : 19] | 8 [0 : 18] | 8 [0 : 17] | 4 [0 : 9] | 4 [0 : 9] | 3 [0 : 8] |
| **All** | 49 [33 : 66] | 45 [30 : 61] | 40 [27 : 54] | 74 [54 : 105] | 68 [49 : 97] | 61 [44 : 87] |

**Table 9.3: Median estimated LAR per 100,000 for all procedure types combined, for males. *figures produced using modified model omitting age adjustment. Figures in brackets represent 95% confidence intervals of risk estimates. Data are for all procedure types combined.**

| | EAR transport | | | ERR transport | | |
|---|---|---|---|---|---|---|
| **Organ** | **ONS S(a)** | **Tennant S(a)** | **Olsen S(a)** | **ONS S(a)** | **Tennant S(a)** | **Olsen S(a)** |
| **Lung** | 65 [44 : 93] | 59 [40 : 85] | 51 [35 : 74] | 163 [109 : 244] | 149 [100 : 224] | 133 [89 : 199] |
| **Lung*** | 25 [17 : 36] | 22 [15 : 32] | 20 [13 : 28] | 62 [42 : 93] | 57 [38 : 86] | 51 [34 : 76] |
| **Stomach** | 9 [6 : 13] | 8 [5 : 12] | 7 [5 : 10] | 1 [1 : 2] | 1 [1 : 1] | 1 [1 : 1] |
| **Liver** | 5 [2 : 12] | 4 [2 : 11] | 4 [1 : 9] | 1 [0 : 3] | 1 [0 : 3] | 1 [0 : 2] |
| **Oesophagus** | 1 [0 : 5] | 1 [0 : 5] | 1 [0 : 4] | 9 [0 : 33] | 8 [0 : 30] | 7 [0 : 27] |
| **Breast** | 93 [67 : 132] | 86 [61 : 121] | 77 [55 : 108] | 59 [32 : 96] | 55 [30 : 90] | 50 [28 : 82] |
| **Thyroid** | n/a | n/a | n/a | 1 [0 : 4] | 1 [0 : 4] | 1 [0 : 4] |
| **Leukaemia** | 4 [0 : 9] | 4 [0 : 9] | 4 [0 : 8] | 4 [0 : 9] | 3 [0 : 8] | 3 [0 : 8] |
| **All** | 65 [51 : 84] | 60 [47 : 77] | 53 [42 : 68] | 111 [85 : 144] | 103 [79 : 133] | 93 [72 : 120] |

Table 9.4: Median estimated LAR per 100,000 for all procedure types combined, for females. *figures produced using modified model omitting age adjustment.

| | Survival function | | |
|---|---|---|---|
| **Organ** | **ONS** | **Tennant** | **Olsen** |
| **Lung** | 43 [20 : 93] | 39 [19 : 85] | 34 [16 : 75] |
| **Lung*** | 16 [8 : 36] | 15 [7 : 32] | 13 [6 : 29] |
| **Stomach** | 3 [2 : 6] | 3 [2 : 5] | 2 [1 : 5] |
| **Liver** | 4 [3 : 9] | 4 [3 : 9] | 3 [2 : 8] |
| **Oesophagus** | 11 [0 : 25] | 10 [0 : 23] | 9 [0 : 21] |
| **Breast** | n/a | n/a | n/a |
| **Thyroid** | 1 [0 : 3] | 1 [0 : 2] | 1 [0 : 2] |
| **Leukaemia** | 5 [0 : 12] | 5 [0 : 11] | 5 [0 : 11] |
| **All** | 66 [47 : 93] | 61 [44 : 86] | 55 [39 : 77] |
| **Summed solid** | 62 [25 : 136] | 57 [24 : 124] | 49 [19 : 111] |
| **Summed solid*** | 35 [13 : 79] | 33 [12 : 71] | 28 [9 : 65] |

Table 9.5: Median estimated LAR (per 100,000) for all procedure types combined, for males, based on the weighted sum of EAR and ERR transports. *figures produced using modified model omitting age adjustment.

| | Survival function | | |
|---|---|---|---|
| **Organ** | **ONS** | **Tennant** | **Olsen** |
| **Lung** | 94 [63 : 138] | 86 [58 : 126] | 76 [51 : 111] |
| **Lung*** | 36 [24 : 53] | 33 [22 : 48] | 29 [19 : 42] |
| **Stomach** | 3 [2 : 5] | 3 [2 : 4] | 3 [2 : 4] |
| **Liver** | 2 [1 : 6] | 2 [1 : 5] | 2 [1 : 4] |
| **Oesophagus** | 7 [0 : 25] | 6 [0 : 23] | 5 [0 : 20] |
| **Breast** | 93 [67 : 132] | 86 [61 : 121] | 77 [55 : 108] |
| **Thyroid** | 1 [0 : 4] | 1 [0 : 4] | 1 [0 : 4] |
| **Leukaemia** | 4 [0 : 9] | 4 [0 : 8] | 3 [0 : 8] |
| **All** | 97 [75 : 126] | 90 [70 : 116] | 81 [63 : 105] |
| **Summed solid** | 200 [133 : 310] | 184 [122 : 283] | 164 [109 : 251] |
| **Summed solid*** | 142 [94 : 225] | 131 [86 : 205] | 117 [77 : 182] |

**Table 9.6: Median estimated LAR (per 100,000) for all procedure types combined, for females, based on the weighted sum of EAR and ERR transports. *figures produced using modified model omitting age adjustment.**

Comparison of the data in Tables 9.3 to 9.6 shows a reduction in estimated LAR where survival functions based on populations with congenital heart disease are used. The effect is relatively small, being around 8% lower where the figures based on UK CHD survival reported by Tennant *et al* [213] are used, and around 18% lower using the Danish CHD survival reported by Olsen [317].

Table 9.7 shows median LAR for procedures conducted using 3rd generation (Siemens Axiom Artis and Artis Zee) machines compared to those conducted on older 2nd and 3rd generation machines. These figures utilise ONS survival rates and standard BEIR VII risk models (i.e. retaining the age adjustment for lung cancer). Overall, there has been a fall of around 77% in estimated risk per examination between these eras. Table 9.8 shows median LAR for summed solid cancers and leukaemia, stratified by procedure type. Data are presented for 3rd generation equipment. Again, patterns are similar to those for $P_{KA}$ or organ doses. The highest risks were for pulmonary valve replacements with overall estimated cancer risks of 213 per 100,000 (1 in 469) for males, and 746 (1 in 134) for females. Corresponding figures for ASD occlusions were 16 (1 in 6250) and 47 (1 in 2127) for males and females respectively. These figures were based on ONS survival statistics. More

accurate estimations would require survival functions specific to each specific condition.

| | Sex and equipment era | | | |
|---|---|---|---|---|
| **Organ** | **Male 1st, 2nd** | **Male 3rd** | **Female 1st, 2nd** | **Female 3rd** |
| **Lung** | 101 [48 : 220] | 22 [10 : 47] | 233 [157 : 344] | 53 [36 : 78] |
| **Stomach** | 7 [4 : 13] | 2 [1 : 3] | 8 [5 : 12] | 2 [1 : 3] |
| **Liver** | 9 [7 : 21] | 2 [2 : 5] | 5 [2 : 13] | 1 [0 : 3] |
| **Oesophagus** | 25 [1 : 57] | 6 [0 : 14] | 15 [0 : 58] | 4 [0 : 15] |
| **Breast** | n/a | n/a | 229 [164 : 324] | 51 [36 : 72] |
| **Thyroid** | 2 [0 : 6] | 0 [0 : 1] | 3 [1 : 11] | 1 [0 : 3] |
| **Leukaemia** | 12 [1 : 28] | 3 [0 : 6] | 9 [1 : 21] | 2 [0 : 5] |
| **All solid** | 156 [112 : 220] | 34 [25 : 49] | 237 [184 : 307] | 55 [43 : 71] |
| **Summed solid** | 144 [60 : 317] | 32 [13 : 70] | 493 [329 : 762] | 112 [73 : 174] |

**Table 9.7: Median LAR (weighted sum of EAR and ERR transports) for two generations of equipment: 3rd (Siemens Axiom Artis/Artis Zee) and 1st and 2nd (Siemens HIcor/BIcor, Philips Integris and Toshiba Infinix). Figures in brackets represent 95% confidence intervals.**

| | Males | | Females | |
|---|---|---|---|---|
| **Procedure:** | **Leukaemia** | **Summed solid** | **Leukaemia** | **Summed solid** |
| **ASD Occlusion** | 1 [0 : 3] | 15 [6 : 33] | 1 [0 : 3] | 48 [33 : 78] |
| **PDA occlusion** | 2 [0 : 5] | 35 [13 : 74] | 2 [0 : 4] | 144 [98 : 224] |
| **Pulm valvuloplasty** | 4 [0 : 10] | 54 [21 : 118] | 3 [0 : 6] | 151 [101 : 233] |
| **Aortic valvuloplasty** | 4 [0 : 8] | 42 [16 : 89] | 3 [0 : 7] | 177 [118 : 274] |
| **PA angioplasty** | 5 [0 : 11] | 71 [29 : 157] | 3 [0 : 7] | 258 [173 : 396] |
| **COA angioplasty** | 5 [0 : 11] | 53 [21 : 117] | 3 [0 : 8] | 199 [134 : 306] |
| **EPS/RFA** | 2 [0 : 5] | 21 [8 : 45] | 2 [0 : 4] | 49 [30 : 76] |
| **EMBx** | 1 [0 : 1] | 5 [2 : 13] | 0 [0 : 1] | 16 [10 : 25] |
| **Coronaries** | 3 [0 : 6] | 24 [10 : 52] | 3 [0 : 6] | 63 [39 : 103] |
| **PVR/pressures** | 1 [0 : 3] | 15 [6 : 33] | 1 [0 : 2] | 41 [28 : 65] |
| **Valve replacement** | 17 [1 : 39] | 196 [83 : 431] | 10 [1 : 24] | 736 [501 : 1114] |
| **Pacemaker** | 0 [0 : 1] | 1 [1 : 4] | 0 [0 : 1] | 7 [4 : 13] |
| **Atrial septostomy** | 1 [0 : 3] | 13 [5 : 27] | 1 [0 : 3] | 72 [46 : 112] |

**Table 9.8: Median LAR (weighted sum of EAR and ERR transports) for 3rd generation equipment (Siemens Axiom Artis/Artis Zee), stratified by procedure type. Figures in brackets represent 95% confidence intervals.**

As with $P_{KA}$ and organ doses, LAR displayed a right skewed distribution, with the majority of procedures associated with a risk of below 200 per 100,000 (i.e. 1 in 500).

Figure 9.3 shows this distribution for the whole cohort and for all procedure types. Fourteen examinations resulted in an estimated LAR of 10,000 or more (i.e. 1 in 10), all of which involved female patients. The mean heart dose in these 14 cases was 746 mGy, while the mean age at exposure was 2.9 years.

Where cumulative LAR was calculated, the median across the whole cohort was 229 per 100,000 (IQR: 82, 592), or about 1 in 436 (1220, 169) for cancers of the lung, stomach, liver, oesophagus, thyroid, breast and leukaemia combined. There was a suggestion of a positive correlation between median combined LAR, and the number of procedures conducted (Spearman's r=0.61, p=0.06). Despite this, of the patients with the five highest cumulative combined LAR estimates (all female), three underwent a single catheterization, typically at an early age. The maximum cumulative LAR was 33,727 per 100,000, or about 1 in 3.

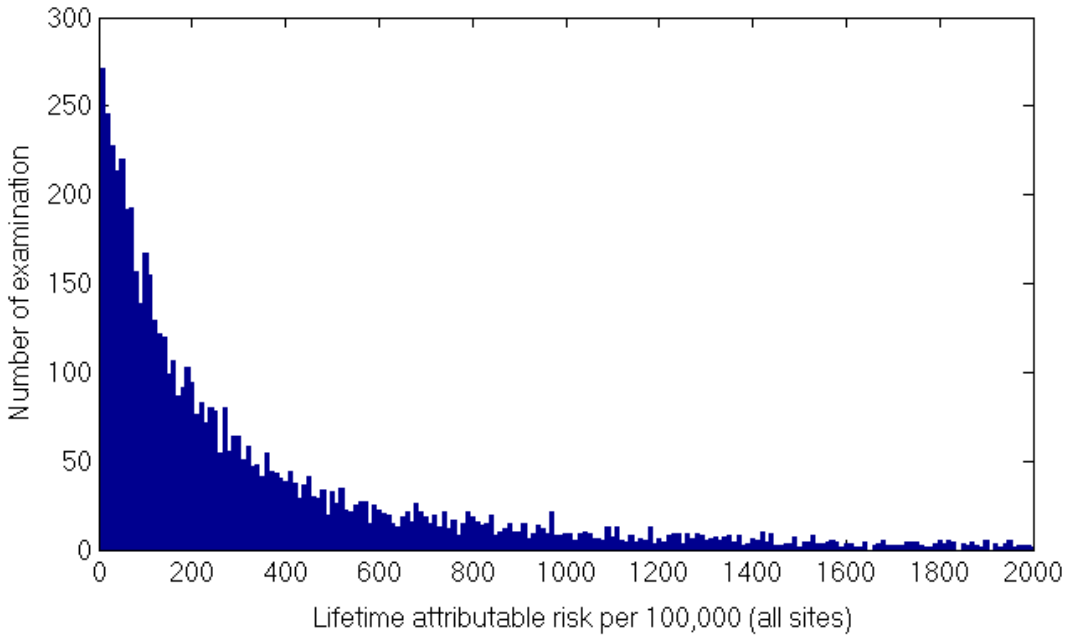


**Figure 9.3: Distribution of estimated lifetime attributable risk of cancer incidence across the whole cohort, for all procedure types.**

*9.4: Discussion*

Many of the patterns in the risk modelling results mirror those for organ doses. This was expected due to the linear relationship assumed between dose and risk. The finding that the highest estimated risks were for the breasts and lungs was expected given that both organs receive relatively high doses and that both appear to be sensitive to radiation induced cancer [45, 139, 291]. Although the thyroid gland is

also considered radiosensitive [45, 294], the low doses received by this organ result in very low estimated risk of thyroid cancer. Risks were not estimated for lymphoma as no EAR or ERR models are available. Nor were risks estimated for cancers of organs for which no doses were calculated, including the colon, bladder, brain or salivary glands. These organs, although apparently susceptible to radiation induced cancer [9, 45, 53], were sufficiently far from the irradiated field that doses and associated risks were assumed to be negligible.

The higher LAR for female patients reflects both the higher risk per unit dose for stomach, lung and thyroid cancer, and the inclusion of breast cancer in the total LAR for females. There is some association between radiation and male breast cancer, but this is limited [318]. Difference in dose between males and females does not appear to be a factor in the discrepancy in LAR. Mean effective doses were approximately the same for male and female cohort members, while median effective dose was 15% higher for males. Previous studies led by Johnson [89], Ait Ali [13] and Beels [12] reported female/male LAR ratios of around 2, 2.4 and 2.7 respectively (these papers are discussed in greater depth below). The larger male/female difference in the current study is most likely due to the use of organ doses to calculate LAR, rather than effective dose. The potentially high risk of breast cancer highlights the importance of radiation protection techniques to reduce breast dose, such as close collimation and use of lung shuttering where appropriate [104]. Avoidance of laterally orientated beam projections may also reduce breast dose, although choice of projections is largely dictated by procedure type.

Across the whole cohort, the combined estimated LAR from cardiac catheterizations for leukaemia and lung, breast, stomach, liver, oesophageal and thyroid cancer was approximately 1 in 1500 and 1 in 500 for males and females respectively, using UK ONS survival rates and retaining the age modifier in BEIR VII models. For recent examinations conducted using modern equipment, equivalent figures are 1 in 2900 and 1 in 900 for males and females respectively. Where accounting for reduced survival of people with congenital heart disease, these risks were reduced by between 10 and 25%. These latter risks were estimated using alternative survival functions. An alternative methodology involves adjusting the upper limit of integration ($a_{max}$) in equations 9.6 and 9.9, allowing the risk of cancer to be estimated up to a particular number of years following exposure. This may be more suitable for

conditions in which survival is especially reduced, such as hypoplastic ventricles [215] or transplantation [211]. LAR as a function of $a_{max}$ has a sigmoid form (Figure 9.4), rising steeply between 40 and 70 years before levelling off. Thus reducing $a_{max}$ to 80 years results in a small decrease in LAR of around 10%. Reducing $a_{max}$ to 50 years, leads to a decrease in LAR by 63%. Patients with a hypoplastic left heart (where the left ventricle fails to develop properly) are not expected to survive beyond their teens [215]. Setting $a_{max}$ to 20 years results in a decrease in LAR of around 95% relative to risks estimated using an $a_{max}$ of 100 years. Figures 9.5 and 9.6 show estimated LAR for coronary angiography examinations, based on median dose for 3rd generation equipment, as $a_{max}$ is adjusted from 5 to 75 years from the age at exposure. Note that the risks at 5 years post exposure are entirely due to leukaemia (which has a 2 year latency period).

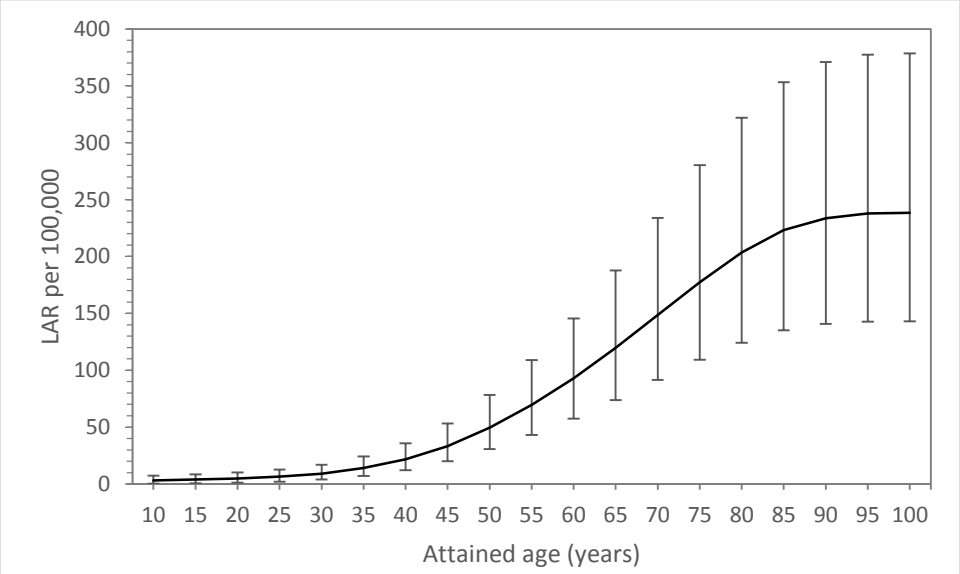


**Figure 9.4: Lifetime attributable risk of cancer from cardiac catheterizations conducted on children who underwent Norwood procedures, as a function of attained age. Error bars represent 95% confidence intervals of risk.**

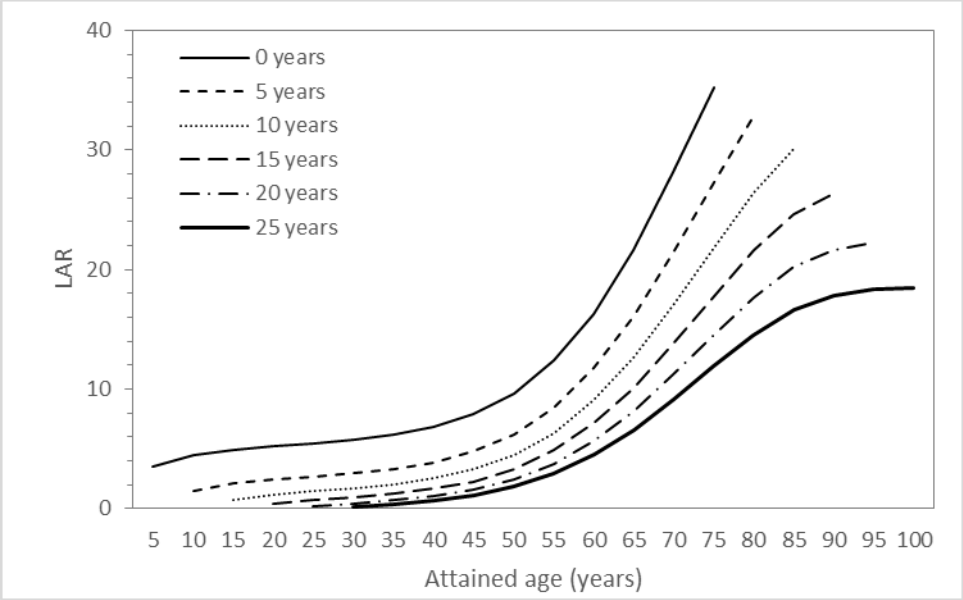


**Figure 9.5: LAR as a function of $a_{MAX}$ (upper limit of integration in Equations 9.23 and 9.26) for coronary angiography examinations at six ages at exposure. Data are for male patients.**

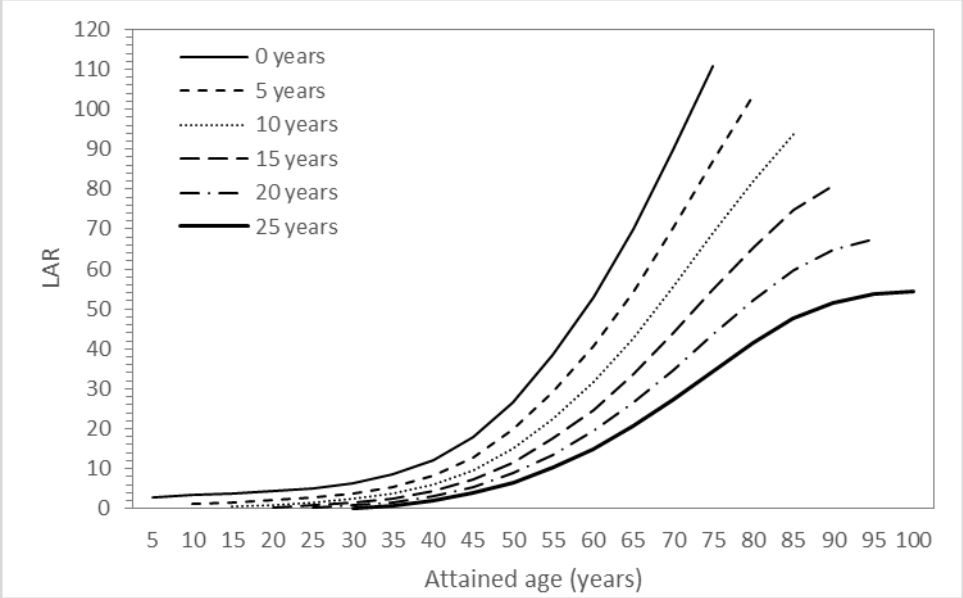


**Figure 9.6 LAR as a function of $a_{MAX}$ for coronary angiography examinations at six ages at exposure. Data are for female patients.**

As with other medical radiation exposures, these risks must be placed in the context of the potential benefits of the diagnostic information provided and the therapeutic benefits of trans-catheter interventions. Radiation protection involves both justification and optimisation [60, 104]. The former is related to decision of whether or not to go ahead with the exposure or nor, based on net benefit to the patient. If the

procedure is considered justified, the process of optimisation seeks to reduce doses to as low as reasonable practicable (ALARP) [16, 104]. The issue of the compromise between radiation dose and image quality has been discussed previously and will be discussed again, later.

### *9.4.1: Uncertainties in risk estimates*

There are a number of sources of uncertainty in risk estimates derived from the modelling approach. The uncertainty in the value of ERR and EAR risk coefficients is reflected in 95% confidence intervals incorporated into these estimates. A linear relationship between radiation dose and excess risk is assumed, with no threshold dose below which there is no risk. This approach remains controversial [58, 59, 311]. There is currently insufficient evidence to confirm or refute alternative proposals. The risks estimated using data derived from nuclear bombing survivors' data tend to be higher than those obtained from studies of children treated with radiotherapy [172] though lower than that suggested by recent studies of children undergoing computed tomography scans [9, 124].

The usage and associated value of the 'dose and dose rate effectiveness factor' (DDREF) is also controversial [59]. Models presented in ICRP 103 [44] utilise a DDREF of 2.0, while those developed by the UNSCEAR 2006 committee [45] use a linear quadratic model, in which a DDREF is implicit (i.e. the models effectively have a DDREF of 1.0). In this study, a factor of 1.5 was applied. Changing this to 2.0 results in a reduction in LAR by 25%. The use of a single DDREF for all cancer sites is a generalisation without adequate evidential support. In particular, in some studies, the risk of breast cancer does not appear to be reduced for fractionated exposures, compared to single acute exposures [158, 314]. Brenner [137] argues that the *apparent* lack of effect of fractionation in studies of patients receiving fluoroscopically guided pneumothorax therapy for tuberculosis is due to the increased radiobiological effectiveness (RBE) of low energy x-ray photos [138, 319]. The energy of fluoroscopic x-rays used in cardiac catheterizations is strongly dependent on filtration. The almost complete removal of photons below around 30 keV with around 0.2 mm of copper and 2.5 mm of aluminium filtration would result in a lower RBE than apparent from studies of fluoroscopic exposures used for TB pneumothorax therapy [154]. It is possible, therefore, that risks for breast cancer have been

underestimated in cases where filtration was lower. Furthermore, recent studies of cancer mortality in nuclear workers [139, 145, 146] and other occupationally exposed groups do not suggest a reduction in risk for protracted exposures, implying a DDREF or 1.0 or less [320].

The decision to use BEIR VII risk models, as opposed to others developed by the ICRP [44] or UNSCEAR [45] was arbitrary. There is currently little to suggest that any one model provides more accurate estimates of the risks at low doses. The differences in LAR estimates obtained using EAR and ERR transports are consistent with those previously reported [49, 321]. The decision to apply either multiplicative or additive transports or the weightings in the combined approach is also arbitrary and lacks common consensus [321]. The ICRP 103 risk models use equal ERR/EAR weightings for liver and stomach cancer and a purely additive model for leukaemia [44], while the current study, the BEIR VII committee [3] and the online risk calculation tool RadRat [322] all utilise 70/30 weightings for all three sites. Wakeford and Little [321] note that when using BEIR VII risk models, the difference in leukaemia risk estimates between EAR and ERR transports are small, but very large when using the alternative risk models reported in the 2006 UNSCEAR report [45]. Fortunately, the contribution of cancers in which EAR and ERR transports differ substantially to overall cancer risks from cardiac catheterizations (stomach and liver in particular) is relatively small.

The BEIR VII risk models assume a monotonically decreasing risk of radiation induced cancer with increasing age at exposure, up to 30 years. As previously mentioned, evidence in support of such an assumption is mixed [129, 196, 197], most notably for organs exposed during cardiac catheterizations, such as the lungs and oesophagus. This is unfortunate given the impact that the exponential age modification term from Equation 9.18 has on estimated risks, as demonstrated by the large reduction in LAR for lung cancer following its omission. The lack of evidence supporting the higher risks among children for lung cancer suggests that these modified figures may be more realistic. For the ICRP 103 risk models, lung cancer risk increases with age at exposure by 17% per decade for the ERR approach and 1% for the EAR approach [44].

Risk estimates based on relative risk transport are also affected by regional variation in background rates. The estimates presented in this study are based on UK-wide

rates and may differ from those obtained using rates specific to the region of residence of individual patients. Regional rates are published by the International Agency for Research on Cancer (IARC) [203]. There is relatively little geographical variation in breast cancer incidence throughout the UK (Figure 9.7), though large differences are apparent for lung cancer (Figure 9.8). It should be noted, however, that the hospital at which procedures are carried out does not necessarily represent the location of residence of the patient. There are no hospitals carrying out paediatric cardiac catheterizations in Wales, for example, meaning Welsh patients must travel to English hospitals such as Alder Hey for these procedures. A similar issue could arise due to differences in ethnicity, which can affect background risk of cancer [323-325]. The impact of variation in the survival function is somewhat smaller, with risks being around 25% lower based on the more pessimistic figures quoted by Olsen and colleagues [317].

Finally, risk estimation must also take into account the uncertainty in dose estimates described in Chapter 8. The largest potential uncertainties are for breast dose, due to the difficulty in predicting the inclusion of breast tissue within the primary beam. As discussed in Chapters 4 and 8, this study has assumed a large increase in breast dose for laterally orientated projections. Thus the breast cancer risks estimated in this chapter may be overly pessimistic.

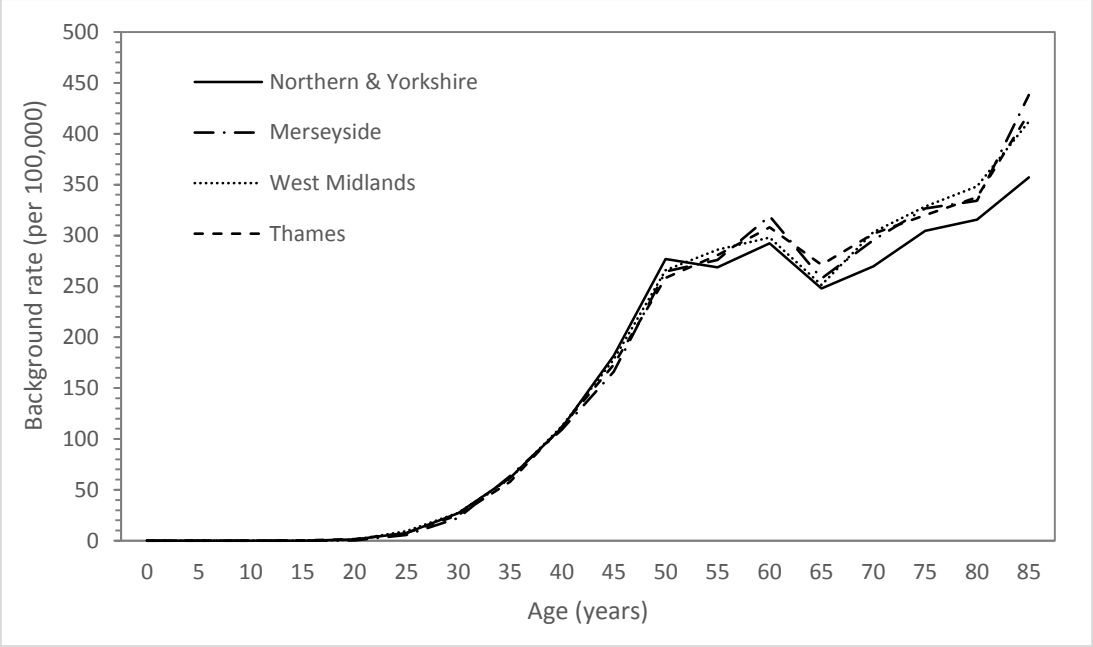


**Figure 9.7: Female breast cancer incidence from four different UK regions. Data obtained from IARC [200]**

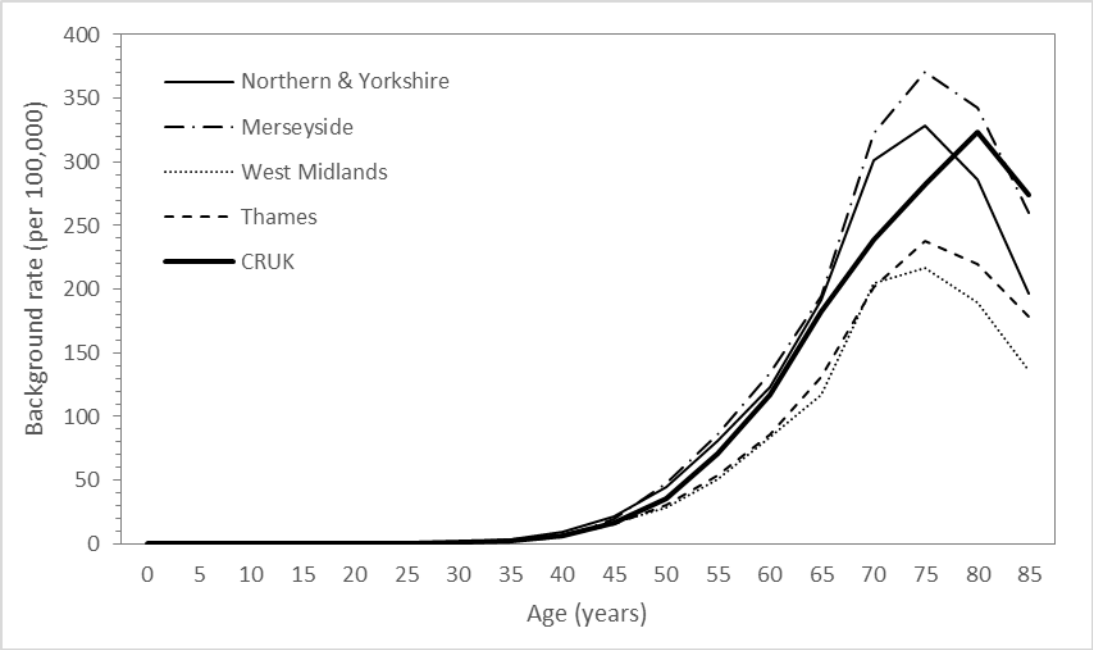


**Figure 9.8: Lung cancer incidence for four different UK regions. Data obtained from IARC [203] and Cancer Research UK [202].**

### *9.4.2: Implications for epidemiological analysis*

The risk estimates for leukaemia and thyroid cancer; the malignancies best suited to an epidemiological analysis of radiation associated risks from childhood exposures

with a relatively short follow-up time, are small. Based on an average UK background incidence rate in the 0-29 year age group of 33 per million people, per year, for leukaemia and 12 for thyroid cancer [202], the expected number of background cases of these two malignancies over a 10 year study period, for a sample of 13,000 subjects, is around 6. The expected number of radiation induced cancers in the same cohort, over the same time period, in the study cohort, was calculated by adjusting the upper limits of integration ($a_{max}$) in Equation 9.23 from 100 to the number of years of follow up. This resulted in a mean 'study period attributable risk' of 7.2 and 1.8 per 100,000 for leukaemia and thyroid cancer respectively (95% CI: 0.6, 17.1 and 0.5, 6.6). Thus, the expected number of radiation induced leukaemia and thyroid cancer cases combined during the study period is 1.17 (95% CI: 0.1, 3.1). Restricting analysis to recently conducted examinations in which doses are relatively low, the number of expected radiation-induced leukaemia and thyroid cancer cases is 0.3 (95% CI: 0.1, 0.8).

A significant increase in leukaemia or thyroid cancer incidence in the study cohort was not expected, based on excess risks predicted by the modelling approach. For other cancer sites, including lung, oesophagus and breast, a longer follow up time is required to enable cohort members to reach the ages at which such diseases become relatively common.

### *9.4.3: Comparison with previous research*

A number of previous studies have estimated lifetime attributable risk of cancer from cardiac catheterizations in children. Ait Ali *et al* [13] estimated LAR for 59 patients undergoing 1548 x-ray procedures, including catheterizations, CT and chest radiographs. For male patients receiving a median cumulative effective dose of 7.1 mSv, the estimated median LAR of cancer incidence was 1 in 804, while for female patients receiving a median effective dose of 9.4 mSv, the median LAR was 1 in 331. The quoted cumulative effective doses do not appear to correspond to the sum of doses for each procedure type. The methodology states that effective doses for catheterizations were estimated using the $E/P_{KA}$ conversion factor of 1.2 mSv/Gy·cm$^2$, which based on the quoted median $P_{KA}$ of 20 Gy·cm$^2$, ought to result in effective doses for catheterizations alone of around 24 mSv. Moreover, the methodology for LAR estimation is unclear, appearing to involve using BEIR VII risk

models to estimate risks from effective dose, rather than individual organ doses. Such a methodology is regarded as improper [326], for the reasons outlined earlier in the chapter, though deserves further analysis. The LAR estimates obtained using the 'All solid cancers' risk coefficients in Tables 9.1 and 9.2, and the mean whole body dose, were 58% lower for females than corresponding estimates obtained by summing LAR for individual sites obtained using respective organ doses, but almost identical for males. Based on the earlier finding that effective dose is, on average, higher than mean whole body dose by a factor of 1.7 (see Chapter 8, section 8.2), using effective dose rather than mean whole body dose with the 'All solid cancers' risk coefficients results in a higher LAR than that obtained by summing risks for individual sites by a factor of 1.7 for males, but brings these figures closer for females (28% lower rather than 58%). Thus, for analyses with both sexes combined, the use of effective dose in BEIR VII risk models results in a crudely similar risk estimate to that obtained using the 'proper' methodology.

Johnson *et al* [89] estimated LAR for 337 children aged under 6 years, undergoing 13,932 procedures, giving a median cumulative effective dose of 2.7 mSv (range 0.1-76.9 mSv). The majority (72%) of exposures were chest radiographs, delivering effective doses of less than 0.03 mSv each. As with the study by Ait Ali *et al* [13], the authors chose to apply effective dose to BEIR VII risk models rather than use individual organ doses. For patients undergoing transplant and Norwood procedures, a separate 'short term' risk estimation was conducted to account for shorter life expectancy. This used an ERR of 0.035 $mSv^{-1}$ derived from the epidemiological analysis of CT-associated risks performed by Mathews *et al* [124], background cancer rates for US adolescents (15-19 years) and assumed exposure at 5 years. The rationale for using this separate ERR, as opposed to using a different survival function, or value of $a_{max}$ is not made clear. The decision to use the ERR from the Mathews study is also questionable. As noted in the literature review, this analysis has drawn criticism, in particular related to the issue of confounding by indication [129, 177, 178]. Using an upwardly biased ERR for patients with shortened life expectancy would achieve the opposite effect to that desired. In reality, shorter life expectancy would mean less time to develop radiation induced cancers and hence lower risk, not higher. Whatever the thinking, the median estimated LAR for the whole cohort was 65 cases per 100,000, or 1 in 1538. For the Norwood and Transplant groups, these figures were 799 and 1677 respectively (1 in 125 and 1 in

60), based on median cumulative effective doses of 63.8 and 28.9 mSv respectively. The LAR estimates for the latter group are high, but then so are the dose estimates for cardiac catheterizations (effective dose of 13.8 and 9.1 mSv for interventional and diagnostic procedures respectively), based on physical measurements in anthropomorphic phantoms.

Beels *et al* [12] estimated LAR for 49 patients aged from 0 to 11.8 years. Unlike Ait Ali *et al* [13] and Johnson *et al* [89], Beels used organ doses, calculated from Monte Carlo simulations (MCNP-X 2.5.0) rather than effective dose. The authors report median estimated LAR figures of 0.076% and 0.205% for males and females respectively (1 in 1316 and 1 in 488). The organ doses used for these estimates were not stated. The median effective dose, based on ICRP 103 weighting factors, was 6.4 mSv, ranging from 0.5 to 53.4 mSv.

Yakoumakis *et al* [107] used the risk of exposure-induced death (REID) estimation tool built in to PCXMC v2.0. This utilises BEIR VII risk models and organ doses transferred from Monte Carlo simulations in the same program. The model uses three sets of background cancer rates; Euro-American, Asian and Finnish, although it is not clear which were used in this case. Aside from calculating REID as opposed to LAR, the upper limits of integration (i.e. $a_{max}$) are set at 120, rather than 100. Yakoumakis's team estimated risks for 53 cardiac catheterizations carried out on patients aged 3 months to 11 years. The median REID estimates for ASD, VSD and PDA occlusions were 0.110%, 0.126% and 0.067% respectively (i.e.1 in 909, 794 and 1493). These risk estimates are quite low, considering the exceptionally high calculated doses (effective dose = 40, 22 and 17 mSv for ASD, VSD and PDA occlusions respectively). The discrepancy in the relative magnitudes of dose and REID between procedure types is striking, but not commented on by the authors.

A number of older studies utilising simpler risk estimation methodologies are also worthy of mention. Bacher and colleagues [8] estimated a median risk of cancer mortality for 60 cardiac catheterizations conducted on patients aged under 10 years of 0.08% (1 in 1250). These figures were derived by multiplying the effective dose, calculated using MCNP4b2 Monte Carlo code, by risk factors quoted in ICRP 60 [67] of 13%/Sv for boys and 16%/Sv for girls. These estimates are similar to those of Yakoumakis *et al* [107] despite the effective doses being 5-10 times lower (these were 4.6 and 6.0 mSv for 'low dose' and 'standard' techniques respectively). The

results of Bacher *et al* should be interpreted with caution, given the simplicity of the risk estimation methodology, which assumes all exposure to have occurred at 10 years. A similar analysis appears to have been performed by Martinez *et al* [94], who arrive at a figure – which is presumably the LAR, though not explicitly stated as such - of 0.07% (1 in 1429) for fatal cancer, based on an estimated effective dose of 5 mSv for 137 patients aged up to 16 years. It is unclear how this estimate of effective dose was derived. The use of cancer mortality in the above studies, rather than incidence, is a further limitation. Although survival of lung and oesophageal cancer remains poor [327], the survival of leukaemia and breast cancer is now sufficiently high [328-330], that risk estimates based on mortality may underestimate the burden associated with radiation exposures.

A final comparison was made between LAR estimates calculated by the current author, those of the BEIR VII committee presented in Tables 12D-1 and 12D-2 of the BEIR VII report [3] and those produced by the RadRat online risk estimation tool developed by the National Cancer Institute (NCI) [315, 322]. The results of this comparison are presented in Table 9.9. The goal was primarily to identify potential errors in the LAR estimation process. All three sources utilise the same BEIR VII models previously described. The BEIR VII example tables and RadRat are based on US background rates and survival curves, rather than UK rates in this study. LAR estimates calculated by the current author are close to those of the BEIR VII report, while those calculated by RadRat are much higher than both.

| | | Male | | | | | Female | | | | | |
|---|---|---|---|---|---|---|---|---|---|---|---|---|
| Age | Study | Lung | Stomach | Liver | Leukaemia | Thyroid | Lung | Stomach | Liver | Leukaemia | Thyroid | Breast |
| 0 y | This | 322 | 182 | 105 | 401 | 192 | 787 | 221 | 61 | 335 | 346 | 1224 |
| | BEIR VII | 314 | 76 | 61 | 237 | 115 | 733 | 101 | 28 | 185 | 634 | 1171 |
| | RadRat | 523 | 272 | 175 | 377 | 297 | 1220 | 328 | 98 | 332 | 1650 | 1810 |
| 5 y | This | 267 | 150 | 86 | 245 | 128 | 657 | 182 | 50 | 202 | 251 | 953 |
| | BEIR VII | 261 | 65 | 50 | 149 | 76 | 608 | 85 | 23 | 112 | 419 | 914 |
| | RadRat | 438 | 225 | 146 | 181 | 198 | 1020 | 271 | 81 | 149 | 1100 | 1420 |
| 10 y | This | 222 | 123 | 71 | 179 | 83 | 549 | 150 | 41 | 151 | 165 | 742 |
| | BEIR VII | 216 | 55 | 43 | 120 | 50 | 504 | 72 | 20 | 86 | 275 | 712 |
| | RadRat | 364 | 184 | 120 | 138 | 130 | 856 | 222 | 45 | 106 | 723 | 1110 |
| 15 y | This | 184 | 101 | 59 | 145 | 54 | 459 | 123 | 34 | 127 | 107 | 578 |
| | BEIR VII | 180 | 46 | 36 | 105 | 33 | 417 | 61 | 16 | 76 | 178 | 553 |
| | RadRat | 302 | 151 | 100 | 116 | 86 | 716 | 182 | 55 | 90 | 470 | 859 |
| 20 y | This | 154 | 83 | 49 | 125 | 34 | 384 | 101 | 28 | 113 | 68 | 448 |
| | BEIR VII | 149 | 40 | 30 | 96 | 21 | 346 | 52 | 14 | 71 | 113 | 429 |
| | RadRat | 252 | 123 | 82 | 104 | 56 | 600 | 149 | 45 | 82 | 299 | 664 |
| 30 y | This | 107 | 56 | 34 | 97 | 13 | 270 | 67 | 19 | 93 | 25 | 265 |
| | BEIR VII | 105 | 28 | 22 | 84 | 9 | 242 | 36 | 10 | 63 | 41 | 253 |
| | RadRat | 176 | 81 | 56 | 92 | 23 | 421 | 98 | 31 | 72 | 112 | 387 |

**Table 9.9: Comparison of three lifetime attributable risk estimates, calculated for an acute exposure of 100 mSv.**

## *9.5: Conclusions*

Risk modelling suggests a median lifetime attributable risk of radiation induced cancer from cardiac catheterizations across the whole cohort of around 1 in 1500 and 1 in 500 for males and females respectively. For more recently conducted procedures with lower doses, these risks fall to around 1 in 2900 and 1 in 900 respectively. These relatively low excess cancer risks ought not to be detectable by epidemiological analysis unless the sample size is especially large, or follow-up time sufficiently long to include breast and lung cancers. The following chapter will discuss the results of matching cohort members to cancer registry data to provide direct epidemiological assessment of cancer risks following cardiac catheterizations.

# Chapter 10: Epidemiology

Excess cancer risks estimated using existing risk models are subject to large uncertainties in the shape of the relationship between radiation dose and cancer. An epidemiological analysis, using empirical data, has the benefit of allowing direct assessment of cancer risks, though has the disadvantages of sensitivity to sample size and confounding factors. The following chapter describes an epidemiological analysis of around 13,000 cohort members. This should be seen as a pilot study, with the aim of evaluating the possibility of a larger scale study involving patients from more UK hospitals and, potentially, a pooled analysis with European studies [331]. Two analyses were carried out; (1) an overall assessment of cancer incidence in the study cohort, and (2) an assessment of the potential impact of radiation doses on these cancer risks. The latter analysis focused only on cancers developing more than 5 years following the first recorded catheterization (2 years for leukaemia).

## *10.1: Methods*

Details of cancer diagnosis and deaths were obtained by linking the cohort with the National Health Service Central Register (NHSCR). This holds records of everyone in Great Britain registered with a general practitioner, and is continuously updated with details of cancer incidence from regional registries, along with births, deaths, marriages and names changes [9]. Some of the 13,564 patients in the cohort could not be matched. Patients at Hospital 6 (n=337) had no Christian name, while 48 patients at other hospitals had no date of birth and 125 were over 22 years at the time of the first procedure (these latter patients were not included in organ dose estimations). A further 222 patients had procedures not considered to be true cardiac catheterizations, including pericardiocentesis and PICC/Hickman insertions. Finally 78 patients were excluded because it was unclear what equipment was used, making dose estimation too unreliable. This left 12,754 patients, contributing 191,865 person years on the 1st of February 2014. The mean patient age on this date was 15.1 years (median = 14.7). 7,562 patients were born within the data collection period at the hospital at which they were first examined. These patients contributed 78,835 person years and had a mean follow-up of 10.4 years (median = 9.3). Details of the cohort are shown in Table 10.1.

| Characteristic | Whole cohort | Transplant | Cases |
|---|---|---|---|
| **Male** | 6335 (50%) | 374 (51%) | 63 (49%) |
| **Female** | 5685 (45%) | 335 (46%) | 62 (48%) |
| **Unknown** | 733 (6%) | 21 (3%) | 4 (3%) |
| **Total** | 12753 | 730 | 129 |
| **Born within study period** | 5295 | 306 | 35 |
| **Mean age 01/02/2014** | 15.1 years | 13.4 years | 23.3 |
| **Born <1980** | 248 (2%) | 59 (8%) | 13 (10%) |
| **Born 1980-1989** | 1557 (12%) | 203 (28%) | 53 (41%) |
| **Born 1990-2009** | 4831 (38%) | 307 (42%) | 42 (33%) |
| **Born 2000-2009** | 4985 (39%) | 144 (20%) | 21 (16%) |
| **Born >2010** | 1132 (9%) | 17 (2%) | 0 (0%) |
| **Mean age at first procedure** | 6 years | 5.1 years | 11.3 |
| **1 procedure** | 9663 (76%) | 229 (30%) | 65 (50%) |
| **2 procedures** | 1747 (14%) | 121 (16%) | 18 (14%) |
| **3 procedures** | 621 (5%) | 77 (10%) | 8 (6%) |
| **4 procedures** | 261 (2%) | 56 (7%) | 7 (5%) |
| **5 procedures** | 154 (1%) | 61 (8%) | 6 (5%) |
| **>5 procedures** | 326 (3%) | 220 (29%) | 26 (20%) |

Table 10.1: Details of the cohort

The standardised incidence ratio (SIR) was calculated as the ratio of observed to expected cases. The expected number of cases was calculated as follows: the sex adjusted average risk of cancer, per 100,000, was obtained for each year, from birth up to the age of the patient on the 1st of February 2014. The mean of these yearly risks was calculated, and this figure multiplied by the patient's age on the 1st of February 2014. If the patient died prior to this date, risks were calculated up to the age at which the patient died. The sum of risks for cohort members was then divided by 100,000 to obtain the expected number of cancer cases. Expected cancer incidence rates were obtained from Cancer Research UK [202]. As explained in Chapter 9, these figures represent UK-wide rates, combining 2013 data from the English, Scottish, Welsh and Northern Irish cancer registries. Confidence intervals for SIR were calculated using the method described by Vandenbroucke [332], defined as $\left(\sqrt{observed} - 1\right)^2$ for the lower limit of observed cases, and $\left(\sqrt{observed + 1} + 1\right)^2$ for the upper limit.

Information on potentially confounding conditions was determined from clinical details, where recorded (Hospitals 1 and 2 only), cause of death if the patient had died, and examination type. Conditions searched for were Down syndrome (trisomy 21), axaxia telangiectasia, Li Fraumeni syndrome, organ transplantation and neurofibromatosis. Patients were considered to have a history consistent with heart transplant if they had undergone coronary angiography and/or endomyocardial heart biopsies, unless stated as having Kawasaki's disease (the other common indication for this procedure in young people).

Survival was calculated for cohort members using the Kaplan Meier method, defined for *n* individuals and *d* deaths in each time interval *i* as:

$$\hat{S}(t) = \prod_{t_i<t} \frac{n_{ti} - d_{ti}}{n_{ti}}$$

Analysis was censored at 40 years of age as data beyond this age was too sparse (39 cohort members (0.3%) had reached this age).

The number of person-years contributed by the cohort to a range of cumulative cardiac dose categories (<5, 5-20, 20-40, 40-80, 80-100, 100-120, 120-140, 140-160, 160-180 and 180-200 mSv) was calculated. Person years were contributed after 5 years following each exposure, to take into account the latency period of radiation induced cancers. A dose response analysis was conducted by dividing the number of cases occurring in each cumulative dose category by the respective number of person years. Relative risk was calculated with respect to the lowest dose category (<5 mSv). Excess relative risks (ERR) was calculated as the relative risk, minus one.

### *10.2: Results*

A total of 141 tumours were identified among eligible patients. The mean age at first procedure among these patients was 11.3 years, compared to 6.0 years for the cohort overall. Nine cohort members were diagnosed with 2 tumours. In 7 of these, the second event was of similar histology to the first, suggesting that the second was simply a reclassification or a transition rather than a second primary malignancy. Excluding these left 133 cases, of which 24 were classified as benign, 'borderline

malignancy' or non-melanoma skin cancers. These were not included in SIR calculations. However, three benign or borderline malignant brain tumours were classed as malignant tumours and included in SIR calculations. Of the 109 malignant events, 12 were classified as '*in situ* carcinoma'. The majority of tumours were of the haematopoietic and lymphoid tissues, including leukaemia and lymphoma (Table 10.2). Among haematological tumours, including borderline malignancies, there were 4 cases of myelodysplastic syndrome (D46, 3 borderline, 1 malignant), 3 Polycythaemia Vera (D45, borderline) and 1 acute panmyelosis with myelofibrosis (C94.4, malignant). The remainder (n=30) were malignant leukaemias, 14 of which were acute myeloid leukaemia (AML), while 9 were acute lymphoblastic leukaemia (ALL). Of the 43 lymphatic tumours, 10 were lymphoproliferative diseases (all classed as borderline malignancies), 7 were Hodgkin lymphomas and 22 were non-Hodgkin lymphomas (NHL), including 15 classified as diffuse large B-cell lymphomas. Of the 20 tumours classified as carcinomas, 11 were of the cervix or exocervix, all but one of which were *in situ* carcinomas. Of the remaining carcinomas, 4 were of the skin (3 basal cell and 1 squamous cell). One papillary adenocarcinoma of the thyroid and one renal cell carcinoma were identified. Among the remaining malignancies were a number of embryonic cancers including 4 each of Wilm's tumours and neuroblastomas, and one hepatoblastoma.

The expected number of malignancies, excluding non-melanoma skin cancer, was calculated as 36.64. The standardised incidence ratio, based on 109 observed malignancies, was 2.97 (95% CI: 2.43, 3.60) (Table 10.3). This figure represents the overall cancer incidence in the cohort, irrespective of radiation exposure. The overall SIR was higher for patients first examined between 2000 and 2010 (3.20, 95% CI: 2.41, 4.17) than for those first examined between 1990 and 1999 (2.78, 95% CI: 2.00, 3.75). For leukaemia, the SIR was 4.30 (95% CI: 2.87, 6.18) based on 30 cases verses 6.98 expected, while for lymphoma it was 5.92 (95% CI: 4.04, 8.38) based on 33 cases verses 5.57 expected. Incidence was significantly raised for cervical cancer (SIR=9.32), but not brain tumours (0.64). The SIR was greater at hospitals carrying out transplants (3.24, 95% CI: 2.60, 3.99) compared to non-transplant hospitals, where SIR was still significantly raised (1.90, 95% CI: 1.09, 3.07). Sixty eight patients developing a malignancy or borderline malignancy (51%) had a clinical history consistent with organ transplantation. Where transplant patients were removed from the analysis, the overall cohort SIR for all malignancies was reduced to 1.67 [95% CI:

1.25, 2.18]. For leukaemia, SIR was reduced to 2.16 [95% CI: 1.16, 3.67], and for lymphoma, SIR was reduced to 1.60 [95% CI: 0.67, 3.19]. Transplant patients underwent more examinations (4.27 per patient) than non-transplant (1.35) and received a higher cumulative dose (median effective dose of 11.2 mSv, compared to 7.7 mSv) (see Chapter 8, section 8.2). The SIR for all sites, where transplant patients were excluded, was slightly higher for patients first examined between 2000 and 2010 (1.62, 95% CI: 1.05, 2.40) than for those first examined between 1990 and 1999 (1.57, 95% CI: 9.97, 2.40).

| Classification | Total | Borderline/Benign | Malignant |
|---|---|---|---|
| Leukaemia | 35 | 5 | 30 |
| Lymphoma | 43 | 10 | 33 |
| Carcinoma | 20 | 4 | 16 |
| Sarcoma | 10 | 1 | 9 |
| Neuroblastoma | 4 | 0 | 4 |
| Wilms tumour | 4 | 0 | 4 |
| Brain | 5 | 5* | |
| Germ cell | 2 | 0 | 2 |
| Others | 10 | 4 | 6 |
| Total | 133 | 24 | 109 |

**Table 10.2: Classification of 169 malignancies and borderline malignancies diagnosed among cohort members. Note *three benign or borderline malignant brain tumours were included as 'malignancies' for the purpose of SIR calculations.**

| | Cancer type | Expected | Observed | SIR [95% CI] |
|---|---|---|---|---|
| Whole cohort | All | 37.04 | 109 | 2.94 [2.41, 3.56] |
| | Leukaemia | 6.98 | 30 | 4.3 [2.87, 6.18] |
| | Lymphoma | 5.57 | 33 | 5.92 [4.04, 8.38] |
| | CNS | 7.87 | 5 | 0.64 [0.19, 1.51] |
| | Cervical | 1.18 | 11 | 9.32 [4.55, 16.89] |
| Excluding transplant patients | All | 32.94 | 55 | 1.67 [1.25, 2.18] |
| | Leukaemia | 6.47 | 14 | 2.16 [1.16, 3.67] |
| | Lymphoma | 5.01 | 8 | 1.6 [0.67, 3.19] |
| | CNS | 7.22 | 3 | 0.42 [0.07, 1.25] |
| | Cervical | 1.01 | 10 | 9.9 [4.63, 18.45] |

**Table 10.3: Observed and expected cancer cases and associated standardised incidence ratio (SIR), for the whole cohort and after excluding patients with a history of transplant.**

Of the 41 tumours with a clearly defined location (Table 10.4), the majority (n=25) were in the abdominal and pelvic region, driven by the 11 cervical carcinomas, 4 neuroblastomas and 4 Wilm's tumours (kidneys). Four malignancies were listed as being in the thoracic region – one peripheral primitive neuroectodermal tumour (pPNET) of the pleura, two ganglioneuroblastomas and one rhabdomyosarcoma. There were no tumours of the lung, breasts, stomach, heart or oesophagus. A further 3 tumours, one melanoma, one synovial sarcoma and one basal cell skin carcinoma, had locations simply listed as 'trunk', meaning chest or abdomen (or both).

| Location | Total | Borderline | Malignant |
|---|---|---|---|
| Head | 5 | 0 | 4 |
| Neck | 2 | 0 | 2 |
| Upper limbs | 2 | 0 | 2 |
| Thorax | 4 | 0 | 4 |
| Trunk | 3 | 0 | 3 |
| Abdominal/pelvic | 25 | 2 | 23 |
| Lower limbs | 0 | 0 | 0 |

Table 10.4: Location of tumours where defined.

One cancer was diagnosed among patients with transposition of the great arteries, verses 1.09 expected. One cancer was diagnosed among patients with Down syndrome (leukaemia), verses 0.18 expected. No malignancies were diagnosed among patients identified as having Tetralogy of Fallot (1.03 expected), Hypoplastic left or right ventricles (0.14 expected), or having undergone Norwood or Fontan procedures (0.06 and 0.37 expected, respectively). The latter operation is associated with liver disease, including hepatocellular carcinoma [333], though no such tumours were identified among this group, or the cohort as a whole. One tumour was diagnosed in a patient identified as having neurofibromatosis. No cases of tuberous sclerosis, ataxia telangiectasia or Li Fraumeni syndrome were identified.

*Association with radiation exposure:*

Almost half of the cases (45%, n=61) were diagnosed before the date of the first recorded catheterization for that patient (maximum of 17.9 years prior). This does not necessarily imply the tumour could not be associated with a catheterization - 5499

patients were born before the earliest recorded procedure at their respective hospital, therefore could have undergone procedures not included within the study. Considering only patients born within the data collection period, 35 developed a malignancy (n=29, SIR=2.59, 95% CI: 1.72, 3.75) or borderline malignancy (n=6). Of these, 17 cases (49%) were still diagnosed before the first recorded catheterization – a similar proportion to the cohort as a whole.

Forty nine patients in the total cohort developed a malignancy (n=36) or borderline malignancy (n=13, including 3 basal cell carcinomas) at least 5 years after the first recorded procedure (solid cancers and lymphoma) or 2 years after the first procedure (leukaemia) (Table 10.5). Of these, 23 (52%) had a history consistent with transplant. None had Down syndrome, tetralogy of Fallot, transposition or had undergone Norwood procedures. The median age at first recorded procedure was 13.3 years (interquartile range: 6.7, 15.9 years), while the mean age was 11.7 years (standard deviation: 6.2 years). The expected number of malignancies developing between 5 years since the first recorded procedure and the 1st of February 2014 was 16.87. The SIR was 2.13 (95% CI: 1.48, 2.97). Fifty five percent of patients (n=27) developing a tumour after the minimum latency period were male.

| Site | Total | Borderline | Malignant |
|---|---|---|---|
| Leukaemia | 8 | 3 | 5 |
| Lymphoma | 18 | 6 | 12 |
| Carcinoma | 15 | 6* | 9 |
| Sarcoma | 1 | 0 | 1 |
| Neuroblastoma | 0 | 0 | 0 |
| Wilms tumour | 0 | 0 | 0 |
| CNS | 3 | 0 | 3 |
| Germ cell | 2 | 0 | 2 |
| Others | 2 | 1 | 1 |
| Total | 49 | 10 | 39 |

**Table 10.5: Cases developing at least 5 years (solid tumours) or 2 years (leukaemia) following the first recorded procedure. *Note – includes 3 basal cell carcinomas.**

Of the 49 patients developing a malignancy or borderline malignancy after the minimum latency period, 38 were born before the earliest date of data collection at their respective hospital. These patients may have undergone further

catheterizations not captured by the study, thus cumulative dose estimates may be underestimates. In Chapter 3 (section 3.3.5), it was found that the mean number of procedures per patient was 1.5, with this figure remaining unchanged when analysis was restricted to patients born within the study period. Considering only patients born within the data collection period, 11 developed a malignancy (n=9) or borderline malignancy (n=2) after the minimum latency period, verses 4.33 malignancies expected. Five of these 11 patients (45%) had a history consistent with transplant. The SIR, excluding borderline cases, was 2.08 (95% CI: 0.92, 4.00). Thus, the standardised incidence ratios for the overall cohort (2.94), those developing malignancies after the minimum latency period (2.13) and the subset of this latter group who were born within the study period (2.08) are reasonably similar. Only the final figure is non-significantly raised. Likewise, the percentage of cases developing in transplant patients is similar in all three analyses - around 50%. As for the cohort as a whole, the SIR was higher for patients first examined between 2000 and 2010 (3.21, 95% CI: 1.88, 5.31) than between 1990 and 2000 (2.31, 95% CI: 1.49, 3.42).

Evidence of an association with radiation exposure is strengthened by a dose response - a proportionality between dose and excess risk. Only exposures occurring more than 5 years (solid cancers) or 2 years (leukaemia) prior to cancer diagnosis contributed toward cumulative dose. A summary of these doses for the 36 patients developing malignancies, not including non-melanoma skin cancer is shown in Table 10.6.

| | Median cumulative dose [IQR] | |
|---|---|---|
| Organ | Cases after latency period | Non-cases |
| Bone marrow | 5.8 [5.3 : 12.1] | 3.8 [1.8 : 8.1] |
| Breasts | 28.9 [19.9 : 64] | 16.6 [6 : 41.8] |
| Heart | 34.2 [24.9 : 61.5] | 21.1 [10.2 : 43.1] |
| Lungs | 42.3 [34.1 : 81.5] | 26.5 [13.6 : 56.7] |
| Lymph nodes | 8.9 [6.5 : 15.9] | 5.4 [2.7 : 10.5] |
| Oesophagus | 32.4 [21.3 : 53] | 19.3 [8.9 : 36.4] |
| Thyroid | 2.1 [1.3 : 3.3] | 1 [0.5 : 2.2] |
| Liver | 13 [10.9 : 22.9] | 7.5 [3.7 : 16.9] |
| Stomach | 7.6 [5 : 11.2] | 4.1 [2.1 : 7.7] |
| Whole body | 8 [6 : 15.2] | 5 [2.5 : 9.9] |
| Effective dose | 14.4 [11.2 : 25.4] | 8.7 [4.4 : 18.7] |

**Table 10.6. Median cumulative doses for cohort members developing malignancies after the minimum latency period of 5 years (solid tumours) or 2 years (leukaemia), compared to equivalent figures for non-cases. Borderline malignancies not included).**

A plot of SIR against cumulative cardiac dose is shown in Figure 10.1 and demonstrates little suggestion of a pattern of increasing risk with increasing dose (p for trend = 0.48). SIR was significantly elevated for the 5-40 and 40-80 mSv dose categories, but not for any others. With the exception of the largest dose category, the percentage of cases developing in patients receiving a heart transplant, steadily increased, ranging from 0% for patients receiving less than 5 mSv to 100% for patients receiving 120-160 mSv (Figure 10.1). There were few cases among patients receiving especially high doses. Of the 191 patients receiving an estimated cumulative cardiac dose of over 250 mSv, none developed a malignancy after the latency period.

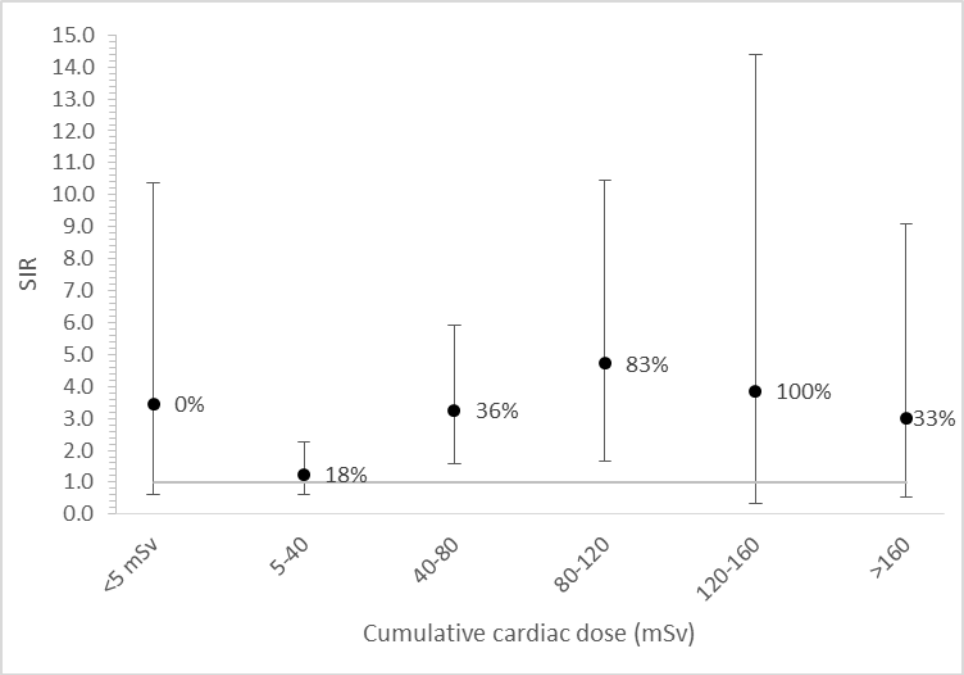


**Figure 10.1: Variation in standardized incidence ratio (SIR) with cumulative cardiac dose. Percentages represent the proportion of cases among transplant recipients.**

The risk of developing a tumour (malignant or borderline/benign, after the latency period) for different cumulative cardiac dose ranges relative to less than 5 mSv was calculated. There is a suggestion of a pattern of increasing risk with increasing dose, especially in the 0-120 mSv range, albeit with very wide confidence intervals (Figure 10.2). Where transplant patients are removed from the analysis, this pattern was replaced by an apparently negative relationship. It should also be noted that many of the cases were of organs remote from the site of irradiation, most notably the 10

cervical cancer cases. Thus this suggestion of a ‘dose response’ should be interpreted with caution.

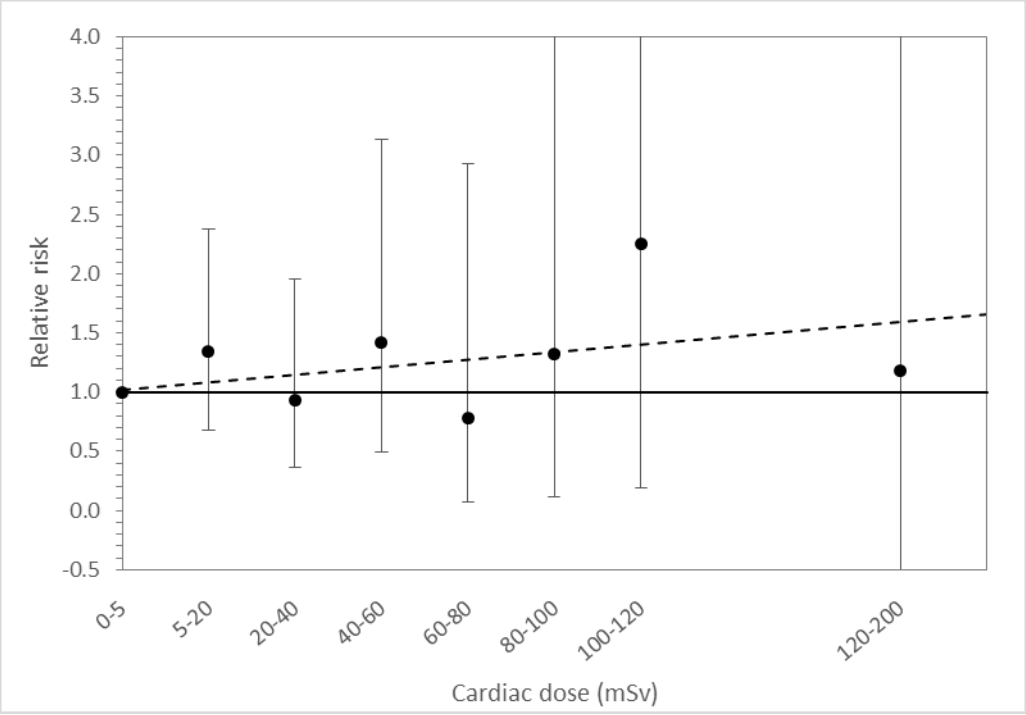


**Figure 10.2: Relative risk of developing a malignant tumour in relation to cumulative cardiac dose.**

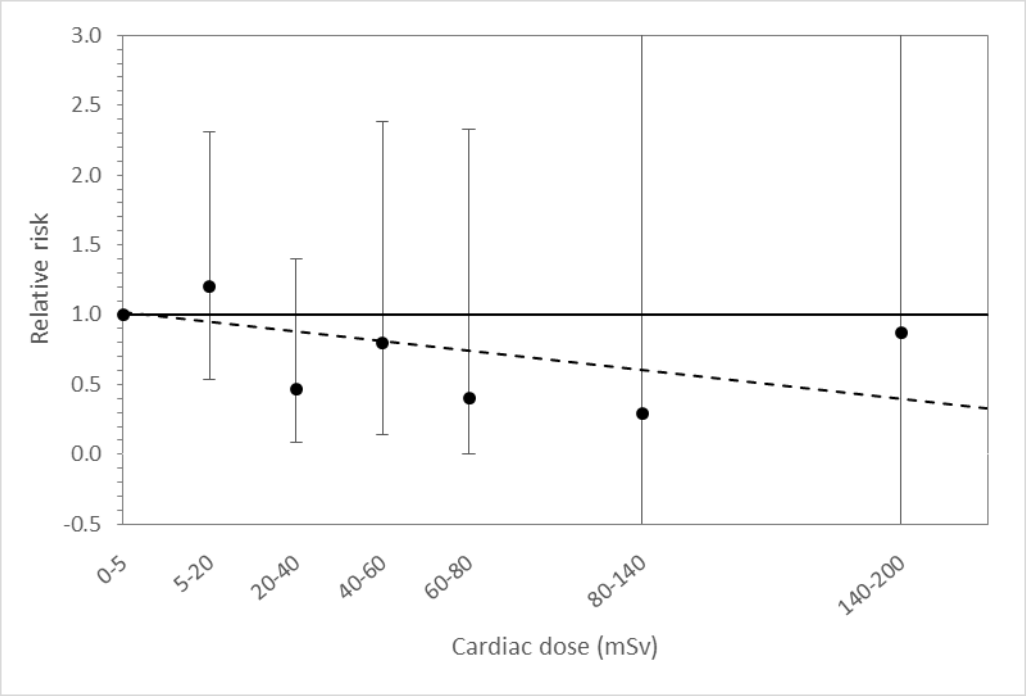


**Figure 10.3: Trend following removal of cases developing in patients receiving a transplanted organ.**

This analysis does not include radiation exposures from other forms of medical imaging (general radiography, computed tomography and nuclear medicine). Information from these procedures was not obtained from participating hospitals as part of this study. Data on CT scans in the UK were gathered as part of a separate study [9]. Linkage was performed between the cardiac and CT cohorts to identify patients who have undergone both cardiac catheterizations and CT scans. Members of both cohorts were assigned non-anonymous identification codes based on the combination of name and date of birth (anonymous ID numbers were then derived from these). Patients with the same non-anonymous ID code were assumed to be the same person. Potentially, two distinct patients could have the same name and date of birth. Although unlikely, this could result in matching errors. Overall, 1848 patients in the cardiac cohort were identified as having undergone at least one CT scan (14% of the total cohort). Of the 131 patients in the cardiac cohort developing a tumour, 70 (53%) had undergone at least one CT scan. Among the 49 patients developing a tumour after the minimum latency period, 23 have received at least one CT scan.

### *10.2.1: Survival of cohort members*

Analysis of survival is largely outside the scope of this thesis. Details of cause of death were primarily analysed to obtain information on confounding conditions. Childhood mortality is a highly sensitive issue [334-336], therefore comparison of death rates between participating hospitals was avoided and only overall details described. In total, 1060 patients were recorded as having died. For 76% of these (n=805), the primary cause of death was listed as being cardiac related or due to congenital disease of the heart or blood vessels. Other causes included cystic fibrosis (n=20), infections (n=10), complications of surgery (n=10) or neoplasm (n=23). Thirty five patients who died had Down syndrome while 30 had Tetralogy of Fallot. Of 132 patients developing a tumour, 36 (27%) are recorded as having died. For these patients, the median number of years between cancer diagnosis and death was 1.8 years (range: 0 to 35 years).

The calculated Kaplan Meier survival function is shown in Figure 10.4. Survival fell rapidly in the first and second years of life, with 361 and 105 deaths respectively,

before levelling off. At 40 years, the survival was just under 92%, compared to 98% in the general UK population.

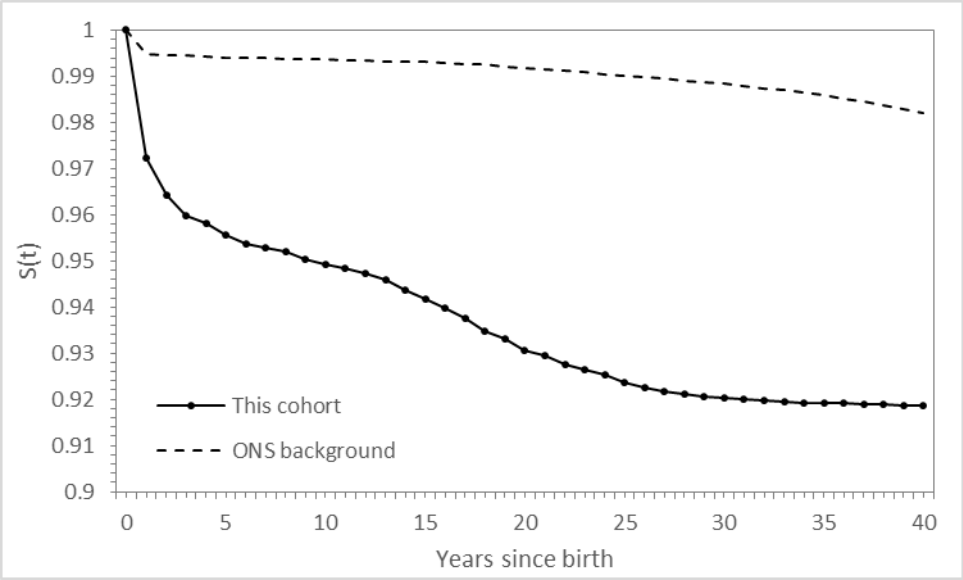


**Figure 10.3: Kaplan Meier survival function for entire cohort, censored at 40 years. ONS=Office for National Statistics.**

### *10.3: Discussion*

Two findings are particularly striking; the significantly raised incidence of malignancies among cohort members compared to the general population and the large impact of organ transplantation on the results. Addressing the first point, the finding of elevated cancer incidence among people with heart disease is not unprecedented. In a recent study by Lee *et al* [337] focusing on 31,961 Taiwanese patients of all ages with CHD between 1998 and 2006, an overall SIR of 1.45 was found (95% CI: 1.25, 1.67). Around half of these patients had undergone a catheterization procedure (48.9%) while 18.9% had undergone a CT scan. The most common cancers were haematological (SIR=4.04) or of the CNS (3.51). In contrast to the current study, the number of cervical cancers was smaller than expected (8 observed verses 15.1 expected) while brain tumour incidence was increased (14 observed verses 4 expected). Lymphomas were not analysed separately. Heart transplants are carried out in Taiwan [338], though it is unclear how many patients in Lee's analysis had undergone this procedure. The SIR in the Taiwanese study is

similar to the equivalent figure in the current study where transplant patients are excluded (1.35).

Bjørge *et al* [233] studied cancer incidence among children born with a range of congenital defects in Scandinavia. The SIR associated with malformations of the heart and blood vessels was slightly raised in Sweden (1.2, 95% CI: 1.0, 1.6) and Norway (1.2, 95% CI: 0.7, 2.0). Carozza et al [339] studied 115,686 patients with congenital abnormalities born in Texas between 1996 and 2005, among whom 239 cancer cases were diagnosed. Half of the cases in this group were leukaemia (n=74) and 15% were of the central nervous system (n=23), while only 3% (n=4) were lymphomas. The incident rate ratio (IRR) was 3.50 (95% CI: 2.81, 4.31). Fisher and his colleagues [340] analysed 222 patients in California with various birth defects, who developed cancer. Of these, 69 cancers developed in patients with malformations of the heart or circulatory system. Hazard ratios were significantly raised, ranging from 3.36 to 4.28. Thus cancer incidence is comparable, albeit somewhat higher among the current cohort than has been suggested in previous research. It should be noted that the current cohort was established from patients undergoing cardiac catheterizations, rather, as with the above mentioned studies, from registers of congenital malformations.

The increased cancer risk among patients undergoing organ transplantation is well known [341], including among childhood recipients [211]. For example, Engels and colleagues studied cancer incidence among solid organ transplant recipients in the United States, using data from the US Scientific Registry of Transplant Recipients (1987-2008) and 13 regional cancer registries. For all ages, a significantly raised SIR of 2.10 was found (95% CI: 2.06, 2.14), while for non-Hodgkin lymphoma this figure was 7.79 (95% CI: 6.89, 8.79) [341]. The rate of malignancies in children receiving heart transplants recorded by the International Society for Heart and Lung Transplantation (ISHLT) is approximately 1% per year of survival, with the majority of these cases being lymphomas [211]. Consistent with the used of immunosuppressive agents, malignancies following organ transplantation tend to be virus-related, including lymphoma, certain skin cancers and cervical cancer [342, 343]. Most notably, there is a strong association between transplantation, Epstein-Barr virus and post-transplant lymphoproliferative disease (PTLD) [344, 345]. In this study, the impact of transplantation was especially pronounced for lymphoma, with the SIR

falling from 5.36 to 1.33 when transplant patients were removed from the analysis. This is an important finding, of relevance to studies examining the potential risks from other medical exposures, including CT scans. An infectious aetiology has long been suspected for leukaemia [346], although the exact infection/mechanism is yet to be identified. The effect of removing transplant patients from the analysis was smaller than for lymphoma, with the SIR falling from 4.07 to 1.92 and remaining significantly raised. Eleven cases of cervical cancer were identified among cohort members in the current study, though only one of these patients appeared to have undergone a transplant. This possibly suggests under-ascertainment of transplantation among the cohort. The identification of transplantation and other potentially confounding conditions was based principally on clinical details and death records. The former were only recorded at two hospitals, while the latter were only available for the cohort members that died. The limitations of this incomplete ascertainment of such confounding conditions is acknowledged, although the quality and completeness of this information is similar, if not better than for studies investigating the risks following CT scans [187, 190, 191]. For example, the German CT study by Krille *et al* [190] used the diagnosis of lymphoproliferative disease to identify cases developing in transplant recipients. This may be unreliable, considering that many of the cases among this group in the current study were B-cell lymphomas, rather than lymphoproliferative disease.

The number of thyroid cancers (a single case) was very small, though expected given the limited sample size and low radiation dose to the thyroid. The absence of any cancers of the lung and oesophagus was also expected given the relatively short follow-up period. There is some evidence of relatively early onset (i.e. under age 35 years) of breast cancer among young people exposed to radiation [129], although no suggestion that the disease can be induced in childhood. Only 189 female cohort members had reached the age of 35 by February 1st 2014, therefore the complete lack of breast cancer cases should not be regarded as a surprising finding at this stage of follow-up. Given the potentially high localised skin doses, potentially reaching several Gray, the small number of skin cancers (especially basal cell carcinoma) was surprising.

More than half of the patients developing a tumour after the minimum latency period were male. The risk estimates described in Chapter 9 using existing risk models

suggested females were around three times more likely to develop radiation induced cancer. However, this gender difference was driven by the impact of breast cancer and the higher risk coefficients for lung cancer in females. Thus a difference in risk by gender ought not to be apparent at this early stage of follow up where lung and breast cancer have not had sufficient time to develop.

Limitations of the cohort were discussed in Section 3.7. In particular, misspelling of names and dates of birth could potentially lead to under ascertainment of cancer rates in the study group. The overall cohort SIR was somewhat higher at hospitals who had provided data in electronic format (3.33) compared to those who provided hand-written log books (2.81), although this comparison ought to be interpreted with caution as these two groups may involve different patient characteristics and doses. A reanalysis of the first UK CT study [9] by Berrington-de-González *et al* [191] found a number of brain tumours, apparently occurring at least 5 years following the first CT scan, were in fact present at the time of the first scan. This suggests cancer registry matching may not be as reliable as could be hoped for.

### *10.4: Conclusion*

Patients undergoing cardiac catheterizations for congenital heart disease are at a significantly increased risk of developing cancer, although it appears that this increase is mostly unrelated to radiation exposure. Future epidemiological analysis of cancer risks following cardiac catheterizations requires rigorous attention to clinical history, most notably transplantation. Ideally, linkage with both transplant and congenital anomaly registries, such as the British Isles Network of Congenital Anomaly Registers (BINOCAR) [347], should be carried out.

# Chapter 11: Discussion

## Summary of main findings:

This study has established a cohort of around 13,500 patients aged under 22 years who have undergone cardiac catheterizations in the UK, comprising around 20,000 individual procedures. The doses from these procedures, as represented by kerma area product ($P_{KA}$), have fallen by a factor up to twenty during the study period, and appear to be relatively low compared to equivalent figures quoted in recent large studies based in the United States. Effective dose and equivalent doses to individual organs were estimated based on a dosimetry system utilising data from Monte Carlo simulations. The results were compared to equivalent figures derived from physical measurements and previous publications. A number of discrepancies were found, which appear to be due to a combination of experimental error and differences in phantom anatomy. Uncertainties in dose estimates were also calculated. These are generally around ±30%, though do not account for uncertainties due to anatomical variation, which are difficult to quantify. The risk of cancer in relation to estimated doses was calculated based on BEIR VII risk models, suggesting an approximate risk of developing cancer of 1 in 1000, per examination, for the overall cohort. For examinations conducted using modern equipment, these risks are reduced to around 1 in 1700, due to lower doses. Estimated risks were higher for females than males by a factor of around 3. This is due to the impact of breast cancer and higher risk per unit dose for other tissues. A number of modifications to the BEIR VII models were investigated, to account for the reduced survival of people with heart disease, and the uncertain relationship between risk and age at exposure. A small epidemiological analysis was performed, suggesting an almost threefold increased risk of cancer in the cohort, compared to the general UK population. There are a number of reasons to suggest that this increase was primarily not related to radiation exposure, most notably the large impact of transplantation and associated immunosuppressant use. Despite the high cancer incidence, the overall survival in the cohort was high, at around 91% after 30 years.

### *Radiation doses:*

The radiation doses from cardiac catheterizations are higher than those of general radiography (i.e. ‘normal’ x-rays), approximately similar to CT and nuclear medicine

[52, 111, 164], and much lower than radiotherapy. The variation in doses from one procedure to the next is higher for cardiac catheterizations, with some procedures delivering organ doses of several hundred mSv. The use of CT as an alternative to cardiac catheterizations could result in an underestimation of collective doses to cohort members. Johnson *et al* [89] estimate proportional contributions to collective effective dose of 35.2, 20.5 and 6.8%, for interventional and diagnostic catheterizations and gated cardiac CT, respectively, based on respective doses per examination of 13.77, 9.10 and 18.28 mSv. These figures are based on an unusually high estimated CT dose relative to catheterizations, compared to that suggested by previous research [111, 167]. Potentially, the contribution to collective dose may be lower than 6.8%, therefore. Ait Ali *et al* [13], recorded 7 CT chest examinations carried out among their cohort of 59 patients, compared to 55 and 40 diagnostic and interventional catheterizations, respectively. Again, this suggests that catheterizations are the dominant source of medical radiation exposure in this patient group. The current study is being run alongside a larger study investigating the risks from CT scans [9], for which data on scans carried out at most UK hospitals are available. Future epidemiology-based risk estimates should incorporate these data.

The large fall in doses over the study period appears to be mainly due to technological factors, including improved detector efficiency, ability to remove antiscatter grids, greater control over frame rates, use of added copper filtration and improved image processing. However, a large variation is also apparent for the same equipment, even when corrected for patient size and procedure type. An especially pronounced variation was apparent between the dose indicators presented in the current study and those of several large, multi-centre American studies [82, 83, 91, 207], where doses appeared to be higher by a factor of between 2 and over 50, depending on procedure type. This was made clear in a paper from this thesis published in the British Journal of Radiology [348]. It is noted that these American studies formed part of multi-centre collaborations on cardiac outcomes, including radiation protection, namely the CCISC (Congenital Cardiovascular Interventional Study Consortium) and $C_3PO$ (Congenital Cardiac Catheterization Project on Outcomes). The fact that radiation doses are so much higher in spite of such initiatives is puzzling. The authors of these studies appear to be unaware of the discrepancies in doses, tending to conduct only limited comparisons with previous research.

Higher doses are not without benefits, however. Increased photon fluence is associated with improved image quality. It is currently unclear if such gains in image quality necessarily lead to better patient outcomes [95], such as increased survival or lower complication rates. Until such information is available, it is not possible to claim high doses are 'too high' – that would require proof of improved patient outcomes due to improved image quality failing to offset the increased risk of radiation induced cancer. This is an exceptionally difficult issue to research, partly because the cancer risks are uncertain, but also due to the difficulty in quantifying patient outcomes. The high survival rates among members of the UK cohort described in this study does not suggest any overt burden caused by the use of low radiation doses.

One of the most interesting findings of the current study was the large increase in breast dose calculated using Monte Carlo simulations, as the beam is rotated towards laterally orientated projections, or where the central ray location is translated in the anterior-posterior direction. This 'cliff' in breast dose was present for all phantom sizes, and to some extent, for different field sizes. Previously published estimates of breast dose or effective dose per unit $P_{KA}$ did not exhibit this feature [88, 92], nor did physical measurements using anthropomorphic phantoms. However, none of these previous studies appear to have investigated the same range of beam angles and field sizes of the current study and may have restricted their analyses to somewhat idealized conditions, i.e. close collimation, deliberately excluding the breasts from the primary field. Clearly, there is scope for large variation in breast dose depending on beam angle, centring point and field size, relating to the exclusion or inclusion of the breasts (in particular the glandular tissues) within the primary beam. It is very difficult to assess from clinical images whether the breasts were included within the primary beam or not. The size and shape of the breasts is also variable and cannot be predicted from patient size (i.e. BMI) alone. The major implication is that breast dose estimates are subject to much larger uncertainties than for other tissues. Techniques for limiting the size of the irradiated field in the lateral projection should be employed, where possible, including collimation and 'lung shuttering'. It is recommended that the anterior chest wall should always be excluded from the primary field of irradiation. The use of lead or lead-free shielding materials to reduce breast dose is unlikely to be practical, as the region of interest would be obscured in other projections.

A further important finding was the potential impact of antiscatter grid usage on patient dose. This was associated with a striking difference in the variation in either organ doses, or $P_{KA}$ per kilogram, between hospitals depending on grid usage. Hospitals claiming to selectively remove grids, report doing so only for small patients below around 10 kg (approximately less than 1 year). However, the pattern of relatively lower doses for smaller patients extended well above 10 kg. This could be potentially explained by radiographers removing grids for larger patients, where they see this as appropriate, though it is likely that other factors are involved. Patterns of antiscatter grid usage are variable within the UK. McFadden *et al* [281] report that 27% of UK hospitals remove grids - 18% for patients under 10 kg, and 9% for 'small children'. The removal of grids for patients below around 10 kg is supported by evidence from a number of studies [217, 222]. The extension of this practice beyond such small patient sizes is more limited [224]. For examinations in which image quality is of less importance, grid removal may be warranted for all patients. Further research in this area would be beneficial.

Organ dose estimates are affected by the phantom models - either physical or computational - upon which they are based. The mathematical phantoms used in PCXMX 2.0 are rather crude. In particular, changes to phantom mass for a given height are not adequately modelled - all organs inflate like a balloon. Some patients in the cohort are obese, with body mass indices of up to 40.0. In these cases, attenuation of the beam by adipose tissue would have the effect of reducing beam intensity before more radiosensitive organs such as the lungs are reached. Although x-ray output, and hence kerma area product, would increase in response to a greater patient thickness, it would be expected that organ doses per unit $P_{KA}$ would be lower. A study investigating the effect of obesity on doses from CT found a 59% decrease in dose for deep lying organs for obese patients (BMI up to 46.4) compared to normal sized patients (BMI of 23.5) [349]. There are two problems that need to be addressed when attempting to correct for changes to body habitus; (1) the level of attenuation provided by adipose tissue, and (2) the distribution of adipose tissue in the body. The first problem is relatively easy to overcome. The attenuation coefficient ($\mu$) of fat can easily be obtained from published data [16] or derived from Hounsfield Units from computed tomography (CT) images. From these values, an estimated reduction in beam intensity per unit thickness of adipose tissue could be calculated analytically. The second problem is considerably more difficult to address; the thickness of

adipose tissue traversed by the beam needs to be determined. Little information on the distribution of fat around the body is available. Again, CT images may provide the best source of information.

Organ dose estimates may also be affected by the administration of iodinated contrast agents. These are designed to increase the attenuation of blood relative to surrounding tissues, thereby increasing subject contrast. The impact of contrast agents on organ doses should not be underestimated. Blood vessels perfuse tissues; they branch into successively smaller arteries and arterioles and capillaries, before regrouping as veins, returning blood to the heart. Almost all tissues have an extensive vascular network (cartilage is avascular). Blood makes up around 60% of the mass of the heart and 43% of the lungs [296]. With the exception of the brain, the whole organ should thus be perfused by contrast agent containing blood following administration (the blood-brain barrier prevents enhancement of the brain in healthy individuals). This would have the effect of increasing x-ray attenuation by organs compared to that simulated by both Monte Carlo simulations and anthropomorphic phantoms in which non contrast enhanced organ densities are assumed. The thorax is the location for the largest arteries and veins in the body as well as the heart itself, therefore the impact of contrast agent administration on dose estimates may be especially important for cardiac catheterizations. The impact of contrast administration would vary between procedures types; almost no effect for electrophysiology studies where contrast is rarely used, small for coronary angiography (the coronary vessels are relatively small) but potentially large for investigations including the right side of the heart and pulmonary vessels. Contrast agents are very rarely used during fluoroscopic imaging and are mostly restricted to acquisitions.

Correcting for contrast agent administration is even more challenging than for body fat. Neither PCXMC Monte Carlo software, nor ATOM anthropomorphic phantoms allow adjustment of the attenuating properties of organs. Furthermore, although whole organs may experience enhancement, this effect is often highly uneven, with greater enhancement occurring where blood vessel density is highest. The heart itself could reasonably be modelled as a single homogenous volume subject to uniform enhancement, but the blood vessel density in the lungs varies from tremendously high around the hilum to fairly low around the lung periphery.

The ideal solution to the issue of both contrast agents and fat distribution is the use of voxel phantoms derived from CT images. These could be specific to the patient for whom dose from a cardiac catheterization is to be calculated. However, such phantoms would represent a single level of contrast agent enhancement and a single level of lung inflation (CT scans are usually acquired on inspiration). The density and shape of organs may not necessarily reflect the respective density and shape during fluoroscopic exposures. Voxel phantoms of a range of patients, or patient specific voxel phantoms would improve central dose estimates and narrow, but not eliminate, associated uncertainties.

This study did not assess doses to the operator in cardiac catheterizations (i.e. cardiologists, radiologists, nurses and radiographers). The risk of cancer and cataracts among operators should not be underestimated [350], especially considering recent findings of studies of nuclear workers suggesting risks are higher than previously supposed at low doses [145, 146]. To some extent, operator dose is related to patient dose [229]. Thus the fall in patient dose found in this study should have been accompanied by a corresponding fall in operator dose.

*Associated risks:*

Cardiac catheterizations are a vital procedure in the treatment and management of acquired and congenital heart diseases. In many cases, the procedure may be lifesaving. In others, quality of life may be significantly improved. Cardiac catheterizations are a proven alternative to surgery [2], with similar success rates and reduced complications [1]. The increased lifetime risk of developing cancer needs to be placed in the context of these benefits. The reduced survival of children with certain heart conditions is also an important factor in risk estimation. Some children, most notably those with a hypoplastic left heart, are unlikely to survive beyond their teens [214, 215], thus have limited time to develop radiation induced cancers. The fact that the lungs, stomach, oesophagus, liver and breasts receive the highest radiation doses from cardiac catheterizations is particularly significant in this sense, as cancers of these organs are all ‘adult’ diseases, tending to occur beyond 30 or 40 years [202]. There is reasonably strong evidence that radiation induced cancers develop at the ages at which they normally occur (i.e. in an unexposed

population) [132]. Second cancers developing after radiotherapy for primary cancer in childhood tend to be other cancers normally occurring in childhood such as sarcomas, brain tumours or leukaemia, unless the follow-up time is long [199, 351]. Excess cancers of the lungs, stomach and oesophagus among atomic bombing survivors did not appear below attained ages of 35 years [169]. Unless patients are likely to survive to at least this age, the risk of radiation induced cancer may be very small and restricted mainly to leukaemia, regardless of how high the doses are. This does not excuse poor radiation protection, however. For many heart conditions, including isolated pulmonary valve stenosis, atrial septal defect or Wolf-Parkinson-White syndrome, survival now approaches that of the general population [213, 214]. The reduction of radiation doses in these patients is especially important. It is pleasing, therefore, that doses for trans-catheter treatment of these conditions has fallen considerably over the last two decades, with the estimated lifetime risk of cancer being generally less than 1 in 1000. There is still scope for further dose reductions, however, such as the increased use of ultrasound or magnetic resonance imaging guidance [2].

Although the epidemiological analysis was small and likely underpowered (in terms of ability to detect radiation induced excess cancers, at least), the work done in establishing the dosimetry system, including gathering data on projection angles and beam energy used in clinical practice, prepares the ground for further research. A number of studies are ongoing to assess the long term risks of diagnostic x-ray exposures [352-355]. These studies mostly focus on computed tomography (CT), with only one other – the French 'Coccinelle' cohort [331, 355] – focusing on cardiac catheterizations. Both the current and French studies have relatively small sample sizes (13,500 and 10,000 respectively), thus limiting statistical power. More European-based studies may follow, allowing the pooling of data.

Studies of people undergoing cardiac catheterizations have a number of advantages for radiation epidemiology. Firstly, individualised dose estimation is possible using data recorded at the time of the examination (i.e. $P_{KA}$). More complete versions of the structured dose reports used in this study, which include details on all exposure events including non-acquisition fluoroscopy are now available [356]. Utilisation of these data could improve central dose estimates by improving information on beam angles and energy used in clinical practice and provide improved information on

uncertainties. Such information may be difficult to acquire for large volumes of patients, and are not available for older examinations (i.e. pre-2011). Automatic recording of structured dose reports in a form suitable for retrospective dose reconstructions would be desirable and has been implemented for CT [357]. No epidemiological studies of cancer risks following CT scans published so far [9, 124, 186, 187, 190] have utilised this methodology, instead using average dose values adjusted for patient size and date of examination. A second advantage is the wide range of doses delivered, per procedure. This allows the relationship between radiation dose and cancer risk to be determined (i.e. a 'dose response'). This is preferable to simply using the number of procedures as a surrogate for radiation dose. A third advantage is the relatively homogenous patient group compared to those undergoing CT scans. This potentially means confounding factors are easier to identify and control for. Unlike CT, cardiac catheterizations are not used in the diagnosis and screening of cancer.

A number of disadvantages of epidemiological studies of these patients must also be acknowledged. Firstly, estimating the radiation doses from cardiac catheterizations is difficult, with large uncertainties. These uncertainties, as indicated by the variation in dose estimates between different studies, appear to be larger than for CT [248]. Incorporation of uncertainties into epidemiological analysis is complex, though the approach used by Lee *et al* [358], in a study investigating the risks from CT scans, could also be applied to cardiac catheterizations. Shared and unshared errors among catheterizations with the same attributes (patient age, equipment type, year, etc.) could be accounted for using a 2 dimensional Monte Carlo (2DMC) approach. Probability density functions (PDFs) could be calculated for scan parameters, based on a sample of examinations with structured dose reports [358]. These could be used to produce multiple realizations of cumulative doses for each cohort member. The concept of multiple dose realizations has been used previously in 'ecological' analyses, such as the study of thyroid cancer incidence among residents of the Semipalatinsk region of Kazakhstan [359] where dose estimates are highly uncertain.

Such uncertainty analysis is hindered by the variable availability of dose indicators over the study period. Much more complete information is available for beam energy and projection angles for recently conducted examinations, where structured dose reports are available. Thus, the increased uncertainty in dose estimates for older examinations should be taken into account. This is partly reflected in the current study in the wider uncertainty limits for beam energy for older equipment.

Secondly, while there may be a narrower range of confounding factors, the impact of these conditions appears to be especially severe. Even a small number of transplant patients in a cohort may result in greatly increased risk of cancer. It is essential therefore that such patients are identified. Although a range of methodologies were utilised in this study (clinical details, examination type, cause of death), it is possible that some transplant cases were missed. Linkage with a transplant registry may be the best solution, although no previous radiation epidemiology studies have achieved this. An alternative source of information is the National Institute for Cardiovascular Outcomes Research (NICOR) [360], who hold data on cardiac catheterizations carried out at all 13 paediatric cardiology centres in the UK, or the British and Irish Network of Congenital Anomaly Researchers (BINOCAR) [347], who hold registers of congenital diseases throughout most of the UK and Ireland. This would allow identification of conditions such as Down syndrome or neurofibromatosis.

Analysis of cancer by individual site may also provide evidence of potential confounding effects. In particular, the large incidence of cervical cancer, a disease not normally associated with radiation exposure [45], and other diseases remote from the site of irradiation, raises suspicions of confounding effects. It may also be possible to take advantage of knowledge of the location of tumours within large organs. For example, the distal oesophagus and lower lobes of the lungs receive higher doses than the proximal oesophagus or upper lung lobes. Likewise, the right breast receives a higher dose than the left. A higher proportion of tumours in the regions of these organs receiving the higher dose may strengthen the association with radiation exposure. No known condition predisposes individual specifically to right sided breast cancer or lower lobe lung cancer.

A third difficulty is the smaller number of cardiac catheterizations carried out compared to CT, which limits sample size. A collaboration with NICOR represents the best opportunity for expanding the study. Even acquiring data from all hospitals

carrying out these procedures in the UK over the last 10-15 years, the sample size is unlikely to exceed around 30,000 patients. Doses have decreased to low levels in recent years, at least in the UK, lowering risks and reducing statistical power for a given sample size. Thus multinational collaboration may be essential to achieve further progress.

Patients receiving the highest doses tended to be examined earlier in the study period, using older equipment, thus accruing a greater number of years of follow-up, compared to recently examined patients receiving smaller doses. Despite this, even accounting for transplantation, the SIR was higher for patients examined in more recent years, with little suggestion of lower statistical power (i.e. in terms of the width of confidence intervals). This unusual finding reinforces the impression that higher cancer rates in this patient group are due to factors other than radiation exposure.

Ongoing research investigating the long term cancer risks from ionising radiation, including the above mentioned medical studies, updates of the Life Span Study, and analysis of occupational and background exposures, will enable risk models such as those described in the BEIR VII report to be refined. This risk projection approach, free from the limitations of small sample sizes, remains the most viable method of calculating excess cancer risks from cardiac catheterizations.

# Appendix 1:

Nature of x-rays:

X-rays, like visible light, are a form of electromagnetic radiation (ER) and can be described to a layperson as a different colour of light, not visible to the human eye. X-rays generally behave in similar ways to other forms of ER, such as infrared or microwaves, though the energy is sufficiently high to cause ionisation of atoms and molecules, including DNA molecules and water. It is this property that means that x-rays are potentially harmful to human health [3]. X-rays are a form of indirectly ionising radiation. They transfer energy to a so-called secondary electron, which, depending on the amount of energy it receives, may have sufficient energy to cause hundreds or thousands of further, direct, ionisations via Coulombic interactions with other electrons.

The nature of electromagnetic radiation was predicted by Maxwell, building on the work of Faraday, Ampere and others. Maxwell developed equations demonstrating that a time varying magnetic field ($\vec{B}$) produces a circulating electric field ($\vec{E}$) [361]:

$$\vec{\nabla}\,\mathrm{X}\,\vec{\mathrm{E}} = -\frac{\partial \vec{B}}{\partial t}$$

And that a circulating magnetic field is produced by an electric current or a time varying electric field [361]:

$$\vec{\nabla}\,\mathrm{X}\,\overrightarrow{B} = \mu_0\left(\vec{J} + \varepsilon_0\frac{\partial \vec{E}}{\partial t}\right)$$

Where the vector $\vec{J}$ is the current density, $\mu_0$ is the magnetic permeability of free space and $\varepsilon_0$ is the electric permittivity of free space. Thus the electric and magnetic fields sustain each other, allowing a disturbance to propagate as a wave, without the need for any medium, or 'aether'. The electric and magnetic components of ER are each described by a wave equation, which can be derived from the above using the Divergence theorem and Stoke's theorem [361]. In three dimensions, the electromagnetic wave equations for electric and magnetic components respectively, are:

$$\nabla^2\vec{\mathrm{E}} = \mu_0\varepsilon_0\frac{\partial^2\vec{\mathrm{E}}}{\partial \mathrm{t}^2}$$

$$\nabla^2\vec{B} = \mu_0\varepsilon_0\frac{\partial^2\vec{B}}{\partial t^2}$$

[362]

Along with other forms of ER, x-rays have properties of both waves and particles. The energy of a particle of ER, known as a *photon*, is given by *hf*, where h is Plank's constant and *f* is the frequency ($s^{-1}$). Photons belong to the class of particles known as Bosons, thus do not obey the Pauli Exclusion Principle (i.e. they 'pile on'). They have a rest mass of zero and propagate at the speed of light ($3x10^8$ $ms^{-1}$).

Exposure factors:

Radiation doses from cardiac catheterizations are modified by a range of factors, many of which also impact image quality. The term 'exposure factors' is generally used to describe the peak tube potential, measured in kilovolts (kV), and tube current, measured in milliamps (mA). The latter parameter determines x-ray intensity in a similar way to a dimmer switch for a lightbulb. The peak tube potential defines the maximum kinetic energy (E, in Joules, J) of electrons as they arrive at the anode:

$$E = e \cdot V$$

Where *e* is the charge of a single electron ($1.602 \times 10^{-19}$ C). X-rays are produced by two mechanisms; (1) Bremsstrahlung, and (2) characteristic interactions. In the former, an electron is deflected off course and decelerated (Bremsstrahlung is German for 'Breaking radiation') by the Coulombic field of target material nuclei, as predicted by Maxwell's general theory of electromagnetic radiation [43]. The strength of this field is proportional to $Z/r^2$, (where Z is the atomic number and r is the proximity of the electron to the nucleus). A portion of the electron's kinetic energy is lost and radiated away as electromagnetic radiation. The proportion of kinetic energy radiated as EM is dependent on the proximity of the electron to the nucleus, up to a maximum of nearly 100% for a direct hit. As accelerating potential is increased, a greater proportion of input energy is converted to x-rays as opposed to heat, such that:

$$Efficiency = 9 \times 10^{-10} \cdot V \cdot Z$$

[16]. Where V is the accelerating potential and Z is the target material atomic number. For a tungsten anode (Z=74), the efficiency ranges from 3.33 x $10^{-3}$ at 50 kV, to 5.33 x $10^{-3}$ at 80 kV. Alongside increased production efficiency, high-energy x-rays are more likely to pass through the tube filtration (both added and inherent). Thus increasing tube potential increases both the energy of x-rays produced and also the intensity.

With regard to the second process of x-ray production - characteristic emissions - the K-edge for tungsten is 73.9 keV [16]. For tube potentials below 74 kV, x-ray output is essentially entirely due to Bremsstrahlung. Due to the impact of inherent (i.e. the tube housing materials) and added filtration of at least 2.5 mm Al equivalent, photons below around 15 keV are entirely removed from the beam [16] and thus play no role in patient interactions. This is desirable, and indeed mandatory, as such low energy photons would add to patient skin dose while contributing nothing to image formation [16]. With further filtration, often with copper (Cu), higher energy photons are removed from the beam, restricting the spectrum to 30 keV or above.

Projection terminology

The beam angles used in x-ray imaging are known as *projections*, and are described by a particular vocabulary, which will be described here:

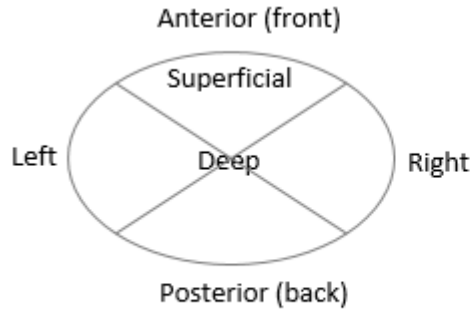


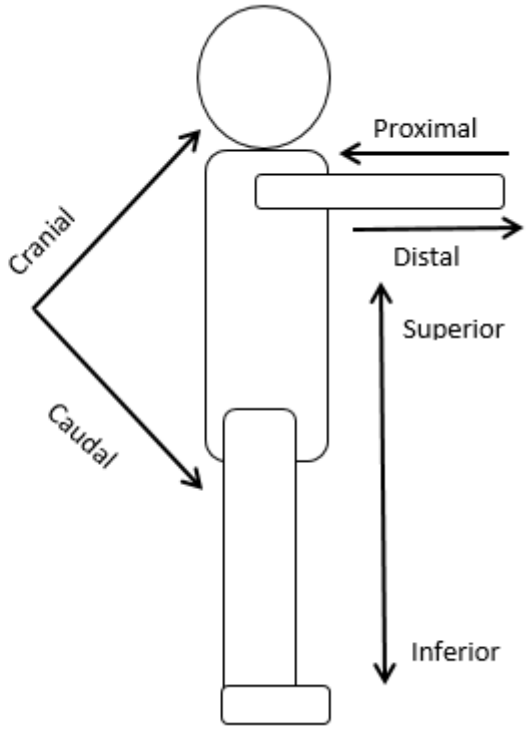


For example, the heart is deep to the skin, while the wrist is distal to the elbow, the knee is proximal to the ankle. The words Cranial and caudal (literally towards the tail) refer to the direction of the beam from source to detector.

The diagram below shows rotational beam angle notation as used in PCXMC, Cardiodose and in Figures showing variation in dose with beam angle in Chapter 4. The arrows denote the direction the x-rays travel in. Thus a 90° rotational angle denotes x-rays entering the posterior and exiting the anterior of the patient, i.e. a posterior-anterior (PA) projection.

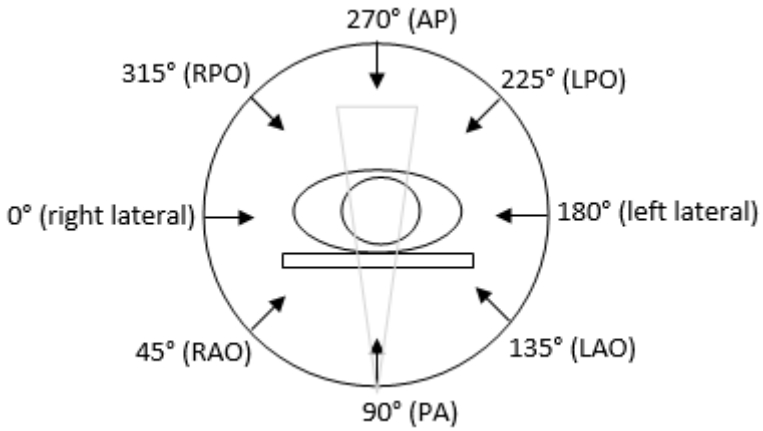


AP=anterior-posterior, LPO=left posterior oblique, RPO=right posterior oblique, RAO=right anterior oblique, LAO=left anterior oblique. The diagram below shows angulation in the cranio-caudal direction. In PCXMC, negative cranio-caudal angulation refers to what is widely regarded as 'cranial' angulation, though in PCXMC, this is referred to as 'caudal x-ray tube'. Likewise, what is widely referred to as 'caudal angulation' is called 'cranial x-ray tube' in PCXMC. This discrepancy has been accounted for in dose calculations.

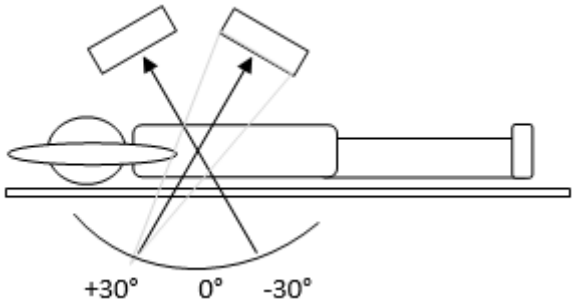


Rotational and cranio-caudal beam angulations can be combined. For example, the 'LAO 40, CAU 25' projection, used in coronary angiography implies a rotational angle of 130° (i.e. 90° plus 40°), combined with 25° degrees of angulation in the caudal direction (i.e. +25° in PCXMC and Cardiodose).

## References:


1. Lock J. Cardiac Catheterization. In: Keane J, Lock, JE, Fyler, DC, editor. NADAS' pediatric cardiology. 2 ed. Philadelphia: Elsevier; 2006.
2. Qureshi S, Redington A, Wren C, Ostman-Smith I, Patel J, Gibbs R, et al. Recommendations of the British Paediatric Cardiac Association for the Therapeutic Cardiac Catheterization in Congenital Heart Disease: British Paediatric Cardiac Association.2012.
3. Committee to Assess Health Risks from Exposure to Low Levels of Ionizing Radiation. Health Risks from Exposures to Low Levels of Ionizing Radiation: BEIR VII Phase 2. Washington D.C: National Research Council of the National Academies2006.
4. Spengler R, Cook D, Clarke E, Olley P, Newman A. Cancer mortality following cardiac catheterization: a preliminary follow-up study on 4,891 irradiated children. Pediatrics. 1983;71(2):235-9.
5. McLaughlin JR, Kreiger N, Sloan MP, Benson LN, Hilditch S, Clarke EA. An historical cohort study of cardiac catheterization during childhood and the risk of cancer. International Journal of Epidemiology. 1993;22(4):584-91.
6. Modan B, Keinan L, Blumstein T, Sadetzki S. Cancer following cardiac catheterization in childhood. International Journal of Epidemiology. 2000;29(3):424-28.
7. Ozasa K, Shimizu Y, Suyama A, Kasagi F, Soda M, Grant EJ, et al. Studies of the mortality of atomic bomb survivors, report 14, 1950-2003: An overview of cancer and noncancer diseases. Radiation Research. 2012;177(3):229-43.
8. Bacher K, Bogaert E, Lapere R, De Wolf D, Thierens H. Patient-specific dose and radiation risk estimation in paediatric cardiac catheterization. Circulation. 2004;111:83-89.
9. Pearce MS, Salotti JA, Little MP, McHugh K, Lee C, Kim KP, et al. Radiation exposure from CT scans in childhood and subsequent risk of leukaemia and brain tumours: a retrospective cohort study. Lancet. 2012;380(9840):499-505.
10. Neofotistou V. Review of patient dosimetry in cardiology. Radiation Protection Dosimetry. 2001;94(1-2):177-82.
11. Pantos I, Patatoukas G, Katritsis D, Efstathopoulos E. Patient Radiation Doses in Interventional Cardiology Procedures. Current Cardiology Reviews. 2009;5(1):1-11.
12. Beels L, Bacher K, De Wolf D, Werbrouck J, Thierens H. γ-H2AX foci as a biomarker for patient X-ray exposure in pediatric cardiac catheterization: Are we underestimating radiation risks? Circulation. 2009;120(19):1903-09.
13. Ait-Ali L, Andreassi M, Foffa I, Spadoni I, Vano E, Picano E. Cumulative patient effective dose and acute radiation-induced chromosomal DNA damage in children with congenital heart disease. Heart. 2010;96:269-74.
14. Geisel D ZE, Rief M, Greupner J, Laule M, Knebel F, Hamm B, Dewey M. DNA double-strand breaks as potential indicators for the biological effects of ionising radiation exposure from cardiac CT and conventional coronary angiography: a randomised, controlled study. Eur Radiol. 2012;22:1641-50.
15. Monell S. Manual of static electricity in x-ray and therapuetic uses. New York: William Beverley Harison, 1897.
16. Busburg J, Siebert J, Leidholdt EJ, Boone J. The Essential Physics of Medical Imaging. 3rd ed. Philadelphia: Lippincott Williams and Wilkins, 2011.
17. Morrish O, Dendy P. Physics for Diagnostic Radiology. 3rd ed: CRC Press; 2011.
18. Dance DR, Evans S, Skinner CL, Bradley A. Diagnostic Radiology with X-rays. In: Flower M, editor. Webb's Physics of Medical Imaging. 2nd ed: Taylor & Francis/CRC Press; 2012.
19. Seibert JA. Flat-panel detectors: how much better are they? Pediatric radiology. 2006;36 Suppl 2:173-81.
20. Cowen AR. Flat-panel Solid-state Digital Radiography. University of Leeds 2010.
21. Trianni A, Bernardi G, Padovani R. Are new technologies always reducing patient doses in cardiac procedures? Radiat Prot Dosimetry. 2005;117(1-3):97-101.

22. Smith BG, Tibby SM, Qureshi SA, Rosenthal E, Krasemann T. Quantification of temporal, procedural, and hardware-related factors influencing radiation exposure during pediatric cardiac catheterization. Catheterization and Cardiovascular Interventions. 2012;80(6):931-36.
23. Block J. Product Overview: Siemens Axiom Artis Interventional Lab. 2012 [17/02/2015]; Available from: http://info.blockimaging.com/bid/90573/Product-Overview-Siemens-Axiom-Artis-Interventional-Lab.
24. Julian D, Campbell Cowan J, McLenachan J. Cardiology. 8 ed: Elsevier Saunders, 2005.
25. Seierstad T, Friberg EG, Lervag C, Widmark A, Wilhelmsen N, Stranden E. Radiation doses to Norwegian heart-transplanted patients undergoing annual coronary angiography. Radiat Prot Dosimetry. 2012;149(4):403-9.
26. Cooper LT, Baughman KL, Feldman AM, Frustaci A, Jessup M, Kuhl U, et al. The role of endomyocardial biopsy in the management of cardiovascular disease: a scientific statement from the American Heart Association, the American College of Cardiology, and the European Society of Cardiology. Endorsed by the Heart Failure Society of America and the Heart Failure Association of the European Society of Cardiology. Journal of the American College of Cardiology. 2007;50(19):1914-31.
27. Choi D, Kim N, Jung M, Kim S. The Results of Transcatheter Occlusion of Patent Ductus Arteriosus: Success Rate and Complications Over 12 Years in a Single Center. Korean Circ J. 2010;40(230-234).
28. Bilkis AA, Alwi M, Hasri S, Haifa AL, Geetha K, Rehman MA, et al. The Amplatzer duct occluder: experience in 209 patients. Journal of the American College of Cardiology. 2001;37(1):258-61.
29. King TD, Thompson SL, Steiner C, Mills NL. Secundum atrial septal defect. Nonoperative closure during cardiac catheterization. JAMA. 1976;235(23):2506-9.
30. Du ZD, Hijazi ZM, Kleinman CS, Silverman NH, Larntz K. Comparison between transcatheter and surgical closure of secundum atrial septal defect in children and adults: results of a multicenter nonrandomized trial. Journal of the American College of Cardiology. 2002;39(11):1836-44.
31. Rashkind WJ, Miller WW. Creation of an atrial septal defect without thoracotomy. A palliative approach to complete transposition of the great arteries. JAMA. 1966;196(11):991-2.
32. Redington A, Booth P, Shore D, Rigby M. Primary balloon dilatation of coarctation of the aorta in neonates. Br Heart J. 1990;64(4):277-81.
33. Sreeram I, Sreeram N, Bennink G. Palliative stent implantation for coarctation in neonates and young infants. . Ann Pediatr Cardiol. 2012;5(2):145-50.
34. Van Son J, Falk V, Schneider P, Smedts F, Mohr F. Repair of coarctation of the aorta in neonates and young infants. J Card Surg. 1997;12(3):139-46.
35. Lock JE, Bass JL, Amplatz K, Fuhrman BP, Castaneda-Zuniga W. Balloon dilation angioplasty of aortic coarctations in infants and children. Circulation. 1983;68(1):109-16.
36. Kan JS, White RI, Jr., Mitchell SE, Gardner TJ. Percutaneous balloon valvuloplasty: a new method for treating congenital pulmonary-valve stenosis. N Engl J Med. 1982;307(9):540-2.
37. Lababidi Z, Wu JR, Walls JT. Percutaneous balloon aortic valvuloplasty: results in 23 patients. Am J Cardiol. 1984;53(1):194-7.
38. Lock JE, Niemi T, Einzig S, Amplatz K, Burke B, Bass JL. Transvenous angioplasty of experimental branch pulmonary artery stenosis in newborn lambs. Circulation. 1981;64(5):886-93.
39. Lock JE, Castaneda-Zuniga WR, Fuhrman BP, Bass JL. Balloon dilation angioplasty of hypoplastic and stenotic pulmonary arteries. Circulation. 1983;67(5):962-7.
40. Parsonnet V. A lifetime pacemaker revisited. N Engl J Med. 2007;357(25):2638-9.
41. Parsonnet V, Driller J, Cook D, Rizvi SA. Thirty-one years of clinical experience with "nuclear-powered" pacemakers. Pacing and clinical electrophysiology : PACE. 2006;29(2):195-200.
42. Chauvel C, Lavergne T, Cohen A, Ducimetiere P, Le Heuzey JY, Valty J, et al. Radioisotopic pacemaker: long-term clinical results. Pacing and clinical electrophysiology : PACE. 1995;18(2):286-92.

43. Khan F. The Physics of Radiation Therapy. 3 ed. Philadelphia: Lippincott Williams and Wilkins, 2003.
44. International Commission on Radiological Protection (ICRP). ICRP Publication 103. The 2007 recommendations of the International Commission on Radiological Protection.2007.
45. United Nations Scientific Committee on the Effects of Atomic Radiation (UNSCEAR). UNSCEAR 2006 Report - Effects of ionizing radiation Annex A: United Nations, 2006.
46. Brenner DJ, Doll R, Goodhead DT, Hall EJ, Land CE, Little JB, et al. Cancer risks attributable to low doses of ionizing radiation: Assessing what we really know. Proceedings of the National Academy of Sciences of the United States of America. 2003;100(SUPPL. 2):13761-66.
47. Wall BF, Kendall GM, Edwards AA, Bouffler S, Muirhead CR, Meara JR. What are the risks from medical X-rays and other low dose radiation? Br J Radiol. 2006;79(940):285-94.
48. Muller H, Mott-Smith L. The frequency of translocations produced by x-rays in Drosophila. Genetics. 1930;15:283–331.
49. Calabrese EJ, O'Connor MK. Estimating Risk of Low Radiation Doses - A Critical Review of the BEIR VII Report and its Use of the Linear No-Threshold (LNT) Hypothesis. Radiat Res. 2014;182(5):463-74.
50. United Nations Scientific Committee on the Effects of Atomic Radiation (UNSCEAR). Hereditary effects of radiation. New York, NY, 2001.
51. The National Lottery. The National Lottery in numbers. [24/11/2014]; Available from: https://www.national-lottery.co.uk/life-changing/project-interesting-numbers.
52. The Royal College of Radiologists. iRefer: Making the best use of clinical radiology. 7th ed2012.
53. Berrington de González A, Darby S. Risk of cancer from diagnostic X-rays: estimates for the UK and 14 other countries. Lancet. 2004;363(9406):345-51.
54. Little MP, Wakeford R, Tawn EJ, Bouffler SD, Berrington de Gonzalez A. Risks associated with low doses and low dose rates of ionizing radiation: why linearity may be (almost) the best we can do. Radiology. 2009;251(1):6-12.
55. Tubiana M, Feinendegen LE, Yang C, Kaminski JM. The linear no-threshold relationship is inconsistent with radiation biologic and experimental data. Radiology. 2009;251(1):13-22.
56. Socol Y, Dobrzynski L, Doss M, Feinendegen LE, Janiak MK, Miller ML, et al. Commentary: ethical issues of current health-protection policies on low-dose ionizing radiation. Dose-response : a publication of International Hormesis Society. 2014;12(2):342-8.
57. Doss M, Little MP, Orton CG. Point/Counterpoint: low-dose radiation is beneficial, not harmful. Med Phys. 2014;41(7):070601.
58. Busby C. Aspects of DNA Damage from Internal Radionuclides, New Research Directions in DNA Repair, Prof. Clark Chen (Ed.). 2013; Available from: http://www.intechopen.com/books/new-research-directions-in-dna-repair/aspects-of-dna-damage-from-internal-radionuclides.
59. Aurengo A, Averbeck D, Bonnin A, Le Guen B, Masse R, Monier R, et al. Dose-effect relationships and estimation of the carcinogenic effects of low doses of ionizing radiation: Académie des Sciences [Academy of Sciences] - Académie nationale de Médecine [National Academy of Medicine]2005.
60. Department of Health. Ionising Radiation (Medical Exposure) Regulations. 2000 [cited 2013 03/05]; Available from: http://www.legislation.gov.uk/uksi/2000/1059/contents/made.
61. International Commission on Radiation Units and Measurements (ICRU). Quantities and units for measurement and calculation in medical x-ray imaging. Journal of the ICRU. 2005;5(2).
62. International Commission on Radiation Units and Measurements (ICRU). Fundamental Quantities and Units for Ionizing Radiation. ICRU report 60. Bethesda, Maryland, USA1998.
63. Brenner DJ, Huda W. Effective Dose: A Useful Concept in Diagostic Radiology? Radiation Protection Dosimetry. 2008;128(4):503-08.
64. United Nations Scientific Committee on the Effects of Atomic Radiation (UNSCEAR). Sources and Effects of Ionizing Radiation. 2008 Report to the General Assembly. Annex 1: Medical Radiation Exposures. New York: United Nations2008.

65. Feinendegen L. The cell dose concept; potential application in radiation protection. Phys Med Biol. 1990;35(5):597-612.
66. International Commission on Radiation Units and Measurements. Report 86: Quantification and Reporting of Low-Dose and other Heterogeneous Exposures. Options for Characterizing Energy Deposition.2011 Contract No.: 2.
67. International Commission on Radiological Protection (ICRP). ICRP Publication 60: Recommendations of the International Commission on Radiological Protection. Oxford.
68. Martin CJ. Interaction of ionising radiations with matter. In: C.J Martin DGS, editor. Practical Radiation Protection in Healthcare: Oxford University Press; 2002.
69. Seuntjens JP, Strydom W, KR. S. Dosimetric Principles, Quantities and Units. In: EB P, editor. Radiation Oncology Physics:A Handbook for Teachers and Students. Vienna: International atomic energy agency.; 2005.
70. International Commission on Radiation Units and Measurements. Patient dosimetry for x rays used in medical imaging. ICRU Report 742005 Contract No.: 2.
71. M Boutillon AMP-R. Re-evaluation of the W value for electrons in dry air. Phys Med Biol 32 213. 1987;32(2):213-19.
72. Toroi P, Komppa T, Kosunen A. A tandem calibration method for kerma–area product meters. Phys Med Biol 2008;53:4941–58.
73. Wagner LK, Fontenla DP, Kimme-Smith C, Rothenberg LN, Shepard J, Boone JM. Recommendations on performance characteristics of diagnostic exposure meters: report of AAPM Diagnostic X-Ray Imaging Task Group No. 6. Med Phys. 1992;19(1):231-41.
74. Balter S. Methods for measuring fluoroscopic skin dose. Pediatric radiology. 2006;36 Suppl 2:136-40.
75. International Electrotechnical Commission. International Standard 60580: Medical electrical equipment – Dose area product meters. Geneva: International Electrotechnical Commission,2000.
76. International Atomic Energy Agency. Dosimetry in Diagnostic Radiology: An International Code of Practice. Vienna: IAEA2007.
77. Poyry P, Komppa T, Kosunen A, editors. Calibration of dose-area product meters for diagnostic x-ray beams. ProcXXXIX Ann Conf Finnish Phys Soc; 2005; Espoo, Finland.
78. Toroi P, Komppa T, Kosunen A, Tapiovaara M. Effects of radiation quality on the calibration of kerma-area product meters in x-ray beams. Phys Med Biol. 2008;53(18):5207-21.
79. International Electrotechnical Commission. IEC report 60601. Medical electrical equipment – Part 2-43: particular requirements for the safety of x-ray equipment for interventional procedures. Geneva: International Electrotechnical Commission2000.
80. Petoussi-Henss N, Zankl M, Drexler G, Panzer W, Regulla D. Calculation of backscatter factors for diagnostic radiology using Monte Carlo methods. Phys Med Biol. 1998;43(8):2237-50.
81. Johnson PB, Borrego D, Balter S, Johnson K, Siragusa D, Bolch WE. Skin dose mapping for fluoroscopically guided interventions. Med Phys. 2011;38(10):5490-9.
82. Verghese GR, McElhinney DB, Strauss KJ, Bergersen L. Characterization of radiation exposure and effect of a radiation monitoring policy in a large volume pediatric cardiac catheterization lab. Catheterization and cardiovascular interventions : official journal of the Society for Cardiac Angiography & Interventions. 2012;79(2):294-301.
83. Ghelani SJ, Glatz AC, David S, Leahy R, Hirsch R, Armsby LB, et al. Radiation dose benchmarks during cardiac catheterization for congenital heart disease in the United States. JACC Cardiovascular interventions. 2014;7(9):1060-9.
84. Axelsson B, Khalil C, Lidegran M, Schuwer P, Mortensson W. Estimating the effective dose to children undergoing heart investigations - a phantom study. British Journal of Radiology. 1999;72:378-83.
85. Schultz FW, Geleijns J, Spoelstra FM, Zoetelief J. Monte Carlo calculations for assessment of radiation dose to patients with congenital heart defects and to staff during cardiac catheterizations. The British journal of radiology. 2003;76(909):638-47.

86. Schmidt PW, Dance DR, Skinner CL, Castellano Smith IA, McNeill JG. Conversion factors for the estimation of effective dose in paediatric cardiac angiography. Phys Med Biol. 2000;45(10):3095-107.
87. Stern S, Rosenstein M, Renaud L. HHS Publication FDA 95-82: Handbook of selected tissue doses for fluoroscopic and cineangiographic examination of the coronary arteries (in SI units). In: US Department of Health and Human Sciences PHS, Food and Drug Administration., editor. Rockville, Maryland, 1995.
88. Struelens L, Vanhavere F, Bacher K, Thierens H. DAP to effective dose conversion in cardiology and vascular/interventional radiology: FCK/University of Ghent, 2012.
89. Johnson JN, Hornik CP, Li JS, Benjamin DK, Jr., Yoshizumi TT, Reiman RE, et al. Cumulative radiation exposure and cancer risk estimation in children with heart disease. Circulation. 2014;130(2):161-7.
90. Clay MA, Campbell RM, Strieper M, Frias PA, Stevens M, Mahle WT. Long-term risk of fatal malignancy following pediatric radiofrequency ablation. Am J Cardiol. 2008;102(7):913-5.
91. Glatz AC, Patel A, Zhu X, Dori Y, Hanna BD, Gillespie MJ, et al. Patient Radiation Exposure in a Modern, Large-Volume, Pediatric Cardiac Catheterization Laboratory. Pediatr Cardiol. 2014;35(5):870-8.
92. Barnaoui S, Rehel JL, Baysson H, Boudjemline Y, Girodon B, Bernier MO, et al. Local Reference Levels and Organ Doses From Pediatric Cardiac Interventional Procedures. Pediatr Cardiol. 2014;35(6):1037-45.
93. McFadden S, Hughes C, D'Helft CI, McGee A, Rainford L, Brennan PC, et al. The establishment of local diagnostic reference levels for paediatric interventional cardiology. Radiography. 2013;19(4):295-301.
94. Martinez LC, Vano E, Gutierrez F, Rodriguez C, Gilarranz R, Manzanas MJ. Patient doses from fluoroscopically guided cardiac procedures in pediatrics. Phys Med Biol. 2007;52(16):4749-59.
95. Barrett HH, Myers KJ, Hoeschen C, Kupinski MA, Little MP. Task-based measures of image quality and their relation to radiation dose and patient risk. Phys Med Biol. 2015;60(2):R1-75.
96. Seibert JA. Tradeoffs between image quality and dose. Pediatric radiology. 2004;34 Suppl 3:S183-95; discussion S234-41.
97. Samei E, Ranger NT, MacKenzie A, Honey ID, Dobbins JT, 3rd, Ravin CE. Detector or system? Extending the concept of detective quantum efficiency to characterize the performance of digital radiographic imaging systems. Radiology. 2008;249(3):926-37.
98. Nickoloff EL. AAPM/RSNA physics tutorial for residents: physics of flat-panel fluoroscopy systems: Survey of modern fluoroscopy imaging: flat-panel detectors versus image intensifiers and more. Radiographics : a review publication of the Radiological Society of North America, Inc. 2011;31(2):591-602.
99. Bernhardt P, Lendl M, Deinzer F. New technologies to reduce pediatric radiation doses. Pediatric radiology. 2006;36 Suppl 2:212-5.
100. Fryback DG, Thornbury JR. The efficacy of diagnostic imaging. Med Decis Making. 1991;11(2):88-94.
101. Thornbury JR. Eugene W. Caldwell Lecture. Clinical efficacy of diagnostic imaging: love it or leave it. AJR Am J Roentgenol. 1994;162(1):1-8.
102. Borik S, Devadas S, Mroczek D, Jin Lee K, Chaturvedi R, Benson LN. Achievable radiation reduction during pediatric cardiac catheterization: How low can we go? Catheterization and cardiovascular interventions : official journal of the Society for Cardiac Angiography & Interventions. 2015.
103. Onnasch DG, Schroder FK, Fischer G, Kramer HH. Diagnostic reference levels and effective dose in paediatric cardiac catheterization. Br J Radiol. 2007;80(951):177-85.
104. Khong PL, Ringertz H, Donoghue V, Frush D, Rehani M, Appelgate K, et al. ICRP publication 121: radiological protection in paediatric diagnostic and interventional radiology. Ann ICRP. 2013;42(2):1-63.

105. Sutton NJ, Lamour J, Gellis LA, Pass RH. Pediatric patient radiation dosage during endomyocardial biopsies and right heart catheterization using a standard "ALARA" radiation reduction protocol in the modern fluoroscopic era. Catheterization and cardiovascular interventions : official journal of the Society for Cardiac Angiography & Interventions. 2014;83(1):80-3.
106. Gellis LA, Ceresnak SR, Gates GJ, Nappo L, Pass RH. Reducing patient radiation dosage during pediatric SVT ablations using an "ALARA" radiation reduction protocol in the modern fluoroscopic era. Pacing and clinical electrophysiology : PACE. 2013;36(6):688-94.
107. Yakoumakis E, Kostopoulou H, Makri T, Dimitriadis A, Georgiou E, Tsalafoutas I. Estimation of radiation dose and risk to children undergoing cardiac catheterization for the treatment of a congenital heart disease using Monte Carlo simulations. Pediatric radiology. 2013;43(3):339-46.
108. Rassow J, Schmaltz A, Hentrich F, Streffer C. Effective dose to patients from paediatric cardiac catheterizations. British Journal of Radiology. 2000;73:172-83.
109. Le Heron JC. Estimation of effective dose to the patient during medical x-ray examinations from measurements of the dose-area product. Phys Med Biol. 1992;37(11):2117-26.
110. Scott-Moncrieff A, Yang J, Levine D, Taylor C, Tso D, Johnson M, et al. Real-World Estimated Effective Radiation Doses From Commonly Used Cardiac Testing and Procedural Modalities. Canadian Journal of Cardiology. 2011;27:613-18.
111. Gherardi GG, Iball GR, Darby MJ, Thomson JD. Cardiac computed tomography and conventional angiography in the diagnosis of congenital cardiac disease in children: recent trends and radiation doses. Cardiology in the young. 2011;21(6):616-22.
112. Karambatsakidou A, Sahlgren B, Hansson B, Lidegran M, Fransson A. Effective dose conversion factors in paediatric interventional cardiology. Br J Radiol. 2009;82(981):748-55.
113. El Sayed MH, Roushdy AM, El Farghaly H, El Sherbini A. Radiation exposure in children during the current era of pediatric cardiac intervention. Pediatric Cardiology. 2012;33(1):27-35.
114. Song S, Liu C, Zhang M. Radiation dose and mortality risk to children undergoing therapeutic interventional cardiology. Acta radiologica (Stockholm, Sweden : 1987). 2014.
115. Yakoumakis EN, Gialousis GI, Papadopoulou D, Makri T, Pappouli Z, Yakoumakis N, et al. Estimation of children's radiation dose from cardiac catheterisations, performed for the diagnosis or the treatment of a congenital heart disease using TLD dosimetry and Monte Carlo simulation. Journal of radiological protection : official journal of the Society for Radiological Protection. 2009;29(2):251-61.
116. Kawasaki T, Fujii K, Akahane K. Estimation of Organ and Effective Doses for Neonate and Infant Diagnostic Cardiac Catheterizations. AJR Am J Roentgenol. 2015;205(3):599-603.
117. Rothkamm K, Löbrich M. Evidence for a lack of DNA double-strand break repair in human cells exposed to very low X-ray doses. Proc Natl Acad Sci USA 2003;100(9):5057-62.
118. Mah LJ, Orlowski C, Ververis K, Vasireddy RS, El-Osta A, Karagiannis TC. Evaluation of the efficacy of radiation-modifying compounds using gammaH2AX as a molecular marker of DNA double-strand breaks. Genome integrity. 2011;2(1):3.
119. Ojima M, Furutani A, Ban N, Kai M. Persistence of DNA double-strand breaks in normal human cells induced by radiation-induced bystander effect. Radiat Res. 2011;175(1):90-6.
120. Collis S, Schwaninger J, Ntambi A, Keller T, Nelson W, Dillehay L, et al. Evasion of early cellular response mechanisms following low level radiationinduced DNA damage. . J Biol Chem. 2004;Nov 26;279(48):49624-32.
121. Grudzenski S RA, Conrad S, Rübe C, Löbrich M. . Inducible response required for repair of low dose radiation damage in human fibroblasts. Cell Biol PNAS. 2010;107(32):14205-10.
122. Andreassi MG. Radiation risk from pediatric cardiac catheterization: friendly fire on children with congenital heart disease. Circulation. 2009;120(19):1847-9.
123. Zyuzikov NA, Coates PJ, Parry JM, Lorimore SA, Wright EG. Lack of nontargeted effects in murine bone marrow after low-dose in vivo X irradiation. Radiat Res. 2011;175(3):322-7.

124. Mathews JD, Forsythe AV, Brady Z, Butler MW, Goergen SK, Byrnes GB, et al. Cancer risk in 680,000 people exposed to computed tomography scans in childhood or adolescence: data linkage study of 11 million Australians. BMJ (Clinical research ed). 2013;346:f2360.
125. Weiss HA, Darby SC, Doll R. Cancer mortality following x-ray treatment for ankylosing spondylitis. International Journal of Cancer. 1994;59(3):327-38.
126. Tao Z, Zha Y, Akiba S, Sun Q, Zou J, Li J, et al. Cancer mortality in the high background radiation areas of Yangjiang, China during the period between 1979 and 1995. J Radiat Res. 2000;41 Suppl:31-41.
127. Doss M. Linear No-Threshold Model VS. Radiation Hormesis. Dose-response : a publication of International Hormesis Society. 2013;11:480-97.
128. Muirhead CR. Exposure assessment: implications for epidemiological studies of ionizing radiation. Radiat Prot Dosimetry. 2008;132(2):134-8.
129. United Nations Scientific Committee on Atomic Radiation (UNSCEAR). Sources, effects and risks of Ionizing radiation, Volume II, Annex B: Effects of radiation exposure of children. New York: United Nations2013.
130. Gilbert ES. Ionising radiation and cancer risks: What have we learned from epidemiology? International Journal of Radiation Biology. 2009;85(6):467-82.
131. Radiation Effects Research Foundation (RERF). Introduction to the Radiation Effects Research Foundation 2007 Available from: http://www.rerf.jp/.
132. Schull WJ. Effects of Atomic Radiation: A Half-Century of Studies from Hiroshima and Nagasaki: Wiley-Liss 1995.
133. Muirhead CR. Studies on the Hiroshima and Nagasaki survivors, and their use in estimating radiation risks. Radiat Prot Dosimetry. 2003;104(4):331-5.
134. Preston DL, Pierce DA, Shimizu Y, Cullings HM, Fujita S, Funamoto S, et al. Effect of recent changes in atomic bomb survivor dosimetry on cancer mortality risk estimates. Radiation Research. 2004;162(4):377-89.
135. Preston D, Shimizu Y, Pierce D, Suyama A, Mabuchi K. Studies of mortality of atomic bomb survivors. Report 13: Solid cancer and noncancer disease mortality: 1950–1997. Radiat Res. 2003;160(4):381-4-7.
136. Kellerer AM, Rühm W, Walsh L. Indications of the neutron effect contribution in the solid cancer data of the A-bomb survivors. Health Physics. 2006;90(6):554-64.
137. Brenner DJ. Does fractionation decrease the risk of breast cancer induced by low-LET radiation? Radiat Res. 1999;151(2):225-9.
138. Heyes GJ, Mill AJ, Charles MW. Enhanced biological effectiveness of low energy X-rays and implications for the UK breast screening programme. Br J Radiol. 2006;79(939):195-200.
139. Cardis E, Vrijheid M, Blettner M, Gilbert E, Hakama M, Hill C, et al. Risk of cancer after low doses of ionising radiation - Retrospective cohort study in 15 countries. British Medical Journal. 2005;331(7508):77-80.
140. Wakeford R. Nuclear worker studies: promise and pitfalls. Br J Cancer. 2014;110(1):1-3.
141. Wakeford R. Radiation in the workplace-a review of studies of the risks of occupational exposure to ionising radiation. Journal of radiological protection : official journal of the Society for Radiological Protection. 2009;29(2A):A61-79.
142. Zablotska LB, Lane RS, Thompson PA. A reanalysis of cancer mortality in Canadian nuclear workers (1956-1994) based on revised exposure and cohort data. Br J Cancer. 2014;110(1):214-23.
143. Cardis E, Vrijheid M, Blettner M, Gilbert E, Hakama M, Hill C, et al. The 15-Country Collaborative Study of Cancer Risk among Radiation Workers in the Nuclear Industry: estimates of radiation-related cancer risks. Radiat Res. 2007;167(4):396-416.
144. Muirhead CR, O'Hagan JA, Haylock RG, Phillipson MA, Willcock T, Berridge GL, et al. Mortality and cancer incidence following occupational radiation exposure: third analysis of the National Registry for Radiation Workers. Br J Cancer. 2009;100(1):206-12.

145. Leuraud K, Richardson DB, Cardis E, Daniels RD, Gillies M, O'Hagan JA, et al. Ionising radiation and risk of death from leukaemia and lymphoma in radiation-monitored workers (INWORKS): an international cohort study. Lancet Haematol. 2015;2(7):e276-e81.
146. Richardson DB, Cardis E, Daniels RD, Gillies M, O'Hagan JA, Hamra GB, et al. Risk of cancer from occupational exposure to ionising radiation: retrospective cohort study of workers in France, the United Kingdom, and the United States (INWORKS). BMJ (Clinical research ed). 2015;351:h5359.
147. Schonfeld SJ, Krestinina LY, Epifanova S, Degteva MO, Akleyev AV, Preston DL. Solid cancer mortality in the techa river cohort (1950-2007). Radiat Res. 2013;179(2):183-9.
148. Bauer S, Gusev BI, Pivina LM, Apsalikov KN, Grosche B. Radiation exposure due to local fallout from Soviet atmospheric nuclear weapons testing in Kazakhstan: solid cancer mortality in the Semipalatinsk historical cohort, 1960-1999. Radiat Res. 2005;164(4 Pt 1):409-19.
149. Kendall GM, Little MP, Wakeford R, Bunch KJ, Miles JC, Vincent TJ, et al. A record-based case-control study of natural background radiation and the incidence of childhood leukaemia and other cancers in Great Britain during 1980-2006. Leukemia. 2013;27(1):3-9.
150. Wrixon AD, Green BMR, Lomas PR, Miles JCH, Cliff KD, EA F, et al. Report No: NRPB-R190: Natural Radiation Exposure in UK Dwellings. : National Radiological Protection Board:1998.
151. Spycher BD, Lupatsch JE, Zwahlen M, Roosli M, Niggli F, Grotzer MA, et al. Background ionizing radiation and the risk of childhood cancer: a census-based nationwide cohort study. Environ Health Perspect. 2015;123(6):622-8.
152. Boice Jr JD, Preston D, Davis FG, Monson RR. Frequent chest X-ray fluoroscopy and breast cancer incidence among tuberculosis patients in Massachusetts. Radiation Research. 1991;125(2):214-22.
153. Hrubec Z, Boice Jr JD, Monson RR, Rosenstein M. Breast cancer after multiple chest fluoroscopies: Second follow-up of Massachusetts women with tuberculosis. Cancer Research. 1989;49(1):229-34.
154. Davis FG, Boice Jr JD, Hrubec Z, Monson RR. Cancer mortality in a radiation-exposed cohort of Massachusetts tuberculosis patients. Cancer Research. 1989;49(21):6130-36.
155. Howe GR, McLaughlin J. Breast cancer mortality between 1950 and 1987 after exposure to fractionated moderate-dose-rate ionizing radiation in the canadian fluoroscopy cohort study and a comparison with breast cancer mortality in the atomic bomb survivors study. Radiation Research. 1996;145(6):694-707.
156. Howe GR. Lung cancer mortality between 1950 and 1987 after exposure to fractionated moderate-dose-rate ionizing radiation in the Canadian fluoroscopy cohort study and a comparison with lung cancer mortality in the atomic bomb survivors study. Radiation Research. 1995;142(3):295-304.
157. Gofman JW, Tamplin AR. Fluoroscopic radiation and risk of primary lung cancer following pneumothorax therapy of tuberculosis. Nature. 1970;227(5255):295-6.
158. Ronckers CM, Doody MM, Lonstein JE, Stovall M, Land CE. Multiple diagnostic X-rays for spine deformities and risk of breast cancer. Cancer Epidemiology Biomarkers and Prevention. 2008;17(3):605-13.
159. Hildreth NG, Shore RE, Hempelmann LH, Rosenstein M. Risk of extrathyroid tumors following radiation treatment in infancy for thymic enlargement. Radiation Research. 1985;102(3):378-91.
160. Shore RE, Woodard E, Hildreth N, Dvoretsky P, Hempelmann L, Pasternack B. Thyroid tumors following thymus irradiation. Journal of the National Cancer Institute. 1985;74(6):1177-84.
161. Shore RE, Hildreth N, Dvoretsky P, Pasternack B, Andresen E. Benign thyroid adenomas among persons X-irradiated in infancy for enlarged thymus glands. Radiation Research. 1993;134(2):217-23.
162. Shore RE, Hildreth N, Dvoretsky P, Andresen E, Moseson M, Pasternack B. Thyroid cancer among persons given x-ray treatment in infancy for an enlarged thymus gland. American Journal of Epidemiology. 1993;137(10):1068-80.

163. Seeram E. Computed Tomography: Physical Principles, Clinical Applications and Quality Control. 3 ed. St. Louis, Missouri: Saunders Elsevier, 2009.
164. Mettler FA, Jr., Huda W, Yoshizumi TT, Mahesh M. Effective doses in radiology and diagnostic nuclear medicine: a catalog. Radiology. 2008;248(1):254-63.
165. Goo HW. Current trends in cardiac CT in children. Acta radiologica (Stockholm, Sweden : 1987). 2013;54(9):1055-62.
166. Lee YW, Yang CC, Mok GS, Wu TH. Infant cardiac CT angiography with 64-slice and 256-slice CT: comparison of radiation dose and image quality using a pediatric phantom. PLoS One. 2012;7(11):e49609.
167. Watson T, Mah E, Schoepf U, King L, Huda W, Hlavacek A. Effective Radiation Dose in Computed Tomographic Angiography of the Chest and Diagnostic Cardiac Catheterization in Pediatric Patients. Pediatr Cardiol. 2012.
168. Leukaemia & Lymphoma Research. Myleodysplastic Syndromes (MDS) (patient information leaflet). Available online at https://leukaemialymphomaresearch.org.uk/booklet/myelodysplastic-syndromes-mds2012.
169. Preston DL, Ron E, Tokuoka S, Funamoto S, Nishi N, Soda M, et al. Solid cancer incidence in atomic bomb survivors: 1958-1998. Radiat Res. 2007;168(1):1-64.
170. Sadetzki S, Chetrit A, Freedman L, Stovall M, Modan B, Novikov I. Long-term follow-up for brain tumor development after childhood exposure to ionizing radiation for tinea capitis. Radiat Res. 2005;163(4):424-32.
171. Karlsson P, Holmberg E, Lundell M, Mattsson A, Holm LE, Wallgren A. Intracranial tumors after exposure to ionizing radiation during infancy: a pooled analysis of two Swedish cohorts of 28,008 infants with skin hemangioma. Radiat Res. 1998;150(3):357-64.
172. Berrington de González A, Gilbert E, Curtis R, Inskip P, Kleinerman R, Morton L, et al. Second solid cancers after radiation therapy: a systematic review of the epidemiologic studies of the radiation dose-response relationship. International journal of radiation oncology, biology, physics. 2013;86(2):224-33.
173. Neglia JP, Robison LL, Stovall M, Liu Y, Packer RJ, Hammond S, et al. New primary neoplasms of the central nervous system in survivors of childhood cancer: a report from the Childhood Cancer Survivor Study. J Natl Cancer Inst. 2006;98(21):1528-37.
174. Taylor AJ, Little MP, Winter DL, Sugden E, Ellison DW, Stiller CA, et al. Population-based risks of CNS tumors in survivors of childhood cancer: the British Childhood Cancer Survivor Study. J Clin Oncol. 2010;28(36):5287-93.
175. Little MP, de Vathaire F, Shamsaldin A, Oberlin O, Campbell S, Grimaud E, et al. Risks of brain tumour following treatment for cancer in childhood: modification by genetic factors, radiotherapy and chemotherapy. International journal of cancer Journal international du cancer. 1998;78(3):269-75.
176. Kutsenko A, Berrington de Gonzalez A, Curtis RE, Rajaraman P. Risk of second benign brain tumors among cancer survivors in the surveillance, epidemiology, and end results program. Cancer Causes Control. 2014;25(6):659-68.
177. Walsh L, Shore R, Auvinen A, Jung T, Wakeford R. Risks from CT scans-what do recent studies tell us? Journal of radiological protection : official journal of the Society for Radiological Protection. 2014;34(1):E1.
178. Boice JD, Jr. Radiation epidemiology and recent paediatric computed tomography studies. Ann ICRP. 2015;44(1 Suppl):236-48.
179. Evans DG. Neurofibromatosis type 2 (NF2): a clinical and molecular review. Orphanet journal of rare diseases. 2009;4:16.
180. Yates JR. Tuberous sclerosis. European journal of human genetics : EJHG. 2006;14(10):1065-73.

181. Meulepas JM, Ronckers CM, Merks J, Weijerman ME, Lubin JH, Hauptmann M. Confounding of the association between radiation exposure from CT scans and risk of leukemia and brain tumors by cancer susceptibility syndromes. Cancer Epidemiol Biomarkers Prev. 2015.
182. Braam KI, Overbeek A, Kaspers GJ, Ronckers CM, Schouten-van Meeteren AY, Van Dulmen-Den Broeder E, et al. Malignant melanoma as second malignant neoplasm in long-term childhood cancer survivors: a systematic review. Pediatr Blood Cancer. 2012;58(5):665-74.
183. Guerin S, Dupuy A, Anderson H, Shamsaldin A, Svahn-Tapper G, Moller T, et al. Radiation dose as a risk factor for malignant melanoma following childhood cancer. Eur J Cancer. 2003;39(16):2379-86.
184. Radiation Effects Research Foundation (RERF). Radiation Effects Research Foundation - a Brief Description 2008. Available from: http://www.rerf.jp/.
185. Harbron RW, Feltbower RG, Glaser A, Lilley J, Pearce MS. Secondary malignant neoplasms following radiotherapy for primary cancer in children and young adults. Pediatric hematology and oncology. 2014;31(3):259-67.
186. Huang WY, Muo CH, Lin CY, Jen YM, Yang MH, Lin JC, et al. Paediatric head CT scan and subsequent risk of malignancy and benign brain tumour: a nation-wide population-based cohort study. Br J Cancer. 2014.
187. Journy N, Rehel JL, Ducou Le Pointe H, Lee C, Brisse H, Chateil JF, et al. Are the studies on cancer risk from CT scans biased by indication? Elements of answer from a large-scale cohort study in France. Br J Cancer. 2015;112(1):185-93.
188. Cardis E, de Basea MB. Comment on 'Are the studies on cancer risk from CT scans biased by indication? Elements of answer from a large-scale cohort study in France'-Evidence of confounding by predisposing factors unclear. Br J Cancer. 2015;112(11):1842-3.
189. Muirhead CR. Response to 'Are the studies on cancer risk from CT scans biased by indication? Elements of answer from a large-scale cohort study in France'. Br J Cancer. 2015;112(11):1841-2.
190. Krille L, Dreger S, Schindel R, Albrecht T, Asmussen M, Barkhausen J, et al. Risk of cancer incidence before the age of 15 years after exposure to ionising radiation from computed tomography: results from a German cohort study. Radiat Environ Biophys. 2015;54(1):1-12.
191. Berrington de González A, Salotti J, McHugh K, Little M, Harbron R, Lee C, et al. The Relationship Between Pediatric CT Scans and Subsequent Risk of Leukemia and Brain Tumors: Assessment of The Impact of Underlying Conditions. British Journal of Cancer. 2015;In Press.
192. Mole RH. Childhood cancer after prenatal exposure to diagnostic X-ray examinations in Britain. British Journal of Cancer. 1990;62(1):152-68.
193. Doll R, Wakeford R. Risk of childhood cancer from fetal irradiation. British Journal of Radiology. 1997;70(FEB.):130-39.
194. Wakeford R, Little MP. Risk coefficients for childhood cancer after intrauterine irradiation: a review. Int J Radiat Biol. 2003;79(5):293-309.
195. Schonfeld SJ, Tsareva YV, Preston DL, Okatenko PV, Gilbert ES, Ron E, et al. Cancer mortality following in utero exposure among offspring of female mayak worker cohort members. Radiation Research. 2012;178(3):160-65.
196. Little MP. Heterogeneity of variation of relative risk by age at exposure in the Japanese atomic bomb survivors. Radiation and Environmental Biophysics. 2009;48(3):253-62.
197. Shuryak I, Sachs R, Brenner D. Cancer Risks After Radiation Exposure in Middle Age. JNCI. 2010;102(21):1628-36.
198. Walsh L. Heterogeneity of variation of relative risk by age at exposure in the Japanese atomic bomb survivors. Radiat Environ Biophys. 2009;48(3):345-7.
199. Diallo I, Haddy N, Adjadj E, Samand A, Quiniou E, Chavaudra J, et al. Frequency distribution of second solid cancer locations in relation to the irradiated volume among 115 patients treated for childhood cancer. International journal of radiation oncology, biology, physics. 2009;74(3):876-83.

200. Gold DG, Neglia JP, Dusenbery KE. Second neoplasms after megavoltage radiation for pediatric tumors. Cancer. 2003;97(10):2588-96.
201. Jenkinson HC, Hawkins MM, Stiller CA, Winter DL, Marsden HB, Stevens MC. Long-term population-based risks of second malignant neoplasms after childhood cancer in Britain. Br J Cancer. 2004;91(11):1905-10.
202. Cancer Research UK. Cancer Incidence by Age. [cited 2013 20/05]; Available from: http://www.cancerresearchuk.org/cancer-info/cancerstats/incidence/age/.
203. Curado MP EB, Shin HR, Storm H, Ferlay J, Heanue M and Boyle P. IARC Scientific Publication No. 160: Cancer Incidence in Five Continents Vol. IX, 2007.
204. Hickman RO, Buckner CD, Clift RA, Sanders JE, Stewart P, Thomas ED. A modified right atrial catheter for access to the venous system in marrow transplant recipients. Surg Gynecol Obstet. 1979;148(6):871-5.
205. Hoshal VL, Jr. Total intravenous nutrition with peripherally inserted silicone elastomer central venous catheters. Arch Surg. 1975;110(5):644-6.
206. World Health Organisation. BMI classification. [cited 2013 11/09]; Available from: http://apps.who.int/bmi/index.jsp?introPage=intro_3.html.
207. Kobayashi D, Meadows J, Forbes TJ, Moore P, Javois AJ, Pedra CA, et al. Standardizing radiation dose reporting in the pediatric cardiac catheterization laboratory-A multicenter study by the CCISC (Congenital Cardiovascular Interventional Study Consortium). Catheterization and cardiovascular interventions : official journal of the Society for Cardiac Angiography & Interventions. 2014.
208. Lilliefors H. On the Kolmogorov-Smirnov test for the exponential distribution with mean unknown. Journal of the American Statistical Association,. 1969;64:387-89.
209. Schmauss D, Weis M. Cardiac allograft vasculopathy: recent developments. Circulation. 2008;117(16):2131-41.
210. Children's Heart Federation. Heart Transplants. 2015 [17/09/2015]; Available from: http://www.chfed.org.uk/how-we-help/information-service/caring-for-heart-children/heart-transplants/.
211. Dipchand AI, Kirk R, Edwards LB, Kucheryavaya AY, Benden C, Christie JD, et al. The Registry of the International Society for Heart and Lung Transplantation: Sixteenth Official Pediatric Heart Transplantation Report--2013; focus theme: age. The Journal of heart and lung transplantation : the official publication of the International Society for Heart Transplantation. 2013;32(10):979-88.
212. Malt EA, Dahl RC, Haugsand TM, Ulvestad IH, Emilsen NM, Hansen B, et al. Health and disease in adults with Down syndrome. Tidsskr Nor Laegeforen. 2013;133(3):290-4.
213. Tennant PW, Pearce MS, Bythell M, Rankin J. 20-year survival of children born with congenital anomalies: a population-based study. Lancet. 2010;375(9715):649-56.
214. Samanek M, Voriskova M. Congenital heart disease among 815,569 children born between 1980 and 1990 and their 15-year survival: a prospective Bohemia survival study. Pediatric Cardiology. 1999;20(6):411-7.
215. British Heart Foundation. Understanding your child's heart Hypoplastic left heart. In: BHF, editor. London2010.
216. British Heart Foundation. Understanding your child's heart Pulmonary atresia with intact ventricular septum. London2010.
217. Tapiovaara MJ, Sandborg M, Dance DR. A search for improved technique factors in paediatric fluoroscopy. Phys Med Biol. 1999;44(2):537-59.
218. Davies AG, Gislason-Lee AJ, Cowen AR, Kengyelics SM, Lupton M, Moore J, et al. Does the use of additional X-ray beam filtration during cine acquisition reduce clinical image quality and effective dose in cardiac interventional imaging? Radiat Prot Dosimetry. 2014;162(4):597-604.
219. Brosi P, Stuessi A, Verdun FR, Vock P, Wolf R. Copper filtration in pediatric digital X-ray imaging: its impact on image quality and dose. Radiol Phys Technol. 2011;4(2):148-55.

220. Bokou C, Schreiner-Karoussou A, Breisch R, Beissel J. Changing from image intensifier to flat detector technology for interventional cardiology procedures: a practical point of view. Radiat Prot Dosimetry. 2008;129(1-3):83-6.
221. Davies AG, Cowen AR, Kengyelics SM, Moore J, Sivananthan MU. Do flat detector cardiac X-ray systems convey advantages over image-intensifier-based systems? Study comparing X-ray dose and image quality. Eur Radiol. 2007;17(7):1787-94.
222. McFadden SL, Hughes CM, Mooney RB, Winder RJ. An analysis of radiation dose reduction in paediatric interventional cardiology by altering frame rate and use of the anti-scatter grid. Journal of radiological protection : official journal of the Society for Radiological Protection. 2013;33(2):433-43.
223. Ubeda C, Vano E, Gonzalez L, Miranda P. Influence of the antiscatter grid on dose and image quality in pediatric interventional cardiology X-ray systems. Catheterization and cardiovascular interventions : official journal of the Society for Cardiac Angiography & Interventions. 2013;82(1):51-7.
224. Partridge J, McGahan G, Causton S, Bowers M, Mason M, Dalby M, et al. Radiation dose reduction without compromise of image quality in cardiac angiography and intervention with the use of a flat panel detector without an antiscatter grid. Heart. 2006;92(4):507-10.
225. Wang Y, Guo T, Liang G, Zhao L, Pan J, Li S, et al. Safe and efectivef guidance by intracardiac echocardiography for transcatheter closure in atrial septal defects. Int J Clin Exp Med. 2015;8(5):8015-9.
226. Kipel G, Arnon R, Ritter SB. Transesophageal echocardiographic guidance of balloon atrial septostomy. J Am Soc Echocardiogr. 1991;4(6):631-5.
227. Bonhoeffer P, Boudjemline Y, Qureshi SA, Le Bidois J, Iserin L, Acar P, et al. Percutaneous insertion of the pulmonary valve. Journal of the American College of Cardiology. 2002;39(10):1664-9.
228. Boothroyd A, McDonald E, Moores BM, Sluming V, Carty H. Radiation exposure to children during cardiac catheterization. British Journal of Radiology. 1997;70(FEB.):180-85.
229. McLaren C. Specific issues in interventional radiology In: Scriven M, Rogers A, editors. Paediatric Radiation Protection; London: The British Institute of Radiology; 2010.
230. Hart D, Hillier M, Wall B. Dose to patients from radiographic and fluoroscopic imaging procedures in the UK - 2005 review. Chilton, Didcott: Health protection Agency, 2007.
231. Hart D, Hillier M, Shrimpton P. Doses to patients from radiographic and fluoroscopic x-ray imaging procedures in the UK - 2010 review. . Chilton, Didcot: Health Protection Agency, 2012.
232. George MR. Hemophagocytic lymphohistiocytosis: review of etiologies and management. J Blood Med. 2014;5:69-86.
233. Bjorge T, Cnattingius S, Lie RT, Tretli S, Engeland A. Cancer risk in children with birth defects and in their families: a population based cohort study of 5.2 million children from Norway and Sweden. Cancer Epidemiol Biomarkers Prev. 2008;17(3):500-6.
234. Balter S, Hopewell JW, Miller DL, Wagner LK, Zelefsky MJ. Fluoroscopically guided interventional procedures: a review of radiation effects on patients' skin and hair. Radiology. 2010;254(2):326-41.
235. Ukisu R, Kushihashi T, Soh I. Skin injuries caused by fluoroscopically guided interventional procedures: case-based review and self-assessment module. AJR Am J Roentgenol. 2009;193(6 Suppl):S59-69.
236. Nicholson R, Tuffee F, Uthappa MC. Skin sparing in interventional radiology: the effect of copper filtration. Br J Radiol. 2000;73(865):36-42.
237. Dragusin O, Gewillig M, Desmet W, Smans K, Struelens L, Bosmans H. Radiation dose survey in a paediatric cardiac catheterisation laboratory equipped with flat-panel detectors. Radiation Protection Dosimetry. 2008;129(1-3):91-95.
238. Sawdy JM, Kempton TM, Olshove V, Gocha M, Chisolm JL, Hill SL, et al. Use of a dose-dependent follow-up protocol and mechanisms to reduce patients and staff radiation exposure in congenital and structural interventions. Catheterization and cardiovascular interventions : official journal of the Society for Cardiac Angiography & Interventions. 2011;78(1):136-42.

239. Edyvean S. National dose registries - an update. IR(ME)R Update; The Royal Society of Medicine, London: British Institute of Radiology; 2014.
240. Edyvean S. PHE patient dose surveys - an update. IR(ME)R Update; IET Birmingham: Austin Court: British Institute of radiology; 2015.
241. International Commission on Radiological Protection (ICRP). Diagnostic reference levels in medical imaging: review and additional advice. Annals of the ICRP. 2001;31(4):33-52.
242. Tapiovaara M, Siiskonen T. PCXMC: A Monte Carlo program for calculating patient doses in medical x-ray examinations. In: STUK - Radiation and Nuclear Safety Authority, editor. Helsinki, Finland2008.
243. Cristy M, Eckerman K. Specific absorbed fractions of energy at various ages from internal photon sources. I. Methods. Oak Ridge Oak Ridge National Laboratory1987
244. Castellano IA, Dance DR, Evans PM. CT dosimetry: getting the best from the adult Cristy phantom. Radiat Prot Dosimetry. 2005;114(1-3):321-5.
245. Servomaa A, Tapiovaara M. Organ Dose Calculation in Medical X Ray Examinations by the Program PCXMC. Radiat Prot Dosimetry 1998;80(1-3):213-19.
246. Hart D, Jones D, Wall B. Normalised Organ Doses for Paediatric X-ray Examinations Calculated using Monte Carlo Techniques. NRPB-SR279. Chilton: NRPB1996.
247. International Commission on Radiation Units and Measurements. Report 74, Appendix F: PCXMC - A PC based Monte Carlo program for calculating patient doses in medical x-ray examinations. Journal of the ICRU. 2005;5(2).
248. Brady Z. Radiation doses and risks from paediatric computed tomography (PhD thesis): RMIT University; 2012.
249. Standring S. Gray's Anatomy: The Anatomical Basis of Clinical Practice. 40 ed: Churchill Livingstone, 2008.
250. Amato E, Lizio D, Settineri N, Di Pasquale A, Salamone I, Pandolfo I. A method to evaluate the dose increase in CT with iodinated contrast medium. Med Phys. 2010;37(8):4249-56.
251. Amato E, Salamone I, Naso S, Bottari A, Gaeta M, Blandino A. Can contrast media increase organ doses in CT examinations? A clinical study. AJR Am J Roentgenol. 2013;200(6):1288-93.
252. Kreft T, Viitala, A, Tapiovaara, M. Excel-pcxmc (2.0) batch run script. 3.0 ed2006, 2009.
253. Medwow. Manufacturer specifications. [20/11/2013]; Available from: http://medwow.com/.
254. Royal College of Paediatrics and Child Health (RCPCH) and the Department of health (DOH). Growth Charts (Males and Females 0-4 and 2-18 years). 2009.
255. Gunn C. Bones and joints : a guide for students. 6 ed. Edinburgh: Elsevier Churchill Livingstone 2012.
256. Cristy M. Active bone marrow distribution as a function of age in humans. Phys Med Biol. 1981;26(3):389-400.
257. Weir J, Abrahams P, Spratt J, Salkowski L. Imaging Atlas of Human Anatomy. 4 ed: Mosby Elsevier, 2011.
258. Lamart S, Imran R, Simon SL, Doi K, Morton LM, Curtis RE, et al. Prediction of the location and size of the stomach using patient characteristics for retrospective radiation dose estimation following radiotherapy. Phys Med Biol. 2013;58(24):8739-53.
259. Martin E, Olson, A,. Radiation exposure to the paediatric patient from cardiac catheterization and angiocardiography. Br J Radiol. 1980;53:100-06.
260. Poludniowski G, Landry G, DeBlois F, Evans PM, Verhaegen F. SpekCalc: a program to calculate photon spectra from tungsten anode x-ray tubes. Phys Med Biol. 2009;54(19):N433-8.
261. Poludniowski GG, Evans PM. Calculation of x-ray spectra emerging from an x-ray tube. Part I. electron penetration characteristics in x-ray targets. Med Phys. 2007;34(6):2164-74.
262. Poludniowski GG. Calculation of x-ray spectra emerging from an x-ray tube. Part II. X-ray production and filtration in x-ray targets. Med Phys. 2007;34(6):2175-86.

263. Brennan PC, O'Leary D. Source to image receptor distance. Br J Radiol. 2006;79(939):266; author reply 66-7.
264. Poletti JL, McLean D. The effect of source to image-receptor distance on effective dose for some common X-ray projections. Br J Radiol. 2005;78(933):810-5.
265. Zankl M, Wittmann A. The adult male voxel model "Golem" segmented from whole-body CT patient data. Radiat Environ Biophys. 2001;40(2):153-62.
266. Banner A. The Calculus Lifesaver: All the Tools You Need to Excel at Calculus (Princeton Lifesaver Study Guides) Princeton University Press, 2007.
267. United Nations Children's Fund (UNICEF) and the World Health Organisation (WHO). Low Birthweight: Country, regional and global estimates. New York, 2004.
268. Valcamonico A, Accorsi P, Sanzeni C, Martelli P, La Boria P, Cavazza A, et al. Mid- and long-term outcome of extremely low birth weight (ELBW) infants: an analysis of prognostic factors. The journal of maternal-fetal & neonatal medicine : the official journal of the European Association of Perinatal Medicine, the Federation of Asia and Oceania Perinatal Societies, the International Society of Perinatal Obstet. 2007;20(6):465-71.
269. Lin PJ. The operation logic of automatic dose control of fluoroscopy system in conjunction with spectral shaping filters. Med Phys. 2007;34(8):3169-72.
270. Siemens A. Guide to Low dose (sales brochure). Unknown publication date.
271. American Association of Physicists in Medicine. AAPM Report no. 125 - Functionality and Operation of Fluoroscopic Automatic Brightness Control/Automatic Dose Rate Control Logic in Modern Cardiovascular and Interventional Angiography Systems. College Park, MD2012.
272. Seissl J, Eschenbacher H, inventors; X-ray diagnostic apparatus with a filter device. United States1997.
273. Clark AL, Brennan AG, Robertson LJ, McArthur JD. Factors affecting patient radiation exposure during routine coronary angiography in a tertiary referral centre. Br J Radiol. 2000;73(866):184-9.
274. Calkins H, Niklason L, Sousa J, el-Atassi R, Langberg J, Morady F. Radiation exposure during radiofrequency catheter ablation of accessory atrioventricular connections. Circulation. 1991;84(6):2376-82.
275. Schueler BA, Julsrud PR, Gray JE, Stears JG, Wu KY. Radiation exposure and efficacy of exposure-reduction techniques during cardiac catheterization in children. American Journal of Roentgenology. 1994;162(1):173-77.
276. Ross R, Joshi V, Carravallah D, Morrow W. Reduced Radiation During Cardiac Catheterization of Infants Using Acquisition Zoom Technology. THE AMERICAN JOURNAL OF CARDIOLOGY. 1997;79:691-93.
277. Broadhead DA, Chapple CL, Faulkner K, Davies ML, McCallum H. The impact of cardiology on the collective effective dose in the North of England. Br J Radiol. 1997;70(833):492-7.
278. Kuon E, Glaser C, Dahm JB. Effective techniques for reduction of radiation dosage to patients undergoing invasive cardiac procedures. Br J Radiol. 2003;76(906):406-13.
279. Al-Haj AN, Lobriguito AM, Rafeh W. Variation in radiation doses in paediatric cardiac catheterisation procedures. Radiat Prot Dosimetry. 2008;129(1-3):173-8.
280. Chida K, Ohno T, Kakizaki S, Takegawa M, Yuuki H, Nakada M, et al. Radiation dose to the pediatric cardiac catheterization and intervention patient. American Journal of Roentgenology. 2010;195(5):1175-79.
281. McFadden SL, Hughes CM, Winder RJ. Variation in radiographic protocols in paediatric interventional cardiology. Journal of radiological protection : official journal of the Society for Radiological Protection. 2013;33(2):313-9.
282. Ubeda C, Miranda P, Vano E. Local patient dose diagnostic reference levels in pediatric interventional cardiology in Chile using age bands and patient weight values. Med Phys. 2015;42(2):615-22.

283. Hufton AP. Diagnostic radiology: patient dosimetry. In: Martin C, Sutton D, editors. Practical radiation protection in healthcare. Oxford, UK: Oxford University Press; 2002.
284. CIRS Tissue Simulation & Phantom Technology. ATOM Dosimetry Phantoms, models 701-706. In: Systems. CIR, editor.2011.
285. Green S, Zamenhof R. Radiation Measurements. In: Martin CJ, Sutton DG, editors. Practical Radiation Protection in Healthcare. Oxford: Oxford University Press; 2002.
286. Thermo Scientific. Harshaw TLD Model 5500 Readers. 2007.
287. Laboratory PM. X-Ray Mass Attenuation Coefficients (Lung, ICRU-44). [10/06/2015]; Available from: http://physics.nist.gov/PhysRefData/XrayMassCoef/ComTab/lung.html.
288. Robertson RJ. Imaging in the evaluation of emphysema. Thorax. 1999;54(5):379.
289. Nunn AA, Davis SD, Micka JA, DeWerd LA. LiF:Mg,Ti TLD response as a function of photon energy for moderately filtered x-ray spectra in the range of 20-250 kVp relative to 60Co. Med Phys. 2008;35(5):1859-69.
290. Harris CK, Elson HR, Lamba MA, Foster AE. Comparison of effectiveness of thermoluminescent crystals LiF:Mg,Ti, and LiF:Mg,Cu,P for clinical dosimetry. Med Phys. 1997;24(9):1527-9.
291. Ronckers CM, Erdmann CA, Land CE. Radiation and breast cancer: a review of current evidence. Breast cancer research : BCR. 2005;7(1):21-32.
292. Preston DL, Kusumi S, Tomonaga M, Izumi S, Ron E, Kuramoto A, et al. Cancer incidence in atomic bomb survivors. Part III. Leukemia, lymphoma and multiple myeloma, 1950-1987. Radiat Res. 1994;137(2 Suppl):S68-97.
293. Wakeford R, Little MP, Kendall GM. Risk of childhood leukemia after low-level exposure to ionizing radiation. Expert review of hematology. 2010;3(3):251-4.
294. Ron E, Lubin JH, Shore RE, Mabuchi K, Modan B, Pottern LM, et al. Thyroid cancer after exposure to external radiation: a pooled analysis of seven studies. Radiat Res. 1995;141(3):259-77.
295. Keiller DA, Martin CJ. Radiation dose to the heart in paediatric interventional cardiology. Journal of radiological protection : official journal of the Society for Radiological Protection. 2015;35(2):257-64.
296. Woodard HQ, White DR. The composition of body tissues. Br J Radiol. 1986;59(708):1209-18.
297. Van Dyk J, Keane TJ, Rider WD. Lung density as measured by computerized tomography: implications for radiotherapy. International journal of radiation oncology, biology, physics. 1982;8(8):1363-72.
298. Long FR, Williams RS, Castile RG. Inspiratory and expiratory CT lung density in infants and young children. Pediatric radiology. 2005;35(7):677-83.
299. Brown RH, Wise RA, Kirk G, Drummond MB, Mitzner W. Lung density changes with growth and inflation. Chest. 2015;148(4):995-1002.
300. The Phantom Laboratory. RANDO® Phantoms Product Guide. 2015 [17/06/2015]; Available from: http://www.phantomlab.com/products/rando.php.
301. Chang K-P, Hung S-H, Chie Y-H, Shiau A-C, Huang R-J. A Comparison of physical and dosimetric properties of lung substitute materials. Medical Physics. 2012;39(4):2013-20.
302. Laussen C. Sedation and Anesthesia in Cardiac Procedures. In: Keane J, Lock, JE, Fyler, DC, editor. NADAS Pediatric cardiolgy. Philadelphia: Saunders Elsevier; 2009.
303. Hwang UJ, Shin DH, Kim TH, Moon SH, Lim YK, Jeong H, et al. The effect of a contrast agent on proton beam range in radiotherapy planning using computed tomography for patients with locoregionally advanced lung cancer. International journal of radiation oncology, biology, physics. 2011;81(4):e317-24.
304. Wertz H, Jakel O. Influence of iodine contrast agent on the range of ion beams for radiotherapy. Med Phys. 2004;31(4):767-73.
305. Zabel-du Bois A, Ackermann B, Hauswald H, Schramm O, Sroka-Perez G, Huber P, et al. Influence of intravenous contrast agent on dose calculation in 3-D treatment planning for

radiosurgery of cerebral arteriovenous malformations. Strahlentherapie und Onkologie : Organ der Deutschen Rontgengesellschaft [et al]. 2009;185(5):318-24.
306. Zanki M, Fill U, Petoussi-Henss N, Regulla D. Organ dose conversion coefficients for external photon irradiation of male and female voxel models. Phys Med Biol. 2002;47(14):2367-85.
307. Johnson PB, Geyer A, Borrego D, Ficarrotta K, Johnson K, Bolch WE. The impact of anthropometric patient-phantom matching on organ dose: a hybrid phantom study for fluoroscopy guided interventions. Med Phys. 2011;38(2):1008-17.
308. Thompson DE, Mabuchi K, Ron E, Soda M, Tokunaga M, Ochikubo S, et al. Cancer incidence in atomic bomb survivors. Part II: Solid tumors, 1958-1987. Radiat Res. 1994;137(2 Suppl):S17-67.
309. Preston DL, Mattsson A, Holmberg E, Shore R, Hildreth NG, Boice JD, Jr. Radiation effects on breast cancer risk: a pooled analysis of eight cohorts. Radiat Res. 2002;158(2):220-35.
310. Kellerer AM, Nekolla EA, Walsh L. On the conversion of solid cancer excess relative risk into lifetime attributable risk. Radiat Environ Biophys. 2001;40(4):249-57.
311. Vaiserman AM. Radiation hormesis: historical perspective and implications for low-dose cancer risk assessment. Dose-response : a publication of International Hormesis Society. 2010;8(2):172-91.
312. Martin CJ. Effective dose: how should it be applied to medical exposures? Br J Radiol. 2007;80(956):639-47.
313. Einstein AJ. Effects of radiation exposure from cardiac imaging: how good are the data? Journal of the American College of Cardiology. 2012;59(6):553-65.
314. ((UNSCEAR) UNSCotEoAR. Sources, Effects and Risks of Ionizing Radiation. UNSCEAR 2013 Report, Volume II, Scientific annex B: Effects of radiation exposure of Children. New York: United Nations2013.
315. Berrington de González A, Iulian Apostoaei A, Veiga L, Rajaraman P, Thomas B, Hoffman F, et al. RadRAT: a radiation risk assessment tool for lifetime cancer risk projection. Journal of radiological protection : official journal of the Society for Radiological Protection. 2012;32(3):205-22.
316. Office for National Statistics. Mortality in England and Wales: Average Life Span, 2010. 2012.
317. Olsen M, Christensen TD, Pedersen L, Johnsen SP, Hjortdal VE. Late mortality among Danish patients with congenital heart defect. American Journal of Cardiology. 2010;106(9):1322-6.
318. Ron E, Ikeda T, Preston DL, Tokuoka S. Male breast cancer incidence among atomic bomb survivors. J Natl Cancer Inst. 2005;97(8):603-5.
319. Heyes GJ, Mill AJ, Charles MW. Mammography-oncogenecity at low doses. Journal of radiological protection : official journal of the Society for Radiological Protection. 2009;29(2A):A123-32.
320. Jacob P, Ruhm W, Walsh L, Blettner M, Hammer G, Zeeb H. Is cancer risk of radiation workers larger than expected? Occup Environ Med. 2009;66(12):789-96.
321. Wakeford R, Kendall GM, Little MP. The proportion of childhood leukaemia incidence in Great Britain that may be caused by natural background ionizing radiation. Leukemia. 2009;23(4):770-6.
322. Berrington de González A, Apostoaei J, Veiga L, Rajaraman P, Thomas BA, Hoffman FO, et al. Radiation Risk Assessment Tool (RadRAT). National Cancer Institute; 2012 [05/10/2105]; Available from: http://dceg.cancer.gov/tools/risk-assessment/radrat.
323. van Laar M, McKinney PA, Stark DP, Glaser A, Kinsey SE, Lewis IJ, et al. Survival trends of cancer amongst the south Asian and non-south Asian population under 30 years of age in Yorkshire, UK. Cancer Epidemiol. 2012;36(1):e13-8.
324. van Laar M, McKinney PA, Parslow RC, Glaser A, Kinsey SE, Lewis IJ, et al. Cancer incidence among the south Asian and non-south Asian population under 30 years of age in Yorkshire, UK. Br J Cancer. 2010;103(9):1448-52.
325. van Laar M, McKinney PA, Parslow RC, Glaser A, Kinsey SE, Lewis IJ, et al. Corrigendum for Cancer incidence among the south Asian and non-south Asian population under 30 years of age in Yorkshire, UK. Br J Cancer. 2013;108(5):1223-24.

326. Harbron RW. Letter by Harbron regarding article, "cumulative radiation exposure and cancer risk estimation in children with heart disease". Circulation. 2015;131(16):e418.
327. Jemal A, Bray F, Center MM, Ferlay J, Ward E, Forman D. Global cancer statistics. CA Cancer J Clin. 2011;61(2):69-90.
328. Cancer Research UK. Statistics and outlook for breast cancer. 2014 [24/11/2015]; Available from: http://www.cancerresearchuk.org/about-cancer/type/breast-cancer/treatment/statistics-and-outlook-for-breast-cancer.
329. Cancer Research UK. Statistics and outlook for acute lymphoblastic leukaemia. 2015 [cited 24/11/2015]; Available from: http://www.cancerresearchuk.org/about-cancer/type/all/treatment/statistics-and-outlook-for-acute-lymphoblastic-leukaemia.
330. Cancer Research UK. Statistics and outlook for acute myeloid leukaemia. 2015 [24/11/2015]; Available from: http://www.cancerresearchuk.org/about-cancer/type/aml/treatment/statistics-and-outlook-for-acute-myeloid-leukaemia.
331. Baysson H, Réhel J, Boudjemline Y, Petit J, Girodon B, Aubert B, et al. Risk of cancer associated with cardiac catheterization procedures during childhood: a cohort study in France. BMC Public Health 2013, 13:266. 2013;13:266.
332. Vandenbroucke J. A shortcut method for calculating the 95 per cent confidence interval of the standardized mortality ratio. Am J Epidemiol. 1982;115(2):303-04.
333. Asrani SK, Warnes CA, Kamath PS. Hepatocellular carcinoma after the Fontan procedure. N Engl J Med. 2013;368(18):1756-7.
334. BBC News. Leeds child heart unit death rates 'worst in England'. 2013 [03/09/2015]; Available from: http://www.bbc.co.uk/news/uk-england-leeds-23086203.
335. BBC News. Bristol scandal surgeon rejects criticism. 2002 [03/09/2015]; Available from: http://news.bbc.co.uk/1/hi/england/2091570.stm.
336. BBC News. Heart scandal 'could happen again'. 2001; Available from: http://news.bbc.co.uk/1/hi/health/1444983.stm.
337. Lee YS, Chen YT, Jeng MJ, Tsao PC, Yen HJ, Lee PC, et al. The risk of cancer in patients with congenital heart disease: a nationwide population-based cohort study in Taiwan. PLoS One. 2015;10(2):e0116844.
338. Wang SS, Wang CH, Chou NK, Chi NH, Huang SC, Yu HY, et al. Current status of heart transplantation in Taiwan. Transplant Proc. 2014;46(3):911-3.
339. Carozza SE, Langlois PH, Miller EA, Canfield M. Are children with birth defects at higher risk of childhood cancers? Am J Epidemiol. 2012;175(12):1217-24.
340. Fisher PG, Reynolds P, Von Behren J, Carmichael SL, Rasmussen SA, Shaw GM. Cancer in children with nonchromosomal birth defects. J Pediatr. 2012;160(6):978-83.
341. Engels EA, Pfeiffer RM, Fraumeni JF, Jr., Kasiske BL, Israni AK, Snyder JJ, et al. Spectrum of cancer risk among US solid organ transplant recipients. JAMA. 2011;306(17):1891-901.
342. Simard JF, Baecklund E, Kinch A, Brattstrom C, Ingvar A, Molin D, et al. Pediatric organ transplantation and risk of premalignant and malignant tumors in Sweden. Am J Transplant. 2011;11(1):146-51.
343. Euvrard S, Kanitakis J, Cochat P, Claudy A. Skin cancers following pediatric organ transplantation. Dermatol Surg. 2004;30(4 Pt 2):616-21.
344. Chinnock R, Webber SA, Dipchand AI, Brown RN, George JF. A 16-year multi-institutional study of the role of age and EBV status on PTLD incidence among pediatric heart transplant recipients. Am J Transplant. 2012;12(11):3061-8.
345. Manlhiot C, Pollock-Barziv SM, Holmes C, Weitzman S, Allen U, Clarizia NA, et al. Post-transplant lymphoproliferative disorder in pediatric heart transplant recipients. The Journal of heart and lung transplantation : the official publication of the International Society for Heart Transplantation. 2010;29(6):648-57.
346. Kinlen LJ. An examination, with a meta-analysis, of studies of childhood leukaemia in relation to population mixing. Br J Cancer. 2012;107(7):1163-8.

347. British Isles Network of Congenital Anomaly Registers. 2011 [05/11/2015]; Available from: http://www.binocar.org/.
348. Harbron RW, Pearce MS, Salotti JA, McHugh K, McLaren C, Abernethy L, et al. Radiation doses from fluoroscopically guided cardiac catheterization procedures in children and young adults in the United Kingdom: a multicentre study. Br J Radiol. 2015;88(1048):20140852.
349. Ding A, Mille MM, Liu T, Caracappa PF, Xu XG. Extension of RPI-adult male and female computational phantoms to obese patients and a Monte Carlo study of the effect on CT imaging dose. Phys Med Biol. 2012;57(9):2441-59.
350. Wagner LK. Overconfidence, overexposure, and overprotection. Radiology. 2004;233(2):307-8.
351. Reulen RC, Frobisher C, Winter DL, Kelly J, Lancashire ER, Stiller CA, et al. Long-term risks of subsequent primary neoplasms among survivors of childhood cancer. JAMA. 2011;305(22):2311-9.
352. Krille L, Zeeb H, Jahnen A, Mildenberger P, Seidenbusch M, Schneider K, et al. Computed tomographies and cancer risk in children: a literature overview of CT practices, risk estimations and an epidemiologic cohort study proposal. Radiat Environ Biophys. 2012;51(2):103-11.
353. Bosch de Basea M, Pearce MS, Kesminiene A, Bernier MO, Dabin J, Engels H, et al. EPI-CT: design, challenges and epidemiological methods of an international study on cancer risk after paediatric and young adult CT. Journal of radiological protection : official journal of the Society for Radiological Protection. 2015;35(3):611-28.
354. Meulepas JM, Ronckers CM, Smets AM, Nievelstein RA, Jahnen A, Lee C, et al. Leukemia and brain tumors among children after radiation exposure from CT scans: design and methodological opportunities of the Dutch Pediatric CT Study. Eur J Epidemiol. 2014;29(4):293-301.
355. Baysson H, Nkoumazok B, Barnaoui S, Rehel JL, Girodon B, Milani G, et al. Follow-up of children exposed to ionising radiation from cardiac catheterisation: the Coccinelle study. Radiat Prot Dosimetry. 2015;165(1-4):13-6.
356. Balter S. Imaging Educational Course: DICOM Dose SR (,etc.). 2011 [updated August 201129/05/2013].
357. Jahnen A, Kohler S, Hermen J, Tack D, Back C. Automatic computed tomography patient dose calculation using DICOM header metadata. Radiat Prot Dosimetry. 2011;147(1-2):317-20.
358. Lee C, Journy N, Tran T, Little M, Moroz B, Pearce M, et al. Organ dose estimation including uncertainty for pediatric and young adult CT scans in the United Kingdom. IARC 50th aniversary conference; Lyon, France2016.
359. Land CE, Kwon D, Hoffman FO, Moroz B, Drozdovitch V, Bouville A, et al. Accounting for shared and unshared dosimetric uncertainties in the dose response for ultrasound-detected thyroid nodules after exposure to radioactive fallout. Radiat Res. 2015;183(2):159-73.
360. NICOR. National Institute for Cardiovascular Outcomes Research. [17/03/2016]; Available from: https://www.ucl.ac.uk/nicor.
361. Fleisch D. A Student's Guide to Maxwell's Equations: Cambridge University Press, 2011.
362. Fleisch D, Kinnaman L. A Student's Guide to Waves: Cambridge University Press 2015.